Title
Microbial Ecology and Bioremediation of 1,4-Dioxane and Chlorinated Solvents Contaminated Groundwater and Soil

Author
Miao, Yu

Publication Date
2019

Peer reviewed|Thesis/dissertation

UNIVERSITY OF CALIFORNIA

Los Angeles

Microbial Ecology and Bioremediation of 1,4-Dioxane and Chlorinated Solvents Contaminated Groundwater and Soil

A dissertation submitted in partial satisfaction of the

requirements for the degree Doctor of Philosophy

in Civil Engineering

by

Yu Miao

2019

ABSTRACT OF THE DISSERTATION

Microbial Ecology and Bioremediation of 1,4-Dioxane and Chlorinated Solvents Contaminated Groundwater and Soil

by

Yu Miao

Doctor of Philosophy in Civil Engineering

University of California, Los Angeles, 2019

Professor Shaily Mahendra, Chair

It is crucial to consider the impact of abiotic and biological remediation technologies on the microbial ecology to predict the success of short-term active treatments and long-term passive attenuation processes. In this research, three bioremediation strategies were tested individually or coupled with chemical remedies in bench- and pilot-scale studies for removing 1,4-dioxane and chlorinated volatile organic compounds (CVOCs), which are widespread co-occurring contaminants in soils and water resources across the U.S., attracting attention because of their potential carcinogenicities. In each project, amplification of taxonomic and functional genes by qPCR as well as metagenomics including high-throughput sequencing were applied to provide reliable information about microbial communities in the ecological matrices as they transitioned

from 1,4-dioxane and CVOC contaminations to exposures from treatment technologies and degradation products.

A comprehensive multiple lines of evidence approach provided evidence of natural attenuation by microorganisms capable of metabolic or co-metabolic degradation of 1,4-dioxane within a large, diffuse plume. A pilot study of bioaugmentation with *Pseudonocardia dioxanivorans* CB1190 through direct injection as well as in-situ bioreactor was successfully conducted at a site impacted by 1,4-dioxane and CVOCs.

Bench-scale microcosms were established to inform pilot-scale ex-situ bioreactors and in-situ propane biosparging at an industrial site. 1,4-Dioxane co-metabolism by indigenous microbes was accelerated by biostimulation with propane and nutrients. Inoculations with CB1190 or propanotroph, *Rhodococcus ruber* ENV425, were eventually outcompeted by native microbes, but gene allocations for xenobiotics and lipid metabolism were enhanced and accompanied rapid 1,4-dioxane degradation rates.

Three synergistic treatment trains: oxidation & catalysis, oxidation & biodegradation, and catalysis & biodegradation, were applied to achieve nearly complete 1,4-dioxane removals even in the presence of inhibitory CVOCs. While oxidant- or nanocatalyst-tolerant microbes were dominant immediately after chemical processes, the microbial community thrived during the biodegradation in a deterministic process over time, presenting higher biodiversity that indicated a more stable community. The post-treatment community carried various functional potentials, such as degradation of CVOCs and aromatic hydrocarbons, as well as nitrogen fixation.

These mechanistic and quantitative data will be valuable for developing synergistic treatments that lead to savings in cost, energy, and substrate amendments for the remediation of contaminant mixtures.

This dissertation of Yu Miao is approved.

Richard Ambrose

Jennifer Ayla Jay

Sanjay Mohanty

Shaily Mahendra, Committee Chair

University of California, Los Angeles

2019

Table of Contents

List of Figures

List of Tables

Acknowledgements

First of all, I would like to express my deepest appreciation to my advisor, Professor Shaily Mahendra, and thank my committee members, Professor Richard Ambrose, Professor Jennifer Ayla Jay, and Professor Sanjay Mohanty. Professor Mahendra introduced me to soil and groundwater bioremediation and provided opportunities and advice on writing proposals and manuscripts. Her guidance, advice, support, mentoring, insights greatly contributed to my academic improvement and research career. In addition to the research, Professor Mahendra is a model example in life that she respects and encourages students, and is optimistic and strong even suffering from the disease. Besides, all my committee members provided endless advice, knowledge, and resources in my 4-year Ph.D. training.

It also gives me great pleasure to thank my collaborators in my research, who generously donated their time to advise me on scientific and engineering questions. I thank Andrew Madison of Golder, Inc. for providing natural attenuation site samples, that was included in Chapter 3. I thank Rebecca Mora, Holly Holbrook, Dr. Francisco Barajas of AECOM, Inc., Dr. Dora Chiang of CDM Smith, Inc., and Dr. Kerry Sublette in University of Tulsa, for providing project about in-situ bioaugmentation that was described in Chapter 4. I thank Dr. Monica Heintz, Caitlin Bell, Jacelyn Saling of Arcadis, Inc. and Dave Favero of RACER Trust, Inc. for providing site samples to conduct bench-scale microcosms study that was involved in Chapter 5 and two submitted manuscripts. I thank Dr. David Adamson and Dr. Charles Newell of GSI Environment, Inc., Dr. Michael Wong and Dr. Kimberly Heck in Rice University, for collaborating on combined treatment trains project that supported Chapter 6, two publications, and one submitted manuscript. I also thank Dr. Claudia Walecka-Hutchison and Dr. Erin Mack of Dow/DuPont, and Jeff Gamlin and William DiGuiseppi of Jacobs, Inc. for other project opportunities.

I would also like to extend my deepest gratitude to Mahendra lab members, who offered me continuous supports throughout my Ph.D. training. I sincerely thank Dr. Phillip Gedalanga for his help when I first stepped in the lab. Phil used his patience and immense knowledge to get me involved in projects smoothly and efficiently, and set a great start for my 4-year study. I would also thank Dr. Meng Wang, who helped me to familiarize with the laboratory, department, campus, and Los Angeles. I thank Nicholas Johnson and Alexandra Polasko, who joined Mahendra lab in the same year with me. Nick is warm-hearted and patient, and Alex is creative and energetic, and both of them inspired and encouraged me on my research. I am also grateful to the former and current group members: Dr. Nancy Merino, Dr. Shu Zhang, Michelle Myers, Dr. Yun Liu, Shashank Kalra, Anjali Lothe, Nik Ortman, Thien Phan, Jamie Liu, Sophia Wang, Ellen O' Connor, Rocio Ambrocio, An Gao, Pia Ramos, Yifan Gao, Jerry Ngo, Catherine Clark, Ivy Kwok, Peibo Guo, Ly Tan, Sylvia Liang, Victor Xue, Dominic Robolino, Alessandro Zulli, and Julia Park.

I would like to thank Dr. Mihyun Park to assign me as teaching assistant in her statistic class, where I learned and practiced teaching strategies. I also would like to thank many people in the Department of Civil and Environmental Engineering, who have helped me a lot in ordering and other graduate school matters: Reba Glover, Jesse Dieker, Dr. Vanessa Thulsiraj, Dr. Ben Rossi, Helen Weary, Dylan Giron, Paula Columbia.

This research was supported by the Strategic Environmental Research and Development Program (SERDP) awards ER-2300, ER-2307, Air Force Civil Engineer Center (contract #FA8903-13-C-0003), and by National Science Foundation Faculty Early Career Development (CAREER) award #1255021. This work used computational and storage services associated with the Hoffman2 Shared Cluster provided by UCLA Institute for Digital Research and Education's Research Technology Group. This research was performed in a renovated collaboratory funded by

the National Science Foundation, Grant Number 0963183, which was awarded under the American Recovery and Reinvestment Act of 2009 (ARRA). This research was also supported by Dow Chemical Company (contract #244633), DuPont Corporate Remediation Group (con- tract #MA-03653-13), Arcadis, Inc. (#B0064480.2017.00502), and a gift from Pfizer Global Engineering to UCLA.

The last but not the least, I am extremely grateful to my family and friends, who always have my back no matter what happens. The 4-year study would not have been accomplished without the support and nurturing of my parents Xiangyang and Xianying, my girlfriend Ruthy, and other relatives and friends. I got blessed from all above.

Vita

EDUCATION

Ph.D. Candidate, Environmental Engineering, University of California, Los Angeles	Expected Aug 2019
M.E., Environmental Engineering, Nanjing University, Nanjing, China	2015
B.E., Environmental Engineering, Ocean University of China, Qingdao, China	2012

PEER-REVIEWED PUBLICATIONS

Miao, Y., Johnson, N.W., Phan, T., Heck, K., Gedalanga, P.B., Adamson, D., Newell, C., Wong, M.S., Mahendra, S., 2020. Monitoring, Assessment, and Prediction of Microbial Shifts in Coupled Catalysis and Biodegradation Treatment for 1,4-Dioxane and Co-contaminants. *Environment International*, submitted.

Miao, Y., Johnson, N.W., Heintz, M., Bell, C.H., Gedalanga, P.B., Favero, D., Mahendra, S., 2020. Profiling microbial community structures in biostimulation and bioaugmentation strategies for treating 1,4-dioxane contaminated groundwater. *Water Research*, submitted.

Horst, J.F., Bell, C.H., Lorenz, A., Heintz, M., **Miao, Y.**, Saling, J., Favero, D., Mahendra, S., 2019. Bioremediation of 1,4-dioxane: Successful demonstration of in situ and ex situ approaches. *Groundwater Monitor & Remediation*, submitted.

Mora, R., **Miao, Y.**, Barajas-Rodriguez, F., Holbrook, H., Anderson, R., Sublette, K., Mahendra, S., 2019. Field bioaugmentation with *Pseudonocardia dioxanivorans* CB1190 metabolizing 1,4-dioxane using in situ bioreactors. *Remediation Journal*, submitted.

Berger, A.W., Valenca, R., **Miao, Y.**, Ravi, S., Mahendra, S., Mohanty, S., 2019 Biochar increases nitrate removal capacity of woodchip biofilters during high-intensity rainfall. *Water Research*, accepted and in press.

Li, J., Cai, M.H., **Miao, Y.**, Luo, G., Li, W.T., Li, Y., Li, A.M., 2019. Bacterial community structure and predicted function in an acidogenic sulfate-reducing reactor: effect of organic carbon to sulfate ratios. *Bioresource Technology*, accepted and in press.

Miao, Y., Johnson, N.W., Gedalanga, P.B., Adamson, D., Newell, C., Mahendra, S., 2019. Response and recovery of microbial communities subjected to oxidative and biological treatments of 1,4-dioxane and co-contaminants. *Water Research*, 149, 74-85.

Miao, Y., Johnson, N.W., Heck, K., Guo, S.J., Powell, C.D., Phan, T., Gedalanga, P.B., Adamson, D.T., Newell, C.J., Wong, M.S., Mahendra, S., 2018. Microbial responses to combined oxidation and catalysis treatment of 1,4-dioxane and co-contaminants in groundwater and soil. *Frontiers of Environmental Science & Engineering*, 12 (5), 1-13.

Miao, Y., Zhang, X.X., Jia, S.Y., Liao, R.H., Li, A.M., 2018. Comprehensive analyses of functional bacteria and genes in a denitrifying EGSB reactor under Cd(II) stress. *Applied Microbiology and Biotechnology*, 102 (19), 8551-8560.

Liao, R., **Miao, Y.**, Li, J., Li, Y., Wang, Z., Du, J., Li, Y., Li, A., Shen, H., 2018. Temperature dependence of denitrification microbial communities and functional genes in an expanded granular sludge bed reactor treating nitrate-rich wastewater. *RSC Advances*, 8 (73), 42087-42094.

Zhao, L.D., Lu, X., Polasko, A., Johnson, N.W., **Miao, Y.**, Yang, Z.M., Mahendra, S., Gu, B.H., 2018. Co-contaminant effects on 1,4-dioxane biodegradation in packed soil column flow-through systems. *Environmental Pollution*, 243, 573-581.

Miao, Y., Guo, X.C., Jiang, W., Zhang, X.X., Wu, B., 2017. Mechanisms of microbial community structure and biofouling shifts under multivalent cations stress in membrane bioreactors. *Journal of Hazardous Materials*, 327, 89-96.

Miao, Y., Wang, Z., Liao, R.H., Shi, P., Li, A.M., 2017. Assessment of phenol effect on microbial community structure and function in an anaerobic denitrifying process treating high concentration nitrate wastewater. *Chemical Engineering Journal*, 330, 757-763.

Jia, S.Y., Zhang, X.X., **Miao, Y.**, Zhao, Y.T., Ye, L., Li, B., Zhang, T., 2017. Fate of antibiotic resistance genes and their associations with bacterial community in livestock breeding wastewater and its receiving river water. *Water Research*, 124, 259-268.

Gedalanga, P., Madison, A., **Miao, Y.**, Richards, T., Hatton, J., DiGuiseppi, W.H., Wilson, J., Mahendra, S., 2016. A multiple lines of evidence framework to evaluate intrinsic biodegradation of 1,4-dioxane. *Remediation Journal*, 27 (1), 93-114.

Miao, Y., Liao, R.H., Zhang, X.X., Wang, Y., Wang, Z., Shi, P., Liu, B., Li, A.M., 2015. Metagenomic insights into Cr(VI) effect on microbial communities and functional genes of an expanded granular sludge bed reactor treating high-nitrate wastewater. *Water Research*, 76, 43-52.

Miao, Y., Liao, R.H., Zhang, X.X., Liu, B., Li, Y., Wu, B., Li, A.M., 2015. Metagenomic insights into salinity effect on diversity and abundance of denitrifying bacteria and genes in an expanded granular sludge bed reactor treating high-nitrate wastewater. *Chemical Engineering Journal*, 277, 116-123.

Guo, X.C.*, **Miao, Y.***, Wu, B., Ye, L., Yu, H.Y., Liu, S., Zhang, X.X., 2015. Correlation between microbial community structure and biofouling as determined by analysis of microbial community dynamics. *Bioresource Technology*, 197, 99-105. **(* Co-First authors)**

Shi, P., Ma, R., Zhou, Q., Li, A.M., Wu, B., **Miao, Y.**, Chen, X., Zhang, X.X., 2015. Chemical and bioanalytical assessments on drinking water treatments by quaternized magnetic microspheres. *Journal of Hazardous Materials*, 285, 53-60.

Jia, S.Y., He, X.W., Bu, Y.Q., Shi, P., **Miao, Y.**, Zhou, H.P., Shan, Z.J., Zhang, X.X., 2014. Environmental fate of tetracycline resistance genes originating from swine feedlots in river water. *Journal of Environmental Science and Health*, 49 (8), 624-631.

Liao, R.H., Li, Y., Wang, Z., **Miao, Y.**, Shen, K., Shi, P., Ma, Y., Li, W.T., Li, A.M., 2014. 454 pyrosequencing analysis on microbial diversity of an expanded granular sludge bed reactor treating high NaCl and nitrate concentration wastewater. *Biotechnology and Bioprocess Engineering*, 19 (1), 183-190.

Liao, R.H., Li, Y., Yu, X.M., Shi, P., Wang, Z., Shen, K., Shi, Q.Q., **Miao, Y.**, Li, W.T., Li, A.M., 2014. Performance and microbial diversity of an expanded granular sludge bed reactor for high sulfate and nitrate waste brine treatment. *Journal of Environmental Sciences*, 26 (4), 717-725.

Liao, R.H., **Miao, Y.**, Hong, Y., Li, Y.M., Shen, Z.Y., Wang, Z.M., 2013. Nitrate reduction using nanoscale zero valent iron supported by porous suspended ceramsite. *Advanced Materials Research*, 726, 677-682.

Wang, Z., Zhang, X.X., Huang, K.L., **Miao, Y.**, Shi, P., Liu, B., Long, C., Li, A.M., 2013. Metagenomic profiling of antibiotic resistance genes and mobile genetic elements in a tannery wastewater treatment plant. *Plos One*, 8 (10).

AWARDS

Outstanding Ph.D. Student in Civil and Environmental Engineering Award	Los Angeles, CA, 06/2019
Travel award for 1,4-Dioxane Working Group Meeting	Detroit, MI, 10/2017
The Excellent Master Thesis in Jiangsu Province	Nanjing, China, 09/2016
The outstanding Graduate of Nanjing University	Nanjing, China, 05/2015
Nanjing University "Meng Lan" Scholarship	Nanjing, China, 03/2015
The Excellent presentation of 2014 Jiangsu Microbiology Council	Nanjing, China, 09/2014

Chapter 1 Introduction and Objectives

1.1 Objectives and Scope

The overall objective of this research was to characterize the microbial ecology shifts and recoveries during bioremediation of groundwater and soil polluted with 1,4-dioxane and chlorinated volatile organic compounds (CVOCs) co-contaminants. In this dissertation, several related research efforts were carried out in bench-scale and pilot-scale reactors, whose specific objectives are described below.

Objective 1: To validate natural attenuation of 1,4-dioxane using biomarker genes for 1,4-dioxane biodegradation in combination with compound-specific stable isotope analyses and spatio-temporal trends of contaminant concentrations and biogeochemical indicators.

Objective 2: To evaluate in-situ bioaugmentation approaches with *Pseudonocardia dioxanivorans* CB1190 for enhancing biodegradation of 1,4-dioxane at a site contaminated with 1,4-dioxane and CVOCs.

Objective 3: To compare performances and microbial community impacts of metabolic and co-metabolic bioaugmentation, as well as biostimuation with oxygen, propane, and nutrients for 1,4-dioxane biodegradation.

Objective 4: To simulate various synergistic treatment trains for 1,4-dioxane and CVOC in laboratory microcosms set up using soil and groundwater collected from a contaminated site, reveal the molecular mechanisms, and analyze microbial community dynamics before, during, and after active treatments.

1.2 Dissertation Overview

This dissertation is organized into seven chapters. A synthesis of published literature leading to the research objectives is presented in Chapter 1. Chapter 2 describes the background and current

research about 1,4-dioxane degradation and metagenomics. Chapter 3 contains results of multiple lines of evidence to validate natural attenuation of 1,4-dioxane and CVOCs, which are included with permission from the *Remediation: The Journal of Environmental Cleanup Costs, Technologies and Techniques* (Gedalanga et al., 2016). The subsurface distribution and 1,4-dioxane degradation performance of CB1190 bioaugmentation via direct injection and immobilization in in-situ bioreactors (ISBRs) is described in Chapter 4. This work has been submitted for publication in *Remediation: The Journal of Environmental Cleanup Costs, Technologies and Techniques* (Mora et al., 2019). Bench-scale biostimulation and bioaugmentation studies leading to pilot-scale ex-situ bioreactors and in-situ biosparging considerations are reported in Chapter 5. Portions of this research have been submitted to *Groundwater Monitor & Remediation* (Horst et al., 2019) and *Water Research* (Miao et al., 2020a). Three separate treatment trains consisting of oxidative, catalytic, and biological processes for the degradation of 1,4-dioxane and CVOCs established in laboratory microcosms are discussed in Chapter 6. Two papers based on this work have already been published (Miao et al., 2018; Miao et al., 2019) and are included in this dissertation with the journal's permission. Another manuscript will be submitted to a special issue "Emerging Contaminants in the Environment: Occurrence, Source and Risks" in *Environment International* (Miao et al., 2020b). A summary of key results along with their significance in environmental engineering and microbiology is provided in Chapter 7. Suggestions for future research in these areas are also included.

1.3 References

Gedalanga, P., Madison, A., Miao, Y., Richards, T., Hatton, J., DiGuiseppi, W.H., Wilson, J., Mahendra, S., 2016. A multiple lines of evidence framework to evaluate intrinsic biodegradation of 1,4-dioxane. Remediation Journal, 27 (1), 93-114.

Horst, J.F., Bell, C.H., Lorenz, A., Heintz, M., Miao, Y., Saling, J., Favero, D., Mahendra, S., 2019. Bioremediation of 1,4-dioxane: Successful demonstration of in situ and ex situ approaches. ndwater Monitor & Remediation, submitted.

Miao, Y., Johnson, N.W., Heintz, M., Bell, C.H., Gedalanga, P.B., Favero, D., Mahendra, S., 2020a. Profiling microbial community structures in biostimulation and bioaugmentation strategies for treating 1,4-dioxane contaminated groundwater. Water Research, submitted.

Miao, Y., Johnson, N.W., Phan, T., Heck, K., Gedalanga, P.B., Adamson, D., Newell, C., Wong, M.S., Mahendra, S., 2020b. Monitoring, assessment, and prediction of microbial shifts in coupled catalysis and biodegradation treatment for 1,4-dioxane and co-contaminants. Environment International, submitted.

Miao, Y., Johnson, N.W., Gedalanga, P.B., Adamson, D., Newell, C., Mahendra, S., 2019. Response and recovery of microbial communities subjected to oxidative and biological treatments of 1,4-dioxane and co-contaminants. Water Research, 149, 74-85.

Miao, Y., Johnson, N.W., Heck, K., Guo, S.J., Powell, C.D., Phan, T., Gedalanga, P.B., Adamson, D.T., Newell, C.J., Wong, M.S., Mahendra, S., 2018. Microbial responses to combined oxidation and catalysis treatment of 1,4-dioxane and co-contaminants in groundwater and soil. Frontiers of Environmental Science & Engineering, 12 (5), 1-13.

Mora, R., Miao, Y., Barajas-Rodriguez, F., Holbrook, H., Anderson, R., Sublette, K., Mahendra, S., 2019. Field bioaugmentation with Pseudonocardia dioxanivorans CB1190 metabolizing 1,4-dioxane using in situ bioreactors. Remediation Journal, submitted.

Chapter 2 Literature Review

2.1 1,4-Dioxane and Co-Contaminants

2.1.1 The Properties of 1,4-Dioxane

Contamination of groundwater by 1,4-dioxane, a cyclic diether, has been increasingly detected across the United States and globally (Anderson et al., 2012, Stepien et al., 2014, Adamson et al., 2015, Manamsa et al., 2016, Mohr et al., 2016, Carrera et al., 2017, Aoyagi et al., 2018, Karges et al., 2018). More recently, its potential carcinogenicity as a Group 2B human carcinogen by all potential exposure routes (IARC, 1999), 1,4-dioxane has been an parameter included in water analyses. Furthermore, the threat of 1,4-dioxane contamination of water supplies have received attention, and the Agency for Toxic Substances and Disease Registry (ATSDR) listed 1,4-dioxane as 214th of the total 275 superfund priority substances (ATSDR, 2017), and The U.S. Environmental Protection Agency (USEPA) recently included 1,4-dioxane on its initial list of 10 "high priority" chemical substances as part of the 2016 amendments to the Toxic Substances Control Act (USEPA, 2016). The challenges of 1,4-dioxane clean-up mainly result from the chemical and physical properties of 1,4-dioxane: miscibility in water, low Henry's law constant (4.88×10^{-6} atm m^3/mol), low adsorption potential on organic matter (log K_{oc} 1.23) (Howard et al., 1990), and low octanol-water partitioning coefficient (Log K_{ow} of -0.27) (Suthersan et al., 2016). Together these properties mean that 1,4-dioxane has both high aqueous mobility and leaching potential in groundwater aquifers (EBC, 2002). Coupled with its chemical recalcitrance, 1,4-dioxane is extremely persistent in groundwater with half-life of 2-5 years, while moderately persistent in surface water with half-life of 56 days (Adamson et al., 2015), thus hardly extracted or adsorbed from water. The cyclic ether structure of 1,4-dioxane carries four carbon atoms and two oxygen atoms, and the oxygen atoms occur directly opposite each other to form symmetrical

ether linkages (Mohr et al., 2016). This structure makes 1,4-dioxane highly stable and relatively refractory, generating long and broad contaminated groundwater plumes (Hatzinger et al., 2017, Chu et al., 2018).

2.1.2 Sources of 1,4-Dioxane and Co-Contaminants

1,4-Dioxane was historically used as a solvent stabilizer for trichloroethane (TCA), and commonly co-occurs with other chlorinated solvents, including trichloroethene (TCE), and dichloroethene (DCE) (Anderson et al., 2012, Adamson et al., 2014). Recent studies have also identified more sources of 1,4-dioxane distinct from chlorinated solvent contaminated sites, including the mouth of the Llobregat River near Barcelona (Carrera et al., 2017), aquatic environment in Germany and Poland (Stepien et al., 2014), landfill leachate (Karges et al., 2018), metal manufacturing/chrome plating plants (Hausladen et al., 2018), and a former landfill site (Gedalanga et al., 2016). 1,4-Dioxane has been broadly detected in groundwater, and Adamson et al. (2014) found that 194 of over 2000 sites in California, USA, contained 1,4-dioxane, and 38% of the 1,4-dioxane-contaminated sites contained plumes equal or larger in size to the chlorinated solvent plumes, indicating both the prevalence and complexity of 1,4-dioxane groundwater contamination.

2.2 Treatment Strategies for 1,4-Dioxane

2.2.1 Biological Treatment

Biodegradation is a promising strategy to destroy various contaminants in soil and groundwater environments by enzymatically-mediated processes during in-situ or ex-situ treatments (Zhang et al., 2017), which may prove to be more economical and sustainable when compared with other treatment alternatives. A substantial number of recent studies have been focused on identifying specific organisms that can biodegrade 1,4-dioxane to better inform

bioremediation strategies, including biostimulation, which provides carbon, nutrient, and oxygen to native microorganisms, or bioaugmentation, which provides specialized bacteria to contaminated sites.

To date, the exploration of anaerobic degradation of 1,4-dioxane has been limited, while aerobic biodegradation has been well studied. Anaerobic biodegradation was only evaluated under iron-reducing conditions by using anaerobic sludge with iron-reducing bacteria present, that could initially degrade 40% of 1,4-dioxane in the microcosm, with complete removal being achieved by adding humic substances and Fe(III) (Pan and Chen, 2006). However, the aerobic biodegradation process is more applicable with two main pathways, metabolism and co-metabolism, differentiated by the role of 1,4-dioxane in cellular growth and energy support for microorganisms, that thus were focused in this study.

2.2.1.1 1,4-Dioxane Metabolic Biodegradation Pathway and Corresponding Microorganisms

Under metabolic biodegradation, microorganisms utilize 1,4-dioxane as the sole carbon and energy sources to grow and thrive, which is advantageous for in-situ biodegradation on the basis of higher rates of transformation, reduced risk of clogging, reduced oxygen demand, and reduced concern for the lack of primary substrate (Barajas-Rodriguez and Freedman, 2018). A wide variety of microorganisms have been identified in bench and field scale studies to have metabolic 1,4-dioxane biodegradation function and summarized by Zhang et al. (2017) and McElroy and Hyman (2019), including *Pseudonocardia dioxanivorans* CB1190 (Mahendra and Alvarez-Cohen, 2005), *Actinomycete* CB1190 (Parales et al., 1994), *Amycolata* sp. CB1190 (Kelley et al., 2001), *Pseudonocardia benzenivorans* B5 (Mahendra and Alvarez-Cohen, 2006), *Mycobacterium* sp. PH-06 (Kim et al., 2009), *Acinetobacter baumannii* DD1 (Huang et al., 2014, Zhou et al., 2016), *Pseudonocardia carboxydivorans* RM-31 (Matsui et al., 2016), *Xanthobacter flavus* DT8 (Chen

et al., 2016), *Afipia* sp. D1 (Sei et al., 2013), *Rhodanobacter* AYS5 (Pugazhendi et al., 2015), *Rhodococcus aetherivorans* JCM 14343^{T} (Inoue et al., 2016, Inoue et al., 2018), *Pseudonocardia* sp. N23 (Yamamoto et al., 2018), etc.

Among these abovementioned 1,4-dioxane-metabolizing bacteria, *Pseudonocardia dioxanivorans* CB1190 (CB1190) is the well-studied at the molecular level and applied in bench scale tests (Jasmann et al., 2017, Miao et al., 2019). CB1190 can use 1,4-dioxane as sole carbon and energy source, but was previously mutated through regulatory, transport, and/or enzyme substrate range alterations from tetrahydrofuran (THF) - degrading organism (Parales et al., 1994). The observed maximum growth rate for CB1190 based on a batch experiment with 1,4-dioxane as the sole carbon and energy source was 90 μg/L/h, with cell yield at 0.09 ± 0.002 g protein/(g dioxane) and energy production at 19 mM ATP/(mM dioxane) (Mahendra and Alvarez-Cohen, 2005). 1,4-Dioxane degradation rates by CB1190 have been reported by Parales et al. (1994) as 19.8 mg dioxane/h/mg protein, by Mahendra and Alvarez-Cohen (2006) as 1.1 mg dioxane/h/mg protein, and by Barajas-Rodriguez and Freedman (2018) as 0.048 mg dioxane/h/mg COD. The varying degradation rates can likely be attributed to the temperature differences between experiments (optimal growth temperature at 30℃) (Mahendra and Alvarez-Cohen, 2005). Moreover, CB1190 was also found to grow slowly on rich media in the absence of 1,4-dioxane (e.g., LB, TSA, and R2A) (Mahendra and Alvarez-Cohen, 2005), and easily form biofilms on the insides and bottom of the flask in liquid medium with appearance of powdery white colonies floating on the liquid surface (Mahendra and Alvarez-Cohen, 2005).

The genome of strain CB1190 consists of a circular 7.1 Mb chromosome with three plasmids, which contain multicomponent monooxygenases and a complete operon encoding THF monooxygenase (THFMO) (Sales et al., 2011), which is similar to the monooxygenase on

Pseudonocardia ENV478 (Masuda et al., 2012). Grostern et al. (2012) proved THFMO was the only upregulated monooxygenase gene cluster located on plasmid pPSED02 in CB1190 during 1,4-dioxane degradation, thus, this gene cluster has also been referred to as dioxane monooxygenase (DXMO) for 1,4-dioxane degradation studies (Gedalanga et al., 2014). DXMO catalyzes 1,4-dioxane in the first step of biodegradation to 2-hydroxy-1,4-dioxane (1,4-dioxane-2-ol), which is then further oxidized to 1,4-dioxane-2-one (lactone), or transferred to 2-hydroxyethoxyacetaldehyde by ring chain tautomerism (Mahendra et al., 2007). Then, both 1,4-dioxane-2-one and 2-hydroxyethoxyacetaldehyde are hydrolyzed and dehydrogenized respectively to 2-hydroxyethoxyacetic acid (HEAA) (Mahendra et al., 2007). Monooxygenases can further hydroxylate HEAA and result in more downstream metabolites that are then easily mineralized to CO_2 via common cellular enzymes, including aldehyde dehydrogenase (ALDH). The 1,4-dioxane biodegradation pathway by CB1190 was first proposed by Mahendra et al. (2007) (Figure 2.1), and has been summarized in recent studies (Zhang et al., 2017, McElroy and Hyman, 2019).

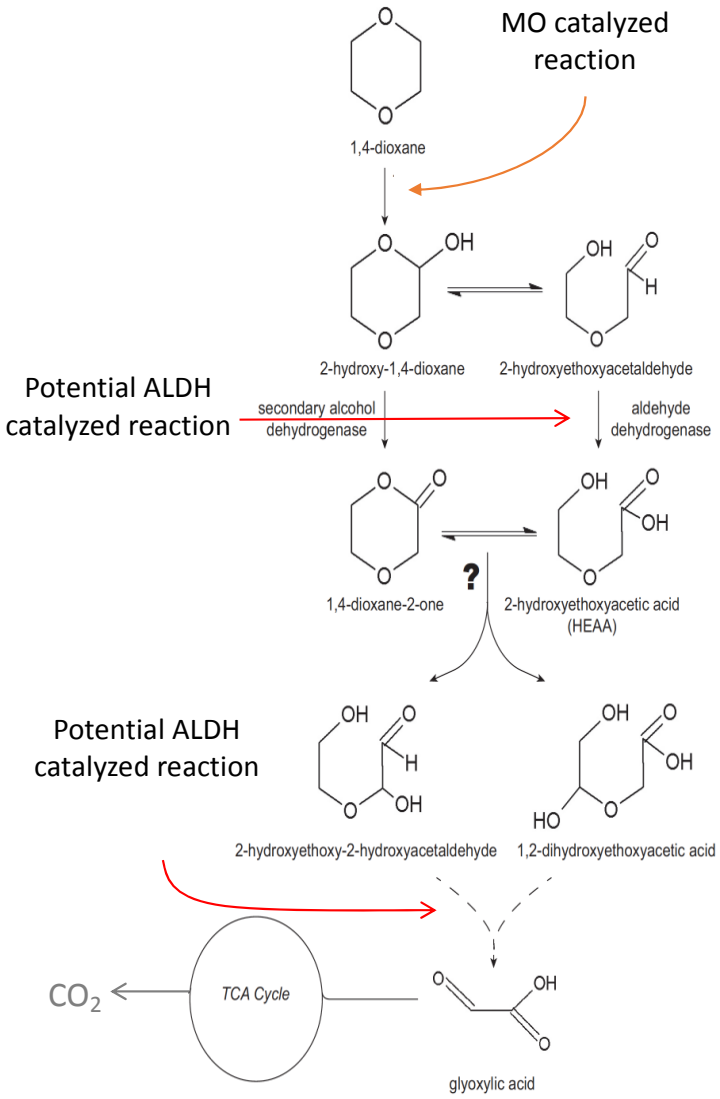

Figure 2.1. 1,4-Dioxane aerobic degradation pathway. A similar pathway was reported for both metabolic and co-metabolic processes, resulting in nearly complete mineralization.

The first study of kinetic of 1,4-dioxane biodegradation by CB1190 indicated whole-cell half saturation constant (K_s) at 160 mg/L (Mahendra and Alvarez-Cohen, 2006), while more recent study determined an order of magnitude lower K_s for CB1190 at 6.32 mg/L, which could be the consequence of the different experiment designs (Barajas-Rodriguez and Freedman, 2018). However, a recent study has tested the survival of CB1190 under low 1,4-dioxane (µg/L level) conditions. Barajas-Rodriguez and Freedman (2018) found decreasing 1,4-dioxane degradation

rates by CB1190 when the concentration of 1,4-dioxane was gradually decreased over time in batch simulations, and the reaction appeared to cease when 1,4-dioxane dipped below 300 μg/L. Thus, CB1190 metabolic biodegradation favors higher initial biomass and higher initial 1,4-dioxane concentrations. Moreover, because of the co-occurrence of chlorinated solvents, 1,4-dioxane degradation by CB1190 was reported in kinetics and mechanistic studies to be inhibited by individual solvents with the order: 1,1-dichloroethene (1,1-DCE) > cis-1,2-diochloroethene (cDCE) > trichloroethene (TCE) > 1,1,1-trichloroethane (TCA) (Zhang et al., 2016). These inhibitory impacts were at the transcriptional level, including down-regulation of both 1,4-dioxane monooxygenase (*dxmB*) and aldehyde dehydrogenase (*aldH*) genes and delayed ATP production (Zhang et al., 2016). Moreover, since CB1190 was unable to degrade TCA or DCE either metabolically or co-metabolically, the inhibition on 1,4-dioxane degradation was not competitive and just relied on the amount of present chlorinated solvents (Mahendra et al., 2013). However, the suppression of 1,4-dioxane degradation by TCA and DCE was found to be reversible in CB1190 cells after removing the chlorinated solvents (Mahendra et al., 2013). Moreover, transition metals were also reported to inhibit 1,4-dioxane biodegradation by monooxygenase-expressing bacteria (Pornwongthong et al., 2014, Zhao et al., 2018).

Several bench scale studies have been conducted to evaluate 1,4-dioxane biodegradation by CB1190 under controlled conditions. Li et al. (2010) bioaugmented microcosms with CB1190 that initially contained 50 mg/L 1,4-dioxane and observed degradation rates of 0.16 ± 0.04 mg dioxane/mg protein/day and 0.021 ± 0.007 mg dioxane/mg protein/day under 14℃ and 4℃, respectively. Polasko et al. (2019) used a co-culture containing the KB-1 consortium and CB1190 to degrade TCE and 1,4-dioxane under varying redox conditions in batch reactors. TCE was completely transformed during the anaerobic phase by the KB-1 culture, followed by 1,4-dioxane

biodegradation by CB1190 once oxygen was amended even after 5 weeks under anaerobic conditions, demonstrating CB1190's ability to remain viable and regain 1,4-dioxane-biodegradation activity even after extended anaerobic periods. Additionally, cis-1,2-DCE was also biotransformed under aerobic conditions by CB1190. Myers et al. (2018) grew CB1190 biofilms on granular activated carbon (GAC), and achieved 99% and 94% reduction of initial 1,4-dioxane in wastewater (from 73.0 to 0.800 mg/L) and groundwater (from 3.6 to 0.220 mg/L) within 2.5 and 5 days, respectively. Zhao et al. (2018) bioaugmented the soil with CB1190 resulting in nearly complete degradation at influent concentrations of 3–10 mg/L 1,4-dioxane and a residence reaction time of 40–80h.

2.2.1.2 1,4-Dioxane Co-Metabolic Biodegradation Pathway and Corresponding Microorganisms

Co-metabolic 1,4-dioxane biodegradation is often carried out by hydrocarbon-metabolizing bacteria that grow on primary substrates that induce monooxygenase activity. Thus, various monooxygenases-expressing strains were identified that could co-metabolize 1,4-dioxane in different initial pathways because of the hydrocarbon substrates. The reported strains capable of 1,4-dioxane co-metabolism and their primary substrates include: propane supporting *Mycobacterium austroafricanum* JOB5 (Mahendra and Alvarez-Cohen, 2006), *Rhodococcus ruber* ENV425 (Vainberg et al., 2006), *Rhodococcus jostii* RHA1 (Hand et al., 2015), *Azoarcus* sp. DD4 (Deng et al., 2018), and *Mycobacterium* sp. ENV421 (Masuda et al., 2012); THF supporting *Flavobacterium* (Sun et al., 2011), *Pseudonocardia* sp. strain ENV478 (Vainberg et al., 2006), *Rhodococcus ruber* strains 219 (Bock et al., 1996), *Rhodococcus ruber* T1 and T5 (SEI et al., 2013), and *Pseudonocardia tetrahydrofuranoxidans* K1 (Mahendra and Alvarez-Cohen, 2006, Bennett et al., 2018); toluene supporting *Burkholderia cepacia* G4 (Mahendra and Alvarez-Cohen,

2006), *Ralstonia pickettii* PKO1 (Mahendra and Alvarez-Cohen, 2006), and *Pseudomonas mendocina* KR1 (Mahendra and Alvarez-Cohen, 2006); isobutane supporting *Rhodococcus rhodochrous* ATCC 21198 (Rolston et al., 2016, Bennett et al., 2018); ethane supporting *Mycobacterium* ENV482 (Hatzinger et al., 2017); and methane supporting *Methylosinus trichosporium* OB3b (Mahendra and Alvarez-Cohen, 2006).

The advantage of co-metabolism is that degradation is less dependent on the concentration of the contaminant at low levels because the microorganism does not depend on it for growth and energy. Some studies in the literature have suggested that co-metabolism may be more effective than metabolism for degrading low levels of 1,4-dioxane. Barajas-Rodriguez and Freedman (2018) found that co-metabolic degradation could degrade 1,4-dioxane to below detection once it fell below 300 μg/L, at a higher rate than CB1190. Moreover, the co-metabolism of 1,4-dioxane was less affected by the co-occurred competitive and toxic chlorinated compounds in field scale studies (Lippincott et al., 2015, Chu et al., 2018). However, the primary substrates are flammable and explosive (alkane gases) or toxic to human health (THF, toluene), and require additional considerations for implementation. Additionally, co-metabolic strains prefer to consume their primary substrates before co-metabolically degrading 1,4-dioxane, e.g., ENV487 consumed propane before degrading 1,4-dioxane (Barajas-Rodriguez and Freedman, 2018). Furthermore, competitive inhibition caused by propane on biodegradation of 1,4-dioxane was significantly higher than inhibition caused by 1,4-dioxane on the utilization of propane, and the propanotrophic cultures had a higher oxygen requirement when degrading 1,4-dioxane compared to CB1190 (Barajas-Rodriguez and Freedman, 2018).

2.2.2 Advanced Oxidation Processes (AOPs)

Conventional chemical oxidants (having a standard oxidation potential of less than 2.0 V) such as chlorine, chloramine, chlorine dioxide, potassium permanganate, and molecular ozone, are not effective at oxidizing 1,4-dioxane. Addressing this issue, advanced oxidation processes (AOPs) involving •OH, $•SO_4^-$, •Cl, and $•Cl_2^-$ shows promise for rapid 1,4-dioxane destruction (McElroy et al., 2019). The •OH is usually generated from combined physical processes and/or chemical reagents (Equation 1, (Li et al., 2017)), including UV irradiation, sonication, ozone (O_3), hydrogen peroxide (H_2O_2), titanium dioxide (TiO_2), and iron (Fe^{2+}/Fe^{3+}) (Ikehata and El-Din, 2006, Ikehata et al., 2006). The $•SO_4^-$ is derived from activated persulfate (Eberle et al., 2016) (Equation 2), and the common activations include heating (Ghauch et al., 2012, Lee et al., 2012), UV irradiation, and sonication (Wang and Liang, 2014), electrochemical activation (Yuan et al., 2014), transition metal amendment (Liang and Lee, 2008), and base activation (Liang and Guo, 2012). Chlorine is used for preoxidation prior to UV disinfection, and constituents in water are exposed to UV and chlorine simultaneously (Fang et al., 2014). The free chlorine is added as chlorine gas (Cl_2) or sodium hypochlorite (NaOCl) to form hypochlorous acid (HOCl) and hypochlorite (OCl^-) (Remucal and Manley, 2016), and •Cl is formed due to the UV photolysis of HOCl and OCl^- (Watts and Linden, 2007) (Equation 3 and 4), which can then react with chloride ions to form $•Cl_2^-$ (Klaning and Wolff, 1985).

$$H_2O_2 \xrightarrow{h\nu} 2•OH \qquad \text{Equation 1.}$$

$$S_2O_8^{2-} \xrightarrow{h\nu} 2•SO_4^- \qquad \text{Equation 2.}$$

$$HOCl \xrightarrow{h\nu} •OH + •Cl \qquad \text{Equation 3.}$$

$$OCl^- \xrightarrow{h\nu} •O^- + •Cl \qquad \text{Equation 4.}$$

The oxidation of 1,4-dioxane by •OH first initiates H- abstraction at either -CH_2 groups to form a 1,4-dioxanyl radical (McElroy et al., 2019). Then, several pathways can proceed in parallel to cause ring opening and yield biodegradable carboxylic acids and aldehydes before complete mineralization to carbon dioxide (Stefan and Bolton, 1998, Jasmann et al., 2016). The •OH could be produced in homogeneous process, including O_3/H_2O_2 (Ikehata et al., 2016, Andaluri and Suri, 2017), UV/O_3 (Ikehata et al., 2016, Shen et al., 2017), and UV/H_2O_2 (Ikehata et al., 2016). The O_3/H_2O_2 treatment with O_3 and H_2O_2 doses of 6 and 1.5 mg/L, respectively, and the UV/H_2O_2 treatment with UV and H_2O_2 doses of 1,000 mJ/cm and 20 mg/L, respectively, were sufficient to degrade 200 μg/L of 1,4-dioxane, 110 μg/L of 1,1-dichloroethene, and 10 μg/L of trichloroethene below their performance standards of 10, 7, and 4 μg/L, respectively (Ikehata et al., 2016). Additionally, in heterogeneous systems, electro-oxidation has been widely studied (Barndok et al., 2014), including boron-doped diamond (BDD) and mixed metal oxide electrodes (Park et al., 2018), as well as TiO_2 pellets in an electric field (Jasmann et al., 2016). Moreover, the Fenton process, which utilizes Fe^{2+} and H_2O_2 to produce •OH (Hermosilla et al., 2012), has been modified and improved with photo-Fenton and zero valent iron to treat 1,4-dioxane contaminated wastewater (Barndok et al., 2016). Microbes have also been identified that are capable of driving the Fenton reaction (Sekar et al., 2016). More combinations are currently being studied based on zerovalent iron-based heterogeneous photo-Fenton processes, e.g., UV/Fe^0/H_2O_2 (Barndok et al., 2018).

Activated persulfate AOPs are considered promising because sulfate radicals are more stable in the subsurface than hydroxyl radicals, allowing for better distribution after injection (Tsitonaki et al., 2010). The potential degradation pathways for 1,4-dioxane were reported to be different under heat-/Fe^{2+}-activated persulfate than for other oxidation processes While the first

transformation product is the same as for hydroxyl radical (1,4-dioxanyl radical), the next intermediate is α-oxyl radical as the precursor of the primary intermediates (Choi et al., 2010). The α-oxyl radical then transforms into glycolaldehyde and glycolic acid in heat-/Fe^{2+}-activated persulfate pathway, and intermediates such as oxalic acid and acetic acid are then mineralized to CO_2 via common cellular metabolic pathways (Zhao et al., 2014). However, Mahendra et al. (2007) found the pathway with α-oxyl radical being transformed to acetaldehyde and acetic acid by an intramolecular reaction and several oxidation steps. Eberle et al. (2016) applied peroxone activated persulfate (PAP) for 1,4-dioxane and chlorinated solvent mixtures, and found the degradation rate followed TCE > 1,4-dioxane > 1,1,1-TCA. Li and Zhu (2016) treated 20 mg/L TCA and 1 mg/L 1,4-dioxane mixtures by using sono-activated persulfate, and observed complete TCA removal in 240 minutes and 88% 1,4-dioxane removal in 300 min. Ouyang et al. (2017) synthesized a nano-magnetite biochar composite (n-Fe_3O_4/biochar) to activate persulfate and degraded 98% 1,4-dioxane with 1.76 mg/L initial concentration in aqueous phase after 120 minutes. Further study is needed to examine the degradation mechanisms in more depth under various activated persulfate oxidation processes versus other oxidation or biodegradation processes. Nevertheless, activated persulfate oxidation of 1,4-dioxane via currently identified pathways is not expected to cause an accumulation of toxic compounds in the environment (Zhao et al., 2014).

Chlorine radicals alone have not be studied for the degradation of 1,4-dioxane, but mixed radicals including •OH, $•SO_4^-$, •Cl, and $•Cl^-_2$ was reported to efficiently degrade 1,4-dioxane, with initial chemicals persulfate and monochloramine (NH_2Cl) under UV activation (Li et al., 2018). However, 1,4-dioxane oxidation proceeded primarily by •OH in the mixed oxidants (Chuang et al., 2017), thus, the role of $•SO_4^-$, •Cl, and $•Cl_2^-$ to 1,4-dioxane removals were relatively small.

In terms of secondary pollution, bromide and chloride compounds are of concern after oxidation because of the potential halogenated organic by-products and halo-oxyanions (Radjenovic and Sedlak, 2015). For example, $\bullet SO_4^-$ could react with chloride to form chlorate (Qian et al., 2016), bromide can be oxidized to bromate by O_3 (Ikehata et al., 2016). BDD electrodes could also oxidize bromide to bromate with metal oxide, and oxidize chloride to perchlorate (Radjenovic and Sedlak, 2015).

2.2.3 Catalysis Processes

As discussed above, AOPs have been applied widely in 1,4-dioxane degradations, however, they require activation by either excess activating chemical additives or sufficiently energetic physical activation processes, and suitable reaction conditions in order to decompose 1,4-dioxane (Choi et al., 2017). Thus, catalytic oxidation methods are being increasingly used to address these issues with various catalysts utilized in different oxidation processes.

Taking hydroxyl radical as an example, it can generated by AOP systems from H_2O_2, dissolved O_2, ozone, or even H_2O under ambient conditions (Shen et al., 2017, Cheng et al., 2018), but can also be generated by the effect of catalysts. The catalysts could be categorized based on the materials (Xu et al., 2019), including metal ions (Zazo et al., 2005, Catrinescu et al., 2017, Cheng et al., 2017), metal or metal oxides (Chiang et al., 2002, Segura et al., 2015, Feng et al., 2018, Kang et al., 2018, Park et al., 2018), activated carbon (Xu et al., 2012), and mixed catalysts (also called catalytic wet peroxide) (Quintanilla et al., 2007, Quintanilla et al., 2010). Thus, the versatile materials applied in 1,4-dioxane degradation processes could induce different performances. Barndok et al. (2016) used solar photocatalysis with an immobilized NF-TiO_2 composite and monodisperse TiO_2 nanoparticles, achieving complete removal of 1,4-dioxane from industrial wastewater, along with 65% and 50% removals of COD and TOC, respectively. Choi et

al. (2017) developed a Pt/CeO_2-ZrO_2-SnO_2/SBA-16 (SBA-16: Santa Barbara Amorphous No. 16) catalyst for the efficient removal of 1,4-dioxane, with 31% residual 1,4-dioxane after reaction at 80°C for 4 h in an air atmosphere without any supply of strongly oxidizing additives or irradiation by UV or ultrasound. Feng et al. (2017) investigated the activation of peroxymonosulfate (PMS) by Pd/Al_2O_3 to degrade 1,4-dioxane, which could be degraded to small-molecular carboxylic acids at pH 7.0. More than 95% of the 1,4-dioxane (initially at 0.55 mM) was degraded after reacting for 60 min with 5.5 mM PMS, 0.2 g/L Pd/Al_2O_3. Scaratti et al. (2018) applied catalytic ozonation in the presence of CuO and increased degradation rates of 1,4-dioxane and total organic carbon by factors of 10.35 and 81.25, respectively, compared with ozone only oxidation. Ramakrishna et al. (2016) utilized the Fe/zeolite-13X catalyst with 6 wt% Fe exhibited the best catalytic activity at 400°C and a GHSV of 24000 h^{-1}, with 97% dioxane conversion and 95% selectivity for the formation of carbon oxides (CO and CO_2). While much work has gone into synthesizing catalysts to meet the various requirements of complex contaminants, more research is needed for the large-scale application of catalysis in the engineered remediation for 1,4-dioxane.

2.3 Metagenomic Technologies

Despite the exhaustive knowledge of intricate molecular mechanisms of most of the cellular processes and the availability of complex culture media, scientists are still able to culture less than 1% of all microorganisms present in diverse natural habitats. Thus, metagenomics based on culture independent methods containing the function-driven and sequence-based analysis target on trapped whole genome from a wide range of habitats (Gabor et al., 2007), combining with potential genomics, bioinformatics, and system biology is a powerful tool for exploring the whole microbial genomes isolated from specific environments (Kumar et al., 2015). Thus, metagenomic tools have allowed us unprecedented insights into natural microbial communities and their potential activities.

2.3.1 Environmental Metagenomics

Metagenomics is defined as the study of environmental microbial communities using a suite of genomic tools to directly access their genetic content (Gilbert et al., 2011), i.e. without prior cultivation and enrichment of specific microbes in the laboratory. Three main technologies support environmental metagenomic analysis, including 1) genetic and/or functional screening of cloned DNA (function-driven); 2) large-scale direct sequencing of environmental samples without pre-cloning (shot gun sequencing); and 3) PCR amplification of specific marker genes (e.g., 16S rRNA) through high throughput sequencing (amplicon sequencing). Although function-driven metagenomics with colonies containing metagenomic DNA are screened for expressed activities, enhancing the understanding of ecological drift theory, it has lagged behind shotgun sequencing because of the comparatively slow advances and heavy workloads in screening technology (Zhou et al., 2015). Therefore, current metagenomics relying on sequencing technologies encompass two types of study: whole genome shotgun (WGS) sequencing of all the genes in the microbial community and amplicon sequencing targeting a single and taxonomically important gene (16S rRNA) (Gilbert and Dupont, 2011).

The next-generation sequencing (NGS) platform developments played critical roles in the success of early metagenomics studies, including 454-FLX (Roche) (Quince et al., 2009), Miseq and Hiseq (Illumina) (Kozich et al., 2013), SOLiD (Applied Biosystems) (Hedges et al., 2011), phyloChip (Hazen et al., 2010), GeoChip (He et al., 2010), mass spectrometry-based proteomics for community analysis (Ram et al., 2005), and metabolite analysis (Cui et al., 2008). Based on theory developed by Zhou et al. (2015), the molecular microbial detection could be grouped into two main categories, open and closed formats (Vieites et al., 2009, Roh et al., 2010), which were also differentiated by sequencing technologies. The open format technologies do not require a

priori sequencing information from the target community (Vieites et al., 2009, Roh et al., 2010), and can potentially reveal new genes, pathways, and taxa. However, the closed format technologies are limited by already known microbial sequences, that require a priori sequence information but will not provide new molecular information. Because natural environments, including soil and groundwater where 1,4-dioxane and chlorinated solvents are primarily found, harbor unknown or uncultured microorganisms, not all sequenced reads can be affiliated to existing databases (Babin et al., 2019), thus open format is mainly discussed in this study with high-throughput sequencing (HTS) technologies.

2.3.2 HTS-based Environmental Metagenomics

The HTS technologies have had the most profound impact on metagenomics because HTS platforms allow massive parallel sequencing where hundreds of thousands to millions of sequencing reactions are performed and detected simultaneously, which results in very high throughput that has expanded the scale and scope of metagenomic studies in a way never explored before (Kumar et al., 2015).

Currently, the majority of microbial ecology with community structure studies apply HTS by focusing on targeted gene sequencing with phylogenetic information (e.g., 16S rRNA) (Sogin et al., 2006, Caporaso et al., 2012). The targeted gene approach is unable to retrieve all the information carried in the whole genome, but allows for greater sequencing depth for 16S rRNA gene than other methods that can provide more comprehensive phylogenetic information. The community DNA is extracted from environmental samples (e.g., samples from soils, sediments, water, bioreactors, or humans) using various extraction and purification methods (Zhou et al., 1996, Hurt et al., 2001). After high-quality DNA is obtained, the 16S rRNA gene can be amplified with conserved primers as reported to fit various sequencing platforms (Klindworth et al., 2013). Each set of primers is

generally barcoded with 6- to 12-mer oligonucleotide tags, as well as sequencing adapters, so that multiple samples can be pooled and sequenced simultaneously (Caporaso et al., 2012). Then, amplified DNA fragments are quantified based on concentrations and equalized to united moles before sequencing. Illumina Miseq 2 × 250 bp or 2 × 300 bp sequencing platforms are currently popular due to lower cost and faster turnaround time. The generated sequence reads are then treated by various bioinformatic tools with different experimental designs and hypotheses. Briefly, the short reads (~300 bp) are assembled after trimming off sequencing required barcodes and adapters, and the assembled contigs are aligned and classified against well-built databases, e.g., SILVA (Quast et al., 2013), GreenGenes (McDonald et al., 2012), and Ribosomal Database Project (Cole et al., 2014). Meanwhile, the artificial error sequences (chimera) are removed to reduce the error rate, and the denoised contigs are then clustered into operational taxonomic units (OTUs), which usually represent the species in community. The last and most important step is to combine the sequenced community with environmental parameters or phenomena, to address the ecological questions and reveal interactions as well as dynamics among community populations, all of which require statistical analyses.

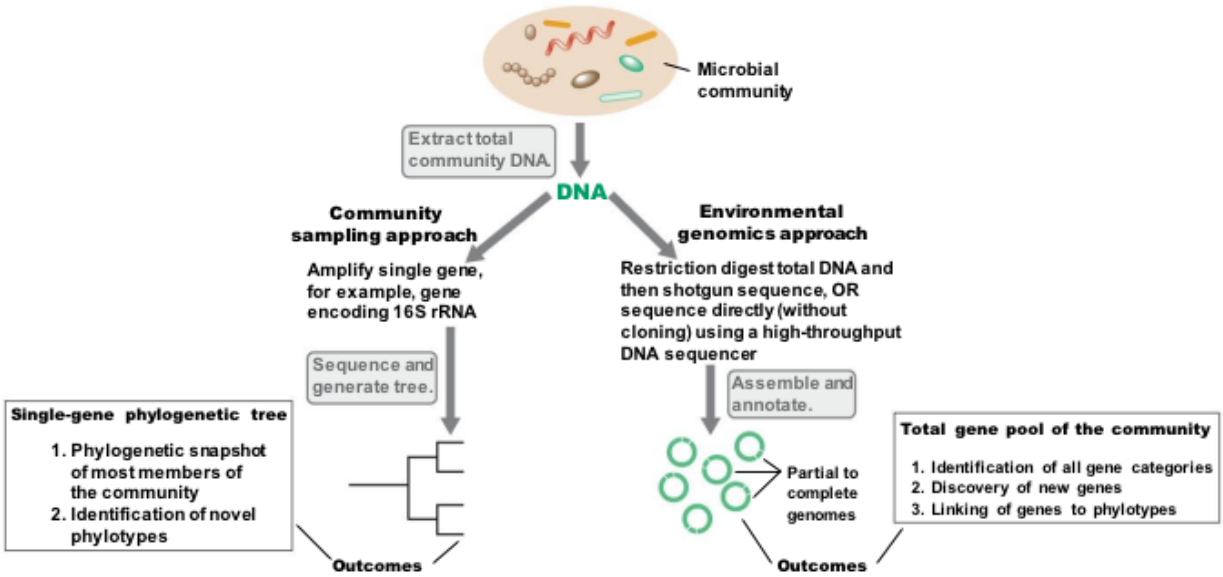

Figure 2.2. Scheme of metagenomics.

Community-level analysis can also be done by shotgun sequencing with thousands to millions of different archaeal, bacterial, and eukaryotic species (Torsvik et al., 2002, Gans et al., 2005). However, more functional features are achieved based on shotgun sequencing, because of the sequencing-by-synthesis technology on random short DNA fragments from the whole genome. The instruments carrying on shotgun sequencing are versatile, but the output data size can be in Gigabyte to Terabyte levels per sample, and can provide the potential to reconstruct whole bacterial or archaeal genomes even without well-built reference database. The critical step to treat shotgun sequencing data is to equip high performance computational tools to run and store large datasets efficiently (Hess et al., 2011, Nagarajan and Pop, 2013). The specific workflows for data processing are varying for each HTS platforms due to the differences in read length, coverage, and accuracy, etc., but the general steps are as follows: 1) reads assembly and gene prediction, 2) functional features identification and quantification, 3) taxonomic classification of functional features, and 4) binning of the whole genomes (Jia et al., 2019, Zhang et al., 2019). Even though the bioinformatic tools have been developed to meet the requirements of the above mentioned workflow, some intrinsic problems still challenge the outcomes of HTS-based research, e.g., absence of any reference genome for assembly of genome sequences from unculturable representatives of metagenomic sequence pool (Zengler and Palsson, 2012) or extremely low coverage of sequencing to discern individual genomes within complex communities (Hess et al., 2011, Wrighton et al., 2012, Castelle et al., 2013). However, The development of new algorithms for extracting useful information out of metagenomic sequence data is so rapid that new updates and developments are reported every couple of weeks and any comprehensive review of this aspect may appear incomplete due to the continuous upgrades and additions of new algorithms (Kumar et al., 2015).

2.3.3 Microbial Community Analysis in Bioremediation

The main focus for the bioremediation of contaminated soil and groundwater has been placed on the elimination of pollutants. However, the goals of remediation are not only to remove pollutants from environments but also to restore the capacity of the soil and groundwater to fulfill important ecological functions (Epelde et al., 2009, Xu et al., 2018). Additionally, bioremediation is often carried out by various microorganisms native to the subsurface, so understanding how bioaugmentation and biostimulation influence the existing populations of contaminant degraders, the diversity and activity of the microbial community, and the ability of inoculants to adapt to new environmental conditions are very important to ensuring effective decontamination (Liu et al., 2012, Taccari et al., 2012). Moreover, it is important to understand the microbial communities involved in the bioremediation of contaminated sites because microbes are the key drivers of bioremediation and the shifts in their structure and activity may affect the fate of pollutants in the environment (Techtmann and Hazen, 2016). Thus, the description of the microbial community and function dynamics provides a basis for the development of effective tools to manage bioremediation as well as predictive models to follow it in progress (Andreolli et al., 2016). Furthermore, the characterization of the involved microorganisms is crucial because the ultimate success of bioremediation greatly depends on soil or groundwater microbial features in terms of activity, abundance, diversity, and community structure. Data obtained from these kinds of studies are useful to the optimization of existing bioremediation strategies and the development of new ones (Pal et al., 2017, Siles and Margesin, 2018). However, the study of microbial communities within contaminated sites is a complex task mainly due to the contamination extending through often discontinuous and heterogenous plumes that have been widely observed at 1,4-dioxane contaminated sites. With increasing attention, more consideration and work has been applied to HTS technology to study the

dynamics of key microbes during bioremediation processes, including natural attenuation (Flocco et al., 2019), bioaugmentation (Roy et al., 2018), and biostimulation (Huang et al., 2019, Zhao et al., 2019).

Therefore, microbial community analysis for bioremediation of 1,4-dioxane and co-contaminant impacted sites could advance our understanding of biodegradation and detoxification, and lead to the identification of new xenobiotic degrading bacteria or catabolic genes for the treatment of complex contaminants. Moreover, microbial community analysis could reveal microbial responses to 1,4-dioxane and co-contaminants under various levels at different sites, allowing for deeper investigation of microbial communities, which is vital in presenting an unbiased view of phylogenetic composition and functional diversity of environmental microbial communities (Zwolinski, 2007).

2.4 References

Adamson, D.T., Anderson, R.H., Mahendra, S., Newell, C.J., 2015. Evidence of 1,4-dioxane attenuation at groundwater sites contaminated with chlorinated solvents and 1,4-dioxane. Environmental Science & Technology, 49 (11), 6510-6518.

Adamson, D.T., Mahendra, S., Walker, K.L., Rauch, S.R., Sengupta, S., Newell, C.J., 2014. A multisite survey to identify the scale of the 1,4-dioxane problem at contaminated groundwater sites. Environmental Science & Technology Letters, 1 (5), 254-258.

Andaluri, G., Suri, R., 2017. Removal of 1,4-dioxane and volatile organic compounds from groundwater using ozone-based advanced oxidation process. Ozone-Science & Engineering, 39 (6), 423-434.

Anderson, R.H., Anderson, J.K., Bower, P.A., 2012. Co-occurrence of 1,4-dioxane with trichloroethylene in chlorinated solvent groundwater plumes at US Air Force installations: Fact or fiction. Integrated Environmental Assessment and Management, 8 (4), 731-737.

Andreolli, M., Albertarelli, N., Lampis, S., Brignoli, P., Khoei, N.S., Vallini, G., 2016. Bioremediation of diesel contamination at an underground storage tank site: a spatial analysis of the microbial community. World Journal of Microbiology & Biotechnology, 32 (1).

Aoyagi, T., Morishita, F., Sugiyama, Y., Ichikawa, D., Mayumi, D., Kikuchi, Y., Ogata, A., Muraoka, K., Habe, H., Hori, T., 2018. Identification of active and taxonomically diverse 1,4-dioxane degraders in a full-scale activated sludge system by high-sensitivity stable isotope probing. The ISME Journal, 12 (10), 2376-2388.

ATSDR, 2017. Support Document to the 2017 Substance Priority List (Candidates for Toxicological Profiles). Division of Toxicology and Human Health Sciences, Atlanta, GA (2017).

Babin, D., Deubel, A., Jacquiod, S., Sorensen, S.J., Geistlinger, J., Grosch, R., Smalla, K., 2019. Impact of long-term agricultural management practices on soil prokaryotic communities. Soil Biology & Biochemistry, 129, 17-28.

Barajas-Rodriguez, F.J., Freedman, D.L., 2018. Aerobic biodegradation kinetics for 1,4-dioxane under metabolic and cometabolic conditions. Journal of Hazardous Materials, 350, 180-188.

Barndok, H., Blanco, L., Hermosilla, D., Blanco, A., 2016. Heterogeneous photo-Fenton processes using zero valent iron microspheres for the treatment of wastewaters contaminated with 1,4-dioxane. Chemical Engineering Journal, 284, 112-121.

Barndok, H., Hermosilla, D., Cortijo, L., Torres, E., Blanco, A., 2014. Electrooxidation of industrial wastewater containing 1,4-dioxane in the presence of different salts. Environmental Science and Pollution Research, 21 (8), 5701-5712.

Barndok, H., Hermosilla, D., Han, C., Dionysiou, D.D., Negro, C., Blanco, A., 2016. Degradation of 1,4-dioxane from industrial wastewater by solar photocatalysis using immobilized NF-TiO_2 composite with monodisperse TiO_2 nanoparticles. Applied Catalysis B-Environmental, 196, 232-232.

Barndok, H., Hermosilla, D., Negro, C., Blanco, A., 2018. Comparison and predesign cost assessment of different advanced oxidation processes for the treatment of 1,4-dioxane-containing wastewater from the chemical industry. ACS Sustainable Chemistry & Engineering, 6 (5), 5888-5894.

Bennett, P., Hyman, M., Smith, C., El Mugammar, H., Chu, M.Y., Nickelsen, M., Aravena, R., 2018. Enrichment with carbon-13 and deuterium during monooxygenase-mediated biodegradation of 1,4-dioxane. Environmental Science & Technology Letters, 5 (3), 148-153.

Bock, C., Kroppenstedt, R.M., Diekmann, H., 1996. Degradation and bioconversion of aliphatic and aromatic hydrocarbons by *Rhodococcus ruber* 219. Applied Microbiology and Biotechnology, 45 (3), 408-410.

Caporaso, J.G., Lauber, C.L., Walters, W.A., Berg-Lyons, D., Huntley, J., Fierer, N., Owens, S.M., Betley, J., Fraser, L., Bauer, M., Gormley, N., Gilbert, J.A., Smith, G., Knight, R., 2012. Ultra-high-throughput microbial community analysis on the Illumina HiSeq and MiSeq platforms. The ISME Journal, 6 (8), 1621-1624.

Carrera, G., Vegue, L., Boleda, M.R., Ventura, F., 2017. Simultaneous determination of the potential carcinogen 1,4-dioxane and malodorous alkyl-1,3-dioxanes and alkyl-1,3-dioxolanes in environmental waters by solid-phase extraction and gas chromatography tandem mass spectrometry. Journal of Chromatography A, 1487, 1-13.

Castelle, C.J., Hug, L.A., Wrighton, K.C., Thomas, B.C., Williams, K.H., Wu, D., Tringe, S.G., Singer, S.W., Eisen, J.A., Banfield, J.F., 2013. Extraordinary phylogenetic diversity and metabolic versatility in aquifer sediment. Nature Communications, 4, 2120.

Catrinescu, C., Chelba, A., Teodosiu, C., Apopei, P., 2017. Removal of diclofenac from secondary wastewater effluents by Fenton based processes. Environmental Engineering and Management Journal, 16 (4), 765-777.

Chen, D.Z., Jin, X.J., Chen, J., Ye, J.X., Jiang, N.X., Chen, J.M., 2016. Intermediates and substrate interaction of 1,4-dioxane degradation by the effective metabolizer *Xanthobacter flavus* DT8. International Biodeterioration & Biodegradation, 106, 133-140.

Cheng, M., Lai, C., Liu, Y., Zeng, G.M., Huang, D.L., Zhang, C., Qin, L., Hu, L., Zhou, C.Y., Xiong, W.P., 2018. Metal-organic frameworks for highly efficient heterogeneous Fenton-like catalysis. Coordination Chemistry Reviews, 368, 80-92.

Cheng, M., Zeng, G.M., Huang, D.L., Lai, C., Liu, Y., Xu, P., Zhang, C., Wan, J., Hu, L., Xiong, W.P., Zhou, C.Y., 2017. Salicylic acid-methanol modified steel converter slag as heterogeneous Fenton-like catalyst for enhanced degradation of alachlor. Chemical Engineering Journal, 327, 686-693.

Chiang, K., Amal, R., Tran, T., 2002. Photocatalytic degradation of cyanide using titanium dioxide modified with copper oxide. Advances in Environmental Research, 6 (4), 471-485.

Choi, J.Y., Lee, Y.J., Shin, J., Yang, J.W., 2010. Anodic oxidation of 1,4-dioxane on boron-doped diamond electrodes for wastewater treatment. Journal of Hazardous Materials, 179 (1-3), 762-768.

Choi, P.G., Nunotani, N., Imanaka, N., 2017. High catalytic efficiency in liquid-phase oxidation of 1,4-dioxane using a Pt/CeO_2-ZrO_2-SnO_2/SBA-16 catalyst. International Journal of Applied Ceramic Technology, 14 (1), 9-15.

Chu, M.Y.J., Bennett, P.J., Dolan, M.E., Hyman, M.R., Peacock, A.D., Bodour, A., Anderson, R.H., Mackay, D.M., Goltz, M.N., 2018. Concurrent treatment of 1,4-dioxane and chlorinated aliphatics in a groundwater recirculation system via aerobic cometabolism. Ground Water Monitoring and Remediation, 38 (3), 53-64.

Chuang, Y.H., Chen, S., Chinn, C.J., Mitch, W.A., 2017. Comparing the UV/Monochloramine and UV/Free chlorine advanced oxidation processes (AOPs) to the UV/Hydrogen peroxide aop under scenarios relevant to potable reuse. Environmental Science & Technology, 51 (23), 13859-13868.

Cole, J.R., Wang, Q., Fish, J.A., Chai, B., McGarrell, D.M., Sun, Y., Brown, C.T., Porras-Alfaro, A., Kuske, C.R., Tiedje, J.M., 2014. Ribosomal Database Project: Data and tools for high throughput rRNA analysis. Nucleic Acids Research, 42 (Database issue), D633-642.

Cui, Q., Lewis, I.A., Hegeman, A.D., Anderson, M.E., Li, J., Schulte, C.F., Westler, W.M., Eghbalnia, H.R., Sussman, M.R., Markley, J.L., 2008. Metabolite identification via the Madison Metabolomics Consortium Database. Nature Biotechnology, 26 (2), 162-164.

Deng, D.Y., Li, F., Wu, C., Li, M.Y., 2018. Synchronic Biotransformation of 1,4-Dioxane and 1,1-Dichloroethylene by a Gram-Negative *Propanotroph Azoarcus* sp DD4. Environmental Science & Technology Letters, 5 (8), 526-532.

EBC, 2002. 1,4-Dioxane risk assessment, final report. European Union Risk Assessment Report, European Chemicals Bureau, Institute for Health and Consumer Protection, 2nd Priority List, Vol. 21, https://echa.europa.eu/documents/10162/a4e83a6a-c421-4243-a8df-3e84893082aa.

Eberle, D., Ball, R., Boving, T.B., 2016. Peroxone activated persulfate treatment of 1,4-dioxane in the presence of chlorinated solvent co-contaminants. Chemosphere, 144, 728-735.

Epelde, L., Mijangos, I., Becerril, J.M., Garbisu, C., 2009. Soil microbial community as bioindicator of the recovery of soil functioning derived from metal phytoextraction with sorghum. Soil Biology and Biochemistry, 41 (9), 1788-1794.

Fang, J.Y., Fu, Y., Shang, C., 2014. The roles of reactive species in micropollutant degradation in the UV/Free chlorine system. Environmental Science & Technology, 48 (3), 1859-1868.

Feng, Y., Lee, P.H., Wu, D.L., Shih, K.M., 2017. Surface-bound sulfate radical-dominated degradation of 1,4-dioxane by alumina-supported palladium (Pd/Al_2O_3) catalyzed peroxymonosulfate. Water Research, 120, 12-21.

Feng, Y., Li, H.L., Lin, L., Kong, L.J., Li, X.Y., Wu, D.L., Zhao, H.Y., Shih, K.M., 2018. Degradation of 1,4-dioxane via controlled generation of radicals by pyrite-activated oxidants: Synergistic effects, role of disulfides, and activation sites. Chemical Engineering Journal, 336, 416-426.

Flocco, C.G., Mac Cormack, W.P., Smalla, K., 2019. Antarctic soil microbial communities in a changing environment: Their contributions to the sustainability of antarctic ecosystems and the bioremediation of anthropogenic pollution. The Ecological Role of Micro-organisms in the Antarctic Environment, 133-161.

Gabor, E., Liebeton, K., Niehaus, F., Eck, J., Lorenz, P., 2007. Updating the metagenomics toolbox. Biotechnology Journal, 2 (2), 201-206.

Gans, J., Wolinsky, M., Dunbar, J., 2005. Computational improvements reveal great bacterial diversity and high metal toxicity in soil. Science, 309 (5739), 1387-1390.

Gedalanga, P., Madison, A., Miao, Y., Richards, T., Hatton, J., DiGuiseppi, W.H., Wilson, J., Mahendra, S., 2016. A multiple lines of evidence framework to evaluate intrinsic biodegradation of 1,4-dioxane. Remediation Journal, 27 (1), 93-114.

Gedalanga, P.B., Pornwongthong, P., Mora, R., Chiang, S.Y.D., Baldwin, B., Ogles, D., Mahendra, S., 2014. Identification of biomarker genes to predict biodegradation of 1,4-dioxane. Applied and Environmental Microbiology, 80 (10), 3209-3218.

Ghauch, A., Tuqan, A.M., Kibbi, N., 2012. Ibuprofen removal by heated persulfate in aqueous solution: A kinetics study. Chemical Engineering Journal, 197, 483-492.

Gilbert, J.A., Dupont, C.L., 2011. Microbial metagenomics: Beyond the genome. Annual Review of Marine Science, 3, 347-371.

Gilbert, J.A., Laverock, B., Temperton, B., Thomas, S., Muhling, M., Hughes, M. (2011). High-Throughput Next Generation Sequencing, pp. 173-183, Springer.

Grostern, A., Sales, C.M., Zhuang, W.Q., Erbilgin, O., Alvarez-Cohen, L., 2012. Glyoxylate metabolism is a key feature of the metabolic degradation of 1,4-dioxane by *Pseudonocardia dioxanivorans* strain CB1190. Applied and Environmental Microbiology, 78 (9), 3298-3308.

Hand, S., Wang, B.X., Chu, K.H., 2015. Biodegradation of 1,4-dioxane: Effects of enzyme inducers and trichloroethylene. Science of the Total Environment, 520, 154-159.

Hatzinger, P.B., Banerjee, R., Rezes, R., Streger, S.H., McClay, K., Schaefer, C.E., 2017. Potential for cometabolic biodegradation of 1,4-dioxane in aquifers with methane or ethane as primary substrates. Biodegradation, 28 (5-6), 453-468.

Hausladen, D.M., Alexander-Ozinskas, A., McClain, C., Fendorf, S., 2018. Hexavalent chromium sources and distribution in California groundwater. Environmental Science & Technology, 52 (15), 8242-8251.

Hazen, T.C., Dubinsky, E.A., DeSantis, T.Z., Andersen, G.L., Piceno, Y.M., Singh, N., Jansson, J.K., Probst, A., Borglin, S.E., Fortney, J.L., Stringfellow, W.T., Bill, M., Conrad, M.E., Tom, L.M., Chavarria, K.L., Alusi, T.R., Lamendella, R., Joyner, D.C., Spier, C., Baelum, J., Auer, M., Zemla, M.L., Chakraborty, R., Sonnenthal, E.L., D'Haeseleer, P., Holman, H.Y., Osman, S., Lu, Z., Van Nostrand, J.D., Deng, Y., Zhou, J., Mason, O.U., 2010. Deep-sea oil plume enriches indigenous oil-degrading bacteria. Science, 330 (6001), 204-208.

He, Z., Deng, Y., Van Nostrand, J.D., Tu, Q., Xu, M., Hemme, C.L., Li, X., Wu, L., Gentry, T.J., Yin, Y., 2010. GeoChip 3.0 as a high-throughput tool for analyzing microbial community composition, structure and functional activity. The ISME Journal, 4 (9), 1167.

Hedges, D.J., Guettouche, T., Yang, S., Bademci, G., Diaz, A., Andersen, A., Hulme, W.F., Linker, S., Mehta, A., Edwards, Y.J., 2011. Comparison of three targeted enrichment strategies on the SOLiD sequencing platform. Plos One, 6 (4), e18595.

Hermosilla, D., Merayo, N., Ordonez, R., Blanco, A., 2012. Optimization of conventional Fenton and ultraviolet-assisted oxidation processes for the treatment of reverse osmosis retentate from a paper mill. Waste Management, 32 (6), 1236-1243.

Hess, M., Sczyrba, A., Egan, R., Kim, T.W., Chokhawala, H., Schroth, G., Luo, S., Clark, D.S., Chen, F., Zhang, T., Mackie, R.I., Pennacchio, L.A., Tringe, S.G., Visel, A., Woyke, T., Wang, Z., Rubin, E.M., 2011. Metagenomic discovery of biomass-degrading genes and genomes from cow rumen. Science, 331 (6016), 463-467.

Howard, P.H., Sage, G., Jarvis, W., Gray, D., 1990. Handbook of environmental fate and exposure data for organic chemicals. Volume II: solvents.

Huang, H.L., Shen, D.S., Li, N., Shan, D., Shentu, J.L., Zhou, Y.Y., 2014. Biodegradation of 1,4-dioxane by a novel strain and its biodegradation pathway. Water Air and Soil Pollution, 225 (9).

Huang, Y., Pan, H., Wang, Q., Ge, Y., Liu, W., Christie, P., 2019. Enrichment of the soil microbial community in the bioremediation of a petroleum-contaminated soil amended with rice straw or sawdust. Chemosphere, 224, 265-271.

Hurt, R.A., Qiu, X., Wu, L., Roh, Y., Palumbo, A.V., Tiedje, J.M., Zhou, J., 2001. Simultaneous recovery of RNA and DNA from soils and sediments. Applied and Environmental Microbiology, 67 (10), 4495-4503.

IARC, 1999. 1,4-Dioxine. IARC Monographs on the Evaluation of Carcinogenic Risks to Humans, Vol. 71, Re-evaluation of Some Organic Chemicals, Hydrazine and Hydrogen Peroxide, IARC, Lyon, France (1999), pp. 589-602.

Ikehata, K., El-Din, M.G., 2006. Aqueous pesticide degradation by hydrogen peroxide/ultraviolet irradiation and Fenton-type advanced oxidation processes: A review. Journal of Environmental Engineering and Science, 5 (2), 81-135.

Ikehata, K., Naghashkar, N.J., Ei-Din, M.G., 2006. Degradation of aqueous pharmaceuticals by ozonation and advanced oxidation processes: A review. Ozone-Science & Engineering, 28 (6), 353-414.

Ikehata, K., Wang-Staley, L., Qu, X.Y., Li, Y., 2016. Treatment of groundwater contaminated with 1,4-dioxane, tetrahydrofuran, and chlorinated volatile organic compounds using advanced oxidation processes. Ozone-Science & Engineering, 38 (6), 413-424.

Inoue, D., Tsunoda, T., Sawada, K., Yamamoto, N., Saito, Y., Sei, K., Ike, M., 2016. 1,4-Dioxane degradation potential of members of the genera *Pseudonocardia* and *Rhodococcus*. Biodegradation, 27 (4-6), 277-286.

Inoue, D., Tsunoda, T., Yamamoto, N., Ike, M., Sei, K., 2018. 1,4-Dioxane degradation characteristics of *Rhodococcus aetherivorans* JCM 14343. Biodegradation, 29 (3), 301-310.

Jasmann, J.R., Borch, T., Sale, T.C., Blotevogel, J., 2016. Advanced electrochemical oxidation of 1,4-dioxane via dark catalysis by novel titanium dioxide (TiO_2) pellets. Environmental Science & Technology, 50 (16), 8817-8826.

Jasmann, J.R., Gedalanga, P.B., Borch, T., Mahendra, S., Blotevogel, J., 2017. Synergistic treatment of mixed 1,4-dioxane and chlorinated solvent contaminations by coupling electrochemical oxidation with aerobic biodegradation. Environmental Science & Technology, 51 (21), 12619-12629.

Jia, S., Wu, J., Ye, L., Zhao, F., Li, T., Zhang, X.-X., 2019. Metagenomic assembly provides a deep insight into the antibiotic resistome alteration induced by drinking water chlorination and its correlations with bacterial host changes. Journal of Hazardous Materials, 120841.

Kang, Y.G., Yoon, H., Lee, W., Kim, E.J., Chang, Y.S., 2018. Comparative study of peroxide oxidants activated by nZVI: Removal of 1,4-Dioxane and arsenic(III) in contaminated waters. Chemical Engineering Journal, 334, 2511-2519.

Karges, U., Becker, J., Puttmann, W., 2018. 1,4-Dioxane pollution at contaminated groundwater sites in western Germany and its distribution within a TCE plume. Science of the Total Environment, 619, 712-720.

Kelley, S.L., Aitchison, E.W., Deshpande, M., Schnoor, J.L., Alvarez, P.J.J., 2001. Biodegradation of 1,4-dioxane in planted and unplanted soil: Effect of bioaugmentation with *Amycolata* sp CB1190. Water Research, 35 (16), 3791-3800.

Kim, Y.M., Jeon, J.R., Murugesan, K., Kim, E.J., Chang, Y.S., 2009. Biodegradation of 1,4-dioxane and transformation of related cyclic compounds by a newly isolated *Mycobacterium* sp PH-06. Biodegradation, 20 (4), 511-519.

Klaning, U.K., Wolff, T., 1985. Laser flash-photolysis of hclo, clo-, hbro, and bro- in aqueous-solution - reactions of Cl-atoms and Br-atoms. Berichte Der Bunsen-Gesellschaft-Physical Chemistry Chemical Physics, 89 (3), 243-245.

Klindworth, A., Pruesse, E., Schweer, T., Peplies, J., Quast, C., Horn, M., Glockner, F.O., 2013. Evaluation of general 16S ribosomal RNA gene PCR primers for classical and next-generation sequencing-based diversity studies. Nucleic Acids Research, 41 (1), e1.

Kozich, J.J., Westcott, S.L., Baxter, N.T., Highlander, S.K., Schloss, P.D., 2013. Development of a dual-index sequencing strategy and curation pipeline for analyzing amplicon sequence data on the MiSeq Illumina sequencing platform. Applied and Environmental Microbiology, 79 (17), 5112-5120.

Kumar, S., Krishnani, K.K., Bhushan, B., Brahmane, M.P., 2015. Metagenomics: Retrospect and prospects in high throughput age. Biotechnology Research International, 2015, 121735.

Lee, Y.C., Lo, S.L., Kuo, J., Lin, Y.L., 2012. Persulfate oxidation of perfluorooctanoic acid under the temperatures of 20-40 degrees C. Chemical Engineering Journal, 198, 27-32.

Li, B.Z., Zhu, J., 2016. Simultaneous degradation of 1,1,1-trichloroethane and solvent stabilizer 1,4-dioxane by a sono-activated persulfate process. Chemical Engineering Journal, 284, 750-763.

Li, M.Y., Fiorenza, S., Chatham, J.R., Mahendra, S., Alvarez, P.J.J., 2010. 1,4-Dioxane biodegradation at low temperatures in Arctic groundwater samples. Water Research, 44 (9), 2894-2900.

Li, W., Jain, T., Ishida, K., Remucal, C.K., Liu, H.Z., 2017. A mechanistic understanding of the degradation of trace organic contaminants by UV/hydrogen peroxide, UV/persulfate and UV/free chlorine for water reuse. Environmental Science: Water Research & Technolog, 3 (2), 377-377.

Li, W., Patton, S., Gleason, J.M., Mezyk, S.P., Ishida, K.P., Liu, H.Z., 2018. UV photolysis of chloramine and persulfate for 1,4-dioxane removal in reverse-osmosis permeate for potable water reuse. Environmental Science & Technology, 52 (11), 6417-6425.

Liang, C.J., Guo, Y.Y., 2012. Remediation of diesel-contaminated soils using persulfate under alkaline condition. Water Air and Soil Pollution, 223 (7), 4605-4614.

Liang, C.J., Lee, I.L., 2008. In situ iron activated persulfate oxidative fluid sparging treatment of TCE contamination - A proof of concept study. Journal of Contaminant Hydrology, 100 (3-4), 91-100.

Lippincott, D., Streger, S.H., Schaefer, C.E., Hinkle, J., Stormo, J., Steffan, R.J., 2015. Bioaugmentation and propane biosparging for in situ biodegradation of 1,4-dioxane. Ground Water Monitoring and Remediation, 35 (2), 81-92.

Liu, P.-W.G., Wang, S.-Y., Huang, S.-G., Wang, M.-Z., 2012. Effects of soil organic matter and ageing on remediation of diesel-contaminated soil. Environmental Technology, 33 (23), 2661-2672.

Mahendra, S., Alvarez-Cohen, L., 2005. *Pseudonocardia dioxanivorans* sp nov., a novel actinomycete that grows on 1,4-dioxane. International Journal of Systematic and Evolutionary Microbiology, 55, 593-598.

Mahendra, S., Alvarez-Cohen, L., 2006. Kinetics of 1,4-dioxane biodegradation by monooxygenase-expressing bacteria. Environmental Science & Technology, 40 (17), 5435-5442.

Mahendra, S., Grostern, A., Alvarez-Cohen, L., 2013. The impact of chlorinated solvent co-contaminants on the biodegradation kinetics of 1,4-dioxane. Chemosphere, 91 (1), 88-92.

Mahendra, S., Petzold, C.J., Baidoo, E.E., Keasling, J.D., Alvarez-Cohen, L., 2007. Identification of the intermediates of in vivo oxidation of 1,4-dioxane by monooxygenase-containing bacteria. Environmental Science & Technology, 41 (21), 7330-7336.

Manamsa, K., Crane, E., Stuart, M., Talbot, J., Lapworth, D., Hart, A., 2016. A national-scale assessment of micro-organic contaminants in groundwater of England and Wales. Science of the Total Environment, 568, 712-726.

Masuda, H., McClay, K., Steffan, R.J., Zylstra, G.J., 2012. Biodegradation of tetrahydrofuran and 1,4-dioxane by soluble diiron monooxygenase in *Pseudonocardia* sp strain ENV478. Journal of Molecular Microbiology and Biotechnology, 22 (5), 312-316.

Masuda, H., McClay, K., Steffan, R.J., Zylstra, G.J., 2012. Characterization of three propane-inducible oxygenases in *Mycobacterium* sp strain ENV421. Letters in Applied Microbiology, 55 (3), 175-181.

Matsui, R., Takagi, K., Sakakibara, F., Abe, T., Shiiba, K., 2016. Identification and characterization of 1,4-dioxane-degrading microbe separated from surface seawater by the seawater-charcoal perfusion apparatus. Biodegradation, 27 (2-3), 155-163.

McDonald, D., Price, M.N., Goodrich, J., Nawrocki, E.P., DeSantis, T.Z., Probst, A., Andersen, G.L., Knight, R., Hugenholtz, P., 2012. An improved Greengenes taxonomy with explicit ranks for ecological and evolutionary analyses of bacteria and archaea. The ISME Journal, 6 (3), 610-618.

McElroy, A., Hyman, M. (2019). Consequences of microbial interactions with hydrocarbons, oils, lipids: Biodegradation and Bioremediation. Handbook of Hydrocarbon and Lipid Microbiology. . (eds), S. R. (ed), pp. 1-30, Springer, Cham.

McElroy, A.C., Hyman, M.R., Knappe, D.R.U., 2019. 1,4-Dioxane in drinking water: emerging for 40 years and still unregulated. Current Opinion in Environmental Science & Health, 7, 117-125.

Miao, Y., Johnson, N.W., Gedalanga, P.B., Adamson, D., Newell, C., Mahendra, S., 2019. Response and recovery of microbial communities subjected to oxidative and biological treatments of 1,4-dioxane and co-contaminants. Water Research, 149, 74-85.

Miao, Y., Johnson, N.W., Heck, K., Guo, S.J., Powell, C.D., Phan, T., Gedalanga, P.B., Adamson, D.T., Newell, C.J., Wong, M.S., Mahendra, S., 2018. Microbial responses to combined oxidation and catalysis treatment of 1,4-dioxane and co-contaminants in groundwater and soil. Frontiers of Environmental Science & Engineering, 12 (5), 1-13.

Mohr, T.K., Stickney, J.A., DiGuiseppi, W.H. (2016). Environmental investigation and remediation: 1,4-dioxane and other solvent stabilizers, CRC Press.

Myers, M.A., Johnson, N.W., Marin, E.Z., Pornwongthong, P., Liu, Y., Gedalanga, P.B., Mahendra, S., 2018. Abiotic and bioaugmented granular activated carbon for the treatment of 1,4-dioxane-contaminated water. Environmental Pollution, 240, 916-924.

Nagarajan, N., Pop, M., 2013. Sequence assembly demystified. Nature Reviews Genetics, 14 (3), 157-167.

Ouyang, D., Yan, J.C., Qian, L.B., Chen, Y., Han, L., Su, A.Q., Zhang, W.Y., Ni, H., Chen, M.F., 2017. Degradation of 1,4-dioxane by biochar supported nano magnetite particles activating persulfate. Chemosphere, 184, 609-617.

Pal, S., Kundu, A., Das Banerjee, T., Mohapatra, B., Roy, A., Manna, R., Sar, P., Kazy, S.K., 2017. Genome analysis of crude oil degrading *Franconibacter pulveris* strain DJ34 revealed its genetic basis for hydrocarbon degradation and survival in oil contaminated environment. Genomics, 109 (5-6), 374-382.

Pan, S., Chen, H., 2006. Anaerobic degradation of 1, 4-dioxane under humic-reducing or Fe (III) reducing conditions. Abstracts of Papers of the American Chemical Society.

Parales, R.E., Adamus, J.E., White, N., May, H.D., 1994. Degradation of 1,4-dioxane by an *Actinomycete* in pure culture. Applied and Environmental Microbiology, 60 (12), 4527-4530.

Park, H., Mameda, N., Choo, K.H., 2018. Catalytic metal oxide nanopowder composite Ti mesh for electrochemical oxidation of 1,4-dioxane and dyes. Chemical Engineering Journal, 345, 233-241.

Polasko, A.L., Zulli, A., Gedalanga, P.B., Pornwongthong, P., Mahendra, S., 2019. A mixed microbial community for the biodegradation of chlorinated ethenes and 1,4-dioxane. Environmental Science & Technology Letters, 6 (1), 49-54.

Pornwongthong, P., Mulchandani, A., Gedalanga, P.B., Mahendra, S., 2014. Transition metals and organic ligands influence biodegradation of 1,4-dioxane. Applied Biochemistry and Biotechnology, 173 (1), 291-306.

Pugazhendi, A., Banu, J.R., Dhavamani, J., Yeom, I.T., 2015. Biodegradation of 1,4-dioxane by *Rhodanobacter* AYS5 and the role of additional substrates. Annals of Microbiology, 65 (4), 2201-2208.

Qian, Y.J., Guo, X., Zhang, Y.L., Peng, Y., Sun, P.Z., Huang, C.H., Niu, J.F., Zhou, X.F., Crittenden, J.C., 2016. Perfluorooctanoic acid degradation using UV-persulfate process: Modeling of the degradation and chlorate formation. Environmental Science & Technology, 50 (2), 772-781.

Quast, C., Pruesse, E., Yilmaz, P., Gerken, J., Schweer, T., Yarza, P., Peplies, J., Glockner, F.O., 2013. The SILVA ribosomal RNA gene database project: improved data processing and web-based tools. Nucleic Acids Research, 41 (Database issue), D590-596.

Quince, C., Lanzén, A., Curtis, T.P., Davenport, R.J., Hall, N., Head, I.M., Read, L.F., Sloan, W.T., 2009. Accurate determination of microbial diversity from 454 pyrosequencing data. Nature Methods, 6 (9), 639.

Quintanilla, A., Casas, J.A., Rodriguez, J.J., 2010. Hydrogen peroxide-promoted-CWAO of phenol with activated carbon. Applied Catalysis B-Environmental, 93 (3-4), 339-345.

Quintanilla, A., Fraile, A.F., Casas, J.A., Rodriguez, J.J., 2007. Phenol oxidation by a sequential CWPO-CWAO treatment with a Fe/AC catalyst. Journal of Hazardous Materials, 146 (3), 582-588.

Radjenovic, J., Sedlak, D.L., 2015. Challenges and opportunities for electrochemical processes as next-generation technologies for the treatment of contaminated water. Environmental Science & Technology, 49 (19), 11292-11302.

Ram, R.J., Verberkmoes, N.C., Thelen, M.P., Tyson, G.W., Baker, B.J., Blake, R.C., 2nd, Shah, M., Hettich, R.L., Banfield, J.F., 2005. Community proteomics of a natural microbial biofilm. Science, 308 (5730), 1915-1920.

Ramakrishna, C., Krishna, R., Gopi, T., Swetha, G., Saini, B., Shekar, S.C., Srivastava, A., 2016. Complete oxidation of 1,4-dioxane over zeolite-13X-supported Fe catalysts in the presence of air. Chinese Journal of Catalysis, 37 (2), 240-249.

Remucal, C.K., Manley, D., 2016. Emerging investigators series: The efficacy of chlorine photolysis as an advanced oxidation process for drinking water treatment. Environmental Science: Water Research & Technology, 2 (4), 565-579.

Roh, S.W., Abell, G.C., Kim, K.H., Nam, Y.D., Bae, J.W., 2010. Comparing microarrays and next-generation sequencing technologies for microbial ecology research. Trends in Biotechnology, 28 (6), 291-299.

Rolston, H., Semprini, L., Thankitkul, S., Azizian, M., Hyman, M., 2016. Kinetic studies of the cometabolism of 1,4-dioxane and chlorinated aliphatic hydrocarbon mixtures by *Rhodococcus Rhodochrous* grown on isobutane. AGU Fall Meeting Abstracts.

Roy, A., Dutta, A., Pal, S., Gupta, A., Sarkar, J., Chatterjee, A., Saha, A., Sarkar, P., Sar, P., Kazy, S.K., 2018. Biostimulation and bioaugmentation of native microbial community accelerated bioremediation of oil refinery sludge. Bioresource Technology, 253, 22-32.

Sales, C.M., Mahendra, S., Grostern, A., Parales, R.E., Goodwin, L.A., Woyke, T., Nolan, M., Lapidus, A., Chertkov, O., Ovchinnikova, G., Sczyrba, A., Alvarez-Cohen, L., 2011. Genome sequence of the 1,4-dioxane-degrading *Pseudonocardia dioxanivorans* strain CB1190. Journal of Bacteriology, 193 (17), 4549-4550.

Scaratti, G., Basso, A., Landers, R., Alvarez, P.J., Puma, G.L., Moreira, R.F., 2018. Treatment of aqueous solutions of 1,4-dioxane by ozonation and catalytic ozonation with copper oxide (CuO). Environmental Technology, 1-13.

Segura, Y., Martinez, F., Melero, J.A., Fierro, J.L.G., 2015. Zero valent iron (ZVI) mediated Fenton degradation of industrial wastewater: Treatment performance and characterization of final composites. Chemical Engineering Journal, 269, 298-305.

Sei, K., Miyagaki, K., Kakinoki, T., Fukugasako, K., Inoue, D., Ike, M., 2013. Isolation and characterization of bacterial strains that have high ability to degrade 1,4-dioxane as a sole carbon and energy source. Biodegradation, 24 (5), 665-674.

Sei, K., Oyama, M., Kakinoki, T., Inoue, D., Ike, M., 2013. Isolation and characterization of tetrahydrofuran-degrading bacteria for 1,4-dioxane-containing wastewater treatment by co-metabolic degradation. Journal of Water Environment Technology, 11 (1), 11-19.

Sekar, R., Taillefert, M., DiChristinaa, T.J., 2016. Simultaneous transformation of commingled trichloroethylene, tetrachloroethylene, and 1,4-dioxane by a microbially driven Fenton reaction in batch liquid cultures. Applied and Environmental Microbiology, 82 (21), 6335-6343.

Shen, W.H., Wang, Y.J., Zhan, J.H., Wang, B., Huang, J., Deng, S.B., Yu, G., 2017. Kinetics and operational parameters for 1,4-dioxane degradation by the photoelectro-peroxone process. Chemical Engineering Journal, 310, 249-258.

Siles, J.A., Margesin, R., 2018. Insights into microbial communities mediating the bioremediation of hydrocarbon-contaminated soil from an Alpine former military site. Applied Microbiology and Biotechnology, 102 (10), 4409-4421.

Sogin, M.L., Morrison, H.G., Huber, J.A., Mark Welch, D., Huse, S.M., Neal, P.R., Arrieta, J.M., Herndl, G.J., 2006. Microbial diversity in the deep sea and the underexplored "rare biosphere". Proceedings of the National Academy of Sciences of the United States of America, 103 (32), 12115-12120.

Stefan, M.I., Bolton, J.R., 1998. Mechanism of the degradation of 1,4-dioxane in dilute aqueous solution using the UV hydrogen peroxide process. Environmental Science & Technology, 32 (11), 1588-1595.

Stepien, D.K., Diehl, P., Helm, J., Thorns, A., Puttmann, W., 2014. Fate of 1,4-dioxane in the aquatic environment: From sewage to drinking water. Water Research, 48, 406-419.

Sun, B.Z., Ko, K., Ramsay, J.A., 2011. Biodegradation of 1,4-dioxane by a *Flavobacterium*. Biodegradation, 22 (3), 651-659.

Suthersan, S., Quinnan, J., Horst, J., Ross, I., Kalve, E., Bell, C., Pancras, T., 2016. Making strides in the management of "Emerging Contaminants". Ground Water Monitoring and Remediation, 36 (1), 15-25.

Taccari, M., Milanovic, V., Comitini, F., Casucci, C., Ciani, M., 2012. Effects of biostimulation and bioaugmentation on diesel removal and bacterial community. International Biodeterioration & Biodegradation, 66 (1), 39-46.

Techtmann, S.M., Hazen, T.C., 2016. Metagenomic applications in environmental monitoring and bioremediation. Journal of Industrial Microbiology & Biotechnology, 43 (10), 1345-1354.

Torsvik, V., Ovreas, L., Thingstad, T.F., 2002. Prokaryotic diversity--magnitude, dynamics, and controlling factors. Science, 296 (5570), 1064-1066.

Tsitonaki, A., Petri, B., Crimi, M., Mosbaek, H., Siegrist, R.L., Bjerg, P.L., 2010. In Situ Chemical Oxidation of Contaminated Soil and Groundwater Using Persulfate: A Review. Critical Reviews in Environmental Science and Technology, 40 (1), 55-91.

USEPA, 2016. Statistics for the New Chemicals Review Program under TSCA. https://www.epa.gov/reviewing-new-chemicals-under-toxic-substances-control-act-tsca/statistics-new-chemicals-review.

Vainberg, S., McClay, K., Masuda, H., Root, D., Condee, C., Zylstra, G.J., Steffan, R.J., 2006. Biodegradation of ether pollutants by *Pseudonocardia* sp strain ENV478. Applied and Environmental Microbiology, 72 (8), 5218-5224.

Vieites, J.M., Guazzaroni, M.E., Beloqui, A., Golyshin, P.N., Ferrer, M., 2009. Metagenomics approaches in systems microbiology. FEMS Microbiology Reviews, 33 (1), 236-255.

Wang, C.W., Liang, C.J., 2014. Oxidative degradation of TMAH solution with UV persulfate activation. Chemical Engineering Journal, 254, 472-478.

Watts, M.J., Linden, K.G., 2007. Chlorine photolysis and subsequent OH radical production during UV treatment of chlorinated water. Water Research, 41 (13), 2871-2878.

Wrighton, K.C., Thomas, B.C., Sharon, I., Miller, C.S., Castelle, C.J., VerBerkmoes, N.C., Wilkins, M.J., Hettich, R.L., Lipton, M.S., Williams, K.H., Long, P.E., Banfield, J.F., 2012. Fermentation, hydrogen, and sulfur metabolism in multiple uncultivated bacterial phyla. Science, 337 (6102), 1661-1665.

Xu, X., Liu, S., Smith, K., Wang, Y., Hu, H., 2019. Light-driven breakdown of 1, 4-Dioxane for potable reuse: A review. Chemical Engineering Journal, 373, 508-518.

Xu, X.H., Liu, X.M., Zhang, L., Mu, Y., Zhu, X.Y., Fang, J.Y., Li, S.P., Jiang, J.D., 2018. Bioaugmentation of chlorothalonil-contaminated soil with hydrolytically or reductively dehalogenating strain and its effect on soil microbial community. Journal of Hazardous Materials, 351, 240-249.

Xu, X.Y., Zeng, G.M., Peng, Y.R., Zeng, Z., 2012. Potassium persulfate promoted catalytic wet oxidation of fulvic acid as a model organic compound in landfill leachate with activated carbon. Chemical Engineering Journal, 200, 25-31.

Yamamoto, N., Saito, Y., Inoue, D., Sei, K., Ike, M., 2018. Characterization of newly isolated *Pseudonocardia* sp N23 with high 1,4-dioxane-degrading ability. Journal of Bioscience and Bioengineering, 125 (5), 552-558.

Yuan, S.H., Liao, P., Alshawabkeh, A.N., 2014. Electrolytic manipulation of persulfate reactivity by iron electrodes for trichloroethylene degradation in groundwater. Environmental Science & Technology, 48 (1), 656-663.

Zazo, J.A., Casas, J.A., Mohedano, A.F., Gilarranz, M.A., Rodriguez, J.J., 2005. Chemical pathway and kinetics of phenol oxidation by Fenton's reagent. Environmental Science & Technology, 39 (23), 9295-9302.

Zengler, K., Palsson, B.O., 2012. A road map for the development of community systems (CoSy) biology. Nature Reviews Microbiology, 10 (5), 366-372.

Zhang, H., Chang, F., Shi, P., Ye, L., Zhou, Q., Pan, Y., Li, A., 2019. Antibiotic resistome alteration by different disinfection strategies in a full-scale drinking water treatment plant deciphered by metagenomic assembly. Environmental Science & Technology, 53 (4), 2141-2150.

Zhang, S., Gedalanga, P.B., Mahendra, S., 2016. Biodegradation kinetics of 1,4-dioxane in chlorinated solvent mixtures. Environmental Science & Technology, 50 (17), 9599-9607.

Zhang, S., Gedalanga, P.B., Mahendra, S., 2017. Advances in bioremediation of 1,4-dioxane-contaminated waters. Journal of Environmental Management, 204, 765-774.

Zhao, L., Hou, H., Fujii, A., Hosomi, M., Li, F.S., 2014. Degradation of 1,4-dioxane in water with heat- and Fe^{2+}-activated persulfate oxidation. Environmental Science and Pollution Research, 21 (12), 7457-7465.

Zhao, L.D., Lu, X., Polasko, A., Johnson, N.W., Miao, Y., Yang, Z.M., Mahendra, S., Gu, B.H., 2018. Co-contaminant effects on 1,4-dioxane biodegradation in packed soil column flow-through systems. Environmental Pollution, 243, 573-581.

Zhao, Y., Bai, Y., Guo, Q., Li, Z., Qi, M., Ma, X., Wang, H., Kong, D., Wang, A., Liang, B., 2019. Bioremediation of contaminated urban river sediment with methanol stimulation: Metabolic processes accompanied with microbial community changes. Science of the Total Environment, 653, 649-657.

Zhou, J., Bruns, M.A., Tiedje, J.M., 1996. DNA recovery from soils of diverse composition. Applied and Environmental Microbiology, 62 (2), 316-322.

Zhou, J., He, Z., Yang, Y., Deng, Y., Tringe, S.G., Alvarez-Cohen, L., 2015. High-throughput metagenomic technologies for complex microbial community analysis: open and closed formats. MBio, 6 (1).

Zhou, Y.Y., Huang, H.L., Shen, D.S., 2016. Multi-substrate biodegradation interaction of 1, 4-dioxane and BTEX mixtures by *Acinetobacter baumannii* DD1. Biodegradation, 27 (1), 37-46.

Zwolinski, M.D., 2007. DNA sequencing: Strategies for soil microbiology. Soil Science Society of America Journal, 71 (2), 592-600.

Chapter 3 Monitoring Tools for Validating Natural Attenuation of 1,4-Dioxane

3.1 Introduction

1,4-Dioxane is a groundwater contaminant often associated with chlorinated solvents, particularly 1,1,1 trichloroethane (TCA) solvent blends (Surprenant, 2002), where it was used to suppress reactivity (Mohr et al., 2010). 1,4-Dioxane has also been used as a solvent and as an additive in ink, paints and other coatings, and was produced as an impurity in various industrial processes including ethoxylated surfactants (products used in detergents, shampoos, and other personal care products), various pesticides and herbicides, and polyester (Mohr et al., 2010). This compound is of environmental and public health concern because it is toxic to kidneys and the liver and because it is "likely to be carcinogenic to humans" (EPA, 2010). Groundwater contamination by 1,4-dioxane is often a result of accidental discharges or improper storage and disposal practices. Because this compound is miscible in water and does not sorb readily to aquifer materials, it is very mobile in the subsurface (Zenker et al., 2003, Mohr et al., 2010), sometimes resulting in large dilute plumes that can only be treated by a limited set of aggressive technologies. Thus, natural in-situ strategies are promising alternatives to remediate 1,4-dioxane in impacted environments.

Successful implementation of natural degradation strategies must address critical points outlined by the U.S. Environmental Protection Agency's (EPA's) Office of Solid Waste and Emergency Response (OSWER) Directive on use of monitored natural attenuation (MNA) (EPA, 1999). Namely, (1) historical site data demonstrating decreasing contaminant trends, (2) hydrogeological and geochemical data that indirectly support natural contaminant removal processes, and (3) microcosm studies for direct support of specific removal mechanisms. Conventional analytical techniques including analyses of trends in concentration and changes in

spatial distribution over time are often used to satisfy the OSWER directives. Further, advanced molecular analyses can provide an additional layer of information to support natural contaminant degradation by the intrinsic microbial population.

Until recently, biodegradation of 1,4-dioxane in the environment was sparsely documented leading many to believe 1,4-dioxane was resistant to microbial-mediated processes. However, several studies have demonstrated a greater potential for biodegradation of this groundwater contaminant (Parales et al., 1994, Zenker et al., 2003, Nakamiya et al., 2005, Mahendra and Alvarez-Cohen, 2006, Vainberg et al., 2006, Kim et al., 2009, Chiang et al., 2012, Masuda et al., 2012). One of the earliest references to 1,4-dioxane biodegradation is from a study attributing its degradation to metabolic and co-metabolic pathways found in *Rhodococcus* sp. and other environmental isolates (Bernhardt and Diekmann, 1991). Additional studies have linked 1,4-dioxane co-metabolism with the presence of a structural analog, tetrahydrofuran (THF) (Sei et al., 2010, Sun et al., 2011, Masuda et al., 2012, Sales et al., 2013). In this situation, 1,4-dioxane biodegradation fortuitously occurs after induction of the necessary enzymes by THF. To date, there are over 30 published papers that document 1,4-dioxane biodegradation in environmental and laboratory studies, and biological degradation of this compound is widely recognized. Indeed, environmental studies focusing on natural in-situ biodegradation of 1,4-dioxane are on the rise (Chiang et al., 2012, Alvarez et al., 2014, Adamson et al., 2015, Lippincott et al., 2015).

Innovative techniques including nucleic acid biomarkers and compound specific isotope analysis (CSIA) provide valuable information on the capacity of microorganisms to degrade contaminants and the specific contaminant removal mechanisms in the environment. Identification and advanced characterization of microorganisms capable of 1,4-dioxane degradation has led to the development of 1,4-dioxane specific biomarkers (Gedalanga et al., 2014, Li et al., 2014).

Specifically, Gene *dxmB* encoding DXMO and *aldH* encoding ALDH have previously been established as biomarkers for 1,4-dioxane biodegradation (Gedalanga et al., 2014). These biomarkers are based on genes that encode bacterial multicomponent monooxygenase and aldehyde dehydrogenase enzymes involved in the metabolic and co-metabolic 1,4-dioxane degradation pathway shown in Figure 3.1 (Mahendra et al., 2007, Grostern et al., 2012). Co-metabolic degradation pathways are catalyzed by monooxygenase enzymes induced by methane (MMO), propane (PrMO), phenol (PHE), tetrahydrofuran (THFMO), and toluene (TOL, T4MO, RMO) monooxygenases (Fishman et al., 2004, Mahendra and Alvarez-Cohen, 2006, Vainberg et al., 2006, Ryan et al., 2007, Masuda et al., 2012). The DNA sequences in the genes that encode THF and 1,4-dioxane monooxygenases are virtually identical, and sequence databases have indicated these gene targets belong to bacteria with a documented capacity for metabolic or co-metabolic 1,4-dioxane degradation. The co-metabolic degradation of 1,4-dioxane degradation by the soluble di-iron methane monooxygenase enzyme (sMMO) has been investigated in detail. The enzyme is used to oxidize methane with oxygen but can also degrade 1,4-dioxane (Mahendra and Alvarez-Cohen, 2006). Quantification of sMMO has been used as evidence to support natural degradation of 1,4-dioxane in a contaminated aquifer (Chiang et al., 2012). Thus, the presence and abundance of specific genetic biomarkers can be an important factor in determining the potential for natural degradation of 1,4-dioxane in contaminated groundwater.

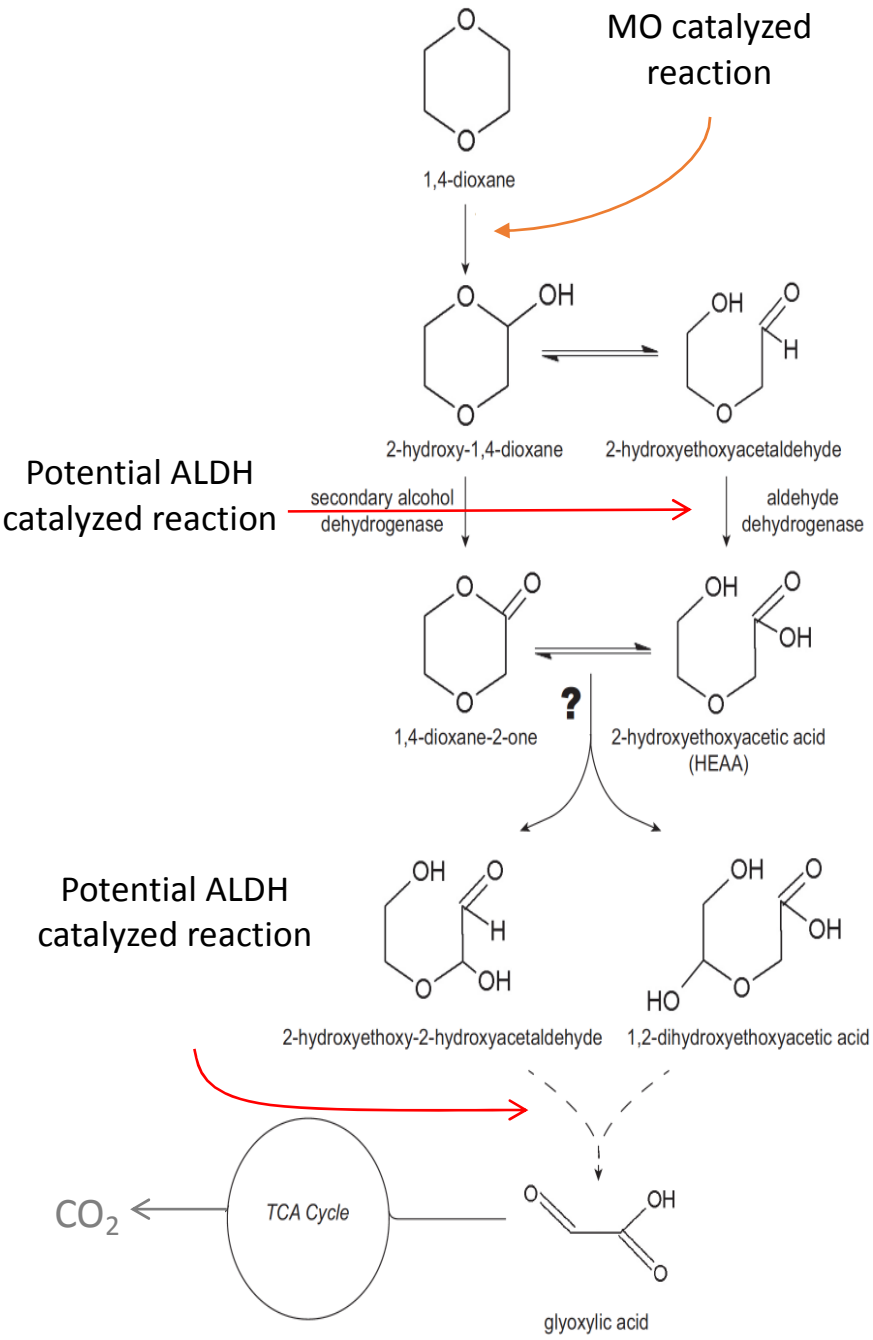

Figure 3.3. 1,4-Dioxane aerobic degradation pathway. Similar pathway was reported for both metabolic and co-metabolic processes, resulting in nearly complete mineralization.

CSIA has also been recently applied to directly monitor 1,4-dioxane biodegradation (Pornwongthong et al., 2011, Pornwongthong et al., In review). CSIA is often used within the environmental remediation field to assess the extent of biodegradation processes and to distinguish

physical processes from biological attenuation processes in the subsurface. CSIA has been applied to a number of contaminants (Hunkeler et al., 2008) including aromatic hydrocarbons (Mancini et al., 2003) and chlorinated compounds (Slater et al., 2001) by measuring the isotopic enrichment of the residual contaminant as degradation proceeds. Thus, by monitoring isotope values of the contaminant along the length of the plume and in comparison to the source material, CSIA has the ability to identify biodegradation of contaminants in the field and to distinguish contaminant mass loss due to biodegradation versus that due to physical processes (e.g., dilution, mixing). Widespread application of CSIA to 1,4-dioxane sites has been limited due to difficulties extracting 1,4-dioxane from water resulting in high method detection limits. However, the extractions and analytical techniques have improved within the past couple of years and CSIA method detection limits are within the 1,4-dioxane concentration range encountered at remediation sites.

In this chapter, the MLOE approach was applied to establish intrinsic biodegradation using biomarkers and CSIA to support more traditional approaches. Establishing intrinsic degradation serves two purposes. First, it is a case study in establishing the in-situ degradation of a compound in accordance with accepted protocols. Second, it will provide a demonstration of natural degradation of 1,4-dioxane in a large plume under field conditions, and provide insights into the biodegradation mechanisms.

3.2 Materials and Methods

3.2.1 Site Description and Conceptual Site Model

The study was conducted using data collected from a former landfill site located in the Midwestern US that accepted industrial waste from 1968 to 1979. The following details the conceptual site model (CSM), which serves to conceptualize the relationship between contaminant

sources and receptors through consideration of potential or actual migration and exposure pathways. The CSM presents the current understanding of the site.

The site is underlain by thick glacial deposits on the order of 350 to 420 feet thick, comprised primarily of outwash sands and gravels with interbedded layers of clay-rich till and lacustrine clays. Groundwater is encountered relatively deep resulting in a substantial vadose or unsaturated zone throughout the site. In the vicinity of the landfill, previous studies indicate that the vadose zone varies from approximately 70 feet thick along the northeastern boundary of the landfill (where localized perched conditions exist) to about 100 feet thick along the western boundary. The retention time of infiltrating water in the vadose zone near the landfill was estimated to range from 6 to 29 years.

The average advective groundwater flow velocity ranges from approximately 0.7 ft/day to 1.0 ft/day, with the aquifer(s) under unconfined to semi-confined conditions. Investigations conducted in the downgradient areas of the site have identified distinct upper and lower clay units. These clay units serve as aquitards isolating the primary flow path (sands and gravels) from groundwater above and below.

A large, dilute groundwater plume primarily comprised of 1,4-dioxane (up to 420 µg/L based on 2015 data) and tetrahydrofuran ([THF] up to 340 µg/L) emanates from the former landfill area and extends downgradient for more than 2 miles. Based on the most recent groundwater quality results (Fall 2015), the main plume of 1,4-dioxane is located between the landfill and the nearest shallow surface water body (<15 feet deep) located approximately 1,700 feet downgradient, as shown on Figure 3.2. The thickness of the 1,4-dioxane plume generally ranges from 50 to 90 feet along the west margin of the landfill to 100 to 150 feet approximately 1,700 to 9,700 feet down

the hydraulic gradient from the landfill. Beyond this distance, the plume thickness decreases to generally less than 50 feet.

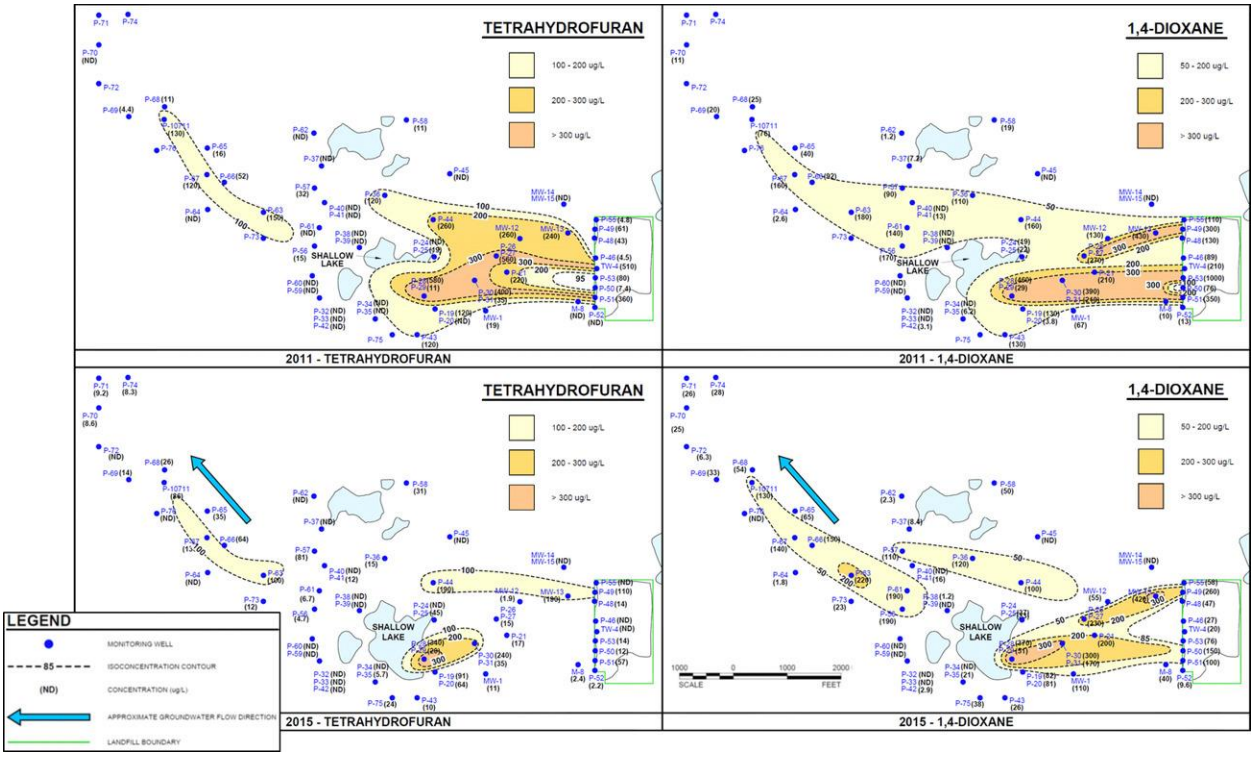

Figure 3.4. 1,4- Dioxane and THF groundwater plume distribution in 2011 and 2015.

Source control measures at the landfill consist of a low permeability cap with an active landfill gas collection system. In concert with the source control measures, regular monitoring has been conducted of an extensive network of 62 monitoring wells that includes wells in the source area, wells in the plume, and sentinel wells. As such, the groundwater plume's chemical and geochemical conditions are well characterized.

3.2.2 Sample Collection

In order to evaluate the intrinsic biodegradation potential of 1,4-dioxane, MLOE data were collected in a phased approach. As part of the regular monitoring activities, groundwater samples for volatile organic compound analysis (including THF and 1,4-dioxane using EPA SW-846 Method 8260 with selective ion monitoring - SIM) and geochemical biological indicator

parameters were collected from 62 monitoring wells using low-flow sampling techniques. Water samples were analyzed for general biogeochemical indicators (pH, specific conductivity [SC], temperature, dissolved oxygen [DO], oxidation-reduction potential [ORP], and alkalinity), potential bacterial electron acceptors (nitrate and sulfate), and potential by-products of anaerobic microbial respiration (ammonia, iron, manganese, and methane). Total organic carbon (TOC) was analyzed to evaluate the presence of organic carbon, which may serve as potential electron donors to support microbial activity. Groundwater samples for molecular analyses were then collected from 29 monitoring wells (i.e., a subset of the 62 well network) across the groundwater plume and sent to the University of California, Los Angeles (UCLA) for characterization. Groundwater samples were also collected from 24 monitoring wells for characterization by ^{13}C CSIA and were submitted to Pace Analytical Services, Inc. (Pittsburgh, PA, USA).

3.2.3 Analysis of 1,4-Dioxane Biomarkers and sMMO Gene Targets

Biomarkers indicating the potential biodegradation of 1,4-dioxane were applied to nucleic acid extracts from 29 groundwater monitoring well samples at this site following the procedure of Gedalanga et al. (2014). Additionally, the presence and abundance of the sMMO gene was determined in groundwater from this site for its potential role in co-metabolism of 1,4-dioxane.

3.2.3.1 Extraction of Total Nucleic Acids

Total nucleic acids were extracted from all samples using a modified phenol chloroform method. Briefly, 4 mL of groundwater was transferred to sterile 15 mL conical tubes and centrifuged at 7,000 × *g* for 10 min. The supernatant was discarded and the pellet was resuspended in 2 mL of 1X phosphate buffered saline and transferred to sterile 2 mL microcentrifuge tubes. Biomass was further pelleted by centrifugation at 13,000 × *g* for 5 min. The supernatant was discarded and 1 mL of phenol, 250 µL of lysis buffer, 100 µL of 10% sodium dodecyl sulfate and

1 g of 0.1 mm silica zirconia beads were added to the biomass. Samples were homogenized using a Mini-Bead Beater-16 (Biospec Products, Bartlesville, OK, USA) and processed with phenol/chloroform/isoamyl alcohol (Gedalanga et al., 2014). Nucleic acids were isolated from crude extracts by precipitation in isopropyl alcohol and resuspended in a final volume of 100 µL in nuclease-free water. DNA concentration and purity were examined on a Nanodrop 2000c Spectrophotometer (Thermo Fisher, Waltham, MA, USA).

3.2.3.2 Gene Abundance Analyses

1,4-Dioxane biomarkers, *dxmB* and *aldH*, along with sMMO encoded gene and total bacterial 16S rRNA gene targets were quantified in DNA extracted from groundwater samples using qPCR. Primer sets for *dxmB*, *aldH*, and sMMO gene were selected from published literature (Lyew and Guiot, 2003, Gedalanga et al., 2014). Standard curves for *dxmB*, *aldH*, and total bacteria 16S rRNA targets were produced using serial dilutions of genomic DNA extracted from a pure culture of the 1,4-dioxane degrading bacterium, *Pseudonocardia dioxanivorans* CB1190 (Mahendra and Alvarez-Cohen, 2005). Genomic DNA from the methane oxidizing bacterium *Methylosinus trichosporium* OB3b (Colby et al., 1977) was used to construct the standard curve for the sMMO gene qPCR assay. Each qPCR reaction included a negative control (no template added) and a positive control to validate the integrity of reagents and assays.

3.2.4 Compound Specific Isotope Analysis

Groundwater samples were collected from 24 monitoring wells across the length of the plume and sent to Pace Analytical Services, Inc. (Pittsburgh, PA) for isotopic analysis of ^{12}C and ^{13}C. 1,4-Dioxane in each sample was first pre-concentrated using purge-and-trap techniques and then analyzed using gas chromatography isotope-ratio mass spectrometry (GC-IRMS). At the time of analysis, the CSIA method detection limit for 1,4-dioxane was 100 µg/L. CSIA samples were

collected in laboratory-provided sample containers using procedures identical to those used for collection of 1,4-dioxane.

3.2.5 Groundwater Temporal and Spatial Trends

Trend analyses were conducted on concentrations of 1,4-dioxane and THF using data from monitoring wells in the source area and the downgradient portion of the plume. The spatial distribution of iron, sulfate, and methane in the groundwater in 2011 was compared to the distribution in 2015. 1,4-Dioxane and THF groundwater trends for representative source and downgradient plume area monitoring wells are shown on Figure 3.3. Linear regression analyses results were calculated for each constituent on each plot by fitting a trend line to each data set. Trends were considered stable, based on the observed attitude of the trend line in relation to horizontal (or flatness of the line) and when the slope of the line was less than +/-0.01 concentration per unit time. Regression analyses were calculated for 5-year (2010 to 2015) and 10-year (2005 to 2015) periods for monitoring wells with a historical record of at least 10 years. Monitoring wells installed within the last 5 years were analyzed for a 2-year (2013 to 2015; minimum of 5 samples) and 5-year (2010 to 2015) monitoring periods.

Evaluations of the temporal changes in the spatial distribution of 1,4-dioxane and geochemical biodegradation attenuation indicators were conducted to support intrinsic biodegradation and attenuation of the groundwater plume. 1,4-Dioxane and THF isopleth maps were prepared for 2011and 2015.

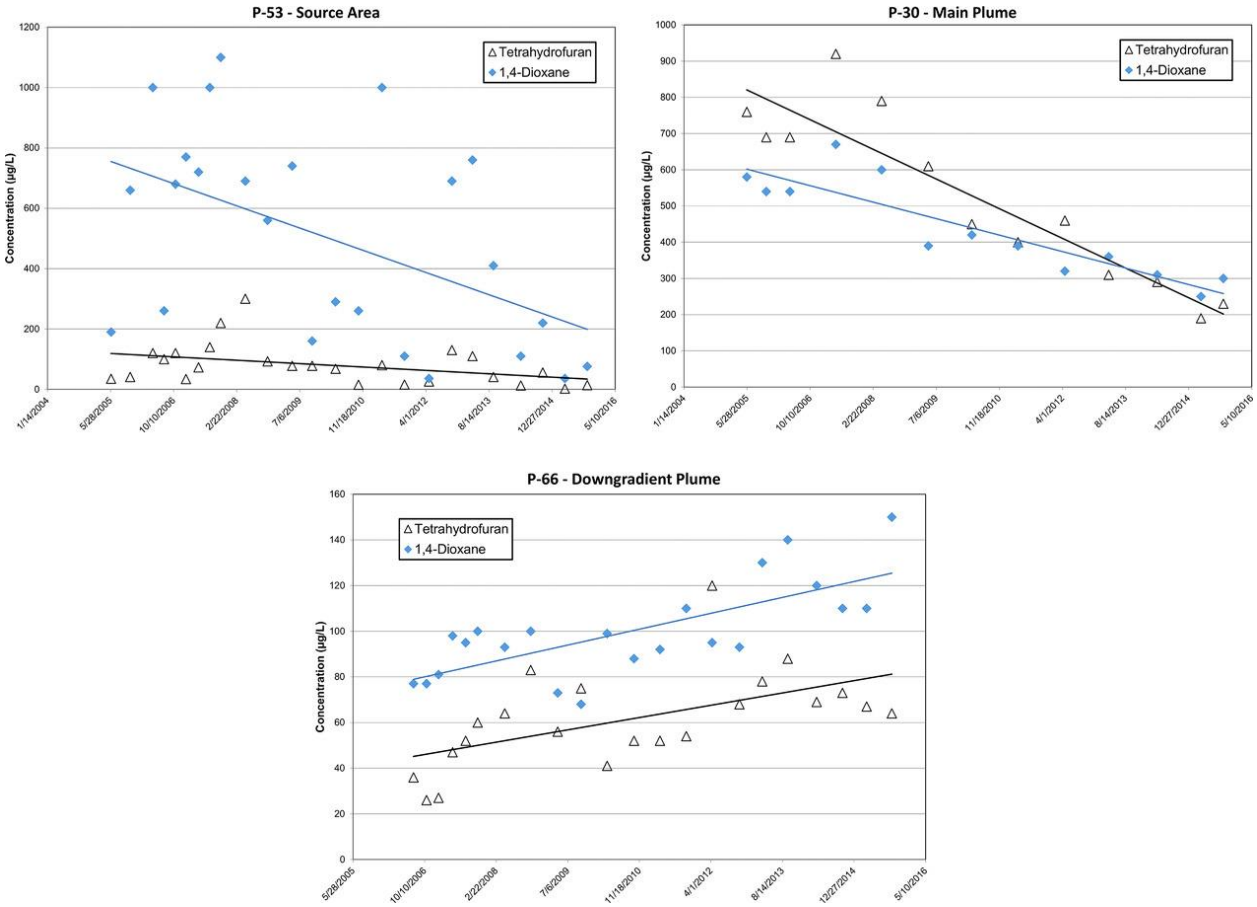

Figure 3.5. 1,4- Dioxane and THF groundwater concentration trends in source and downgradient plume areas.

3.2.6 Source and Plume Mass Estimates

Hydrogeologic time series simulations of groundwater contaminant distribution of 1,4-dioxane (2004 to 2015) and THF (2002 to 2015) were conducted using field data to estimate the plume masses for each constituent and to evaluate the temporal mass changes. The simulations were created using Environmental Visualization System/Mining Visualization System (EVS/MVS) modeling software, version 9.93 by C-Tech Corporation (Boggstown, IN, USA). Plume mass for 1,4-dioxane and THF was estimated using relative differences for three iso-concentration volumes; 200 µg/L, 85 µg/L, and 20 µg/L on an annual basis for the time period of interest. For the purposes of these estimates, the mass within the main plume area (near source)

was considered to be within the >200 µg/L iso-concentration volume, and the mass of the total plume was considered to be within the >20 µg/L iso-concentration volume.

3.2.7 Fate and Transport Modeling

Groundwater flow and fate and transport modeling was conducted as an additional line of evidence to evaluate 1,4-dioxane groundwater plume conditions. MODFLOW, a widely used United States Geologic Survey (USGS) computer code for numerical, 3-D, finite-difference groundwater flow models, was used to simulate the groundwater flow in the study area. MT3DMS, a modular 3-D transport model that can simulate advection, dispersion, and chemical reactions of dissolved constituents was used to simulate the fate and transport of 1,4-dioxane.

Simulations were conducted beginning in 1970, shortly after the landfill commenced operations. The numerical flow model was calibrated to historic hydrogeological data and observed hydraulic heads across the monitoring well network. For the solute transport component of the model, the base scenario for the solute transport model employed source area concentrations for the southern, central, and northern areas of the landfill shown in Table 3.1 that vary over time, consistent with analytical sampling results. The solute transport component of the model was calibrated to the 2015 groundwater sampling analytical results. As part of the numerical modeling effort, dispersion and dilution processes were simulated. Further, based on the results as detailed below, simulation of 1,4-dioxane biodegradation processes was required, which were simulated using first-order decay kinetics (half-life for 1,4-dioxane was set to 3,500 days).

Table 3.1. Estimates of 1,4-dioxane concentrations (µg/L) in the source area that were used to set up the mathematical model.

Time Period	Period 1	Period 2	Period 3
Year	1970 - 1980	1980 - 2006	2006 - 2014
Concentration (µg/L), South Area	3500	1500	500
Concentration (µg/L), Central Area	1200	900	300
Concentration (µg/L), North Area	1000	800	600

3.3 Results

3.3.1 Presence and Abundance of 1,4-Dioxane Biomarkers and sMMO Gene Targets in Groundwater Monitoring Wells

Groundwater samples from 29 monitoring wells collected in September 2015 were screened for the presence and abundance of 1,4-dioxane biomarkers genes which encoded DXMO and ALDH, and sMMO (Figure 3.4, 3.5, 3.6, 3.7). Positive detections for *dxmB* and/or *aldH* were observed in 14 of 15 monitoring wells that were located within the plume with detectable levels of 1,4-dioxane. Six of eight monitoring wells positive for the *dxmB* biomarker were located within portions of the plume where 1,4-dioxane concentrations were greater than 50 µg/L whereas only 4 of these 8 wells had THF concentrations above 50 µg/L. Gene *aldH* detections were found in 9 of 13 and 8 of 13 monitoring wells where 1,4-dioxane and THF concentrations were greater than 50 µg/L, respectively. In addition, 5 of 6 wells positive for both *dxmB* and *aldH* were observed in samples collected from monitoring wells where 1,4-dioxane levels were greater than 50 µg/L (Figure 3.4 and 3.5). The single well with both *dxmB* and *aldH* present outside of this range was located in monitoring well P-46 with a 1,4-dioxane and THF concentration of 27 µg/L and <2 µg/L, respectively. The absence of 1,4-dioxane biomarkers in monitoring wells with > 50 µg/L 1,4-dioxane were anomalous and accounted for 8 of 14 wells lacking biomarker detections.

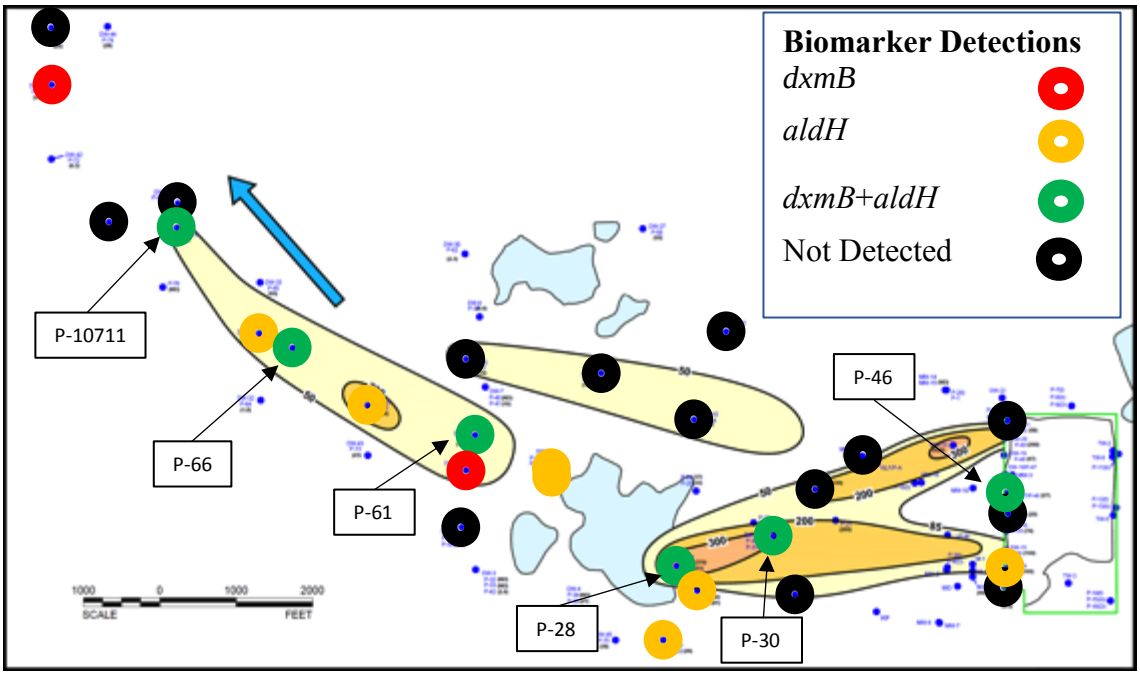

Figure 3.6. *dxmB* and *aldH* biomarker detections in groundwater collected September 2015 track well within the 1,4-dioxane plume.

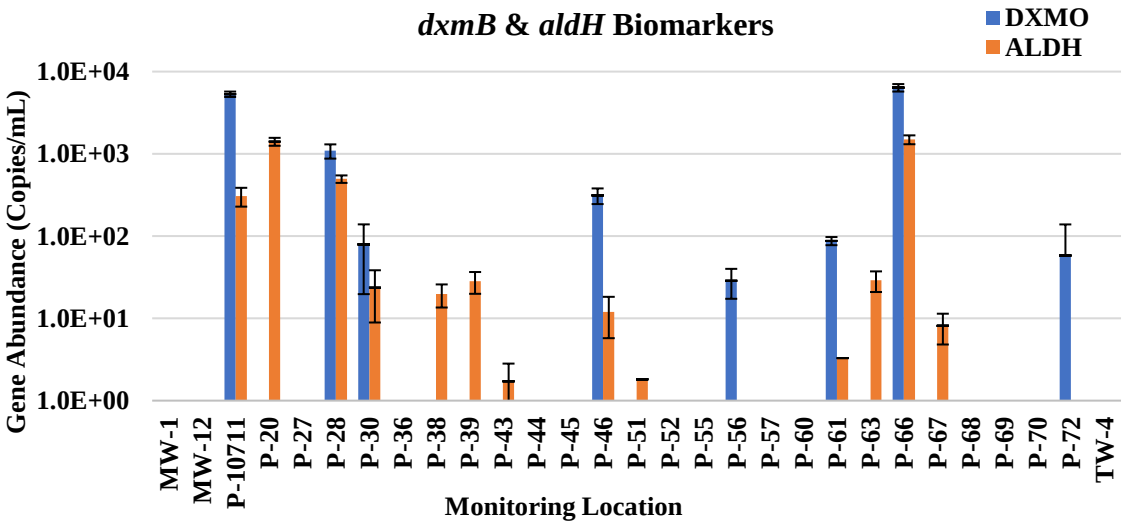

Figure 3.7. Abundance of 1,4-dioxane biomarkers, *dxmB* and *aldH*, in samples collected from KL Ave. Landfill.

Total bacteria and sMMO gene were present throughout the site (Figure 3.6 and 3.7). These targets were highly prevalent in monitoring wells resulting in positive detections in 26 of 29

surveyed wells. The total bacteria primer set was more sensitive to inhibition with 7 of 29 sampled wells determined to be negative for this gene target while sMMO was only negative in 2 of these wells. In addition, the sMMO gene target was present in 9 of 12 monitoring wells with 1,4-dioxane concentrations below 50 µg/L.

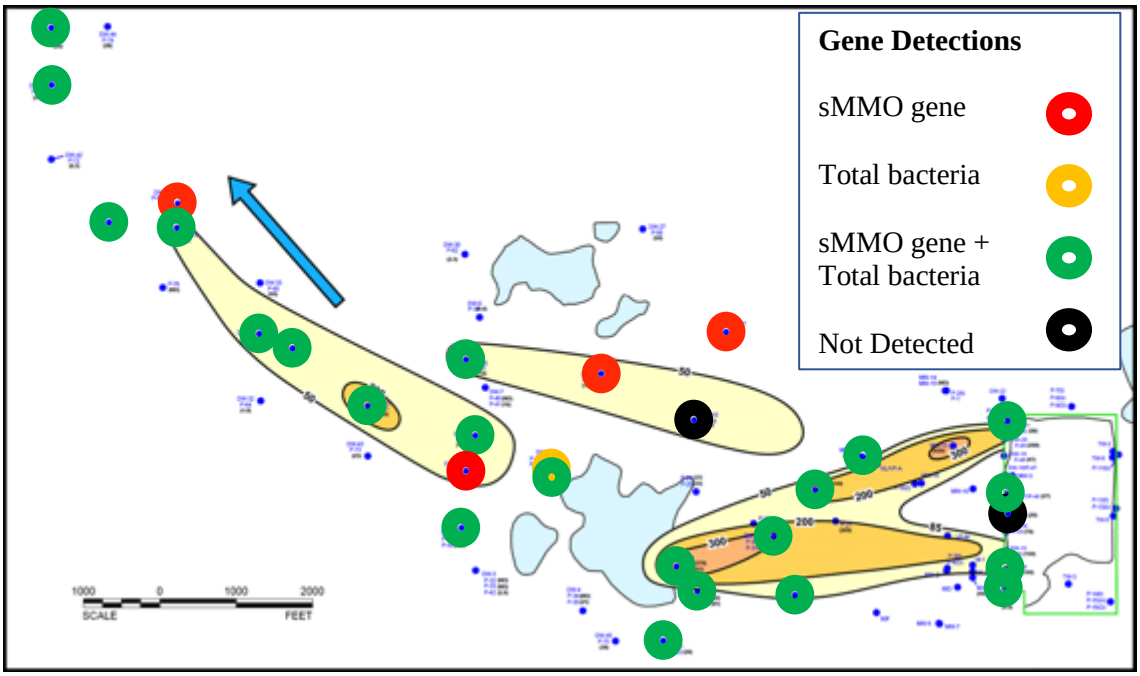

Figure 3.8. Presence of sMMO gene and total bacteria in a 1,4-dioxane contaminated aquifer collected in September 2015.

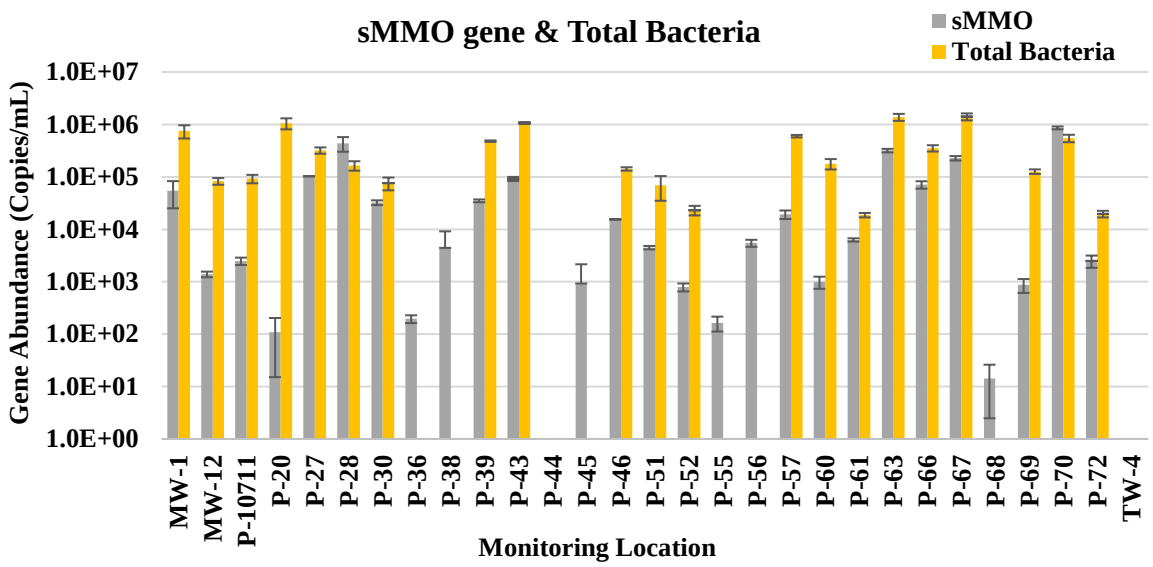

Figure 3.9. Abundance of sMMO gene and total bacteria populations in samples collected from KL Ave. Landfill.

The abundance of 1,4-dioxane biomarkers, sMMO gene, and total bacteria 16S rRNA gene targets are presented in Table 3.2. All standard curves used in qPCR analyses had an r^2 value and PCR efficiency greater than 0.97 and 0.90, respectively. The results in Table 3.2 are the average of two analytical replicates and error is presented as the range of duplicate measurements. The method detection limits for *dxmB*, *aldH*, and sMMO were respectively 1.5×10^1, 2.7×10^1, and 3.1×10^1 copies/mL. *dxmB* was present in concentrations ranging from 2.9×10^1 to 6.4×10^3 copies/mL, while *aldH* concentrations ranged between 2.0×10^1 to 1.5×10^3 copies/mL. Most notably, *dxmB* and *aldH* were both present and abundant at six locations with detectable levels of 1,4-dioxane: P-10711, P-28, P-30, P-46, P-61, and P-66. Monitoring locations P-66, P-10711, and P-28 corresponded to 1,4-dioxane concentrations of 150 µg/L, 130 µg/L, and 370 µg/L, respectively. THF was also positive in these same wells at 64 µg/L, 86 µg/L, and 340 µg/L, respectively. As expected, *aldH* was present in more locations than *dxmB* due to the high specificity of *dxmB* for 1,4-dioxane degrading bacteria and the broad specificity of *aldH* for a

number of different bacteria carrying the gene encoding aldehyde dehydrogenase. The results for total bacteria 16S rRNA and sMMO gene indicate there is high abundance of bacteria in these samples ranging from 1.9×10^4 to 1.4×10^6 bacterial cells/mL. Additionally, the abundance of microorganisms carrying sMMO gene ranged between 1.4×10^1 to 8.6×10^5 cells/mL. The sMMO gene microorganisms were clearly dominant in monitoring wells P-28, P-30, and P-70 occupying over 40% of the total bacterial population. Further, *dxmB*-carrying microorganisms consisted of up to 5.8% of the microbial community.

Table 3.2. Gene abundance for *dxmB*, *aldH*, sMMO gene, total bacterial and contaminant concentrations in groundwater samples.

Location	*dxmB*		*aldH*		sMMO		TB		1,4-Dioxane (µg/L)	THF (µg/L)
	Mean	Error	Mean	Error	Mean	Error	Mean	Error		
Detection Limit	1.46E+01		2.70E+01		3.14E+01		9.81E+02			
Reporting Limit	***3.35E+01***		***3.64E+01***		***4.31E+02***		***1.41E+03***			
Negative Control	BDL	BDL	BDL	BDL	BDL	BDL	9.81E+02	2.57E+02		
MW-12	BDL	BDL	BDL	BDL	1.39E+03	1.71E+02	8.28E+04	1.22E+04	55	1.9
MW-1	BDL	BDL	BDL	BDL	5.41E+04	2.89E+04	7.53E+05	2.13E+05	110	11
P-10711	5.32E+03	4.01E+02	3.07E+02	7.92E+01	2.48E+03	3.96E+02	9.24E+04	1.70E+04	130	86
P-20	BDL	BDL	1.41E+03	1.56E+02	1.09E+02	9.40E+01	1.06E+06	2.52E+05	81	64
P-27	BDL	BDL	BDL	BDL	1.03E+05	8.54E+02	3.21E+05	4.43E+04	230	15
P-28	1.09E+03	2.14E+02	4.95E+02	5.19E+01	4.38E+05	1.36E+05	1.65E+05	3.37E+04	370	340
P-30	7.93E+01	5.96E+01	2.37E+01	1.48E+01	3.23E+04	3.39E+03	7.62E+04	2.09E+04	300	240
P-36	BDL	BDL	BDL	BDL	1.96E+02	3.31E+01	BDL	BDL	120	15
P-38	BDL	BDL	1.97E+01	6.15E+00	4.42E+03	4.72E+03	BDL	BDL	1.2	<2
P-39	BDL	BDL	2.82E+01	8.36E+00	3.50E+04	2.15E+03	4.80E+05	1.51E+04	<1	<2
P-43	BDL	BDL	1.72E+00	1.10E+00	9.18E+04	8.13E+03	1.06E+06	4.61E+04	26	10
P-44	BDL	BDL	BDL	BDL	BDL	BDL	BDL	BDL	160	190
P-45	BDL	BDL	BDL	BDL	9.25E+02	1.22E+03	BDL	BDL	<1	<2
P-46	3.13E+02	6.75E+01	1.20E+01	6.27E+00	1.54E+04	2.50E+02	1.42E+05	1.06E+04	27	<2
P-51	BDL	BDL	1.82E+00	-	4.48E+03	3.38E+02	6.93E+04	3.43E+04	100	57
P-52	BDL	BDL	BDL	BDL	7.89E+02	1.37E+02	2.32E+04	4.81E+03	9.6	2.2
P-55	BDL	BDL	BDL	BDL	1.64E+02	5.19E+01	BDL	BDL	58	<2
P-56	2.87E+01	1.13E+01	BDL	BDL	5.47E+03	8.41E+02	BDL	BDL	190	4.7
P-57	BDL	BDL	BDL	BDL	1.93E+04	3.58E+03	5.98E+05	3.20E+04	110	81
P-60	BDL	BDL	BDL	BDL	9.90E+02	2.57E+02	1.78E+05	4.01E+04	<1	<2

P-61	8.75E+01	9.92E+00	3.29E+00	-	6.28E+03	4.57E+02	1.87E+04	1.78E+03	190	6.7
P-63	BDL	BDL	2.91E+01	8.18E+00	3.18E+05	2.47E+04	1.38E+06	2.11E+05	220	100
P-66	6.39E+03	6.65E+02	1.49E+03	1.85E+02	7.10E+04	1.15E+04	3.53E+05	4.85E+04	150	64
P-67	BDL	BDL	8.11E+00	3.29E+00	2.28E+05	2.20E+04	1.41E+06	2.14E+05	140	130
P-68	BDL	BDL	BDL	BDL	1.43E+01	1.18E+01	BDL	BDL	54	26
P-69	BDL	BDL	BDL	BDL	8.68E+02	2.56E+02	1.27E+05	1.27E+04	33	14
P-70	BDL	BDL	BDL	BDL	8.62E+05	5.35E+04	5.47E+05	8.87E+04	25	8.6
P-72	5.81E+01	8.07E+01	BDL	BDL	2.50E+03	6.57E+02	1.97E+04	2.84E+03	6.3	<2
TW-4	BDL	BDL	BDL	BDL	BDL	BDL	BDL	BDL	20	<2

"-" = Amplification in only 1 of 2 duplicate samples

Bold Italics = Below reporting limit

Gene *dxmB*, *aldH*, and sMMO gene RNA transcripts were quantified in all groundwater samples received from KL Ave. Landfill (Table 3.3). The abundance of RNA transcripts is not a direct measure of gene expression; however, these targets are more associated with activity of the functional gene target. Our results show that most monitoring locations at KL Ave. Landfill were negative for *dxmB*, *aldH*, and sMMO gene transcripts. The very low levels of RNA transcripts quantified at these locations is attributed a number of factors including the instability of RNA and already low levels of *dxmB* and *aldH* harboring bacteria. However, several sites indicate positive detections for these gene targets. Gene *dxmB* was detected in P-10711, P-20, P-36, P-56 (J), and P-66. Monitoring location P-66 had the highest concentrations of DXMO transcripts. This site was also positive for *aldH* transcripts suggesting the appropriate functional genes for 1,4-dioxane biodegradation are present and active.

The results for *dxmB* at P-20 and P-36 are interesting because these locations were positive for RNA transcripts, but negative for gene abundance. This finding indicates potential inhibition in the DNA extracts that were removed during RNA isolation. P-56 was also positive for *dxmB* RNA transcripts, albeit below the reporting limit. This also corresponds to a positive result for *dxmB* gene abundance and negative *aldH* genes and RNA transcripts. These results indicate the presence of native 1,4-dioxane degrading bacteria at this location and the presence of an inhibitor preventing active biodegradation.

Quantification of sMMO gene RNA transcripts in KL Ave. Landfill groundwater samples determined relatively low detections of this target in all samples. This is rather surprising given the concentration of sMMO genes detected in the gene abundance analysis (Figure 3.7 and Table 3.2). Groundwater samples from P-70 had the highest sMMO gene RNA transcripts in all samples

analyzed. This suggests that methane oxidizing bacteria are present and active and the potential for co-metabolism of 1,4-dioxane exists at this location.

Table 3.3. Abundance of RNA transcripts for 1,4-dioxane biomarkers and sMMO gene in KL AVE. Landfill.

Location	*dxmB* (Copies/mL)		*aldH* (Copies/mL)		sMMO (Copies/mL)	
	Mean	Range	Mean	Range	Mean	Range
MW-1	BDL	BDL	BDL	BDL	BDL	BDL
MW-12	BDL	BDL	BDL	BDL	BDL	BDL
P-10711	3.76E+01	-	BDL	BDL	BDL	BDL
P-20	9.83E+01	2.50E+01	1.77E+01 J	-	BDL	BDL
P-27	BDL	BDL	BDL	BDL	1.99E+01 J	-
P-28	BDL	BDL	BDL	BDL	BDL	BDL
P-30	BDL	BDL	BDL	BDL	BDL	BDL
P-36	2.26E+02	5.71E+01	4.00E+01	3.37E+01	1.47E+01 J	-
P-38	BDL	BDL	BDL	BDL	BDL	BDL
P-39	BDL	BDL	BDL	BDL	BDL	BDL
P-43	BDL	BDL	BDL	BDL	2.22E+01 J	-
P-44	BDL	BDL	BDL	BDL	BDL	BDL
P-45	BDL	BDL	BDL	BDL	BDL	BDL
P-46	BDL	BDL	BDL	BDL	BDL	BDL
P-51	BDL	BDL	BDL	BDL	BDL	BDL
P-52	BDL	BDL	BDL	BDL	BDL	BDL
P-55	BDL	BDL	BDL	BDL	BDL	BDL
P-56	2.03E+01 J	-	BDL	BDL	BDL	BDL
P-57	BDL	BDL	BDL	BDL	BDL	BDL
P-60	BDL	BDL	BDL	BDL	BDL	BDL
P-61	BDL	BDL	BDL	BDL	BDL	BDL
P-63	BDL	BDL	BDL	BDL	BDL	BDL
P-66	4.42E+02	1.22E+02	2.60E+02	7.67E+01	3.00E+01 J	1.52E+00
P-67	BDL	BDL	BDL	BDL	1.23E+02 J	-
P-68	BDL	BDL	BDL	BDL	BDL	BDL
P-69	BDL	BDL	BDL	BDL	BDL	BDL
P-70	BDL	BDL	BDL	BDL	3.83E+03	1.01E+02
P-72	BDL	BDL	BDL	BDL	BDL	BDL
TW4	BDL	BDL	2.54E+01 J	-	BDL	BDL

NEC	BDL	BDL	BDL	BDL	BDL	BDL
NTC	BDL	BDL	BDL	BDL	BDL	BDL

NEC = No enzyme control
NTC = No template control
BDL = Below detection limit
J = Below reporting limit
"-" = Amplification in only 1 of 2 duplicate samples

We determined the relative expression of *dxmB*, *aldH*, and sMMO gene in groundwater samples collected from KL Ave. Landfill and these results are presented in Figures 3.8 and 3.9. The expression of target genes was determined relative to the housekeeping gene, *rpoD*, and relative to the RNA transcripts at monitoring location P-39. While both P-38 and P-39 were candidate locations for normalization, P-39 was chosen due to the likelihood of qPCR inhibitors at P-38 (Table 3.2; total bacteria = BDL). One caveat of this approach in low biomass environments is associated with the error introduced when quantifying relative differences in gene expression for samples that are below the detection limit for the target genes, but have varying concentrations of the housekeeping gene. This situation may result in over or under estimations of gene expression. Because of this limitation, only locations that were positive for RNA transcripts will be considered relevant results.

Overall, the expression of *dxmB, aldH*, and sMMO gene were very low relative to the housekeeping gene *rpoD* and their levels at location P-39. P-10711, P-20, and P-36 had positive detections for *dxmB*, but *dxmB* remains at levels similar to the control location (Figure 3.8). Interestingly, *aldH* is much lower at P-20 suggesting the presence of an inhibitor that prevents 1,4-dioxane biodegradation.

Monitoring location P-66 is the most promising of all the samples analyzed. P-66 had high concentrations of gene abundance and RNA transcripts (Tables 3.2 and 3.3). In addition, the relative gene expression for *dxmB* and *aldH* are among the highest observed in environmental

samples. Expression of *dxmB* and *aldH* was approximately 2 orders of magnitude higher than the control (Figure 3.9). This finding suggests that microorganisms containing the dioxane monooxygenase and aldehyde dehydrogenase enzymes necessary for 1,4-dioxane metabolism and co-metabolism are both present and active at this location.

Interestingly, the only location exhibiting high expression for sMMO gene was P-70. The abundance of sMMO genes and RNA transcripts at this location was 8.62×10^5 copies/mL and 3.83×10^3 copies/mL, respectively. This finding suggests that this location has an abundant and active methane oxidizing microbial population. Further, the soluble methane monooxygenase is highly expressed indicating the potential for 1,4-dioxane co-metabolism at this location.

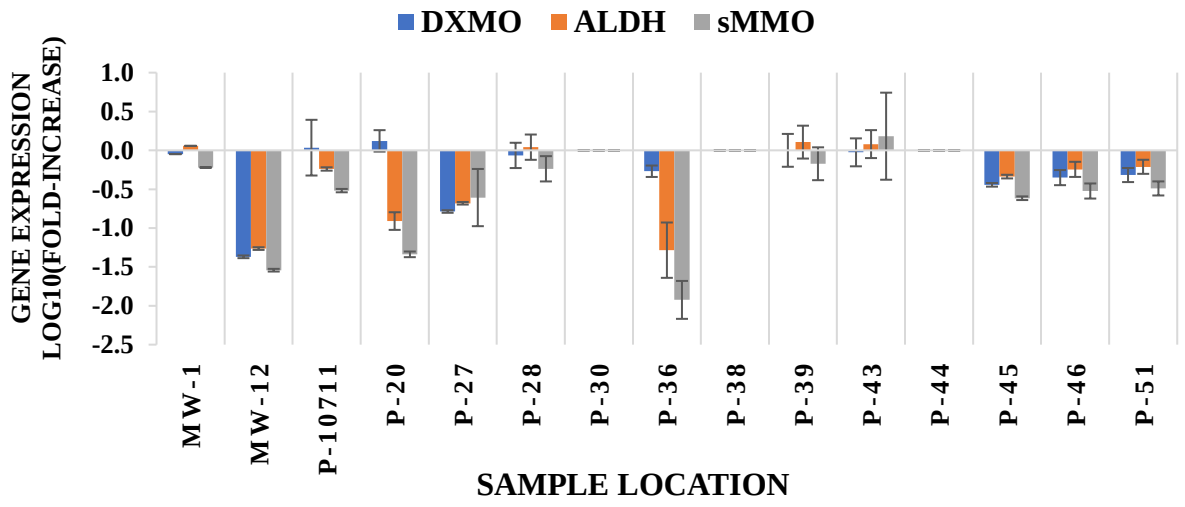

Figure 3.10. Relative expression of 1,4-dioxane biomarkers and sMMO gene in KL Ave. Landfill samples (MW-1 – P-51).

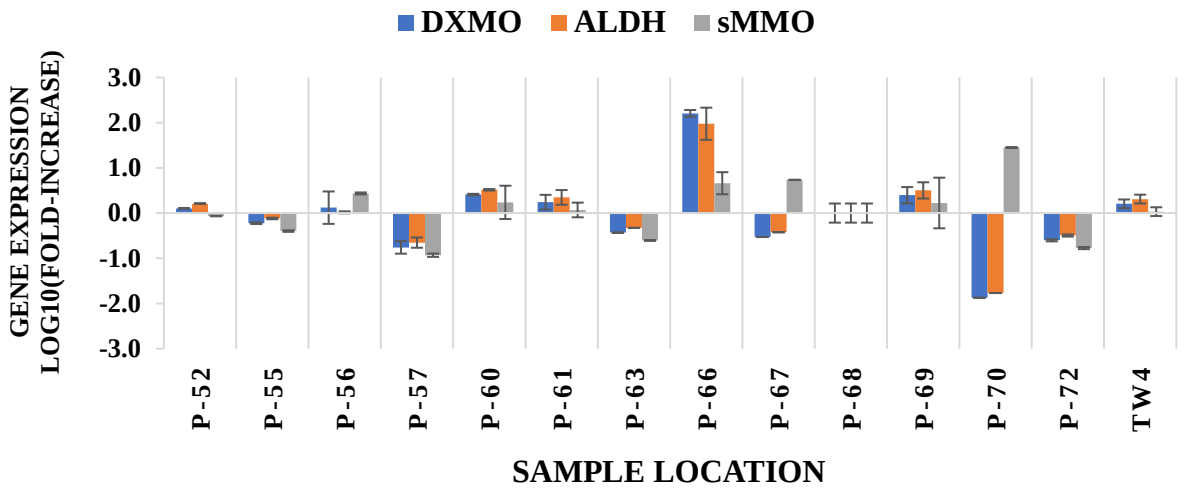

Figure 3.11. Relative gene expression of 1,4-dioxane biomarkers and sMMO gene at KL Ave. Landfill (P-52 – TW4).

3.3.2 CSIA

The CSIA results are presented in Figure 3.10. Values of $\delta^{13}C$ isotopic fractionation of 1,4-dioxane ranged from -29.15 ‰ to -31.80 ‰. Higher values (less negative) of $\delta^{13}C$ indicate 1,4-dioxane biodegradation processes are likely occurring. The extent of 1,4-dioxane depletion was calculated as the fraction of 1,4-dioxane remaining by dividing the current 1,4-dioxane concentration (Fall 2015) by the maximum 1,4-dioxane concentration detected since 2006. As detailed in published literature (Ahad et al., 2000, Slater et al., 2001, Mancini et al., 2003, Pornwongthong et al., 2011), a simple Rayleigh model can describe the relationship between isotopic fractionation and the fraction of 1,4-dioxane remaining after biodegradation. The site data can be fit to the Rayleigh model to extract a site-specific enrichment factor ε. The site-specific enrichment factor can then be compared to that reported by Pornwongthong et al. (-1.73 ± 0.14) for a pure culture of a 1,4-dioxane-degrading bacterium (Pornwongthong et al., 2011, Pornwongthong et al., In review).

As shown in Figure 3.10, there is spread in the data with decreasing fraction of 1,4-dioxane remaining; however, there is a clear trend that $\delta^{13}C$ values increase with increasing attenuation of 1,4-dioxane, which is indicative of biodegradation of 1,4-dioxane by the intrinsic microbial community. A best fit to the Rayleigh model is shown as a green line, which exemplifies the increase in $\delta^{13}C$ values with decreasing fraction of 1,4-dioxane remaining. For comparative purposes, the Rayleigh model using the enrichment factor ε for the pure culture (Pornwongthong et al., 2011) is shown as a purple line. As expected, there is a difference between the site data and the literature model, which is likely because site groundwater contains a consortium of microorganisms potentially capable of 1,4-dioxane degradation where the literature value is for a pure culture. Additionally, there are physical attenuation processes that operate at field scale, such as dispersion and dilution, which attenuate without fractionating the 1,4-dioxane (Hunkeler et al., 2008). Regardless, the CSIA data suggest an increase in $\delta^{13}C$ values with decreasing fraction of 1,4-dioxane, which is a secondary line of evidence that intrinsic biodegradation is occurring within the downgradient groundwater plume.

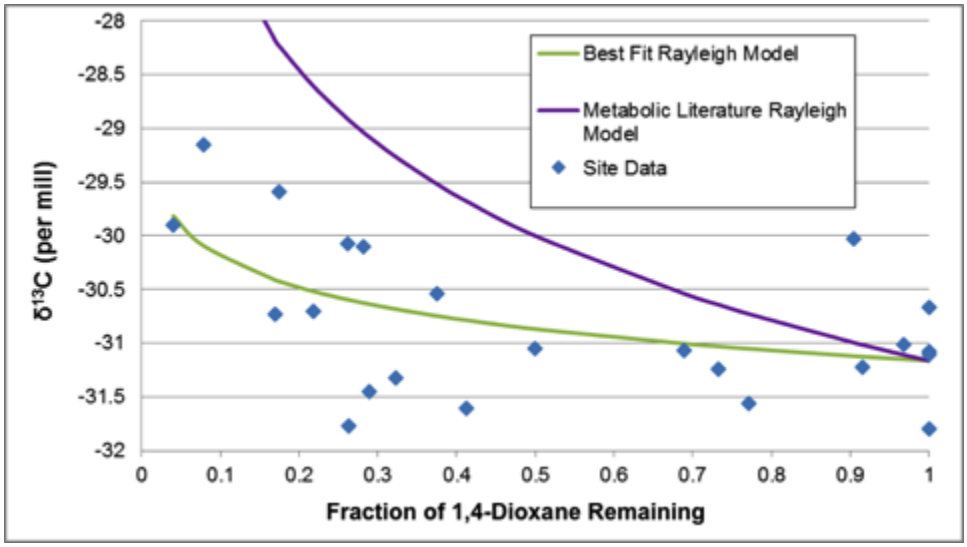

Figure 3.12. CSIA results for *Pseudonocardia dioxanivorans* CB1190 pure culture (purple) and site-specific (green) biodegradation of 1,4-dioxane.

3.3.3 1,4-Dioxane Groundwater Temporal and Spatial Trends

As shown in Figure 3.2, the lateral extent of the 1,4-dioxane plume has decreased significantly between 2011 and 2015. 1,4-Dioxane concentrations at monitoring wells on the landfill margin (Figure 3.2) have substantially declined during this time period such that 1,4-dioxane was detected above 100 µg/L in only two monitoring wells in 2015 (P-49 and P-50) while 1,4-dioxane was detected above 100 µg/L in six wells in 2011 (P-48, P-49, P-51, P-53, P-55, TW-4). These data are supported by temporal trend analyses conducted for all source area wells (M-8, MW-13, P-46, P-48, P-49, P-50, P-51, P-52, P-53, P-55, TW-4), which indicate that 1,4-dioxane concentrations are decreasing or stable between 2005 and 2015. 1,4-Dioxane depletion is also occurring immediately downgradient of the landfill margin as evidenced by the development of isolated plume areas in the vicinity of and downgradient of the shallow, unidentified lake presented on Figure 3.2. Based on the concentration trend analyses, 1,4-dioxane concentrations between 2010 and 2015 are decreasing or stable in 92% of monitoring wells located between the landfill margin and the downgradient shallow lake. Downgradient of the shallow lake, 1,4-dioxane concentrations between 2013 and 2015 are decreasing or stable in 88% of monitoring wells.

3.3.4 Source and Plume Mass Estimates

Source and plume mass estimates were conducted using EVS/MVS modeling software calibrated to time series groundwater distribution of 1,4-dioxane and THF indicated that source and plume mass for each contaminant have decreased significantly. As shown in Table 3.4, the total mass of 1,4-dioxane near the source area of the plume has decreased by 82% since 2004, while the total mass of THF in the source area has decreased by 99% since 2002. The model estimates also indicate that masses of 1,4-dioxane and THF in the entire plume have decreased by 38% and 80%, respectively. These estimates agree with temporal trend analyses and the spatial

changes of the 1,4-dioxane and THF plumes indicating that natural degradation of both contaminants is occurring within the source and downgradient plume areas. Further, the temporal trends and plume mass estimates indicated that THF plume collapse (between 2011 and 2013) closely preceded the contraction of the 1,4-dioxane plume, such that once THF levels in the plume decreased below 100 µg/L in most areas, the 1,4-dioxane plume contraction accelerated.

Table 3.4. Near source mass and total plume mass percent reductions between 2002 and 2015.

Compound	Percent Reduction Near Source Mass (2002 to 2015)	Percent Reduction Total Plume Mass (2002 to 2015)
THF	99%	80%
1,4-Dioxane	82%	38%

3.3.5 Geochemical Biodegradation Attenuation Indicators

The rate of intrinsic biodegradation of 1,4-dioxane is strongly dependent on the geochemical conditions of the impacted aquifer. A suite of natural attenuation indicator parameters has been collected consistently since 2001 to assess the potential for intrinsic biodegradation. Changes in the distribution and concentrations of these parameters can be used to assess groundwater geochemical conditions and temporal changes in these conditions. Review of analytical data and field sampling parameters indicated that there are two generalized areas within the groundwater plume that have distinctive geochemical conditions as compared to background as shown on Figure 3.11. The first area includes the portion of the groundwater plume immediately downgradient of the landfill. Sulfate-reducing conditions and potentially methanogenic conditions prevail in this area as indicated by depressed levels of sulfate due to utilization as an electron acceptor. Additionally, elevated levels of iron resulting from microbial iron-reduction and elevated levels of methane resulting from methanogenesis indicate that reducing conditions dominate. Analytical data from 2015 indicate that geochemical conditions are becoming more aerobic over

time as indicated by rebounding sulfate levels and a reduced area where sulfate is depleted. This shift towards weakening reducing conditions is also demonstrated by decreasing methane levels.

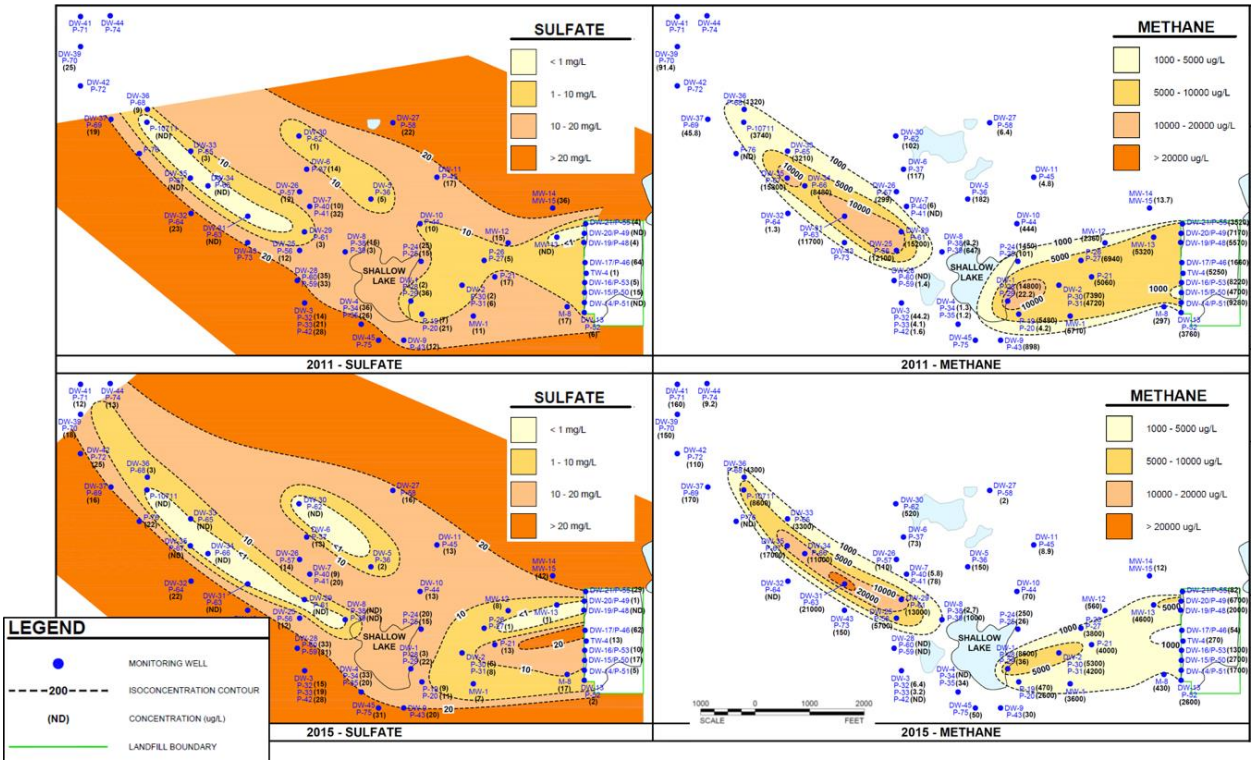

Figure 3.13. Sulfate and methane distribution in 2011 and 2015.

The second area that has distinctive geochemical conditions as compared to background conditions is located downgradient of the shallow lake. Similar to the area immediately downgradient of the landfill, this portion of the groundwater plume is dominated by sulfate-reducing and methanogenic conditions as evidenced by elevated levels of iron and methane and depletion of sulfate. As compared to the area immediately downgradient of the landfill, the areal extent of reducing conditions is narrower and there is a significant redox gradient (i.e., from reducing to oxidizing conditions) present along the fringes.

3.3.6 Fate and Transport Modeling

The model simulation results for the base scenario (i.e., Fall 2015 analytical results and plume extent) are shown on Figure 3.12, and display a reasonable match between the 1,4-dioxane plume

core concentrations and plume extent compared with the observed data distribution. Importantly, when only physical attenuation processes (i.e., dispersion and dilution) were considered in the solute transport model, the base scenario model simulations could not match the plume extent or plume concentrations. It was necessary to add a 1,4-dioxane biodegradation process (i.e., half-life decay) to calibrate the model to the field data. Therefore, similar to the MLOE presented above that converge to suggest that intrinsic biodegradation of 1,4-dioxane is occurring, the fate and transport model base scenario provides additional evidence that 1,4-dioxane biodegradation is occurring within the groundwater plume.

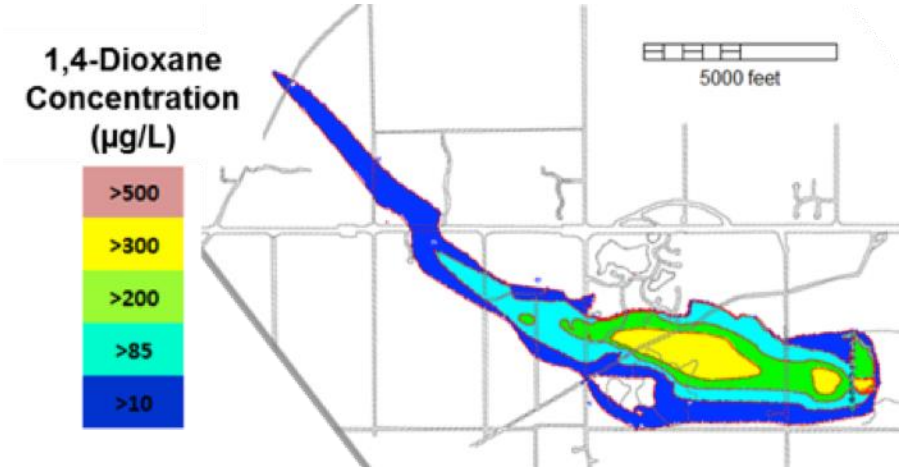

Figure 3.14. 1,4-Dioxane fate and transport model simulation results.

3.4 Discussion

Recent studies demonstrate that microbial degradation of 1,4-dioxane can occur naturally in-situ by native microbial populations through metabolic and co-metabolic processes. In this study, the application of molecular techniques to groundwater samples revealed that *dxmB* and *aldH* carrying microorganisms are present and abundant along the length of the groundwater plume at levels that are at the high range or in excess of all environmental samples in published literature. It should also be noted that 1,4-dioxane is comingled with THF at this site. THF can serve as a primary substrate for bacteria during co-metabolism of 1,4-dioxane for several microorganisms

(Vainberg et al., 2006, Sei et al., 2010, Sun et al., 2011, Sales et al., 2013). Historical trends indicate that THF and 1,4-dioxane levels within the plume have decreased concomitantly; though, following the THF plume collapse, decreases in 1,4-dioxane concentrations at most monitoring locations in the plume since 2013 was more evident (Figure 3.3). This may suggest both metabolic and co-metabolic 1,4-dioxane biodegradation pathways are active at this site. The presence of both *dxmB* and *aldH* has been established as a strong indicator of 1,4-dioxane biodegradation (Gedalanga et al., 2014). Remarkably, our 1,4-dioxane biomarkers were highly associated with monitoring well locations with detectable levels for 1,4-dioxane and THF, although THF concentrations were typically lower. Figure 3.4 shows the locations where *dxmB* and *aldH* carrying microorganisms were detected as well as the locations where both gene targets were observed. Importantly, detections of both *dxmB* and *aldH* are largely absent in monitoring locations with < 50 µg/L. This finding indicates a high specificity for 1,4-dioxane degrading bacteria to environments with 1,4-dioxane concentrations that are able to sustain this group of microorganisms. The downgradient well (P-72) with a positive detection for only *dxmB* was also positive for 1,4-dioxane (6.3 µg/L). Gene *dxmB* was detected at very low levels in this monitoring well with a relatively large error. This suggests that *dxmB* and *aldH* carrying microorganisms were present at levels near or below our detection limits because 1,4-dioxane concentrations may not have been sufficient to support an abundant 1,4-dioxane degrading bacterial population at this location.

In comparison to the total bacteria counts, *dxmB* carrying microorganisms constituted up to 5.8% of the total bacterial community, which is significant as a previous study has shown that 1,4-dioxane degrading bacteria (carrying *dxmB*) as low as 2% of the total population were able to consume high levels of 1,4-dioxane (Gedalanga et al., 2014). This site is unique to have > 5% of

the bacterial population with the *dxmB* gene. This finding may also be attributed to the co-occurrence of 1,4-dioxane and THF because the genes encoding the monooxygenase enzymes responsible for 1,4-dioxane and THF biodegradation are virtually identical. Thus, it is not possible to differentiate between metabolic and co-metabolic 1,4-dioxane biodegradation at this site. The coincidence and high abundance of both *dxmB* and *aldH* genes at six monitoring locations (P-10711, P-28, P-30, P-46, P-61, and P-66) indicate that microorganisms containing the enzymes necessary for 1,4-dioxane metabolism were present at the site. Increasing 1,4-dioxane concentrations at P-66 (Figure 3.3) indicate that the microbial-mediated degradation rate of 1,4-dioxane at this location may not be higher than the flux of 1,4-dioxane to this area.

High levels of sMMO genes were also observed in nearly all groundwater samples collected from the site indicating that there is significant capacity for co-metabolism of 1,4-dioxane. Additionally, sMMO gene detections were independent of 1,4-dioxane concentrations suggesting this gene target is not a good indicator of microorganisms that rely on 1,4-dioxane for carbon and energy. In contrast, the high association of both *dxmB* and *aldH* for locations in the plume with 1,4-dioxane lends further support for these biomarkers as indicators of 1,4-dioxane biodegradation.

These findings suggest that 1,4-dioxane is likely being degraded by a consortium of microorganisms at the site via metabolic and co-metabolic processes. Further, these data likely underestimate the potential for microbial mediated 1,4-dioxane degradation as this work focused solely on groundwater samples. Since bacteria prefer to grow on solid substrates, the abundance of 1,4-dioxane-degrading microorganisms detected in the groundwater samples likely underestimates the total biomass of these organisms in the system. The presence of 1,4-dioxane-degrading microorganisms throughout the plume, and especially at the fringe of the plume where a redox gradient is present between the aerobic (limited concentrations of oxygen) and anaerobic

(methanogenic) conditions, suggests that microbes have established themselves within the groundwater plume to utilize these conditions for metabolism. Microbes that can metabolize 1,4-dioxane and methane oxidizers are likely well established in micro-niche environments within the site to exploit hypoxic conditions (i.e., dissolved oxygen levels below the detection limit) for metabolism. Further, although not specifically tested for in this study, the concomitant collapse of the 1,4-dioxane plume and the THF plume also suggests that co-metabolic degradation of 1,4-dioxane may be enhanced by microbes metabolizing THF.

The results of the molecular analyses indicating the occurrence of intrinsic biodegradation of 1,4-dioxane across the plume are supported by the CSIA data. Values for $\delta^{13}C$ increased marginally with attenuation of 1,4-dioxane. The 1.5‰ to 2‰ enrichment factor observed in the CSIA data is close to that reported in a previous study (Pornwongthong et al., 2011) of metabolic degradation of 1,4-dioxane.

Spatial and temporal trends of 1,4-dioxane concentrations throughout the plume overwhelmingly demonstrate that 1,4-dioxane concentrations in the plume are decreasing or, at a minimum, stable, while the overall size of the plume has decreased significantly since 2011. The 1,4-dioxane plume contraction was preceded by contraction of the THF plume which declined below 100 µg/L in most portions of the historical plume. Following the THF plume collapse between 2011 and 2013, contraction of the 1,4-dioxane plume has accelerated suggesting preferential biodegradation of THF over 1,4-dioxane by the indigenous microbial community (Sun et al., 2011, Masuda et al., 2012). The contraction of the 1,4-dioxane plume correlates with a geochemical shift towards more aerobic conditions more favorable for 1,4-dioxane biodegradation due to a decreased flux of dissolved methane from the landfill resulting from source control measures. Source and plume mass estimates indicate that since 2002, the 1,4-dioxane source mass

near the landfill has decreased by 82% while the total 1,4-dioxane plume mass has decreased by 38%. In the vicinity of the landfill margin, geochemical conditions have shifted since 2011 towards more natural and aerobic conditions that promote the enhanced biodegradation of 1,4-dioxane. This shift is evidenced by decreasing levels of dissolved methane and increasing levels of sulfate in landfill margin wells and monitoring wells located downgradient towards the shallow lake, which suggests a shift from methanogenic and sulfate-reducing conditions towards more oxidizing conditions. Since oxidizing conditions are required for intrinsic biodegradation of 1,4-dioxane, this shift is expected to enhance the rate of attenuation of these compounds. *dxmB* and *aldH* carrying microorganisms were detected coincidentally in monitoring wells P-28 and P-30 indicating that a population capable of 1,4-dioxane metabolic degradation is present in this area and can potentially be enhanced by the shift toward aerobic geochemical conditions.

The analytical results from groundwater samples show that the position of the downgradient extent of the 1,4-dioxane plume is stable and the position has been maintained for five years. Groundwater modeling indicates that the stability of the downgradient plume cannot be explained by hydrodynamic process (e.g., dilution and dispersion) alone, providing further evidence that microbial degradation is likely an important mechanism. Downgradient of a surface water body located approximately mid-plume, the 1,4-dioxane plume is narrow and there is a significant redox gradient (anaerobic to aerobic) present along the edges of this plume, which favors 1,4-dioxane biodegradation. *dxmB* and *aldH* carrying microorganisms were detected at high levels in this section of the plume and the gene abundance analyses demonstrated microorganisms capable of 1,4-dioxane metabolism are present at monitoring locations P-10711 and P-66.

3.5 Conclusions

The MLOE framework outlined in this study combined new technologies with traditional data analyses and successfully demonstrated that intrinsic biodegradation of 1,4-dioxane occurs at this site. While the role of THF in 1,4-dioxane biodegradation was not the focus of this study, the evidence collected suggests that THF-driven co-metabolism is possible. Molecular biological tools demonstrated that microorganisms capable of both co-metabolizing (sMMO, DXMO/THFMO) and metabolically degrading (DXMO/ALDH) 1,4-dioxane are present and abundant at the site. Notably, the detections of *dxmB* and *aldH* tracked the 1,4-dioxane plume with reasonable accuracy, strongly suggesting the presence of 1,4-dioxane stimulated these markers and implying the microorganisms were degrading 1,4-dioxane. The detections of sMMO gene were widespread and non-specific to 1,4-dioxane, which was expected because co-metabolism is stimulated by the primary substrate (in this case, methane) rather than by the degradation of the co-metabolic substrate. CSIA analysis detected a weak enrichment of ^{13}C in 1,4-dioxane as it was depleted with distance downgradient. Available evidence suggests ^{13}C enrichment in 1,4-dioxane will be weak because the indigenous mixed bacterial consortium may not be as selective for the light carbon isotope as the pure culture in the laboratory. The CSIA results provide additional evidence that a biochemical degradation process is active at this site. Coupled with the historical data that demonstrate 1,4-dioxane concentrations and plume mass have declined, the results from this case study strongly indicate that intrinsic biodegradation of 1,4-dioxane is occurring at this site. This case study further implies that intrinsic metabolic and co-metabolic biodegradation of 1,4-dioxane should be considered at more sites with favorable biogeochemical conditions using a MLOE framework, especially as long-term monitoring data become available to better support observation of degradation. The innovative molecular biological tools, including biomarkers of

1,4-dioxane degradation and improved CSIA techniques, are critical in demonstrating degradation and should be considered when planning an intrinsic degradation study for 1,4-dioxane.

3.6 References

Adamson, D.T., Anderson, R.H., Mahendra, S., Newell, C.J., 2015. Evidence of 1,4-dioxane attenuation at groundwater sites contaminated with chlorinated solvents and 1,4-dioxane. Environmental Science & Technology, 49 (11), 6510-6518.

Ahad, J.M.E., Lolla, B.S., Edwards, E.A., Slater, G.F., Sleep, B.E., 2000. Carbon isotope fractionation during anaerobic biodegradation of toluene: Implications for intrinsic bioremediation. Environmental science & technology, 26 (34), 892-896.

Alvarez, P.J., Li, M., Mathieu, J., 2014. Developing and validating genetic catabolic probes for monitored natural attenuation of 1,4-dioxane with a one-year timeframe. DTIC Document.

Bernhardt, D., Diekmann, H., 1991. Degradation of dioxane, tetrahydrofuran and other cyclic ethers by an environmental *Rhodococcus* strain. Applied Microbiology and Biotechnology, 36 (1), 120-123.

Chiang, S.Y., Mora, R., Diguiseppi, W.H., Davis, G., Sublette, K., Gedalanga, P., Mahendra, S., 2012. Characterizing the intrinsic bioremediation potential of 1,4-dioxane and trichloroethene using innovative environmental diagnostic tools. Journal of Environmental Monitoring, 14 (9), 2317-2326.

Colby, J., Stirling, D.I., Dalton, H., 1977. The soluble methane mono-oxygenase of *Methylococcus capsulatus* (Bath). Its ability to oxygenate n-alkanes, n-alkenes, ethers, and alicyclic, aromatic and heterocyclic compounds. Biochemical Journal, 165 (2), 395-402.

EPA, 1999. Final OSWER Directive: Use of Monitored Natural Attenuation at Superfund, RCRA Corrective Action, and Underground Storage Tank Sites; OSWER Directive 9200.4-17P. Office of Solid Waste and Emergency Response.

EPA, 2010. Toxicological Review of 1,4-Dioxane (CAS No. 123-91-1) In Support of Summary Information on the Integrated Risk Information System (IRIS), EPA/635/R-09/005-F.

Fishman, A., Tao, Y., Wood, T.K., 2004. Toluene 3-monooxygenase of *Ralstonia pickettii* PKO1 is a para-hydroxylating enzyme. Journal of Bacteriology, 186 (10), 3117-3123.

Gedalanga, P.B., Pornwongthong, P., Mora, R., Chiang, S.Y., Baldwin, B., Ogles, D., Mahendra, S., 2014. Identification of biomarker genes to predict biodegradation of 1,4-dioxane. Applied and Environmental Microbiology, 80 (10), 3209-3218.

Grostern, A., Sales, C.M., Zhuang, W.-Q., Erbilgin, O., Alvarez-Cohen, L., 2012. Glyoxylate metabolism is a key feature of the metabolic degradation of 1,4-dioxane by *Pseudonocardia dioxanivorans* strain CB1190. Applied and Environmental Microbiology, 78 (9), 3298-3308.

Hunkeler, D., Meckenstock, R.U., Sherwood Lollar, B., Schmidt, T.C., Wilson, J., Schmidt, T., Wilson, J., 2008. A guide for assessing biodegradation and source identification of organic ground water contaminants using compound specific isotope analysis (CSIA). Office of Research Development, National Risk Management Research Laboratory, US Environmental Protection Agency.

Kim, Y.-M., Jeon, J.-R., Murugesan, K., Kim, E.-J., Chang, Y.-S., 2009. Biodegradation of 1,4-dioxane and transformation of related cyclic compounds by a newly isolated *Mycobacterium* sp. PH-06. Biodegradation, 20 (4), 511-519.

Li, M., Mathieu, J., Liu, Y., Van Orden, E.T., Yang, Y., Fiorenza, S., Alvarez, P.J., 2014. The abundance of tetrahydrofuran/dioxane monooxygenase genes (*thmA*/*dxmA*) and 1,4-dioxane degradation activity are significantly correlated at various impacted aquifers. Environmental Science & Technology Letters, 1 (1), 122-127.

Lippincott, D., Streger, S.H., Schaefer, C.E., Hinkle, J., Stormo, J., Steffan, R.J., 2015. Bioaugmentation and propane biosparging for in situ biodegradation of 1,4-dioxane. Ground Water Monitoring and Remediation, 35 (2), 81-92.

Lyew, D., Guiot, S., 2003. Effects of aeration and organic loading rates on degradation of trichloroethylene in a methanogenic-methanotrophic coupled reactor. Applied Microbiology & Biotechnology, 61 (3), 206-213.

Mahendra, S., Alvarez-Cohen, L., 2005. *Pseudonocardia dioxanivorans* sp. nov., a novel actinomycete that grows on 1,4-dioxane. International Journal of Systematic and Evolutionary Microbiology, 55 (2), 593-598.

Mahendra, S., Alvarez-Cohen, L., 2006. Kinetics of 1,4-dioxane biodegradation by monooxygenase-expressing bacteria. Environmental Science & Technology, 40 (17), 5435-5442.

Mahendra, S., Petzold, C.J., Baidoo, E.E., Keasling, J.D., Alvarez-Cohen, L., 2007. Identification of the intermediates of in vivo oxidation of 1,4-dioxane by monooxygenase-containing bacteria. Environmental Science & Technology, 41 (21), 7330-7336.

Mancini, S.A., Ulrich, A.C., Lacrampe-Couloume, G., Sleep, B., Edwards, E.A., Lollar, B.S., 2003. Carbon and hydrogen isotopic fractionation during anaerobic biodegradation of benzene. Applied & Environmental Microbiology, 69 (1), 191-198.

Masuda, H., McClay, K., Steffan, R.J., Zylstra, G.J., 2012. Biodegradation of tetrahydrofuran and 1,4-dioxane by soluble diiron monooxygenase in *Pseudonocardia* sp. strain ENV478. Journal of Molecular Microbiology and Biotechnology, 22 (5), 312-316.

Mohr, T., Stickney, J., Diguiseppi, B. (2010). Environmental investigation and remediation: 1,4-Dioxane and other solvent stabilizers, CRC Press, Boca Raton FL.

Nakamiya, K., Hashimoto, S., Ito, H., Edmonds, J.S., Morita, M., 2005. Degradation of 1,4-dioxane and cyclic ethers by an isolated fungus. Applied and Environmental Microbiology, 71 (3), 1254-1258.

Parales, R., Adamus, J., White, N., May, H., 1994. Degradation of 1,4-dioxane by an *Actinomycete* in pure culture. Applied and Environmental Microbiology, 60 (12), 4527-4530.

Pornwongthong, P., Paradis, G.L., Mahendra, S., 2011. Stable carbon isotope fractionation during 1,4-dioxane biodegradation. Proceedings of the Water Environment Federation, 111-116(116).

Pornwongthong, P., Paradis, G.L., Mahendra, S., In review. Development and application of compound-specific carbon isotope analysis method for validating 1,4-dioxane biodegradation. Environmental Science & Technology.

Ryan, M.P., Pembroke, J.T., Adley, C.C., 2007. *Ralstonia pickettii* in environmental biotechnology: Potential and applications. Journal of Applied Microbiology, 103 (4), 754-764.

Sales, C.M., Grostern, A., Parales, J.V., Parales, R.E., Alvarez-Cohen, L., 2013. Oxidation of the cyclic ethers 1,4-dioxane and tetrahydrofuran by a monooxygenase in two *Pseudonocardia* species. Applied and Environmental Microbiology, 79 (24), 7702-7708.

Sei, K., Kakinoki, T., Inoue, D., Soda, S., Fujita, M., Ike, M., 2010. Evaluation of the biodegradation potential of 1,4-dioxane in river, soil and activated sludge samples. Biodegradation, 21 (4), 585-591.

Slater, G.F., Lollar, B.S., Sleep, B.E., Edwards, E.A., 2001. Variability in carbon isotopic fractionation during biodegradation of chlorinated ethenes: implications for field applications. Environmental Science & Technology, 35 (5), 901-907.

Sun, B., Ko, K., Ramsay, J.A., 2011. Biodegradation of 1,4-dioxane by a *Flavobacterium*. Biodegradation, 22 (3), 651-659.

Surprenant, K.S., 2002. Dioxane. In Ullmann's Encyclopedia of Industrial Chemistry.

Vainberg, S., McClay, K., Masuda, H., Root, D., Condee, C., Zylstra, G.J., Steffan, R.J., 2006. Biodegradation of ether pollutants by *Pseudonocardia* sp. strain ENV478. Applied and Environmental Microbiology, 72 (8), 5218-5224.

Zenker, M.J., Borden, R.C., Barlaz, M.A., 2003. Occurrence and treatment of 1,4-dioxane in aqueous environments. Environmental Engineering Science, 20 (5), 423-432.

Chapter 4 In-situ Bioaugmentation to Enhance Biodegradation of 1,4-Dioxane

4.1 Introduction

Bioaugmentation is one of the biological methods used for removal of organic and inorganic pollutants from contaminated matrices (Innemanova et al., 2018), with four common strategies: adding the pure bacterial strain, adding the microbial consortium, introducing well-designed genetically modified organisms (GMO), and cloning biodegradation-relevant genes in a vector to be transferred and expressed in indigenous microorganisms (El Fantroussi and Agathos, 2005). The basic premise for this artificial intervention is that the metabolic capacities of the indigenous microbial community already present in the environments but dysfunctional in cleanup will be increased by an exogenously enhanced microorganisms, thus leading to a wider processes of productive biodegradation reactions as well as enhanced microbial activity (Safdari et al., 2018), and resulting in enhanced degradation of target pollutants. Bioaugmentation has been considered as a safe and economical means of remediation of contaminated sites (Tyagi et al., 2011) and applied in various conditions, e.g., PAH-contaminated soil (Innemanova et al., 2018), chlorothalonil-contaminated soil (Xu et al., 2018), activated sludge nitrification (Figdore et al., 2018), ammonia contained industrial wastewater (Raper et al., 2018), etc.

However, bioaugmentation by adding exogenous degrading strains is usually affected by many abiotic and biotic factors, such as the type of pollutant, the characteristics of the exogenous degrader, and environmental factors, such as chlorinated solvents in 1,4-dioxane plumes (Onneby et al., 2010), because the laboratory inoculants are produced under optimal conditions. Moreover, the bioaugmented strains usually need to compete with indigenous microorganisms for nutrients and space, which may lead to poor survivability and adaptability of the added strains (Szulc et al., 2014). Meanwhile, the elimination of pollutants by the bioaugmented stains can alleviate the

selective pressure of agrochemicals on the other microorganism in the same niches (Wan et al., 2014). Furthermore, complex interactions such as niche-based and stochastic-neutral processes (Ju et al., 2017) among the members living in the same microbial community will also determine their function and affect both the rate of degradation and the identity of the final products of pollutants (Zelezniak et al., 2015, Jiao et al., 2016), and the by-products and/or bioaugmented strains may alter metabolic dependence in microbial consortia, leading to a common influence on the co-occurred taxon.

The use of carrier materials often provides a physical support for microorganisms, along with a better access to nutrients, moisture and aeration, which extends the survival rate of the microbes (Mishra et al., 2001). Microbial cell immobilization may offer a better survival rate by shielding cells under stressed environmental conditions, usually enabling a faster and more efficient biodegradation as compared to free living cells (Obuekwe and Al-Muttawa, 2001, Moslemy et al., 2002). Moreover, this process may use the characteristics of microorganisms to form biofilms on the surface of various materials, reduce risk of genetic mutations, and increase tolerance to high pollutant concentrations (Dzionek et al., 2016). From an applied perspective, using a complex microbial consortia rather than a pure culture for the bioremediation is more advantageous as it provides the metabolic diversity and robustness needed for field applications (Nyer et al., 2002, Rahman et al., 2002).

Even CB1190 has been well studied in the degradation of 1,4-dioxane under co-contaminants stress (Mahendra et al., 2013, Zhang et al., 2016), treating actual 1,4-dioxane contaminated groundwater by augmenting CB1190 was rarely reported, especially the pilot or field applications. The decision to implement bioaugmentation for 1,4-dioxane largely depends on the degrading capability of the indigenous microbes and the extent of contamination of the site to be treated. As

several examples show, successful laboratory studies concerning bioremediation do not necessarily lead to reproducible in-situ decontamination (Balba et al., 1998, El Fantroussi and Agathos, 2005). Thus, in this chapter, CB1190 was used to test the feasibility of its application in pilot scale with bioaugmentation in an 1,4-dioxane contaminated site, with multiple bioaugmentation events. The objectives in this task were to i) validate distributions of bioaugmented CB1190 in the subsurface; ii) explore the 1,4-dioxane removal performances in the plume by mobile bioaugmented CB1190; iii) evaluate the effectiveness of biodegradation of 1,4-dioxane by immobilized CB1190 in in-situ bioreactors (ISBRs) with Bio-Sep beads packed bed. The results of this chapter could help to set example for future full-scale bioaugmentation applications for 1,4-dioxane biodegradations.

4.2 Materials and Methods

4.2.1 Site Information

The study area is located in southern US, adjacent to an airport (Figure 4.1). The proposed study area for the technology demonstration is located in area of concern (AOC) 1, on the eastern side of Building 1 (Figure 4.2). Historically, two vapor degreasers were housed within (or near) Building 1 for solvent reuse; the former trichloroethene (TCE) degreaser was located sub-grade within a sump while the former trichloroethene (TCA) degreaser was above grade. Environmental investigations conducted to date have identified volatile organic compound (VOC) and 1,4-dioxane groundwater plumes originating from the former vapor degreaser locations and migrating east-northeast in the direction of groundwater flow towards Mingo Creek. Locations of temporary

wells installed by AECOM, Inc. (AECOM) in July and August 2013 as well as permanent monitoring wells near AOC 1 are shown on Figure 4.3.

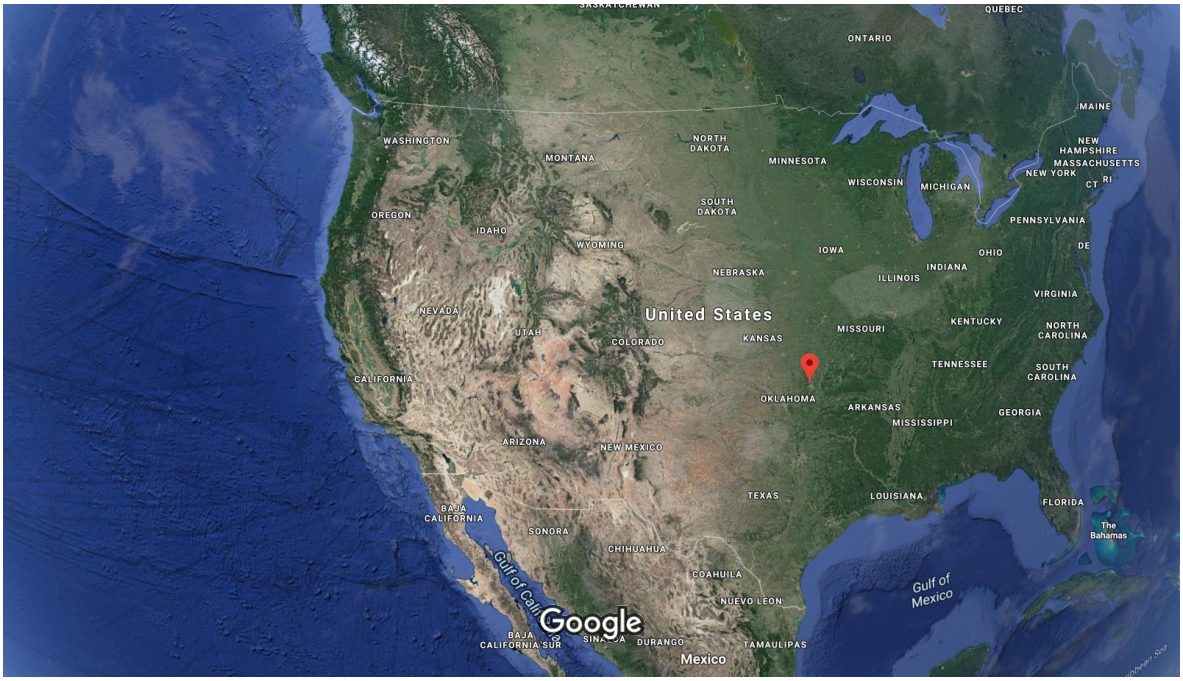

Figure 4.15. The location of study area.

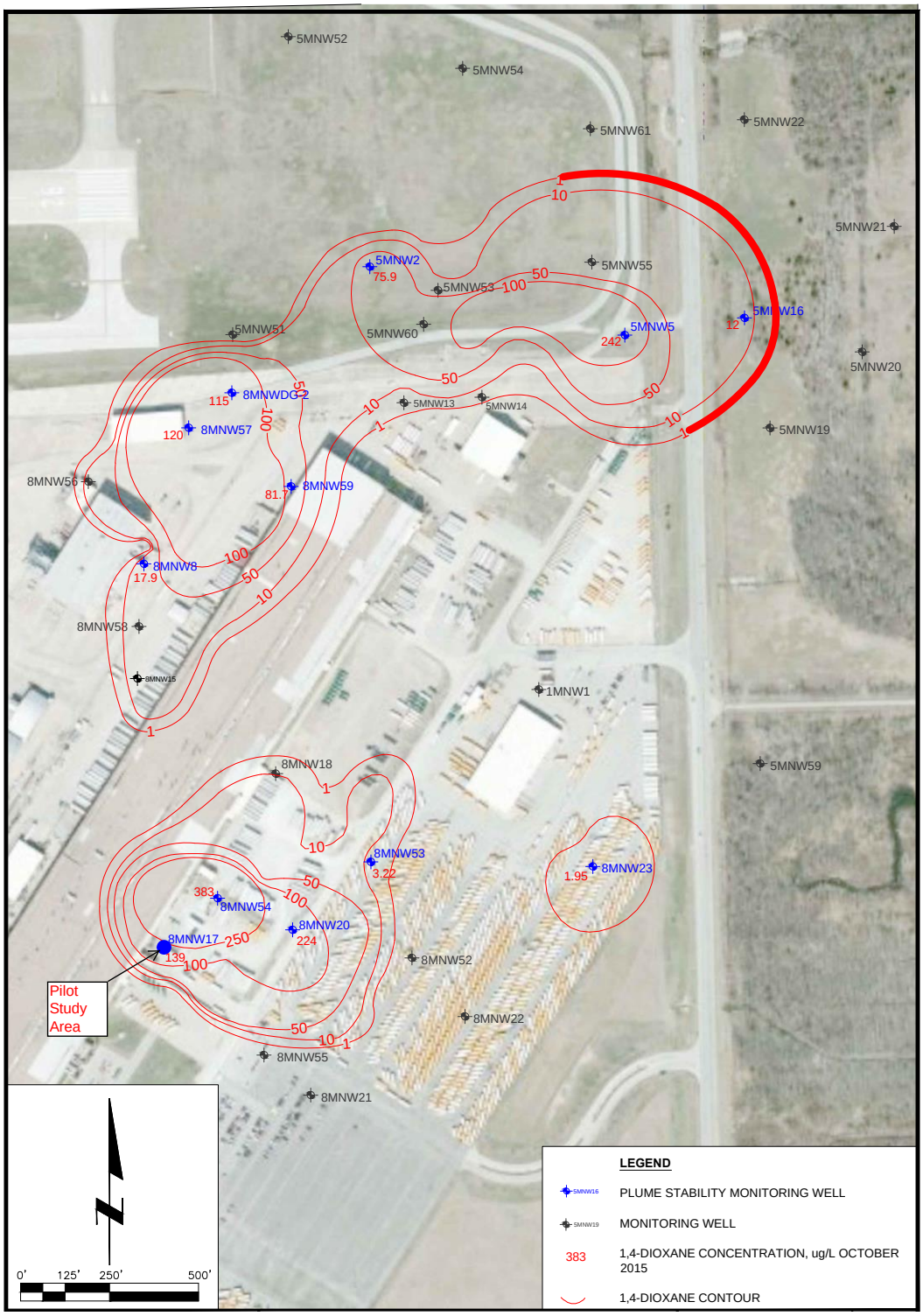

Figure 4.16. 1,4-Dioxane concentrations in groundwater.

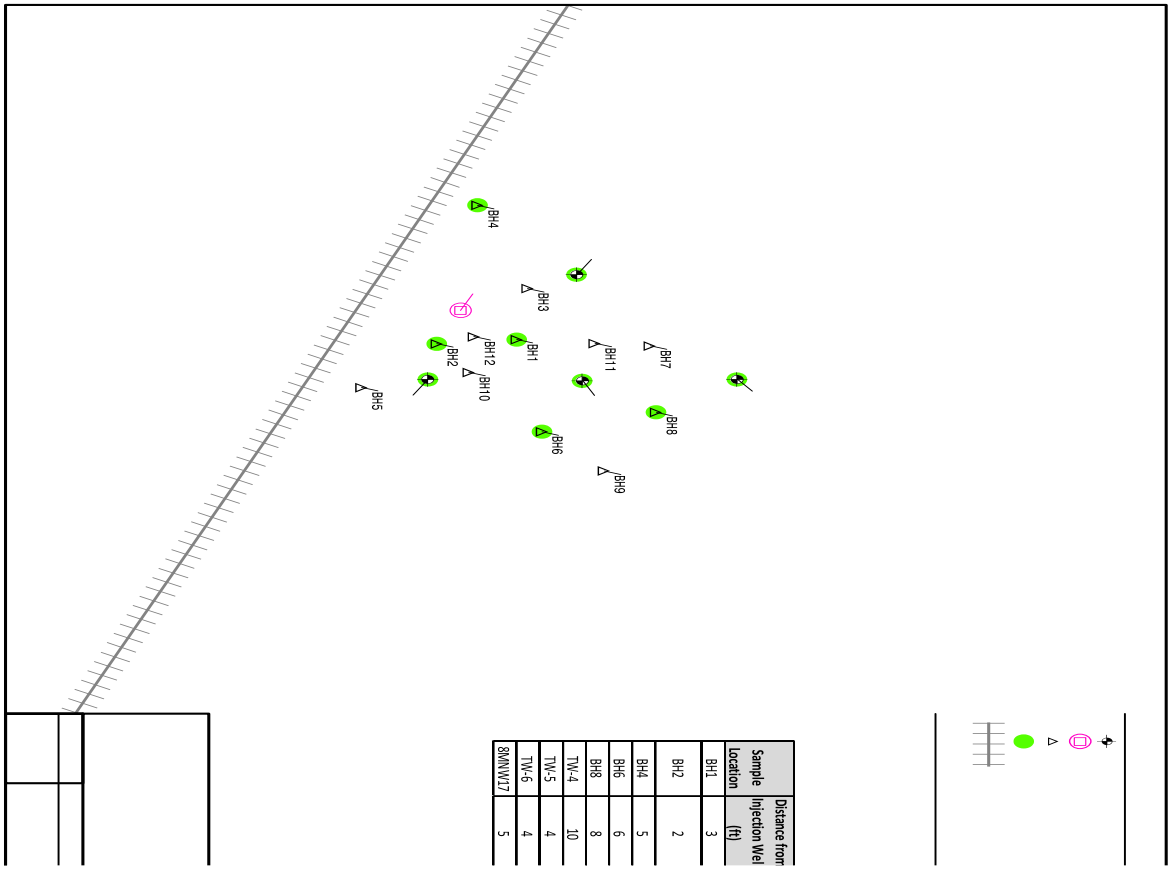

Figure 4.17. Study area and well locations for CB1190 distribution evaluation.

For the site assessment, three areas in the western portion of AOC 1, adjacent to Building 1, were identified and evaluated as possible locations for the technology demonstration (Figure 4.2) due to elevated 1,4-dioxane concentrations and the presence of a gravel layer in the subsurface, based on existing borehole logs. Within each area, three proposed direct push boring locations were selected based upon available site data. The field activities included lithology evaluation via direct push borings, installation of temporary wells for groundwater sampling, installation of an injection well, and performance of slug tests, as described in Section 4.7.1.

4.2.2 Bioaugmentation Culture Preparation

In order to scale-up the volume of CB1190 culture for field implementation, the team engaged the bioaugmentation laboratory, SiREM. SiREM is most well-known for broadly commercializing the KB-1 culture, which contains *Dehalococcoides*, spp. and degrades chlorinated solvents.

UCLA sent a sample of CB1190 to SiREM for scale-up. An initial culture was started at SiREM using a 10 %t inoculum to 30 mL fresh anaerobic mineral salts medium and 1,4-dioxane was amended to 100 mg/L. Initial culture scale-up was conducted using sterile glass flasks shaken on an orbital shaker (~125-150 revolutions per minute [rpm]) at room temperature. Sterile foam plugs were used to allow air exchange and headspace in the flasks was no less than 50%. The CB1190 culture was sampled and analyzed for 1,4-dioxane concentration one to three times per week to confirm 1,4-dioxane degradation and guide re-amendment of 1,4-dioxane.

Subsequent CB1190 culture scale-up was conducted by doubling the culture volume into fresh media (50%) inoculum and feeding 1,4-dioxane. After approximately five feedings, the culture was again doubled in volume. Once the culture volume exceeded 500 mL, culture was transferred to multiple containers: either glass 2 L glass jugs or 5 L glass carboys shaken on an orbital shaker or magnetic stir plate. Subsequent scale-up was conducted in multiple 10 L and 20 L Nalgene autoclavable carboys with baffled magnetic stirrers. Larger containers have screw cap closures to maintain sterility and are kept closed, and were opened under sterile conditions in a laminar flow hood to exchange the headspace. Culture continued to be sampled and analyzed for 1,4-dioxane concentration one to three times per week and re-amended with 1,4-dioxane as needed. Due to practical/logistical limitations of the laboratory, the scale-up volume of CB1190 bioaugmentation culture was approximately 25 L for the field implementation (Figure 4.4). The culture's activity and purity were checked at UCLA as described in Section 4.7.2.

Figure 4.18. On site CB1190 culture shipped from SiREM.

4.2.3 Field Bioaugmentation Procedures

The distribution evaluation targeted a 5-foot radius of influence around injection well 8IW01. Prior to bioaugmentation, approximately 60 gallons of groundwater (equivalent to 10% of the effective pore volume of the targeted treatment area) was extracted from well 8IW01 and stored in a 100-gallon tank on site. An in-situ submerged oxygen curtain (iSOC) was deployed in the tank to increase dissolved oxygen levels in the extracted groundwater using a pressurized air tank and diammonium phosphate was added to the injected solution as a nutrient.

A sump pump was deployed in the tank and discharge tubing was lowered into the screen interval of 8IW01 (18 feet to 23 feet bgs). Immediately prior to injection, concentrated Rhodamine WT dye was introduced to the injection well as a slug. One carboy (plastic 5-gallon container), containing approximately 15 liters of culture, was poured into the discharge tubing using a funnel and gravity flow, followed by approximately 30 gallons of the amended groundwater. The process was then repeated for the remaining 15 liters of culture and 30 gallons of amended groundwater (Figure 4.5). During injection (Figure 4.6), up to 5 feet of mounding was observed in the injection well as 4 directions and the flow rate was noted to be approximately 2 gallons per minute (gpm) to 3 gpm. After injection of the amended culture was complete, the discharge tubing was removed

and the iSOC was deployed in the injection well, along with a dissolved oxygen sensor to allow remote monitoring of dissolved oxygen concentrations in the well. Remote sensor readings indicated adequate dissolved oxygen concentrations in the injection well during procedure.

Figure 4.19. Mixing CB1190 culture with extracted groundwater.

Figure 4.20. Injecting mixed CB1190 culture through direct push rods.

4.2.4 Distribution Evaluation and in-situ Bioaugmentation Field Activities

Prior to the start of the bioaugmentation event, groundwater samples were collected from the injection well (8IW01), monitoring well 8MNW17, and the three test wells (TW-4 through TW-6). Samples were sent to offsite laboratories for analysis of 1,4-dioxane, VOCs, and microbial parameters including CB1190-like 16S rRNA, dioxane monooxygenase (DXMO) encoded gene (*dxmB*), and alcohol dehydrogenase (ALDH) encoded gene (*aldH*). Biotraps™ were deployed in the test wells and monitoring wells. Following collection of groundwater samples, a direct push technology (DPT) rig was used to collect continuous core samples to evaluate distribution of the injected culture. One month after bioaugmentation, groundwater samples were collected from the injection well, monitoring well, and test wells and Biotraps were retrieved and sent to offsite laboratories for analysis. Sampling locations, shown on Figure 4.7, were selected based on real-time evaluation of field observations. The locations of subsequent borings were driven by the presence or absence of Rhodamine WT dye (Figure 4.8). The initial points (identified as BH1 through BH3) were located approximately 2 feet to 3 feet from injection well 8IW01. Groundwater samples were analyzed for 1,4-dioxane, VOCs, and microbial parameters, and Biotraps were analyzed for just microbial parameters.

Figure 4.21. Sampling wells.

Figure 4.22. Samples with and without presence of rhodamine dye.

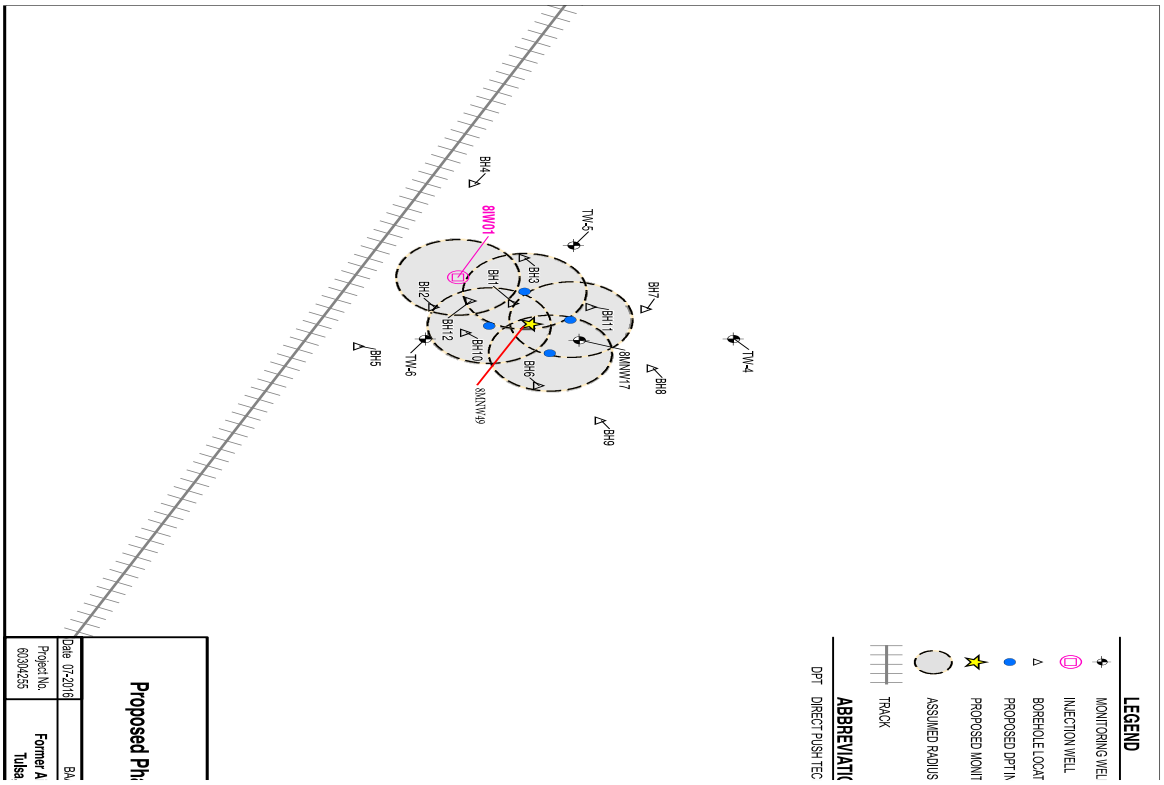

Figure 4.23. Study area and well distribution for bioaugmentation implement.

During the in-situ bioaugmentation pilot study (Figure 4.9), higher frequency monitoring was performed to better understand the effects of bioaugmentation. Samples were collected immediately following injection and 1, 2, 4, 6, and 8 weeks post-injection.

4.2.5 Growth of CB1190 on Bio-Sep Beads in Bench-Scale Reactor

Pure CB1190 cultures were prepared by diluting preserved glycerol stocks in sterile 2 L screw-cap bottles containing 1 L ammonia mineral salt (AMS) medium following previous recipe (Parales et al., 1994, Mahendra and Alvarez-Cohen, 2005), with 100 mg/L 1,4-dioxane amended as the sole carbon and energy source. Bacterial cultures were incubated at 30°C with 150 rpm of agitation to maintain aerobic conditions, and 100 mg/L 1,4-dioxane was re-amended once it was undetectable in the culture (< 1.0 mg/L). The active CB1190 was harvested after 5 cycles addition of 1,4-dioxane with estimated degradation rates of 70-80 mg 1,4-dioxane/(L·day), and liquid

culture was collected for future molecular analysis. The purity of harvested CB1190 was checked on Reasoner's 2A (R2A) agar plates before inoculating the experimental bottles.

The Bio-Sep beads were synthesized at University of Tulsa, and selected as the support material for CB1190 biofilms. The growing process involved using 2 L flasks (in triplicate) with 1000 sterile beads, and 300 mL liquid culture (containing AMS+CB1190) containing around 100 mg/L 1,4-dioxane (Labeled as ABCD). All flasks were incubated at 30°C with 150 rpm of agitation, and liquid samples were collected periodically to measure 1,4-dioxane and biomass. The growth of CB1190 on the beads was confirmed after 30 days of growth by monitoring 1,4-dioxane biodegradation activity as a surrogate. This activity assay was conducted by first separating the inoculated beads from the liquid, and gently washing them up to three times with 100 mL AMS. The washed beads were then resuspended in 300 mL fresh AMS containing approximately 100 mg/L 1,4-dioxane in a new flask (labeled as Washed Beads). 1,4-Dioxane was measured periodically to check the activity of attached CB1190. A viability test was conducted following the activity assay in both ABCD and Washed Beads flasks by monitoring and gradually decreasing the amount of amended 1,4-dioxane to achieve concentrations of 20 mg/L, 2 mg/L, and 0.3 mg/L. All beads were washed again and merged into fresh AMS after viability test with 0.3 mg/L 1,4-dioxane spike.

4.2.6 Adsorption and Desorption Test on Bio-Sep Beads

The adsorption process was conducted with the similar composition with ABCD in 2 L flasks except the beads were kept abiotic (labeled as ABD). The flasks were incubated at 30°C with 150 rpm of agitation, and liquid samples were collected periodically to measure 1,4-dioxane and calculate adsorption rate. After the 1,4-dioxane concentration was stable in liquid, the presumed CB1190 attached beads were separated with liquid, and washed by 100 mL AMS gently up to

three times, then, 300 mL fresh AMS without 1,4-dioxane were added. The flasks were maintained in the same condition to adsorption process, and 1,4-dioxane was measured periodically to calculate the desorption rate.

4.2.7 ISBR Construction and Deployment

Bio-Sep beads were incubated in bench scale reactors with pure CB1190 culture for 4 weeks with multiple 1,4-dioxane feedings. CB1190 attached beads were washed by fresh AMS and incubated for 12 hours to desorb 1,4-dioxane, and wash-desorption process was conducted three times. Afterwards, beads were dried by sterile paper towel on the sieve for 3 hours, with paper change and beads shuffle in every 30 minutes. Total ~3.6 kg Bio-Sep beads were sent to University of Tulsa, and Dr. Sublette constructed the two CB1190 ISBRs as well as the two control ISBRs per the schematics shown in (Figure 4.10). Following construction, the ISBRs were sent immediately to the site for deployment. As mentioned above, one CB1190 ISBR and one control ISBR were deployed in both well 8IW01 and 8MNW17. Representatives from Bio-Enhance were onsite to assist with deployment of the ISBRs as well as setting up the aboveground equipment. A single control box was installed aboveground and connected to an electrical supply. Tubing connections ran from the control box down to each ISBR to supply nutrients and air. The control box was housed in a temporary shed along with a small air compressor and metering pump. When the ISBRs were retrieved at the end of operation, all aboveground tubing and equipment were removed from the site.

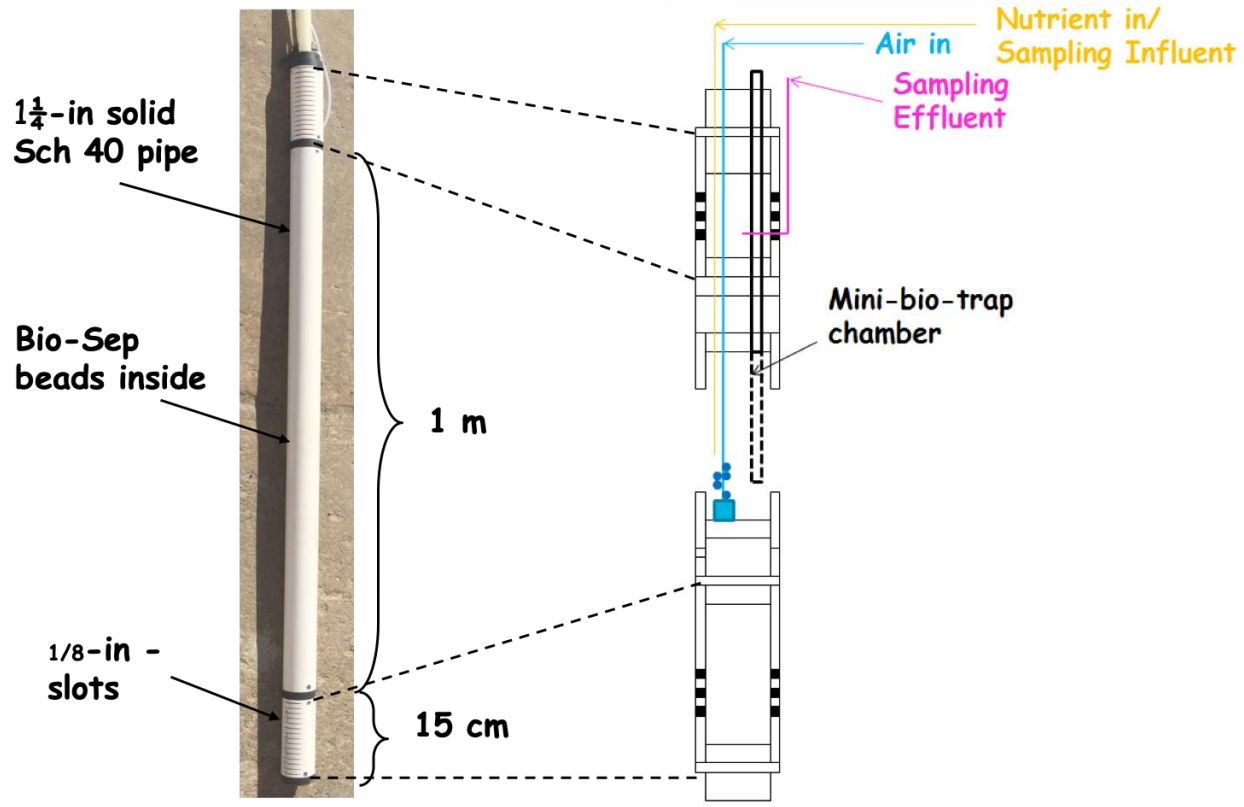

Figure 4.24. Schematics of customized in-situ bioreactor.

4.2.8 Monitoring Program during ISBR Operations

Baseline and post-deployment samples of Bio-Sep beads were collected and analyzed for 1,4-dioxane biomarkers as well as 1,4-dioxane that has adsorbed to the Bio-Sep beads. Nucleic acids were extracted from the Bio-Sep beads to evaluate the presence and activity of the dioxane biomarkers associated with CB1190. The adsorbed 1,4-dioxane on the Bio-Sep beads from the CB1190 ISBRs and control ISBRs were compared to help evaluate whether CB1190 is utilizing and biodegrading 1,4-dioxane on the Bio-Sep beads. The baseline and post-deployment adsorbed 1,4-dioxane on the Bio-Sep beads from the control ISBR were compared to help evaluate whether Bio-Sep beads could concentrate 1,4-dioxane in-situ.

Due to the size of the ISBRs and number of Bio-Sep beads required for nucleic acids extraction, only 4 mini-biotraps could be installed inside the ISBR and retrieved for sampling.

Baseline samples of Bio-Sep beads were collected during ISBR construction and sent to the laboratory just prior to ISBR deployment. The first post-deployment mini-biotrap was collected from each ISBR approximately 2 weeks after deployment and results were compared to baseline, and the next mini-biotrap was collected at 6 or 8 weeks post-deployment when groundwater samples from the ISBR effluent show a significant change in 1,4-dioxane concentrations compared to baseline.

Groundwater samples were collected from the influent and effluent of each ISBR (both CB1190 and controls). The samples were analyzed for field parameters (dissolved oxygen [DO], oxidation-reduction potential [ORP], temperature, pH and specific conductance) in the field and for 1,4-dioxane and VOCs by the offsite laboratory. Field parameters were monitored to ensure maintenance of favorable conditions for 1,4-dioxane biodegradation inside the ISBRs (e.g., aerobic conditions and fairly neutral pH). 1,4-Dioxane data from the influent and effluent of the ISBRs was compared and evaluated for any changes as groundwater circulates upward through the ISBR. The changes in the CB1190 ISBRs were compared to the changes in their associated control ISBRs to evaluate what amount of change could be associated with in-situ biodegradation of 1,4-dioxane by CB1190.

4.2.9 Analytical Methods

Liquid samples were collected periodically, and preserved with hydrochloric acid. 1,4-Dioxane (1-1000 µg/L) was monitored using an Agilent 6890 gas chromatograph equipped with an Agilent 5973 mass spectrometer (GC-MS) and a Restek Rxi-624Sil MS GC column (30 m × 0.25 mm id × 1.4 µm). The collected aqueous samples were prepared for GC-MS analysis using a frozen micro-extraction procedure as previously described (Li et al., 2011), and 5 µL of processed sample was injected into the GC-MS equipped with a pulsed split-less injection with an inlet temperature of

150°C, 77 kPa, a pulsed pressure of 170 kPa for 2 min, and a purge flow of 15.0 mL/min. The oven temperature was initially held constant at 35°C for 5 min, then increased to 100 °C at a rate of 20 °C/min, and further increased to 275°C at a rate of 50°C/min. The mass-selective detector (MSD) was operated with an electron multiplier (EM) offset of 400 and EM voltage of 2000. The MS quadrupole was set to 150°C with a source for 230°C (Zhang et al., 2016).

1,4-Dioxane concentrations over than 1000 μg/L were measured using a Hewlett-Packard 6890 gas chromatograph equipped with a flame ionization detector (GC-FID) (Hewlett-Packard, Atlanta, GA) with a Restek® Stabilwax-DB capillary column (30 m × 0.53 mm ID × 1 μm; Restek, Bellefonte, PA) as described in Pornwongthong et al. (2014). Briefly, liquid samples (100 μL) were collected and filtered through 0.2-μm-pore Fisher brand nylon syringe filters. 2 μL of the filtrate was directly injected into the GC-FID. The injector and detector were maintained at a temperature of 220°C and 250°C, respectively. The oven was programmed to rise from 80°C to 140°C at a ramp rate of 20°C/min, and held for 1 minute at 140°C. The 1,4-dioxane retention time was approximately 3.5 minutes.

4.2.10 Nucleic Acids Extraction

The nucleic acids contain DNA and RNA, that can describe gene abundances and expressions, respectively. The total nucleic acids were extracted based on modified phenol/chloroform/isoamyl alcohol method (Gedalanga et al., 2014). Briefly, 500 μL of slurry samples were centrifuged at 13000 x g for 3 min, and the supernatant was discarded. The centrifuged precipitants were lysed by adding 250 μL of lysis buffer (50 mM sodium acetate, 10 mM EDTA [pH 5.1]), 100 μL 10% sodium dodecyl sulfate, 1.0 mL pH 8.0 buffer-equilibrated phenol, and 1 g of 100 μm-diameter zirconia−silica beads (Biospec Products, Bartlesville, OK, USA), followed by heating at 65°C for 2 min, bead beating for 2 min with a Mini-Beadbeater 16 (Biospec Products, Bartlesville, OK, USA),

incubating for 8 min at 65°C, and bead beating again for 2 min. The lysate was collected by centrifugation at 13000 x g for 5 min, followed by phenol/chloroform/isoamyl alcohol purification and chloroform−isoamyl alcohol purification. Precipitation of total nucleic acids was performed by addition of 0.1 volume of 3 M sodium acetate and 1 volume of isopropanol followed by incubation at −20°C overnight. Nucleic acid pellets were collected by centrifugation at 4°C for 30 min at 20000 x g. The precipitate was washed with 70% ethanol and resuspended in 100 μL of DNase- and RNase-free water. The concentrations of total nucleic acids were determined by a Nanodrop 2000C spectrophotometer (Thermo Scientific, Wilmington, DE, USA). Afterwards, 30 μL of extracts were transferred into the new snap-cap tube, and RNA reverse transcription was performed by using EasyScript Plus^{TM} cDNA Synthesis Kit (Lamda Biotech, St. Louis, MO, USA) after DNA was removed by using RapidOut DNA Removal Kit (Thermo Fisher Scientific, Waltham, MT, USA) according to the manufacturer's introductions.

4.2.11 Quantitative Polymerase Chain Reaction (qPCR) Assay

To quantify CB1190 biomass and functional gene abundances and expressions, CB1190-like 16S rRNA gene and 1,4-dioxane biomarker genes (*dxmB* and *aldH*) were selected because of the significance of 1,4-dioxane monooxygenase (DXMO) and aldehyde dehydrogenase (ALDH) enzymes in the 1,4-dioxane biodegradation pathways as described previously (Gedalanga et al., 2014, Gedalanga et al., 2016, Zhang et al., 2016). All reactions were run on a StepOnePlus thermocycler (Life Technologies, Carlsbad, CA) using a total volume of 20 μL containing 1 × Luminaris Color HiGreen-HiROX qPCR Master Mix (Thermo Scientific, Waltham, MA), 0.3 μM primers, and 2 μL of DNA/cDNA (1-10 ng/μL) template. The cycling parameters to amplify the gene fragment started with holding at 50°C for 2 min and 95°C for 10 min, followed by 40 cycles of 95°C for 15 s and annealing at 60°C for 45 s. All reactions were accompanied by a melt-curve analysis to confirm the

specificity of qPCR products. Standard curves were produced using serial dilutions of genomic DNA extracted from a pure culture of the CB1190 (Gedalanga et al., 2016).

4.4 Results

4.4.1 Distribution of Bioaugmented CB1190

Field parameter and chemistry results are shown on Table 4.1. During baseline sampling, dissolved oxygen concentrations in all wells were at or slightly below 1.0 milligram per liter (mg/L). One month after bioaugmentation and deployment of the iSOC in injection well 8IW01, the dissolved oxygen concentration in 8IW01 increased to 11.59 mg/L (with the iSOC online) and to 3 mg/L in 8MNW17, located slightly more than 5 feet away from the injection well. However, dissolved oxygen concentrations in the three 1-inch diameter test wells remained at or below 1 mg/L, indicating insufficient oxygen for CB1190.

Unlike dissolved oxygen, ORP increased significantly in all wells, and pH also increased approximately 1 standard unit in most wells following bioaugmentation. In the injection well, the pH increased to 8.6, which was slightly above conditions conducive to reduction biodegradation of 1,4-dioxane by CB1190 (pH of 4 to 8). Concentrations of VOCs and 1,4-dioxane in groundwater generally did not change between baseline and 1-month post bioaugmentation in any of the wells, suggesting that either no significant degradation occurred, or, if it did occur, concentrations rebounded rapidly.

Table 4.5. Field Groundwater geochemistry analytical results.

Sample Name	TW- 4	TW- 5	TW- 6	8MNW17	8IW01	TW- 4	TW- 5	TW- 6	8MNW17	8IW01
Field Event		**January 2016 (Pre- bioaugmentation)**					**February 2016 (1- month Post- bioaugmentation)**			
Sample Date	1/12/2016	1/12/2016	1/12/2016	1/12/2016	1/12/2016	2/15/2016	2/15/2016	2/15/2016	2/15/2016	2/15/2016
Field Parameters (AECOM)										
Temperature	21.78	21.79	21.34	20.65	21.45	21.65	21.97	21.75	21.31	21.7
Specific Cond (mS/cm)	1.413	1.415	1.440	1.422	1.436	1.40	1.41	1.42	1.42	1.46
DO (mg/L)	0.85	0.64	0.98	1.07	1.00	1.17	0.71	0.77	3.00	11.59
pH	7.23	7.25	7.22	7.19	7.39	8.17	8.10	7.95	7.95	8.6
ORP (mV)	- 41.7	- 53.3	- 58.7	14.3	- 61.8	109	90.8	93	95	92
Turbidity (NTU)	6.12	5.93	1.03	1.54	5.08	8.40	7.22	7.64	6.47	11.6
Chemical (UCLA)										
1,4- Dioxane (µg/L)	238.20	244.70	384.30	324.00	355.50	122.10	129.00	181.37	150.14	190.14
TCE (µg/L)	2,616.70	2,126.20	5,230.80	3,484.00	3,486.30	1,068.77	1,295.20	2,349.11	1,543.19	1,149.07
cDCE (µg/L)	122.80	108.30	209.40	179.90	166.90	48.68	37.54	59.22	52.77	57.78
1,1- DCE (µg/L)	636.40	219.20	262.10	<100	<100	4.47	5.25	7.58	5.37	2.99
Chemical (TestAmerica)										
1,4- Dioxane (µg/L)	140	150	280	170 J	240/230	130	140	210	170	200
TCA (µg/L)	2.0 J	2.0 J	9.4 J	< 1.7	4.8 J/4.3 J	2.1 J	1.9 J	8.7 J	2.7 J	1.6 J
TCE (µg/L)	1,500	1,500	3,500	2,300	2,800/2,800	1,600	1,700	3,600	2,000	1,500
cDCE (µg/L)	17	17	33	22 J	27/25	15 J	17	32	19	15
1,1- DCE (µg/L)	460	480	900	640	750/710	520	530	850	520	300
VC (µg/L)	< 0.84	< 0.84	< 2.1	< 2.1	< 2.1/< 2.1	< 0.84	< 0.84	< 2.1	< 2.0	< 0.84

/	denotes duplicate sample
<	less than
µg/L	micrograms per liter cDCE cis - 1,2 - DCE
DCE	dichloroethene
DO	dissolved oxygen
J	result was less than the reporting limit but greater than the method detection limit
mS/cm	microsiemens per centimeter
mV	millivolts
NTU	nepholematic turbidity unit

Table 4.6. Field Groundwater molecular microbial analytical results.

Sample Name	TW- 4	TW- 5	TW- 6	8MNW17	8IW01	TW- 4	TW- 5	TW- 6	8MNW17	8IW01
Field Event	**January 2016 (Pre- bioaugmentation)**					**February 2016 (1- month Post- bioaugmentation)**				
Sample Date	1/12/2016	1/12/2016	1/12/2016	1/12/2016	1/12/2016	2/15/2016	2/15/2016	2/15/2016	2/15/2016	2/15/2016
DNA from Groundwater (copies/mL) (UCLA)										
dxmB	< 1,800	< 1,800	< 1,800	< 1,800	< 1,800	< 242	< 242	< 242	< 242	< 242
aldH	-	-	-	-	-	< 242	< 242	< 242	< 242	< 242
CB1190 16S	290 J	14,000	140 J	590 J	2,100	87 J	30 J	164 J	18.4 J	134 J
DNA from Biotrap Beads (copies/bead) (UCLA)										
dxmB	-	-	-	-	-	674	122	510	594	-
aldH	-	-	-	-	-	< 7.36	< 7.36	< 7.36	< 7.36	-
CB1190 16S	-	-	-	-	-	4,130	938	1,700	1,100	-
cDNA from Biotrap Beads (copies/bead) (UCLA)										
dxmB	-	-	-	-	-	14.3	< 7.36	< 7.36	< 7.36	-
aldH	-	-	-	-	-	< 7.36	< 7.36	< 7.36	< 7.36	-
CB1190 16S	-	-	-	-	-	91.4	13.9	20.5	5.05 J	-
mRNA from Biotrap Beads (gene copies/bead) (Microbial Insights)										
dxmB	-	-	-	-	-	< 250	< 250	< 250	< 250	-
aldH	-	-	-	-	-	< 250	< 250	< 250	< 250	-

- not analyzed
< less than
ALDH alcohol dehydrogenase
CB1190 *Pseudonocardia dioxanivorans* CB1190
cDNA complimentary deoxyribonucleic acid
copies/mL copies per milliliter
DXMO dioxane monooxygenase
J result was less than the reporting limit but greater than the method detection limit
mRNA messenger

Groundwater samples were collected immediately prior to bioaugmentation. Post bioaugmentation microbial samples included groundwater from the monitoring wells, Biotraps retrieved from well 8MWN17 and the three test wells, and soil collected from boreholes during the distribution evaluation. The primary targets for microbial analysis were *dxmB* and *aldH*, both of which were not detected in any of the baseline groundwater samples. Groundwater and Biotrap microbial results are shown on Table 4.2.

DNA samples were extracted from the groundwater samples sent to UCLA. Post bioaugmentation sampling results did not detect *dxmB* or *aldH* in any of the wells above the detection limit of 242 copies/mL, including the injection well. Moreover, *dxmB* and *aldH* were not detected on Biotrap beads by analyzing mRNA indicating no activity of the degradative enzymes. Results for cDNA were similar, only with the exception of a low detection of *dxmB* in TW-4. These results also supported little to no activity of the degradative enzymes. However, DNA extracts detected *dxmB* in the Biotraps from all four wells at abundances ranging from 122 to 674 copies/bead. These results indicated that the injected CB1190 was distributed to these locations (5 feet to at least 10 feet away from the injection well), but was not active. Figure 4.11 shows the locations where *dxmB* was detected in DNA following bioaugmentation. The concentrations of *dxmB* that were detected in Biotrap samples are significantly (approximately five orders of magnitude) lower than those associated with 1,4-dioxane degradation. The highest concentration of *dxmB* was detected in TW-4, which was also the only location where *dxmB* was detected in cDNA, while *aldH* was not detected in any of the Biotrap samples. Soil sample analytical results are shown on Table 4.3, and *dxmB* was detected in 6 out of 14 soil samples, ranging from 141 to 433 Copies/g. Figure 4.3 shows the locations (both boreholes and monitoring wells) where *dxmB* was detected (shaded in green). Based on *dxmB*,

CB1190 was distributed at least 10 feet away (TW-4), with preferential distribution to the east and northeast, similar to the general groundwater flow direction at the site.

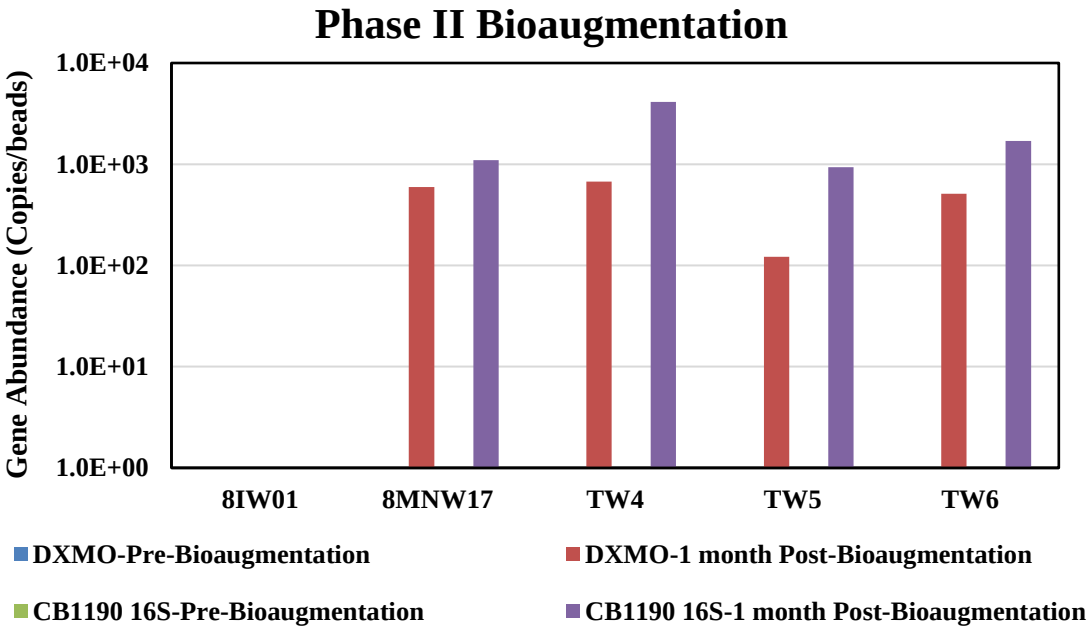

Figure 4.25. Gene abundance in CB1190 distribution test after 1-month bioaugmentation.

Table 4.7. Soil sample analytical results.

Sample Name (sample interval)	Sample Date	*dxmB* (copies/g)	*aldH* (copies/g)	CB1190 16S (copies/g)
BH1 (18'- 20')	2/16/2016	433 J	< 452	1,410
BH2 (16'- 19')	2/16/2016	141 J	< 452	843
BH2 (20'- 21')	2/16/2016	359 J	< 452	1,470
BH3 (17'6"- 20')	2/16/2016	< 452	< 452	3,830
BH4 (19'7"- 20'6")	2/16/2016	418 J	< 452	2,770
BH6 (17'4"- 19')	2/16/2016	< 452	< 452	1,190
BH6 (16'9"- 18'9")	2/16/2016	283 J	< 452	194 J
BH7 (17'5"- 18'2")	2/16/2016	< 452	< 452	827
BH8 (17'9"- 20'5")	2/16/2016	190 J	< 452	1,390
BH9 (17- 19')	2/16/2016	< 452	< 452	863
BH10 (17'- 20')	2/16/2016	< 452	< 452	170 J
BH11 (18'- 19')	2/16/2016	< 452	< 452	356 J
BH12 (18'- 19'3")	2/16/2016	< 452	< 452	191 J
BH12 (19'- 19'9")	2/16/2016	< 452	< 452	821

J result was less than the reporting limit but greater than the method detection limit

4.4.2 Mobile CB1190 in-situ Bioaugmentation Pilot Study

Prior to the in-situ bioaugmentation, the baseline data indicated only 2.11×10^3 copies/mL CB1190 left near the injection well 8IW01, and the abundance immediately increased to 1.12×10^6 copies/mL after injection (Figure 4.12). Moreover, the detection of CB1190 was increasing over time in the downstream wells with the order of distances to 8IW01. Similarly, the gene transcripts of *dxmB* and *aldH* reached to 2.39×10^5 and 1.57×10^4 copies/mL after injection in 8IW01, and other wells in the following monitoring activities. However, both abundance and transcript of CB1190 steadily declined over time in 8 weeks, while the total bacteria were increased and stable in monitoring wells (Figure 4.13). The injected culture contained elevated concentrations of 1,4-dioxane, causing temporary/localized increases in 1,4-dioxane groundwater concentrations over 800 μg/L in 8IW01 (Figure 4.14), which also impacted 1,4-dioxane concentrations in 8MNW17. However, the accidentally spiked 1,4-dioxane decreased to baseline level in two weeks in both 8IW01 and 8MNW17, and continuously reduced and stabilized at 180-200 μg/L in 12 weeks. The detected 1,4-dioxane in 8MNW49 and TW-4 were steady during the bioaugmentation event, even with the boosted *dxmB* and *aldH* abundances and transcripts. In addition, dissolved oxygen was adequate in two wells right after injection and the third (8MNW17) within 4 weeks. Oxidation reduction potential (ORP) values were greater than 100 millivolts in all three wells within 2 weeks of bioaugmentation (Table 4.4).

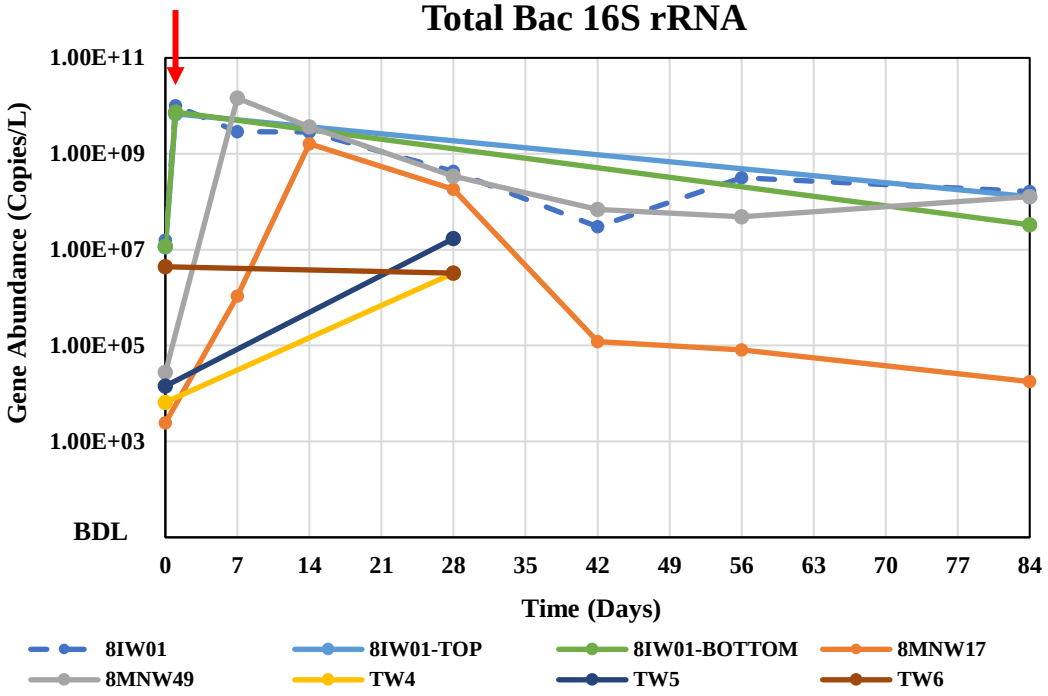
Total Bac 16S rRNA
Gene Abundance (Copies/L)
1.00E+11
1.00E+09
1.00E+07
1.00E+05
1.00E+03
BDL
0
7
14
21
28
35
42
49
56
63
70
77
84
Time (Days)
8IW01
8IW01-TOP
8IW01-BOTTOM
8MNW17
8MNW49
TW4
TW5
TW6

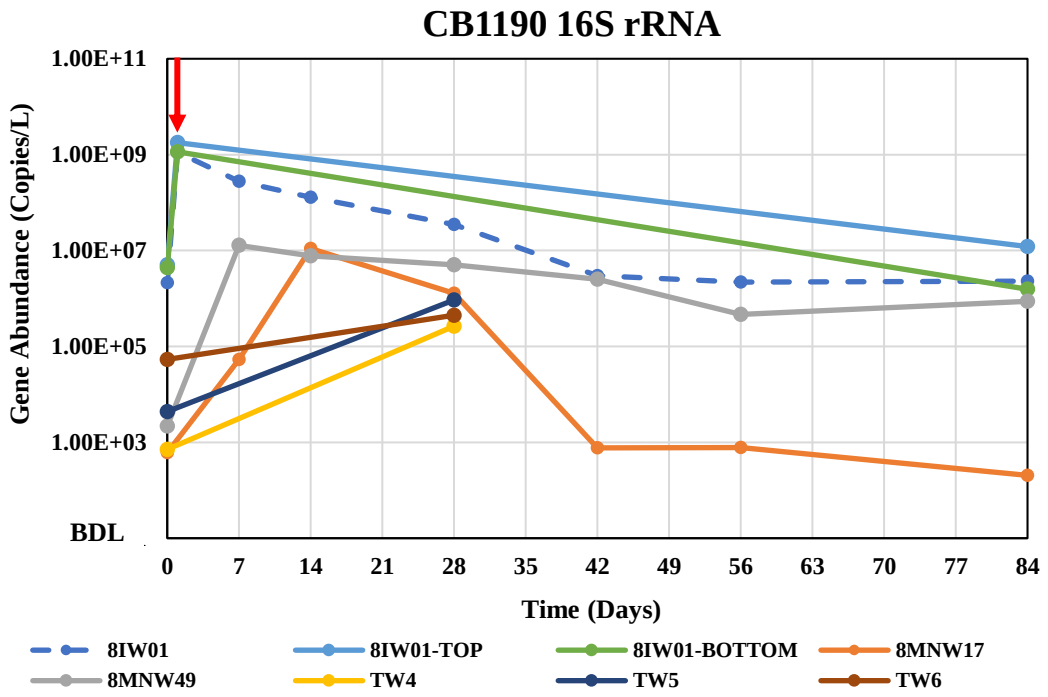
CB1190 16S rRNA
Gene Abundance (Copies/L)
1.00E+11
1.00E+09
1.00E+07
1.00E+05
1.00E+03
BDL
0
7
14
21
28
35
42
49
56
63
70
77
84
Time (Days)
8IW01
8IW01-TOP
8IW01-BOTTOM
8MNW17
8MNW49
TW4
TW5
TW6

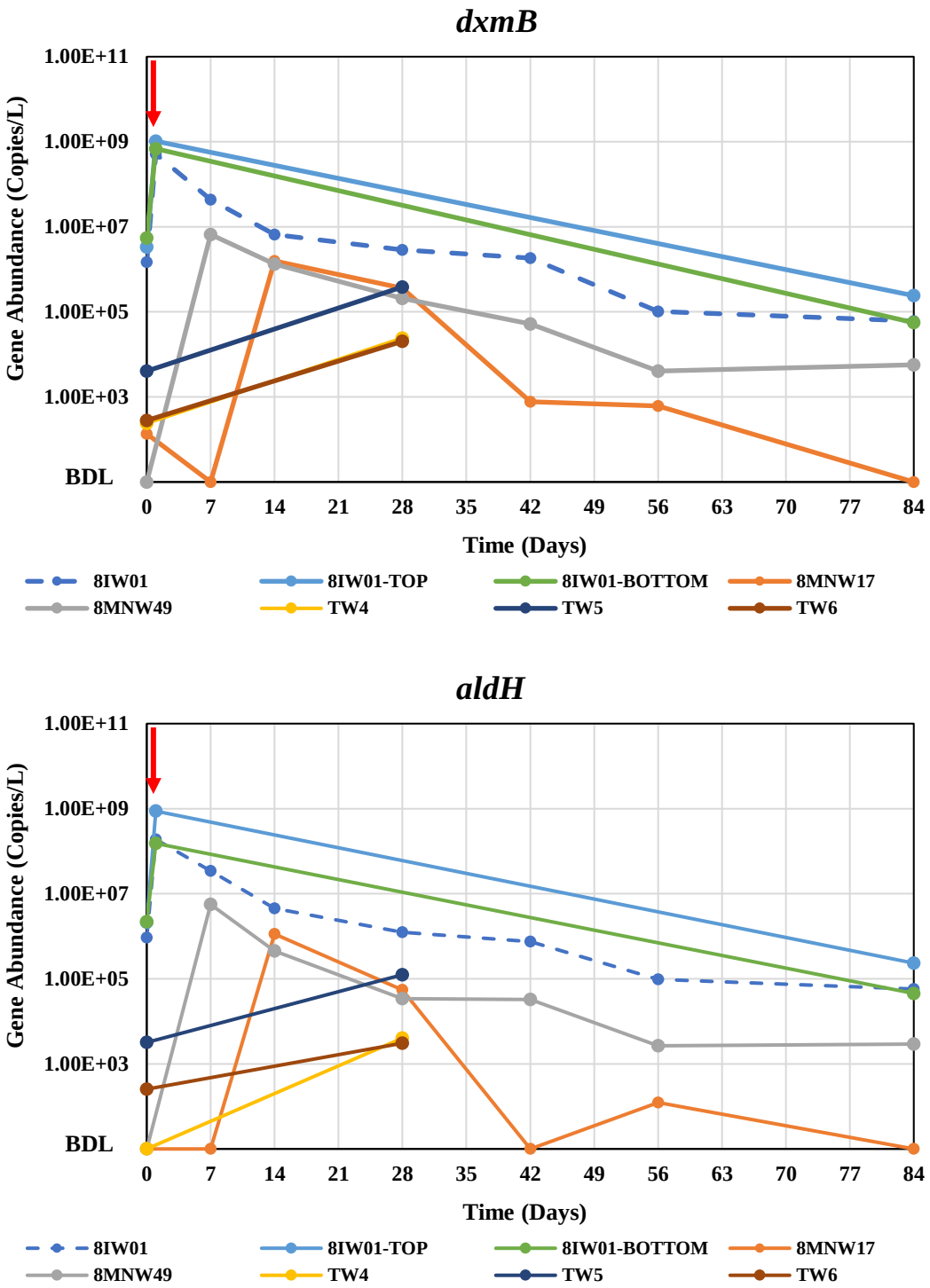

Figure 4.26. Gene abundance in the 12-week bioaugmentation implement.

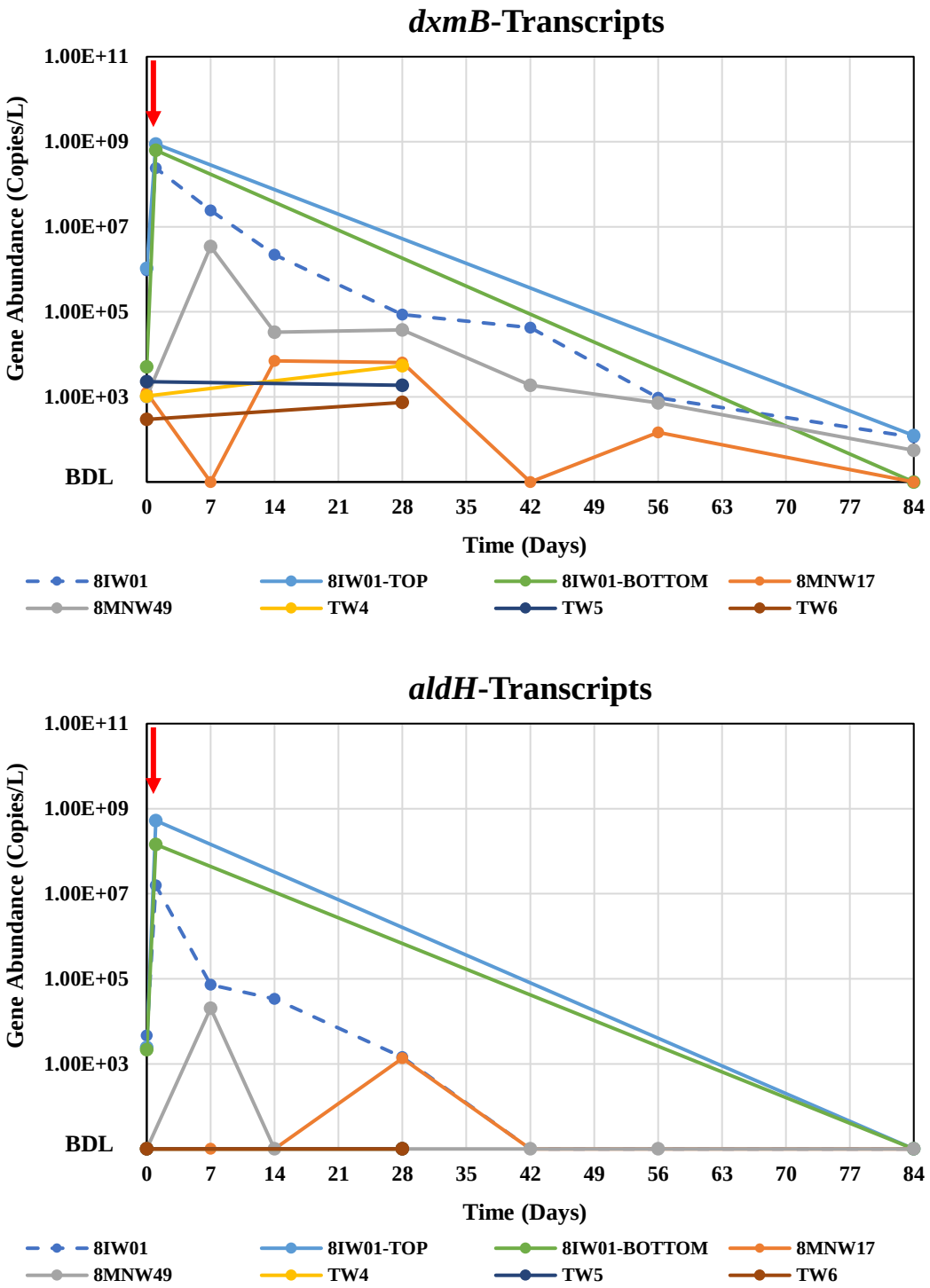

Figure 4.27. Gene transcript in the 12-week bioaugmentation implement.

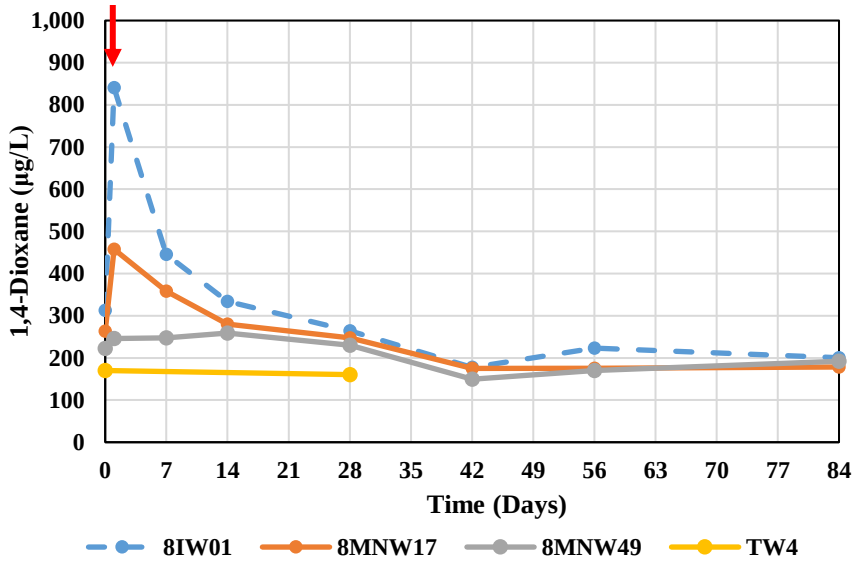

Figure 4.28. 1,4-Dioxane concentrations in the 12-week bioaugmentation implement.

Table 4.8. Field Groundwater geochemistry analytical results after bioaugmentation.

Sample Name	8IW01	8MNW49	8MNW17	TW-4	TW-5	TW-6	8IW01	8MNW49	8MNW17
Field Event			**Phase 3 Baseline**				**Immediately Post Injection**		
Sample Date	8/31/2016	8/31/2016	8/31/2016	8/31/2016	8/31/2016	8/31/2016	9/1/2016	9/1/2016	9/1/2016
Field Parameters (AECOM)									
Temperature	24.87	26.06	24.89	24.11	24.21	23.64	-	-	-
Specific Cond (mS/cm)	1.42	1.44	1.43	1.41	1.40	1.44	-	-	-
DO (mg/L)	0.71	2.32	1.95	1.42	0.98	1.09	-	-	-
pH	6.95	7.40	7.43	6.70	7.04	7.00	-	-	-
ORP (mV)	203	197	87.3	213	139	200	-	-	-
Turbidity (NTU)	5.3	3.4	43	5.6	17.8	1.0	-	-	-
Chemical (UCLA)									
1,4-Dioxane (µg/L)	313	222	263	170	200	305	841	246	458
Chemical (Test America)									
1,4-Dioxane (µg/L)	180	160 M	170	110	110	190	440 D	170	310 D
TCA (µg/L)	3.2 J D	3.5 J D	3.5 J D	0.99 J D	1.0 J D	9.9 J D	-	-	-
TCE (µg/L)	2,600 D	2,300 D	2,500 D	1,400 D	1,400 D	3,300 D	-	-	-
cDCE (µg/L)	22 D	20 D	20 D	12 D	13 D	28 D	-	-	-
1,1-DCE (µg/L)	620 D	610 D	590 D	370D	370 D	170 D	-	-	-
VC (µg/L)	<20	<20	<20	<10	<10	<20	-	-	-

Sample Name	8IW01	8MNW49	8MNW17	8IW01	8MNW49	8MNW17
Field Event	**1-week Post Injection**			**2-week Post Injection**		
Sample Date	9/8/2016	9/8/2016	9/8/2016	9/13/2016	9/13/2016	9/13/2016
Field Parameters (AECOM)						
Temperature	25.38	26.98	25.46	25.42	26.38	25.2
Specific Cond (mS/cm)	2.224	1.454	1.554	1.874	1.446	1.483
DO (mg/L)	7.07	1.78	0.81	7.08	1.36	0.55
pH	7.62	7.65	7.25	8.02	7.71	7.18
ORP (mV)	143.3	82.4	70.5	145.4	124.9	127.2
Turbidity (NTU)	-	-	-	-	2.16	3.79
Chemical (UCLA)						
1,4-Dioxane (µg/L)	445	248	359	334	259	280
Chemical (Test America)						
1,4-Dioxane (µg/L)	270 D	190	240 D	250 D	180	210 D
TCA (µg/L)	-	-	-	-	-	-
TCE (µg/L)	-	-	-	-	-	-
cDCE (µg/L)	-	-	-	-	-	-
1,1-DCE (µg/L)	-	-	-	-	-	-
VC (µg/L)	-	-	-	-	-	-

Sample Name	8IW01	8MNW49	8MNW17	TW-4	TW-5	TW-6	8IW01	8MNW59	8MNW17	8IW01	8MNW59	8MNW17
Field Events			4-week Post Injection				6-week Post Injection			8-week Post Injection		
Sample Date	9/27/2016	9/27/2016	9/27/2016	9/27/2016	9/27/2016	9/27/2016	10/12/2016	10/12/2016	10/12/2016	10/25/2016	10/25/2016	10/25/2016
Field Parameters (AECOM)												
Temperature	25.18	25.08	25.85	25.23	23.98	23.2	25.13	22.17	23.07	24.16	23.88	24.57
Specific Cond (mS/cm)	1.541	1.496	1.104	1.299	1.30	1.531	1.389	1.339	0.665	1.423	1.76	0.634
DO (mg/L)	7.58	1.55	4.8	3.86	0.42	1	8.32	1.30	4.01	8.45	2.26	3.15
pH	7.54	7.23	7.4	7.22	7.15	6.19	8.02	7.69	7.23	7.491	7.33	6.9
ORP (mV)	105.1	97.3	58.7	3.5	23.7	75.4	131.6	139.9	137.4	103.3	65.7	66.7
Turbidity (NTU)	2.1	1.6	8.67	4.94	3.67	1.0	5.63	3.15	33.9	3.66	4.15	14.5
Chemical (UCLA)												
1,4-Dioxane (µg/L)	264	230	248	160	186	269	142	152	159	223	170	175
Chemical (Test America)												
1,4-Dioxane (µg/L)	190 D	180 D	170	120	120	200 D	180	180	110	150 D	170	170 J
TCA (µg/L)	-	-	-	-	-	-	-	-	-	-	-	-
TCE (µg/L)	-	-	-	-	-	-	-	-	-	-	-	-
cDCE (µg/L)	-	-	-	-	-	-	-	-	-	-	-	-
1,1-DCE (µg/L)	-	-	-	-	-	-	-	-	-	-	-	-
VC (µg/L)	-	-	-	-	-	-	-	-	-	-	-	-

-	not analyzed	**M**	manual integrated compound	**1,1-DCE**	1,1-dichloroethene
<	Not detected at or above the detection limit shown	**mg/L**	milligrams per liter	**DO**	dissolved oxygen
µg/L	micrograms per liter	**mS/cm**	microsiemens per centimeter	**J**	result was less than the reporting limit but greater than the method detection limit
cDCE	cis-1,2-dichloroethene	**mV**	millivolts	**TCA**	1,1,1-trichloroethane
D	the reported sample is from a dilution	**NTU**	nepholematic turbidity unit	**TCE**	Trichloroethene

4.4.3 1,4-Dioxane Adsorption and Desorption on Bio-Sep Beads

The adsorption was conducted for 5 days and bottles were initially spiked at around 73.24 mg/L 1,4-dioxane, and then decreased by 64%, presumably due to adsorption (Figure 4.15). The washed beads were placed in fresh AMS without 1,4-dioxane, and elevated 1,4-dioxane concentrations were observed in 20 hours, showing desorption of 1,4-dioxane off the beads into the aqueous phase, and reached to equilibrium after then (Figure 4.16).

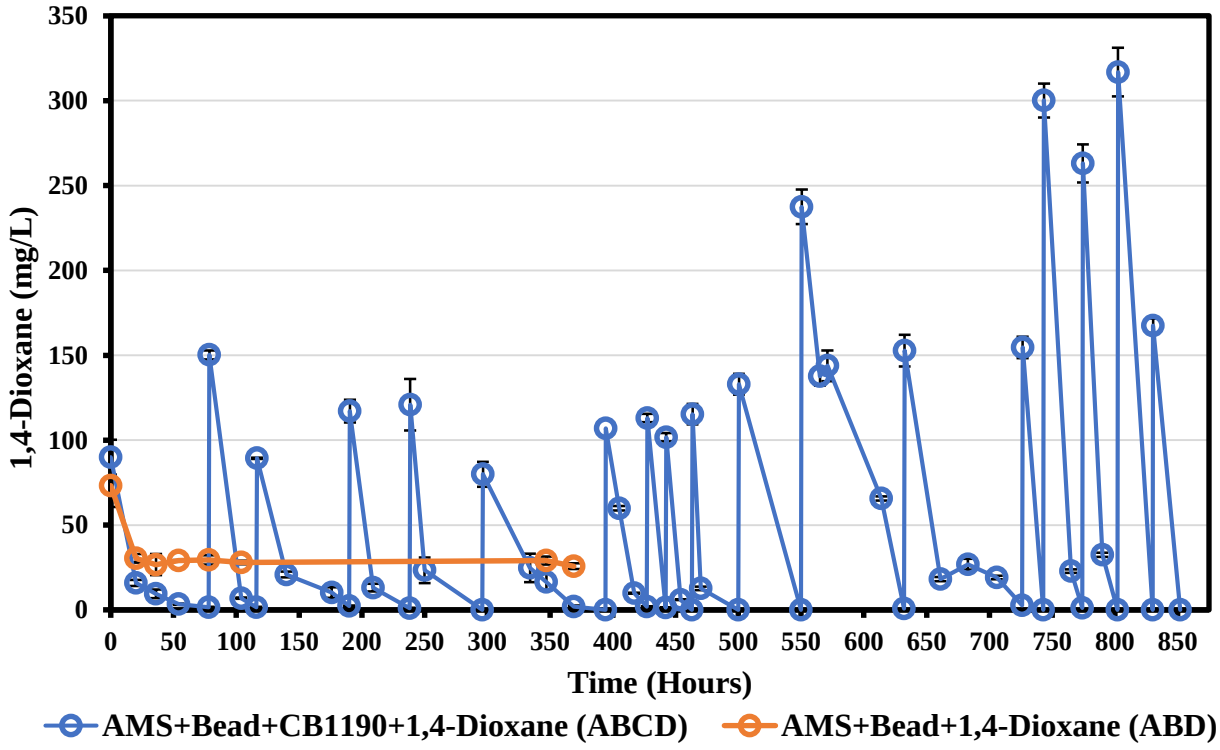

Figure 4.29. 1,4-Dioxane concentrations in CB1190 growing on beads and 1,4-dioxane adsorption processes. Error bars represent the standard deviation of analytical triplicates.

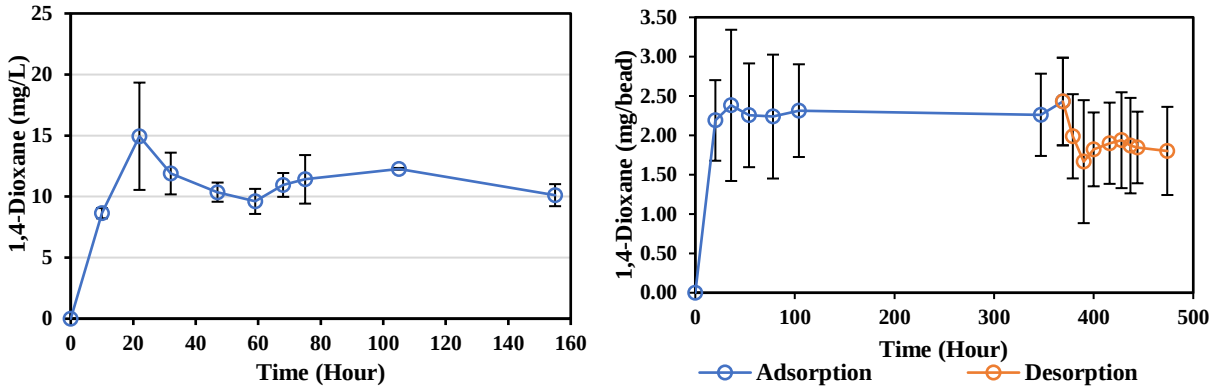

Figure 4.30. 1,4-Dioxane readily desorbed from abiotic bio-trap beads that were previously exposed to 1,4-dioxane. Error bars represent the standard deviation of duplicate reactors.

4.4.4 Attachment and Activity of CB1190 on Bio-Sep Beads

Reactors containing AMS medium, beads, CB1190, and 1,4-dioxane (ABCD) were used to grow CB1190 on the beads for over 30 days. 1,4-Dioxane was continuously removed by the bioaugmented beads (Figure 4.15), indicating the active CB1190 the reactors. After growth, liquid and beads were separated for activity test and the washed beads were consolidated and resuspended in fresh AMS containing 1,4-dioxane, which decreased rapidly from 104.32 mg/L to 28.61 mg/L in first 8 hours (Figure 4.17). Moreover, 1,4-dioxane concentrations were observed to continuously decrease in the reactors (Figure 4.18), demonstrating that CB1190 biofilms on the beads or detached cells could degrade 1,4-dioxane after transferring to a new environment.

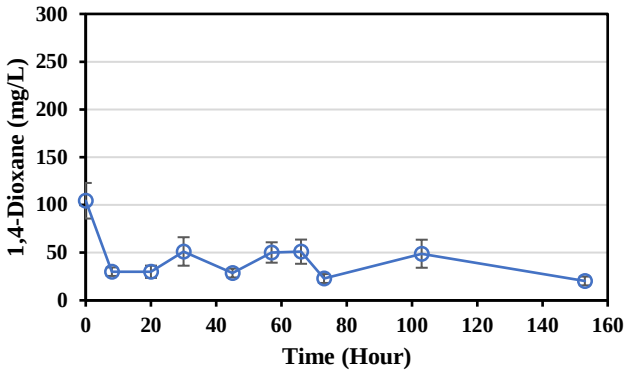

Figure 4.31. 1,4-Dioxane concentration at the start of the activity assay (~150 hours). Error bars represent the standard deviation of analytical triplicates.

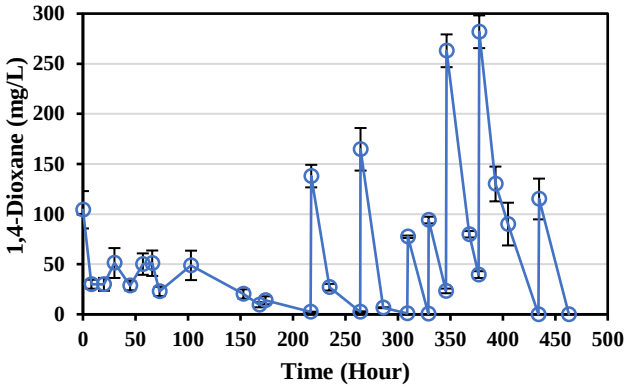

Figure 4.32. 1,4-dioxane concentrations during the whole process of activity assay showing high degradation capability. Error bars represent the standard deviation of analytical triplicates.

Afterwards, lower levels of 1,4-dioxane ranging from ~20 mg/L to ~0.3 mg/L were used to test CB1190's biodegradation potential at lower concentrations. The results showed the constant removal of 1,4-dioxane, further confirming the activity CB1190 attached on the beads and in the liquid (Figure 4.19).

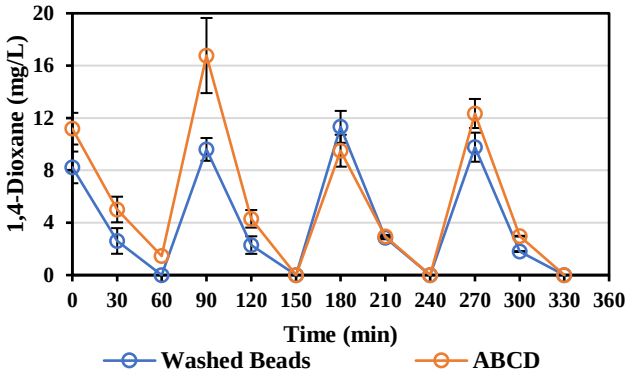

A

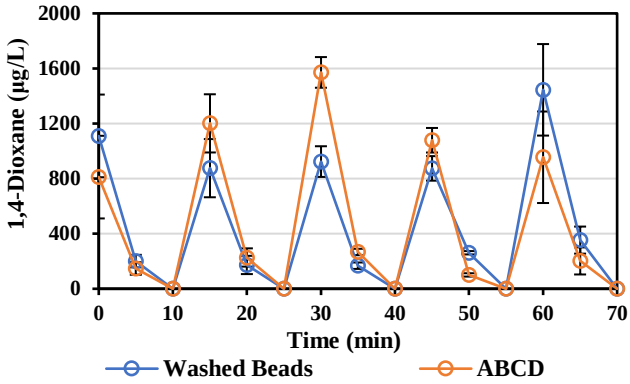

B

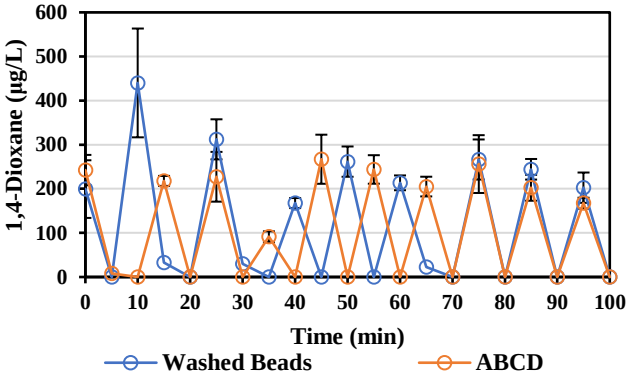

C

Figure 4.33. 1,4-Dioxane concentrations during the CB1190 viability test with gradually lowered spiking concentrations at 20 mg/L (A), 2 mg/L (B), and 0.3 mg/L (C).

However, after the viability test and consolidation of the washed beads into fresh AMS, a large amount of 1,4-dioxane was detected in 24 hours in all reactors. Desorption continued even after multiple bead washing steps, but eventually decreased to below detection in 30 days (Figure 4.20). The 1,4-dioxane accumulation is likely due to the lack of planktonic cells that could have been

responsible, in part, for the degradation of the previously desorbing 1,4-dioxane. This steady state condition was likely disrupted after the washing steps due to the removal of planktonic cells and the typically slower biodegradation rates associated with biofilm cells. However, the growing and eventually detaching CB1190 from the beads to the aqueous phase enhanced the degradation.

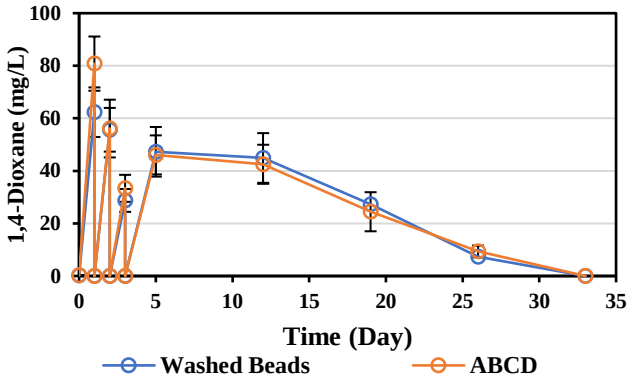

Figure 4.34. Desorbed 1,4-dioxane in fresh AMS from washed beads after viability test, and potential degradation by CB1190 on beads and in liquid.

3.4.5 Gene Abundances and Transcripts

Total nucleic acids were extracted from beads and liquid, respectively, for gene abundance quantification and expression analysis. The initial biomass of prepared pure CB1190 culture was 3.31×10^{6} copies/mL with *dxmB* and *aldH* expressed at 3.98×10^{4} and 4.32×10^{4} copies/mL, respectively (Figure 4.21). More samples were collected during the incubation process at hour 400, and both gene abundance and transcription showed increasing trends (*dxmB* abundances and transcripts reached to 2.73×10^{8} and 7.30×10^{7} copies/mL, respectively; *aldH* abundances and transcripts reached to 6.40×10^{7} and 3.95×10^{6} copies/mL, respectively).

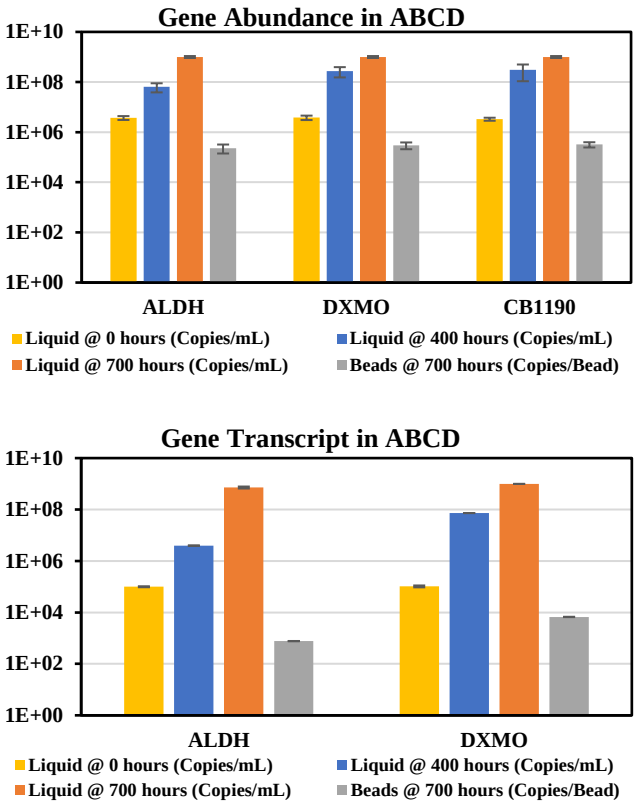

Figure 4.35. Gene abundances and transcripts in CB1190 growing process.

The continuous increase of biomass indicates the growth of CB1190 in the aqueous phase with a final density of over 10^9 copies/mL at hour 700, while attached CB1190 reached 3.21×10^5 copies/bead. The transcripts of *dxmB* and *aldH* were 6.69×10^3 and 7.66×10^2 copies/bead, respectively (Figure 4.21). This confirmed the growth of CB1190 on beads, and supports the argument that desorbed 1,4-dioxane accumulated in washed beads flasks due to the removal of relatively higher biomass in the aqueous phase. However, the evidence has demonstrated that bead-associated CB1190 could detach and resuspend in the aqueous phase after transferring the washed beads to fresh AMS medium. Detached CB1190 reached transcription levels of 7.43×10^7 and 6.43×10^6 copies/mL, respectively, for *dxmB* and *aldH* in 20 days after bead washing and transfer (Figure 4.22).

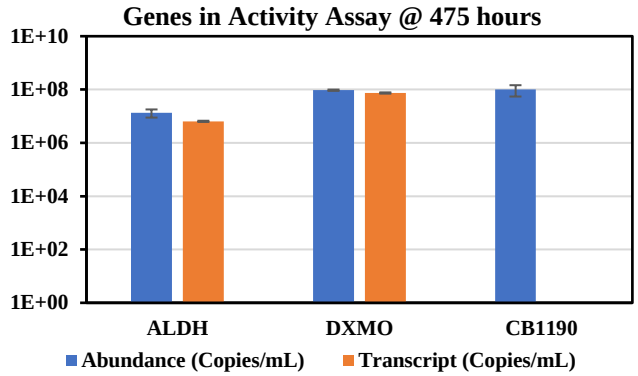

Figure 4.36. Gene abundances and transcripts in aqueous phase at the end of activity assay.

Similarly, the CB1190 in aqueous phase kept growing during the viability test, despite the lower levels of 1,4-dioxane (Figure 4.23). However, attached CB1190 on the beads showed slight decreases in both abundance and transcripts after ~0.3 mg/L 1,4-dioxane viability test (Figure 4.24), compared with the data at hour 700 (Figure 4.21).

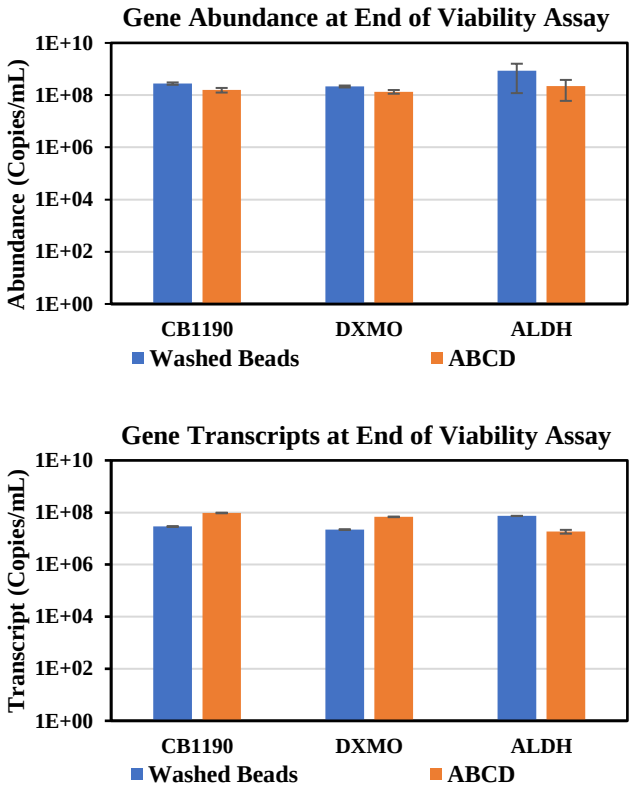

Figure 4.37. Gene abundances and transcripts in aqueous phase at the end of viability assay.

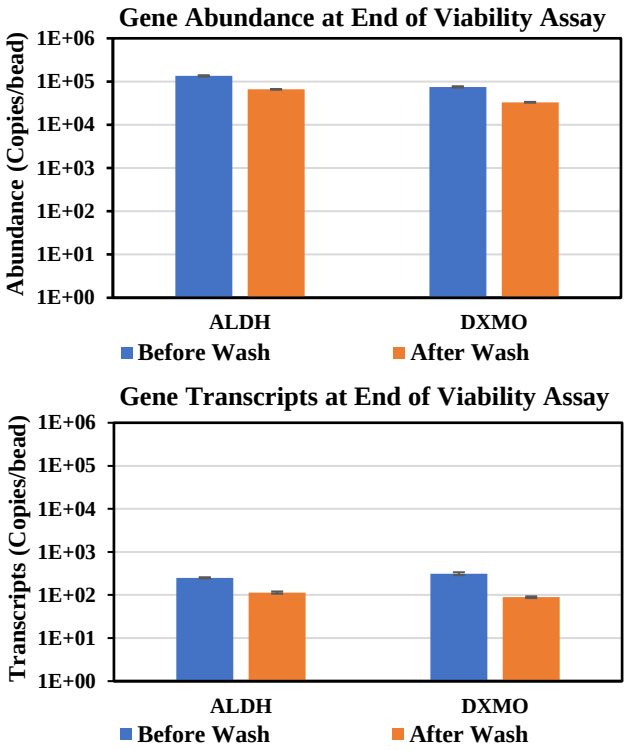

Figure 4.38. Gene abundances and transcripts on the beads at the end of viability assay and after washes, respectively.

4.4.6 In-situ Bioreactor (ISBR) in Pilot Study

The ISBR was designed as packed bed bioreactor containing CB1190 loaded Bio-Sep beads, and air was sparged into bottom to create air lift for circulation of groundwater through the bioreactor, and nutrient was injected into bioreactor from surface equipment. The 6 months ISBR field demonstration showed promising results that the attached CB1190 remained abundant (10^4 - 10^5 copies/bead) and active (10^1 – 10^3 copies/bead) on the beads (Figure 4.25), and the adsorbed 1,4-dioxane sharply decreased in the first week of demonstration (Figure 4.25). However, the 1,4-dioxane in the groundwater through the ISBRs was not removed as much as that on the beads during the monitoring time (Figure 4.26).

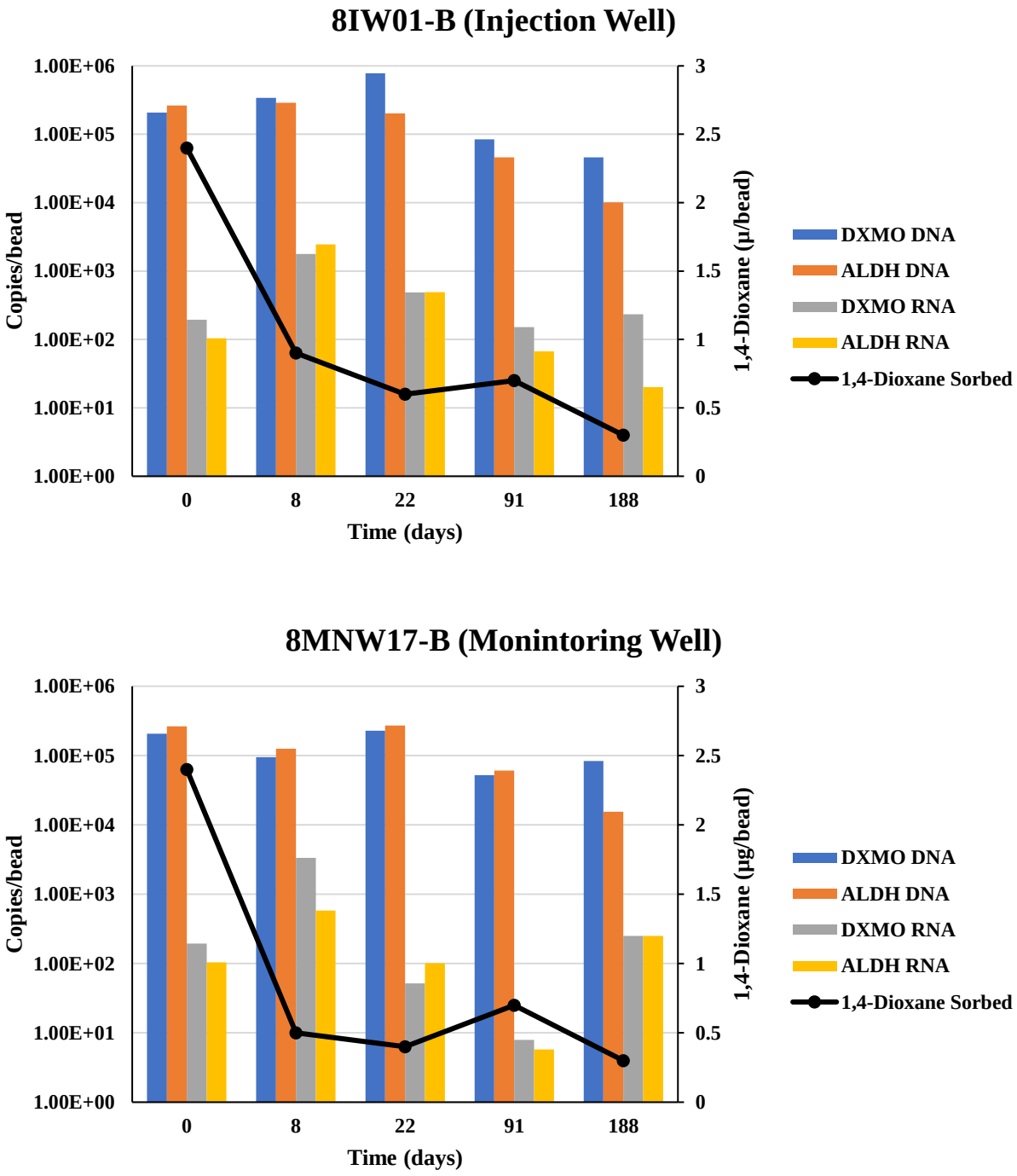

Figure 4.39. Gene abundances, transcripts, and adsorbed 1,4-dioxane on the bead in injection and monitoring wells over the 6 month demonstration.

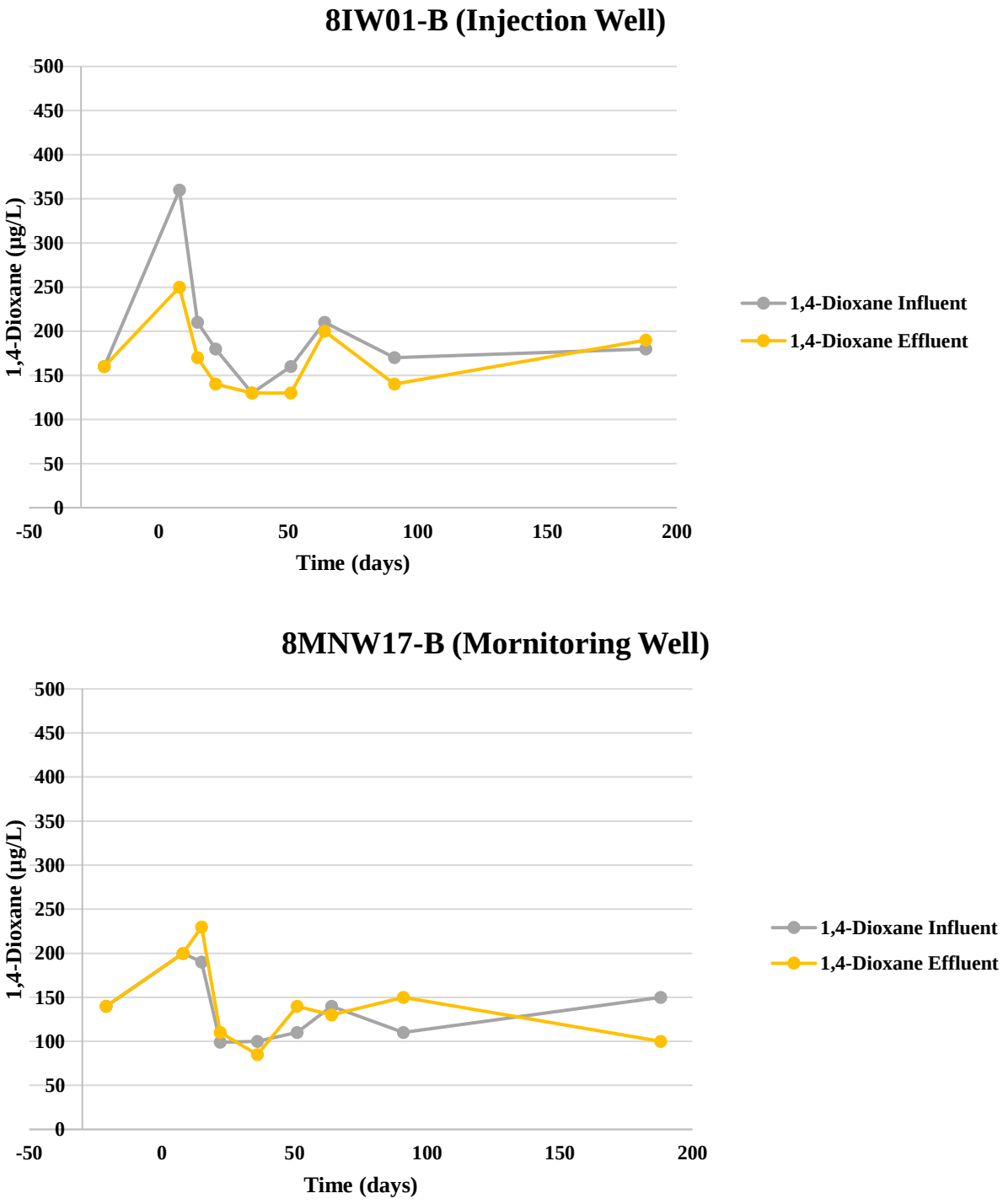

Figure 4.40. 1,4-Dioxane concentrations in groundwater through the ISBR in injection and monitoring wells over the 6 month demonstration.

4.5 Discussion

ORP increased significantly in all wells, it is possible that this increase indicates a trend toward more aerobic conditions; however, native aerobes may be consuming the dissolved oxygen. This pH increase may have been related to the injection of DAP. The lack of detection in well 8IW01 could indicate that the chase water used after injection of the culture may have pushed the culture completely out of the well. This may be because *aldH* is associated with the second half of the 1,4-dioxane degradation pathway and since 1,4-dioxane degradation has likely not occurred yet at the site, *aldH* was not induced.

The growth difference could be attributed the preference of CB1190 to grow in the liquid phase as planktonic cells or suspended flocs, or that CB1190 produces less extracellular polymeric substances (EPS) that are necessary to anchor the cells to solid surfaces (Myers, 2016). Moreover, some detachment occurred over the course of CB1190 growing on the beads, which was likely due to a combination of mechanical removal by rotary shaker-induced shear forces (Figure 3.27), detachment as part of biofilm lifecycles, and stress-mediated detachment caused by local nutrient deficiencies (Myers et al., 2018). Thus, the CB1190 attached beads could be applied in the pilot study with one of the roles as the CB1190 carriers to keep active and viable CB1190 even with low concentrations of 1,4-dioxane, and consistently migrate CB1190 to contacted groundwater for long-term 1,4-dioxane biodegradation. Moreover, the carriers are intended to offer a protective niche for inoculated CB1190 and hence reduce competition with indigenous microorganisms (Chen et al., 2012), and to keep the 1,4-dioxane contamination from spreading within the plume.

Figure 4.41. Morphological changes of beads in liquids before (right) and after (left) reaction.

4.6 Conclusions

The bioaugmentation strategy with 1,4-dioxane-metabolizing bacteria is an efficient method to degrade contaminant in-situ, compensating the lack or insufficiency of catabolic capability in indigenous microbes. The feasibility study indicated that injected CB1190 (> 10^7 copies/mL) was distributed at least 10 feet away from the injection well and followed preferential pathways, while only low cell densities were detected, supported by biomarker genes abundances and transcripts either in groundwater (< 242 copies/mL), or on Biotrap beads (122-674 copies/beads), or in the soil (141-433 copies/g). The second phase was implemented with the increased injection cell density, along with oxygen and diammonium phosphate nutrient, while the 1,4-dioxane showed decreasing trend in the first 8 weeks, but stabilized at ~100 μg/L with lower *dxmB* abundances and transcripts. Then, the third phase using in-situ bioreactor (ISBR) embedded with granular activated carbon (GAC) based Bio-Sep beads was conducted with immobile CB1190,

and the gene abundances and transcripts were stable in 200 days with significant decrease of adsorbed 1,4-dioxane on the beads. The bioaugmentation implement validated feasibility of in-situ 1,4-dioxane metabolizing process, but the parameter still needs to be optimized to achieve higher efficiency.

4.7 Supporting Information

4.7.1 Field Activities

4.7.1.1 Lithology Evaluation

At each of the nine boreholes, continuous cores were advanced using direct push drilling methods until bedrock refusal. Each core was logged using Unified Soil Classification System (USCS) methods and photographed. Headspace readings were collected using a photoionization detector (PID). The lithology of the study area was generally consistent with previous investigations. Based upon the continuous cores collected, the lithology can be divided into the following three zones:

- Vadose Zone (0 to 15 feet [ft] below ground surface [bgs]): Composed of clay, sandy clay, and silty clay (re-worked from previous construction activities and undisturbed) grading to silt between 12 and 15 ft bgs.
- Saturated Zone (15 to 23 ft bgs): Groundwater is encountered in the study area between 15 and 16 feet bgs. The saturated zone is made of up silt and sandy silt interbedded with discontinuous clayey sand, silty sandy, gravelly clay and gravelly silt beds. The gravel layers range in thickness from an inch (Area 3 and Area 1) to half a foot (Area 2). This zone has features which best fit the Aquiclude classification.
- Weathered Shale: The shale was encountered across the site at depths ranging from 21 to 25 ft bgs.

The lithology and location (close proximity to Mingo Creek) of the study area was indicative of a fluvial depositional environment. The saturated zone's composition of a fine-grained soil (clay and silt) with interbedding of clayey and silty gravel and sand was indicative of a flood plain and stream bank (low energy) environment, which experienced occasional flood events. During flood (high energy) events, a nearby creek would "jump" its bed, depositing a mixture of channel deposits (sand and gravel) and with low energy fine-grained deposits, resulting in discontinuous lenses of coarse-grained sediments with varying amounts of fines. This sort of depositional environment created an aquifer with highly variable hydraulic conductivities.

4.7.1.2 Temporary Well Installation and Sampling

The groundwater recharge rate at all direct push borehole locations was not sufficient to collect enough groundwater for the selected laboratory analysis, thus temporary monitoring wells were installed at each boring location. These temporary wells were identified as TW-1 through TW-9 (Figure 4.3).

Groundwater samples were collected from TW-1, -2, and -3 in Area 1 using a peristaltic pump and analyzed for VOCs and 1,4-dioxane. Based on the consistency of the analytical results in these wells, it was determined that only one temporary well in each of the other areas (TW-4 in Area 2 and TW-8 in Area 3) needed to be sampled for laboratory analysis. While elevated 1,4-dioxane concentrations are desired for the technology demonstration, the elevated VOC concentrations in Area 1 could cause inhibition of 1,4-dioxane biodegradation. In particular, recent work by UCLA has identified 1,1-dichloroethene (1,1-DCE) as a primary VOC that can inhibit 1,4-dioxane biodegradation (Zhang et al., 2016).

4.7.1.3 Injection Well Installation and Sampling

Area 2 was selected as the best candidate for performing the technology demonstration project based on 1) the 6-inch gravel zone that was encountered during direct push drilling and 2) the lower concentrations of VOCs that can potentially inhibit 1,4-dioxane biodegradation. Therefore, an injection well (8IW01) was installed in Area 2 and the temporary monitoring wells in Area 2 were completed as permanent monitoring wells. Temporary wells in the other two Area 1 were removed and backfilled with cement-bentonite grout.

For the injection well, an approximately 10-inch diameter borehole was advanced to the targeted depth (refusal at bedrock at approximately 23 ft bgs). Continuous split spoon samples were collected for the purpose of lithologic logging and collection of soil for the UCLA laboratory testing. Once the borehole was advanced to depth, the injection well was constructed using 4-inch diameter Schedule 40 polyvinyl chloride (PVC) screen and riser and up to 5 ft of 0.010-inch slot screen. The location of injection well 8IW01 is shown on Figure 4.3.

Injection well 8IW01 and the Area 2 monitoring wells were developed using a combination of swabbing and over pumping, after at least a period of 24 hours had elapsed since setting the annular seal. Injection well 8IW01 and previously existing monitoring well 8MNW17 in Area 2 were sampled using low-flow sampling techniques. Groundwater samples were analyzed for 1,4-dioxane by UCLA and additional groundwater volume was collected from injection well 8IW01 for the UCLA laboratory testing. Analytical results for wells 8IW01 and 8MNW17 are included in Table 4.1.

4.7.1.4 Slug Tests

Three rising head and two falling head tests were conducted at injection well 8IW01 prior to low-flow sampling. Slug test data were collected using submersible, data logging pressure

transducer to measure changes in head. The head change was induced by inserting a 3.1 foot-long slug constructed from Schedule 40 polyvinyl chloride (PVC) filled with sand into the water column for rising head tests and removing the slug for falling head tests. Slug test data were analyzed using spreadsheets developed by the United States Geological Survey (USGS) that estimate hydraulic conductivity and transmissivity using the Bouwer and Rice model. The average hydraulic conductivity at injection well 8IW01 within the screened zoned was 13.2 feet per day with a transmissivity of 1,145 gallons per day per foot (gpd/ft). Falling and rising head tests were also conducted at directly adjacent monitoring well 8MNW17. The tests conducted at 8MNW17, using the same methods and equipment as well 8IW01, resulted in an average hydraulic conductivity of 1 foot per day and an average transmissivity of 85 gpd/ft.

The hydraulic conductivity and transmissivity results from both of these wells were relatively low and roughly correspond to a unit that is made up of silt, silty sand, and medium sand. Injection well 8IW01 appeared to be screened in the thickest part of the clayey gravel/gravelly clay lens, thus resulting in slightly higher hydraulic conductivity and transmissivities, while 8MNW17 and the temporary wells appeared to be screened on the edges of this clayey gravel/gravelly clay lens. The results of the test data support that the lithology of this unit was an aquiclude with many discontinuous coarse layers

4.7.2 Culture Conditions

During culture scale-up, SiREM provided samples of the scaled-up culture to UCLA to confirm 1,4-dioxane biodegradation. Upon receiving a subset of SiREM CB1190, cultures were fed 1,4-dioxane and incubated at 30 degrees Celsius (°C). Biodegradation kinetics in the seed culture were confirmed and microcosms were established for a new bioaugmentation event using SiREM and UCLA-prepared cultures of CB1190. The results without biomass normalization

indicated that SiREM cultures outperformed the strain prepared at UCLA. In addition, the nutrient amendments continued to be an integral factor that improves biodegradation performance.

To further investigate the differences in strain performance, samples were analyzed for the abundance of dioxane monooxygenase (DXMO), alcohol dehydrogenase (ALDH), and soluble methane monooxygenase (sMMO) genes related to 1,4-dioxane biodegradation. Gene *dxmB* and *aldH* were at least double the concentration in the SiREM cultures which could explain the improved rates of 1,4-dioxane biodegradation. Surprisingly, sMMO gene targets were quantified in SiREM CB1190 DNA extracts. While the concentrations are below the reporting limit for this assay, this result led us to test the purity of the SiREM CB1190 culture on Reasoner's 2A agar.

Plating cultures on R2A medium allows the growth of a wide range of bacteria. Identification of mixed cultures is determined based on the observation of different physical or morphological characteristics in the bacteria that colonize the petri dish, whereas pure cultures will appear uniform. Pure cultures of CB1190 typically grow in very small colonies with a white powder-like texture and these colonies are observed in the UCLA-prepared CB1190. However, SiREM cultures show several different bacteria displaying difference in color, shape, and texture indicating some level of mixed microbial growth. These results support the quantification of sMMO genes since this sequence should not be amplified in pure cultures of CB1190. Based on the 1,4-dioxane biodegradation ability of the SiREM-prepared CB1190 prepared culture, the presence of additional bacteria is not considered a concern.

4.8 References

Balba, M.T., Al-Awadhi, N., Al-Daher, R., 1998. Bioremediation of oil-contaminated soil: Microbiological methods for feasibility assessment and field evaluation. Journal of Microbiological Methods, 32 (2), 155-164.

Chen, B.L., Yuan, M.X., Qian, L.B., 2012. Enhanced bioremediation of PAH-contaminated soil by immobilized bacteria with plant residue and biochar as carriers. Journal of Soils and Sediments, 12 (9), 1350-1359.

Dzionek, A., Wojcieszynska, D., Guzik, U., 2016. Natural carriers in bioremediation: A review. Electronic Journal of Biotechnology, 23, 28-36.

El Fantroussi, S., Agathos, S.N., 2005. Is bioaugmentation a feasible strategy for pollutant removal and site remediation? Current Opinion in Microbiology, 8 (3), 268-275.

Figdore, B.A., Stensel, H.D., Winkler, M.-K.H., 2018. Comparison of different aerobic granular sludge types for activated sludge nitrification bioaugmentation potential. Bioresource Technology, 251, 189-196.

Gedalanga, P., Madison, A., Miao, Y., Richards, T., Hatton, J., DiGuiseppi, W.H., Wilson, J., Mahendra, S., 2016. A multiple lines of evidence framework to evaluate intrinsic biodegradation of 1,4-dioxane. Remediation Journal, 27 (1), 93-114.

Gedalanga, P.B., Pornwongthong, P., Mora, R., Chiang, S.Y.D., Baldwin, B., Ogles, D., Mahendra, S., 2014. Identification of biomarker genes to predict biodegradation of 1,4-dioxane. Applied and Environmental Microbiology, 80 (10), 3209-3218.

Innemanova, P., Filipova, A., Michalikova, K., Wimmerova, L., Cajthaml, T., 2018. Bioaugmentation of PAH-contaminated soils: A novel procedure for introduction of bacterial degraders into contaminated soil. Ecological Engineering, 118, 93-96.

Jiao, S., Liu, Z.S., Lin, Y.B., Yang, J., Chen, W.M., Wei, G.H., 2016. Bacterial communities in oil contaminated soils: Biogeography and co-occurrence patterns. Soil Biology & Biochemistry, 98, 64-73.

Ju, F., Lau, F., Zhang, T., 2017. Linking microbial community, environmental variables, and methanogenesis in anaerobic biogas digesters of chemically enhanced primary treatment sludge. Environmental Science & Technology, 51 (7), 3982-3992.

Li, M.Y., Conlon, P., Fiorenza, S., Vitale, R.J., Alvarez, P.J.J., 2011. Rapid analysis of 1,4-dioxane in groundwater by frozen micro-extraction with gas chromatography/mass spectrometry. Ground Water Monitoring and Remediation, 31 (4), 70-76.

Mahendra, S., Alvarez-Cohen, L., 2005. *Pseudonocardia dioxanivorans* sp nov., a novel actinomycete that grows on 1,4-dioxane. International Journal of Systematic and Evolutionary Microbiology, 55, 593-598.

Mahendra, S., Grostern, A., Alvarez-Cohen, L., 2013. The impact of chlorinated solvent co-contaminants on the biodegradation kinetics of 1,4-dioxane. Chemosphere, 91 (1), 88-92.

Mishra, S., Jyot, J., Kuhad, R.C., Lal, B., 2001. In situ bioremediation potential of an oily sludge-degrading bacterial consortium. Current Microbiology, 43 (5), 328-335.

Moslemy, P., Neufeld, R.J., Guiot, S.R., 2002. Biodegradation of gasoline by gellan gum-encapsulated bacterial cells. Biotechnology and Bioengineering, 80 (2), 175-184.

Myers, M.A., 2016. 1,4-Dioxane Biodegradation Using Bioaugmented Granular Activated Carbon, UCLA.

Myers, M.A., Johnson, N.W., Marin, E.Z., Pornwongthong, P., Liu, Y., Gedalanga, P.B., Mahendra, S., 2018. Abiotic and bioaugmented granular activated carbon for the treatment of 1,4-dioxane-contaminated water. Environmental Pollution, 240, 916-924.

Nyer, E.K., Payne, F., Suthersan, S., 2002. Environment vs. bacteria or let's play 'name that bacteria'. Ground Water Monitoring and Remediation, 23 (1), 36-45.

Obuekwe, C.O., Al-Muttawa, E.M., 2001. Self-immobilized bacterial cultures with potential for application as ready-to-use seeds for petroleum bioremediation. Biotechnology Letters, 23 (13), 1025-1032.

Onneby, K., Jonsson, A., Stenstrom, J., 2010. A new concept for reduction of diffuse contamination by simultaneous application of pesticide and pesticide-degrading microorganisms. Biodegradation, 21 (1), 21-29.

Parales, R.E., Adamus, J.E., White, N., May, H.D., 1994. Degradation of 1,4-dioxane by an *Actinomycete* in pure culture. Applied and Environmental Microbiology, 60 (12), 4527-4530.

Pornwongthong, P., Mulchandani, A., Gedalanga, P.B., Mahendra, S., 2014. Transition metals and organic ligands influence biodegradation of 1,4-dioxane. Applied Biochemistry and Biotechnology, 173 (1), 291-306.

Rahman, K.S.M., Banat, I.M., Thahira, J., Thayumanavan, T., Lakshmanaperumalsamy, P., 2002. Bioremediation of gasoline contaminated soil by a bacterial consortium amended with poultry litter, coir pith, and rhamnolipid biosurfactant. Bioresource Technology, 81 (1), 25-32.

Raper, E., Stephenson, T., Anderson, D., Fisher, R., Soares, A., 2018. Industrial wastewater treatment through bioaugmentation. Process Safety and Environmental Protection, 118, 178-187.

Safdari, M.S., Kariminia, H.R., Rahmati, M., Fazlollahi, F., Polasko, A., Mahendra, S., Wilding, W.V., Fletcher, T.H., 2018. Development of bioreactors for comparative study of natural attenuation, biostimulation, and bioaugmentation of petroleum-hydrocarbon contaminated soil. Journal of Hazardous Materials, 342, 270-278.

Szulc, A., Ambrozewicz, D., Sydow, M., Lawniczak, L., Piotrowska-Cyplik, A., Marecik, R., Chrzanowski, L., 2014. The influence of bioaugmentation and biosurfactant addition on bioremediation efficiency of diesel-oil contaminated soil: Feasibility during field studies. Journal of Environmental Management, 132, 121-128.

Tyagi, M., da Fonseca, M.M.R., de Carvalho, C.C.C.R., 2011. Bioaugmentation and biostimulation strategies to improve the effectiveness of bioremediation processes. Biodegradation, 22 (2), 231-241.

Wan, R., Wang, Z., Xie, S.G., 2014. Dynamics of communities of bacteria and ammonia-oxidizing microorganisms in response to simazine attenuation in agricultural soil. Science of the Total Environment, 472, 502-508.

Xu, X.H., Liu, X.M., Zhang, L., Mu, Y., Zhu, X.Y., Fang, J.Y., Li, S.P., Jiang, J.D., 2018. Bioaugmentation of chlorothalonil-contaminated soil with hydrolytically or reductively dehalogenating strain and its effect on soil microbial community. Journal of Hazardous Materials, 351, 240-249.

Zelezniak, A., Andrejev, S., Ponomarova, O., Mende, D.R., Bork, P., Patil, K.R., 2015. Metabolic dependencies drive species co-occurrence in diverse microbial communities. Proceedings of the National Academy of Sciences of the United States of America, 112 (51), E7156-E7156.

Zhang, S., Gedalanga, P.B., Mahendra, S., 2016. Biodegradation kinetics of 1,4-dioxane in chlorinated solvent mixtures. Environmental Science & Technology, 50 (17), 9599-9607.

Chapter 5 Comparison of Different Bioaugmentation and Biostimulation Strategies

5.1 Introduction

Soil and groundwater contamination with 1,4-dioxane are receiving increased regulatory attention due to its potential carcinogenicity and widespread occurrence at thousands of contaminated sites (Anderson et al., 2012, Suthersan et al., 2016). 1,4-Dioxane has been used as an industrial solvent for inks, adhesives, fats, waxes (Barajas-Rodriguez and Freedman, 2018), and also as an impurity in some industrial and personal care products such as antifreeze and aircraft deicing fluids, paints and varnishes, deodorants, shampoos, and detergents (Mohr et al., 2016). Because of the low Henry's Law constant and low organic carbon partitioning coefficient (Hatzinger et al., 2017), as well as hydrophilic and miscible characteristics, 1,4-dioxane has low adsorption to soil particles, and moves rapidly in the groundwater with large dilute plumes (Adamson et al., 2015). The heterocyclic structure of 1,4-dioxane's molecule with two ether band makes it refractory and resistant to biodegradation (Tian et al., 2014).

Bioremediation is a potential promising method for cleanup of 1,4-dioxane contaminated sites, because of the environmental friendly and effective cost without extra energy and chemical consumptions (Barajas-Rodriguez and Freedman, 2018), and both laboratory and field evidences have reported mineralization of 1,4-dioxane by microbiomes under various conditions (Zhang et al., 2016, Hatzinger et al., 2017). A wide variety of microbes have been studied well as 1,4-dioxane metabolizer that use it as the sole source of carbon and energy (McElroy and Hyman, 2019), and the best-characterized metabolizer is *Pseudonocardia dioxanivorans* CB1190, which is able to u completely mineralize 1,4-dioxane via a monooxygenase-catalyzed reaction, has been widely studied in laboratory for 1,4-dioxane removal kinetics (Mahendra and Alvarez-Cohen, 2005, Zhang et al., 2016). Moreover, co-metabolic pathway is also a non-toxic process (Mahendra et al.,

2007), that 1,4-dioxane can be catalyzed by bacteria grown on other carbon sources (Mahendra and Alvarez-Cohen, 2006). Among the primary substrates, tetrahydrofuran (THF) metabolizing strains were firstly studied to co-metabolize 1,4-dioxane because of the structural similarities between 1,4-dioxane and THF, and various bacteria were identified to co-metabolically degrade 1,4-dioxane after fed by THF, including *Rhodococcus ruber* 219 (Bock et al., 1996), T1 and T5 (Sei et al., 2013), *Pseudonocardia* sp. ENV478 (Vainberg et al., 2006), and K1 (Mahendra and Alvarez-Cohen, 2006). More co-metabolic degraders were found to grow based on alkanes, e.g., ethane metabolizer *Mycobacterium* ENV482 (Hatzinger et al., 2017), methane metabolizer *Methylosinus trichosporium* OB3b (Mahendra and Alvarez-Cohen, 2006), propane metabolizers *Mycobacterium austroafricanum* JOB5 (Lan et al., 2013) and *Rhodococcus ruber* ENV425 (Lippincott et al., 2015). However, the abundance of 1,4-dioxane biodegrading bacteria is low in sewage treatments plants (Gedalanga et al., 2014) and natural groundwater (Sei et al., 2010), implying that intrinsic biodegradation is not a viable remediation method (Lippincott et al., 2015), and likely to require a significant time investment if used as part of a long-term site management strategy (Adamson et al., 2015). Thus, engineered processes, bioaugmentation, which could compensate the insufficient functional microbes in the native conditions by adding pre-adapted pure bacterial strain, is the alternative for efficient and enhanced 1,4-dioxane removals.

Moreover, besides a competent microbe able to degrade the contaminant carbon source, other environmental parameters also must be taken into account e.g. water, oxygen, and utilizable nitrogen and phosphorous sources. Thus, biostimulation strategy, which could make up the environmental limitations in various contaminated sites (Chu et al., 2018), is considered to optimize biogeochemical parameters and accelerates the decontamination rate. The decision to implement either or both of these techniques for bioremediation largely depends on the degrading

capability of the indigenous microbes and the extent of contamination of the site to be treated (Tyagi et al., 2011), and both strategies have been applied to promote in-situ or bench-scale biodegradation of 1,4-dioxane at military bases (Lippincott et al., 2015, Sadeghi et al., 2016, Hatzinger et al., 2017). However, the direct comparisons among those strategies to stimulate 1,4-dioxane degradation, as well as influences on microbial ecology, are rarely reported, especially with the actual contaminated environmental samples.

The implementation of efficacious above-mentioned bioaugmentation and biostimulation strategies rely on artificially added degraders and intrinsic microbes, respectively, that can impact or be impacted by innate microbial community dynamics, structures, and functions (Kao et al., 2016). Thus, it is crucial to monitor the community to find out functional microbes that take charges of decontaminations, as well as contaminants or environmental factors that induce the shifts or of microbial community structures (Ju et al., 2017). Moreover, a complete degradation of the pollutants depends on the interaction of diverse microorganisms collectively and bacteria could evolve to utilize a variety of pollutants or byproducts (Shah et al., 2013), thus it's essential to check connections between and within functional guilds and linkages to performances (Vanwonterghem et al., 2014, Ju et al., 2017). Additionally, in the long-term view, the post bioaugmentation and biostimulation microbes will merge into natural condition and undertake fundamental biogeochemical cycles, thus the realistic environmental risk assessment of remaining microbes and further predictions of functioning are critical to evaluate the strategies before deployments (Miao et al., 2018). This next-generation sequencing (NGS) technology targeting on functional and sequence-based analysis of the collective microbial genomes has been widely used in researches related wastewater treatments (Miao et al., 2018), groundwater treatments (Kao et al., 2016), and soil remediations (Li et al., 2018), providing immense and comprehensive information regarding

bacterial community compositions and dynamics (Ju et al., 2017), as well as functional shifts (Liu et al., 2018). Therefore, sequencing technology is an enhanced tool to fulfill above molecular gaps from functional and structural aspects in specific 1,4-dioxane contaminated sites with bioaugmentation and biostimulation strategies.

The bench-scale study in this chapter tested the hypotheses that co-metabolism of 1,4-dioxane will induce different microbial community and functional genes changes with metabolic process, and biostimulation with oxygen and propane will enhance biodegradation of 1,4-dioxane. Besides, inorganic nutrient addition was set as additive to biostimulation process since insufficient quantities of inorganic nutrients, such as nitrogen and phosphate, have previously been observed to limit the biodegradation of 1,4-dioxane in environments (Lippincott et al., 2015). Conventional biotechnology and amplicon sequencing were used to explore basic knowledge of biodegradation from molecular aspects and to expand understanding of the dynamic microbial systems found in 1,4-dioxane contaminated environments. This controlled condition study can provide insight about the microbes and their growth requirements, before any on-site intervention for decontamination is carried out, thus, the results will serve as theoretical supports for future in-situ metabolic and co-metabolic biological treatment strategies for 1,4-dioxane.

5.2 Materials and Methods

5.2.1 Site Description

The contaminated site is located at Northern US, working as an industrial land with vehicle factories and productions during 1985-2006. The 1,4-dioxane contamination source was located south of the area known as the “coliseum”. The coliseum is a subfloor of the former Plant structure that was constructed to a depth of 15 to 20 feet below grade, formerly used to house equipment for stamping automobile parts. The lower 1,4-dioxane plumes was approximately 2,400 feet long and

migrated from the source to the south-southwest within the deep overburden and weathered bedrock zones at depths typically between 65 to 75 ft below ground surface, and the 1,4-dioxane's concentration was up to 510 μg/L.

5.2.2 Culture Preparations

1,4-Dioxane metabolizer *Pseudonocardia dioxanivorans* CB1190 (CB1190) was incubated in the sterilized 1 L conical baffled flask with 200 mL ammonium mineral salts (AMS) medium solution (Parales et al., 1994) and 100 mg/L 1,4-dioxane; meanwhile, co-metabolizing propanotrophic bacterium, *Rhodococcus ruber* ENV425 (ENV425), was grown in sterile 1 L serum bottles with septa and crimp seals, with 200 mL AMS and 10% (vol/vol) headspace propane serving as sole carbon and energy source. All cultures were incubated at 30°C in a rotating incubator with shaking speed of 150 rpm, and concentrations of 1,4-dioxane (liquid) and propane (gas in headspace) in bottles were monitored over time using a Hewlett-Packard 6890 gas chromatograph equipped with a flame ionization detector (GC-FID) (Agilent Technologies, Santa Clara, CA, USA). CB1190 was treated with 1,4-dioxane to grow and harvested when 1,4-dioxane degradation rate reached ~80 mg/L/day. ENV425 was kept feeding propane to maintain viability and harvested when optimal density was over 3.0 (NanoDrop® ND-1000, NanoDrop Technologies, Willmington, DE, USA), then washed three by fresh AMS medium with 1:5 volume ratio to remove extracellular polymeric substances (EPSs) before using in microcosm study.

5.2.3 Microcosm Establishments and Operations

Total five experimental sets of microcosms were established with four duplicated in each condition, including killed control, bioaugmentation with CB1190, bioaugmentation with ENV425, biostimulation with oxygen, and biostimulation with propane. The actual site materials were assembled in 1 L glass serum bottles sealed by screw-cap Mininert™ valves to allow repetitive

samplings and the addition of amendments, e.g., oxygen, propane, 1,4-dioxane, etc. Approximately 50g homogenized soil were added to each bottle, and 250 mL site groundwater were added into biostimulation bottles, while 225 mL site groundwater as well as 25 mL cultures were added into bioaugmentation bottles. Around 20% (vol/vol) headspace propane (~12 mg/L dissolved propane) was sparged into propane-biostimulation bottles, and was re-sparged periodically. Similarly, oxygen was also sparged when dissolved oxygen was below 3 mg/L. The extra AMS were added in biostimulation bottles after 90 days, to test the impact of nutrients on 1,4-dioxane removals under biostimualtion conditions. In bioaugmentation conditions, 1,4-dioxane was added periodically to keep bacterial viability and test the reproducibility.

5.2.4 Sample Collections, Analytic Measurements, and Molecular Experiments

The mixed slurry samples (1000 μL) were collected along with microcosm operations, and stored at −80°C before further analysis. 1,4-Dioxane was extracted by using frozen micro-extraction method (Li et al., 2011), and measured on a Hewlett-Packard 6890 Chromatograph Plus coupled with a mass spectrometer detector and Supelco SPB-1 column (30 m x 0.53 mm id x 1 μm) by a 7693A ALS autosampler under pulse splitless mode, following parameters and methods in previous study (Miao et al., 2018). Dissolved oxygen was measured by using an oxygen and carbon dioxide analyzer (Quantek Instrument, Grafton, MA), while propane was measured by direct headspace injection using a GC-FID. The total nucleic acids were extracted from 500 μL slurry samples based on modified phenol/chloroform/isoamyl alcohol method (Gedalanga et al., 2016), and RNA reverse transcription was performed by using EasyScript Plus^{TM} cDNA Synthesis Kit (Lamda Biotech, St. Louis, MO, USA) after DNA was removed by using RapidOut DNA Removal Kit (Thermo Fisher Scientific, Waltham, MT, USA) according to the manufacturer's introductions. The DNA or RNA extracts of four triplicates bottles were mixed before quantitative polymerase chain reaction (qPCR),

with four pairs of primer (Table 5.1) targeting on total 16S rRNA gene, and functional biomarker genes, dioxane monooxygenase (DXMO) gene (*dxmB*), propane monooxygenase (PrMO) gene (*prmA*), and aldehyde dehydrogenase (ALDH) gene (*aldH*). All qPCR reactions were processed in 20 μL system using Luminaris^{TM} Color HiGreen master mixes (Thermo Fisher Scientific, Waltham, MT, USA), following previous established programs for each gene (Gedalanga et al., 2014, Miao et al., 2019).

Table 5.9. Gene primers and annealing temperatures.

Gene/Enzyme	For-Primer (5'→3')	Rev-Primer (5'→3')	Annealing temperature (°C)
dxmB/dioxane monooxygenase (DXMO)	CCAAACGGGCGTCAGTCAT	AGAACGTGCGCTCCCAAAG	60
aldH/aldehyde dehydrogenase (ALDH)	ACCAAGGACCTCACCTCGTA	AACGGATGCGCGTTGTTC	60
prm1A/propane monooxygenase (PrMO)	GAAGAGTCGTGGAAGCAGATC	GTACTTGTACTCGAACCACTCG	58
Universal 16S rRNA gene	ATGGCTGTCGTCAGCT	ACGGGCGGTGTGTAC	53

5.2.5 Amplicon Sequencing and Data Analysis

The hypervariable V4 region of 16S rRNA gene of each sample was amplified triplicate with region-specific primers that included the Illumina flow-cell adapter based on protocol present in (Caporaso et al., 2012), and the amplicons belonging to the same sample were pooled in equimolar mass and sequenced in duplicate per sample on Illumina Miseq platform (Laragen, Inc., Culver City, CA, USA) with Miseq V4 regents and PE250 strategy (pair-end sequenced 2 × 250).

The generated 16S rRNA gene reads were analyzed by Mothur workflow (Schloss et al., 2009) following previous established pipeline (Miao et al., 2018, Miao et al., 2019). The contigs were assembled from paired-end reads by using "make.contigs". Then the successfully formed contigs were trimmed by using "trim.seqs" with zero ambiguous bases and an average quality cutoff at 30 (Chao et al., 2016). Sequencing reads were denoised with chimera, Chloroplast-Mitochondria-

unknown-Archaea-Eukaryota reads and the length was permitted at ~300 bp with the maximum number of homopolymers per sequence at 8. The filtered reads were assigned to OTUs based on average neighbor algorithm in cluster process with greater than or equal to 97% sequence identity, and then were taxonomically classified with Silva 16S rRNA gene training set (v128), while the OTU with less than 10 reads were excluded from downstream analyses. Although the analyses were processed using the relative abundance, each sample was randomly sub-sampled to normalize the reads number at 25000. Afterwards, the results were assembled into one OTU-table with abundances information of individual OTUs and higher taxon under all conditions.

The microbial composition was based on the OTU-table and visualized on circular phylogenetic trees for direct comparisons among different samples by using "metacoder" package (Foster et al., 2017, Miao et al., 2017). The α-diversity was represented by rarefaction curve based on Mothur, and the β-diversity including Bray-Curtis dissimilarity index, weighted and unweighted Unifrac distances were calculated and visualized on non-metric multidimensional scaling (NMDS) and principal coordinate analysis (PCoA) by R (v3.5.0) with "phyloseq" package (McMurdie and Holmes, 2013, Miao et al., 2019). To compare the community correlation between CB1190 and ENV425 bioaugmentation conditions, as well as oxygen and propane biostimulation conditions, procrustes analysis was performed using the protest function with 999 permutations to verify significance based on OTU-table by R (v3.5.0) with "vegan" and "labdsv" packages. The M^2 value is the sum of the squared distances between matched sample pairs, and the P value was obtained by recalculating the M^2 value and comparing the original M^2 value with the simulated distribution (Zhao et al., 2018).

To better understand the potential functional features from the observed microbes in the bioaugmentation and biostimulation processes, the 16S rRNA gene sequences were used to calculate

the metabolic cycles and pathways in the Kyoto Encyclopedia of Genes and Genomes (KEGG) by the "tax4fun2" package in R (v3.5.0) (Wemheuer et al., 2018). The package depends on assigning the OTUs to reference sequences in the NCBI RefSeq database, and the taxonomic abundance were transformed to metabolic capabilities using the pre-computed KEGG profiles, obtaining the relative abundance of the enzyme-encoding genes in KEGG pathways and orthologues.

The network analysis was used to show the correlations between OTUs and functions, including pathways or monooxygenase-encoding genes. A correlation matrix was constructed based on the all possible pairwise Spearman's rank correlations, with correlation coefficient (ρ) over 0.8 and P value less than 0.01 (Ju et al., 2017), after adjusting the P values with reduced positive false discovery rate (FDR) (Benjamini and Hochberg, 1995). Then, all the statistically robust pairwise correlations were input into the interactive platform Gephi (v 0.9.2) (Bastian et al., 2009), and the nodes were colored according to taxa or functions and proportional to the number of connections.

5.3 Results

5.3.1 1,4-Dioxane Removal Performances

Bioaugmented CB1190 and ENV425 showed efficient removal performances that degraded ~90% 1,4-dioxane in 1.5 days, which was below detection limits within 7 days (Figure 5.1A). More 1,4-dioxane was spiked at day 15 to replenish the contaminant concentration at ~550 µg/L, and was undetectable when measured at day 30. Under biostimulation within 7 days, 1,4-dioxane was rapidly degraded from 345 µg/L to 251 µg/L after initial propane addition, and decreased from 354 µg/L to 235 µg/L in the bottles aerated with oxygen (Figure 5.1A). Afterwards, 1,4-dioxane removals tended to be fluctuated under both conditions in the rest of experiments, and finally reached to 170 µg/L and 207 µg/L under oxygen and propane stimulation, respectively. However, after 90 days when more ammonia and phosphate nutrients were added in oxygen and propane bottles respectively,

biostimulation with propane achieved significant 1,4-dioxane removals within 60 days, while oxygen biostimulated bottles only showed steadily decreases of 1,4-dioxane, and substantial oxygen and propane usages were also observed (Figure 5.1B and 5.1C).

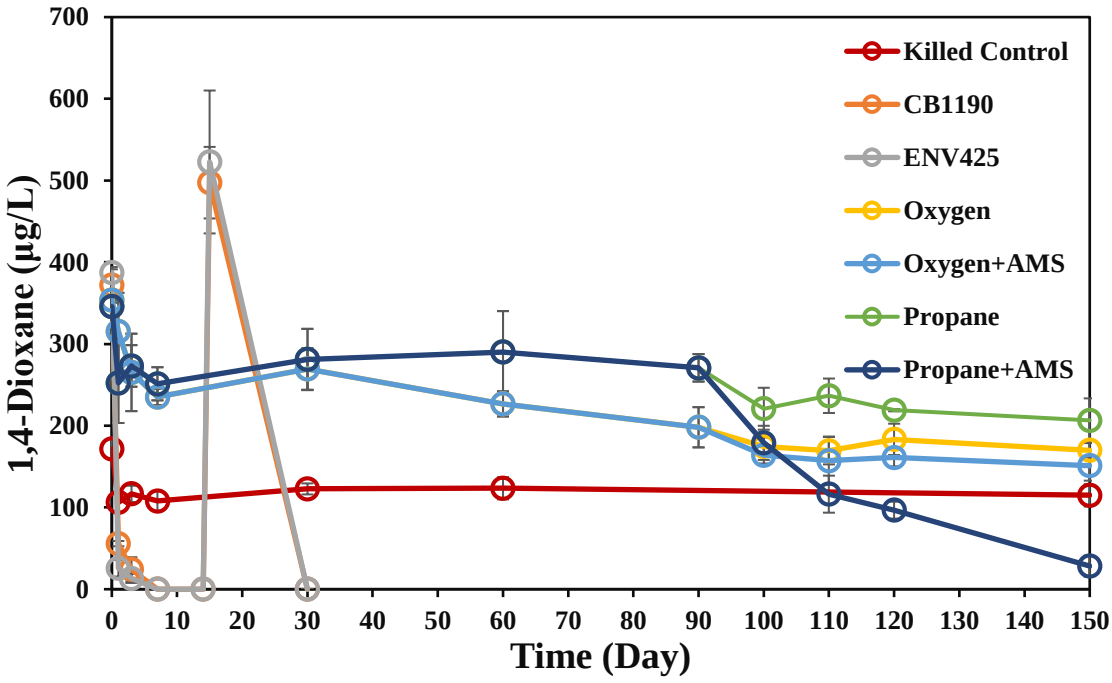

A

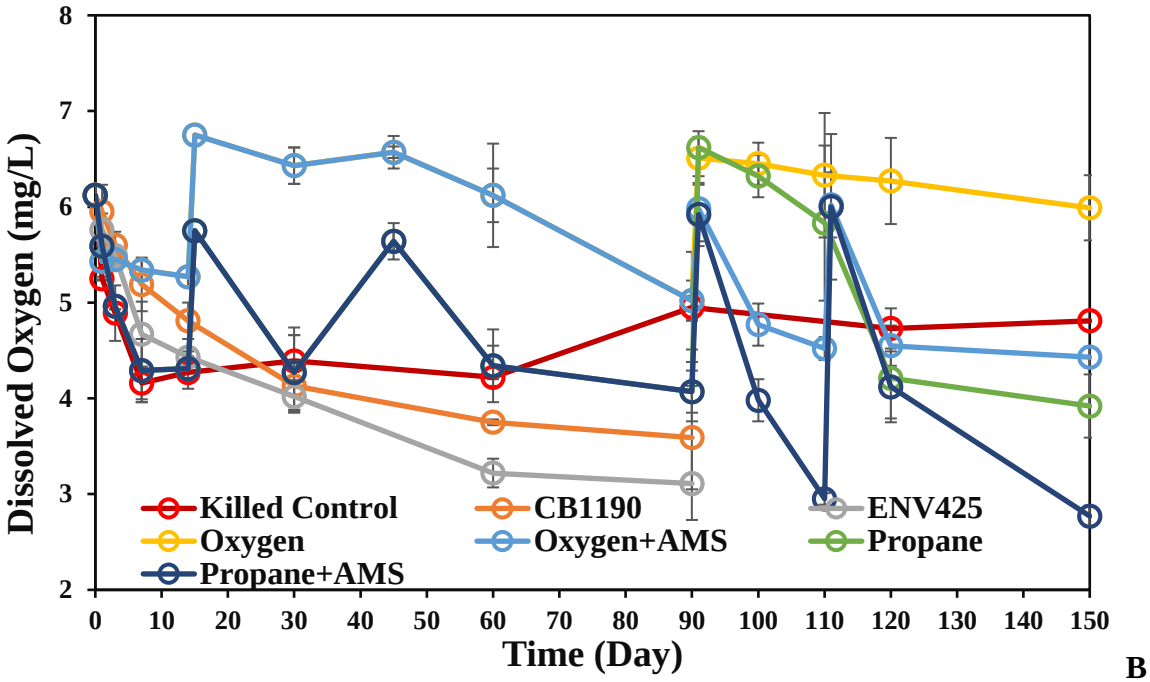

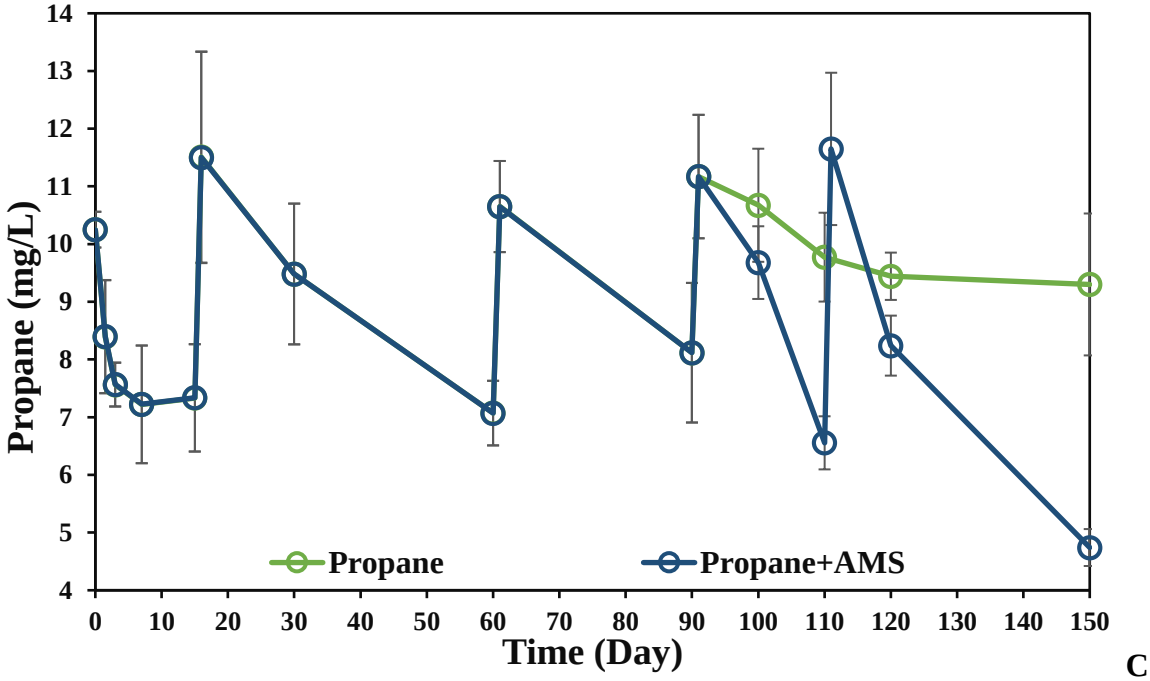

Figure 5.42. 1,4-Dioxane removals (A), dissolved oxygen levels (B), and propane concentrations (C) under all conditions during the treatment process.

Dissolved oxygen was consumed in 30 days for both bioaugmentation treatments, but ENV425 bottles had higher consumption rate at 0.067 $mg \cdot L^{-1} \cdot day^{-1}$ (Figure 5.1B). This indicated equal

performance of metabolic and co-metabolic processes on these environmental samples, and showed the potential continuous capabilities to biodegrade 1,4-dioxane in bioaugmented microcosms even after one week (day 8-15) when 1,4-dioxane was below the detection level. Propane was observed to be degraded but without 1,4-dioxane degradation in biostimulation microcosms, and dissolved oxygen was reduced faster under propane stimulation in the first week, along with the relatively fast 1,4-dioxane removal, and periodically sparging with ~12 mg/L propane seemed to enhanced oxygen reductions. Higher rates of oxygen and propane consumptions were observed after nutrient additions in biostimulation bottles, indicating the thrive of propanotrophs or other aerobic microbes.

5.3.2 Functional Biomarker Genes

Three functional biomarker genes were picked to analyze and indicate the 1,4-dioxane biodegradation potentials under different conditions during the treatment. Bioaugmented ENV425 and CB1190 initially elevated biomass, followed by a decreasing abundance of total bacteria over time that could be dependent on the bioavailable substances in microcosms (Figure 5.2A). Meanwhile, biomass in CB1190 added microcosms showed lower abundance than that at ENV425 microcosms, indicating the potential wider carbon sources for ENV425's growth. Biomass under biostimulation slightly increased along with time, demonstrating the lag period of indigenous bacteria responding to oxygen and propane. Moreover, the rapid growth of biomass was observed when nutrients were added under biostimulation, illuminating the limits of nutrients for these environmental samples.

The *dxmB* genes were abundant and expressed only in CB1190 bioaugmented microcosms, while lower under other conditions (Figure 5.2B), but the relative expression of *dxmB* were inhibited at day 7 and day 30. Interestingly, *dxmB*'s relative expression was stimulated after nutrients were added in non-bioaugmented microcosms, indicating the potential role of indigenous microorganisms

carrying *dxmB*-like monooxygenase in removing 1,4-dioxane from these samples. The *aldH* genes had higher abundance and relative expression than that of *dxmB* (Figure 5.2D), and *aldH*'s relative expression was kept high under propane sparged condition. Gene *prmA* was abundant under ENV425 bioaugmented conditions, but less from indigenous propanotrophic bacteria, but were stimulated upon nutrient addition after 90 days in propane biostimulated bottles (Figure 5.2C).

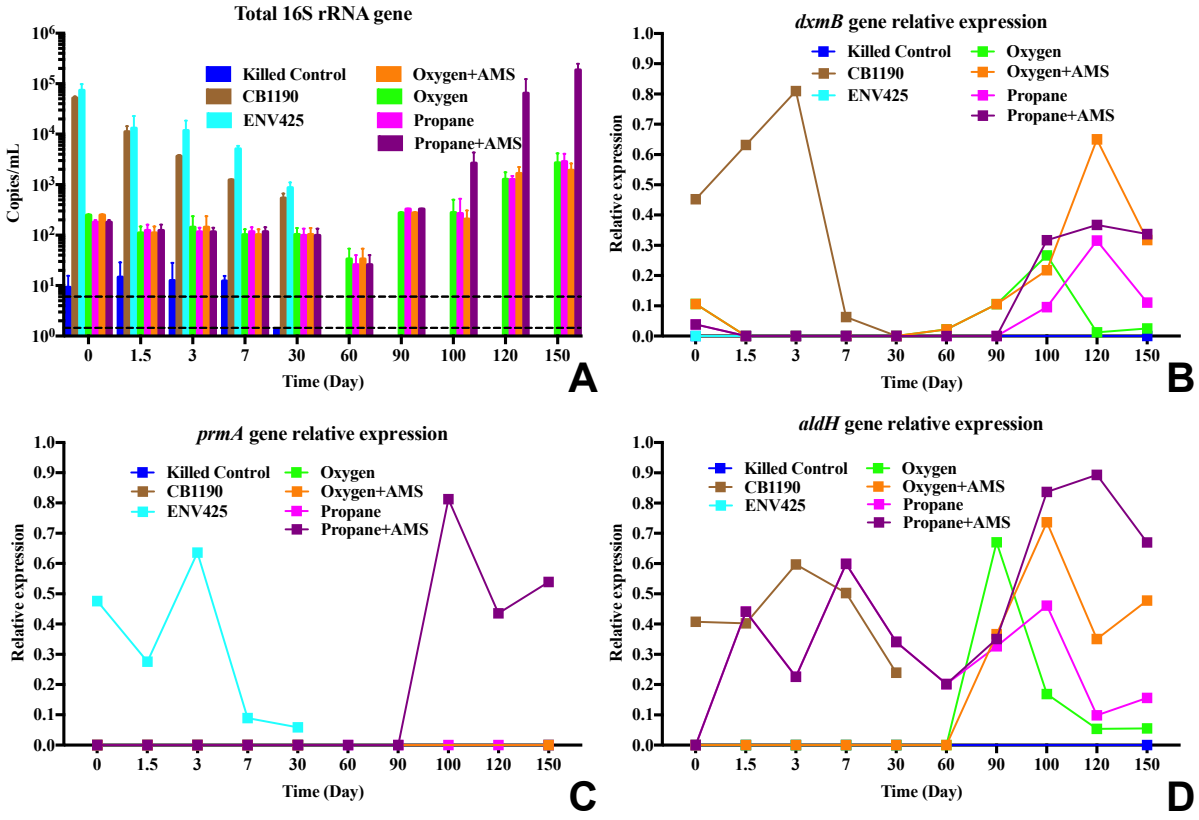

Figure 5.43. The abundance of total 16S rRNA gene (A), and relative expression of dioxane monooxygenase gene *dxmB* (B), propane monooxygenase gene *prmA* (C), and aldehyde dehydrogenase gene *aldH* (D). The relative expression was calculated based on ratio of gene transcript abundance to gene abundance.

5.3.3 Microbial Diversity, Composition, and Interaction

The alpha biodiversity was represented by rarefaction curves showing that the diversity under bioaugmentation conditions were thrived at certain time points. In ENV425 bioaugmented bottles,

biodiversity was high at day 3 and day 60 (Figure 5.3), indicating the degradation of 1,4-dioxane as well as other hydrocarbons, and accumulated byproducts fed other indigenous microorganisms. However, biodiversity was highest at day 60 with CB1190 bioaugmentation, and could be attributed that more 1,4-dioxane was added (~550 μg/L) at day 15, thus the bacteria might have used the 1,4-dioxane and its intermediates to grow and peak at day 60. After that, lack of carbon sources might restrict the biodiversity, and the microbial community experienced lag phase over time. Under oxygen biostimulation, biodiversity was obviously increased after 150 days, both under w/ and w/o nutrients conditions. The trend of biodiversity could be attributed to thriving of minor indigenous microorganisms, that utilized hydrocarbons and nutrient amendment. However, microbial competition, lag responses to O_2, as well as different O_2 consumptions might result in thrive or elimination of microbes, that fluctuated biodiversity in the first 90 days. Surprisingly, biodiversity under propane biostimulation was stable for the first few days, but blossomed at 30 days, that could be related to the rapid 1,4-dioxane removals in the first 7 days and suggest microorganisms were active potentially resulting in the generation of more intermediates. However, biodiversity stared to decrease after 30 days, indicating the dominance of propanotrophs along with propane sparging that occupied more nutrients in original samples.

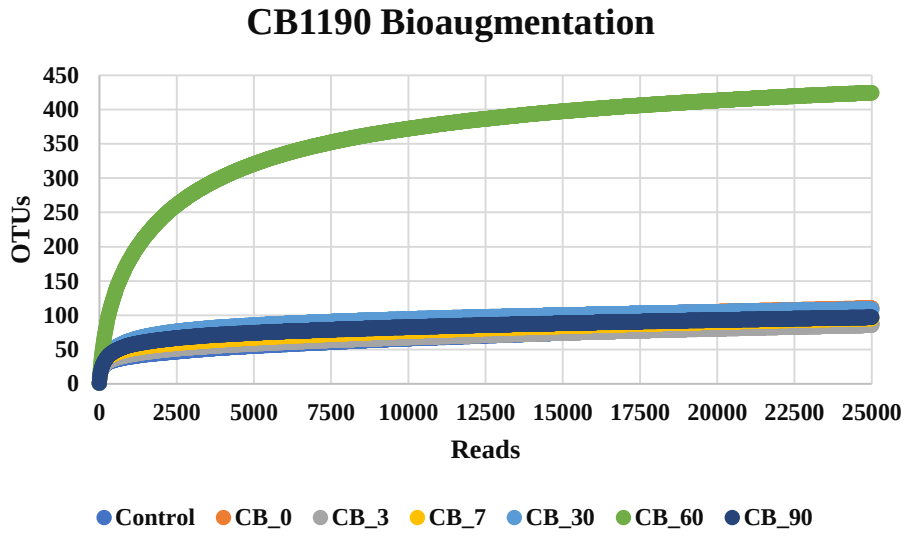
CB1190 Bioaugmentation
OTUs
450
400
350
300
250
200
150
100
50
0
0
2500
5000
7500
10000
12500
15000
17500
20000
22500
25000
Reads
Control
CB_0
CB_3
CB_7
CB_30
CB_60
CB_90

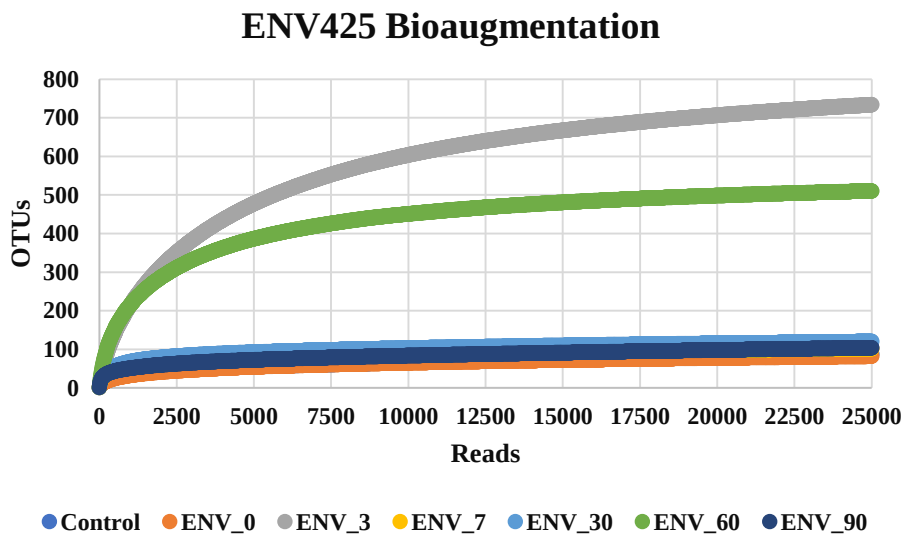
ENV425 Bioaugmentation
OTUs
800
700
600
500
400
300
200
100
0
0
2500
5000
7500
10000
12500
15000
17500
20000
22500
25000
Reads
Control
ENV_0
ENV_3
ENV_7
ENV_30
ENV_60
ENV_90

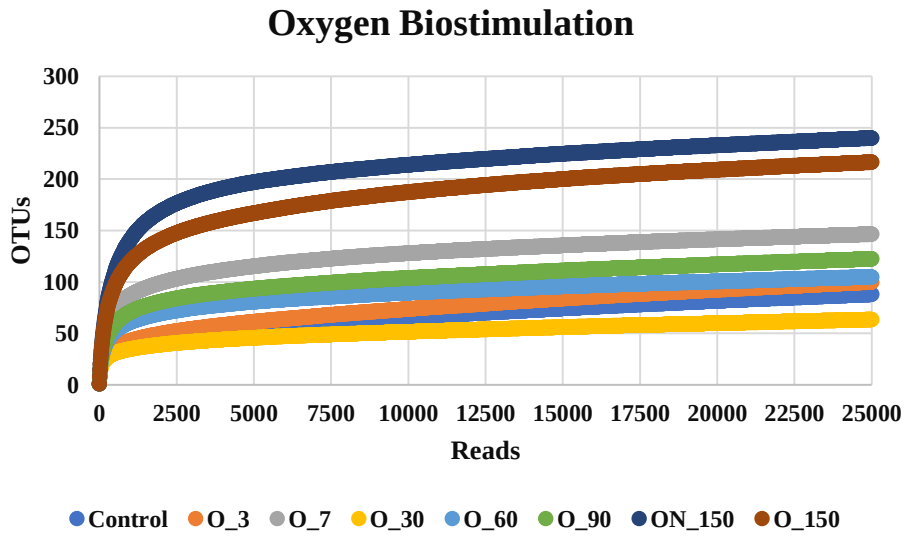
Oxygen Biostimulation
OTUs
300
250
200
150
100
50
0
0
2500
5000
7500
10000
12500
15000
17500
20000
22500
25000
Reads
Control
O_3
O_7
O_30
O_60
O_90
ON_150
O_150

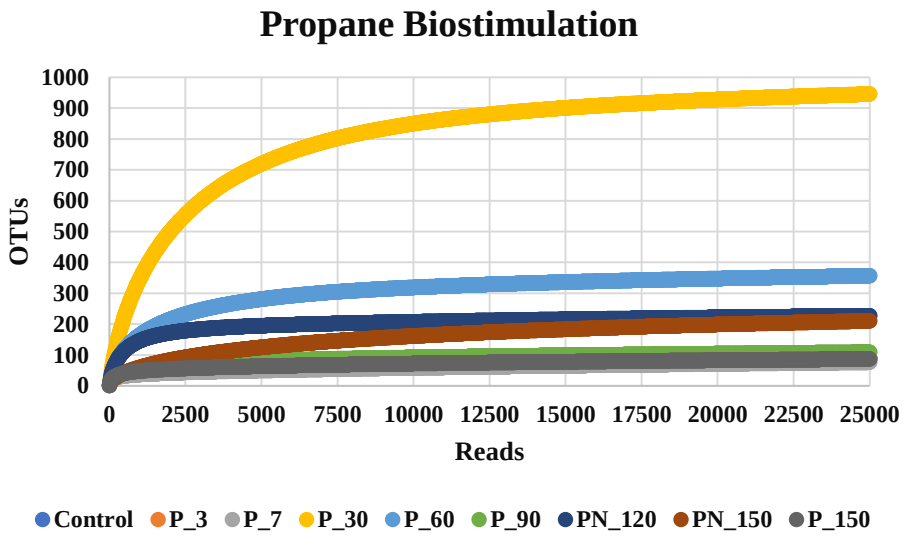

Figure 5.44. Rarefaction curve represents the α diversity under all conditions.

The taxonomic classification at taxon level showed all detected microbes in phylogenetic trees under CB1190-bioaugmentation (Figure 5.4) and ENV425-bioaugmentation (Figure 5.5) condition over time, describing the shift of microbial compositions. The original unamended slurry mainly contained genera *Hydrogenobacter* (20.58%), *Aeribacillus* (8.65%), *Staphylococcus* (7.80%), *Stenotrophomonas* (7.69%), and *Bacillus* (7.14%). The bioaugmented *Pseudonocardia* and *Rhodococcus* immediately became the dominant bacterium after spiking into microcosms, occupying 36.96% and 78.61% of the microbial community, respectively, but both dominant microorganisms eventually decreased with time. Genus *Rhodococcus* decreased relatively slower and was still dominant at day 30 with 23.38% of the total population, while genus *Pseudonocardia* was eliminated rapidly and dropped to 1.12% in 3 days, then, microbial compositions fluctuated along with time and under both bioaugmentations.

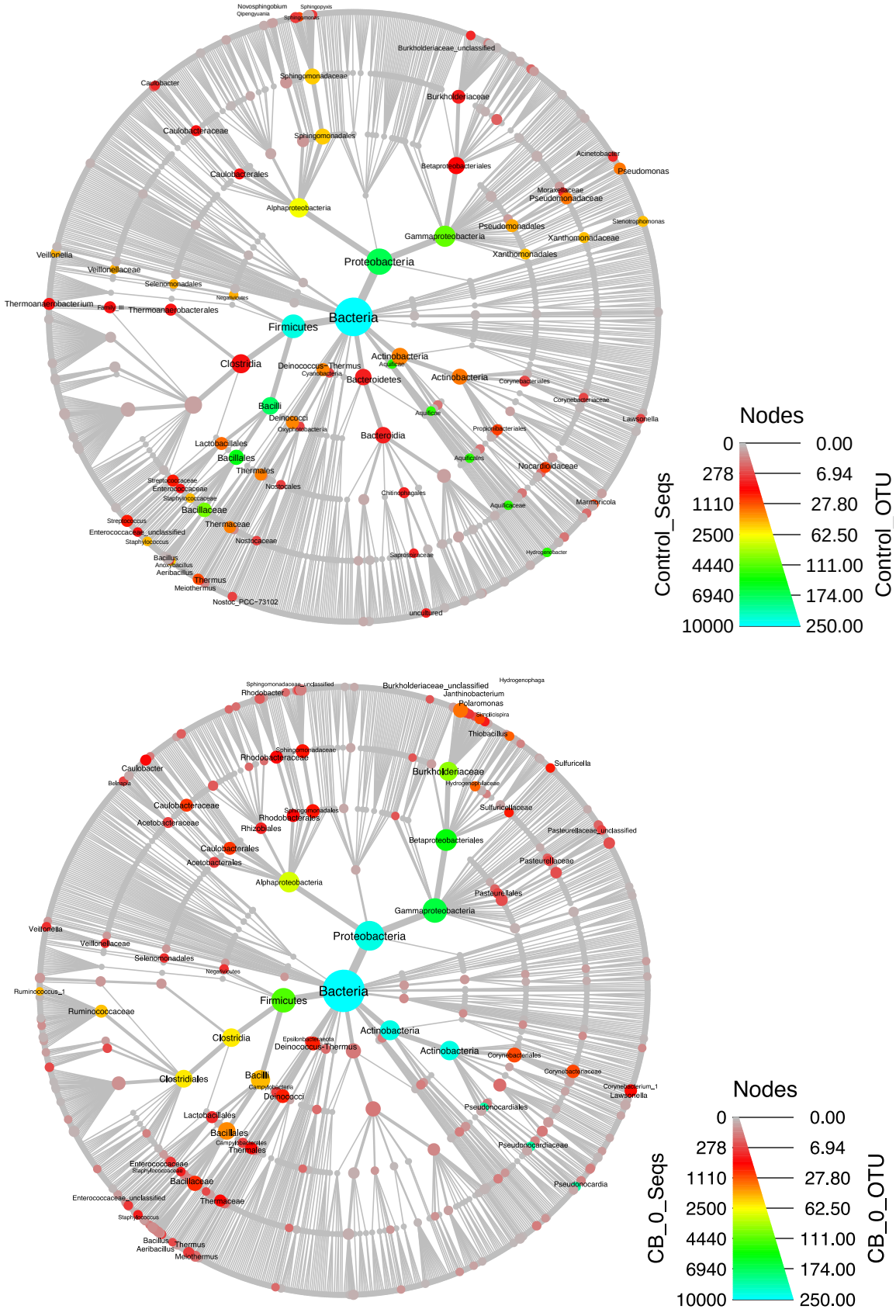
Bacteria
Proteobacteria
Firmicutes
Actinobacteria
Bacteroidetes
Alphaproteobacteria
Gammaproteobacteria
Betaproteobacteriales
Burkholderiaceae
Burkholderiaceae_unclassified
Sphingomonadaceae
Caulobacteraceae
Caulobacterales
Sphingomonadales
Pseudomonadales
Pseudomonadaceae
Xanthomonadaceae
Xanthomonadales
Moraxellaceae
Acinetobacter
Pseudomonas
Stenotrophomonas
Lawsonella
Veillonellaceae
Veillonella
Selenomonadales
Negativicutes
Thermoanaerobacterium
Thermoanaerobacterales
Family_III
Clostridia
Deinococcus-Thermus
Deinococci
Cyanobacteria
Oxyphotobacteria
Bacteroidia
Bacilli
Lactobacillales
Bacillales
Thermales
Streptococcaceae
Enterococcaceae
Staphylococcaceae
Streptococcus
Enterococcaceae_unclassified
Staphylococcus
Bacillaceae
Bacillus
Anoxybacillus
Aeribacillus
Thermaceae
Thermus
Meiothermus
Nostocales
Nostocaceae
Nostoc_PCC-73102
Chitinophagales
Saprospiraceae
uncultured
Aquificae
Aquificales
Aquificaceae
Hydrogenobacter
Propionibacteriales
Corynebacteriales
Corynebacteriaceae
Nocardioidaceae
Marmoricola
Novosphingobium
Qipengyuania
Sphingopyxis
Sphingomonas
Caulobacter
Nodes
0
278
1110
2500
4440
6940
10000
0.00
6.94
27.80
62.50
111.00
174.00
250.00
Control_Seqs
Control_OTU
Sphingomonadaceae_unclassified
Rhodobacter
Hydrogenophaga
Janthinobacterium
Polaromonas
Pirellulales
Thiobacillus
Rhodobacteraceae
Caulobacter
Belnapia
Caulobacteraceae
Acetobacteraceae
Rhodobacterales
Rhizobiales
Caulobacterales
Acetobacterales
Sulfuricella
Sulfuricellaceae
Hydrogenophilaceae
Pasteurellaceae_unclassified
Pasteurellaceae
Pasteurellales
Ruminococcus_1
Ruminococcaceae
Clostridia
Clostridiales
Epsilonbacteraeota
Campylobacteria
Campylobacterales
Pseudonocardiales
Pseudonocardiaceae
Pseudonocardia
Corynebacterium_1
CB_0_Seqs
CB_0_OTU

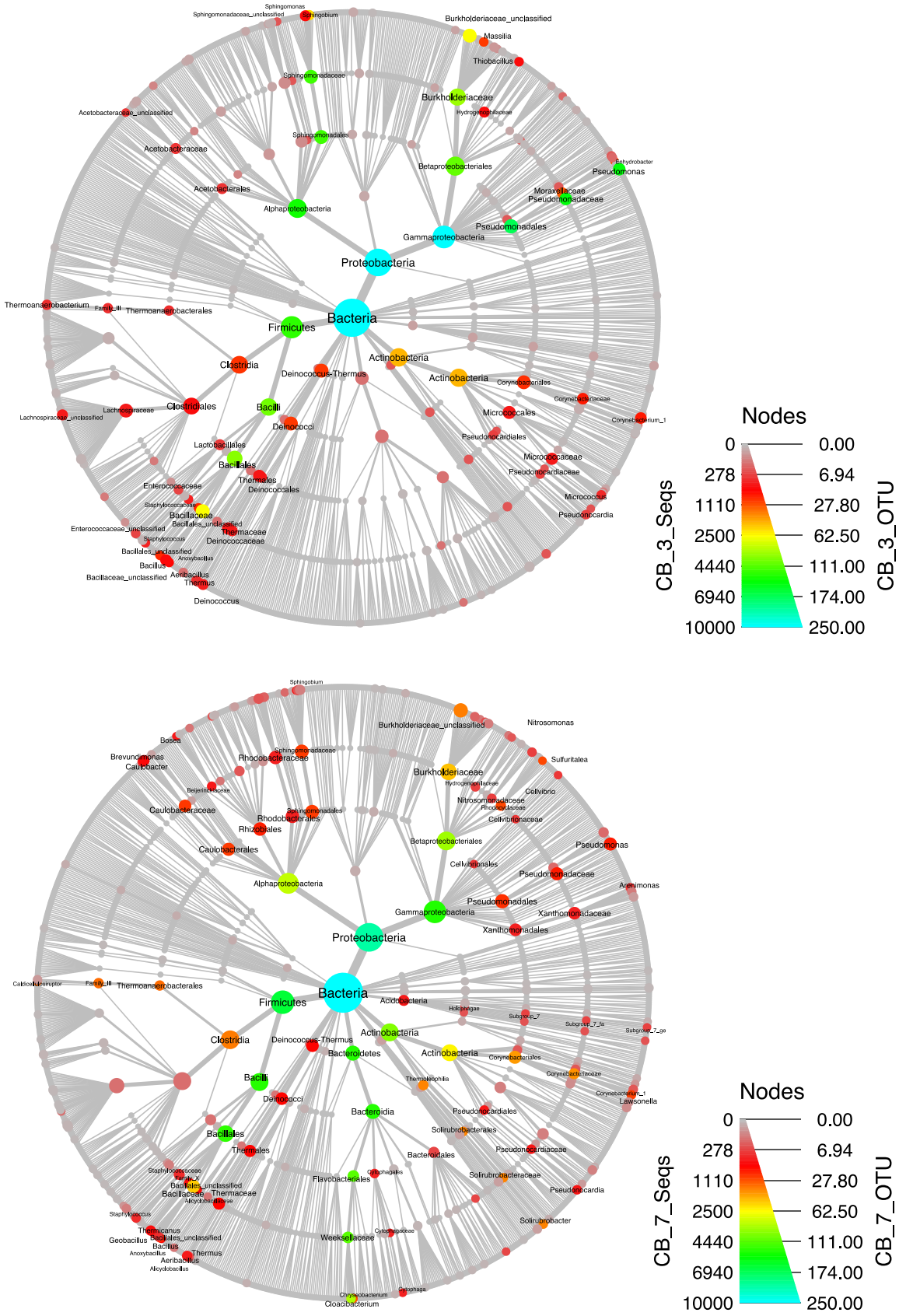
Sphingomonas
Sphingomonadaceae_unclassified
Sphingobium
Burkholderiaceae_unclassified
Massilia
Thiobacillus
Sphingomonadaceae
Burkholderiaceae
Hydrogenophilaceae
Acetobacteraceae_unclassified
Sphingomonadales
Acetobacteraceae
Betaproteobacteriales
Ephydrobacter
Pseudomonas
Acetobacterales
Moraxellaceae
Pseudomonadaceae
Alphaproteobacteria
Pseudomonadales
Gammaproteobacteria
Proteobacteria
Thermoanaerobacterium
Family_III
Thermoanaerobacterales
Bacteria
Firmicutes
Actinobacteria
Clostridia
Deinococcus-Thermus
Actinobacteria
Corynebacteriales
Corynebacteriaceae
Clostridiales
Lachnospiraceae
Lachnospiraceae_unclassified
Bacilli
Micrococcales
Corynebacterium_1
Deinococci
Pseudonocardiales
Lactobacillales
Micrococcaceae
Bacillales
Pseudonocardiaceae
Thermales
Enterococcaceae
Deinococcales
Micrococcus
Staphylococcaceae
Pseudonocardia
Bacillaceae
Bacillales_unclassified
Enterococcaceae_unclassified
Thermaceae
Staphylococcus
Deinococcaceae
Bacillales_unclassified
Anoxybacillus
Bacillus
Aeribacillus
Bacillaceae_unclassified
Thermus
Deinococcus
Nodes
0
278
1110
2500
4440
6940
10000
0.00
6.94
27.80
62.50
111.00
174.00
250.00
CB_3_Seqs
CB_3_OTU
Sphingobium
Burkholderiaceae_unclassified
Nitrosomonas
Bosea
Sulfuritalea
Brevundimonas
Sphingomonadaceae
Rhodobacteraceae
Caulobacter
Burkholderiaceae
Hydrogenophilaceae
Beijerinckiaceae
Cellvibrio
Nitrosomonadaceae
Caulobacteraceae
Sphingomonadales
Rhodobacterales
Rhodocyclaceae
Cellvibrionaceae
Rhizobiales
Betaproteobacteriales
Caulobacterales
Pseudomonas
Cellvibrionales
Pseudomonadaceae
Alphaproteobacteria
Arenimonas
Pseudomonadales
Gammaproteobacteria
Xanthomonadaceae
Xanthomonadales
Proteobacteria
Caldicellulosiruptor
Family_III
Thermoanaerobacterales
Bacteria
Firmicutes
Acidobacteria
Holophagae
Subgroup_7
Subgroup_7_fa
Subgroup_7_ge
Clostridia
Deinococcus-Thermus
Actinobacteria
Bacteroidetes
Actinobacteria
Corynebacteriales
Corynebacteriaceae
Bacilli
Thermoleophilia
Corynebacterium_1
Deinococci
Lawsonella
Bacteroidia
Pseudonocardiales
Solirubrobacterales
Bacillales
Thermales
Pseudonocardiaceae
Bacteroidales
Staphylococcaceae
Cytophagales
Solirubrobacteraceae
Flavobacteriales
Pseudonocardia
Bacillales_unclassified
Bacillaceae
Thermaceae
Alicyclobacillaceae
Staphylococcus
Solirubrobacter
Thermicanus
Geobacillus
Bacillales_unclassified
Weeksellaceae
Cytophagaceae
Bacillus
Anoxybacillus
Thermus
Aeribacillus
Alicyclobacillus
Chryseobacterium
Cytophaga
Cloacibacterium
Nodes
0
278
1110
2500
4440
6940
10000
0.00
6.94
27.80
62.50
111.00
174.00
250.00
CB_7_Seqs
CB_7_OTU

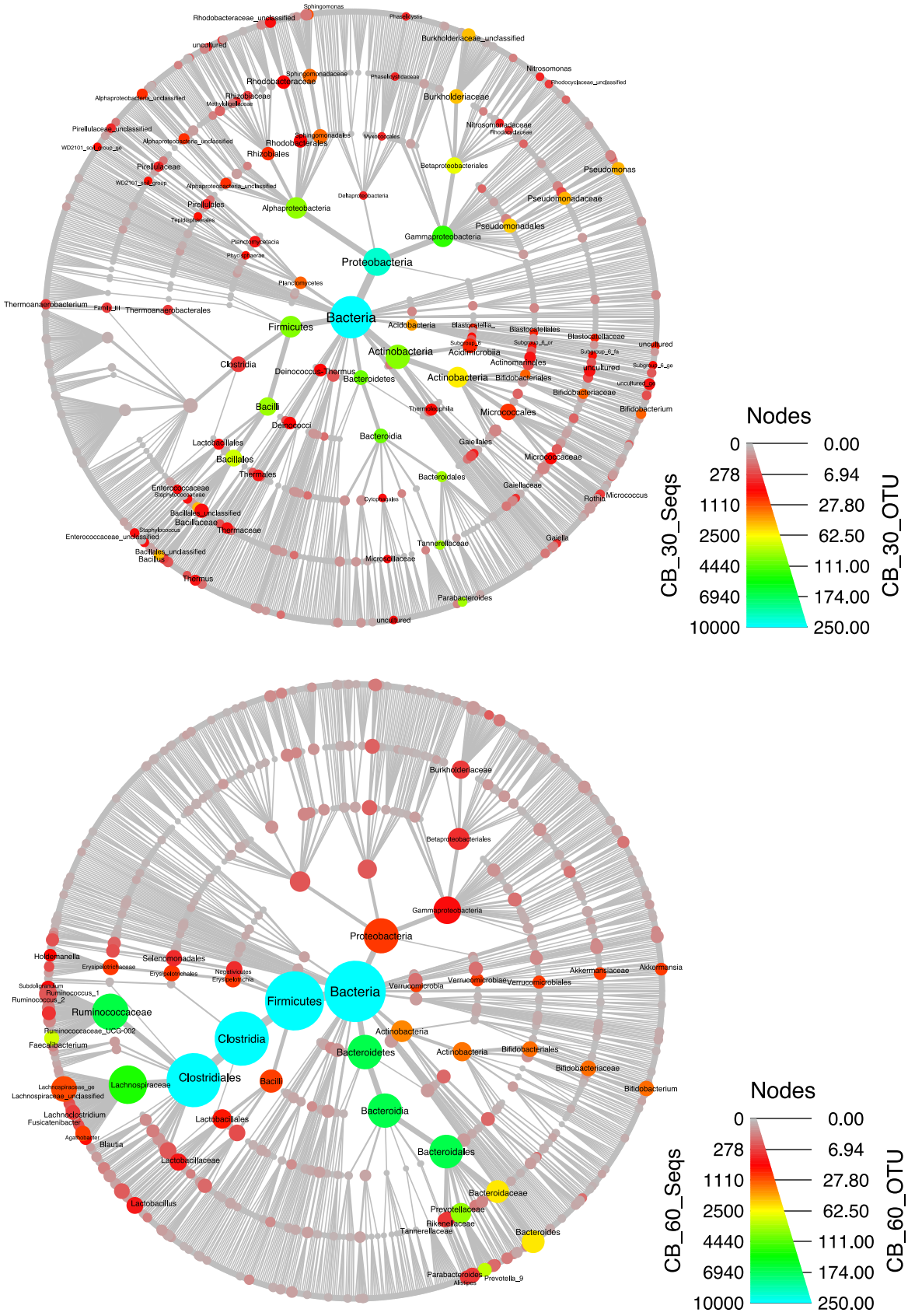
Bacteria
Proteobacteria
Firmicutes
Actinobacteria
Bacteroidetes
Gammaproteobacteria
Alphaproteobacteria
Betaproteobacteriales
Pseudomonadales
Pseudomonadaceae
Pseudomonas
Burkholderiaceae
Rhodobacteraceae
Rhizobiales
Sphingomonadales
Nitrosomonas
Nitrosomonadaceae
Clostridia
Clostridiales
Bacilli
Lactobacillales
Lactobacillaceae
Lactobacillus
Ruminococcaceae
Ruminococcus_2
Faecalibacterium
Lachnospiraceae
Blautia
Bacteroidia
Bacteroidales
Bacteroidaceae
Bacteroides
Prevotellaceae
Tannerellaceae
Parabacteroides
Actinobacteria
Bifidobacteriales
Bifidobacteriaceae
Bifidobacterium
Micrococcales
Micrococcaceae
Rothia
Micrococcus
Gaiellales
Gaiellaceae
Gaiella
Acidobacteria
Acidimicrobiia
Actinomarinales
Blastocatellia_
Blastocatellales
Blastocatellaceae
Thermoanaerobacterium
Thermoanaerobacterales
Family_III
Clostridia
Deinococcus-Thermus
Deinococci
Thermales
Bacteroidia
Bacteroidales
Cytophagales
Enterococcaceae
Staphylococcaceae
Staphylococcus
Enterococcaceae_unclassified
Bacillales_unclassified
Bacillaceae
Thermaceae
Bacillales_unclassified
Bacillus
Thermus
Tannerellaceae
Microbacteriaceae
Parabacteroides
uncultured
Nodes
0
278
1110
2500
4440
6940
10000
0.00
6.94
27.80
62.50
111.00
174.00
250.00
CB_30_Seqs
CB_30_OTU
Burkholderiaceae
Betaproteobacteriales
Gammaproteobacteria
Proteobacteria
Bacteria
Firmicutes
Clostridia
Clostridiales
Bacilli
Lactobacillales
Lactobacillaceae
Lactobacillus
Ruminococcaceae
Ruminococcaceae_UCG-002
Faecalibacterium
Lachnospiraceae
Blautia
Lachnoclostridium
Fusicatenibacter
Bacteroidetes
Bacteroidia
Bacteroidales
Bacteroidaceae
Bacteroides
Prevotellaceae
Tannerellaceae
Parabacteroides
Actinobacteria
Bifidobacteriales
Bifidobacteriaceae
Bifidobacterium
Verrucomicrobia
Verrucomicrobiae
Verrucomicrobiales
Akkermansiaceae
Akkermansia
Selenomonadales
Erysipelotrichaceae
Holdemanella
Ruminococcus_1
Ruminococcus_2
Nodes
0
278
1110
2500
4440
6940
10000
0.00
6.94
27.80
62.50
111.00
174.00
250.00
CB_60_Seqs
CB_60_OTU

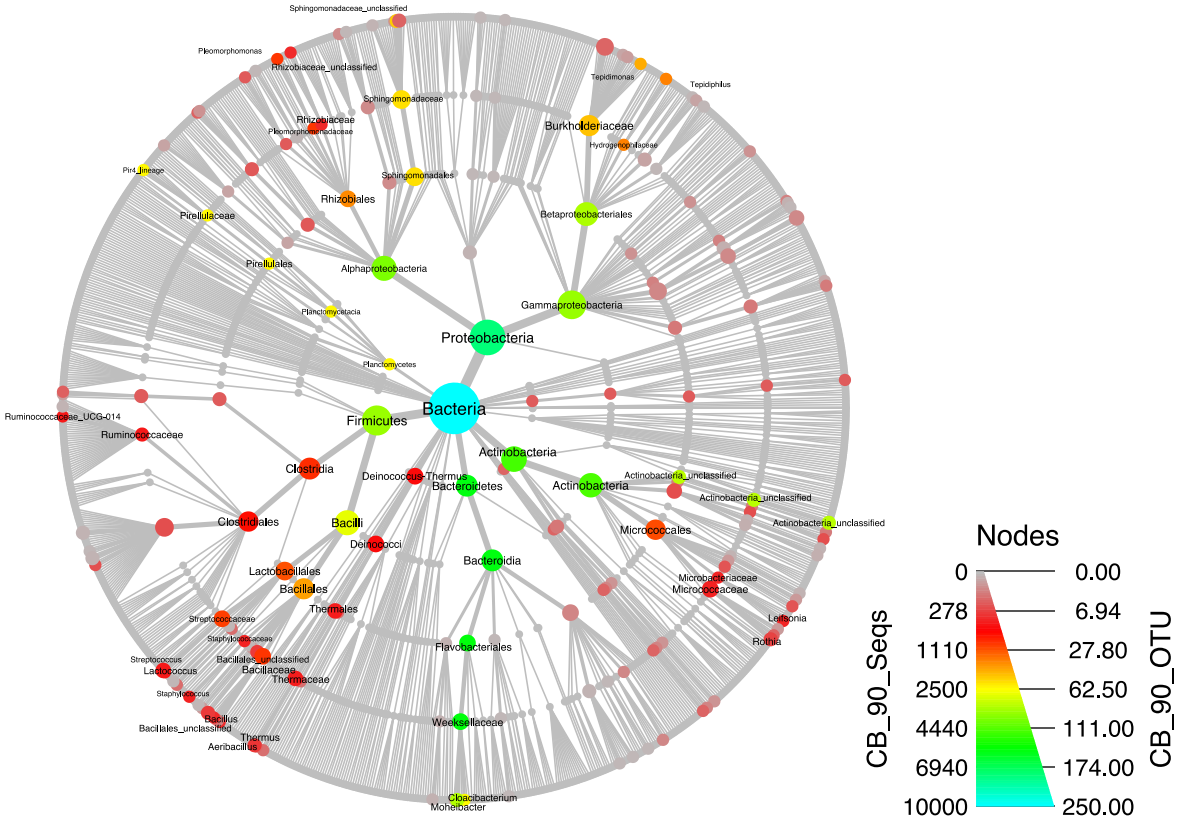

Figure 5.45. Number of reads and OTUs assigned in specific taxon under CB1190-bioaugmentation condition, and the cladograms from top to bottom correspond to the order of time. Each node represents a taxon used to classify OTUs and the edges determine where it fits in the overall taxonomic hierarchy. Node color indicates the number of reads and node diameter is proportional to the number of OTUs classified in that taxa.

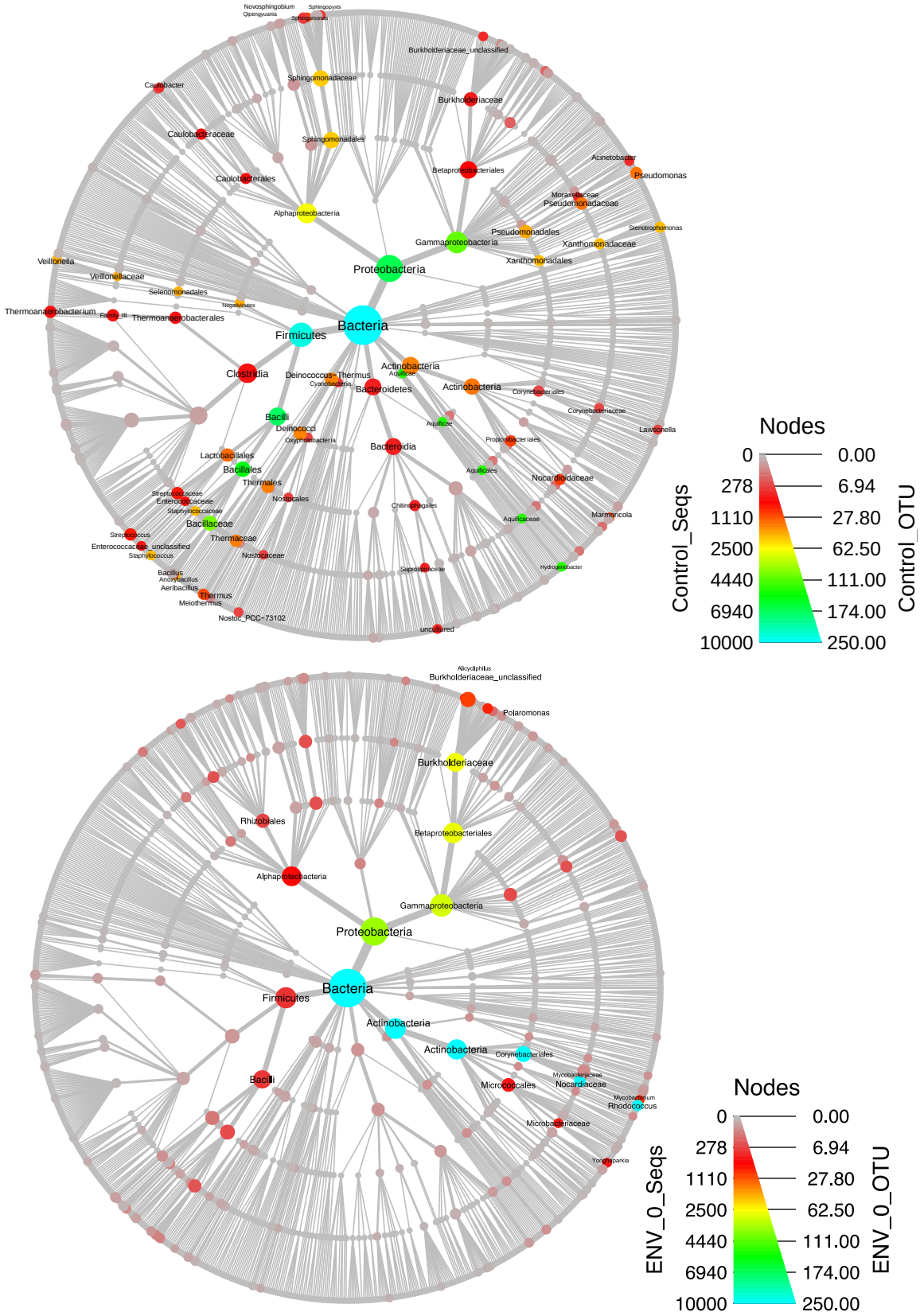
Novosphingobium
Qipengyuania
Sphingopyxis
Sphingomonas
Burkholderiaceae_unclassified
Caulobacter
Sphingomonadaceae
Burkholderiaceae
Caulobacteraceae
Sphingomonadales
Betaproteobacteriales
Acinetobacter
Pseudomonas
Caulobacterales
Moraxellaceae
Pseudomonadaceae
Alphaproteobacteria
Pseudomonadales
Stenotrophomonas
Gammaproteobacteria
Xanthomonadaceae
Xanthomonadales
Veillonella
Proteobacteria
Veillonellaceae
Selenomonadales
Negativicutes
Thermoanaerobacterium
Family_III
Thermoanaerobacterales
Bacteria
Firmicutes
Clostridia
Deinococcus-Thermus
Actinobacteria
Aquificae
Cyanobacteria
Bacteroidetes
Actinobacteria
Coriobacteriales
Corynebacteriales
Bacilli
Deinococci
Aquificae
Lawsonella
Oxyphotobacteria
Propionibacteriales
Bacteroidia
Lactobacillales
Aquificales
Bacillales
Thermales
Nocardioidaceae
Streptococcaceae
Enterococcaceae
Nostocales
Chitinophagales
Staphylococcaceae
Aquificaceae
Marmoricola
Bacillaceae
Streptococcus
Thermaceae
Enterococcaceae_unclassified
Staphylococcus
Nostocaceae
Saprospiraceae
Hydrogenobacter
Bacillus
Anoxybacillus
Aeribacillus
Thermus
Meiothermus
Nostoc_PCC-73102
uncultured
Nodes
0
278
1110
2500
4440
6940
10000
0.00
6.94
27.80
62.50
111.00
174.00
250.00
Control_Seqs
Control_OTU
Alicyclophilus
Burkholderiaceae_unclassified
Polaromonas
Burkholderiaceae
Rhizobiales
Betaproteobacteriales
Alphaproteobacteria
Gammaproteobacteria
Proteobacteria
Bacteria
Firmicutes
Actinobacteria
Actinobacteria
Corynebacteriales
Bacilli
Mycobacteriaceae
Micrococcales
Nocardiaceae
Mycobacterium
Rhodococcus
Microbacteriaceae
Yonghaparkia
Nodes
0
278
1110
2500
4440
6940
10000
0.00
6.94
27.80
62.50
111.00
174.00
250.00
ENV_0_Seqs
ENV_0_OTU

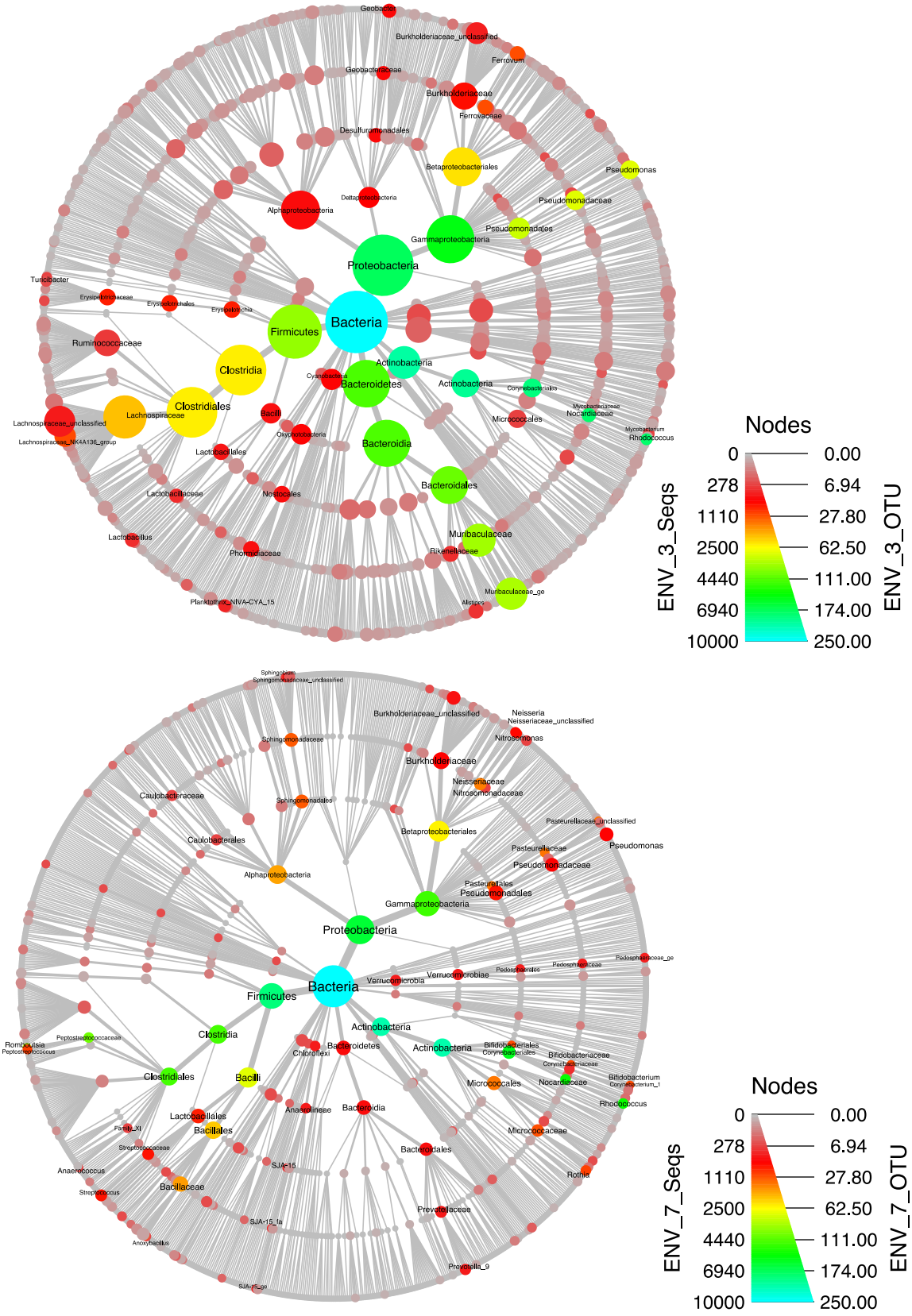
Geobacter
Burkholderiaceae_unclassified
Ferrovum
Geobacteraceae
Burkholderiaceae
Ferrovaceae
Desulfuromonadales
Betaproteobacteriales
Pseudomonas
Deltaproteobacteria
Alphaproteobacteria
Pseudomonadaceae
Pseudomonadales
Gammaproteobacteria
Proteobacteria
Tuncibacter
Erysipelotrichaceae
Erysipelotrichales
Erysipelotrichia
Firmicutes
Bacteria
Ruminococcaceae
Clostridia
Actinobacteria
Cyanobacteria
Bacteroidetes
Actinobacteria
Corynebacteriales
Clostridiales
Lachnospiraceae
Bacilli
Micrococcales
Mycobacteriaceae
Nocardiaceae
Mycobacterium
Rhodococcus
Lachnospiraceae_unclassified
Lachnospiraceae_NK4A136_group
Oxyphotobacteria
Bacteroidia
Lactobacillales
Bacteroidales
Lactobacillaceae
Nostocales
Muribaculaceae
Lactobacillus
Rikenellaceae
Phormidiaceae
Muribaculaceae_ge
Planktothrix_NIVA-CYA_15
Alistipes
Nodes
0
278
1110
2500
4440
6940
10000
0.00
6.94
27.80
62.50
111.00
174.00
250.00
ENV_3_Seqs
ENV_3_OTU
Sphingobium
Sphingomonadaceae_unclassified
Burkholderiaceae_unclassified
Neisseria
Neisseriaceae_unclassified
Sphingomonadaceae
Nitrosomonas
Burkholderiaceae
Neisseriaceae
Caulobacteraceae
Sphingomonadales
Nitrosomonadaceae
Pasteurellaceae_unclassified
Betaproteobacteriales
Caulobacterales
Pasteurellaceae
Pseudomonas
Pseudomonadaceae
Alphaproteobacteria
Pasteurellales
Pseudomonadales
Gammaproteobacteria
Proteobacteria
Pedosphaeraceae_ge
Pedosphaeraceae
Pedosphaerales
Verrucomicrobia
Verrucomicrobiae
Bacteria
Firmicutes
Actinobacteria
Clostridia
Peptostreptococcaceae
Romboutsia
Peptostreptococcus
Chloroflexi
Bacteroidetes
Actinobacteria
Bifidobacteriales
Corynebacteriales
Bifidobacteriaceae
Corynebacteriaceae
Clostridiales
Bacilli
Micrococcales
Nocardiaceae
Bifidobacterium
Corynebacterium_1
Rhodococcus
Anaerolineae
Bacteroidia
Lactobacillales
Micrococcaceae
Family_XI
Bacillales
Bacteroidales
Streptococcaceae
SJA-15
Anaerococcus
Rothia
Bacillaceae
Streptococcus
Prevotellaceae
SJA-15_fa
Anoxybacillus
Prevotella_9
SJA-15_ge
Nodes
0
278
1110
2500
4440
6940
10000
0.00
6.94
27.80
62.50
111.00
174.00
250.00
ENV_7_Seqs
ENV_7_OTU

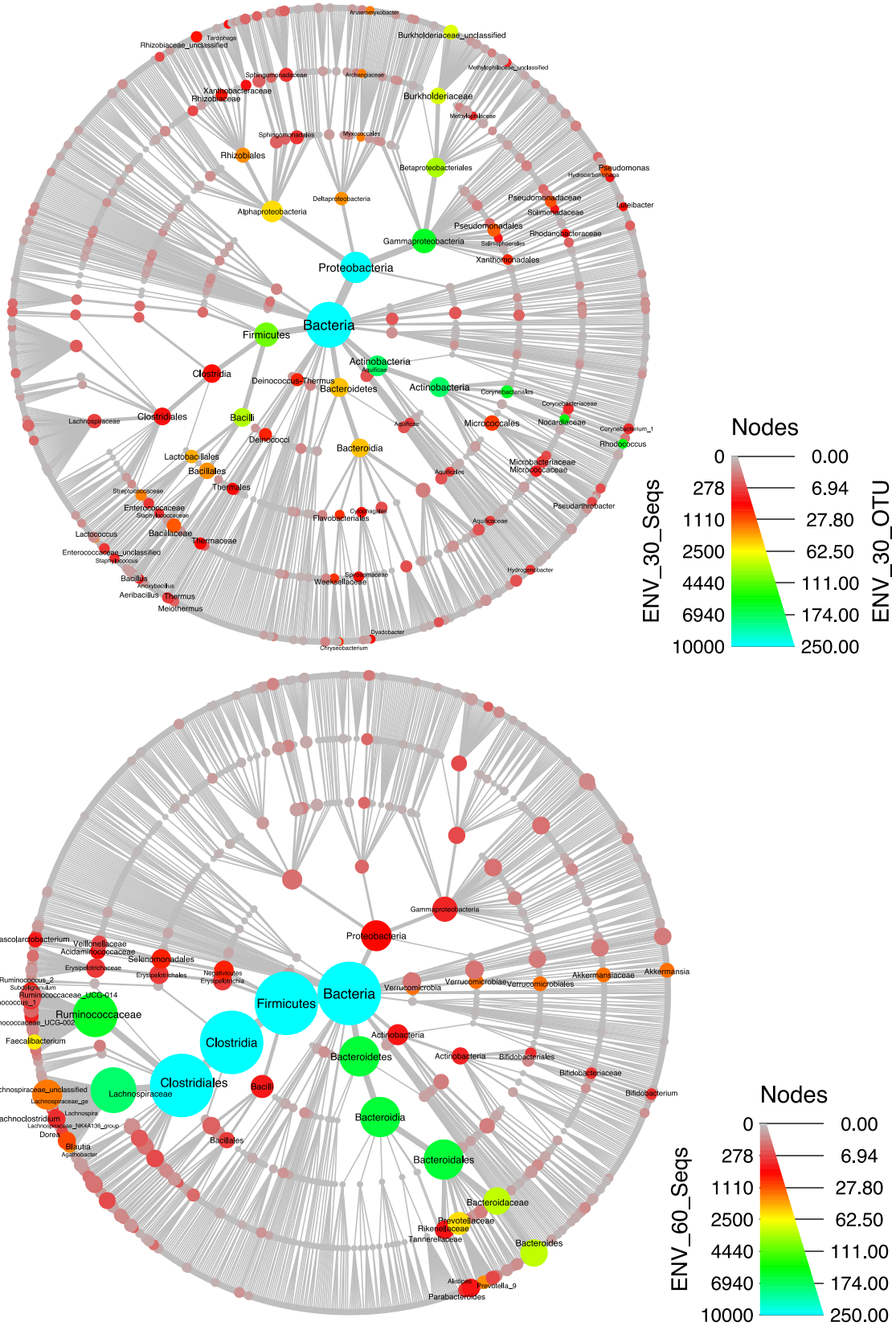
Nodes
0
278
1110
2500
4440
6940
10000
0.00
6.94
27.80
62.50
111.00
174.00
250.00
ENV_30_Seqs
ENV_30_OTU
Nodes
0
278
1110
2500
4440
6940
10000
0.00
6.94
27.80
62.50
111.00
174.00
250.00
ENV_60_Seqs
ENV_60_OTU

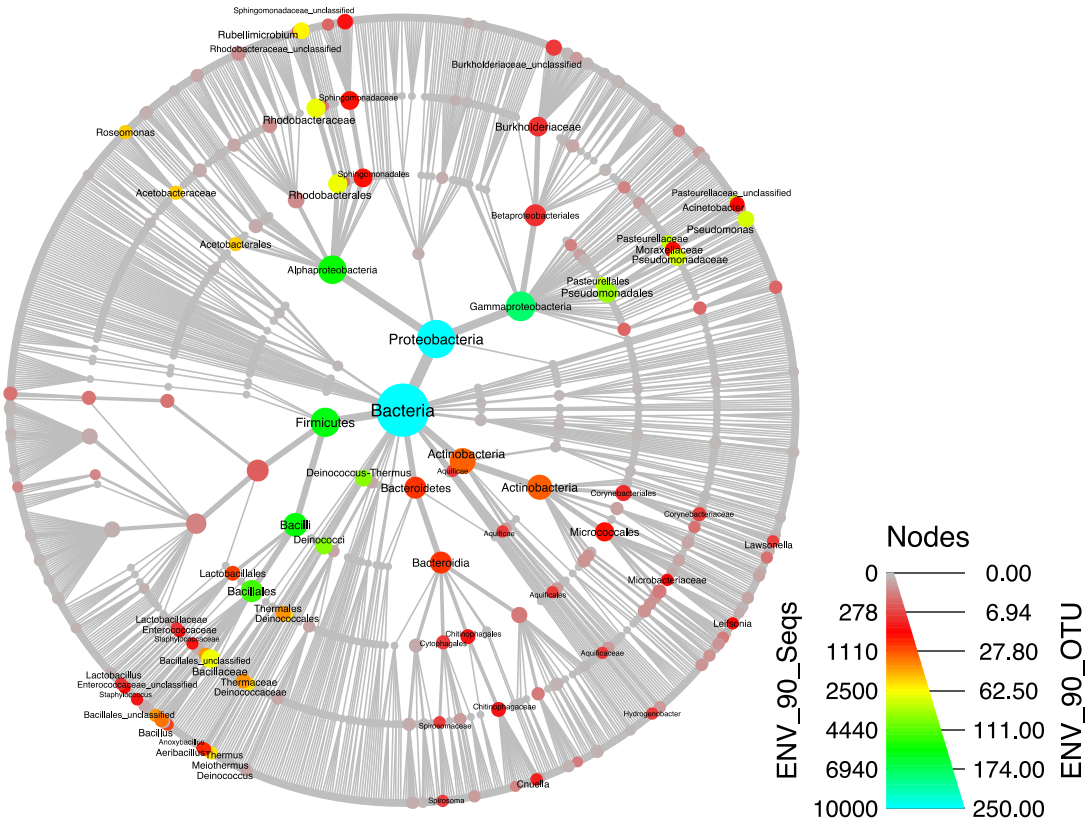

Figure 5.46. Number of reads and OTUs assigned in specific taxon under ENV425-bioaugmentation condition, and the cladograms from top to bottom correspond to the order of time. Each node represents a taxon used to classify OTUs and the edges determine where it fits in the overall taxonomic hierarchy. Node color indicates the number of reads and node diameter is proportional to the number of OTUs classified in that taxa.

Under oxygen biostimulation, microorganisms changed with no clear trends, while nutrient addition selected for similar bacteria that dominated under stimulation with oxygen alone at day 150, such as *Prevotella*_9, *Faecalibacterium*, and *Bacteroides*, etc. (Figure 5.6). This demonstrated that the addition of nutrients could stimulate more minor bacteria and this was also reflected by increases in biodiversity. Unfortunately, increases in minor bacterial groups had no significant benefit for 1,4-dioxane removal. However, dominant microorganisms under propane stimulation after nutrient addition were genera *Mycobacterium* and *Methyloversatilis* at day 150 (Figure 5.7).

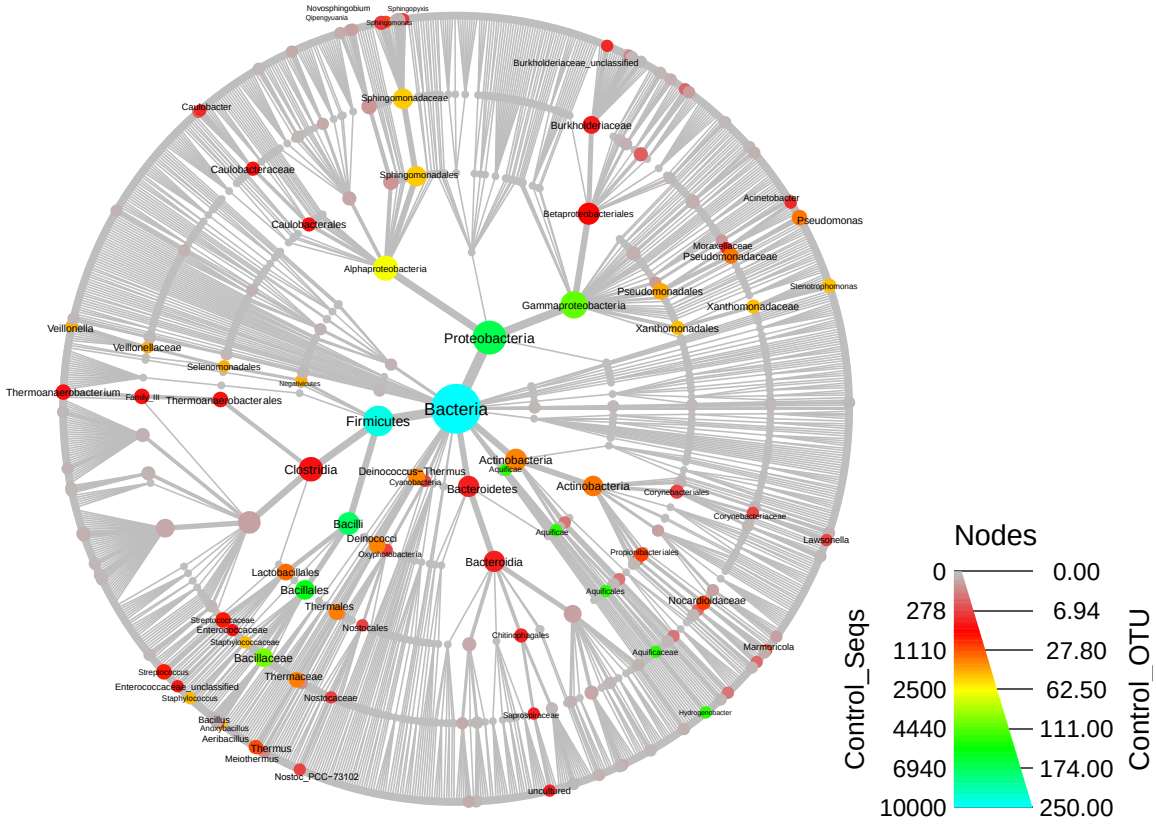

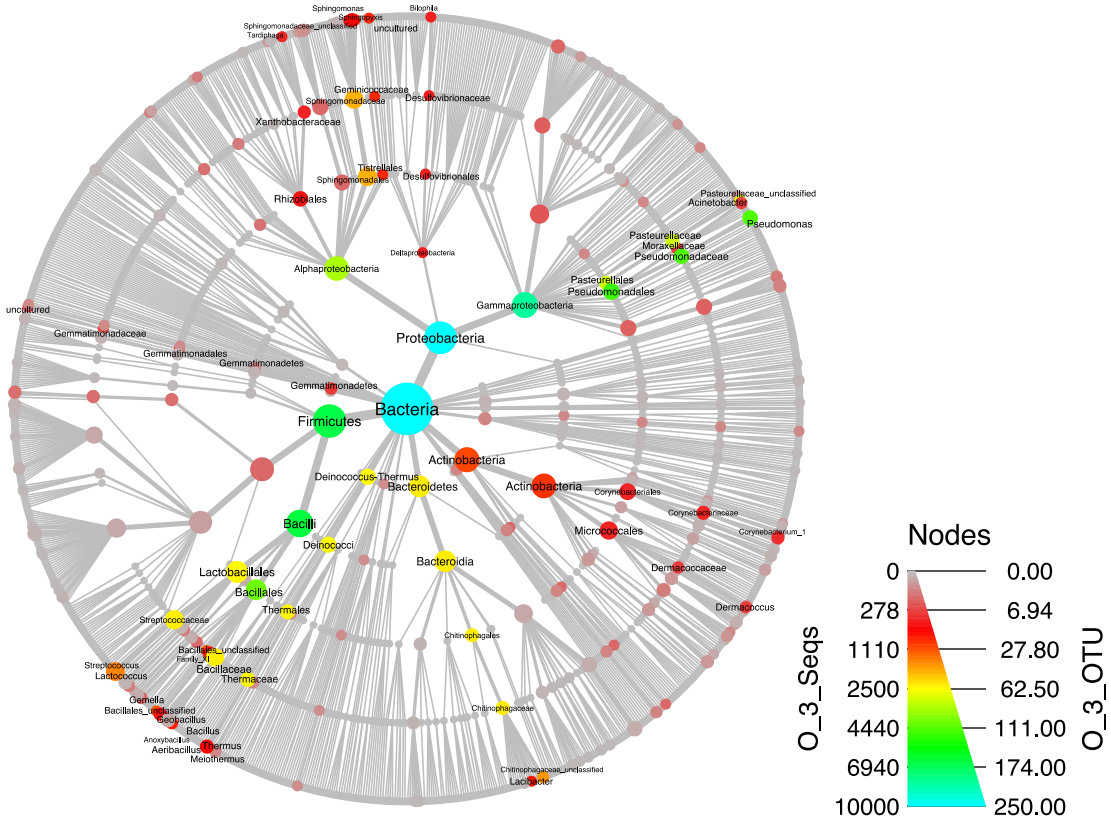
Bacteria
Proteobacteria
Firmicutes
Actinobacteria
Bacteroidetes
Deinococcus-Thermus
Gammaproteobacteria
Alphaproteobacteria
Deltaproteobacteria
Bacteroidia
Bacilli
Clostridia
Actinobacteria
Micrococcales
Corynebacteriales
Corynebacterium_1
Dermabacteraceae
Dermabacter
Pasteurellaceae_unclassified
Acinetobacter
Pseudomonas
Pasteurellaceae
Moraxellaceae
Pseudomonadaceae
Pasteurellales
Pseudomonadales
Rhizobiales
Sphingomonadales
Desulfovibrionales
Tistrellales
Xanthobacteraceae
Sphingomonadaceae
Geminicoccaceae
Desulfovibrionaceae
Sphingomonas
Sphingopyxis
Bilophila
uncultured
Tardiphaga
Sphingomonadaceae_unclassified
uncultured
Gemmatimonadaceae
Gemmatimonadales
Gemmatimonadetes
Lactobacillales
Bacillales
Thermales
Streptococcaceae
Streptococcus
Lactococcus
Bacillales_unclassified
Family_XI
Bacillaceae
Thermaceae
Gemella
Bacillales_unclassified
Geobacillus
Bacillus
Anoxybacillus
Aeribacillus
Thermus
Meiothermus
Deinococci
Chitinophagales
Chitinophagaceae
Chitinophagaceae_unclassified
Lactobacillales
Nodes
0
278
1110
2500
4440
6940
10000
0.00
6.94
27.80
62.50
111.00
174.00
250.00
O_3_Seqs
O_3_OTU

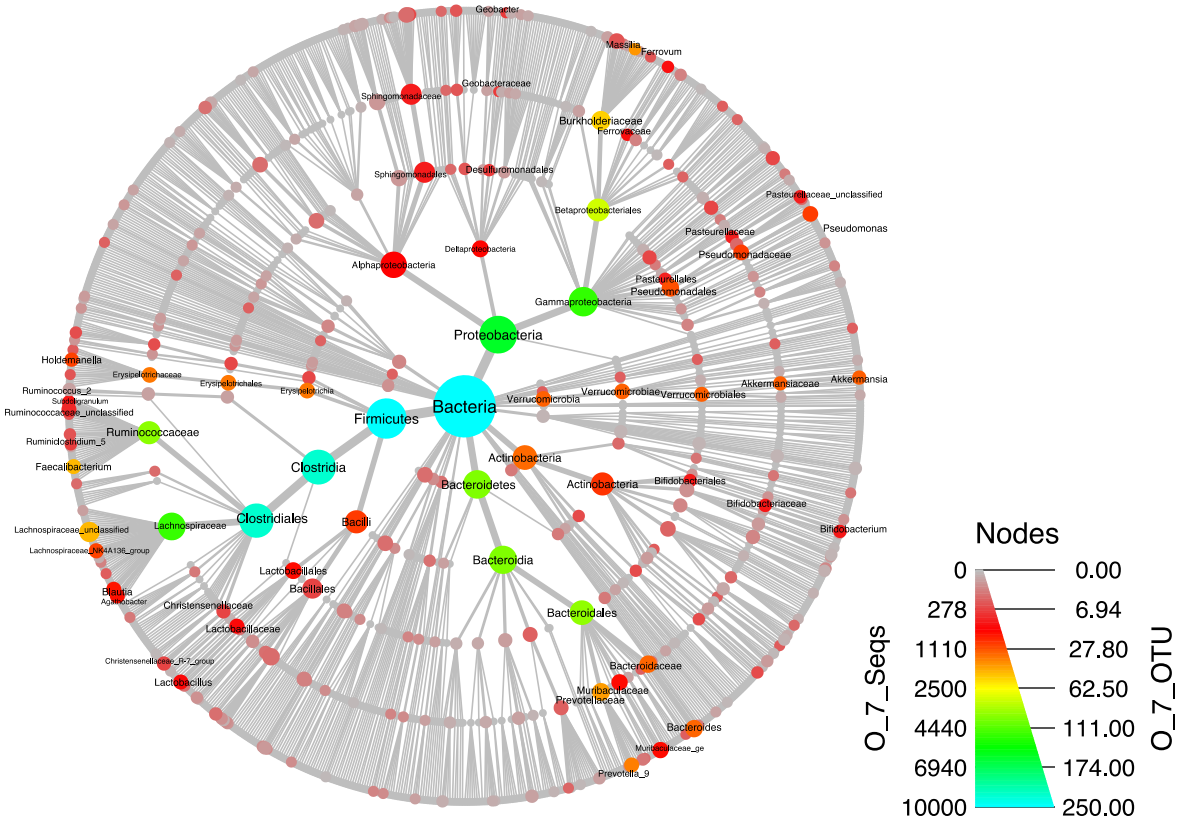
Bacteria
Proteobacteria
Firmicutes
Actinobacteria
Bacteroidetes
Gammaproteobacteria
Alphaproteobacteria
Deltaproteobacteria
Betaproteobacteriales
Bacteroidia
Bacteroidales
Clostridia
Clostridiales
Bacilli
Lactobacillales
Bacillales
Bifidobacteriales
Bifidobacteriaceae
Bifidobacterium
Verrucomicrobia
Verrucomicrobiae
Verrucomicrobiales
Akkermansiaceae
Akkermansia
Pasteurellaceae_unclassified
Pseudomonas
Pasteurellaceae
Pseudomonadaceae
Pasteurellales
Pseudomonadales
Sphingomonadales
Desulfuromonadales
Sphingomonadaceae
Geobacteraceae
Geobacter
Massilia
Ferrovum
Burkholderiaceae
Ferrovaceae
Holdemanella
Erysipelotrichaceae
Erysipelotrichales
Erysipelotrichia
Ruminococcus_2
Subdoligranulum
Ruminococcaceae_unclassified
Ruminococcaceae
Ruminiclostridium_5
Faecalibacterium
Lachnospiraceae_unclassified
Lachnospiraceae
Lachnospiraceae_UCG-4136_group
Blautia
Agathobacter
Christensenellaceae
Christensenellaceae_R-7_group
Lactobacillaceae
Lactobacillus
Bacteroidaceae
Muribaculaceae
Prevotellaceae
Bacteroides
Muribaculaceae_ge
Prevotella_9
Nodes
0
278
1110
2500
4440
6940
10000
0.00
6.94
27.80
62.50
111.00
174.00
250.00
O_7_Seqs
O_7_OTU

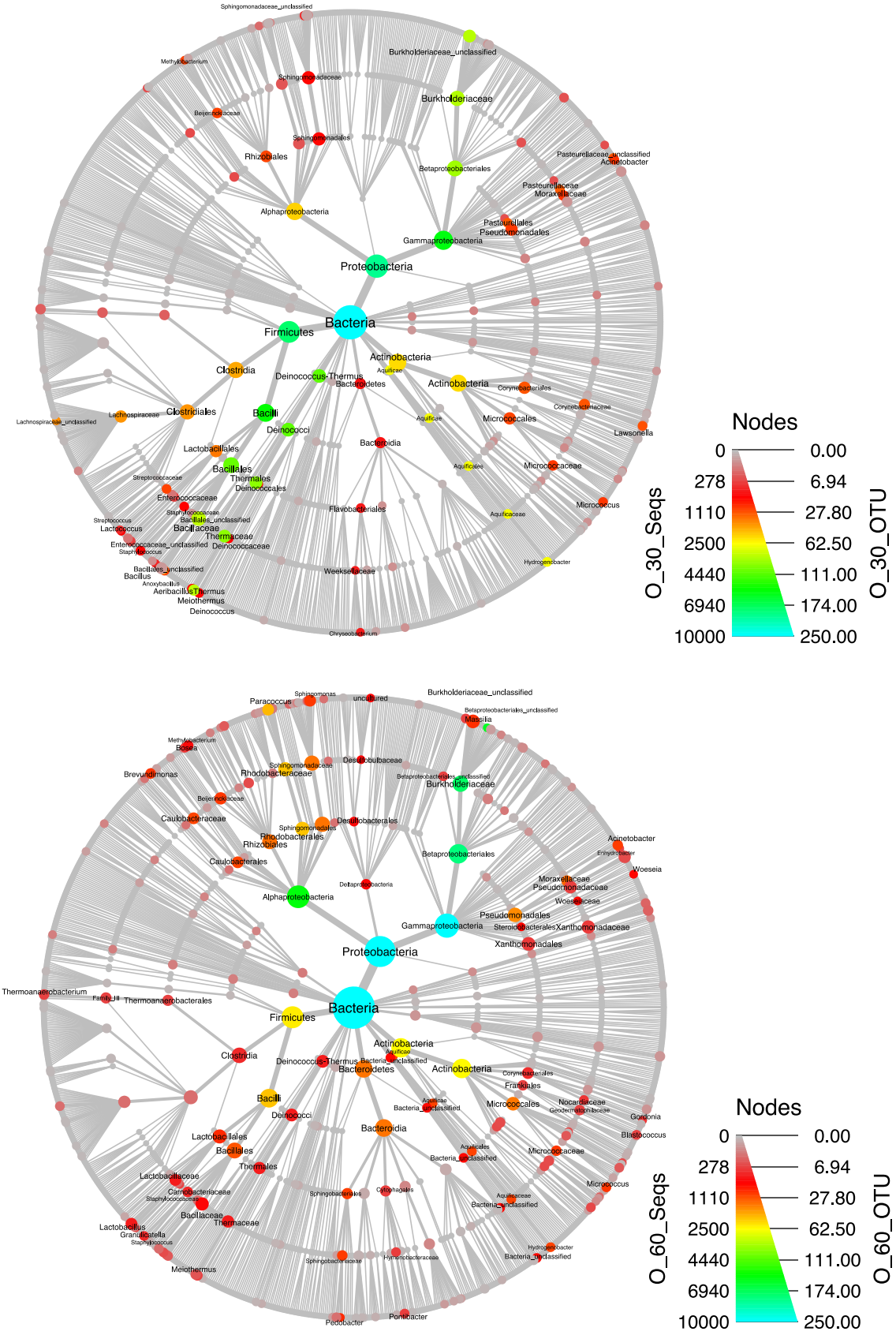
Bacteria
Proteobacteria
Gammaproteobacteria
Alphaproteobacteria
Betaproteobacteriales
Burkholderiaceae
Burkholderiaceae_unclassified
Rhizobiales
Sphingomonadales
Sphingomonadaceae
Pasteurellaceae
Moraxellaceae
Pseudomonadales
Pasteurellaceae_unclassified
Acinetobacter
Firmicutes
Clostridia
Clostridiales
Bacilli
Lactobacillales
Bacillales
Thermales
Deinococci
Deinococcus-Thermus
Bacteroidetes
Bacteroidia
Flavobacteriales
Actinobacteria
Corynebacteriales
Micrococcales
Micrococcaceae
Micrococcus
Lawsonella
Aquificae
Aquificales
Aquificaceae
Hydrogenobacter
Weeksellaceae
Chryseobacterium
Meiothermus
Deinococcus
Aeribacillus
Thermus
Bacillus
Lactococcus
Enterococcaceae
Streptococcaceae
Lachnospiraceae
Lachnospiraceae_unclassified
Nodes
0
278
1110
2500
4440
6940
10000
0.00
6.94
27.80
62.50
111.00
174.00
250.00
O_30_Seqs
O_30_OTU

Bacteria
Proteobacteria
Gammaproteobacteria
Alphaproteobacteria
Betaproteobacteriales
Burkholderiaceae
Burkholderiaceae_unclassified
Rhizobiales
Rhodobacteraceae
Caulobacterales
Caulobacteraceae
Desulfobacterales
Desulfobulbaceae
Pseudomonadales
Xanthomonadales
Xanthomonadaceae
Moraxellaceae
Pseudomonadaceae
Acinetobacter
Woeseia
Firmicutes
Clostridia
Bacilli
Lactobacillales
Bacillales
Thermales
Deinococci
Deinococcus-Thermus
Bacteroidetes
Bacteroidia
Actinobacteria
Micrococcales
Micrococcaceae
Micrococcus
Nocardiaceae
Gordonia
Blastococcus
Frankiales
Corynebacteriales
Aquificae
Aquificales
Thermoanaerobacterales
Thermoanaerobacterium
Meiothermus
Pontibacter
Peddobacter
Nodes
0
278
1110
2500
4440
6940
10000
0.00
6.94
27.80
62.50
111.00
174.00
250.00
O_60_Seqs
O_60_OTU

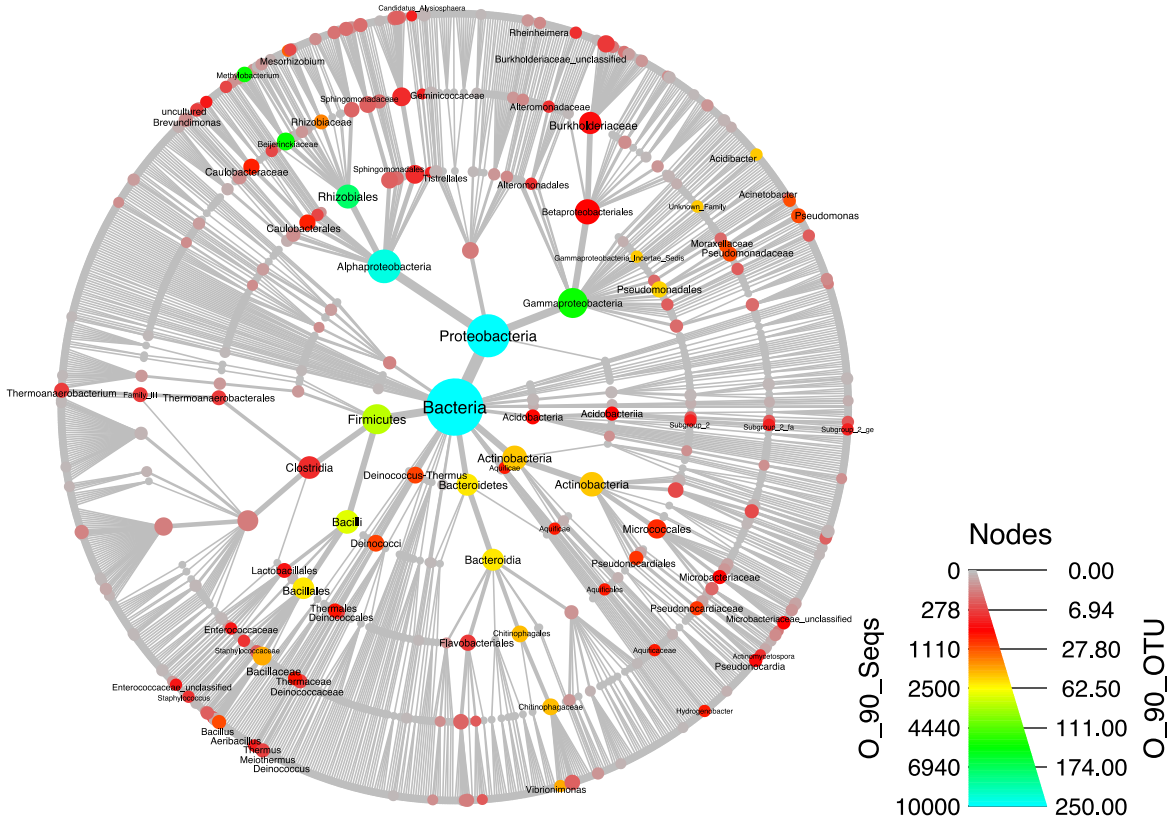
Candidatus_Alysosphaera
Rheinheimera
Burkholderiaceae_unclassified
Mesorhizobium
Methylobacterium
Sphingomonadaceae
Gaiellales
Alteromonadaceae
uncultured
Brevundimonas
Rhizobiaceae
Burkholderiaceae
Beijerinckiaceae
Acidibacter
Caulobacteraceae
Sphingomonadales
Rhizobiales
Alteromonadales
Acinetobacter
Betaproteobacteriales
Unknown_Family
Pseudomonas
Caulobacterales
Moraxellaceae
Pseudomonadaceae
Alphaproteobacteria
Gammaproteobacteria_Incertae_Sedis
Pseudomonadales
Gammaproteobacteria
Proteobacteria
Thermoanaerobacterium
Family_III
Thermoanaerobacterales
Bacteria
Firmicutes
Acidobacteria
Acidobacteriia
Subgroup_2
Subgroup_2_fa
Subgroup_2_ge
Clostridia
Actinobacteria
Deinococcus-Thermus
Bacteroidetes
Actinobacteria
Bacilli
Micrococcales
Deinococci
Bacteroidia
Pseudonocardiales
Lactobacillales
Microbacteriaceae
Bacillales
Thermales
Deinococcales
Pseudonocardiaceae
Microbacteriaceae_unclassified
Enterococcaceae
Chitinophagales
Flavobacteriales
Staphylococcaceae
Aquimicrobium
Actinomycetospora
Pseudonocardia
Bacillaceae
Thermaceae
Enterococcaceae_unclassified
Deinococcaceae
Staphylococcus
Chitinophagaceae
Hydrocarboniphaga
Bacillus
Aeribacillus
Thermus
Meiothermus
Deinococcus
Vibrionimonas
Nodes
0
278
1110
2500
4440
6940
10000
0.00
6.94
27.80
62.50
111.00
174.00
250.00
O_90_Seqs
O_90_OTU

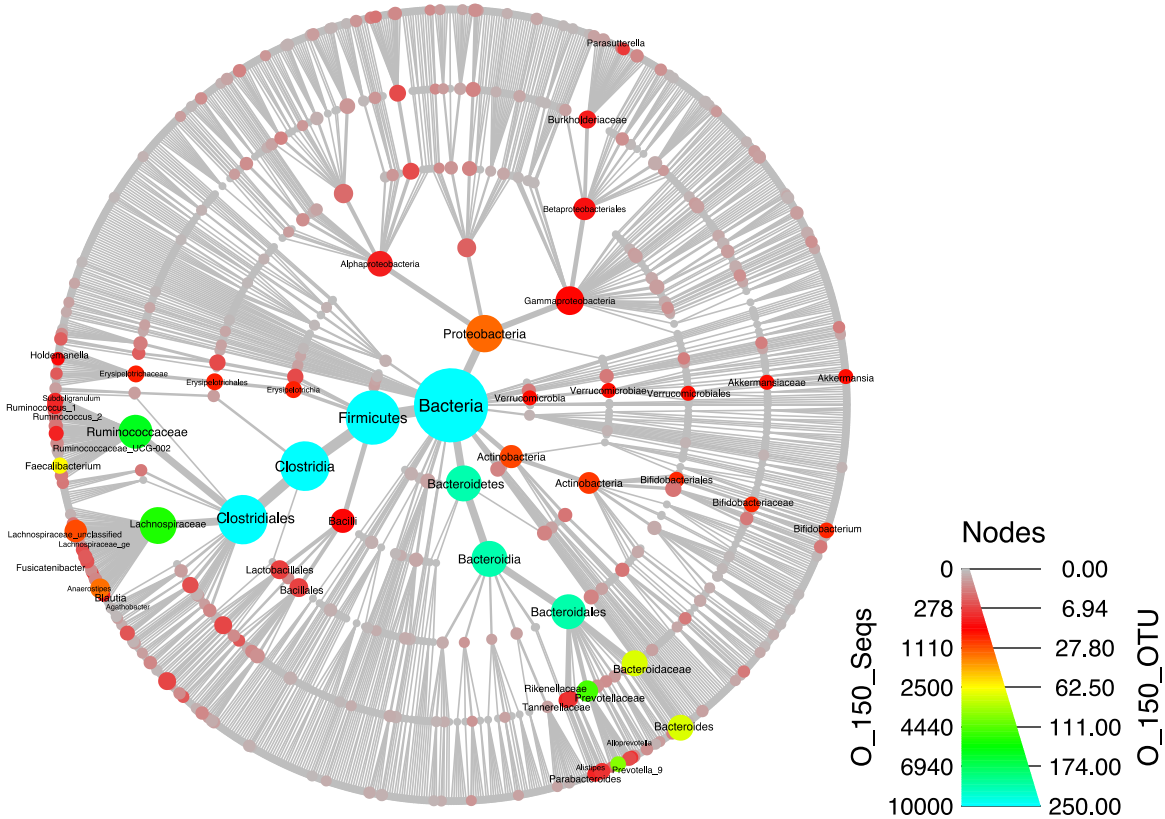
Parasutterella
Burkholderiaceae
Betaproteobacteriales
Alphaproteobacteria
Gammaproteobacteria
Proteobacteria
Holdemanella
Erysipelotrichaceae
Erysipelotrichales
Erysipelotrichia
Akkermansiaceae
Akkermansia
Verrucomicrobia
Verrucomicrobiae
Verrucomicrobiales
Bacteria
Firmicutes
Subdoligranulum
Ruminococcus_1
Ruminococcus_2
Ruminococcaceae
Ruminococcaceae_UCG-002
Actinobacteria
Clostridia
Faecalibacterium
Bacteroidetes
Actinobacteria
Bifidobacteriales
Bifidobacteriaceae
Bifidobacterium
Lachnospiraceae
Clostridiales
Bacilli
Lachnospiraceae_unclassified
Lachnospiraceae_ge
Bacteroidia
Fusicatenibacter
Lactobacillales
Anaerostipes
Bacillales
Blautia
Agathobacter
Bacteroidales
Bacteroidaceae
Rikenellaceae
Prevotellaceae
Tannerellaceae
Bacteroides
Alloprevotella
Alistipes
Prevotella_9
Parabacteroides
Nodes
0
278
1110
2500
4440
6940
10000
0.00
6.94
27.80
62.50
111.00
174.00
250.00
O_150_Seqs
O_150_OTU

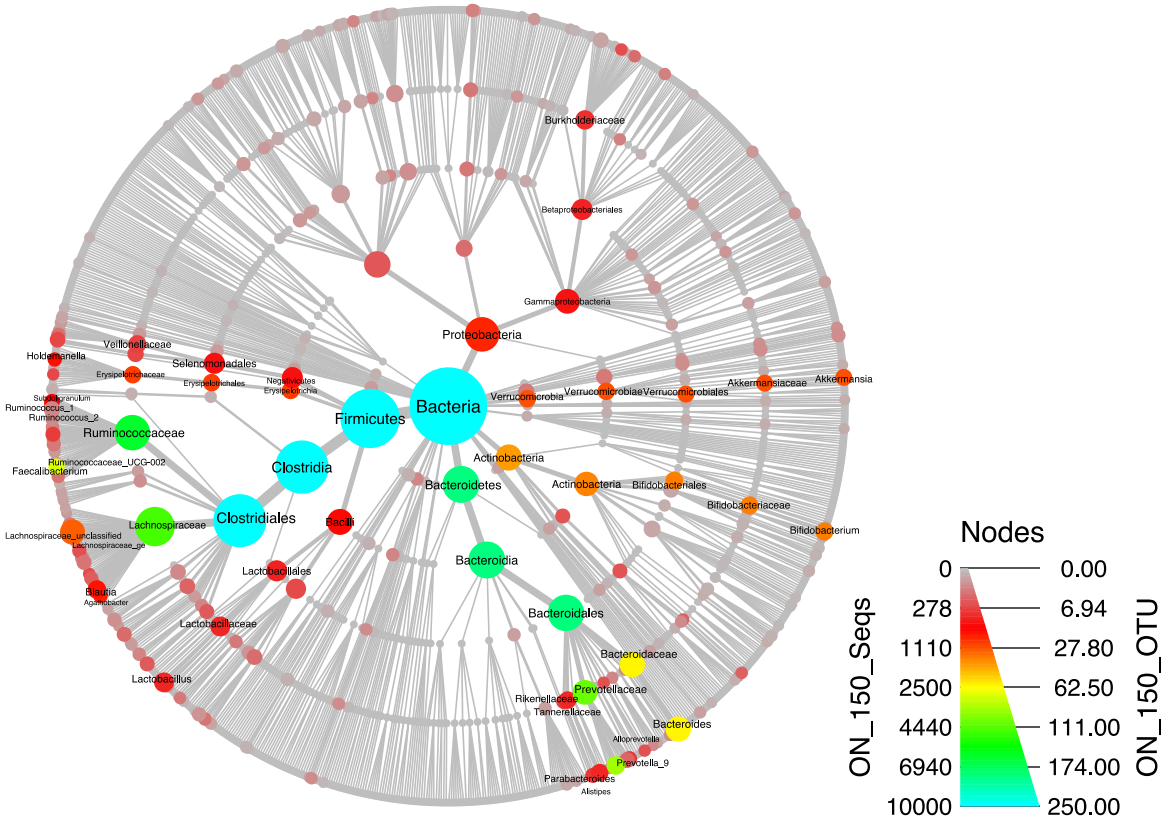

Figure 5.47. Number of reads and OTUs assigned in specific taxon under oxygen-biostimulation condition, and the cladograms from top to bottom correspond to the order of time. Each node represents a taxon used to classify OTUs and the edges determine where it fits in the overall taxonomic hierarchy. Node color indicates the number of reads and node diameter is proportional to the number of OTUs classified in that taxa.

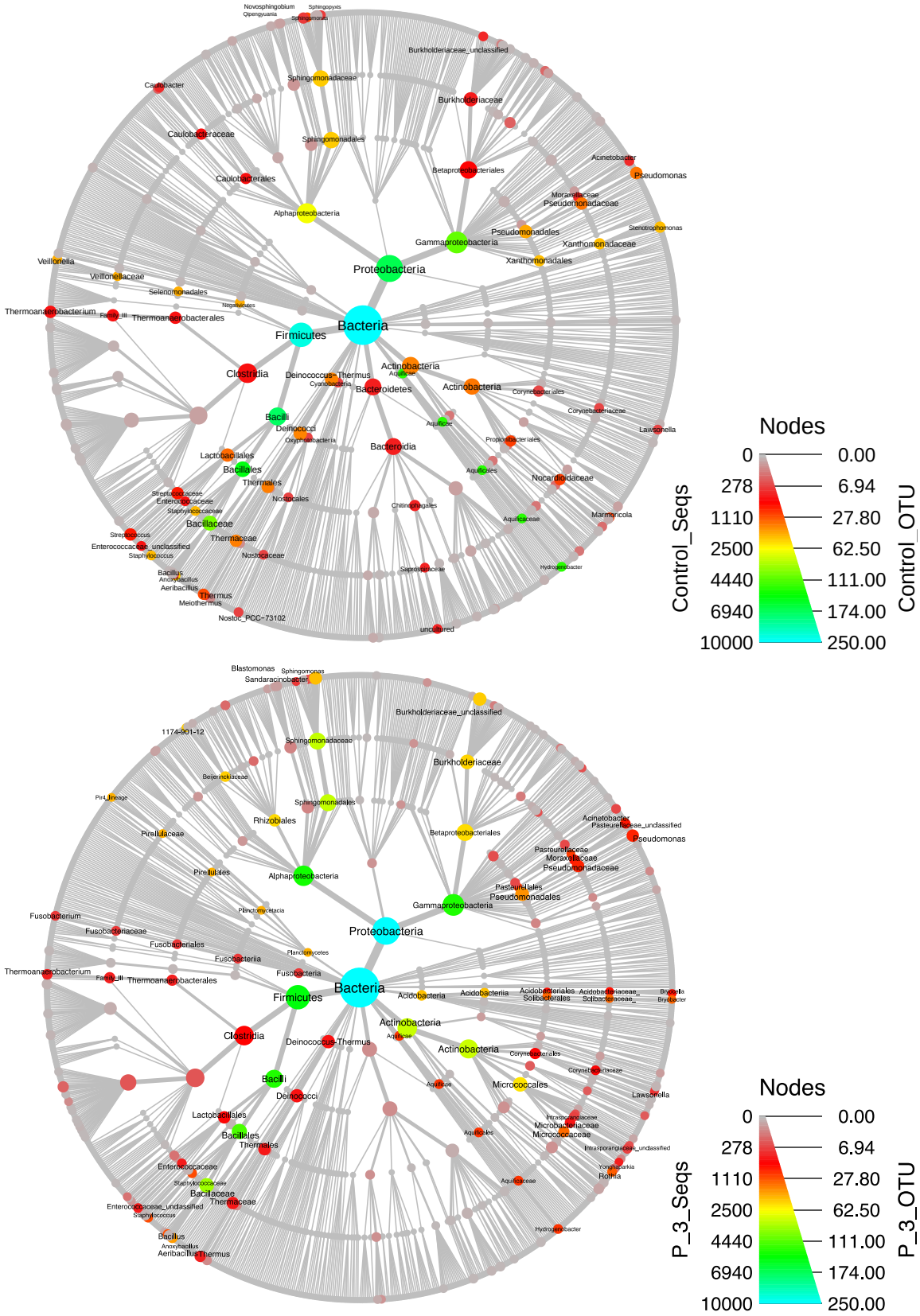
Nodes
0
278
1110
2500
4440
6940
10000
0.00
6.94
27.80
62.50
111.00
174.00
250.00
Control_Seqs
Control_OTU
P_3_Seqs
P_3_OTU
Bacteria
Proteobacteria
Firmicutes
Actinobacteria
Bacteroidetes
Clostridia
Bacilli
Gammaproteobacteria
Alphaproteobacteria
Betaproteobacteriales
Burkholderiaceae
Burkholderiaceae_unclassified
Sphingomonadaceae
Sphingomonadales
Caulobacteraceae
Caulobacterales
Pseudomonadales
Pseudomonadaceae
Moraxellaceae
Xanthomonadaceae
Xanthomonadales
Acinetobacter
Pseudomonas
Stenotrophomonas
Veillonellaceae
Veillonella
Selenomonadales
Thermoanaerobacterales
Thermoanaerobacterium
Family_III
Negativicutes
Deinococcus-Thermus
Deinococci
Cyanobacteria
Oxyphotobacteria
Aquificae
Aquificales
Corynebacteriales
Corynebacteriaceae
Lawsonella
Propionibacteriales
Nocardioidaceae
Marmoricola
Bacteroidia
Chitinophagales
Saprospiraceae
Hydrogenobacter
Lactobacillales
Bacillales
Thermales
Streptococcaceae
Enterococcaceae
Staphylococcaceae
Nostocales
Bacillaceae
Thermaceae
Streptococcus
Enterococcaceae_unclassified
Staphylococcus
Nostocaceae
Bacillus
Anoxybacillus
Aeribacillus
Thermus
Meiothermus
Nostoc_PCC-73102
uncultured
Blastomonas
Sphingomonas
Sandaracinobacter
1174-901-12
Beijerinckiaceae
Pir4_lineage
Rhizobiales
Pirellulaceae
Pirellulales
Planctomycetacia
Planctomycetes
Fusobacteriaceae
Fusobacteriales
Fusobacteriia
Fusobacteria
Fusobacterium
Acidobacteria
Acidobacteriia
Solibacterales
Acidobacteriales
Micrococcales
Micrococcaceae
Microbacteriaceae
Intrasporangiaceae
Intrasporangiaceae_undassified
Yonghaparkia
Rothia
Pasteurellaceae
Pasteurellales
Pasteurellaceae_unclassified

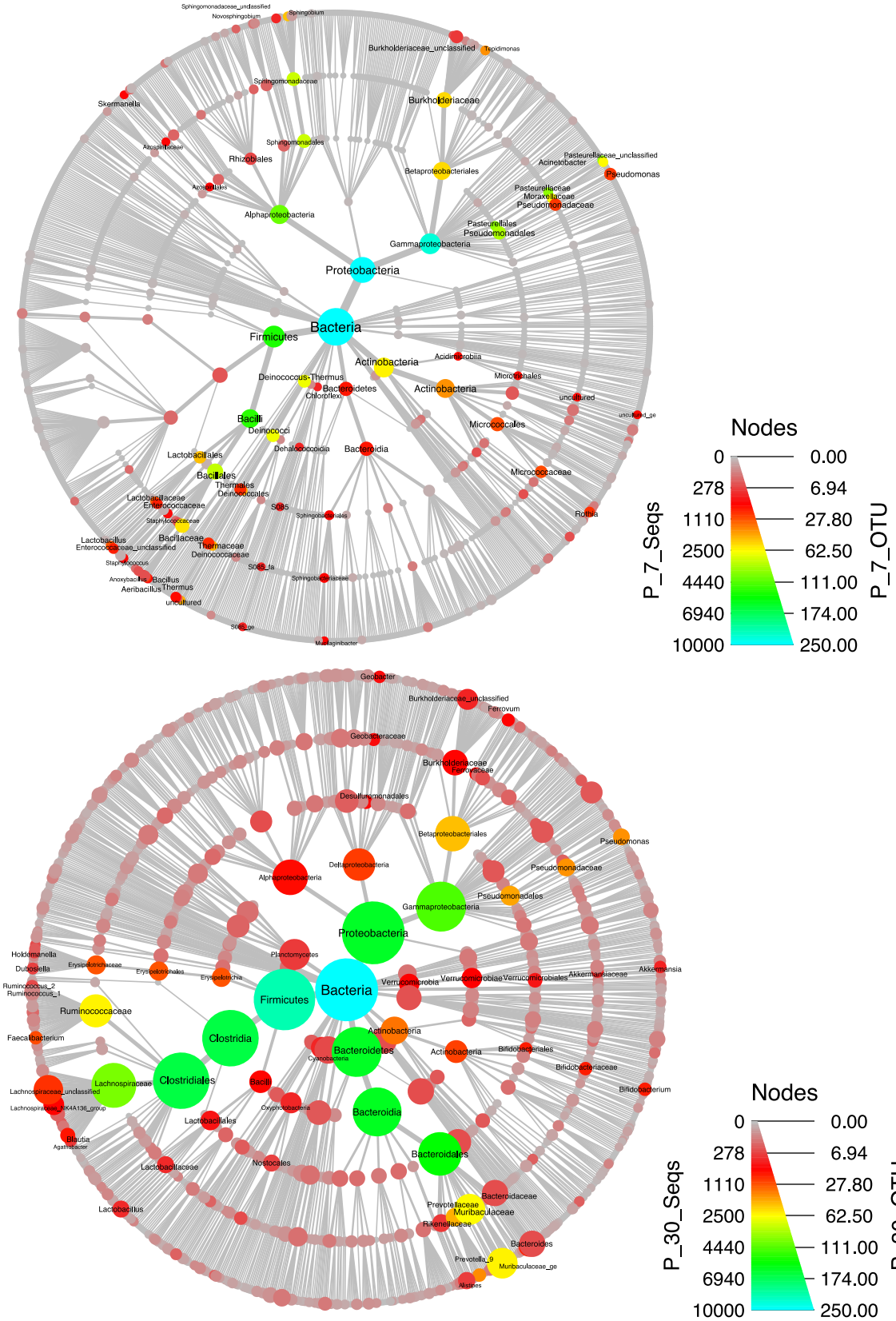
Nodes
0
278
1110
2500
4440
6940
10000
0.00
6.94
27.80
62.50
111.00
174.00
250.00
P_7_Seqs
P_7_OTU
Nodes
0
278
1110
2500
4440
6940
10000
0.00
6.94
27.80
62.50
111.00
174.00
250.00
P_30_Seqs
P_30_OTU

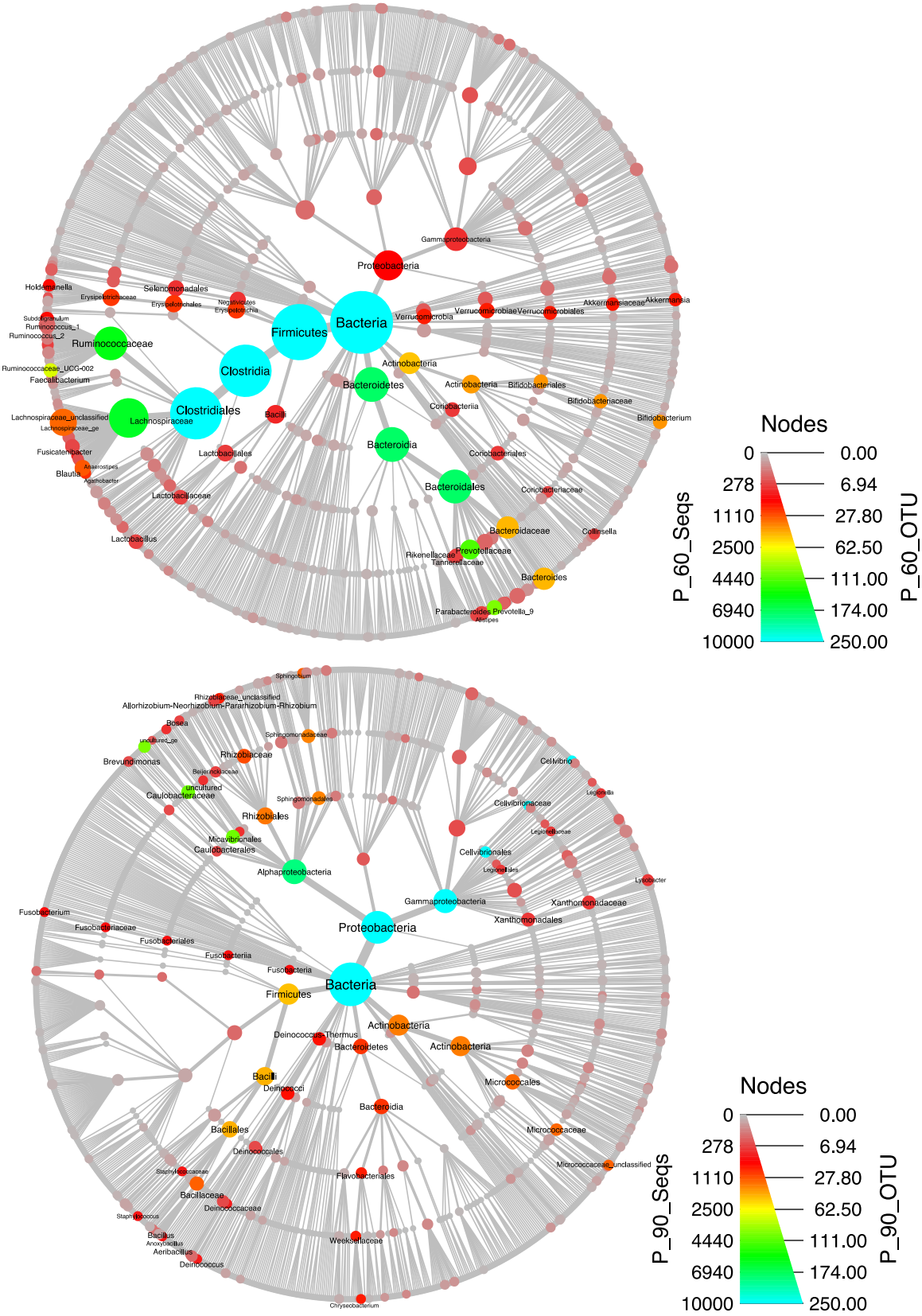
Bacteria
Proteobacteria
Gammaproteobacteria
Firmicutes
Clostridia
Clostridiales
Lachnospiraceae
Ruminococcaceae
Bacteroidetes
Bacteroidia
Bacteroidales
Bacteroidaceae
Prevotellaceae
Rikenellaceae
Tannerellaceae
Actinobacteria
Bifidobacteriales
Bifidobacteriaceae
Bifidobacterium
Coriobacteriia
Coriobacteriales
Coriobacteriaceae
Collinsella
Verrucomicrobia
Verrucomicrobiae
Verrucomicrobiales
Akkermansiaceae
Akkermansia
Selenomonadales
Erysipelotrichaceae
Erysipelotrichales
Erysipelotrichia
Holdemanella
Subdoligranulum
Ruminococcus_1
Ruminococcus_2
Ruminococcaceae_UCG-002
Faecalibacterium
Lachnospiraceae_unclassified
Lachnospiraceae_ge
Fusicatenibacter
Blautia
Anaerostipes
Agathobacter
Bacilli
Lactobacillales
Lactobacillaceae
Lactobacillus
Parabacteroides
Prevotella_9
Alistipes
Nodes
0
278
1110
2500
4440
6940
10000
0.00
6.94
27.80
62.50
111.00
174.00
250.00
P_60_Seqs
P_60_OTU
Proteobacteria
Gammaproteobacteria
Alphaproteobacteria
Bacteria
Firmicutes
Actinobacteria
Bacteroidetes
Bacteroidia
Bacilli
Rhizobiales
Rhizobiaceae
Caulobacteraceae
Sphingomonadales
Sphingomonadaceae
Caulobacterales
Micavibrionales
Cellvibrionales
Cellvibrionaceae
Cellvibrio
Legionellales
Legionellaceae
Legionella
Xanthomonadales
Xanthomonadaceae
Lysobacter
Fusobacteriia
Fusobacteriales
Fusobacteriaceae
Fusobacterium
Micrococcales
Micrococcaceae
Micrococcaceae_unclassified
Deinococcus-Thermus
Deinococci
Deinococcales
Deinococcaceae
Bacillales
Bacillaceae
Staphylococcaceae
Staphylococcus
Bacillus
Anoxybacillus
Aeribacillus
Flavobacteriales
Weeksellaceae
Chryseobacterium
Sphingobium
Rhizobiaceae_unclassified
Allorhizobium-Neorhizobium-Pararhizobium-Rhizobium
Rosea
uncultured_ge
Brevundimonas
Beijerinckiaceae
uncultured
Nodes
0
278
1110
2500
4440
6940
10000
0.00
6.94
27.80
62.50
111.00
174.00
250.00
P_90_Seqs
P_90_OTU

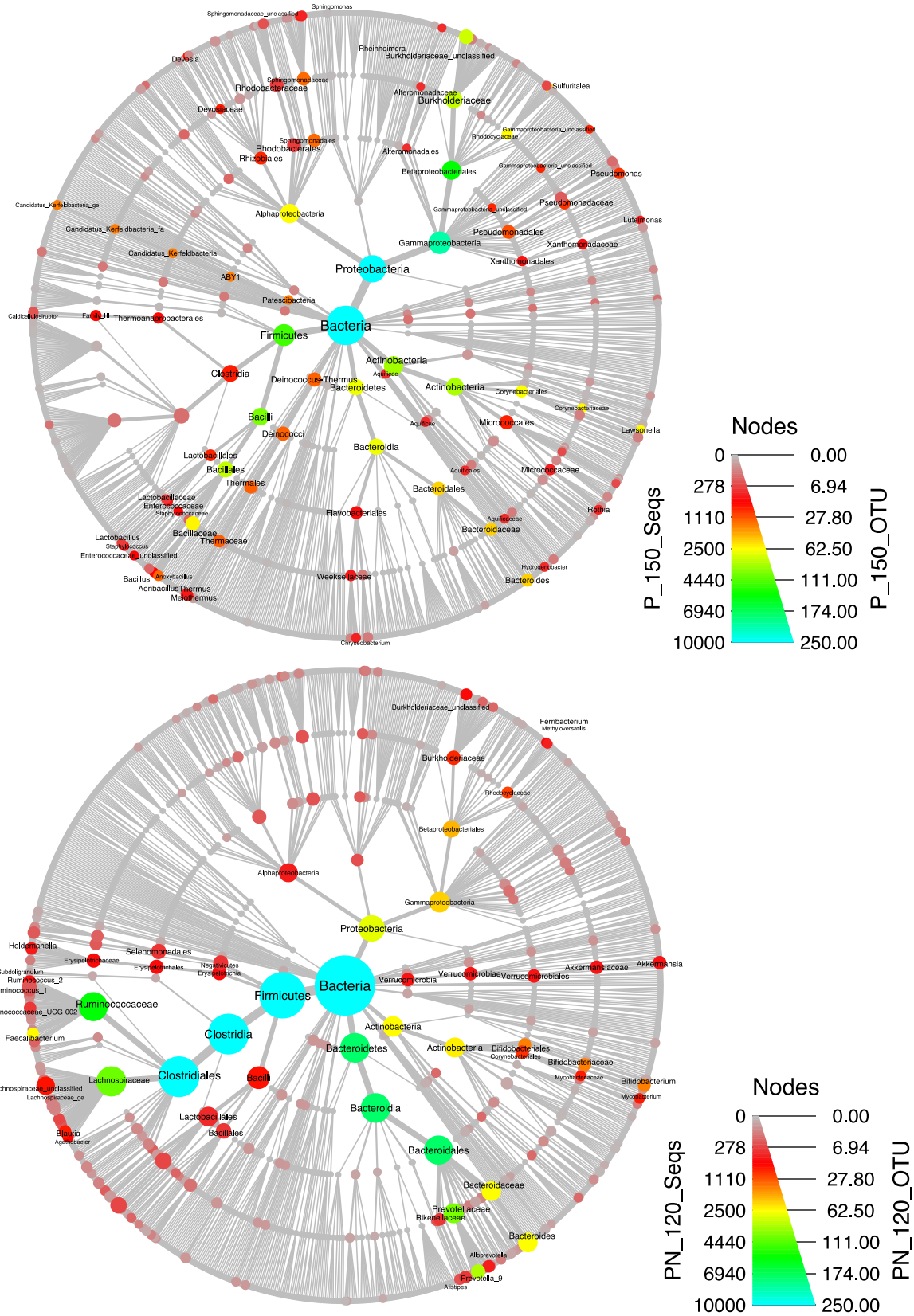
Nodes
P_150_Seqs
P_150_OTU
0
278
1110
2500
4440
6940
10000
0.00
6.94
27.80
62.50
111.00
174.00
250.00
Bacteria
Proteobacteria
Firmicutes
Actinobacteria
Bacteroidetes
Alphaproteobacteria
Gammaproteobacteria
Clostridia
Bacilli
Bacteroidia
Clostridiales
Bacteroidales
Lactobacillales
Bacillales
Ruminococcaceae
Lachnospiraceae
Bacteroidaceae
Prevotellaceae
Rikenellaceae
Bacteroides
Prevotella_9
Alloprevotella
Faecalibacterium
Ruminococcus_1
Ruminococcus_2
Ruminococcaceae_UCG-002
Lachnospiraceae_unclassified
Lachnospiraceae_ge
Blautia
Holdemanella
Selenomonadales
Negativicutes
Erysipelotrichia
Erysipelotrichales
Erysipelotrichaceae
Subdoligranulum
Verrucomicrobia
Verrucomicrobiae
Verrucomicrobiales
Akkermansiaceae
Akkermansia
Actinobacteria
Bifidobacteriales
Bifidobacteriaceae
Bifidobacterium
Corynebacteriales
Mycobacteriaceae
Mycobacterium
Nodes
PN_120_Seqs
PN_120_OTU
0
278
1110
2500
4440
6940
10000
0.00
6.94
27.80
62.50
111.00
174.00
250.00
Bacteria
Proteobacteria
Firmicutes
Actinobacteria
Bacteroidetes
Alphaproteobacteria
Gammaproteobacteria
Clostridia
Bacilli
Bacteroidia
Clostridiales
Bacteroidales
Lactobacillales
Bacillales
Ruminococcaceae
Lachnospiraceae
Bacteroidaceae
Prevotellaceae
Rikenellaceae
Bacteroides
Prevotella_9
Alloprevotella
Faecalibacterium
Ruminococcus_1
Ruminococcus_2
Ruminococcaceae_UCG-002
Lachnospiraceae_unclassified
Lachnospiraceae_ge
Blautia
Holdemanella
Selenomonadales
Negativicutes
Erysipelotrichia
Erysipelotrichales
Erysipelotrichaceae
Subdoligranulum
Verrucomicrobia
Verrucomicrobiae
Verrucomicrobiales
Akkermansiaceae
Akkermansia
Actinobacteria
Bifidobacteriales
Bifidobacteriaceae
Bifidobacterium
Corynebacteriales
Mycobacteriaceae
Mycobacterium
Burkholderiaceae_unclassified
Ferribacterium
Methylbversatilis
Burkholderiaceae
Rhodocyclaceae
Betaproteobacteriales

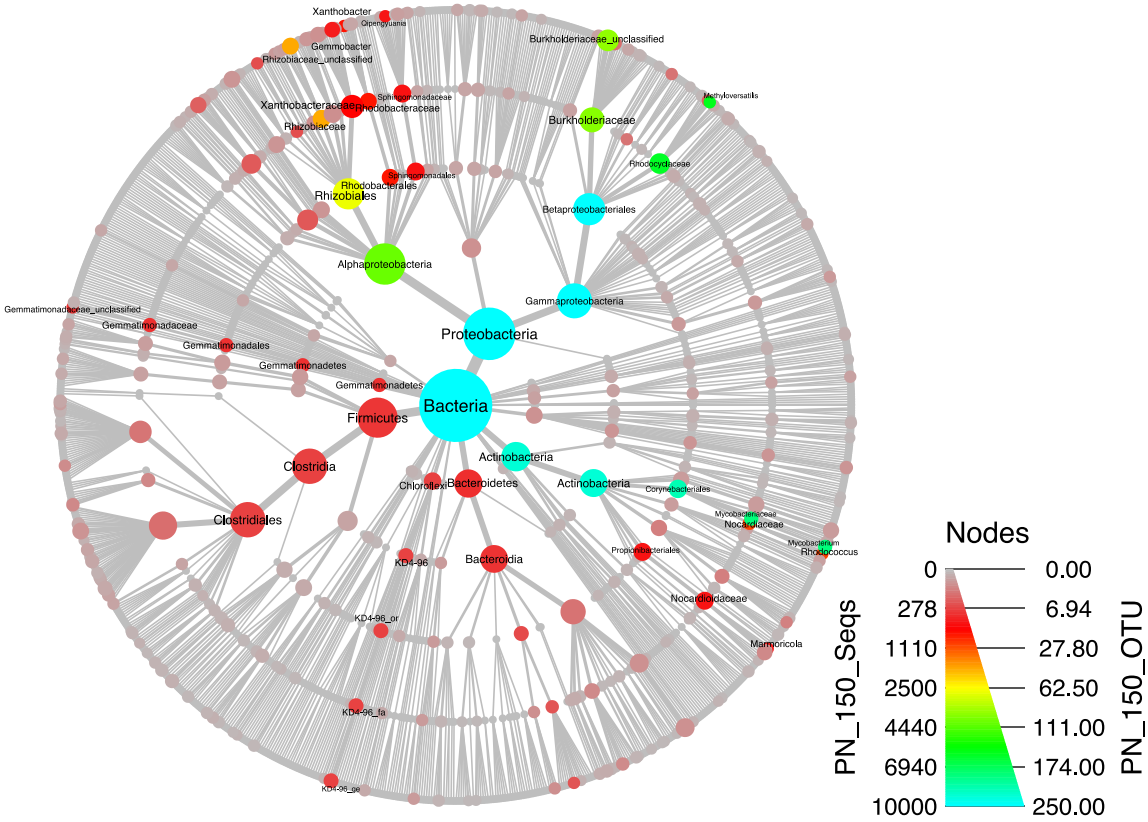

Figure 5.48. Number of reads and OTUs assigned in specific taxon under propane-biostimulation condition, and the cladograms from top to bottom correspond to the order of time. Each node represents a taxon used to classify OTUs and the edges determine where it fits in the overall taxonomic hierarchy. Node color indicates the number of reads and node diameter is proportional to the number of OTUs classified in that taxa.

The structural correlations between conditions were computed and visualized based on procrustes analyses. When CB1190 bioaugmentation and ENV425 bioaugmentation were considered, Bray-Curtis distances calculated from abundance metrics of bacterial OTUs presented insignificant (M^2 = 0.452, P > 0.05) correlations, and biostimulated conditions also showed insignificant (M^2 = 0.669, P > 0.05) correlations among microbial community profiles (Figure 5.8). This insight for overall correlations among microbial community compositions deciphered that

microbes developed inconsistently between metabolic and co-metabolic bioaugmentation process, even the spiked cultures were eliminated.

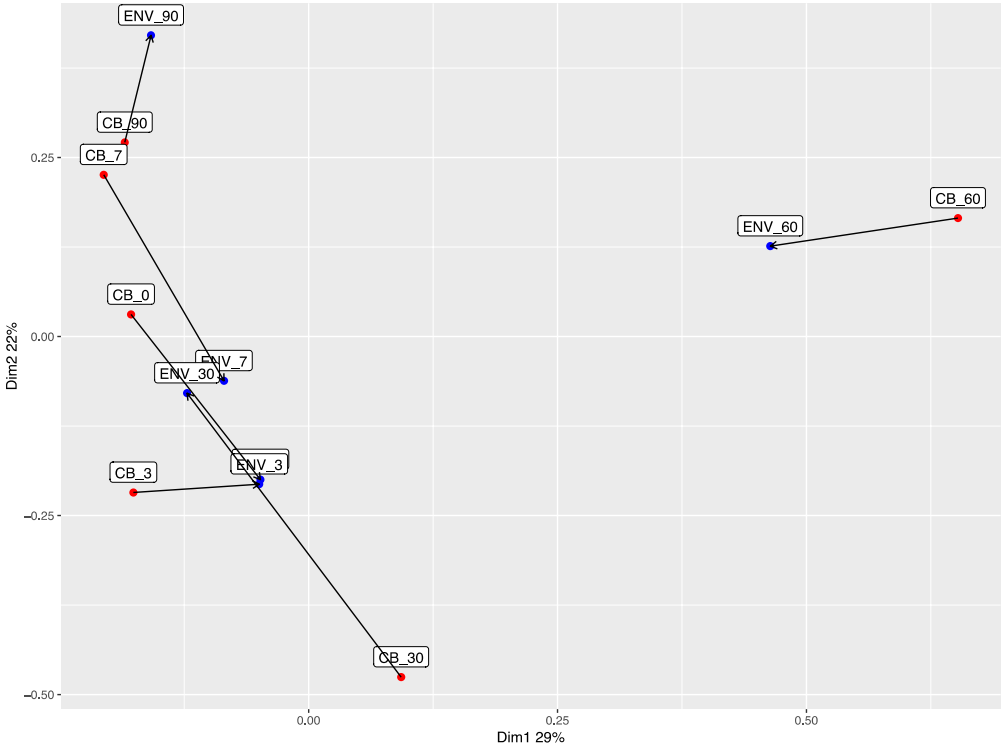

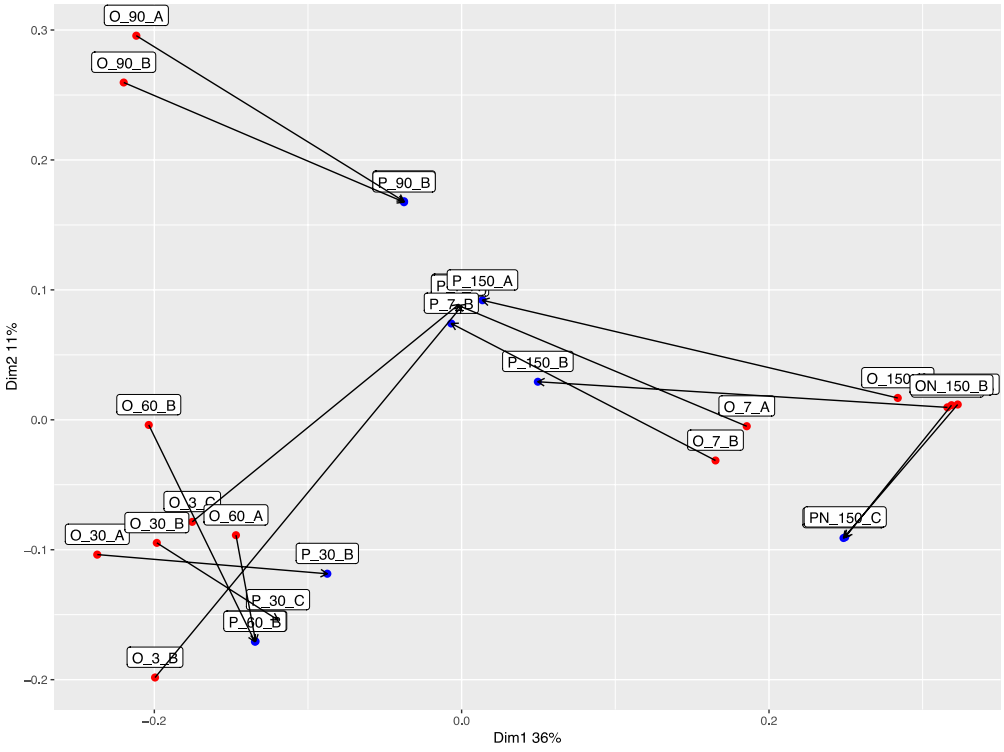

Figure 5.49. Procrustes analysis of the correlation of microbial community between different conditions based on the Bray-Curtis results of all OTUs abundances.

The microbial community correspondence between oxygen- and propane-stimulated conditions showed the different changing trends of microorganisms responding to the abiotic factors. The detailed microbial dynamics were also presented by using PCoA (Figure 5.9) that microbial memberships and abundances were distributed in unorganized directions in the course of time. Under bioaugmentation conditions, microbial membership separated at day 3, indicating the different instant microbial responses to 1,4-dioxane metabolizer and co-metabolizer, corresponding to the intensive 1,4-dioxane removals. Afterwards, types of microbes in both conditions isolated at day 60 (Figure 5.9 and 5.10), that could be attributed to the degradation of re-spiked1,4-dioxane, as stressful factor that integrated microbial community. When take microbial abundances into consideration, microbes in ENV425 bioaugmented condition distributed wider along with time, comparing with CB1190-bioaug's, and the abundance of microbial community inclined to be identical from day 60 to 90 under two conditions (Figure 5.10), exhibiting the potential temporal succession that niche-based selection.

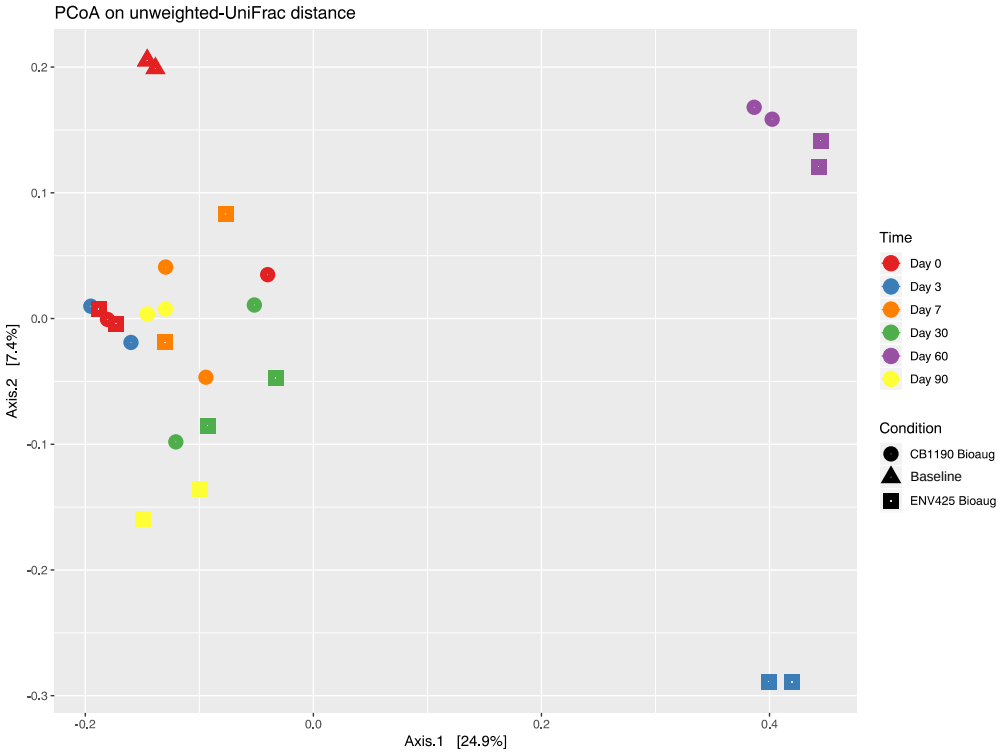
PCoA on unweighted-UniFrac distance
Axis.2 [7.4%]
Axis.1 [24.9%]
0.2
0.1
0.0
-0.1
-0.2
-0.3
-0.2
0.0
0.2
0.4
Time
Day 0
Day 3
Day 7
Day 30
Day 60
Day 90
Condition
CB1190 Bioaug
Baseline
ENV425 Bioaug

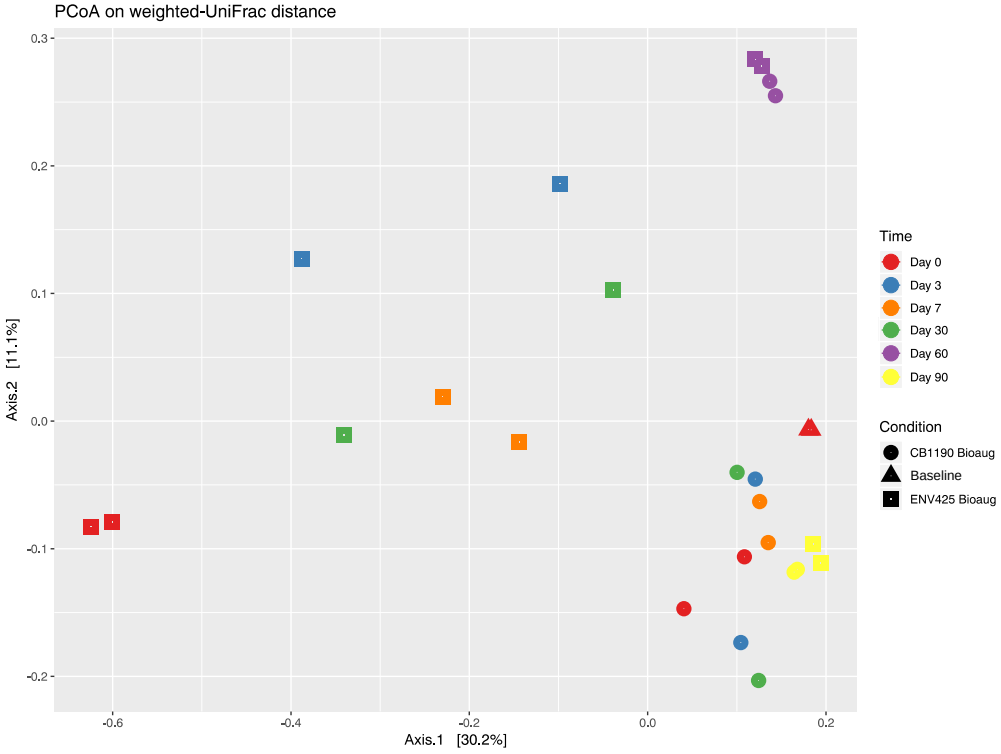
PCoA on weighted-UniFrac distance
Axis.2 [11.1%]
Axis.1 [30.2%]
0.3
0.2
0.1
0.0
-0.1
-0.2
-0.6
-0.4
-0.2
0.0
0.2
Time
Day 0
Day 3
Day 7
Day 30
Day 60
Day 90
Condition
CB1190 Bioaug
Baseline
ENV425 Bioaug

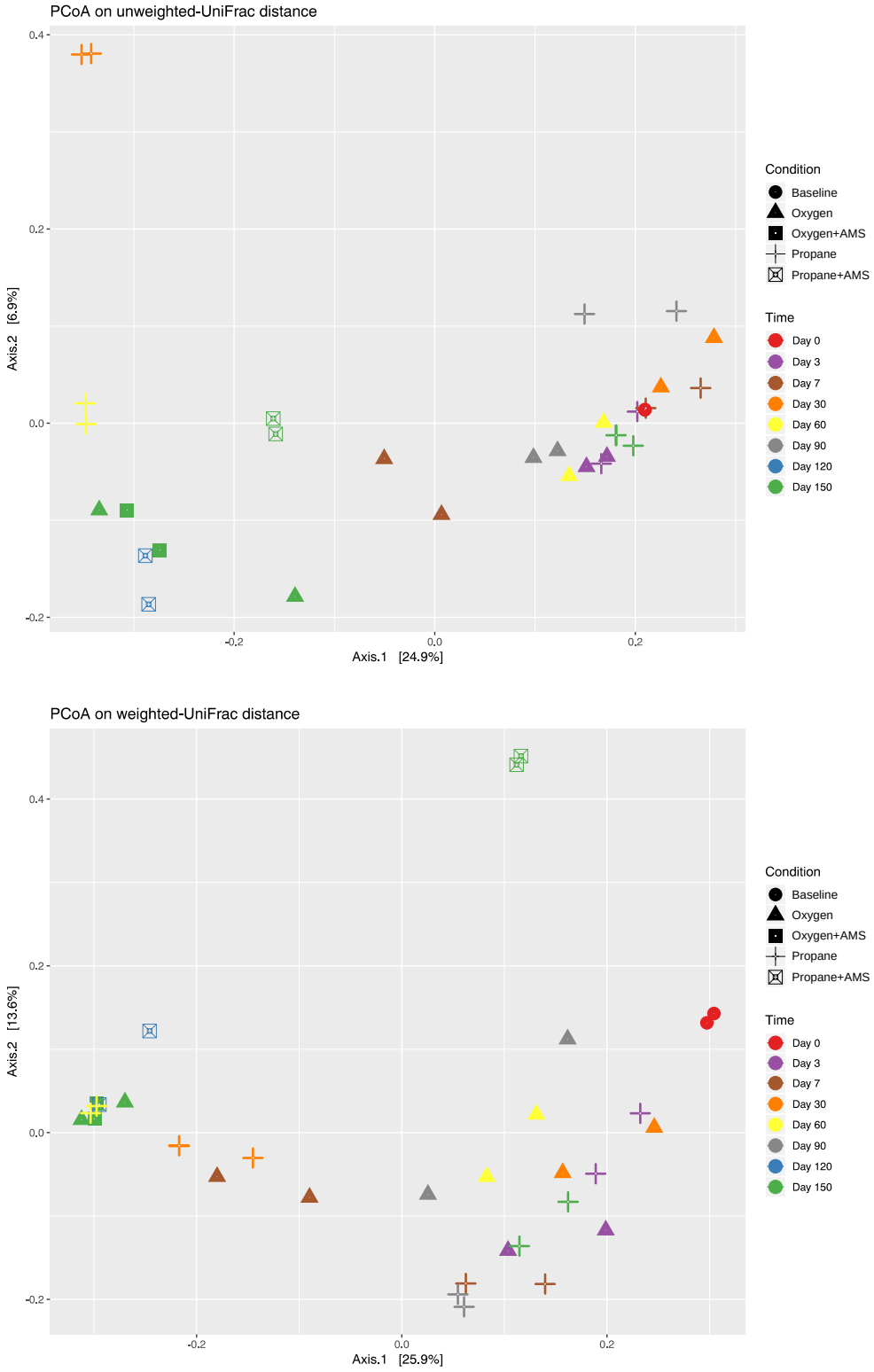

Figure 5.50. Dynamics of the microbial community at each time point under all conditions at the OTUs level during the treatment. PCoA biplots show UniFrac distances (weighted and unweighted)

based on qualitative (i.e., phylogeny) measures of microbial community with and without quantitative (i.e., abundance) measures.

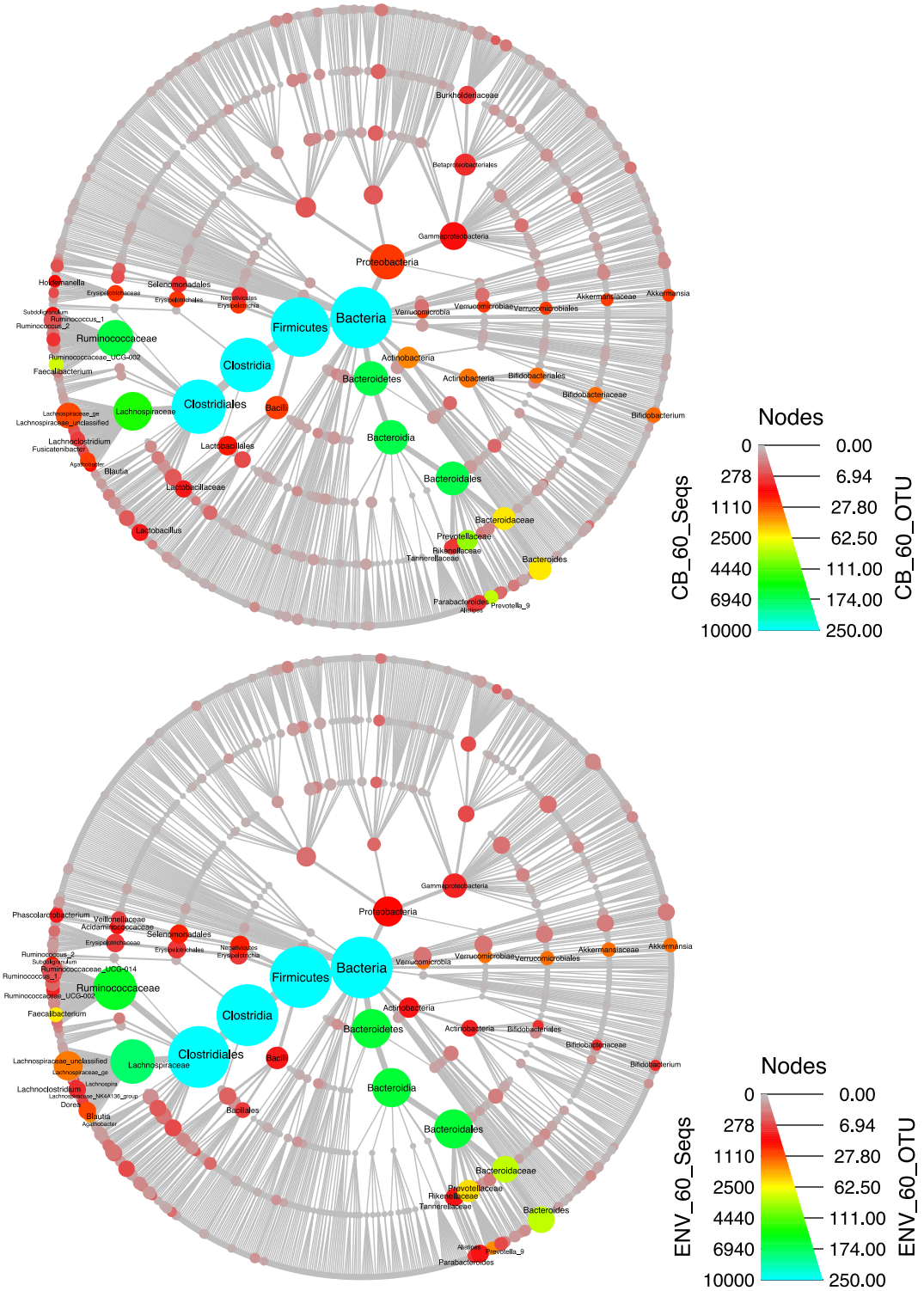

Figure 5.51. Number of reads and OTUs assigned in specific taxon under bioaugmentation conditions at day 60. Each node represents a taxon used to classify OTUs and the edges determine where it fits in the overall taxonomic hierarchy. Node color indicates the number of reads and Node diameter is proportional to the number of OTUs classified in that taxon.

The cluster analysis described similarity among samples under the same condition. Microbial communities in microcosms bioaugmented with CB1190 returned to their near-original state after 3 days, indicating the short-term shock of spiked CB1190 (Figure 5.11). The lag phase of CB1190 impacts on the whole community was shown on day 30 and 60, at which, communities were clustered differently. Moreover, community tended to be original condition after 90 days, demonstrating the self-resilience of the community, and the weak competes of CB1190. However, the microbial community developed separately after day 7, showing the slow utilization of byproducts that accumulated after first few days. Unlikely, spiked ENV425 at day 0 was relatively closed to original condition (Figure 5.11), even with different dominant bacteria, while clear dissimilarity was observed after 3 days, indicating the lag response of indigenous bacterium to ENV425 shocks. The oxygen condition caused fluctuation of microbial populations that the similarity was changed periodically, which could be explained by the fluctuation of biodiversity as well as dominant microorganisms. However, propane sparging started to separate microorganisms after 30 days, and added nutrients intensified the segregations. Similarly, community after nutrients addition was divergent under both biostimulated conditions, demonstrating the thrives of bacteria.

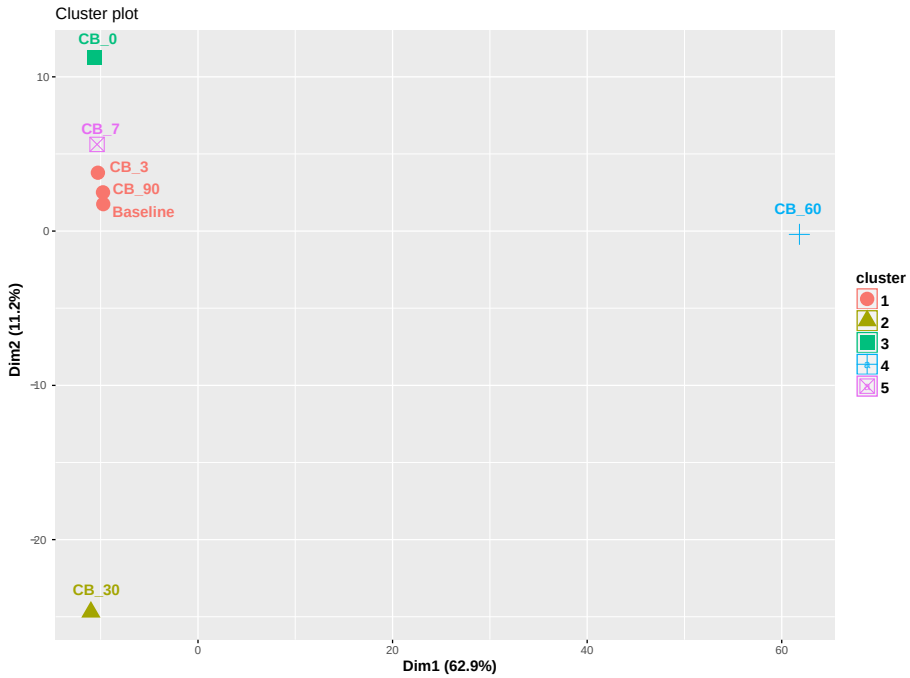

CB1190

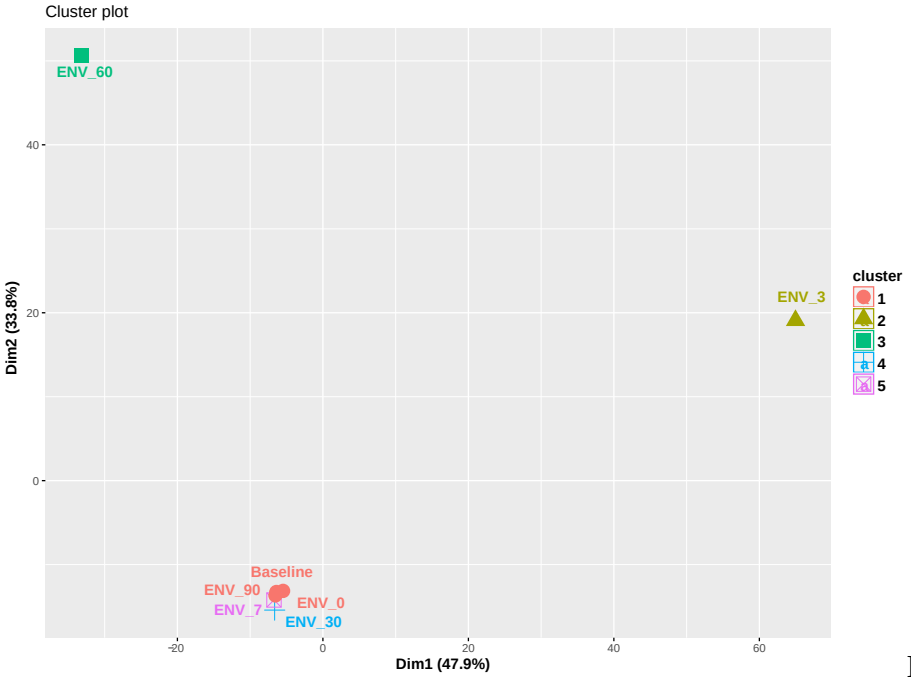

ENV425

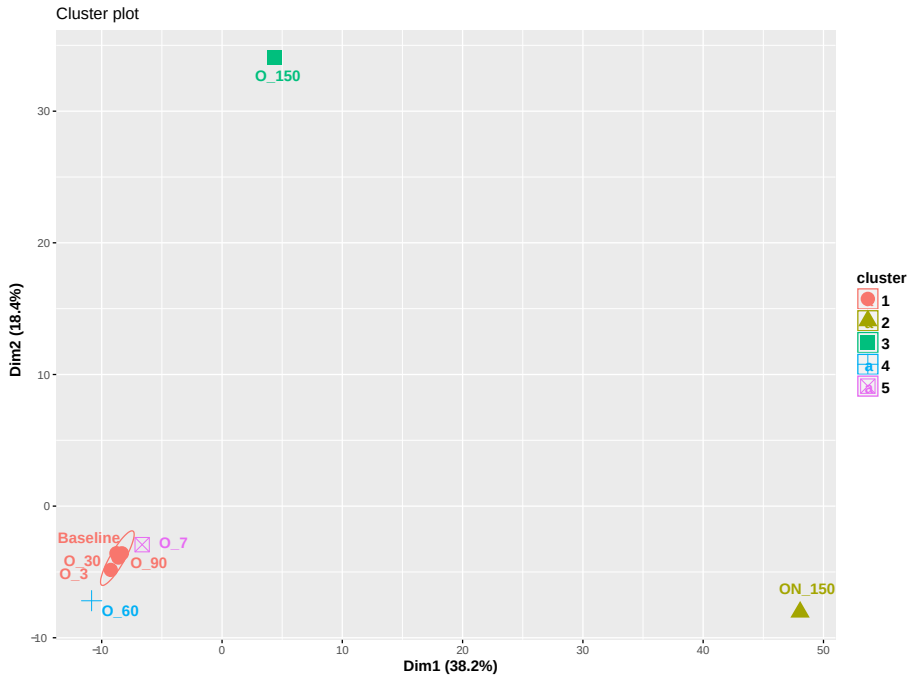

Oxygen

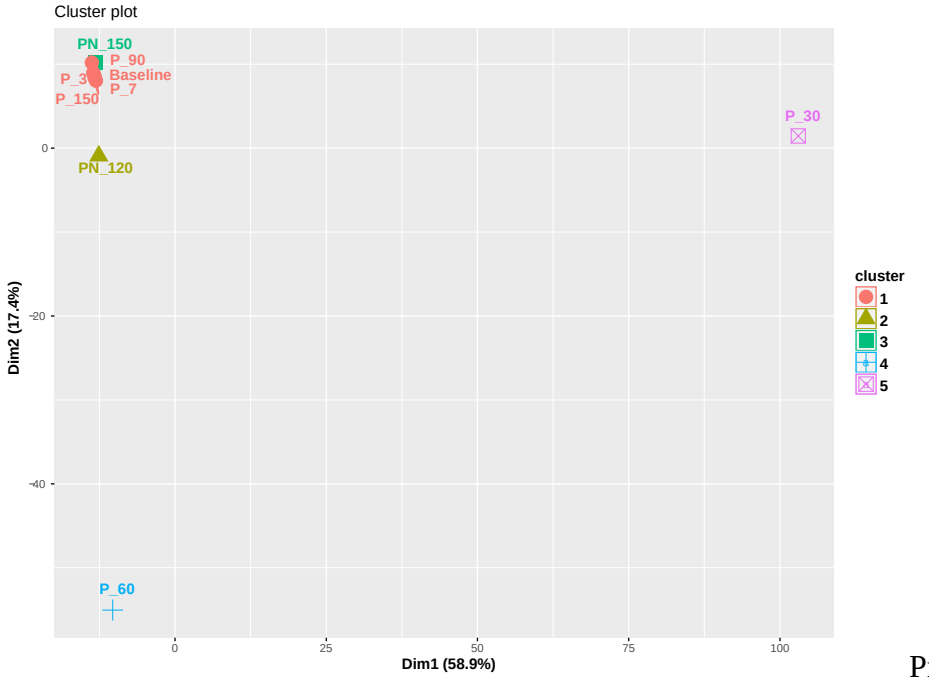

Propane

Figure 5.52. Cluster analysis among samples at each time point under all conditions during the treatment (average OTUs). All samples were classified to OTUs level and pooled together to show integral shift among conditions and time points.

5.3.4 Bacterial Functioning Potentials in Bioaugmentation and Biostimulation

The functional potentials of the bacterial community in the bioaugmentation and biostimulation processes, including pathways and enzyme-encoded genes, were derived from Tax4Fun2 based on OTUs. In the mapped data, a total of 340 groups at the level 3 pathways and 8358 KEGG orthologues (KOs) were found across all samples, mainly classified as pathways in metabolism, environmental information processing, and cellular processes, etc. on level 1. When looked at into the overall patterns, functions tended to rebound back to original level after bioaugmention process, and were stable under biostimulation process before nutrients were added with propane (Figure 5.12), validated by relative abundances of genes involved in each functional pathway on each level. This phenomenon was attributed to functional redundancy, and the low efficient of 1,4-dioxane removals during the oxygen only or propane only biostimulation process could result from the constant of functions as usual, and stimulators only triggered community changes. This decoupling between microbial functions and community compositions was also confirmed under biostimulation conditions by rare connections between microbes and genes involving in pathways in Spearman's rank-based network analysis (Figure 5.13).

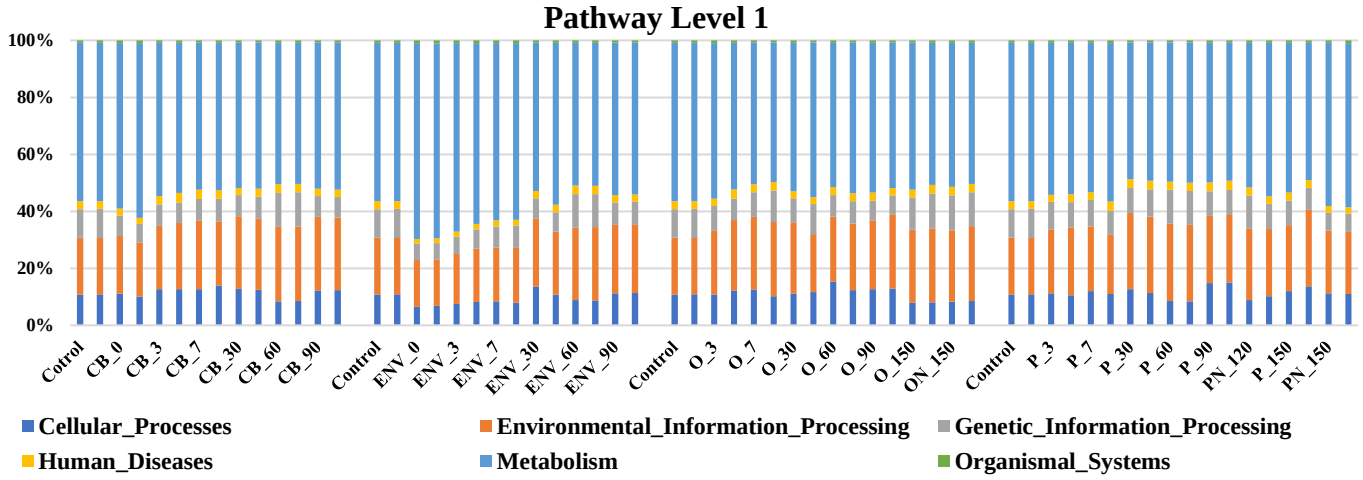

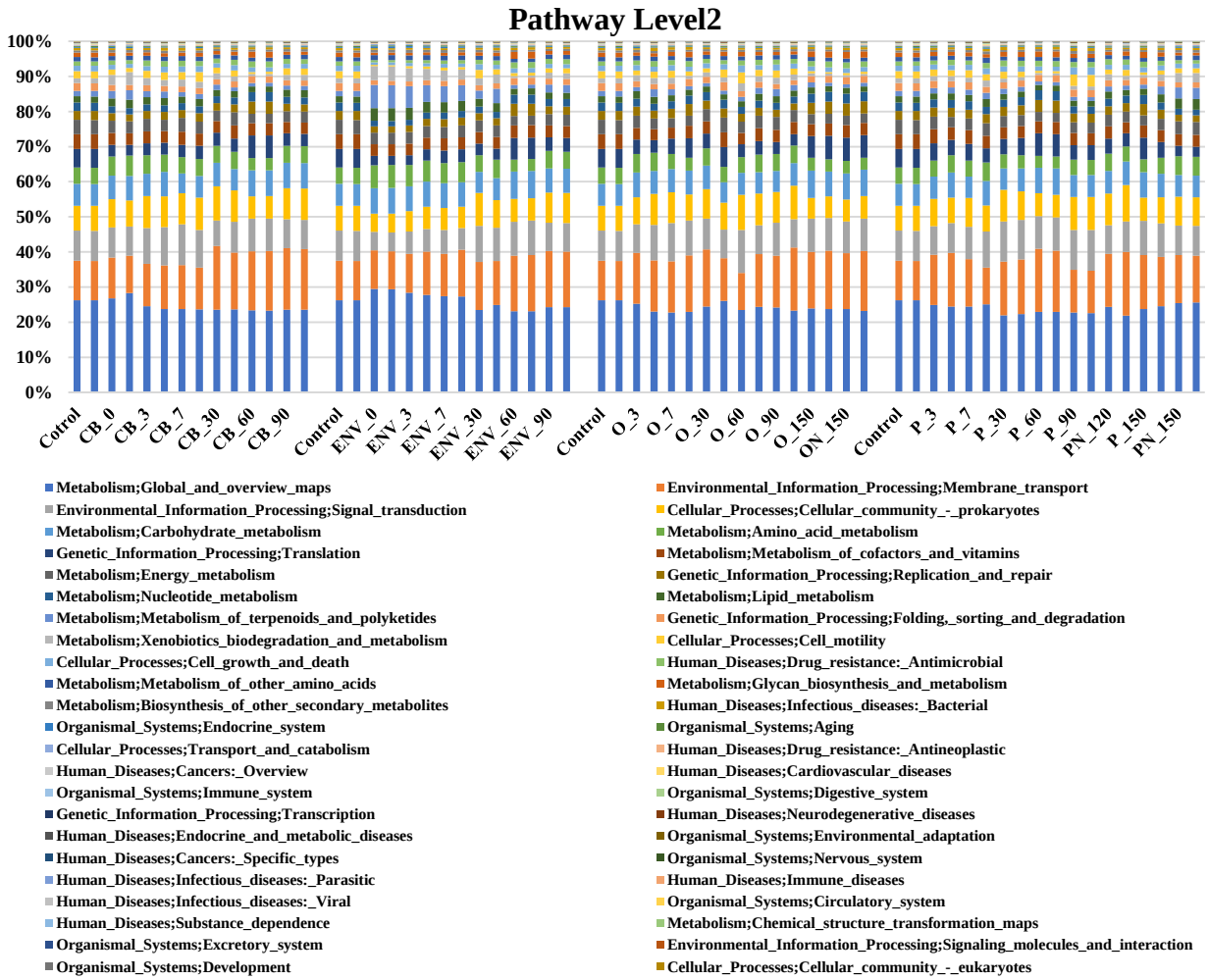

Figure 5.53. Relative abundance of each pathway on level 1 and 2 in Metabolism pathway under all conditions. The duplicates of each sample were listed, and every two bars belong to one sample.

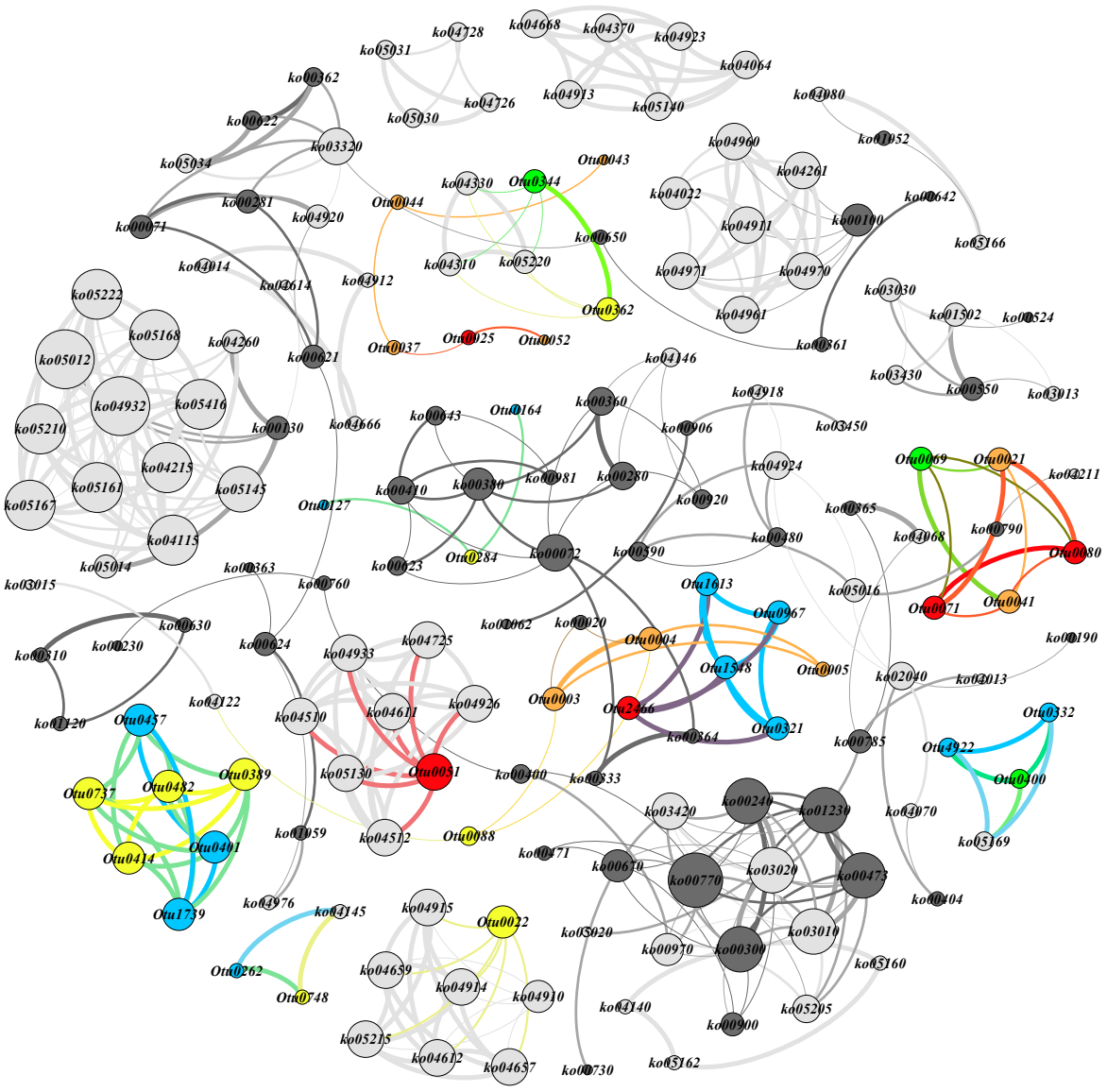

Propane-Biostimulation

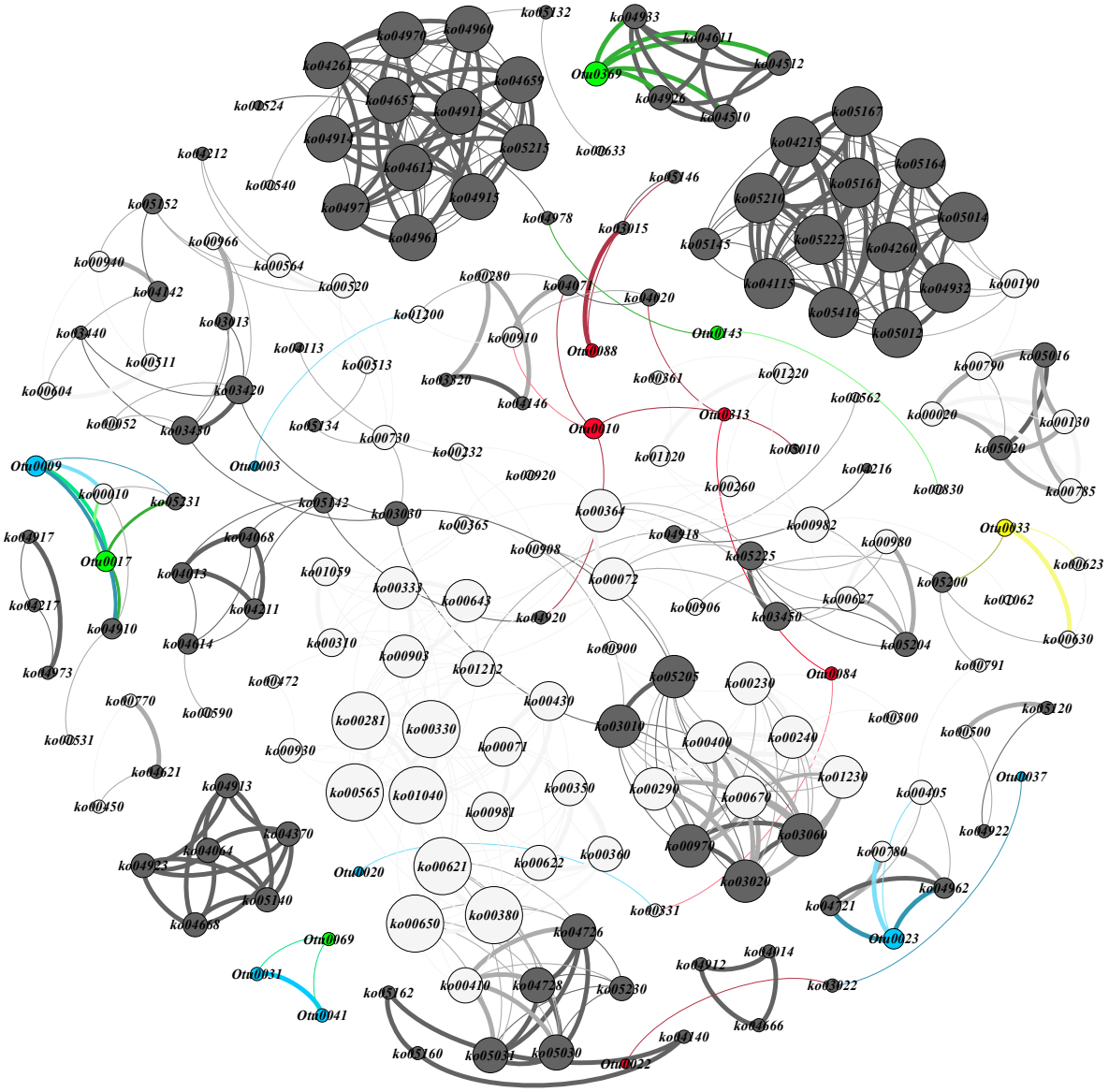

Oxygen-Biostimulation

Figure 5.54. The network analysis revealing the co-occurrence patterns among pathways and microbial taxa. The nodes were colored according to Metabolism pathways (dark), non-Metabolism pathway (grey) and OTUs (colourful). A connection represents a strong (Spearman' s correlation coefficient r > 0.8) and significant (P < 0.01) correlation. The size of each node is proportional to the number of connections.

When zoomed into metabolism pathway, carbohydrate metabolism, amino acid metabolism, lipid metabolism, xenobiotics biodegradation and metabolism, and metabolism of terpenoids and polyketides were found to increase after adding CB1190 and ENV425 (Table 5.2), explaining the high efficiency of 1,4-dioxane degradation. However, lipid metabolism, xenobiotics biodegradation and metabolism, and metabolism of terpenoids and polyketides decreased along with time, indicating the elimination of xenobiotic compounds as well as by-products. However, membrane transport pathway containing ABC transporters on level 3 was found to increase at day 30 and be abundant to the end of the experiment. This increase could be response of biodiversity boost from functional aspect, indicating more survival bacteria. In oxygen stimulated condition, the pathways on level 2 showed fluctuations along with time, even after nutrients additions. However, propane with nutrient biostimulation mode accumulated genes in lipid metabolism, xenobiotics biodegradation and metabolism, and metabolism of terpenoids and polyketides, after 60 days when nutrient was added, comparing to propane-only condition.

Table 5.10. Relative abundance of top 20 abundant level 2 pathway at each sampling point under conditions.

Level 1	Level2	Control	CB_0	CB_3	CB_7	CB_30	CB_60	CB_90
Metabolism	Global_and_overview_maps	26.22%	27.53%	24.15%	23.69%	23.58%	23.31%	23.55%
Environmental_Information_Processing	Membrane_transport	11.27%	11.10%	12.25%	12.22%	17.20%	16.93%	17.40%
Environmental_Information_Processing	Signal_transduction	8.56%	8.44%	10.55%	11.16%	7.96%	9.22%	8.25%
Cellular_Processes	Cellular_community_-_prokaryotes	7.11%	7.77%	8.94%	9.01%	9.38%	6.42%	8.92%
Metabolism	Carbohydrate_metabolism	6.21%	6.82%	6.64%	5.91%	6.38%	7.35%	7.22%
Metabolism	Amino_acid_metabolism	4.68%	5.66%	5.10%	4.75%	4.88%	3.49%	4.85%
Genetic_Information_Processing	Translation	5.29%	3.17%	3.42%	3.65%	3.76%	6.47%	3.55%
Metabolism	Metabolism_of_cofactors_and_vitamins	4.20%	3.35%	3.36%	3.61%	3.53%	3.47%	3.21%
Metabolism	Energy_metabolism	4.07%	3.48%	3.39%	3.65%	3.32%	2.71%	3.05%
Genetic_Information_Processing	Replication_and_repair	2.57%	2.05%	2.23%	2.33%	2.19%	3.45%	2.15%
Metabolism	Nucleotide_metabolism	2.37%	1.83%	1.88%	1.97%	2.02%	2.71%	1.91%
Metabolism	Lipid_metabolism	1.77%	2.33%	2.09%	1.96%	1.80%	1.59%	2.08%
Metabolism	Xenobiotics_biodegradation_and_metabolism	1.40%	3.31%	1.94%	1.83%	1.56%	0.58%	1.60%
Genetic_Information_Processing	Folding, sorting_and_degradation	2.17%	1.57%	1.62%	1.69%	1.57%	1.94%	1.50%
Cellular_Processes	Cell_motility	2.03%	1.32%	2.06%	2.48%	1.70%	0.61%	1.81%
Metabolism	Metabolism_of_terpenoids_and_polyketides	1.58%	2.45%	1.77%	1.34%	1.28%	1.06%	1.20%
Human_Diseases	Drug_resistance:_Antimicrobial	1.25%	1.15%	1.64%	1.51%	1.42%	1.68%	1.37%
Cellular_Processes	Cell_growth_and_death	1.54%	1.24%	1.47%	1.66%	1.38%	1.31%	1.33%
Metabolism	Metabolism_of_other_amino_acids	1.23%	1.24%	1.29%	1.32%	1.24%	1.06%	1.21%
Metabolism	Glycan_biosynthesis_and_metabolism	1.28%	0.95%	0.96%	1.01%	0.96%	1.74%	0.92%

Level 1	Level2	Control	ENV_0	ENV_3	ENV_7	ENV_30	ENV_60	ENV_90
Metabolism	Global_and_overview_maps	26.22%	29.41%	28.05%	27.38%	24.17%	23.15%	24.28%
Environmental_Information_Processing	Membrane_transport	11.27%	10.87%	11.73%	12.65%	13.13%	15.88%	15.93%
Environmental_Information_Processing	Signal_transduction	8.56%	5.37%	6.38%	6.50%	9.86%	9.74%	8.08%
Metabolism	Carbohydrate_metabolism	6.21%	7.31%	7.15%	7.04%	6.17%	7.78%	6.89%
Cellular_Processes	Cellular_community_-_prokaryotes	7.11%	5.25%	6.07%	6.15%	8.61%	6.43%	8.57%
Metabolism	Amino_acid_metabolism	4.68%	6.50%	6.06%	5.70%	4.97%	3.44%	4.91%
Genetic_Information_Processing	Translation	5.29%	2.68%	2.97%	3.63%	3.26%	6.11%	3.89%
Metabolism	Metabolism_of_terpenoids_and_polyketides	1.58%	6.52%	5.50%	4.52%	3.21%	1.06%	2.20%
Metabolism	Metabolism_of_cofactors_and_vitamins	4.20%	3.26%	3.29%	3.46%	3.28%	3.57%	3.40%
Metabolism	Energy_metabolism	4.07%	3.31%	3.33%	3.29%	3.34%	2.69%	3.22%
Metabolism	Lipid_metabolism	1.77%	3.62%	3.19%	2.85%	2.34%	1.70%	1.85%
Metabolism	Xenobiotics_biodegradation_and_metabolism	1.40%	4.06%	3.47%	2.91%	2.23%	0.61%	1.68%
Genetic_Information_Processing	Replication_and_repair	2.57%	1.78%	1.93%	2.22%	2.05%	3.42%	2.30%
Metabolism	Nucleotide_metabolism	2.37%	1.61%	1.73%	1.94%	1.83%	2.65%	2.10%
Genetic_Information_Processing	Folding, sorting_and_degradation	2.17%	1.32%	1.39%	1.57%	1.54%	1.96%	1.71%
Metabolism	Metabolism_of_other_amino_acids	1.23%	1.41%	1.38%	1.34%	1.22%	1.01%	1.26%
Cellular_Processes	Cell_growth_and_death	1.54%	0.78%	0.89%	1.04%	1.43%	1.32%	1.21%
Human_Diseases	Drug_resistance:_Antimicrobial	1.25%	0.64%	0.87%	0.94%	1.25%	1.73%	1.43%
Cellular_Processes	Cell_motility	2.03%	0.38%	0.64%	0.75%	1.95%	0.84%	1.33%
Metabolism	Glycan_biosynthesis_and_metabolism	1.28%	0.68%	0.79%	0.89%	1.00%	1.91%	1.00%

Level 1	Level2	Control	O_3	O_7	O_30	O_60	O_90	O_150	ON_150
Metabolism	Global_and_overview_maps	26.22%	24.12%	22.83%	25.29%	23.88%	23.73%	23.82%	23.49%
Environmental_Information_Processing	Membrane_transport	11.27%	14.56%	15.36%	14.21%	12.86%	16.38%	16.37%	16.44%
Environmental_Information_Processing	Signal_transduction	8.56%	9.10%	10.41%	8.44%	10.20%	8.67%	9.39%	9.18%
Cellular_Processes	Cellular_community_-_prokaryotes	7.11%	8.32%	8.11%	8.05%	9.52%	9.21%	6.03%	6.36%
Metabolism	Carbohydrate_metabolism	6.21%	6.76%	6.70%	6.26%	6.18%	6.21%	7.45%	7.42%
Genetic_Information_Processing	Translation	5.29%	3.87%	4.96%	4.91%	3.75%	3.29%	6.40%	6.54%
Metabolism	Amino_acid_metabolism	4.68%	5.20%	3.97%	4.63%	4.73%	4.94%	3.59%	3.51%
Metabolism	Metabolism_of_cofactors_and_vitamins	4.20%	3.25%	3.34%	3.85%	3.46%	3.49%	3.46%	3.52%
Metabolism	Energy_metabolism	4.07%	3.25%	2.83%	3.83%	3.38%	3.52%	2.80%	2.70%
Genetic_Information_Processing	Replication_and_repair	2.57%	2.44%	2.93%	2.53%	2.24%	1.98%	3.37%	3.46%
Metabolism	Nucleotide_metabolism	2.37%	2.08%	2.31%	2.44%	2.00%	1.94%	2.65%	2.73%
Genetic_Information_Processing	Folding, sorting_and_degradation	2.17%	1.60%	1.86%	2.05%	1.69%	1.45%	1.87%	1.98%
Metabolism	Lipid_metabolism	1.77%	2.04%	1.69%	1.56%	1.80%	1.81%	1.68%	1.63%
Cellular_Processes	Cell_motility	2.03%	1.57%	1.61%	1.68%	2.45%	1.91%	0.53%	0.60%
Cellular_Processes	Cell_growth_and_death	1.54%	1.44%	1.51%	1.50%	1.68%	1.56%	1.35%	1.32%
Human_Diseases	Drug_resistance:_Antimicrobial	1.25%	1.47%	1.55%	1.21%	1.42%	1.40%	1.62%	1.67%
Metabolism	Metabolism_of_terpenoids_and_polyketides	1.58%	1.69%	1.35%	1.08%	1.47%	1.80%	1.26%	1.05%
Metabolism	Xenobiotics_biodegradation_and_metabolism	1.40%	1.69%	1.25%	1.32%	1.90%	1.66%	0.71%	0.57%
Metabolism	Glycan_biosynthesis_and_metabolism	1.28%	1.01%	1.41%	1.11%	1.09%	0.92%	1.70%	1.82%
Metabolism	Metabolism_of_other_amino_acids	1.23%	1.31%	1.05%	1.18%	1.23%	1.19%	1.08%	1.06%

Level 1	Level2	Control	P_3	P_7	P_30	P_60	P_90	P_150	PN_120	PN_150
Metabolism	Global_and_overview_maps	26.22%	24.69%	24.77%	22.09%	22.95%	22.66%	23.13%	24.15%	25.56%
Environmental_Information_Processing	Membrane_transport	11.27%	14.81%	11.95%	15.45%	17.69%	12.10%	16.61%	14.69%	13.44%
Environmental_Information_Processing	Signal_transduction	8.56%	8.30%	9.78%	11.38%	9.37%	11.51%	8.37%	9.66%	8.45%
Cellular_Processes	Cellular_community_prokaryotes	7.11%	7.50%	7.78%	8.57%	6.45%	9.39%	9.76%	7.02%	8.22%
Metabolism	Carbohydrate_metabolism	6.21%	6.71%	6.56%	6.31%	7.41%	6.27%	6.57%	6.97%	6.17%
Genetic_Information_Processing	Translation	5.29%	4.65%	4.37%	4.59%	6.39%	4.18%	4.02%	5.32%	2.90%
Metabolism	Amino_acid_metabolism	4.68%	4.77%	4.92%	3.92%	3.40%	4.30%	4.58%	4.11%	5.36%
Metabolism	Metabolism_of_cofactors_and_vitamins	4.20%	3.79%	3.77%	3.36%	3.45%	3.43%	3.30%	3.44%	3.34%
Metabolism	Energy_metabolism	4.07%	3.29%	3.44%	3.19%	2.64%	3.05%	3.18%	3.02%	3.65%
Genetic_Information_Processing	Replication_and_repair	2.57%	2.58%	2.57%	2.67%	3.43%	2.48%	2.41%	2.92%	1.92%
Metabolism	Nucleotide_metabolism	2.37%	2.25%	2.19%	2.19%	2.71%	2.06%	2.13%	2.34%	1.64%
Metabolism	Lipid_metabolism	1.77%	1.81%	2.01%	1.61%	1.54%	1.65%	1.88%	2.08%	2.99%
Genetic_Information_Processing	Folding_sorting_and_degradation	2.17%	1.93%	1.87%	1.76%	1.90%	1.99%	1.69%	1.80%	1.44%
Cellular_Processes	Cell_motility	2.03%	1.81%	1.98%	1.74%	0.59%	3.31%	1.50%	0.95%	1.38%
Metabolism	Metabolism_of_terpenoids_and_polyketides	1.58%	1.59%	1.68%	1.47%	1.01%	1.06%	1.28%	1.67%	3.21%
Cellular_Processes	Cell_growth_and_death	1.54%	1.41%	1.58%	1.52%	1.30%	2.08%	1.40%	1.41%	1.33%
Human_Diseases	Drug_resistance:_Antimicrobial	1.25%	1.36%	1.41%	1.64%	1.63%	1.51%	1.54%	1.45%	1.03%
Metabolism	Xenobiotics_biodegradation_and_metabolism	1.40%	1.39%	1.57%	1.06%	0.57%	1.05%	1.46%	1.29%	2.65%
Metabolism	Glycan_biosynthesis_and_metabolism	1.28%	1.11%	1.10%	1.35%	1.67%	1.16%	1.13%	1.47%	0.79%
Metabolism	Metabolism_of_other_amino_acids	1.23%	1.21%	1.33%	1.09%	1.04%	1.18%	1.14%	1.13%	1.33%

Network analysis was further applied in biostimulation process to show strong (coefficients > 0.8) and significant ($p < 0.01$) connections between microbes (OTUs) and monooxygenases, since they are the critical enzyme in first step of 1,4-dioxane biodegradation (Mahendra and Alvarez-Cohen, 2006). Again, because of the fluctuation of microbe against functional redundancy, only a few OTUs significantly connected with monooxygenases (Figure 5.14). For example, under bioaugmentation conditions, spiked CB1190 had positive correlations with anthranilate 3-monooxygenase, aurachin C monooxygenase, and 4-nitrophenol 2-monooxygenase, while ENV425 showed positive correlations with methane and propane related monooxygenases, in line with its cometabolic capability. However, under propane biostimulated condition, no clear correlations were found even for accumulated genera *Mycobacterium* and *Methyloversatilis*, that could be attributed that they carried existing abundant monooxygenases (propane monooxygenases) or other enzymes that catalyzed 1,4-dioxane.

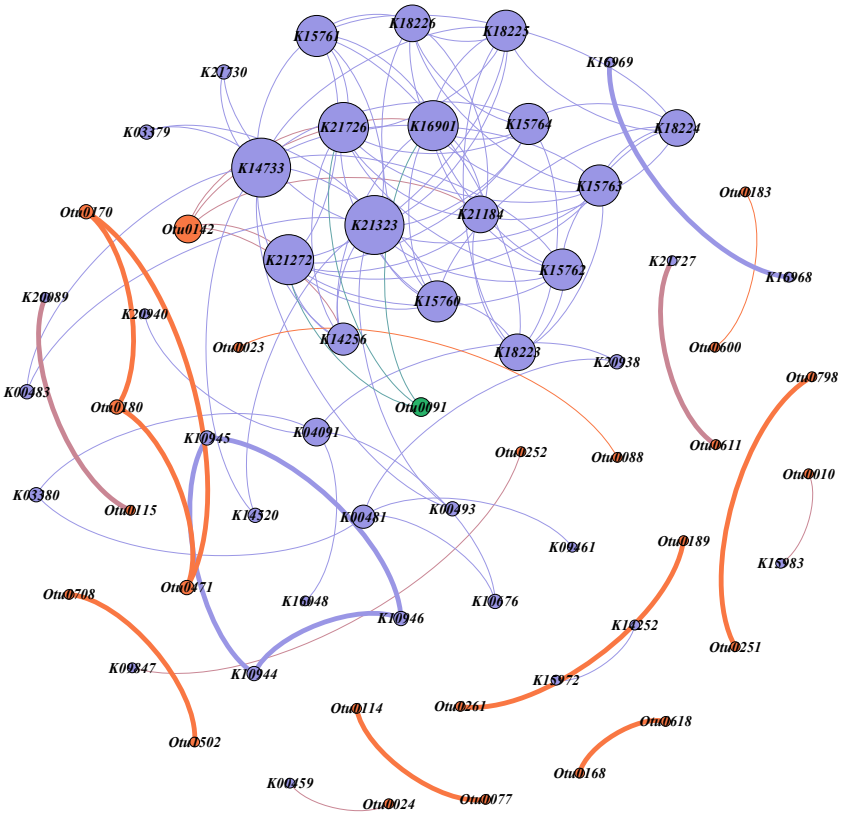

CB1190

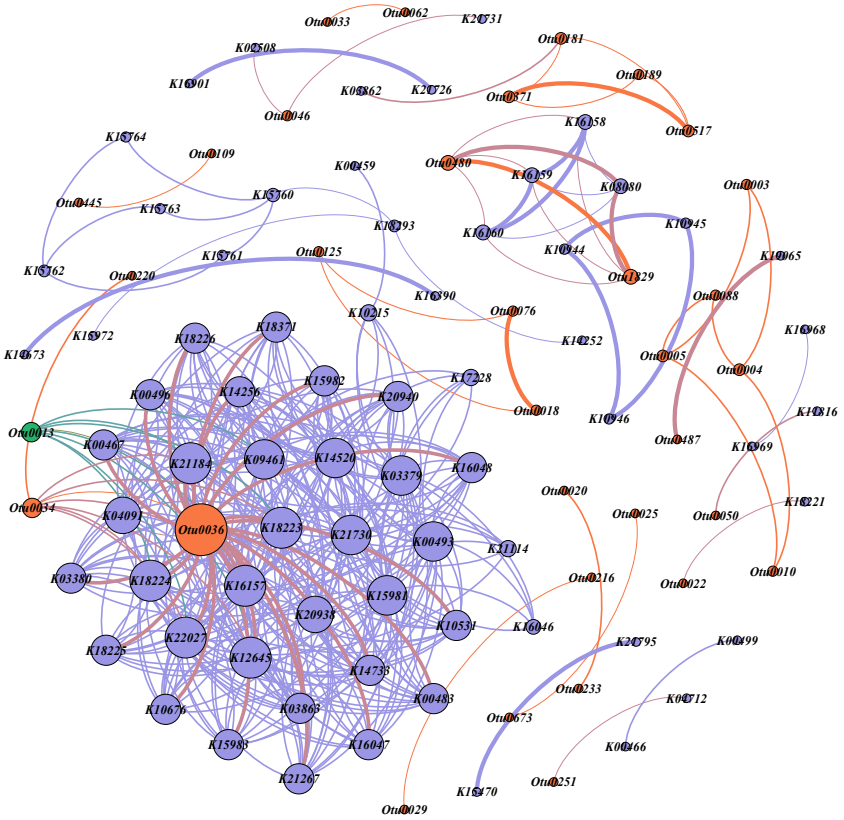

ENV425

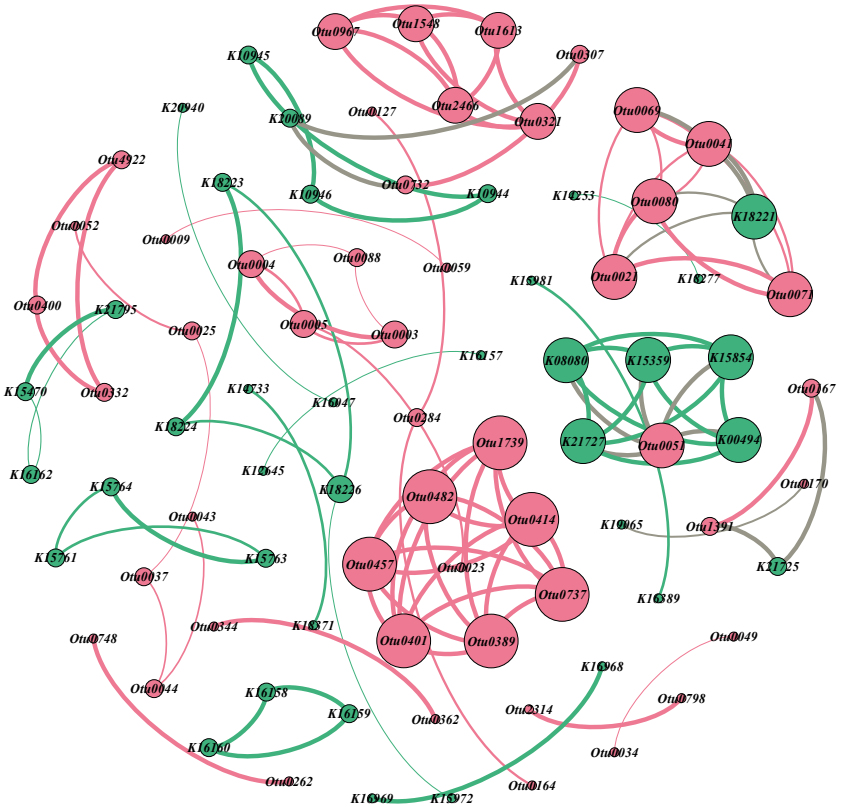

Oxygen

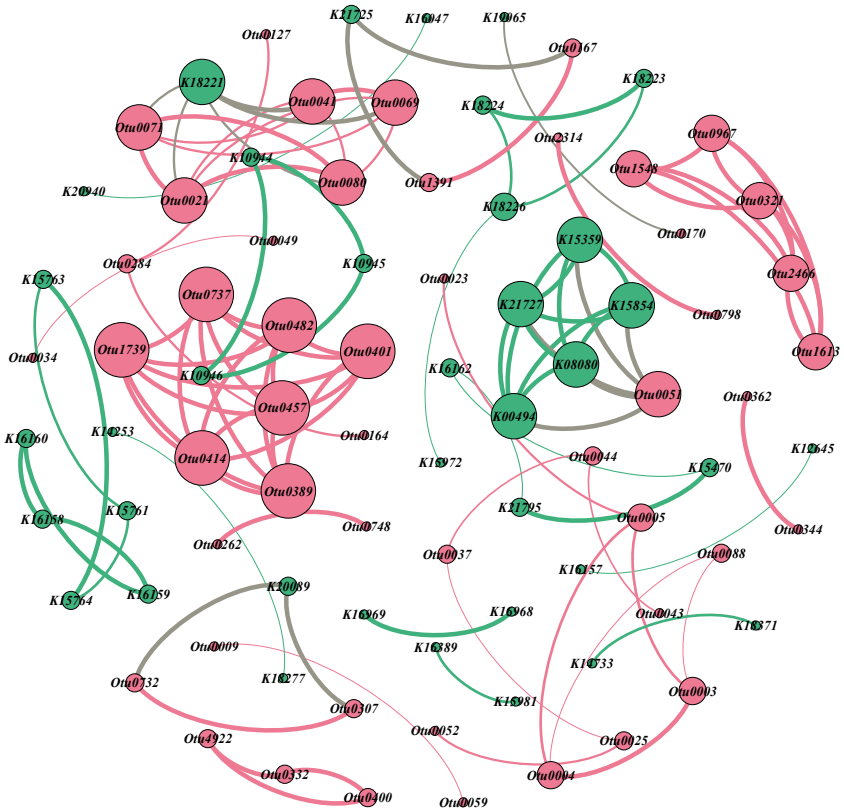

Propane

Figure 5.55. The network analysis revealing the co-occurrence patterns among monooxygenases and microbial taxa. The nodes were colored according to monooxygenase types and OTUs. A connection represents a strong (Spearman's correlation coefficient r > 0.8) and significant (P < 0.01) correlation. The size of each node is proportional to the number of connections.

5.4 Discussion

Bioaugmented CB1190 and ENV425 showed efficient removal performances, and 1,4-dioxane metabolizer CB1190 has been widely reported as a high efficient degrader in previous studies (Mahendra and Alvarez-Cohen, 2005, Miao et al., 2019), that monooxygenase firstly catalyzes 1,4-dioxane (Mahendra and Alvarez-Cohen, 2006, Gedalanga et al., 2014). The propanotroph ENV425 has previously been linked to 1,4-dioxane degradations with propane sparging (Lippincott et al., 2015), and the cell viability could still last more than 30 days in this study, even in the absence of propane, indicating this extensive co-metabolism could supply low levels of energy sufficient to

sustain ENV425 (Chu et al., 2018), which was similar to propanotroph *Mycobacterium austroafricanum* JOB5 (JOB5) (Mahendra et al., 2007). Moreover, 1,4-dioxane was studied to be co-metabolic biodegradation in aquifer with methane or ethane (Hatzinger et al., 2017), as well as propane and 1-butanol (Hand et al., 2015) as primary substrates, that could induce the expression of different oxygenases.

Under biostimulation conditions, 1,4-dioxane showed steadily degradation, and only ~50% removals were achieved in 150 days, that was similar to previous studies that Lippincott et al. (2015) observed no 1,4-dioxane degradation in oxygen or oxygen with propane amended microcosms, and propane pre-incubated microcosms with groundwater were able to degrade 1,2-dibromoethane with a low rate and extent (Hatzinger et al., 2015). This could be attributed to the complicated indigenous microbial community that propane was utilized by propanotrophs while putative propane monooxygenase was insufficient to oxidize 1,4-dioxane or had high affinity to other dissolved organic compounds. Additionally, for the co-metabolic process, the primary substances usually work as a competitive inhibitors of the biodegradation of the targeting contaminants (Hatzinger et al., 2018), that propane in this study might slow or cease 1,4-dioxane degradation. However, the accelerated degradation rate after AMS addition indicated that indigenous microbes are capable of growing on the propane and degrading 1,4-dioxane efficiently, but only in the presence of sufficient ammonia and phosphate nutrients, consistent with previous studies (Hatzinger et al., 2015, Hatzinger et al., 2018).

Propane was observed to be degraded but without 1,4-dioxane degradation in biostimulation microcosms, and based on model simulation, inhibition caused by propane on co-metabolism of 1,4-dioxane was significantly higher than inhibition caused by 1,4-dioxane on propane utilization (Barajas-Rodriguez and Freedman, 2018). However, higher rates of oxygen and propane

consumptions were observed after nutrient additions in biostimulation bottles, indicating the thrive of propanotrophs or other aerobic microbes, and the previous inadequate amounts of inorganic nutrients could also limit the biodegradation of alkane gases (Hatzinger et al., 2015).

The more abundant ENV425 than CB1190 could be attributed to broader carbon sources for ENV425's growth, and Barajas-Rodriguez and Freedman (2018) reported that CB1190 would be more competitive when 1,4-dioxane turned to be low, while ENV425 depended more strongly on the amount of propane. The rapid growth of biomass was observed when nutrients were added under biostimulation, and previous study found that ammonium nutrients had significant enhancements on indigenous microbiomes, even better than organic nitrogen (Wang et al., 2018).

The relative expression of *dxmB* declined after 1,4-dioxane was removed, and this was consistent with descriptions that *dxmB* activity responds to 1,4-dioxane concentrations (Gedalanga et al., 2014). Gene *aldH* is not specific to 1,4-dioxane biodegradation and could be induced by aldehydes that are produced by any reactions other than 1,4-dioxane degradation (Jung et al., 2016), explaining high abundance of *aldH* than that of *dxmB.* Furthermore, because of propanotrophic bacteria carrying *aldH* (Masuda et al., 2012), *aldH*'s relative expression was kept high under propane sparged condition. Gene *prmA* was stimulated upon nutrient addition after 90 days in propane biostimulated bottles that was consistent with previous study in which Hatzinger et al. (2017) suggested propanotrophs could be resilient to a shortage of nutrients when treating N-nitrosodimethylamine (NDMA) and N-nitrodimethylamine (NTDMA) in a field-scale fluidized bed bioreactor.

The change of biodiversity was related to accumulated byproducts that could feed other indigenous microorganisms, and the affinity towards 1,4-dioxane was higher in the propanotrophic cultures than in CB1190 (Barajas-Rodriguez and Freedman, 2018), resulting in higher biodiversity

in ENV425 bioaugmented bottles. Under oxygen biostimulation conditions, the trend of biodiversity could not only be attributed to intermediates and nutrients, but also microbial competition, lag responses to O_2, as well as different O_2 consumptions, that also could be applied in propane biostimulated microcosms. However, dominance of propanotrophs along with propane sparging might occupy more nutrients in original samples over time. The most dominant genus in original sample, *Hydrogenobacter*, was a well-studied aerobic hydrogen-oxidizing bacterium, and can survive at extreme thermophilic environments (Sharma et al., 2015). Both bioaugmented *Pseudonocardia* and *Rhodococcus* eventually decreased with time, but genus *Rhodococcus* decreased relatively slower, since strains of *Rhodococcus* are able to catabolize a wide range of compounds and produce bioactive steroids, acrylamide, and acrylic acid (McLeod et al., 2006), that allow them to thrive under a variety of conditions with the capability to metabolize various hydrocarbons. However, genus *Pseudonocardia* could be more dependent on 1,4-dioxane for metabolism, thus its abundance rapidly declined when 1,4-dioxane was degraded after 3 days. Moreover, microbial compositions fluctuated along with time and under both bioaugmentations, indicating the potential differences of intermediates utilization and efficiency, as well as interactions among microorganisms. Under oxygen biostimulation, more minor bacteria were observed to thrive after the addition of nutrients, and it is common that rare taxa replaced previously dominant or metabolically similar taxa in a short period, even within the constant environments (Fernandez-Gonzalez et al., 2016). Furthermore, and propane-growing genus *Mycobacterium* accumulated with sufficient nutrient and propane, which has been widely reported to be able to degrade 1,4-dioxane (Deng et al., 2018, He et al., 2018), and may have contributed to the rapid 1,4-dioxane removal after the nutrient addition.

This procrustes analyses for overall correlations among microbial community compositions deciphered that microbes developed inconsistently between metabolic and co-metabolic bioaugmentation process, even the spiked cultures were eliminated, indicating the different impacts of external cultures on indigenous microbes, that could be attributed to various biotransformation products. Alidina et al. (2014) have studied that adaption phase to primary substrate would affect microbial compositions, and the adaption phase could be interpreted as post-bioaugmentation process, where microbes adapted metabolic or co-metabolic products. Moreover, the interactions between augmented bacteria and indigenous microorganisms could also differentiate the microbial compositions, e.g., CB1190 was found to co-occur with Rhizobiales, Bacillales, and Sphingobacteriales (Miao et al., 2019).

Under bioaugmentation conditions, microbial membership separated at day 3, indicating the different instant microbial responses to 1,4-dioxane metabolizer and co-metabolizer, and Festa et al. (2016) have studied that PAH-degrading strain could cause a drastic change on soil microbial community when using bioaugmentation strategy. Afterwards, stressful factor could integrate the microbial community, which was also described by Wang et al. (2014) that an evident shift in the soil bacterial and fungal community structures due to adding indole. When taken microbial abundances into consideration, microbes in ENV425 bioaugmented condition distributed wider along with time, that could be related to the wide range of primary or co-metabolic substrates and tolerances to several stress of the genus *Rhodococcus* and its species (Cappelletti et al., 2016). The co-metabolism process could allow the growth of various microbes independent of the target contaminants, and have advantages over growth-linked biodegradation when contaminant concentrations are low (Hatzinger et al., 2018). Thus, ENV425 could not only target on 1,4-dioxane, but also other carbon sources in the groundwater, whose catabolites might benefit more other

microorganisms. The identical microbial composition in the later bioaugmentation exhibited the potential temporal succession that niche-based selection with similar developments of compositions and diversities over time (Miao et al., 2019), because of absence of obvious environmental variations (Louca et al., 2018), e.g., the diminished original bioaugmented bacteria and 1,4-dioxane in this study. This indicated that the community had the identical potential to normal condition even after different biological augmentations, and the previous investigation also found that the remediated soil had a similar microbial community composition and distribution to that in the normal soil (Wu et al., 2011). Wang et al. (2014) studied indole-contaminated soil and found that bioaugmented strain could increase microbial diversity with some restoration of the resident microbial community. The restoration to original robustness of microbial community was also observed in organic biomixture packed columns treating pesticides, attributed to the adaption of microorganisms in the biopurification systems (Diez et al., 2017). Furthermore, the dormant microorganisms persisting in the soil may also contribute to the community resilience after bioaugmentation and 1,4-dioxane spikes (Jones and Lennon, 2010). Besides, microbes and their respiration products could create the oxidation-reduction condition that eventually harbored the restoring community (Shade et al., 2012).

The functional potentials of the bacterial community in the bioaugmentation and biostimulation processes were predicted by Tax4Fun2 based on OTUs, but not all sequenced reads could be affiliated to existing KEGG database because of the unknown or uncultured microorganisms (Babin et al., 2019), The dominant pathways including metabolism, environmental information processing, and cellular processes were similar to previous soil study (Zhou et al., 2019). The functional redundancy was in the sense that functions could be performed by multiple coexisting, taxonomically distant microorganisms (Louca et al., 2017), such as variable microbial communities in this study. Purahong et al. (2018) also found a strong OTUs shift in wood-inhabiting fungal community after

nitrogen addition, while the functional redundancy was in the treatment. The reason was that functions were largely determined by the environment and type of ecosystem, and were less sensitive to taxonomic variations (Louca et al., 2018), which actually were considered as complementary to functional community structure within the functional groups (Louca et al., 2016). Stimulators only triggered community changes, and the broad functions may be more functionally redundant and thus better buffered against taxonomic shifts caused by biotic or abiotic disturbance (Blanco et al., 2015), or adaptions to selective pressure through physiological changes and genetic evolution respectively (Schimel et al., 2007). Anantharaman et al. (2016) observed no correlation between number or relative abundance of microorganism controlling the specific step of a pathway and total energy yields associated with that step, in river aquifer system. This decoupling between microbial functions and community compositions was also observed in engineered system with controlled environments, where overall functionality was maintained while dominant microorganisms changed (Vanwonterghem et al., 2016), and taxonomic turnover might only weakly affect micro-ecological functioning (Langenheder et al., 2005). Therefore, the main driver for biodegradation was the enhance of functions by artificially added strains or nutrients, e.g., genes in pathways of metabolism in this study, in both bioaugmentation or biostimulation processes.

The abundant carbohydrate metabolism, amino acid metabolism, lipid metabolism, xenobiotics biodegradation and metabolism, and metabolism of terpenoids and polyketides could explain the high efficiency of 1,4-dioxane degradation like previous bioaugmentation strategy (Chi et al., 2018), and this could be related to some specific compounds (e.g., toluene, steroid, benzoate, xylene, styrene, etc.) degradation function genes (level 3) or horizontal transfer genes Bai et al. (2016). However, lipid metabolism, xenobiotics biodegradation and metabolism, and metabolism of terpenoids and polyketides decreased along with time, indicating the elimination of xenobiotic compounds as well

as by-products, since these functional genes were indicators of the presence of xenobiotics and their metabolites (Bai et al., 2014, Li et al., 2016). However, the abundant membrane transport pathway containing ABC transporters at the end demonstrated the potential substrates transport across cellular membranes as well as cell viability and growth (Lyons et al., 2017). Moreover, the more bioavailable substrate produced in the early bioaugmentation process could also be easier utilized by the microbiomes, that also enhanced these gene pathways (Lyons et al., 2017). The fluctuations of pathways on level 2 under oxygen stimulated condition indicated the wide consumptions of nutrient and oxygen during biostimulation process that could not specially benefit 1,4-dioxane biodegradation, such as increasing specific genes (e.g., xenobiotics degradation genes), and the slow decreasing trend of 1,4-dioxane could be attributed to the entire higher gene expression or bacterial growth. However, the accumulated genes in lipid metabolism, xenobiotics biodegradation and metabolism, and metabolism of terpenoids and polyketides was found after nutrient addition, and this validated that not only propane, but also nutrient could increase bioavailability and biodegradation rate by stimulate native propanotrophs in microcosms.

The network analysis only showed few connections between microbes and pathways or monooxygenases, further confirming the decoupling between microbial compositions and functions. Moreover, even with the stable abundances of specific enzymes under propane and nutrient conditions, the activities might depend on bioavailable phosphate and nitrogen, that explains the high 1,4-dioxane removals.

5.5 Conclusions

1,4-Dioxane is expected to be present in groundwater from numerous historical industrial releases, and this study demonstrated and evaluated effective strategies using metabolic or co-metabolic bioaugmentations, as well as propane and nutrient spiked biostimulations.

Pseudonocardia dioxanivorans CB1190 as well as *Rhodococcus ruber* ENV425 resulted in rapid biodegradation of 1,4-dioxane to below detection limits within 7 days, and biostimulation with propane only caused 1,4-dioxane removals after sufficient nutrient was added, while oxygen spikes couldn't enhance 1,4-dioxane biodegradation efficiently even with extra nutrient. Genes regarding to 1,4-dioxane degradations, *dxmB, aldH,* and *prmA,* were all stimulated to express after nutrient addition, while biomass was reduced in bioaugmentation conditions. Microbial community analysis pictured that augmented genera *Pseudonocardia* and *Rhodococcus* were overwhelmed by other native bacteria over time with *Pseudonocardia* being replaced faster than *Rhodococcus,* and various bacterial groups became predominant over time in the biostimulated microcosms, while after nutrients were added, genera *Mycobacterium* and *Methyloversatilis* were accumulated in propane-stimulated microcosms when microbiomes distributed similarly in microcosms that were stimulated by oxygen and supplemented with nutrients. Functional potential analysis showed enhanced genes allocation for different pathways directly involved in metabolism after bioaugmentation or nutrient addition, while functional redundancy was predicted to happen in the rest of treatment process.

Nutrients and bioaugmentation induced community dynamics and metabolic interplay might be involved in accelerated bioremediation, that have been reported in bench or pilot scale studies, while this study firstly used sequencing technology to profile the overall molecular mechanisms behind the treatment process, and pinpointed functional bacteria, metabolic pathways, and microbial trajectories, that could improve remediation decision-making and regulate further engineered work.

5.6 References

Adamson, D.T., Anderson, R.H., Mahendra, S., Newell, C.J., 2015. Evidence of 1,4-dioxane attenuation at groundwater sites contaminated with chlorinated solvents and 1,4-dioxane. Environmental Science & Technology, 49 (11), 6510-6518.

Alidina, M., Li, D., Drewes, J.E., 2014. Investigating the role for adaptation of the microbial community to transform trace organic chemicals during managed aquifer recharge. Water Research, 56, 172-180.

Anantharaman, K., Brown, C.T., Hug, L.A., Sharon, I., Castelle, C.J., Probst, A.J., Thomas, B.C., Singh, A., Wilkins, M.J., Karaoz, U., Brodie, E.L., Williams, K.H., Hubbard, S.S., Banfield, J.F., 2016. Thousands of microbial genomes shed light on interconnected biogeochemical processes in an aquifer system. Nature Communications, 7.

Anderson, R.H., Anderson, J.K., Bower, P.A., 2012. Co-occurrence of 1,4-dioxane with trichloroethylene in chlorinated solvent groundwater plumes at US Air Force installations: Fact or fiction. Integrated Environmental Assessment and Management, 8 (4), 731-737.

Babin, D., Deubel, A., Jacquiod, S., Sorensen, S.J., Geistlinger, J., Grosch, R., Smalla, K., 2019. Impact of long-term agricultural management practices on soil prokaryotic communities. Soil Biology & Biochemistry, 129, 17-28.

Bai, Y.H., Chang, Y.Y., Liang, J.S., Chen, C., Qu, J.H., 2016. Treatment of groundwater containing Mn(II), Fe(II), As(III) and Sb(III) by bioaugmented quartz-sand filters. Water Research, 106, 126-134.

Bai, Y.H., Qi, W.X., Liang, J.S., Qu, J.H., 2014. Using high-throughput sequencing to assess the impacts of treated and untreated wastewater discharge on prokaryotic communities in an urban river. Applied Microbiology and Biotechnology, 98 (4), 1841-1851.

Barajas-Rodriguez, F.J., Freedman, D.L., 2018. Aerobic biodegradation kinetics for 1,4-dioxane under metabolic and cometabolic conditions. Journal of Hazardous Materials, 350, 180-188.

Bastian, M., Heymann, S., Jacomy, M., 2009. Gephi: an open source software for exploring and manipulating networks. Icwsm, 8, 361-362.

Benjamini, Y., Hochberg, Y., 1995. Controlling the false discovery rate: a practical and powerful approach to multiple testing. Journal of the Royal Statistical Society. Series B (Methodological), 289-300.

Blanco, J.A., Lo, Y.-H., Roy, S. (2015). Biodiversity in Ecosystems: Linking Structure and Function, BoD–Books on Demand.

Bock, C., Kroppenstedt, R.M., Diekmann, H., 1996. Degradation and bioconversion of aliphatic and aromatic hydrocarbons by *Rhodococcus ruber* 219. Applied Microbiology and Biotechnology, 45 (3), 408-410.

Caporaso, J.G., Lauber, C.L., Walters, W.A., Berg-Lyons, D., Huntley, J., Fierer, N., Owens, S.M., Betley, J., Fraser, L., Bauer, M., Gormley, N., Gilbert, J.A., Smith, G., Knight, R., 2012. Ultra-high-throughput microbial community analysis on the Illumina HiSeq and MiSeq platforms. The ISME Journal, 6 (8), 1621-1624.

Cappelletti, M., Fedi, S., Zampolli, J., Di Canito, A., D'Ursi, P., Orro, A., Viti, C., Milanesi, L., Zannoni, D., Di Gennaro, P., 2016. Phenotype microarray analysis may unravel genetic determinants of the stress response by *Rhodococcus aetherivorans* BCP1 and *Rhodococcus opacus* R7. Research in Microbiology, 167 (9-10), 766-773.

Chao, Y.Q., Liu, W.S., Chen, Y.M., Chen, W.H., Zhao, L.H., Ding, Q.B., Wang, S.Z., Tang, Y.T., Zhang, T., Qiu, R.L., 2016. Structure, variation, and co-occurrence of soil microbial communities in abandoned sites of a rare earth elements mine. Environmental Science & Technology, 50 (21), 11481-11490.

Chi, X., Li, J.Z., Wang, X., Zhang, Y.F., Leu, S.Y., Wang, Y., 2018. Bioaugmentation with *Clostridium tyrobutyricum* to improve butyric acid production through direct rice straw bioconversion. Bioresource Technology, 263, 562-568.

Chu, M.Y.J., Bennett, P.J., Dolan, M.E., Hyman, M.R., Peacock, A.D., Bodour, A., Anderson, R.H., Mackay, D.M., Goltz, M.N., 2018. Concurrent treatment of 1,4-dioxane and chlorinated aliphatics in a groundwater recirculation system via aerobic cometabolism. Ground Water Monitoring and Remediation, 38 (3), 53-64.

Deng, D.Y., Li, F., Li, M.Y., 2018. A novel propane monooxygenase initiating degradation of 1,4-dioxane by *Mycobacterium dioxanotrophicus* PH-06. Environmental Science & Technology Letters, 5 (2), 86-91.

Diez, M.C., Elgueta, S., Rubilar, O., Tortella, G.R., Schalchli, H., Bornhardt, C., Gallardo, F., 2017. Pesticide dissipation and microbial community changes in a biopurification system: influence of the rhizosphere. Biodegradation, 28 (5-6), 395-412.

Fernandez-Gonzalez, N., Huber, J.A., Vallino, J.J., 2016. Microbial communities are well adapted to disturbances in energy input. Msystems, 1 (5).

Festa, S., Coppotelli, B.M., Morelli, I.S., 2016. Comparative bioaugmentation with a consortium and a single strain in a phenanthrene-contaminated soil: Impact on the bacterial community and biodegradation. Applied Soil Ecology, 98, 8-19.

Foster, Z.S., Sharpton, T.J., Grünwald, N.J., 2017. Metacoder: An R package for visualization and manipulation of community taxonomic diversity data. PLoS Computational Biology, 13 (2), e1005404.

Gedalanga, P., Madison, A., Miao, Y., Richards, T., Hatton, J., DiGuiseppi, W.H., Wilson, J., Mahendra, S., 2016. A multiple lines of evidence framework to evaluate intrinsic biodegradation of 1,4-dioxane. Remediation Journal, 27 (1), 93-114.

Gedalanga, P.B., Pornwongthong, P., Mora, R., Chiang, S.Y.D., Baldwin, B., Ogles, D., Mahendra, S., 2014. Identification of biomarker genes to predict biodegradation of 1,4-dioxane. Applied and Environmental Microbiology, 80 (10), 3209-3218.

Hand, S., Wang, B., Chu, K.H., 2015. Biodegradation of 1,4-dioxane: effects of enzyme inducers and trichloroethylene. Environmental Science & Technology, 520, 154-159.

Hatzinger, P.B., Banerjee, R., Rezes, R., Streger, S.H., McClay, K., Schaefer, C.E., 2017. Potential for cometabolic biodegradation of 1,4-dioxane in aquifers with methane or ethane as primary substrates. Biodegradation, 28 (5-6), 453-468.

Hatzinger, P.B., Begley, J.F., Lippincott, D.R., Bodou, A., Forbes, R., 2018. In situ bioremediation of 1,2-dibromoethane (EDB) in groundwater to part-per-trillion concentrations using cometabolism. Journal of Contaminant Hydrology, 218, 120-129.

Hatzinger, P.B., Lewis, C., Webster, T.S., 2017. Biological treatment of N-nitrosodimethylamine (NDMA) and N-nitrodimethylamine (NTDMA) in a field-scale fluidized bed bioreactor. Water Research, 126, 361-371.

Hatzinger, P.B., Streger, S.H., Begley, J.F., 2015. Enhancing aerobic biodegradation of 1,2-dibromoethane in groundwater using ethane or propane and inorganic nutrients. Journal of Contaminant Hydrology, 172, 61-70.

He, Y., Mathieu, J., da Silva, M.L., Li, M., Alvarez, P.J., 2018. 1,4 - Dioxane - degrading consortia can be enriched from uncontaminated soils: prevalence of *Mycobacterium* and soluble di - iron monooxygenase genes. Microbial Biotechnology, 11 (1), 189-198.

Jones, S.E., Lennon, J.T., 2010. Dormancy contributes to the maintenance of microbial diversity. Proceedings of the National Academy of Sciences of the United States of America, 107 (13), 5881-5886.

Ju, F., Lau, F., Zhang, T., 2017. Linking microbial community, environmental variables, and methanogenesis in anaerobic biogas digesters of chemically enhanced primary treatment sludge. Environmental Science & Technology, 51 (7), 3982-3992.

Jung, J., Philippot, L., Park, W., 2016. Metagenomic and functional analyses of the consequences of reduction of bacterial diversity on soil functions and bioremediation in diesel-contaminated microcosms. Scientific Reports, 6.

Kao, C.-M., Liao, H.-Y., Chien, C.-C., Tseng, Y.-K., Tang, P., Lin, C.-E., Chen, S.-C., 2016. The change of microbial community from chlorinated solvent-contaminated groundwater after biostimulation using the metagenome analysis. Journal of hazardous materials, 302, 144-150.

Lan, R.S., Smith, C.A., Hyman, M.R., 2013. Oxidation of cyclic ethers by alkane - grown *Mycobacterium vaccae* JOB5. Remediation Journal, 23 (4), 23-42.

Langenheder, S., Lindstrom, E.S., Tranvik, L.J., 2005. Weak coupling between community composition and functioning of aquatic bacteria. Limnology and Oceanography, 50 (3), 957-967.

Li, B., Wu, W.-M., Watson, D.B., Cardenas, E., Chao, Y., Phillips, D., Mehlhorn, T., Lowe, K., Kelly, S.D., Li, P., 2018. Bacterial community shift and coexisting/coexcluding patterns revealed by network analysis in a uranium-contaminated site after bioreduction followed by reoxidation. Applied and Environmental Microbiology, 84 (9), e02885-02817.

Li, D., Sharp, J.O., Drewes, J.E., 2016. Influence of wastewater discharge on the metabolic potential of the microbial community in river sediments. Microbial ecology, 71 (1), 78-86.

Li, M.Y., Conlon, P., Fiorenza, S., Vitale, R.J., Alvarez, P.J.J., 2011. Rapid analysis of 1,4-dioxane in groundwater by frozen micro-extraction with gas chromatography/mass spectrometry. Ground Water Monitoring and Remediation, 31 (4), 70-76.

Lippincott, D., Streger, S.H., Schaefer, C.E., Hinkle, J., Stormo, J., Steffan, R.J., 2015. Bioaugmentation and propane biosparging for in situ biodegradation of 1,4-dioxane. Ground Water Monitoring and Remediation, 35 (2), 81-92.

Liu, X., Wu, Y., Wilson, F.P., Yu, K., Lintner, C., Cupples, A.M., Mattes, T.E., 2018. Integrated methodological approach reveals microbial diversity and functions in aerobic groundwater microcosms adapted to vinyl chloride. FEMS Microbiology Ecology, 94 (9), fiy124.

Louca, S., Jacques, S.M.S., Pires, A.P.F., Leal, J.S., Srivastava, D.S., Parfrey, L.W., Farjalla, V.F., Doebeli, M., 2017. High taxonomic variability despite stable functional structure across microbial communities. Nature Ecology & Evolution, 1 (1).

Louca, S., Parfrey, L.W., Doebeli, M., 2016. Decoupling function and taxonomy in the global ocean microbiome. Science, 353 (6305), 1272-1277.

Louca, S., Polz, M.F., Mazel, F., Albright, M.B.N., Huber, J.A., O'Connor, M.I., Ackermann, M., Hahn, A.S., Srivastava, D.S., Crowe, S.A., Doebeli, M., Parfrey, L.W., 2018. Function and functional redundancy in microbial systems. Nature Ecology & Evolution, 2 (6), 936-943.

Lyons, P.P., Turnbull, J.F., Dawson, K.A., Crumlish, M., 2017. Phylogenetic and functional characterization of the distal intestinal microbiome of rainbow trout *Oncorhynchus mykiss* from both farm and aquarium settings. Journal of Applied Microbiology, 122 (2), 347-363.

Mahendra, S., Alvarez-Cohen, L., 2005. *Pseudonocardia dioxanivorans* sp. nov., a novel actinomycete that grows on 1,4-dioxane. International Journal of Systematic and Evolutionary Microbiology, 55 (Pt 2), 593-598.

Mahendra, S., Alvarez-Cohen, L., 2006. Kinetics of 1,4-dioxane biodegradation by monooxygenase-expressing bacteria. Environmental Science & Technology, 40 (17), 5435-5442.

Mahendra, S., Petzold, C.J., Baidoo, E.E., Keasling, J.D., Alvarez-Cohen, L., 2007. Identification of the intermediates of in vivo oxidation of 1,4-dioxane by monooxygenase-containing bacteria. Environmental Science & Technology, 41 (21), 7330-7336.

Masuda, H., McClay, K., Steffan, R.J., Zylstra, G.J., 2012. Characterization of three propane-inducible oxygenases in *Mycobacterium* sp strain ENV421. Letters in Applied Microbiology, 55 (3), 175-181.

McElroy, A., Hyman, M. (2019). Consequences of microbial interactions with hydrocarbons, oils, lipids: Biodegradation and bioremediation. handbook of hydrocarbon and lipid microbiology. (eds), S. R. (ed), pp. 1-30, Springer, Cham.

McLeod, M.P., Warren, R.L., Hsiao, W.W.L., Araki, N., Myhre, M., Fernandes, C., Miyazawa, D., Wong, W., Lillquist, A.L., Wang, D., Dosanjh, M., Hara, H., Petrescu, A., Morin, R.D., Yang, G., Stott, J.M., Schein, J.E., Shin, H., Smailus, D., Siddiqui, A.S., Marra, M.A., Jones, S.J.M., Holt, R., Brinkman, F.S.L., Miyauchi, K., Fukuda, M., Davies, J.E., Mohn, W.W., Eltis, L.D., 2006. The complete genome of *Rhodococcus* sp RHA1 provides insights into a catabolic powerhouse. Proceedings of the National Academy of Sciences of the United States of America, 103 (42), 15582-15587.

McMurdie, P.J., Holmes, S., 2013. phyloseq: an R package for reproducible interactive analysis and graphics of microbiome census data. Plos One, 8 (4), e61217.

Miao, Y., Johnson, N.W., Gedalanga, P.B., Adamson, D., Newell, C., Mahendra, S., 2019. Response and recovery of microbial communities subjected to oxidative and biological treatments of 1,4-dioxane and co-contaminants. Water Research, 149, 74-85.

Miao, Y., Johnson, N.W., Heck, K., Guo, S., Powell, C.D., Phan, T., Gedalanga, P.B., Adamson, D.T., Newell, C.J., Wong, M.S., Mahendra, S., 2018. Microbial responses to combined oxidation and catalysis treatment of 1,4-dioxane and co-contaminants in groundwater and soil. Frontiers of Environmental Science & Engineering, 12 (5), 1-13.

Miao, Y., Wang, Z., Liao, R.H., Shi, P., Li, A.M., 2017. Assessment of phenol effect on microbial community structure and function in an anaerobic denitrifying process treating high concentration nitrate wastewater. Chemical Engineering Journal, 330, 757-763.

Miao, Y., Zhang, X.-X., Jia, S., Liao, R., Li, A., 2018. Comprehensive analyses of functional bacteria and genes in a denitrifying EGSB reactor under Cd (II) stress. Applied Microbiology and Biotechnology, 102 (19), 8551-8560.

Mohr, T.K., Stickney, J.A., DiGuiseppi, W.H. (2016). Environmental investigation and remediation: 1,4-dioxane and other solvent stabilizers, CRC Press.

Parales, R.E., Adamus, J.E., White, N., May, H.D., 1994. Degradation of 1,4-dioxane by an *Actinomycete* in pure culture. Applied and Environmental Microbiology, 60 (12), 4527-4530.

Purahong, W., Wubet, T., Kahl, T., Arnstadt, T., Hoppe, B., Lentendu, G., Baber, K., Rose, T., Kellner, H., Hofrichter, M., Bauhus, J., Kruger, D., Buscot, F., 2018. Increasing N deposition

impacts neither diversity nor functions of deadwood-inhabiting fungal communities, but adaptation and functional redundancy ensure ecosystem function. Environmental Microbiology, 20 (5), 1693-1710.

Sadeghi, V., Mora, R., Jacob, P., Chiang, S.Y., 2016. Characterizing in situ methane‐enhanced biostimulation potential for 1,4‐dioxane biodegradation in groundwater. Remediation Journal, 27 (1), 115-132.

Schimel, J., Balser, T.C., Wallenstein, M., 2007. Microbial stress-response physiology and its implications for ecosystem function. Ecology, 88 (6), 1386-1394.

Schloss, P.D., Westcott, S.L., Ryabin, T., Hall, J.R., Hartmann, M., Hollister, E.B., Lesniewski, R.A., Oakley, B.B., Parks, D.H., Robinson, C.J., Sahl, J.W., Stres, B., Thallinger, G.G., Van Horn, D.J., Weber, C.F., 2009. Introducing mothur: Open-source, platform-independent, community-supported software for describing and comparing microbial communities. Applied and Environmental Microbiology, 75 (23), 7537-7541.

Sei, K., Kakinoki, T., Inoue, D., Soda, S., Fujita, M., Ike, M., 2010. Evaluation of the biodegradation potential of 1,4-dioxane in river, soil and activated sludge samples. Biodegradation, 21 (4), 585-591.

Sei, K., Oyama, M., Kakinoki, T., Inoue, D., Ike, M., 2013. Isolation and characterization of tetrahydrofuran-degrading bacteria for 1, 4-dioxane-containing wastewater treatment by co-metabolic degradation. Journal of Water and Environment Technology, 11 (1), 11-19.

Shade, A., Read, J.S., Youngblut, N.D., Fierer, N., Knight, R., Kratz, T.K., Lottig, N.R., Roden, E.E., Stanley, E.H., Stombaugh, J., Whitaker, R.J., Wu, C.H., McMahon, K.D., 2012. Lake microbial communities are resilient after a whole-ecosystem disturbance. The ISME Journal, 6 (12), 2153-2167.

Shah, V., Zakrzewski, M., Wibberg, D., Eikmeyer, F., Schlüter, A., Madamwar, D., 2013. Taxonomic profiling and metagenome analysis of a microbial community from a habitat contaminated with industrial discharges. Microbial Ecology, 66 (3), 533-550.

Sharma, A., Jani, K., Shouche, Y.S., Pandey, A., 2015. Microbial diversity of the Soldhar hot spring, India, assessed by analyzing 16S rRNA and protein-coding genes. Annals of Microbiology, 65 (3), 1323-1332.

Suthersan, S., Quinnan, J., Horst, J., Ross, I., Kalve, E., Bell, C., Pancras, T., 2016. Making strides in the management of "Emerging Contaminants". Ground Water Monitoring and Remediation, 36 (1), 15-25.

Tian, G.-P., Wu, Q.-Y., Li, A., Wang, W.-L., Hu, H.-Y., 2014. Enhanced decomposition of 1,4-dioxane in water by ozonation under alkaline condition. Water Science and Technology, 70 (12), 1934-1940.

Tyagi, M., da Fonseca, M.M.R., de Carvalho, C.C.C.R., 2011. Bioaugmentation and biostimulation strategies to improve the effectiveness of bioremediation processes. Biodegradation, 22 (2), 231-241.

Vainberg, S., McClay, K., Masuda, H., Root, D., Condee, C., Zylstra, G.J., Steffan, R.J., 2006. Biodegradation of ether pollutants by *Pseudonocardia* sp strain ENV478. Applied and Environmental Microbiology, 72 (8), 5218-5224.

Vanwonterghem, I., Jensen, P.D., Dennis, P.G., Hugenholtz, P., Rabaey, K., Tyson, G.W., 2014. Deterministic processes guide long-term synchronised population dynamics in replicate anaerobic digesters. The ISME Journal, 8 (10), 2015.

Vanwonterghem, I., Jensen, P.D., Rabaey, K., Tyson, G.W., 2016. Genome-centric resolution of microbial diversity, metabolism and interactions in anaerobic digestion. Environmental Microbiology, 18 (9), 3144-3158.

Wang, H., Zhao, Y., Wei, Y.Q., Zhao, Y., Lu, Q., Liu, L.N., Jiang, N., Wei, Z.M., 2018. Biostimulation of nutrient additions on indigenous microbial community at the stage of nitrogen limitations during composting. Waste Management, 74, 194-202.

Wang, H.W., Dai, C.C., Zhu, H., Wang, X.X., 2014. Survival of a novel endophytic fungus *Phomopsis liquidambari* B3 in the indole-contaminated soil detected by real-time PCR and its effects on the indigenous microbial community. Microbiological Research, 169 (12), 881-887.

Wemheuer, F., Taylor, J.A., Daniel, R., Johnston, E., Meinicke, P., Thomas, T., Wemheuer, B., 2018. Tax4Fun2: a R-based tool for the rapid prediction of habitat-specific functional profiles and functional redundancy based on 16S rRNA gene marker gene sequences. bioRxiv, 490037.

Wu, Z.J., Zou, L.D., Lu, D.N., Liu, Z., 2011. Restoration of taxonomic and functional genes after bioaugmentation of petroleum contaminated soil. Journal of Environmental Monitoring, 13 (10), 2904-2913.

Zhang, S., Gedalanga, P.B., Mahendra, S., 2016. Biodegradation kinetics of 1,4-dioxane in chlorinated solvent mixtures. Environmental Science & Technology, 50 (17), 9599-9607.

Zhao, R., Feng, J., Yin, X., Liu, J., Fu, W., Berendonk, T.U., Zhang, T., Li, X., Li, B., 2018. Antibiotic resistome in landfill leachate from different cities of China deciphered by metagenomic analysis. Water Research, 134, 126-139.

Zhou, H., Zhang, D.G., Jiang, Z.H., Sun, P., Xiao, H.L., Wu, Y.X., Chen, J.G., 2019. Changes in the soil microbial communities of alpine steppe at Qinghai-Tibetan Plateau under different degradation levels. Science of the Total Environment, 651, 2281-2291.

Chapter 6 Treatment Trains for 1,4-Dioxane and Co-Contaminants' Degradation

6.1 Introduction

1,4-Dioxane soil and groundwater contamination, caused by improper disposal and historical usage, has been a growing concern in recent decades (Suthersan et al., 2016). 1,4-Dioxane widely worked as the solvent and stabilizer for 1,1,1-trichloroethane (TCA) (Mohr et al., 2010), but was also found to be associated with trichloroethylene (TCE) (Anderson et al., 2012), and 1,1-dichloroethene (1,1-DCE) (Adamson et al., 2015) in contaminated aquifers. Conventional treatment methods such as air stripping and soil vapor extraction are largely ineffective because 1,4-dioxane is highly polar and has high aqueous solubility (Mohr et al., 2010). Biodegradation of 1,4-dioxane has been reported in several laboratory studies (Mahendra and Alvarez-Cohen, 2005, 2006, Vainberg et al., 2006, Mahendra et al., 2007, Li et al., 2010, Lan et al., 2013, Sekar et al., 2016, Zhang et al., 2017). Recent studies describe that 1,4-dioxane biodegradation may play a significant role in natural attenuation in several contaminated aquifers (Adamson et al., 2015, Li et al., 2015), and a former landfill site (Gedalanga et al., 2016). However, the abundance of 1,4-dioxane biodegrading bacteria were low in both sewage treatments plants (Gedalanga et al., 2014) and natural groundwater (Sei et al., 2010), meaning that intrinsic biodegradation is likely to require a significant time investment if used as part of a long-term site management strategy (Adamson et al., 2015). Additionally, co-occurring chlorinated volatile organic compounds (CVOCs) and heavy metals (Cd(II), Cu(II), and Ni(II)) inhibited the biodegradation of 1,4-dioxane (Mahendra et al., 2013, Pornwongthong et al., 2014, Zhang et al., 2016). The properties of soil and groundwater with comingled 1,4-dioxane and CVOC plumes pose unique challenges to engineered 1,4-dioxane remediation processes due to scale- (Lobo et al., 2014) and cost- (Choi et al., 2017)

limitations of chemical oxidation technologies and negative impacts of chlorinated solvents on microorganisms that can perform bioremediation processes (Zhang et al., 2016).

Currently, ex-situ 1,4-dioxane treatments have focused on various methods, such as bioaugmented sorption (Myers et al., 2018), and abiotic method, such as advanced oxidation processes (AOPs), which are capable of generating hydroxyl radicals (•OH) as potent and nonselective oxidants (Chitra et al., 2012, Eberle et al., 2016) and can take advantage of the aqueous miscibility of 1,4-dioxane. Importantly, AOPs may provide oxygen and decrease the concentrations of co-contaminants (Eberle et al., 2016), both of which could benefit aerobic microorganisms. However, there are critical limitations for full scale practical application, such as the consumption of oxidative reagents and the need for additional energy inputs in the form of UV radiation sources (Choi et al., 2017). Catalytic oxidation attempts to address these limitations by the addition of inorganic catalysts that speed up oxidation rates and reduce the overall supply of any additives or irradiation for oxidants (Choi et al., 2017). To date, the developed materials including Ti/IrO_2−Ta_2O_5 (Jasmann et al., 2017), Pt/CeO_2-ZrO_2-SnO_2/SBA-16 (Choi et al., 2017), Pd/Al_2O_3 (Feng et al., 2017), and photocatalytically active TiO_2 (Barndok et al., 2016) have been tested in 1,4-dioxane ex-situ remediation. Additionally, Tungstated zirconia (WO_x/ZrO_2) has improved activity and higher stability than previously studied catalysts (Soultanidis et al., 2010), without the requirement of a precious metal or a light source, and has been used to treat 1,4-dioxane with hydrogen peroxide (H_2O_2) by activating H_2O_2 into reactive oxygen species on its metal oxide surface and reacting with 1,4-dioxane co-adsorbed to Lewis-acidic sites on the catalyst surface (Adamson et al., 2017).

Treatment train technologies provide many alternatives for the remediation of sites with complex soil or groundwater contamination (Lobo et al., 2014). To date, oxidative-biological (Xu

et al., 2016, Wang et al., 2017, Medina et al., 2018, Miao et al., 2019) and electrochemical-biological (Lobo et al., 2014, Jasmann et al., 2017) treatment strategies have been studied in soil and groundwater contaminations. However, given the broad physicochemical properties of contaminant mixtures and microbial communities across different sites, applying general decontamination methods achieve cost-effective remediation management becomes very challenging. This problem is especially difficult when attempting to include bioremediation steps that generally rely on a recovery in the functionality of the soil microbial community for optimal performance (Lobo et al., 2014). The concept of a treatment train with oxidation and catalysis processes has rarely been applied in soil and groundwater 1,4-dioxane remediation that could optimize use of both oxidants and catalysts. To date, coupling chemical oxidation and bioremediation has produced successful results indicating improved remediation efficiencies for in-situ remediation of soil contaminated with diesel (Kim and Lee, 2012, Sutton et al., 2014), as well as polycyclic aromatic hydrocarbons (PAHs) (Medina et al., 2018). However, few studies have examined the behavior of systems that combine the technologies for treating emerging contaminants, such as 1,4-dioxane and CVOC mixtures. There are several factors that could influence the performance of a combined oxidation-biodegradation treatment train, including the soil type (Sutton et al., 2014), decreases in the persistence of oxidants, and the generated radical species in the presence of oxidized molecules (Deng et al., 2015). Although more efficient H_2O_2 use and higher 1,4-dioxane degradation activity were achieved, the performance of WO_x/ZrO_2 under CVOCs stress as well as its further impacts on biodegradation are still unknown. Therefore, a novel synergistic catalysis-biodegradation treatment train was considered to target 1,4-dioxane and CVOCs mixtures.

The responses of indigenous microorganisms to treatment trains are not well understood in soil and groundwater. Closing this knowledge gap is important, because these microbes act as environmental indicators and are responsible for fundamental ecosystem processes and potential natural attenuation of environmental contaminants. Therefore, potential shifts in microbial community due to the application of an oxidation/catalysis/biodegradation treatment train must be considered and thoroughly evaluated before further in-situ deployment of this promising strategy (Chen et al., 2016). Additionally, environmental constraints can trigger a microbial response observable through different forms among the community. Microbial community analysis can provide comprehensive insights into the compositions of microorganisms and the microbial responses to contaminants and the reagents used during treatment. Based on metagenomics, microbial community analysis allows a realistic assessment of individual or combined impacts of oxidants, catalysts, and contaminants on microbial communities, and consequently leads to a better environmental risk assessment (Simonin and Richaume, 2015). This analytical method has been widely used in the fields of wastewater treatment (Miao et al., 2015), soil bioremediation (Lefevre et al., 2016), and in treatment efforts that target various contaminants, such as CVOCs mixed with metals (Nemecek et al., 2016). However, microbial community analysis has not been widely applied to emerging contaminants, especially on 1,4-dioxane and its co-contaminants. Moreover, environmental assessments of soil remediation by conventional chemical oxidation with respect to microbial ecology are rare (Chen et al., 2016) and limited to the combined treatment train technologies.

With the aim of filling the engineered technological and analytical gaps described above, this chapter evaluated oxidation-catalysis, oxidation-biodegradation, and catalysis-biodegradation treatment trains in ex situ bench-scale microcosms constructed using actual contaminated soil and

groundwater, with the objectives to (1) analyze the diversity and microbial community composition shifts during each step in the treatment train, (2) identify microbes that could act as key indicators in different conditions or treatment phases, (3) determine the relationships among the targeting functions, contamination removals, and microorganisms, and (4) explore microbial dynamics, co-occurrence and co-exclusion patterns among microbial taxa in the biodegradation process. By addressing the above questions, this study will validate a proposed novel engineered 1,4-dioxane remediation technology and provide comprehensive insights into molecular mechanisms to guide the application of in-situ remediation management strategies.

6.2 Materials and Methods

6.2.1 Site Identification and Contaminants

Groundwater and soil samples were taken from a site located in the southern United States where groundwater and soil are impacted by previous military and industrial activities including vapor degreasing. Contaminants of concern (COCs) include COVCs, such as TCA, TCE, 1,1-dichloroethane (1,1-DCA), 1,2-dichloroethane (1,2-DCA), 1,1-dichloroethene (1,1-DCE), and cis-1,2-dichloroethene (cis-DCE), and emerging contaminant 1,4-dioxane. Concentrations of COCs at temporary and permanent monitoring wells in the vicinity of the proposed demonstration area are summarized in Table 6.1.

Table 6.11. Groundwater concentrations in the vicinity of the demonstration area (Courtesy: AECOM 2014).

COC	Groundwater Concentrations (July-August 2013) (μg/L)					
	TW43	TW44	TW45	8MNW17	8MNW20	8MNW54*
TCE	14,700/15,700	486 J	7.12	7,080	17,400/17,000	1,310
TCA	164/156	<0.5	<0.5	67.3	4.23/4.18	91.5
1,4-DX	620/680	91	62/63	270	147/145	351 J
cDCE	120/119	0.822 F	19.9/18.9	69.1	31.4/30.6	105 M
1,1-DCE	3,600/3,630	7.07	18.6/17.1	1,720	2,330/2,910 J	296 F
1,1-DCA	7.26/6.54	5.77	68.2/65	8.59	3.96/3.87	6.81
1,2-DCA	<5	4.04 F	<5	13.2	37.3/36.3	24.4

Notes:
*Monitoring well 8MNW54 installed adjacent to location of temporary well TW43.
/ denotes duplicate sample
DCA dichloroethane
cDCE cis-1,2-dichloroethene
F qualifier indicating concentration in excess of detection limit and below reporting limit
J qualifier indicating estimated concentration
M qualifier indicating matrix effect

6.2.2 Microcosm Constructions and Conditions

The bench scale microcosm study was conducted in 250 mL glass bottles with screw-cap Mininert™ valves, containing 50 mL groundwater and 10 g soil that collected from the site. Two levels of contaminants (500 and 5000 μg/L) were spiked individually and in mixtures to mimic natural conditions (Table 6.2). These two levels were selected because they represent a low-to-moderate concentration and a high concentration, respectively, using typical contaminated groundwater plume concentration ranges for 1,4-dioxane and CVOCs described in Adamson et al. (2015). This resulted in four sets of microcosms, including high 1,4-dioxane high CVOCs (H-DX/H-CV), high 1,4-dioxane low CVOCs (H-DX/L-CV), low 1,4-dioxane low CVOCs (L-DX/L-CV), and low 1,4-dioxane-only (L-DX). A bioaugmentation set (Bioaug) was also prepared as a positive biodegradation control by adding 1,4-dioxane metabolizing and mineralizing bacterial strain

Pseudonocardia dioxanivorans CB1190 (CB1190) (Mahendra and Alvarez-Cohen, 2005, 2006, Mahendra et al., 2007) and incubated with high 1,4-dioxane and low CVOCs initial concentrations. A heat-sterilized control set was also prepared to correct for abiotic loss corrections.

Table 6.12. Initial 1,4-dioxane and CVOCs concentrations under each condition. The 1,4-dioxane concentration were measured using GC-MS and GC-FID, while the CVOCs were calculated prior to the study based on dilutions.

Contaminant Mixtures	Abbreviation	1,4-Dioxane (µg/L) *	TCE (µg/L) #	1,1-DCE (µg/L) #	cis-1,2-DCE (µg/L) #
High DX/High CVOC	H-DX/H-CV	7300 ± 430	5000	5000	5000
High DX/Low CVOC	H-DX/L-CV	6980 ± 410	500	500	500
Low DX/Low CVOC	L-DX/L-CV	1130 ± 70	500	500	500
Low DX Only	L-DX	1080 ± 80	0	0	0
Bioaugmentation	Bioaug	6660 ± 720	500	500	500

* Concentrations were measured on GC-MS and GC-FID.

Concentrations were calculated based on dilution from stock CVOCs solutions.

6.2.3 Combined Oxidation and Catalysis (OC) Treatment Train

The oxidation phase involved amending site materials with H_2O_2. With H_2O_2 as the oxidant treating site groundwater and soil, microcosm bottles also contained 100 mg $FeSO_4 \cdot 7H_2O$, and 10% sulfuric acid was used to adjust pH value to 4.5. Partial 1,4-dioxane removals were achieved after incubating at room temperature for 12 hours with 100 rpm agitation, and some 1,4-dioxane was available for the subsequent treatment step. The H_2O_2 oxidation process was quenched with NaOH after 12 hours. The original site aqueous 1,4-dioxane concentration was 404.7 µg/L (the results of H_2O_2 dose tests are listed in Table 6.3) and the optimal dose of H_2O_2 was 0.96 mM for the unamended groundwater and soil mixture samples.

Table 6.13. Optimization test of hydrogen peroxide.

8MNW54 + TW1	
Hydrogen Peroxide Added	**Percent Degradation**
77.62 mM	Full
38.81 mM	Full
19.40 mM	Full
9.55 mM	Full
4.78 mM	Full
1.19 mM	90.0%
1.07 mM	Full
0.96 mM	71.4%
0.96 mM	59.4%
0.84 mM	47.7%
0.48 mM	30.8%
0.06 mM	None

The catalysis treatment portion was conducted with tungstated zirconia of one composition (20 wt% WO_3 supported on ZrO_2 (*i.e.* 20 g WO_3 per 100 g of total WO_3 and ZrO_2), commercially available from MEL Chemicals, "WO_x/ZrO_2") (Heck et al., 2018). The bottles were then dosed with 1600 μL 30% H_2O_2, and the bottles stirred for another 24 hours (Adamson et al., 2017).

The sampling timeline of this study was shown in Table S4. Briefly, the slurry samples under each condition were collected before oxidation (original state, Control), post-oxidation state (OC1), and post-catalysis state (OC2). At each time point, liquid (200 μL, stored at -20°C) and mixed soil-water samples (300 μL, stored at -80°C) were collected from each microcosm for later 1,4-dioxane and total nucleic acid analysis.

6.2.4 Combined Oxidation and Biodegradation (OB) Treatment Train

Hydrogen peroxide (H_2O_2) was selected as the oxidant, and the optimal dose for unamended groundwater and soil mixture slurry was 0.96 mM (dose tests prior to microcosms are summarized in Table 6.3). The microcosms were first established with different concentrations of 1,4-dioxane and CVOCs, then H_2O_2 was added and oxidation process conducted with continuous 100 rpm agitation at room temperature with pH at 4.5 (100 mg $FeSO_4 \cdot 7H_2O$ and 10% sulfuric acid), simulating the Fenton type reaction. The oxidation process lasted for 12 hours based on the dose test to achieve expected partial 1,4-dioxane removals (~50%), then was quenched with NaOH, and the remaining 1,4-dioxane in the microcosms was incubated for following 9-week biodegradation process (30°C, 150 rpm shaking). CB1190 was added before and after oxidation process, and ~5000 μg/L 1,4-dioxane was added in microcosms whenever 1,4-dioxane dropped below detection limit during the incubation period, to maintain bacterial viability and test the reproducibility in CB1190-augmented bottles.

Four time points were selected during the combined treatment train for DNA extraction (300 μL slurry), including before oxidation (OB1) and after oxidation (OB2, day 0), middle of biodegradation (OB3, day 17) where 1,4-dioxane was first depleted and second batch of CB1190 was added, and the end of biodegradation (OB4, day 63).

6.2.5 Combined Catalysis and Biodegradation (CB) Treatment Train

The doses of H_2O_2 and WO_x/ZrO_2 were first tested on natural slurry (Table 6.4). Briefly, significant (> 10%) degradation of 1,4-dioxane was observed for doses greater than 155 μM H_2O_2 and higher catalyst concentrations appeared to be more useful for 1,4-dioxane degradation. Therefore, a catalyst dose of 8 g_{cat}/L and H_2O_2 dose of 310 μM, which achieved a ~20% reduction in the 1,4-dioxane concentration, were chosen for the microcosms.

Table 6.14. Catalyst and H_2O_2 dosing experiments on 1,4-dioxane.

H_2O_2 (μM)	WO_x/ZrO_2 (g_{cat} L^{-1})		
	2	4	8
0	0%		
4.78	7%		
9.55	9%		
19.4	7%		
38.81	7%		
77.62	4%		
155	13%	11%	11%
310	13%		21%

In the microcosms, 400 mg of WO_x/ZrO_2 catalyst (20% WO_x, w/w) was added along with 1600 μL 30% (w/w) H_2O_2 in each bottle, and stirred for 24 hours, then quenched with NaOH. 500 μL samples of soil-groundwater slurry were collected before (CB0) and after (CB1) the catalysis phase, 200 μL of which was used for 1,4-dioxane measurements, and the remaining was used for total nucleic acids extraction. Afterward, the same microcosm bottles were continuously incubated at 30°C and shaken at 150 rpm for 17 weeks to represent a subsequent biodegradation phase. Samples were collected at the middle (day 63, CB2) and the end (day 119, CB3) of the biodegradation phase. For the bioaugmentation condition, CB1190 was added at the middle of biodegradation phase, immediately before the CB2 sampling.

6.2.6 Analytical Methods for 1,4-Dioxane and CVOCs

1,4-Dioxane (1-1000 μg/L) was monitored using an Agilent 6890 gas chromatograph equipped with an Agilent 5973 mass spectrometer (GC-MS) and a Supelco SPB-1 Sulfur column (30 m × 0.32 mm id ×4 μm). The collected aqueous samples were prepared for GC-MS analysis using a frozen micro-extraction procedure as previously described (Li et al., 2011), and 5 μL of processed sample was injected into the GC-MS equipped with a pulsed split-less injection with an inlet temperature of 150°C, 77 kPa, a pulsed pressure of 170 kPa for 2 min, and a purge flow of 15.0 mL/min. The oven

temperature was initially held constant at 35°C for 5 min, then increased to 100°C at a rate of 20 °C/min, and further increased to 275°C at a rate of 50°C/min. The mass-selective detector (MSD) was operated with an electron multiplier (EM) offset of 400 and EM voltage of 2000. The MS quadrupole was set to 150°C with a source for 230°C (Zhang et al., 2016).

1,4-Dioxane concentrations were measured using a Hewlett-Packard 6890 gas chromatograph equipped with a flame ionization detector (GC-FID) (Hewlett-Packard, Atlanta, GA) with a Restek® Stabilwax-DB capillary column (30 m x 0.53 mm ID x 1 μm; Restek, Bellefonte, PA) as described in Pornwongthong et al. (2014). Briefly, liquid samples (100 μL) were collected and filtered through 0.2-μm-pore Fisherbrand nylon syringe filters. 2 μL of the filtrate was directly injected into the GC-FID. The injector and detector were maintained at a temperature of 220°C and 250°C, respectively. The oven was programmed to rise from 80°C to 140°C at a ramp rate of 20°C/min, and held for 1 minute at 140°C. The 1,4-dioxane retention time was approximately 3.5 minutes.

A Varian 3500 capillary gas chromatograph equipped with an ECD was used to quantify TCE, TCA, and 1,1-DCE (100-5000 μg/L; Agilent DB-5 capillary column, 30 m × 0.25 mm × 0.25 μm). Samples were analyzed by direct headspace injection (50 μL) to the injection port (260°C), with the detector was kept at 310°C. The oven temperature was held at 35℃ 30 min with a column flow rate of 9.6 mL/min. Samples containing cDCE (ranging from 500 to 5000 μg/L) were analyzed by GC-FID by direct headspace injection (10 μL). The flow rate was 1.7 mL/min. The oven temperature was initially held at 100°C for 1 min and then increased at a thermal incline of 25°C /min and held at a final temperature of 150°C for 30 s (Zhang et al., 2016).

6.2.7 DNA Extraction, PCR Amplification and Illumina Miseq Sequencing

FastDNA™ Spin Kit for Soil (MP Biomedicals, USA) was used to extract DNA from stored slurry according to the manufacturer's instructions and microspectrophotometry (NanoDrop® ND-1000, NanoDrop Technologies, Willmington, Delaware, USA) was used to measure the concentration and purity of extracts (Miao et al., 2015).

Universal 16S rRNA gene was amplified to quantify total bacterial biomass in microcosms, and the CB1190-like 16S rRNA gene was used to quantify the abundance of the 1,4-dioxane metabolizer *Pseudonocardia dioxanivorans* CB1190 or closely related bacteria (Gedalanga et al., 2014). Reactions were conducted using a StepOnePlus thermocycler (Life Technologies, Carlsbad, California, USA) with a total reaction volume of 20 μL, containing qPCR Master Mix (10 μL, 2× Luminaris Color HiGreen-HiROX, Thermo Scientific, Waltham, Massachusetts, USA), forward (0.5 μL, 10 μM) and reverse primers (0.5 μL, 10 μM) (Table 5.5), 7 μL of ddH_2O, and 2 μL of DNA template. The annealing temperatures for both genes were 60°C and 50°C, respectively, and melt-curve analyses at 81.5-83.6°C were considered to ensure specificity of amplification to target genes, with genome DNA of *Pseudonocardia dioxanivorans* CB1190 as standard in qPCR.

Table 6.15. Primer sequences and annealing temperatures.

Gene	For-Primer (5'→3')	Rev-Primer (5'→3')	Annealing temperature (°C)
dxmB/dioxane monooxygenase (DXMO)	CCAAACGGGCGTCAGTCAT	AGAACGTGCGCTCCCAAAG	60
aldH/aldehyde dehydrogenase (ALDH)	ACCAAGGACCTCACCTCGTA	AACGGATGCGCGTTGTTC	60
CB1190-like 16S rRNA	CCAAACGGGCGTCAGTCAT	AGAACGTGCGCTCCCAAAG	60
Universal 16S rRNA	ATGGCTGTCGTCAGCT	ACGGGCGGTGTGTAC	53
16S rRNA gene V3-V4 region	TCGTCGGCAGCGTCAGATGTGTATAA GAGACAGCCTACGGGNGGCWGCAG	GTCTCGTGGGCTCGGAGATGTGTATAAGA GACAGGACTACHVGGGTATCTAATCC	55

The hypervariable V3-V4 regions of 16S rRNA gene (Table 6.5) were chosen to be sequenced on the Illumina Miseq platform (Klindworth et al., 2013). Each condition had triplicate DNA

samples from triplicate microcosm bottles, respectively. The three DNA samples were mixed and analyzed via duplicate PCR reactions. Thus, each condition had two PCR products. The PCR reaction system was 50 μL containing 2 × EasyTaq® PCR SuperMix (25 μL), forward primer (2 μL, 10 μM) and reverse primer (2 μL, 10 μM), 40 ng sample genomic DNA and 21 μL double deionized H_2O, with annealing at 55°C. PCR products were sent to Laragen, Inc. (Culver City, California) for further purification and additions of sample specific dual-index barcodes, then pooled and run Illumina Miseq sequencing, using MiSeq v3 reagents to generate paired 300-bp reads.

6.2.8 Bioinformatics and Statistical Analyses

The generated sequences of 16S rRNA genes were grouped and preprocessed in Mothur software (v 1.40.0), and quality controlled the assembled paired-end reads with criteria: (i) an average quality cutoff at Q30; (ii) ambiguous bases at 0 (Chao et al., 2016); (iii) minimum length at 400 bp (Schloss et al., 2009). The chimeras were detected and identified by using "chimera.vsearch", and assembled reads that aligned and classified to chloroplasts, mitochondria, or Eukaryota based on Silva database were discarded by using "remove.lineage". Finally, the number of remaining quality-controlled reads in each sample were normalized to 30,000, and all datasets have been submitted to Metagemonics Rapid Annotation using Subsystem Technology (MG-RAST) server. The normalized sequences were further clustered into different operational taxonomic units (OTUs) with command "cluster.split" at 0.03 cutoff (97% similarity), producing a total of 3412 OTUs after removing singletons (an OTU with one read), and the taxonomy of each OTU was blast against Silva database by using "classify.otu".

The α-diversity indices (Shannon, Chao1, ace, etc.) were calculated by the "summary.single", and the relative abundance of taxa was calculated in each sample. UniFrac distances metrics (weighted and unweighted) calculated by "unifrac.weighted", was used to indicate pairwise

similarities among samples, and triplicates of each sample were shown by using principal coordinates analysis (PCoA).

The cluster analysis (CA) was also based on average relative abundance of 97% similarity OTUs (0.97-OTUs), and data were clustered using the Clara algorithm (Kaufman and Rousseeuw, 2009). This method was based on partitioning around medoids (PAM), which refers to an object within a cluster minimizing the sum of dissimilarities among all cluster observations, and can show distinct discontinuities among samples.

The linear discriminant analysis (LDA) effect size (LEfSe) method was used to determine the taxa that were most likely to explain differences among groups, with consideration of standard tests for statistical significance, as well as additional tests encoding biological consistency and effect relevance (Segata et al., 2011), and the determining taxon was defined as the representative biomarker of the specific group.

The microbial functions were predicted by using Tax4Fun (Aßhauer et al., 2015) based on generated OTUs table and OTUs taxonomy, with R package "tax4fun". Pathways and genes related to 1,4-dioxane and CVOCs degradation in KEGG ortholog were searched and picked manually with enzyme commission (EC) number.

Network analysis based on correlations, which was previously applied to study microbial co-occurrence/co-exclusion species-species associations (SSA) patterns (Chao et al., 2016, Ju et al., 2017), was calculated using an average relative abundance of 97% similarity OTUs (0.97-OTUs). The algorithm was based on the non-parametric Spearman's rank correlation with strict coefficients at ± 0.6 and significant cutoff p-value at 0.01 (Barberan et al., 2012). Random incidence (R%) and observed incidence (O%) of taxa co-occurrence were statistically checked on order level based on previous methods (Ju and Zhang, 2015). The O% was defined as ratio of the number of observed

edges (E_0) between two orders to total number of edges (E), and the R% was conducted by following formula:

$$R = \frac{2 \times N_1 \times N_2}{N \times (N-1)}$$

Where N_1 and N_2 represented order1's and order2's OTUs' number in the network, and N is total nodes in the network. The ratio of O% to R% (O/R), was used as criteria of nonrandom SSA between two different orders (Ju et al., 2017).

Supervised regression model based on machine learning is a powerful tool to explore the patterns in complicated datasets, and can predict treatment process utilizing the microbial community, as well as implicit the community development in the course of time. 1,4-Dioxane and CVOCs prediction models were constructed by the Random Forest (RF) regression as a function of the changes in OTUs abundances data (Metcalf et al., 2016, Belk et al., 2018). Four sampling points were categorized by numbers (CB0=day 0, CB1=day 1, CB2=day 63, and CB3=day 119). Sample replicates belonging to the same conditions were pooled together to train the model, and 10-fold cross-validation (CV) was performed to tune and evaluate the models (Metcalf et al., 2016), then the model was tested by randomly picked samples. The accuracy of models is measured as R^2 and mean absolute error (MAE) (Belk et al., 2018). Multiple conditions were picked with purposes to train the regression models, and the remaining condition(s) were used to test the model or to be predicted. The modeling results were compiled and graphics were generated in R environments following previous work (Belk et al., 2018).

All visualizations were made by using R (v 3.4.0) with packages "phyloseq" (McMurdie and Holmes, 2013) for PCoA, "ComplexHeatmap" (Gu et al., 2016) for heatmap organization, "factoextra" and "cluster" (Miao et al., 2017) for cluster analysis (CA), "Hmisc" (Miao et al., 2017)

for correlation analysis. The circular networks were visualized by Gephi (v 0.9.2) (Bastian et al., 2009).

6.3 Results

6.3.1 Oxidation and Catalysis Treatment Train

6.3.1.1 1,4-Dioxane Removal and Gene Abundance Changes in OC Train

1,4-Dioxane concentrations under H-DX/H-CV and H-DX/L-CV conditions were spiked to 6759 and 7358 μg/L, respectively, and were 1109 and 1002 μg/L for L-DX/L-CV and L-DX conditions, respectively (Figure 6.1). However, the 12-hour oxidation process degraded 87.44%, 85.13%, 85.83%, and 84.56% 1,4-dioxane under H-DX/H-CV, H-DX/L-CV, L-DX/L-CV, and L-DX conditions, respectively, indicating the high efficiency of oxidation on different levels of 1,4-dioxane, even with the presence of the CVOCs. In the following catalysis process, catalyst was added with more dose of H_2O_2, and reacted for 24 hours, then ~20% of remaining 1,4-dioxane was removed. All conditions showed similar 1,4-dioxane removals, even various initial CVOCs concentrations. The overall degradation rates were promising (~90%), confirming the high efficiency of coupled treatment technologies for 1,4-dioxane degradation, even with the presence of CVOCs or various initial 1,4-dioxane levels.

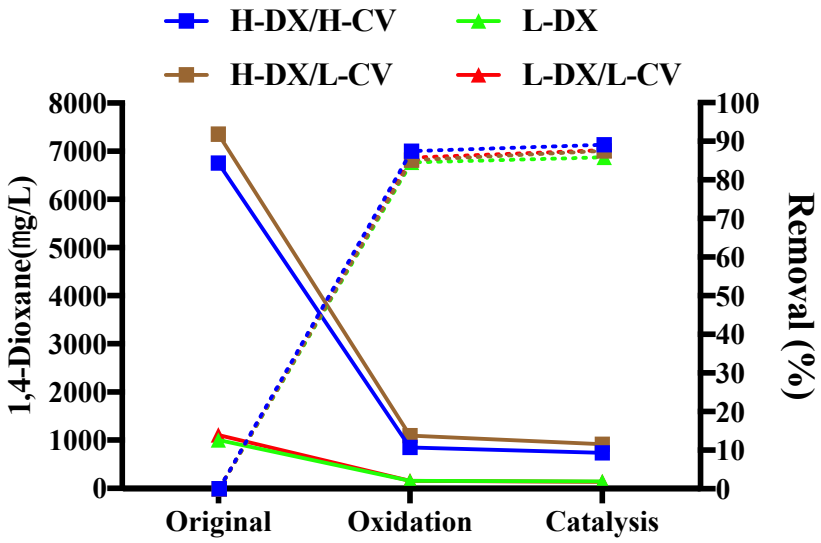

Figure 6.56. Removal performances of 1,4-dioxane in microcosms constructed from well 8MNW54 during oxidation-catalysis treatment train under different 1,4-dioxane and CVOCs concentrations. The solid line belonged to left Y-axis indicating 1,4-dioxane concentrations, and the dot line belonged to right Y-axis indicating 1,4-dioxane removals after each treatment process. Each condition was conducted with triplicate microcosms.

The inhibitory impacts of chemical reactions on biomass quantities were clear under H-DX/H-CV and H-DX/L-CV conditions, while under L-DX/L-CV and L-DX conditions, more microorganisms survived after catalysis (Figure 6.2). This indicated that the catalysis to treat higher concentration of 1,4-dioxane exhibited more pressure on microbiomes. To predict potential biodegradation, CB1190-like rRNA genes were quantified, which originally were 10^2 copies/mL slurry, but were nearly obliterated during oxidation process, indicating their vulnerability to peroxide and the cessation of 1,4-dioxane biodegradation processes.

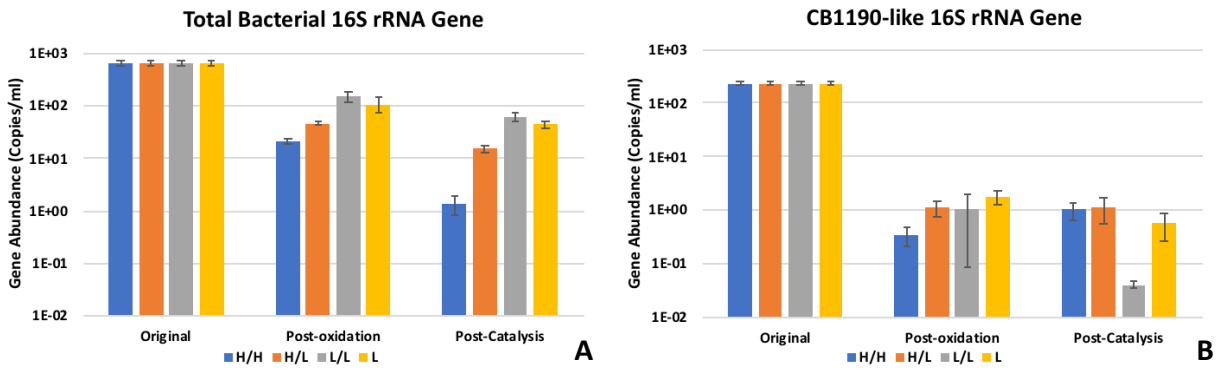

Figure 6.57. Total bacterial 16S rRNA gene (A) and CB1190-like 16S rRNA gene (B) abundance under different conditions during oxidation-catalysis process. Y-axis is in log scale.

6.3.1.2 Microbiome Distributions and Biodiversity Shifts

While 1,4-dioxane removals were not distinguished among different conditions, dominant microorganisms were differentiated during the process. Phylum *Proteobacteria* were most abundant before treatment (72.44%), but were sequentially decreased after the oxidation and catalysis processes under all conditions, except for L-DX, where *Proteobacteria* were kept at 59% (Figure 6.3). Both phyla *Actinobacteria* (12.62%) and *Firmicutes* (0.56%) abundance increased after the oxidation process, but decreased during the catalysis process. However, after the oxidation process, *Firmicutes* abundance increased less under L-DX condition comparing with other conditions, and *Actinobacteria* showed larger increases in low 1,4-dioxane concentration microcosms comparing with high 1,4-dioxane concentration microcosms. In contrast, *Bacteroidetes* (10.60%) abundance initially decreased during the oxidation process (less than 3% under each condition), but increased after the catalysis process. Interestingly, *Cyanobacteria* (0.03%) abundance did not increase until after the catalysis process under CVOCs-spiked conditions, while kept marginal abundance under the low 1,4-dioxane-only condition during whole train, demonstrating the selective impacts of CVOCs on *Cyanobacteria* in microcosms.

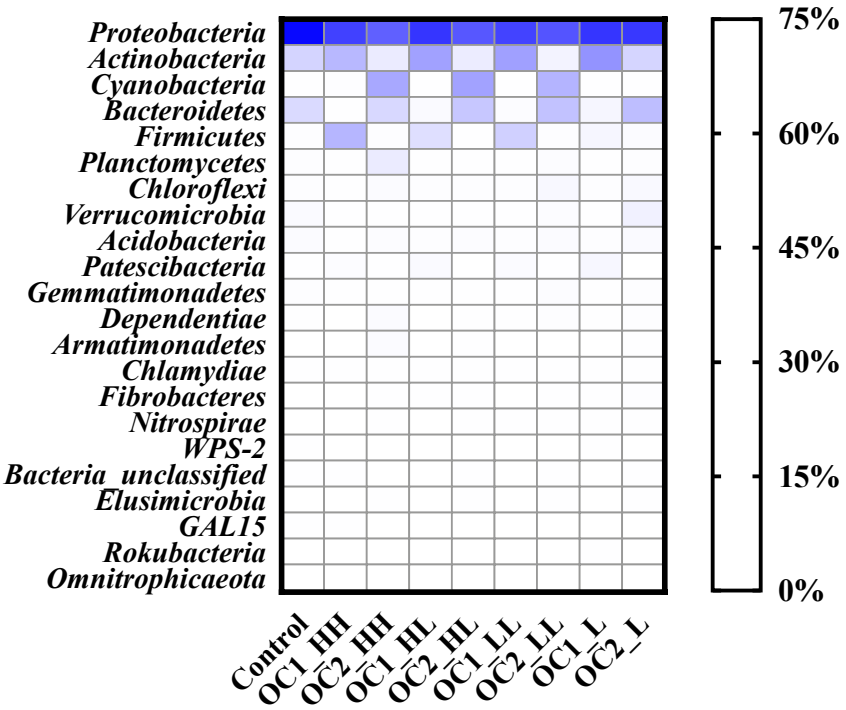

Figure 6.58. Relative abundance of all taxa on phylum level at each time points under all conditions. Control is original state, OC1 is post-oxidation state, and OC2 is post-catalysis state.

On further taxonomic classification level (Figure 6.4), genus *Pseudomonas* was dominantly abundant, occupying 46.78% before treatments, but decreased to below 5% after the oxidation process and below 1% after the catalysis process under all conditions. This indicates that the chemical reactions had a larger impact on *Pseudomonas* distributions than those imposed by the presence of either 1,4-dioxane or CVOCs. Some originally minor genera showed tolerant capabilities to oxidation, such as *Massilia* (0.01%), *Rhodococcus* (6.93%), *Paenibacillus* (0.01%), *Pseudarthrobacter* (0.45%), and *Williamsia* (0.91%), all of which increased after oxidation but decreased after catalysis. However, 1,4-dioxane and CVOCs were involved in the oxidative tolerance, as *Massilia* increased to 47.54% and 1.17% under H-DX/H-CV and L-DX conditions, respectively, indicating that high concentrations of 1,4-dioxane, CVOCs and oxidant facilitated the survival of *Massilia*. However, *Rhodococcus* had the highest relative abundance under L-DX

condition compared with other conditions after oxidation, showing opposing trends with *Massilia*, demonstrating sensitivity of *Rhodococcus* to high doses of 1,4-dioxane and CVOCs combinations. The genera that increased after the catalysis process were defined as catalyst-tolerant microorganisms, including *Cylindrospermum* (0.01%), *Novosphingobium* (0.50%), *Lacibacter* (1.90%), Sphingomonas (2.66%), and *Devosia* (0.23%). Similar to oxidative tolerance, 1,4-dioxane and CVOCs also had associated impacts on catalyst-tolerant microorganisms, such as *Cylindrospermum* and *Novosphingobium*, that favored high 1,4-dioxane and CVOCs concentrations, while *Lacibacter* had no clear trends. Genera *Sphingomonas* (2.66%) and *Devosia* showed potential simultaneous oxidative and catalyst tolerances through their stability after oxidation and increased abundance after catalysis, but both preferred relatively lower CVOCs exposure. Interestingly, under the L-DX condition, genus *Pseudarthrobacter* also demonstrated catalyst-tolerance, but was suppressed after catalysis under all other conditions.

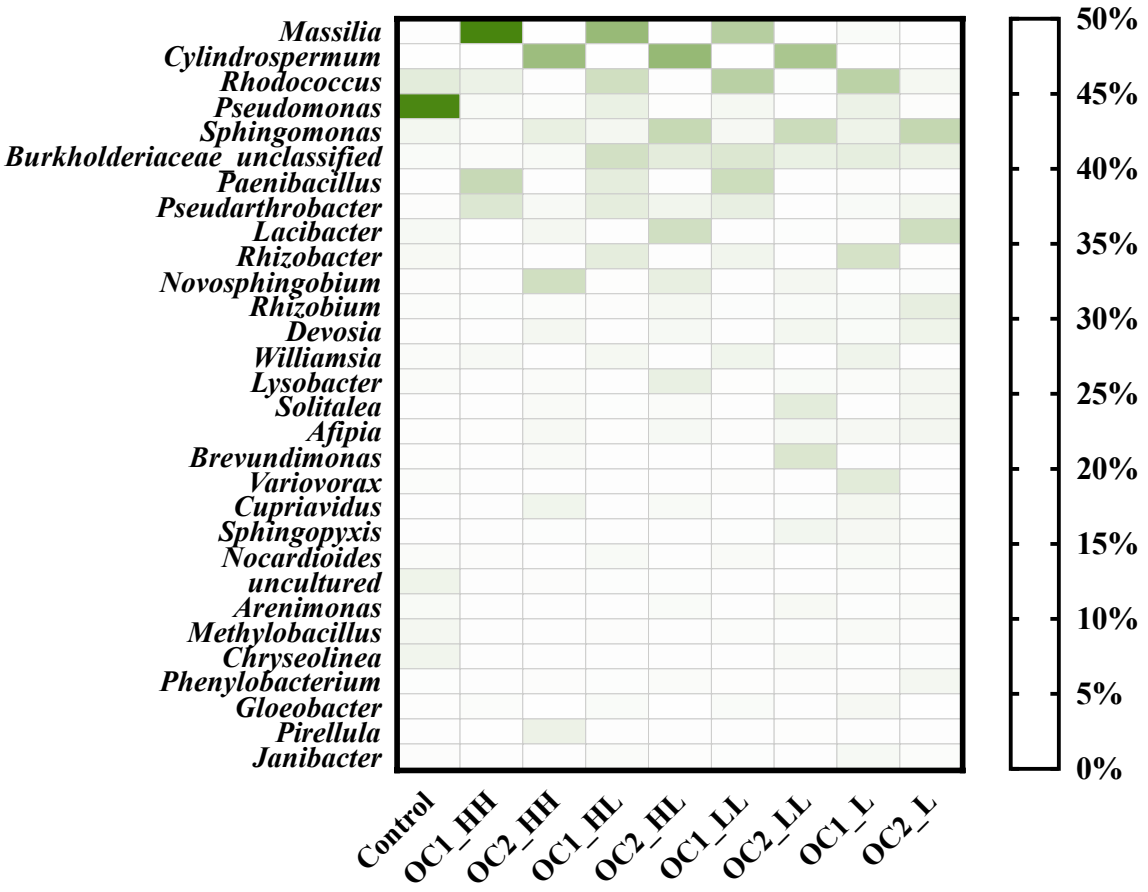

Figure 6.59. Trends of dynamics of microbial community with the 30 most abundant genera at each time point under all conditions. Control is original state, OC1 is post-oxidation state, and OC2 is post-catalysis state.

The biodiversity plotted by rarefaction curves under each condition was used to show direct microbial community shifts during the treatment train associated with 1,4-dioxane and CVOCs (Figure 6.5). Under H-DX/H-CV condition, biodiversity was reduced directly after oxidation process, and remained unchanged after catalysis, while diversity under H-DX/L-CV and L-DX/L-CV conditions maintained constant levels after oxidation, but decreased after catalysis. However, under L-DX condition, biodiversity was stimulated after oxidation process and decreased after catalysis, but remained higher than the initial diversity.

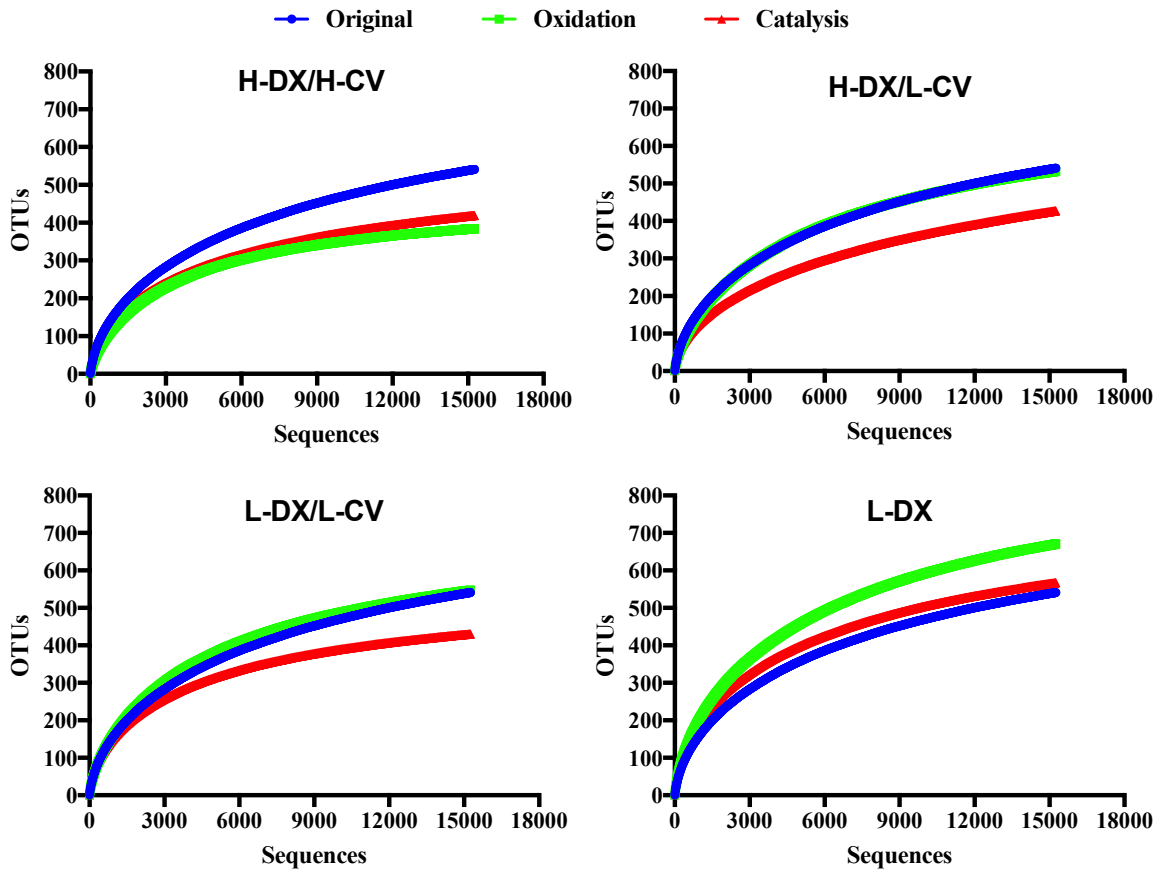

Figure 6.60. Rarefaction curves (average OTUs) during oxidation-catalysis treatment train under different 1,4-dioxane and CVOCs concentrations.

6.3.1.3 Microbial Community Dynamics and Representative Biomarkers

Based on taxonomic classification, specific microorganisms varied under different conditions along with the OC treatment train. Thus, the overall relationships based on a cluster analysis (CA) were used to describe condition-microorganism similarity. Microbial communities were clearly differentiated by oxidation and catalysis treatments (Figure 6.6), while within the same treatment process, L-DX condition stood out from the other conditions, becoming an individual cluster. This separation demonstrated the community was also determined by the concentrations of 1,4-dioxane and CVOCs. Indeed, CVOCs could be the potential driver for this structural shift. In addition, all OC2 samples were in greater proximity than the OC1 or Control samples, indicating the stronger

impact of the oxidation process on structural shift beyond the differences induced by different 1,4-dioxane and CVOCs levels. Moreover, principal coordinates analysis (PCoA) on weighted and unweighted Unifrac distances between states also showed that communities shifted away from original state, and segregated after different treatment states (Figure 6.7). Similar to cluster analysis, microbial compositions under L-DX condition were isolated from other conditions after the oxidation process. PCoA analysis also demonstrated that the H-DX/H-CV condition (Figure 6.7, green triangles) was different than H-DX/L-CV and L-DX/L-CV conditions, which were observed to be in closer proximity on cluster analysis. This pattern in the PCoA results further highlights the impact of CVOCs within the same treatment. In addition, the oxidation process had similar impacts to the microbial communities in terms of both microbial membership (unweighted, Figure 6.7B) and abundance (weighted, Figure 6.7A), while the catalysis process had a greater impact on microbial membership as evidenced by less separation of the L-DX condition in the weighted analysis (Figure 6.7A) compared to the unweighted analysis (Figure 6.7B). This is consistent with the cluster analysis that showed that close grouping of all post-catalysis treatments (Figure 6.6, OC2).

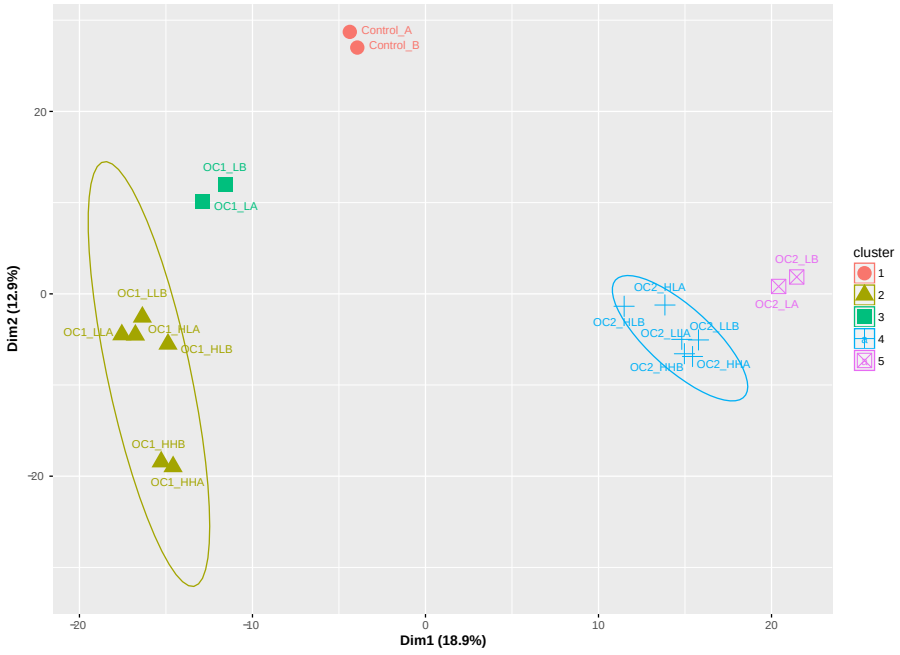

Figure 6.61. Cluster analysis among samples at each time point under all conditions during oxidation-catalysis treatment train (average OTUs). All samples were classified to OTUs level and pooled together to show integral shift among conditions and time points. Control is original state, OC1 is post-oxidation state, and OC2 is post-catalysis state.

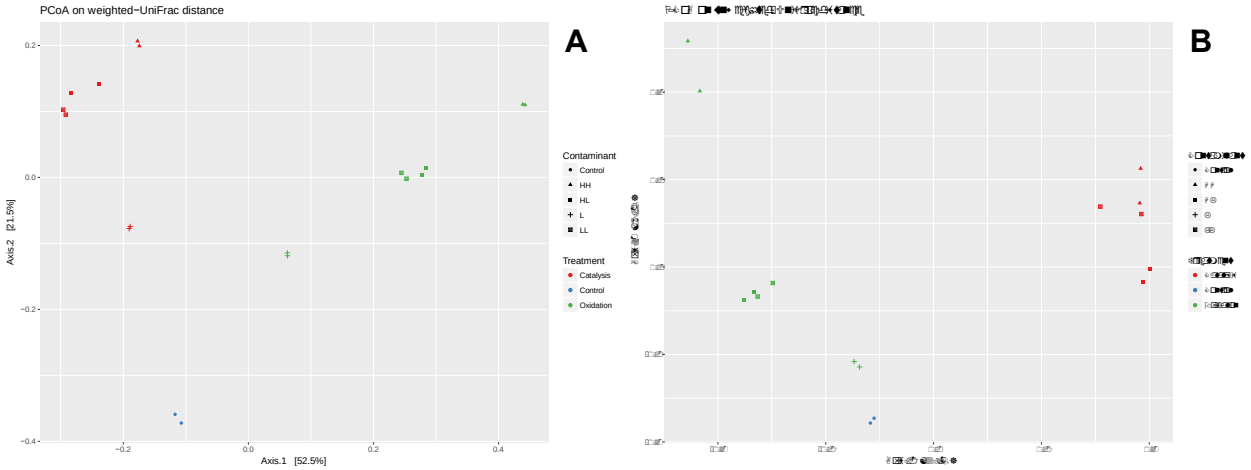

Figure 6.62. Dynamics of microbial community at each time point under all conditions at the 0.97-OTUs level during oxidation-catalysis treatment train. PCoA biplots show weighted (A) and unweighted (B) UniFrac distances were namely qualitative (i.e., phylogeny) measures of microbial dynamics with and without quantitative (i.e., abundance) measures.

LEfSe was used to highlight the representative microbes in different groups (states or conditions). When focusing on treatment states, genus *Pseudomonas* was identified as the biomarker at original state, while *Massilia*, *Rhodococcus*, *Williamsia*, and *Paenibacillus* were found accumulated at post-oxidation state, and *Sphingomonas*, *Brevundimonas*, and *Devosia* were selected after catalysis process (Figure 6.8 and 6.9). Furthermore, based on the biomarkers highlighted in each treatment state, the comparison among conditions showed that L-DX had 29 unique biomarkers, more than other conditions (Figure 6.10), explaining the isolation of L-DX on PCoA and CA. Similarly, unique enriched genera were found under specific conditions (Figure 6.11 and 6.12). LEfSe covered the whole microbial community based on 0.97-OTUs classification, thus statistically

showed not only dominant microorganisms, but also included minor representative microbes with their higher taxonomic ranks.

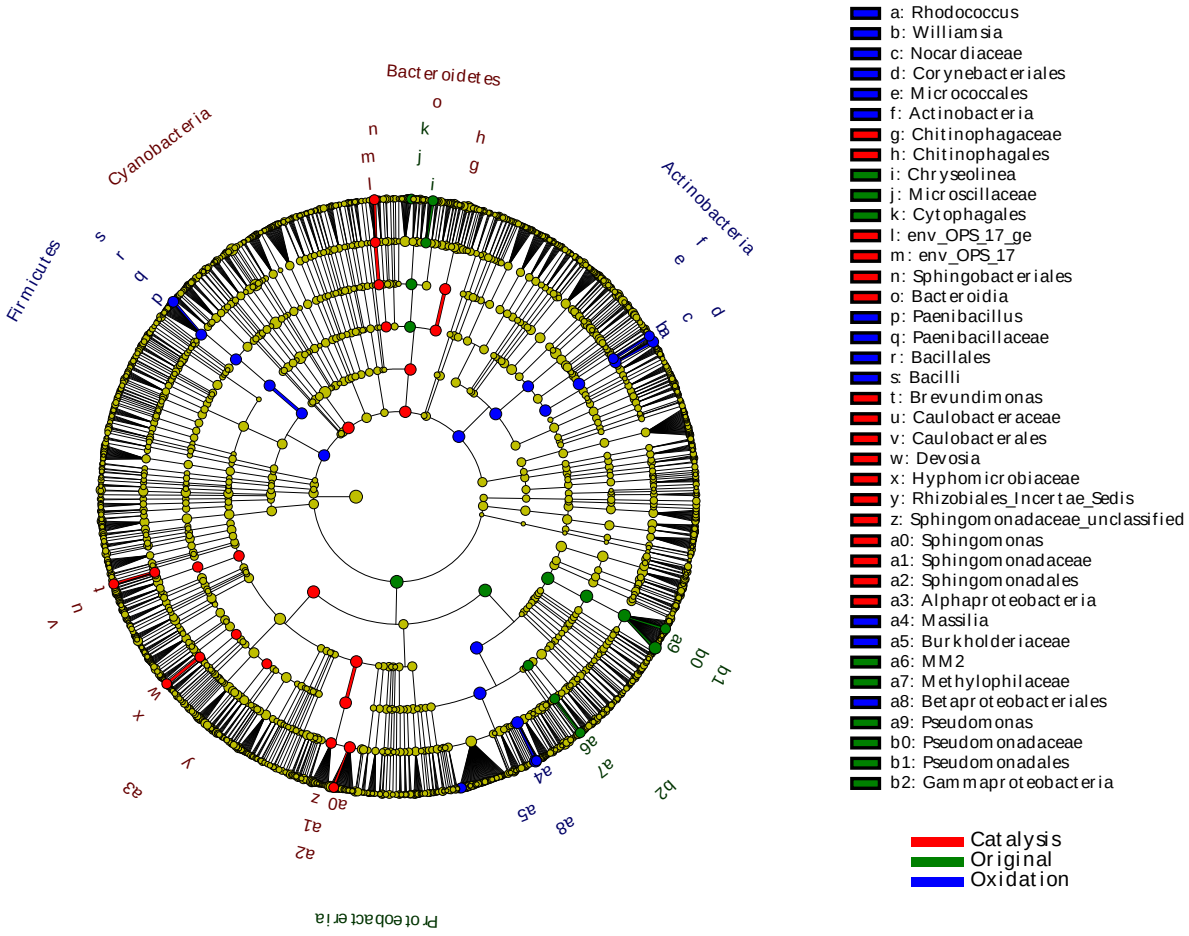

Figure 6.63. Taxonomic cladogram obtained using LEfSe analysis of the 16S sequences indicating the phylogenetic distribution of microbial lineages associated with the three treatment states, and only the taxa meeting a significant LDA threshold value of >4 are shown. Differences are represented in the unique color of each state (green for original state, blue for post-oxidation state, red for post-catalysis state, and yellow nonsignificant), and highlighted taxa indicate enrichment of that taxa within the treatment state that corresponds to the highlighting color (shading and label). Circles represent phylogenetic levels from phylum to species (OTUs) inside out, and each circle's diameter is proportional to the taxon's abundance.

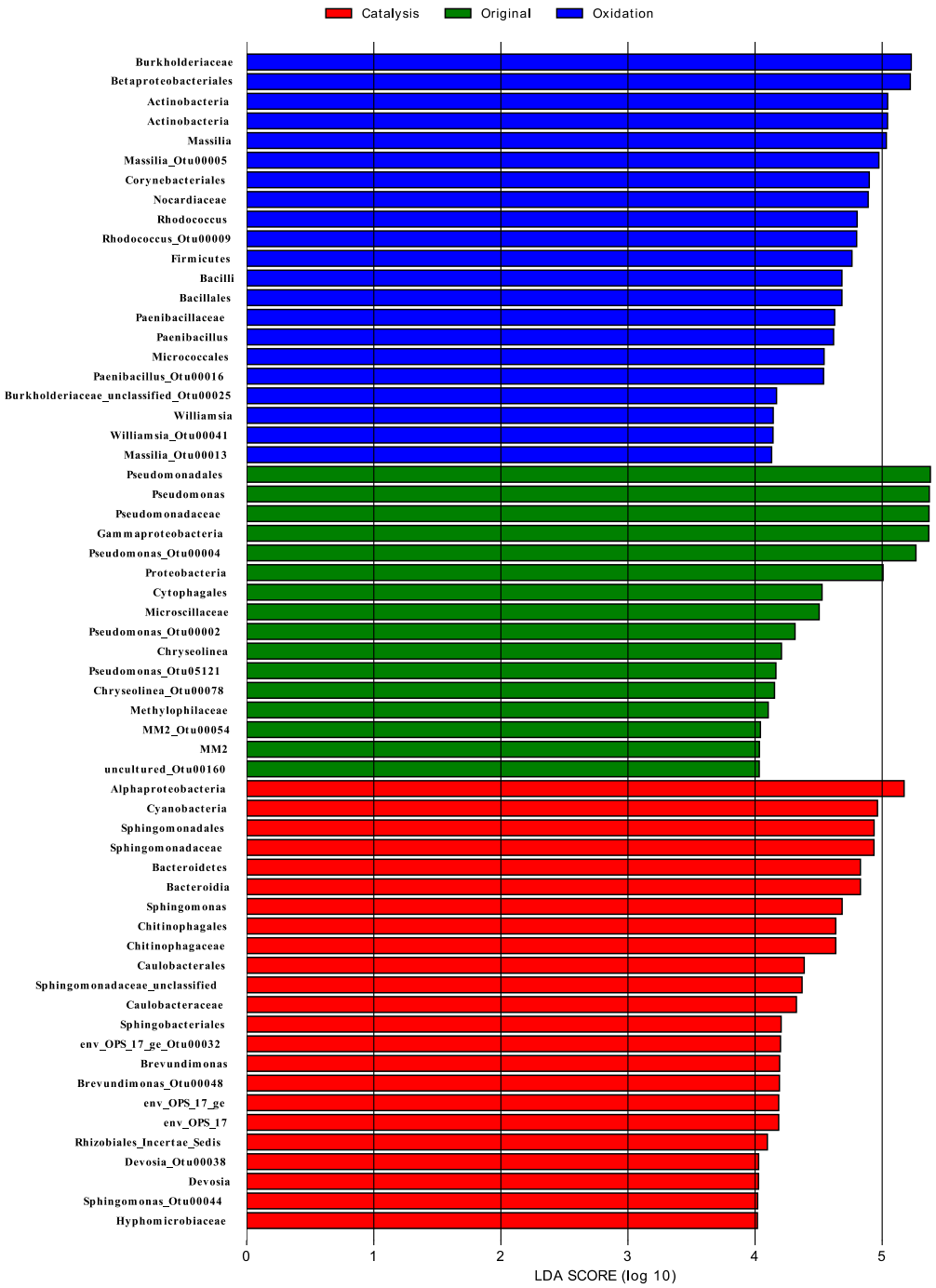

Figure 6.64. Histogram of the LDA scores computed for taxon differentially abundant among treatment processes including original, oxidation and catalysis. LEfSe scores can be interpreted as the degree of consistent difference in relative abundance between taxa in the two groups of analyzed microbial communities. Only the taxa with meeting a significant LDA threshold value of >4 are shown.

Figure 6.65. Histogram of the LDA scores computed for taxon differentially abundant among conditions. LEfSe scores can be interpreted as the degree of consistent difference in relative abundance between taxa in the two groups of analyzed microbial communities. Only the taxa with meeting a significant LDA threshold value of >4 are shown.

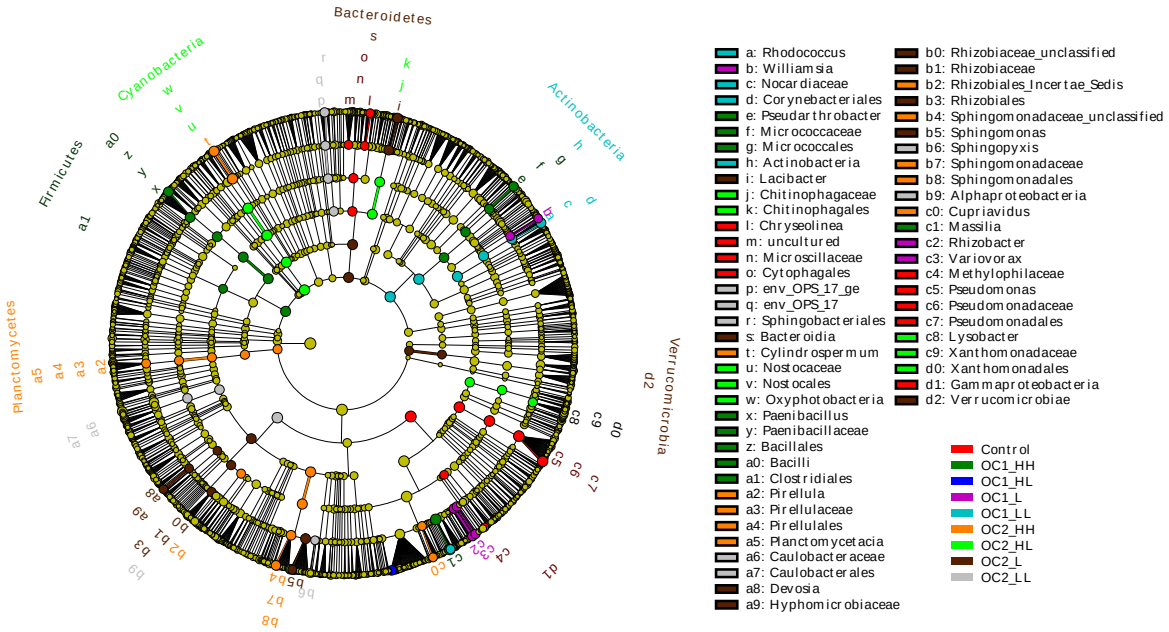

Figure 6.66. Taxonomic cladogram obtained using LEfSe analysis of the 16S sequences indicating the phylogenetic distribution of microbial lineages associated with each time point under specific condition, and only the taxa meeting a significant LDA threshold value of >4 are shown. Differences are represented in the unique color of each time point under specific condition, and highlighted taxa indicate enrichment of that taxa within the treatment state that corresponds to the highlighting color (shading and label). Circles represent phylogenetic levels from phylum to species (OTUs) inside out, and each circle's diameter is proportional to the taxon's abundance.

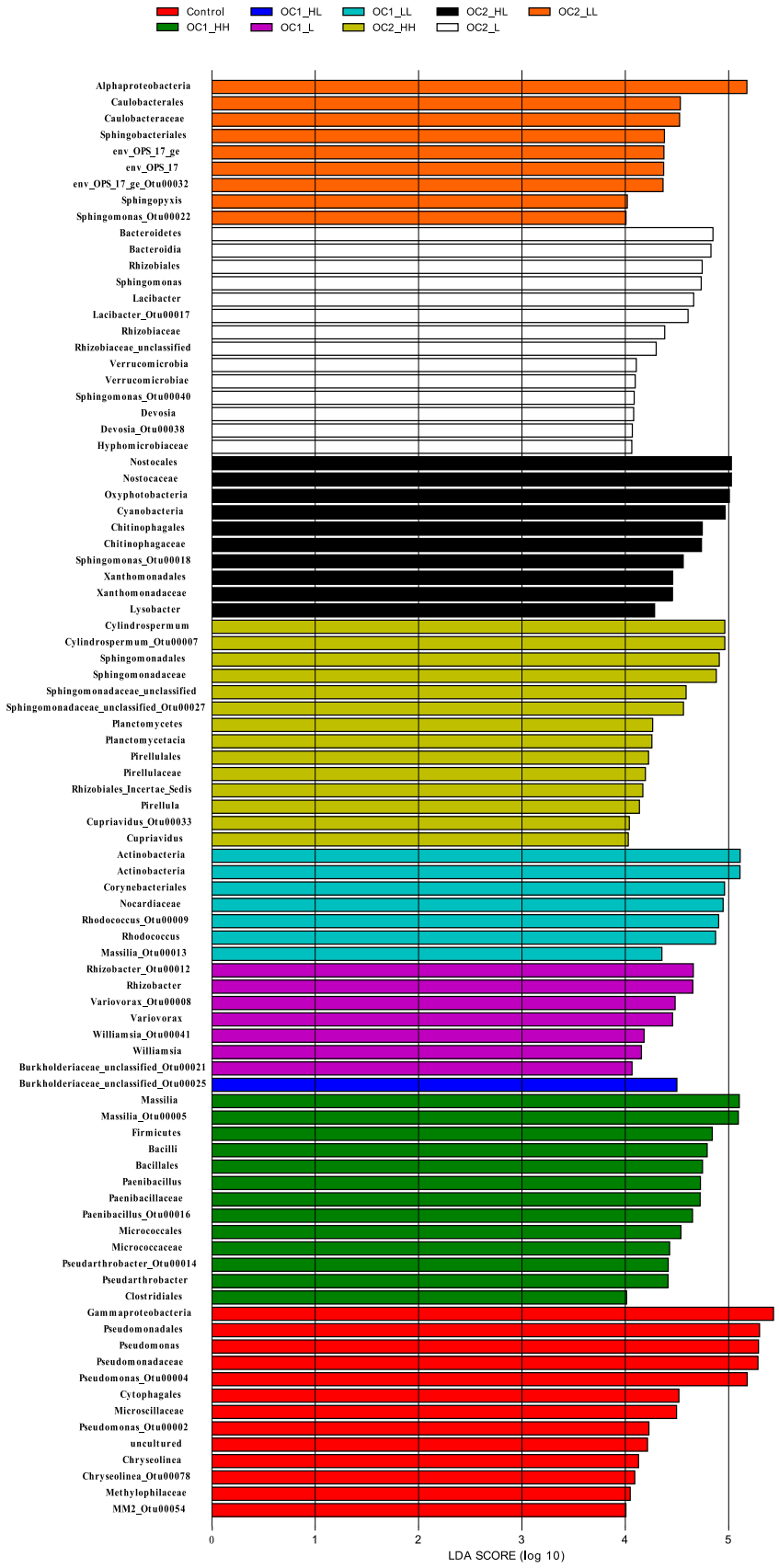
Control
OC1_HL
OC1_LL
OC2_HL
OC2_LL
OC1_HH
OC1_L
OC2_HH
OC2_L
Alphaproteobacteria
Caulobacterales
Caulobacteraceae
Sphingobacteriales
env_OPS_17_ge
env_OPS_17
env_OPS_17_ge_Otu00032
Sphingopyxis
Sphingomonas_Otu00022
Bacteroidetes
Bacteroidia
Rhizobiales
Sphingomonas
Lacibacter
Lacibacter_Otu00017
Rhizobiaceae
Rhizobiaceae_unclassified
Verrucomicrobia
Verrucomicrobiae
Sphingomonas_Otu00040
Devosia
Devosia_Otu00038
Hyphomicrobiaceae
Nostocales
Nostocaceae
Oxyphotobacteria
Cyanobacteria
Chitinophagales
Chitinophagaceae
Sphingomonas_Otu00018
Xanthomonadales
Xanthomonadaceae
Lysobacter
Cylindrospermum
Cylindrospermum_Otu00007
Sphingomonadales
Sphingomonadaceae
Sphingomonadaceae_unclassified
Sphingomonadaceae_unclassified_Otu00027
Planctomycetes
Planctomycetacia
Pirellulales
Pirellulaceae
Rhizobiales_Incertae_Sedis
Pirellula
Cupriavidus_Otu00033
Cupriavidus
Actinobacteria
Actinobacteria
Corynebacteriales
Nocardiaceae
Rhodococcus_Otu00009
Rhodococcus
Massilia_Otu00013
Rhizobacter_Otu00012
Rhizobacter
Variovorax_Otu00008
Variovorax
Williamsia_Otu00041
Williamsia
Burkholderiaceae_unclassified_Otu00021
Burkholderiaceae_unclassified_Otu00025
Massilia
Massilia_Otu00005
Firmicutes
Bacilli
Bacillales
Paenibacillus
Paenibacillaceae
Paenibacillus_Otu00016
Micrococcales
Micrococcaceae
Pseudarthrobacter_Otu00014
Pseudarthrobacter
Clostridiales
Gammaproteobacteria
Pseudomonadales
Pseudomonas
Pseudomonadaceae
Pseudomonas_Otu00004
Cytophagales
Microscillaceae
Pseudomonas_Otu00002
uncultured
Chryseolinea
Chryseolinea_Otu00078
Methylophilaceae
MM2_Otu00054
0
1
2
3
4
5
LDA SCORE (log 10)

Figure 6.67. Histogram of the LDA scores computed for taxon differentially abundant among specific conditions after each treatment state. LEfSe scores can be interpreted as the degree of consistent difference in relative abundance between taxa in the two groups of analyzed microbial communities. Only the taxa with meeting a significant LDA threshold value of >4 are shown.

6.3.2 Oxidation and Biodegradation Treatment Train

6.3.2.1 Microcosm Performance and Biomarker Detection

H_2O_2 was an effective oxidant for the 12-hour oxidation period under each condition, and high 1,4-dioxane reductions between 80%-82% were achieved except for the H-DX/H-CV condition where only 50% of the 1,4-dioxane was removed (Figure 6.13). In the H-DX/H-CV condition, 9.45% of the initial TCA remained after oxidation, while CVOCs were completely removed after 12-hour oxidation in all other conditions. The biodegradation phase following the AOP phase lasted for another 9 weeks, and 1,4-dioxane was stable in each non-bioaugmented microcosm, without apparent indigenous 1,4-dioxane removals. Under bioaugmentation, 1,4-dioxane was spiked to 2919 µg/L at day 17 (OB3) after the initial dose of 1,4-dioxane had been depleted, and CB1190 (1:10 v/v) was added at same time. 1,4-Dioxane was monitored to below detection continuously at days 30, 42 and 63 (OB4), respectively, and both 1,4-dioxane and CB1190 had to be spiked again at days 30 and 42, respectively (Figure 6.13). No significant 1,4-dioxane removals were observed during the treatment train under each condition in the heat-sterilized abiotic control microcosms (Table 6.6).

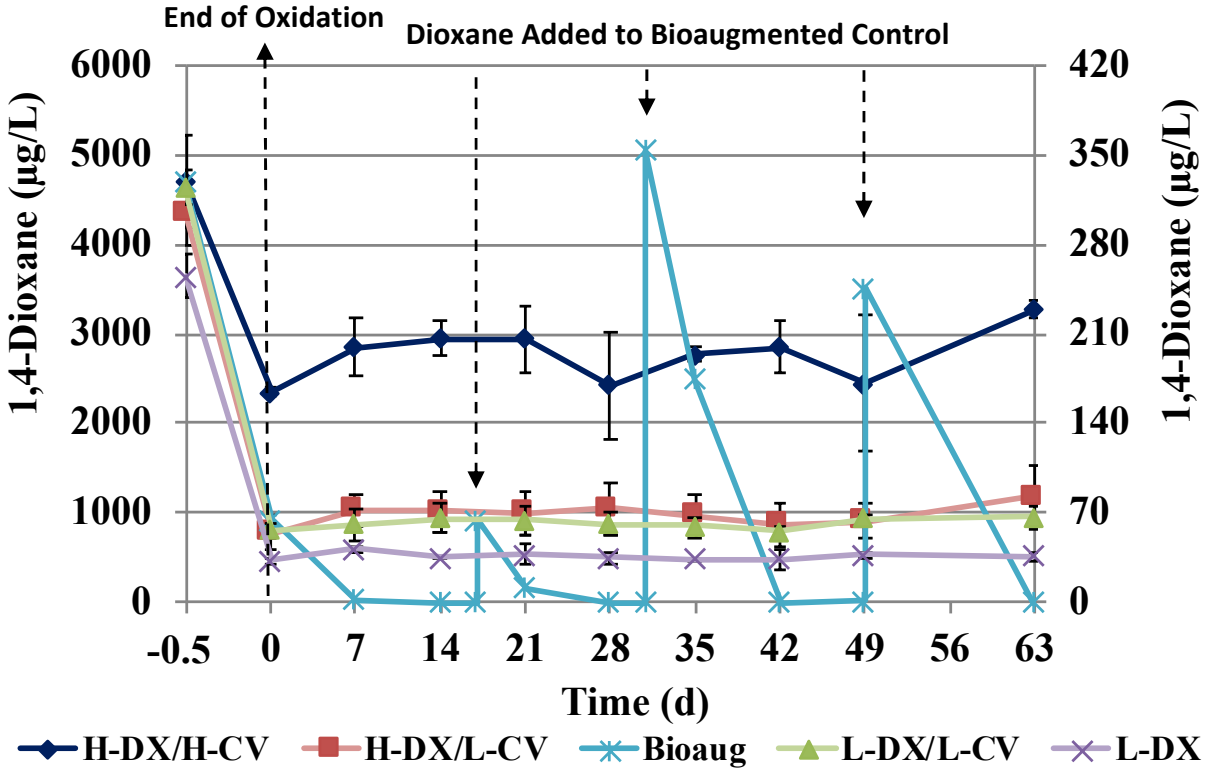

Figure 6.68. Removal performances of 1,4-dioxane in microcosms constructed from well 8MNW54 during oxidation-biodegradation process under different 1,4-dioxane and CVOC concentrations. The left Y-axis indicates high level of 1,4-dioxane and connects with H-DX/H-CV, H-DX/L-CV, and Bioaug. The right Y-axis indicates low level of 1,4-dioxane and connects with L-DX/L-CV and L-DX.

Table 6.16. 1,4-Dioxane concentrations in heat-sterilized abiotic control microcosms during the treatment train under each condition.

Conditions	1,4-dioxane concentrations (µg/L)						
	Before oxidation	After oxidation	Day 7	Day 21	Day 35	Day 49	Day 63
H-DX/H-CV	4892	2505	2548	2883	2887	2589	2568
H-DX/L-CV	4780	605	620	691	617	664	642
L-DX/L-CV	287	35	41	50	48	40	40
L-DX only	234	31	42	35	39	39	40

The biomarker genes *dxmB* and *aldH* were only observed in the bioaugmentation microcosms, and were consistent with spiked CB1190 at each feeding time point. In addition, both *dxmB* and *aldH* were inhibited by three to four orders of magnitude directly after the oxidation phase, but increased during the post-AOP biodegradation phase and reached to 3.75×10^6 copies/mL and 2.22×10^6 copies/mL, respectively (Figure 6.14).

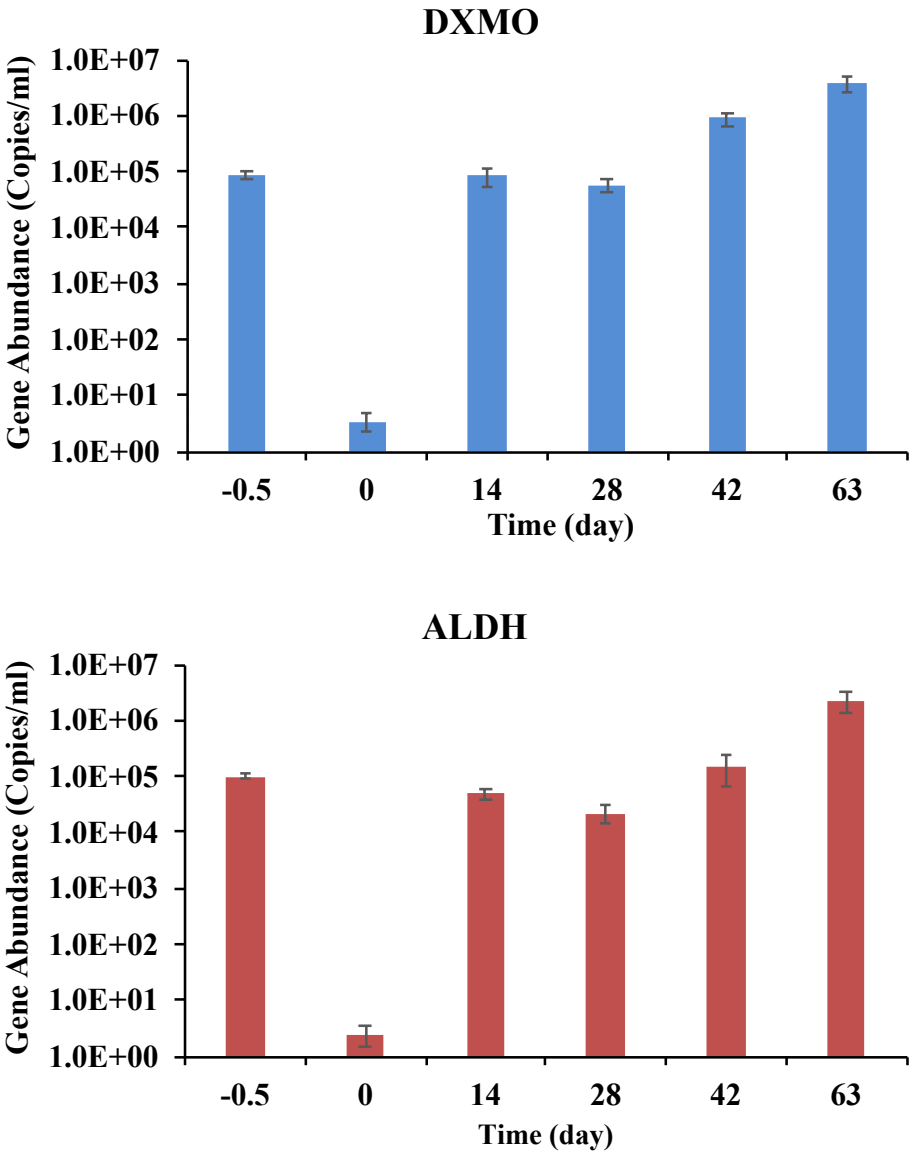

Figure 6.69. Biomarkers *dxmB* (encoding DXMO) and *aldH* (encoding ALDH) gene abundance under bioaugmentation condition during oxidation-biodegradation process.

6.3.2.2 Associations among Microcosm Performances and Microbial α-Diversity

Both Spearman's rank and Pearson's linear correlations showed no significant connections among biodiversity, richness, and 1,4-dioxane concentrations (Table 6.7). However, the Shannon index indicated that biodiversity under all conditions was reduced significantly (p-value < 0.05) during the oxidation phase, except for the H-DX/H-CV condition (Figure 6.15, Table 6.8). Afterwards, during the first stage of the biodegradation phase from OB2 (day 0) to OB3 (day 17), the biodiversity was relatively stable under H-DX/H-CV, H-DX/L-CV and L-DX/L-CV, but increased significantly under L-DX and Bioaug conditions. Rapid and significant increases of biodiversity were observed after 9-week incubation of biodegradation from OB3 to OB4 (day 63) under all conditions.

The richness metrics represented by the Chao1 index and observed species (0.97 OTU) depict the change of species along with treatment trains, both of which kept decreasing from OB1 to OB3 under all conditions with CVOCs. Under low 1,4-dioxane-only condition, the richness of microbial community started to recover from OB2 to OB3, which occurred earlier than in microcosms with CVOCs (Figure 6.15, Table 6.8).

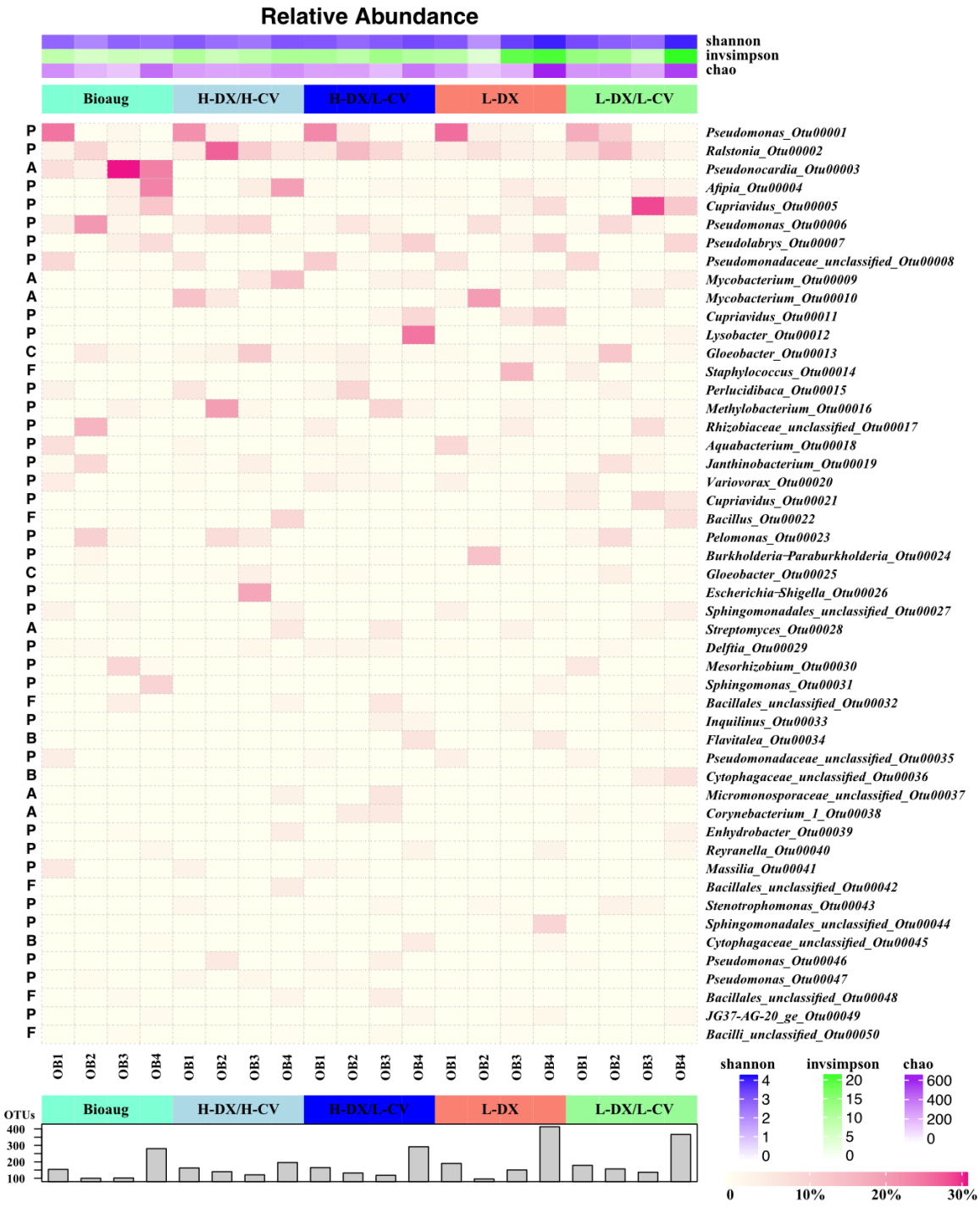

Figure 6.70. Trends of dynamics of microbial community richness, diversity and most abundant 50 species (0.97-OTUs) at each time points under all conditions. OTUs information are listed in Table S8. Phylum information are in left column as, P: Proteobacteria, A: Actinobacteria, C: Cyanobacteria, F: Firmicutes, and B: Bacteroidetes.

Table 6.17. Pearson and Spearman correlations between richness/diversity and 1,4-dioxane under different conditions.

Methods	Indices	HH		HL		L		LL		Bioaug	
		R	p-value	R	p-value	R	p-value	R	p-value	R	p-value
Pearson	invsimpson	0.412	0.588	0.229	0.771	-0.294	0.706	-0.017	0.983	0.540	0.46
	shnnon	0.318	0.682	0.196	0.804	-0.016	0.984	0.102	0.898	-0.070	0.93
	Chao1	-0.096	0.904	-0.063	0.937	-0.084	0.916	-0.225	0.775	0.102	0.898
	sob	0.014	0.986	-0.027	0.973	-0.097	0.903	-0.179	0.821	-0.276	0.724
Spearman	invsimpson	0.4	0.6	0.4	0.6	0.4	0.6	0.6	0.4	-0.4	0.6
	shnnon	0	1	0.8	0.2	0.4	0.6	0.6	0.4	0.4	0.6
	Chao1	0.4	0.6	0	1	0.8	0.2	0	1	0.2	0.8
	sob	0	1	0.6	0.4	0.8	0.2	0.6	0.4	0.8	0.2

Table 6.18. Differences of richness and biodiversity between each consecutive time points under each condition. The "obs" is observed species, and the "Chao" is Chao_1 index.

HH_obs	OB1	OB2	OB3	HH_Chao	OB1	OB2	OB3	HH_shannon	OB1	OB2	OB3
OB2	0.31			OB2	0.502			OB2	0.165		
OB3	0.06	0.39		OB3	0.904	0.557		OB3	0.009	0.566	
OB4	0.24	0.06	0.01	OB4	0.341	0.183	0.284	OB4	0.565	0.077	0.002
AUG_obs	OB1	OB2	OB3	AUG_Chao	OB1	OB2	OB3	AUG_shannon	OB1	OB2	OB3
OB2	0.002			OB2	0.013			OB2	0		
OB3	0.002	0.841		OB3	0	0.26		OB3	0.035	0	
OB4	<0.01	<0.01	<0.01	OB4	0.098	<0.01	<0.01	OB4	<0.01	<0.01	<0.01
HL_obs	OB1	OB2	OB3	HL_Chao	OB1	OB2	OB3	HL_shannon	OB1	OB2	OB3
OB2	0.004			OB2	0.663			OB2	<0.01		
OB3	<0.01	0.119		OB3	0.047	0.018		OB3	0.61	<0.01	
OB4	<0.01	<0.01	<0.01	OB4	0.002	0.006	<0.01	OB4	0.066	<0.01	0.04
L_obs	OB1	OB2	OB3	L_Chao	OB1	OB2	OB3	L_shannon	OB1	OB2	OB3
OB2	<0.01			OB2	0			OB2	0		
OB3	0.034	0.008		OB3	0.046	0.042		OB3	0.003	0	
OB4	<0.01	<0.01	<0.01	OB4	<0.01	<0.01	<0.01	OB4	<0.01	<0.01	0.001
LL_obs	OB1	OB2	OB3	LL_Chao	OB1	OB2	OB3	LL_shannon	OB1	OB2	OB3
OB2	0.263			OB2	0.867			OB2	0.001		
OB3	0.055	0.345		OB3	0.292	0.313		OB3	<0.01	0.014	
OB4	<0.01	<0.01	<0.01	OB4	<0.01	0.006	<0.01	OB4	<0.01	<0.01	<0.01

6.3.2.3 Taxonomic Profiles Shift in Treatment Trains

The taxonomic classification showed that the most abundant phyla before oxidation were Proteobacteria, Actinobacteria, Firmicutes, Cyanobacteria, and Bacteroidetes (Figure 6.16). The relative abundance of Proteobacteria (class Gammaproteobacteria) was reduced during the oxidation phase under all conditions, except H-DX/H-CV, where Proteobacteria (class Betaproteobacteria) increased by 10% with decreasing Actinobacteria. Under Bioaug, H-DX/H-CV, and H-DX/L-CV conditions, Proteobacteria decreased at OB3, but increased with low 1,4-dioxane-only spikes. When comparing conditions with the same initial 1,4-dioxane concentration, the presence of lower levels of CVOCs induced a rebound of Proteobacteria (class Alphaproteobacteria) at OB4, which was in contrast to the trend observed at higher CVOC levels. Phylum Actinobacteria was observed to increase during the biodegradation phase under Bioaug and H-DX/H-CV conditions, but was found to decrease under L-DX condition. Phylum Firmicutes carrying the class Bacilli showed opposite trends to Proteobacteria along with treatment trains under each condition, and only accumulated under H-DX/H-CV condition at OB4. Phylum Cyanobacteria carrying the class Gloeobacteria accumulated after oxidation at OB2 and only continuously increased under H-DX/H-CV conditions, while Phylum Bacteroidetes carrying the classes Sphingobacteriia and Cytophagia was abundant after biodegradation at OB4.

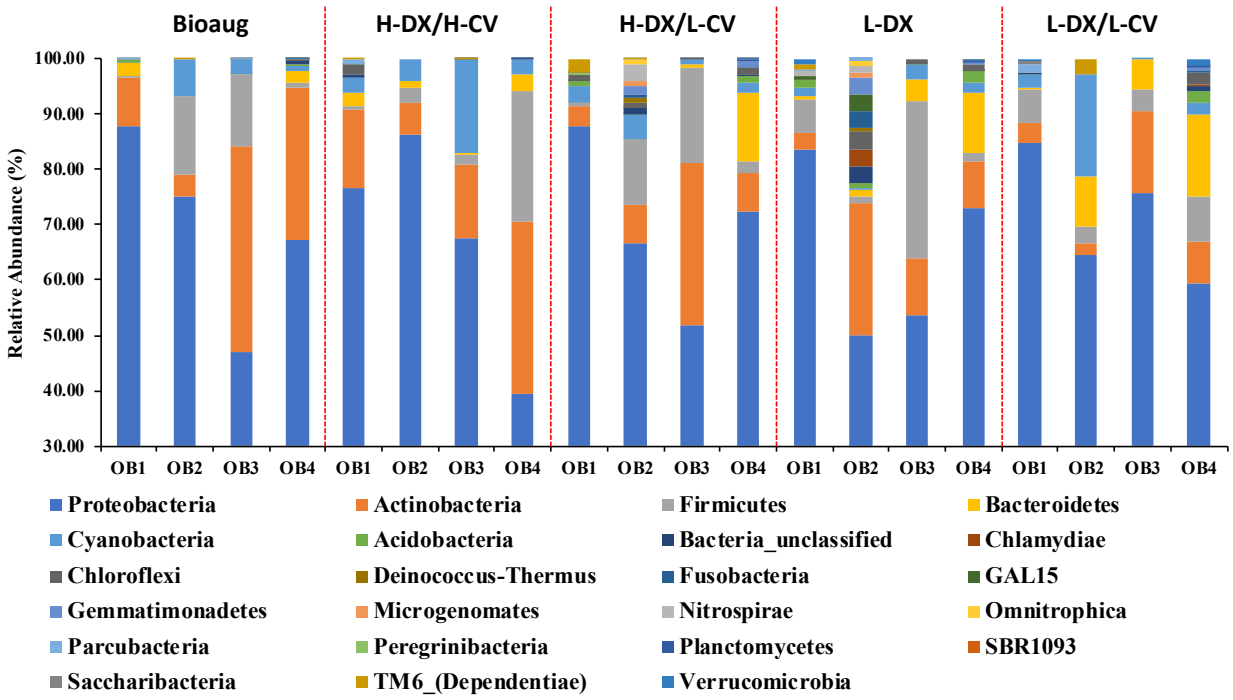

Figure 6.71. Taxonomic classification on phylum level at each time point under all conditions. Since Proterobacteria occupied at least 30% in each sample, the relative abundance (Y-axis) started from 30% for higher resolution for low-abundant phyla.

At genus and species (0.97-OTUs) levels (Figure 6.15), some originally highly abundant genera were inhibited by the oxidant exposure, and continued to decrease for the duration of the incubation, including *Pseudomonas*, *Massilla*, *Aquabacterium*, *Variovorax*, and an unclassified genus in *Pseudomonadaceae*. Genus *Pseudomonas* was the dominant microorganism at the beginning, but inhibited by the chemical oxidation phase, and kept decreasing during the biodegradation phase. Interestingly, two main OTUs in *Pseudomonas* showed opposite responses to oxidation: *Pseudomonas cerasi* 58 (OTU1) was reduced while *Pseudomonas azotoformans* NBRC 12693 (OTU6) increased; but both OTUs decreased at OB3 and OB4. Genus *Ralstonia* was the only abundant genus demonstrating oxidative tolerance and increased in abundance after oxidation under all conditions, while decreasing relatively during the post-AOP phase. Other genera demonstrating

oxidative tolerance were only observed under specific conditions, such as *Pelomonas* under Bioaug, H-DX/H-CV, and L-DX/L-CV; *Janthinobacterium* under Bioaug and L-DX/L-CV; *Streptococcus* under Bioaug and H-DX/L-CV; *Gloeobacter* under Bioaug, H-DX/H-CV, and L-DX/L-CV, etc. Notably, genus *Mycobacterium*, which was dominant under L-DX condition at OB2, showed early inhibition under H-DX/H-CV condition, but grew abundant again during the biodegradation phase for the H-DX/H-CV condition. Moreover, during the initial stage of biodegradation from OB2 to OB3, various genera recovered in distinct ways from prior exposure to oxidant radicals. Along with the post-AOP burst of biodiversity, more genera thrived and interacted during the 7-week incubation, showing different responses to operational conditions, and abundant *Cupriavidus*, *Pseudolabrys*, *Sphingomonas* continued to accumulate through OB4 under all conditions. *Pseudonocardia dioxanivorans* CB1190 was spiked at OB1 but was expected to be inhibited after oxidation. During the biodegradation phase, CB1190 was still a minor member of the overall microbial population, reaching to 23.67% at OB4 even after second spike at OB3 (day 17) to reach 32.80%.

5.3.2.4 Microbial Population Dynamics Linked to Treatment Trains

The microbial community shifted rapidly along with time during the whole treatment train incubation. Results indicate that time was a better variable for explaining the dynamics of the microbial community (Figure 6.17B, 6.17D, color-coded) than the presence and/or concentration or co-contaminants (Figure 6.18). PCoA biplots based on Unifrac distances described that both microbial membership (unweighted) and abundance (weighted) developed along with treatment trains under different conditions. Furthermore, the oxidation phase clearly influenced the microbial community both in terms of membership and abundance. The bacterial membership (unweighted, Figure 6.17C, 6.17D) seemed to separate more apparently than bacterial abundance (weighted, Figure 6.17A, 6.17B) during the biodegradation phase, and this was consistent with the Venn

diagram showing that more species were identified at OB4 (Figure 6.19). When taking the conditions into consideration, the community in H-DX/H-CV condition (triangles in Figure 6.17A and 6.17C) changed more slowly than in other conditions, while the community in the L-DX condition (cross in Figure 6.17A and 6.17C) evolved relatively faster compared to other conditions. Moreover, the members at OB3 tended to merge with OB2 (Figure 6.17D), while the abundances were in relative proximity to OB4 (Figure 6.17C), indicating the unstable impacts under different conditions. Interestingly, microbiomes at OB4 showed more clear boundaries among conditions, and the linear connections based Pearson correlation showed that samples at OB4 only had solid connections within same conditions (purple in Figure 6.20A). Additionally, impact from oxidation reduced the connections among samples under different conditions when comparing between OB1 (green in Figure 6.20A) and OB2 (thinner edge of blue in Figure 6.20A), while the signs of recovery could be found at OB3 (orange in Figure 6.20A), since more connections were re-built. The cluster analyses based on unsupervised classification (ungrouped) depicted the relative distance of each sample, and microbial community structure showed deviations under different conditions at OB4 with relatively further shifts than the rest of the samples (Figure 6.20B). In clustered samples collected at OB1, OB2 and OB3, samples belonging to OB2 and OB3 were closely related regardless of the conditions (Figure 6.21).

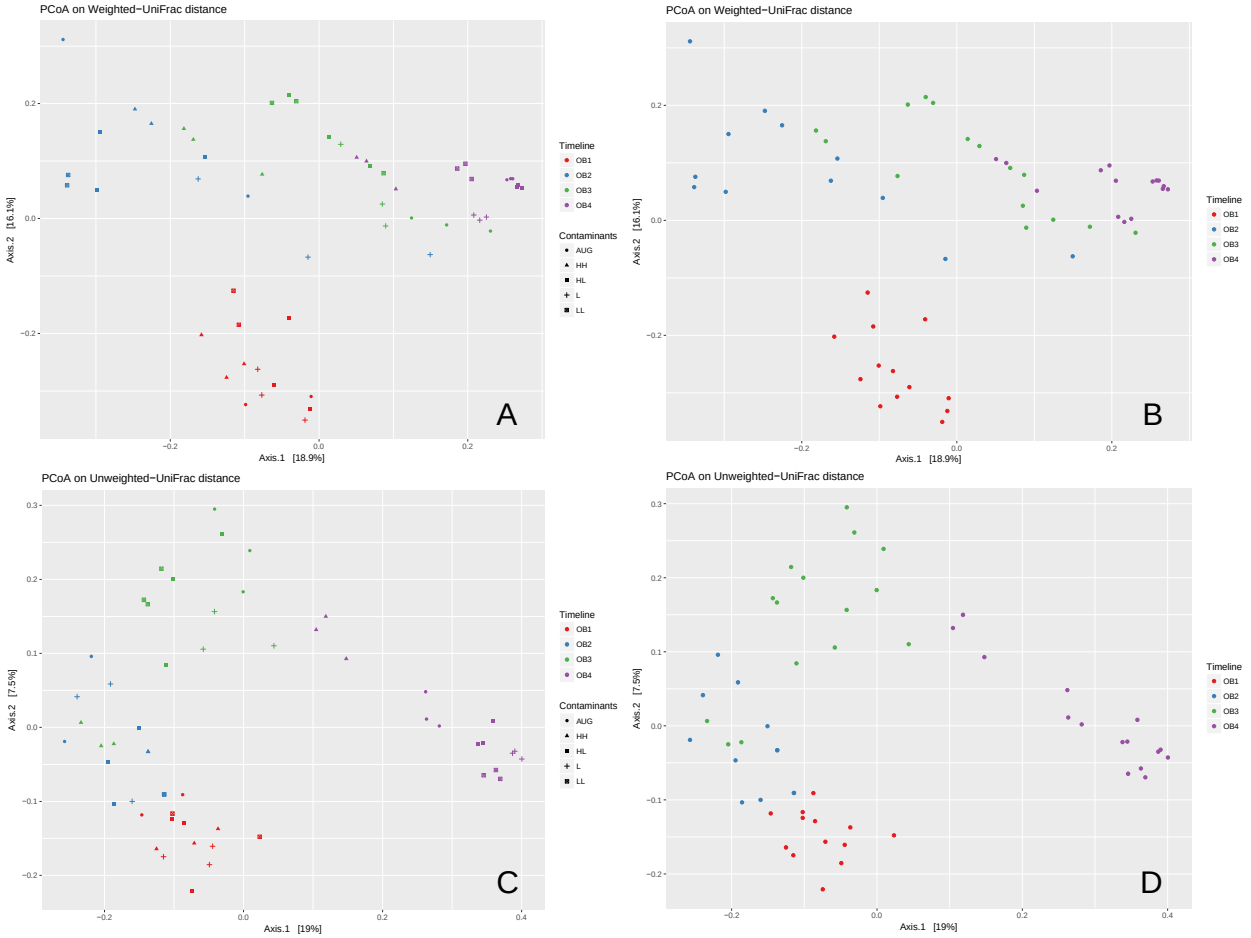

Figure 6.72. Dynamics of microbial community at each time point under all conditions at the 0.97-OTUs level. PCoA biplots show weighted (A and B) and unweighted (C and D) UniFrac distances were namely qualitative (i.e., phylogeny) measures of microbial dynamics with and without quantitative (i.e., abundance) measures. (A and C) The samples were colored by time and shaped by conditions. (B and D) The samples were only colored by time.

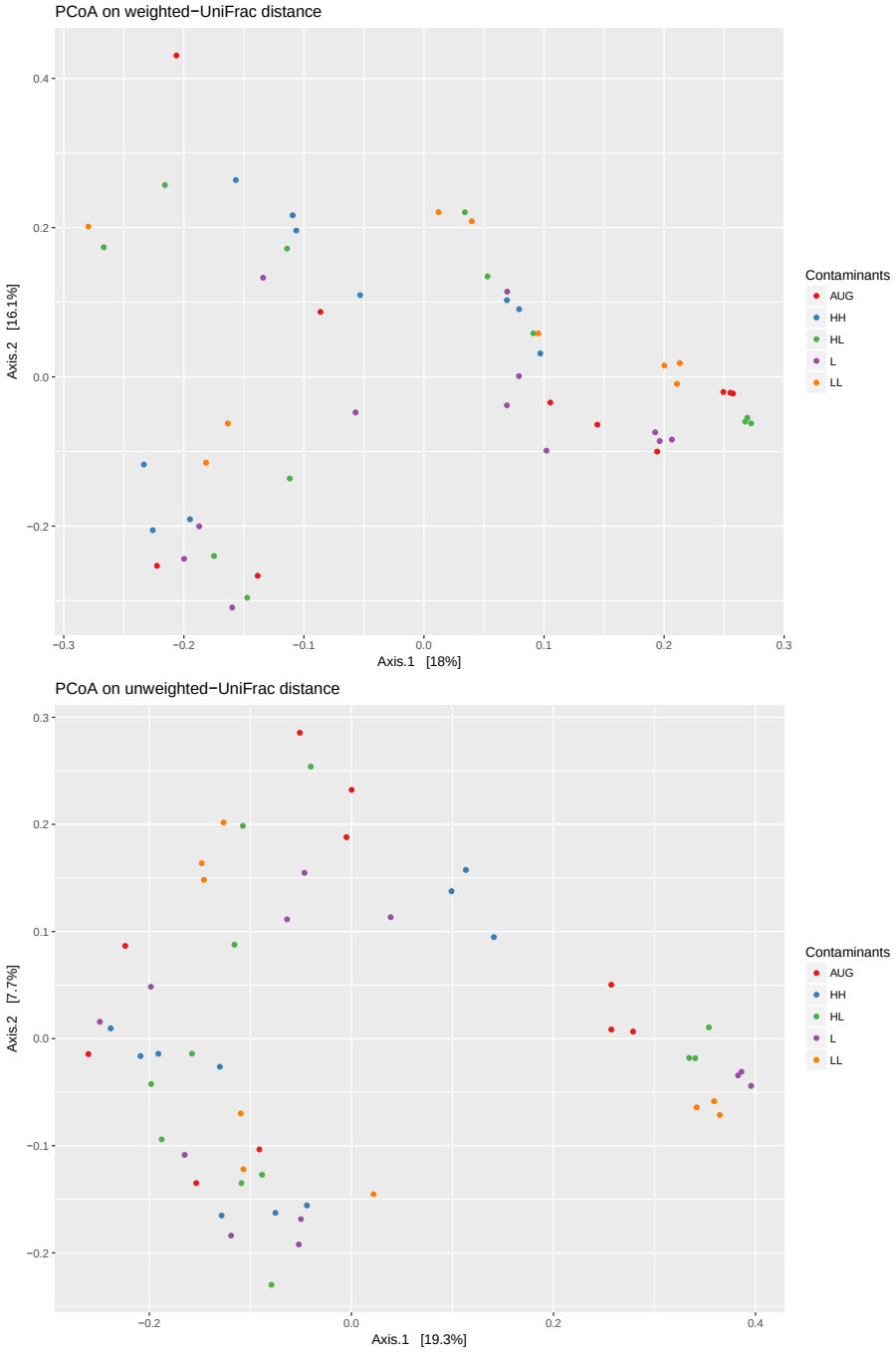

Figure 6.73. Dynamics of microbial community at each time point under all conditions at the 0.97-OTUs level. PCoA biplots showed weighted (Upper) and unweighted (Lower) UniFrac distances were namely qualitative (i.e., phylogeny) measures of microbial dynamics with and without quantitative (i.e., abundance) measures. All samples were colored by conditions.

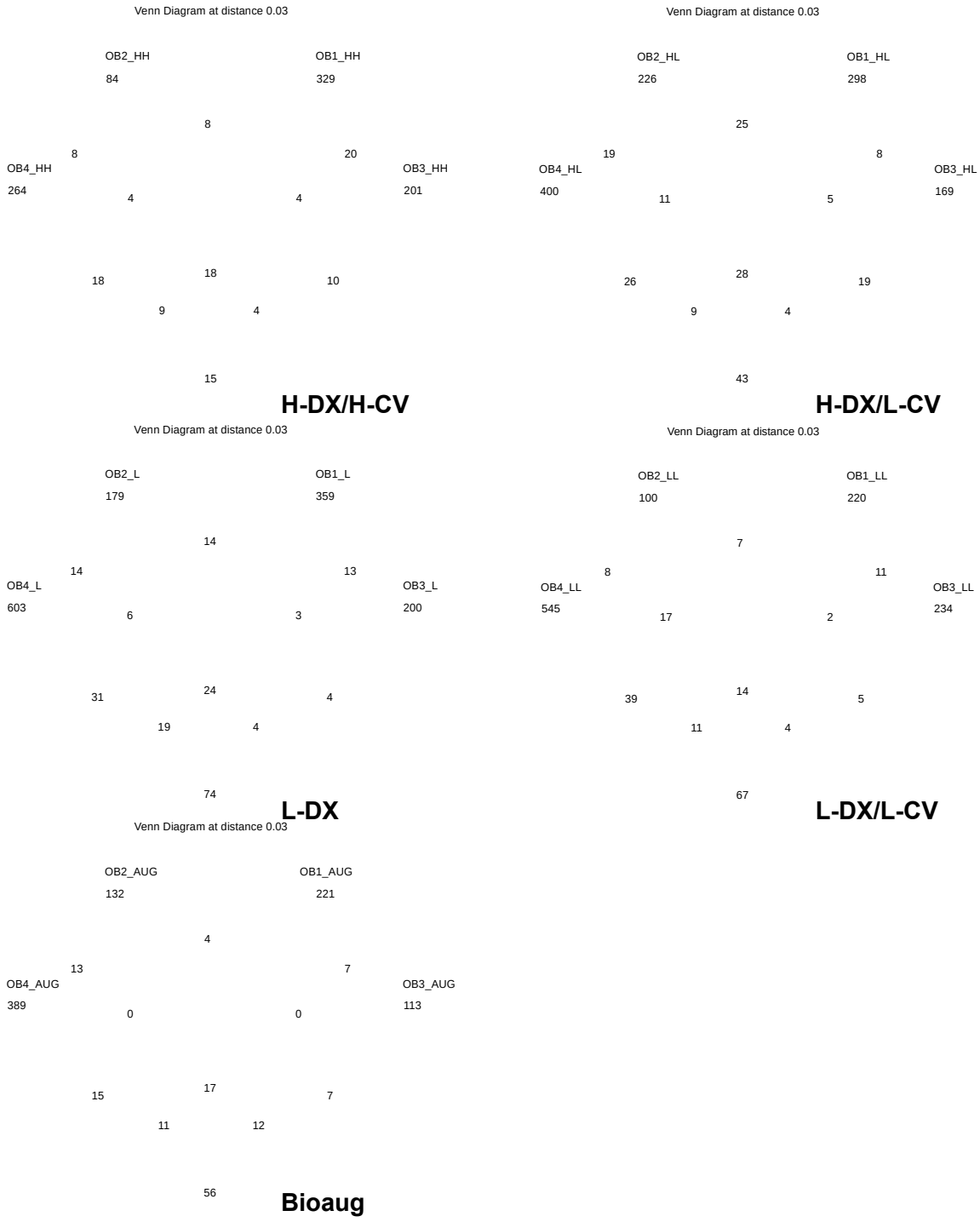

Figure 6.74. Number of species (0.97-OTU) in one sample or shared among couples of samples. Pink is OB1, green is OB2, purple is OB3, and yellow is OB4.

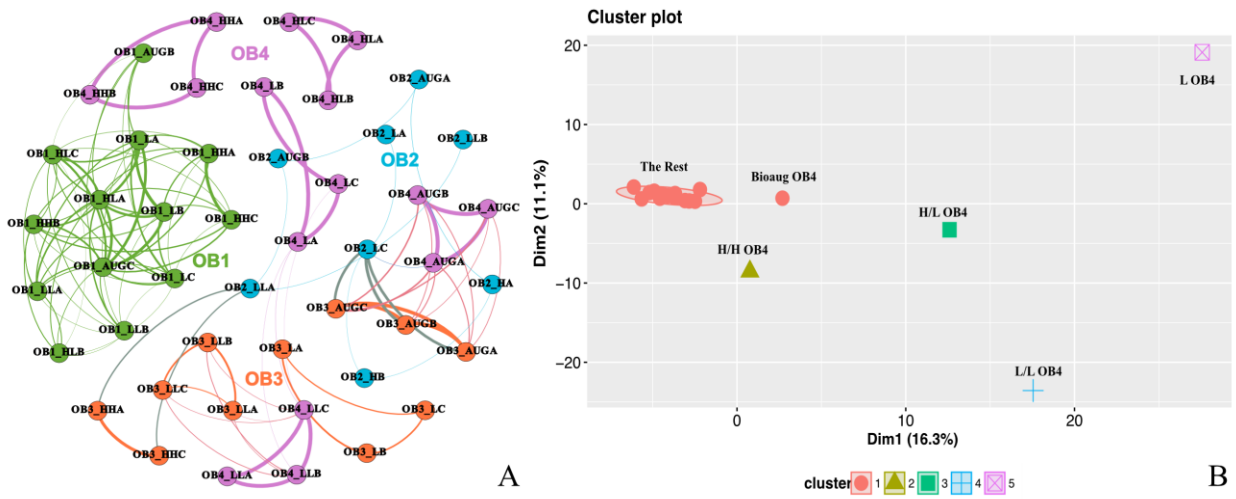

Figure 6.75. Network and cluster analyses among samples at each time point under all conditions. (A) The node in network are colored by each time point, and the connections represented a strong (R > 0.6) and significant (p-value < 0.01) correlations. The thickness of each edge is proportional to the p-value. (B) Cluster analysis pools all samples at different time points under different conditions and shows integral shift among conditions and time points.

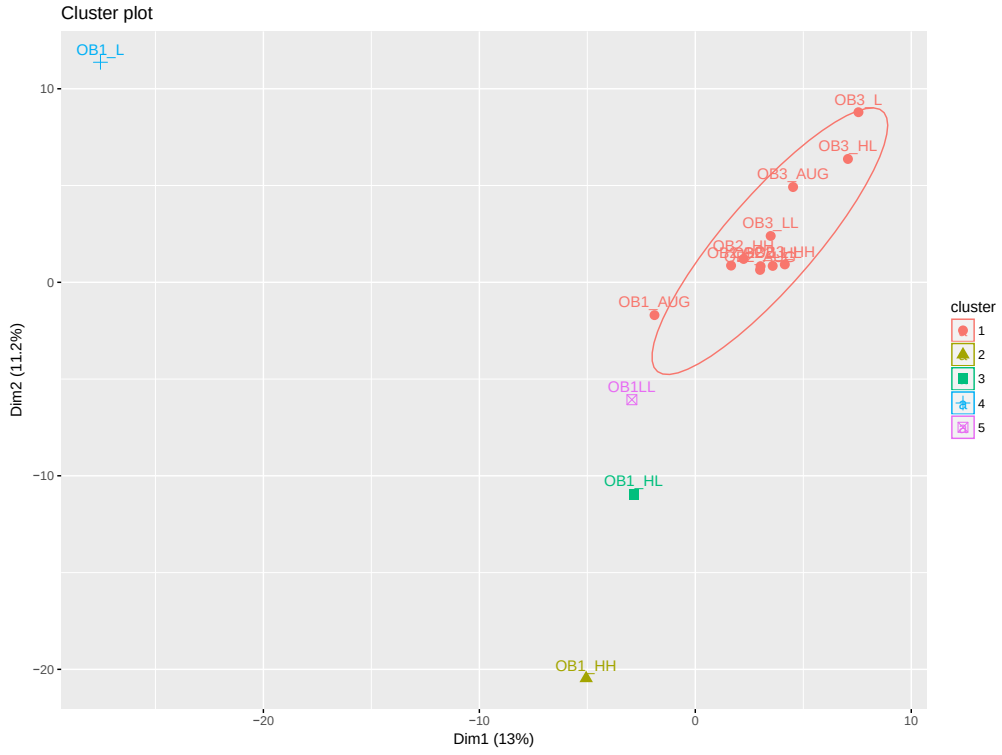

Figure 6.76. Cluster analysis based on all samples at OB1, OB2 and OB3 under all conditions.

6.3.2.5 Co-Occurrence and Co-Exclusion Patterns in the Combined Treatment Trains

In networks constructed based on the OTUs that totaled over 1% in all samples, only the strong (coefficients > 0.6 or < -0.6) and significant ($p < 0.01$) correlations were presented, which generally indicated the role of cooperative and competitive relations in guiding community dynamics. The output positive network contained 711 pairs of Spearman correlations between 168 OTUs (Figure 6.22), while the negative had 69 strong pairs between 51 OTUs (Figure 6.23). The OTUs in the positive network (co-occurrence) were mainly distributed into 12 phyla, which was consistent with the trend of taxonomic classification that Proteobacteria (54.17%), Actinobacteria (13.10%), Firmicutes (14.29%), Cyanobacteria (2.98%), and Bacteroidetes (8.33%) were the top five most abundant phyla. Among them, Proteobacteria had 220 connections and 142 of 220 were intra-phylum (within phylum) pairs, and this ratio were 22 of 83 and 11 of 76 for Firmicutes and Actinobacteria, respectively (Figure 6.22A). When compared against the network grouped by phyla (Figure 6.22A), most niches were occupied by multiple interacted phyla, except for module III where mostly matched a whole part of Proteobacteria. For example, phyla Proteobacteria and Cyanobacteria (OTU13, 25, 69, 88, and 95, yellow in Figure 6.22A) shared in same niche (Module V), and module II contained Proteobacteria, Firmicutes (OTU32, 48, 50, 58, 70, green in Figure 6.22A), and Actinobacteria (OTU9, 28, 37, 87, 153, orange in Figure 6.22A). Moreover, the co-exclusion pattern showed unmodularized distribution of phyla, demonstrating the inter- or intra-phylum competitions within community. OTU60 (Comamonadaceae_unclassified), 72 (*Ramlibacter*), 73 (*Hydrogenophaga*), and 138 (Comamonadaceae_unclassified) belonging to Proteobacteria showed competitions with Proteobacteria OTU23 (*Pelomonas*), respectively, occupying the Module II in negative networks (blue in Figure 23B). Moreover, OTU6 (*Pseudomonas*) and 19 (*Janthinobacterium*) in

Proteobacteria had more dense negative connections (large nodes in Figure 6.23A) with inter- or intra-phylum OTUs in Module III (purple in Figure 6.23B).

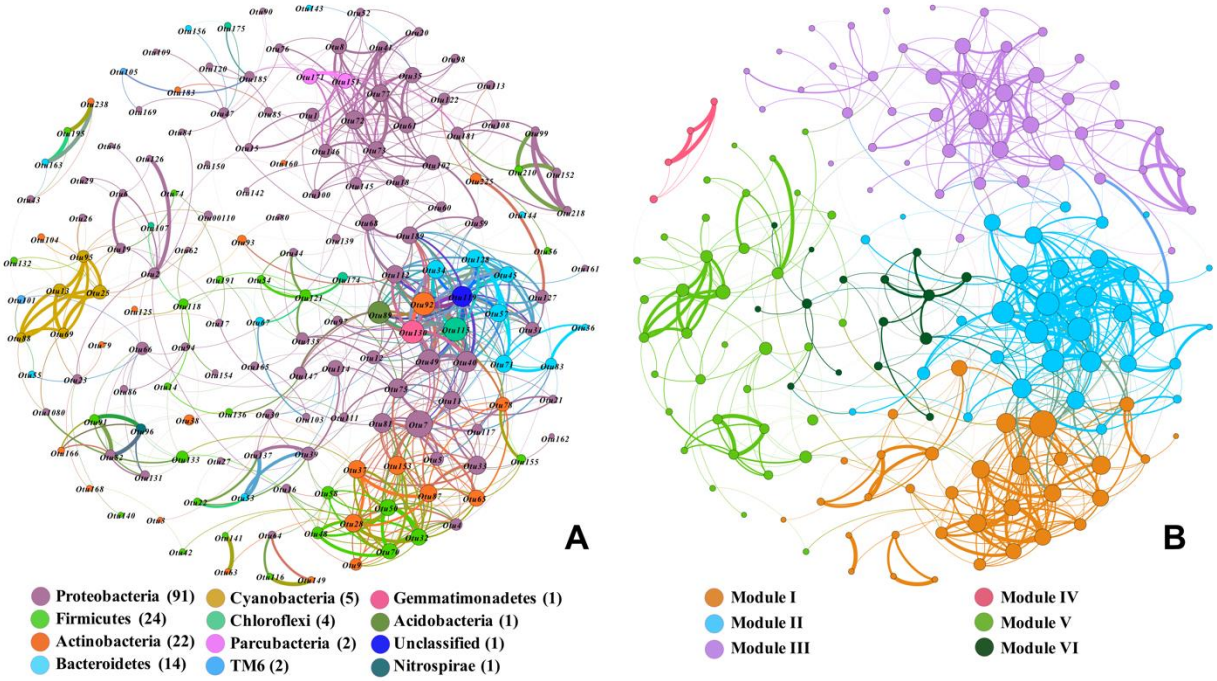

Figure 6.77. Correlation-based network analysis of species co-occurrence patterns in all samples, with significant (p-value < 0.01) and strong correlations (R > 0.6) between 0.97-OTU. The size of each node (0.97-OTUs) is proportional to the number of connections, and the thickness of each edge between two nodes is proportional to the strength of correlation. Left: network colored by phylum, number of OTUs follows label; Right: network colored by modules calculated by Gephi modularity toolkit, and nodes within the same module were more densely connected together than to the rest of the network.

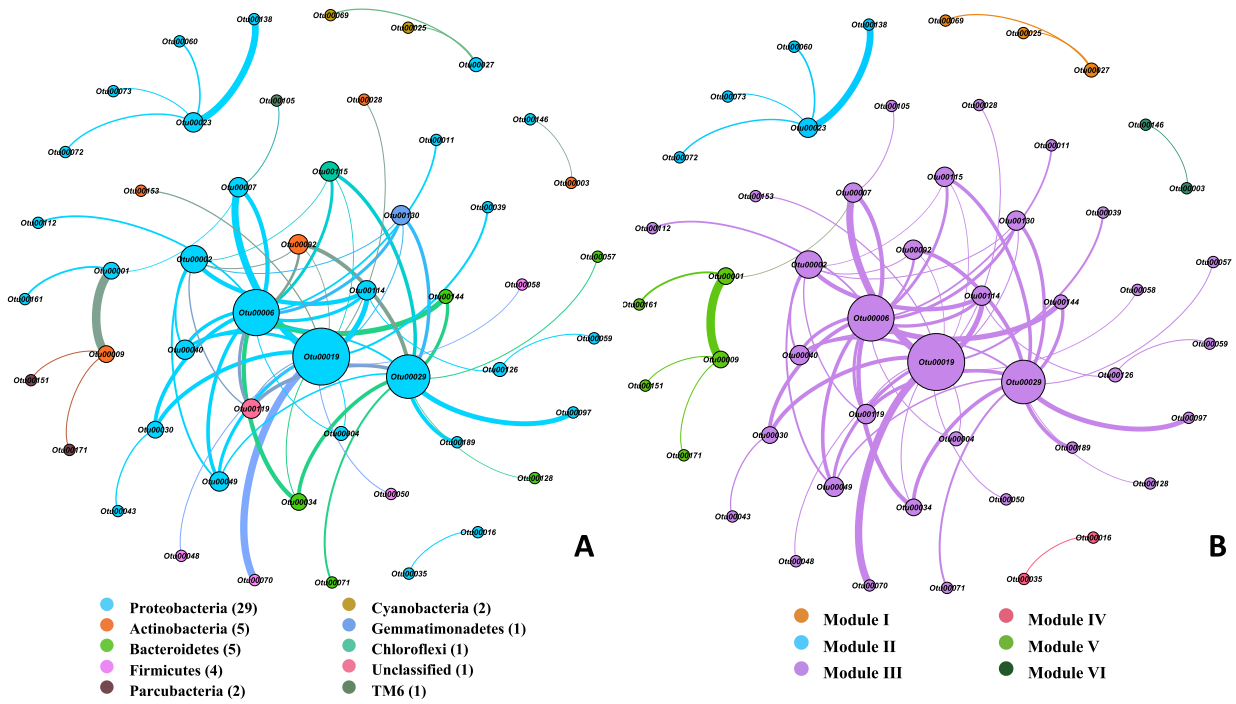

Figure 6.78. Correlation-based network analysis of species co-exclusion patterns in all samples, with significant (p-value < 0.01) and strong correlations (R < -0.6) between 0.97-OTU. The size of each node (0.97-OTUs) is proportional to the number of connections, and the thickness of each edge between two nodes is proportional to the strength of correlation. Left: network colored by phylum, number of OTUs follows label; Right: network colored by modules calculated by Gephi modularity toolkit, and nodes within the same module were more densely connected together than to the rest of the network.

Detailed network and statistical analyses were applied to the microbial community under Bioaug condition to explore the connections of bioaugmented CB1190 with other OTUs, coupled with incidence analysis to reveal the observed/random connections. The output network was constructed with 405 pairs of strong connections among 81 OTUs, in which 356 pairs were positive and 49 pairs were negative (Figure 6.24A). The spiked CB1190 removed 1,4-dioxane efficiently and showed negative correlations with species belonged to *Gloeobacter*, *Ralstonia*, *Mycobacterium*, *Janthinobacterium*, etc. (Figure 6.25). Moreover, the CB1190 strongly connected

with a few co-occurring genera (i.e., *Cupriavidus*), that were observed to share in the same module, indicating their close interactions (Figure 6.24B). This was also confirmed by incidence analysis between OTUs from different orders. CB1190's higher rank taxon Pseudonocardiales tended to co-occur with Rhizobiales (O/R = 4.33), Bacillales (O/R = 4.00) and Sphingobacteriales (O/R = 3.00) (Table 6.9).

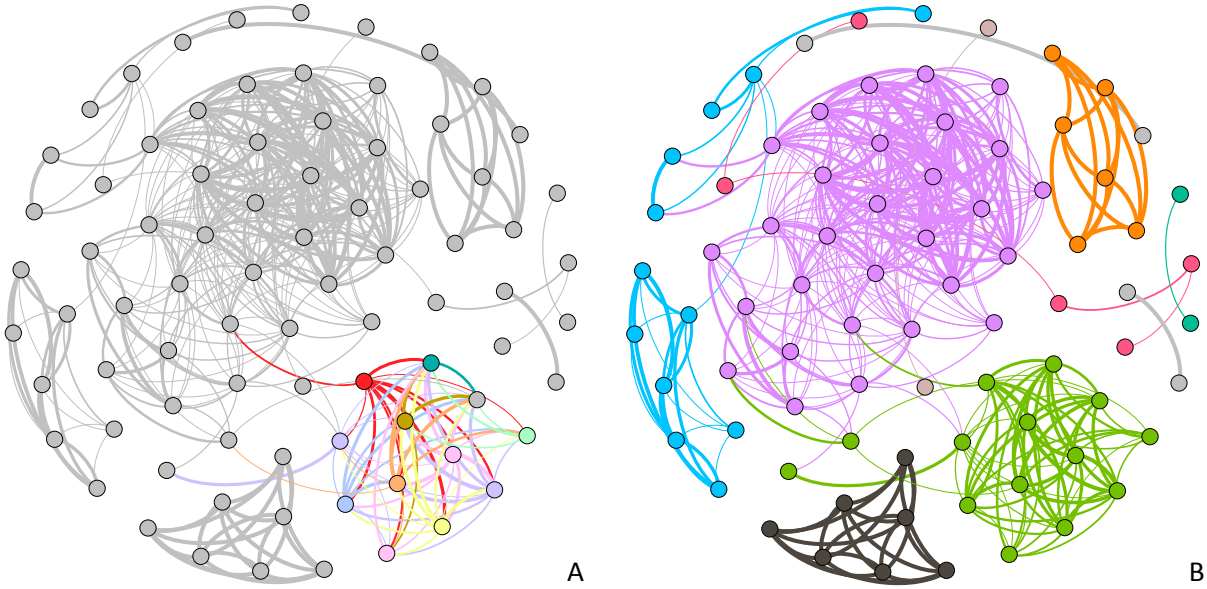

Figure 6.79. Correlation-based network analysis of species co-occurrence patterns under Bioaug condition, with significant (p-value < 0.01) and strong correlations (R > 0.8) between 0.97-OTU. The thickness of each edge between two nodes was proportional to strength of correlation. Left: network colored by orders having connections with CB1190 (Red); Right: network colored by modules calculated by Gephi modularity toolkit.

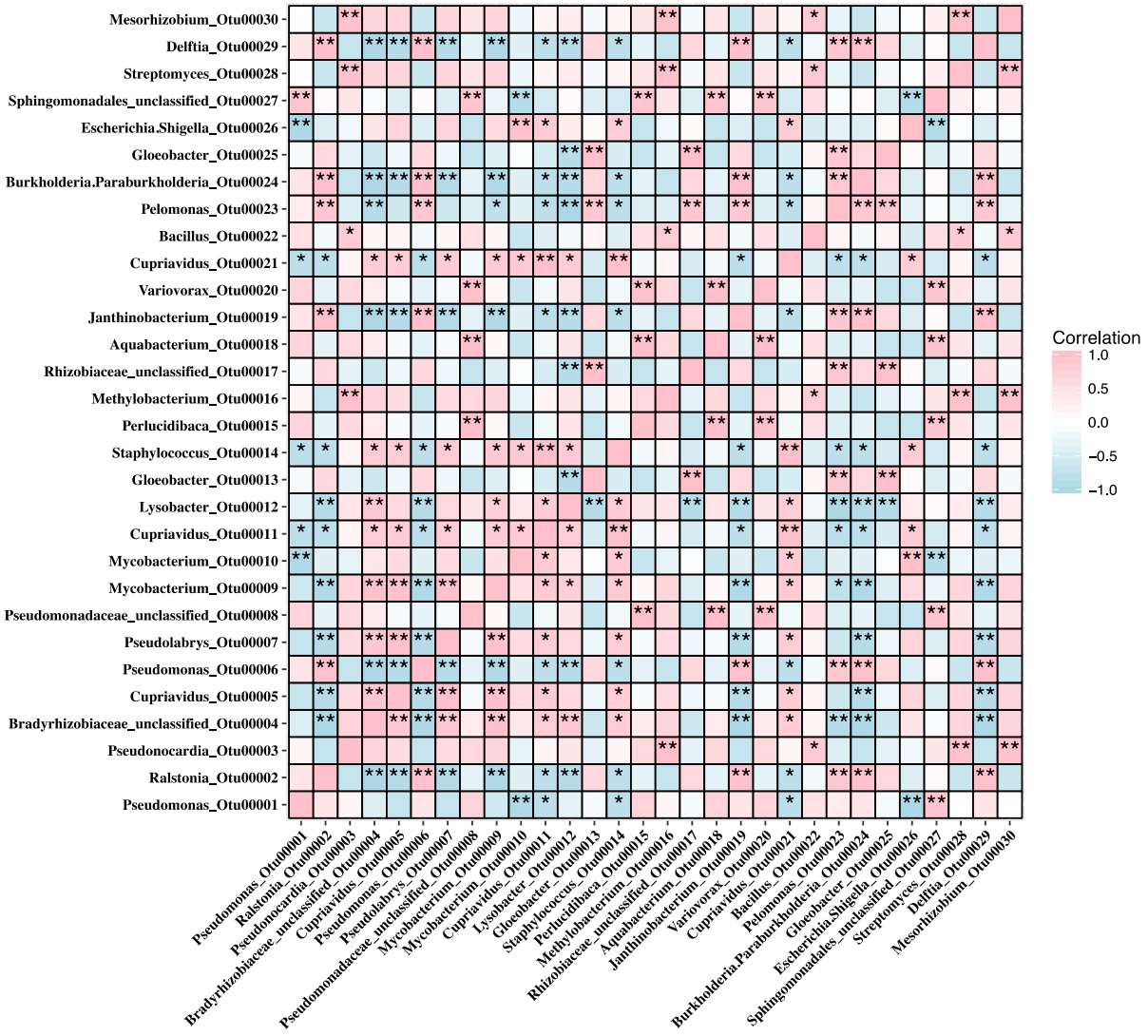

Figure 6.80. Significance of correlation among species under different conditions. * indicates $p<0.05$, and ** indicated $p<0.01$. The top 30 abundant species under Bioaug condition were pooling together and calculated with Spearman's rank correlation coefficient.

Table 6.19. Incidence of significant (P-value < 0.01) and strong (Spearman's rank correlation > 0.6) co-occurring patterns between 0.97-OTUs in bioaugmentation condition. The observed co-occurring incidence (O%) of two orders (i.e., nodes; N) was calculated as the relative percentage of the number of observed edges (E_0) between them in total number of edges (E) in the network, while the random co-occurring incidence (R%) was theoretically calculated by considering the taxa frequencies (i.e., n(N1) and n(N2)) and random associations. Over 2 edges were listed.

Nodes Affiliation		Positive SSA Network (N=81, E=405)					
N1	N2	E_0	N2	N1	R	O	O/R
Pseudonocardiales	Rhizobiales	13	12	2	0.74%	3.21%	4.33
	Burkholderiales	2	16	2	0.99%	0.49%	0.50
	Bacillales	5	5	2	0.31%	1.23%	4.00
	Bacilli_unclassified	2	3	2	0.19%	0.49%	2.67
	Sphingobacteriales	3	4	2	0.25%	0.74%	3.00
	Streptomycetales	2	1	2	0.06%	0.49%	8.00
	Sphingomonadales	2	4	2	0.25%	0.49%	2.00
	Rhodospirillales	2	4	2	0.25%	0.49%	2.00

6.3.3 Catalysis and Biodegradation Treatment Train

6.3.3.1 Coupled Catalysis-Biological Treatment and Biomarker Analysis

The 24-hour catalysis phase removed ~20% 1,4-dioxane under all conditions as expected (Figure 6.26); meanwhile, over 60% TCE, 50% 1,1-DCE, and 50% cis-1,2-DCE were also removed (Figure 6.26, Table 6.10). Even though the reaction was completely quenched in the catalysis phase, 1,4-dioxane concentrations decreased continuously in the first two weeks of biodegradation, and higher 1,4-dioxane degradation rates were found with lower CVOC

concentrations, but without apparent decreasing trends after a 17-week biodegradation period. However, at the end of biodegradation phase, TCE and cis-1,2-DCE were removed to below detection limits, and 1,1-DCE was only present under the H/H condition. The Bioaug condition only showed removal of 1,4-dioxane after CB1190 was added at day 63, where 1,4-dioxane started to drop from 5000 µg/L to below 1000 µg/L in four weeks, and slowly declined to below 4 µg/L. The *dxmB* gene was negatively detected in naturally simulated conditions, while *aldH* gene was detected at relatively low levels before CB1190 spikes (Figure 6.27). After the addition of CB1190, both *dxmB* and *aldH* gene abundances increased from day 63 to day 91 and remained stable afterward, with *aldH* showing higher abundances than *dxmB* during the second half of the biodegradation phase.

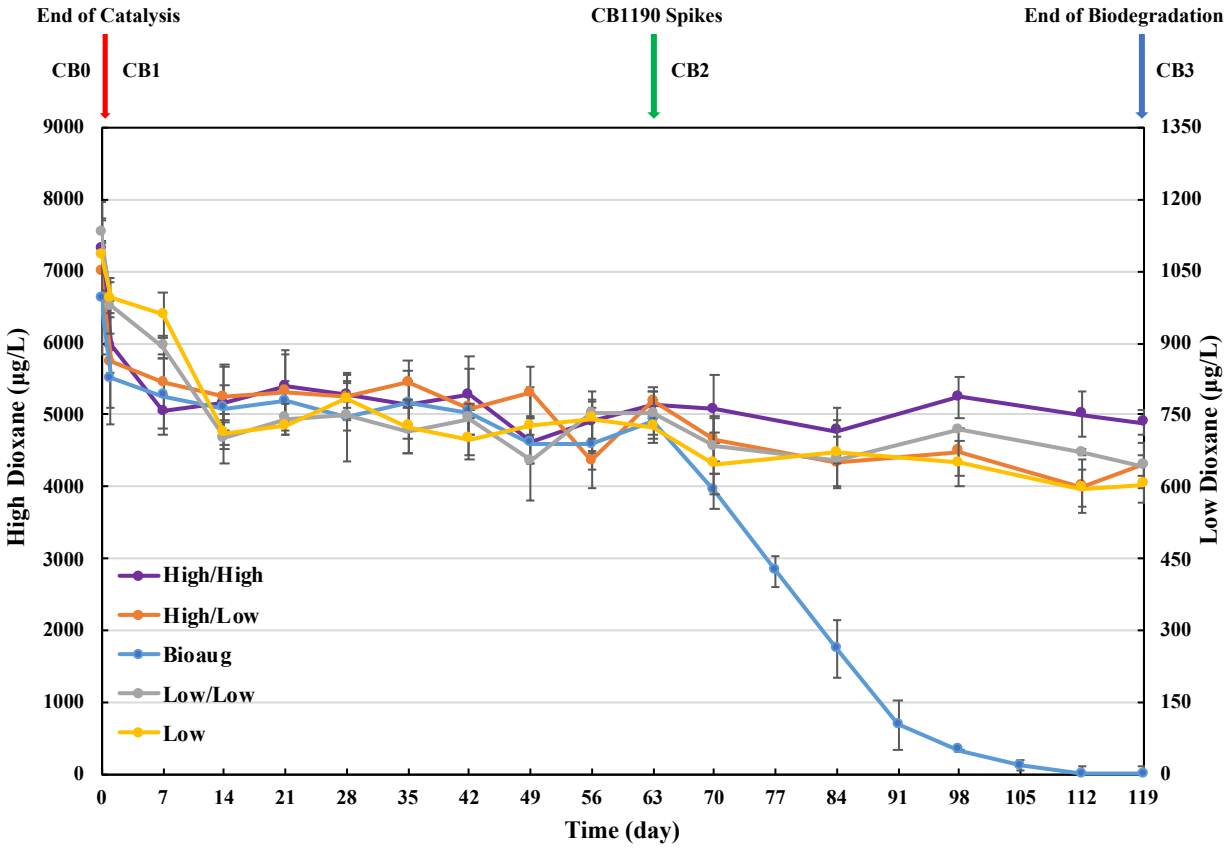

Figure 6.81. Removal performances of 1,4-dioxane in microcosms during catalysis-biodegradation process under different 1,4-dioxane and CVOCs concentrations. The left Y-axis indicates high level of 1,4-dioxane and connects with H-DX/H-CV, H-DX/L-CV, and Bioaug. The right Y-axis indicates low level of 1,4-dioxane and connects with L-DX/L-CV and L-DX. The red array indicates the end of catalysis phase, and the green array indicates the CB1190 spikes.

Table 6.20. CVOCs concentrations after catalysis phase and biodegradation phase.

Conditions	TCE (µg/L)			1,1-DCE (µg/L)			cis-1,2-DCE (µg/L)		
	Before catalysis (CB0) #	After catalysis (CB1) *	After Biodegradation (CB3) *	Before catalysis (CB0) #	After catalysis (CB1) *	After Biodegradation (CB3) *	Before catalysis (CB0) #	After catalysis (CB1) *	After Biodegradation (CB3) *
H-DX/H-CV	5000	1054±77	BD	5000	2202±315	1290±470	5000	1976±208	BD
H-DX/L-CV	500	34±25	BD	500	45±35	BD	500	14±5	BD
L-DX/L-CV	500	115±63	BD	500	174±100	BD	500	272±118	BD
Bioaug	500	107±33	BD	500	152±47	BD	500	154±40	BD

* Concentrations were measured on GC-MS or GC-FID.

Concentrations were calculated based on dilution from stock CVOCs solutions.

BD: Below detection

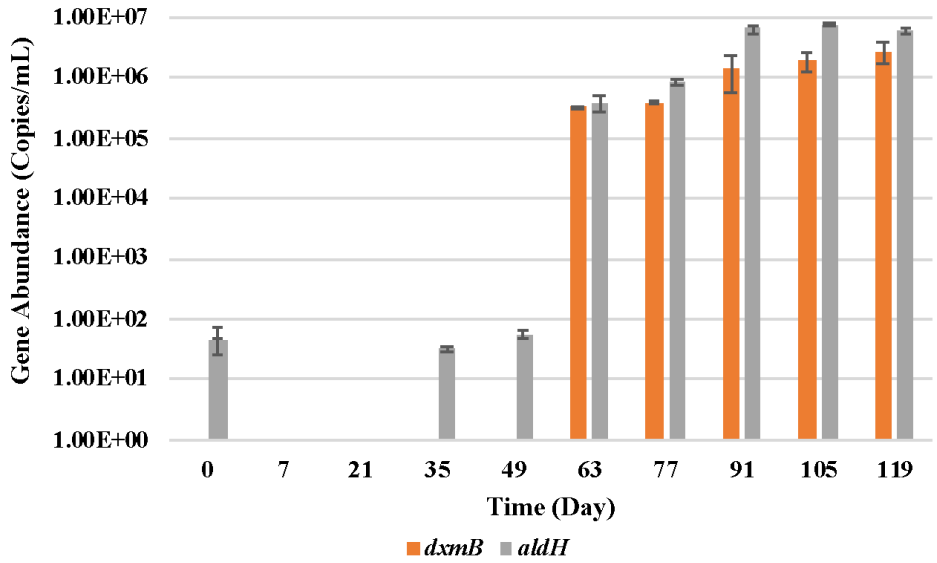

Figure 6.82. Abundances of biomarker genes, *dxmB* encoding dioxane monooxygenase (DXMO) and *aldH* encoding aldehyde dehydrogenase (ALDH), under bioaugmentation condition during catalysis-biodegradation process. CB1190 was spiked at day 63.

6.3.3.2 Microbial Community Dynamics during the Treatment Train

The whole treatment train was composed of five conditions that were monitored at four time points, and the Unifrac distance including membership (unweighted) and abundance (weighted) shown on PCoA displayed more differences over time (Figure 6.28, color-coded) than among conditions (Figure 6.28, shape-coded). This was also consistent with ENVFIT analysis that only time variables showed significant influences on both membership (R^2 = 0.89, P-value = 0.001) and abundance (R^2 = 0.80, P-value = 0.001). The original (CB0) and post-catalysis (CB1) microbes distributed separately, and microbes were more proximal from week 9 (CB2) to week 17 (CB3) than that from post-catalysis (CB1) to week 9 (CB2), demonstrating the relatively stronger shift of the microbial community right after the catalysis. The abundances of microbes under the three non-bioaugmented but CVOC-containing conditions were clustered together, demonstrating the potential control of CVOCs on the growth of microbes at the late biodegradation stage.

Figure 6.83. Dynamics of microbial community at each time point under all conditions at the 0.97-OTUs level. PCoA biplots showing weighted and unweighted UniFrac distances were namely qualitative (i.e., phylogeny) measures of microbial dynamics with and without quantitative (i.e., abundance) measures. The samples were color-coded by treatments (time) and shape-coded by contaminants (conditions).

Inoculation of CB1190 under the Bioaug condition also changed the abundance of microbes because its high abundance helped it to dominate the microbial community and compress the relative abundances of other microbes. However, even with the impact of CB1190 on the community, the microbial memberships were similar to those observed in the other conditions. When compared without phylogenetic information, all naturally simulated conditions were adjacent in the second biodegradation stage, based on Bray-Curtis distances (Figure 6.29). Moreover, no representative taxa were differently distributed among different naturally simulated conditions when LEFSE analysis using Kruskall-Wallis test (with strict Wilcoxon test), while representative microbes were differentiated when grouped by treatment phases (Figure 5.30 and 5.31).

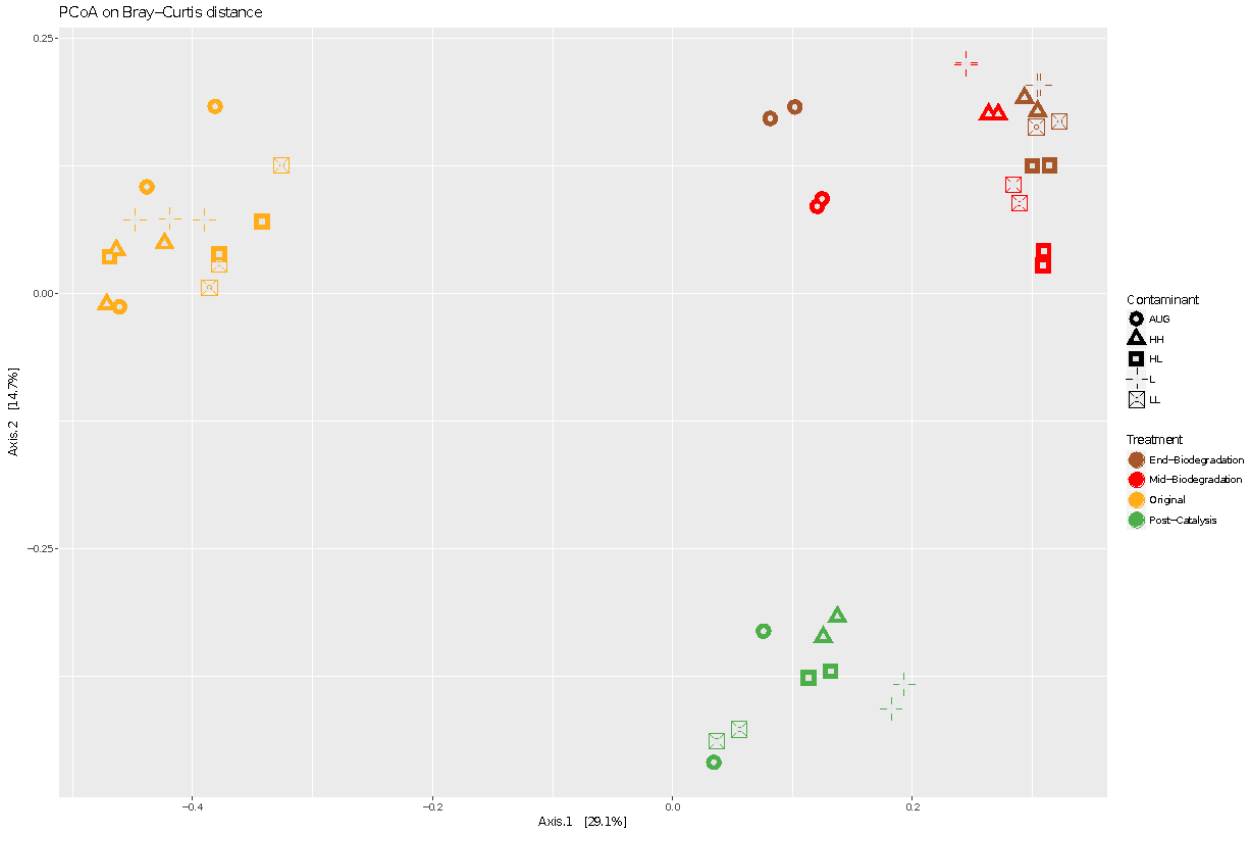

Figure 6.84. Dynamics of microbial community at each time point under all conditions at the 0.97-OTUs level. PCoA showing Bray-Curtis distances, and the samples were color-coded by treatments (time) and shape-coded by contaminants (conditions).

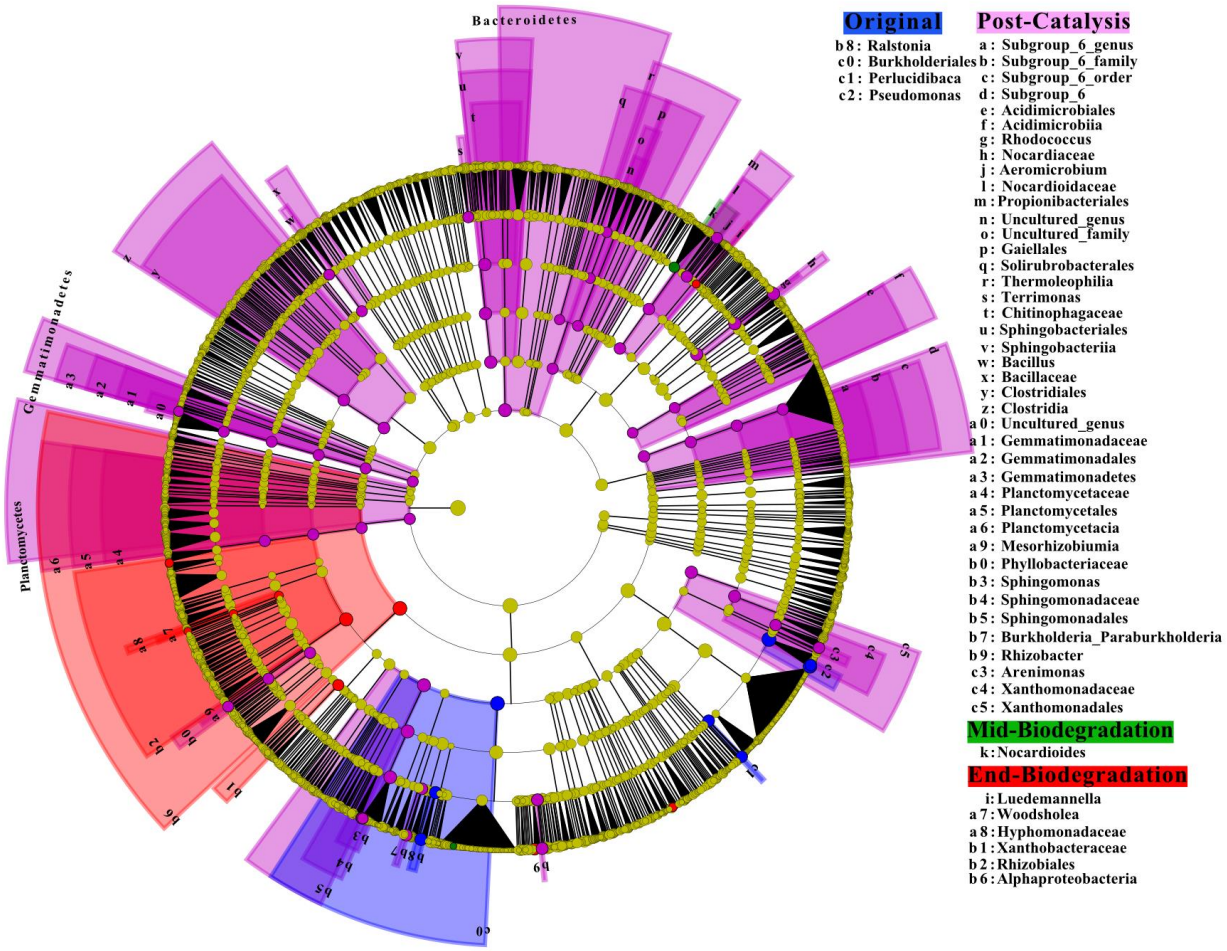

Figure 6.85. Taxonomic cladogram obtained using LEfSe analysis of the 16S sequences indicating the phylogenetic distribution of microbial lineages associated with the three treatment states, and only the taxa meeting a significant LDA threshold value of > 4 are shown. Differences are represented in the unique color of each condition, and highlighted taxa indicate enrichment of that taxa within the treatment state that corresponds to the highlighting color (shading and label). Circles represent phylogenetic levels from phylum to species (OTUs) inside out, and each circle's

diameter is proportional to the taxon's abundance. The annotations reach to genus level, more representative taxa were listed in Figure 6.31.

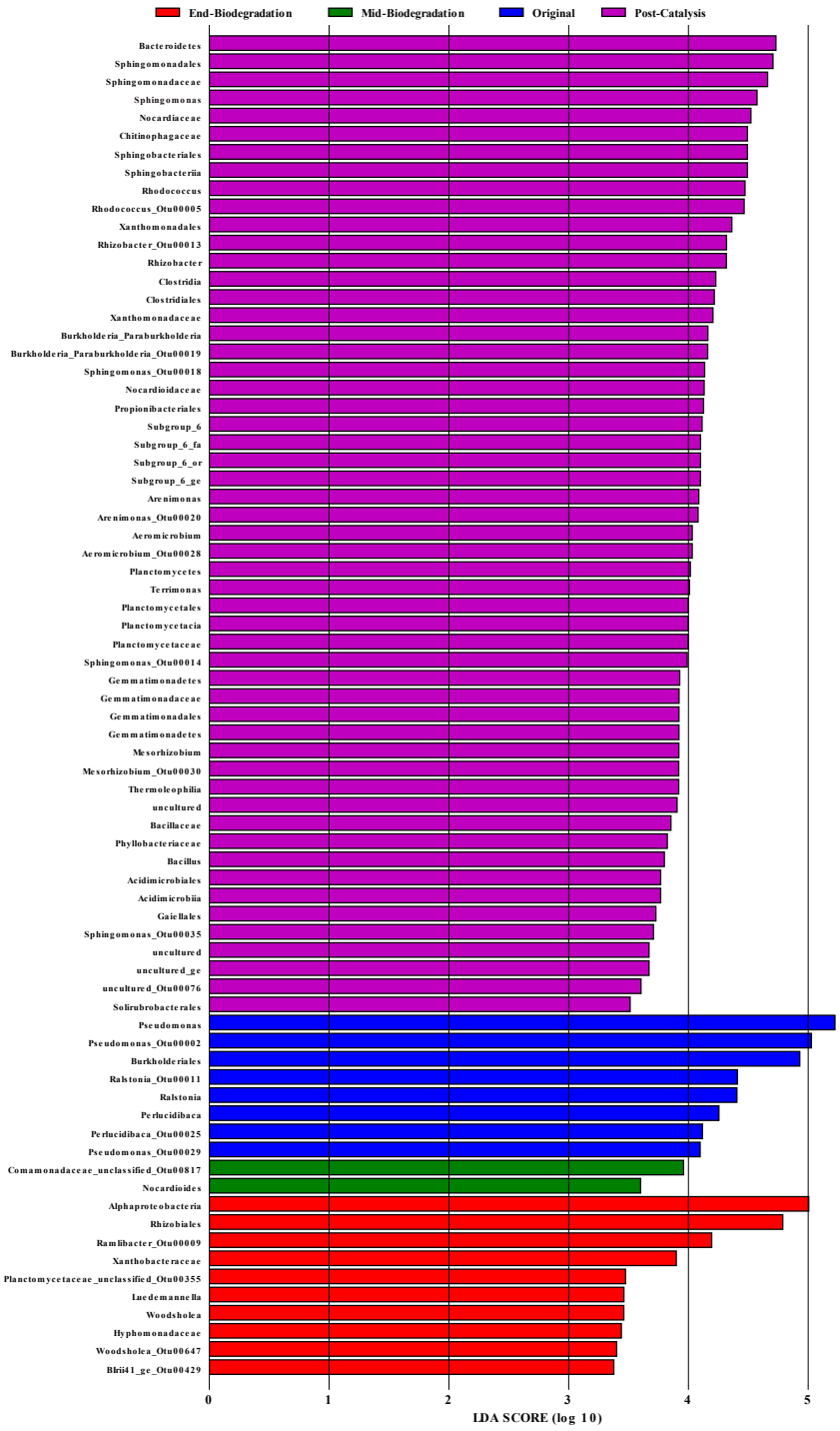

Figure 6.86. Histogram of the LDA scores computed for taxon differentially abundant among specific conditions after each treatment state. LEfSe scores can be interpreted as the degree of

consistent difference in relative abundance between taxa in the two groups of analyzed microbial communities. Only the taxa with meeting a significant LDA threshold value of >3 are shown.

6.3.3.3 Temporal and Conditional Distributions of Bacteria

The microbial community under the Bioaug condition showed signs of change due to the influence of CB1190 which was added at day 63 (20.16%), but dropped to 17.18% by the end of the biodegradation phase (Figure 6.32), even playing a large role in 1,4-dioxane biodegradation. Under the four naturally simulated conditions, *Pseudomonas*, *Ralstonia*, and *Perlucidibaca* were the main genera before treatment and then reduced by the catalysis phase. However, *Pseudomonas* was able to recover during the biodegradation phase, eventually becoming dominant, especially under the L-DX only condition. More genera, such as *Sphingomonas*, *Rhodococcus*, *Lacibacter*, *Rhizobacter*, *Arenimonas*, *Aeromicrobium*, and *Mesorhizobium*, thrived after the catalysis phase, demonstrating their potential catalysis-tolerances in the microcosms, but then decreased by the end of the biodegradation phase. After the completion of the biodegradation phase, *Ramlibacter* and *Methylobacillus* were found to accumulate under all conditions, while *Pseudarthrobacter* was only more abundant under the L-DX only condition. Additionally, the specific 1,4-dioxane and CVOC combinations and levels promoted specific microbes, e.g., both *Ohtaekwangia* and *Rhodoplanes* increased during biodegradation under both H/H and L/L conditions, and both *Bradyrhizobium* and *Acidovorax* preferred higher 1,4-dioxane during the biodegradation phase. The diversity and richness of the microbial community were stable after the catalysis phase, but increasing under all conditions during the first stage of biodegradation (Figure 6.32), and the remaining 1,1-DCE under the H/H condition further reduced the richness during the second stage of biodegradation.

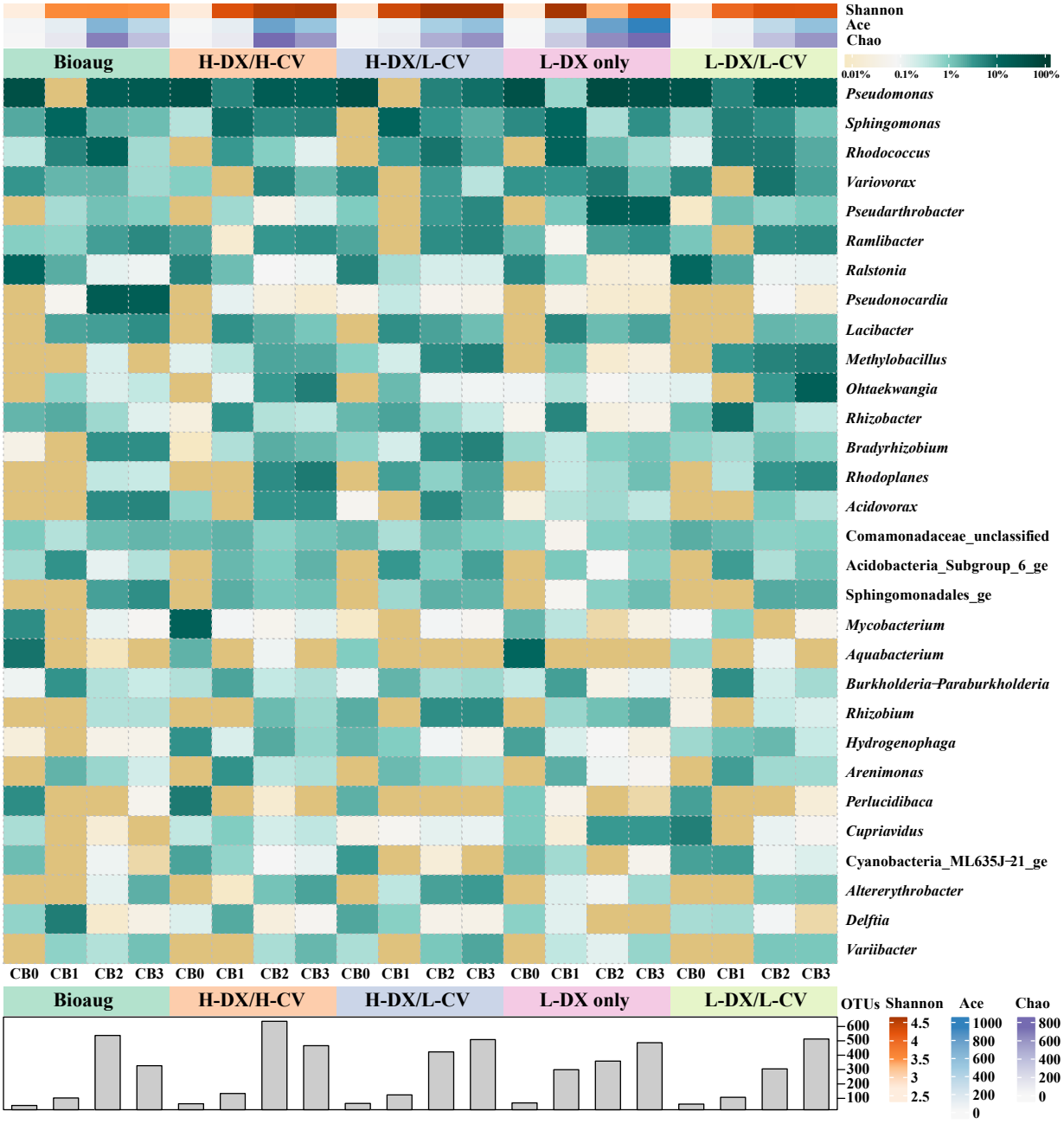

Figure 6.87. Trends of dynamics of microbial community richness, diversity and most abundant 30 species (0.97-OTUs) at each time points under all conditions.

6.3.3.4 Predictive Functional Features of the Bacterial Community

Tax4Fun was used in this study to find and identify a total of 6317 functional genes and 279 pathways based on KEGG databases. In non-metric multidimensional scaling (NMDS) of various

distances methods, both pathways and genes were only differentiated by the catalysis phase, but did not show differentiation when compared with samples from later time points (green in Figure 6.33). The methane metabolism pathway was more abundant than toluene degradation pathway, as well as COVCs related pathways, while their abundances were stable during the treatment process (Figure 6.34).

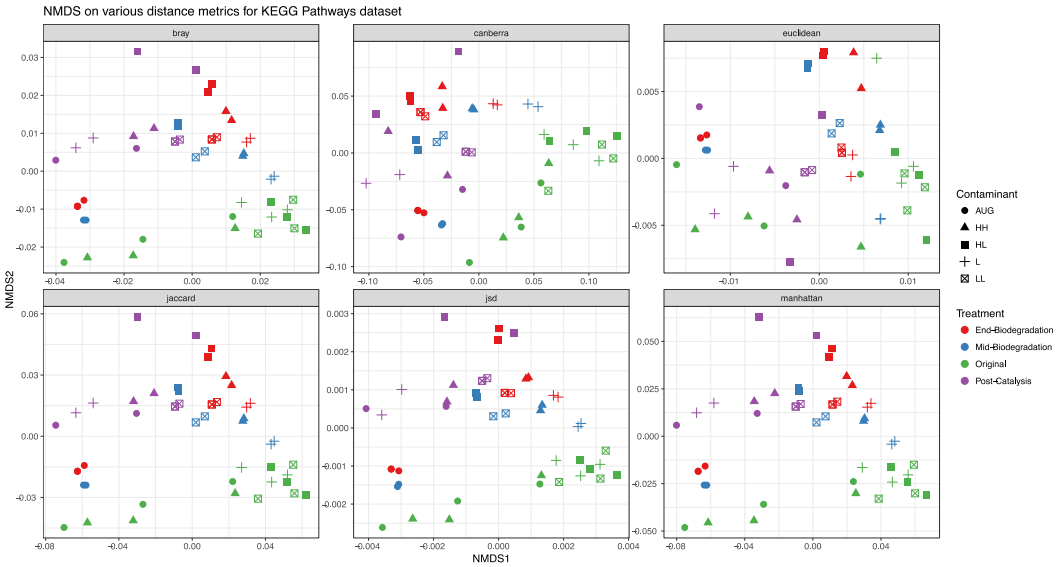

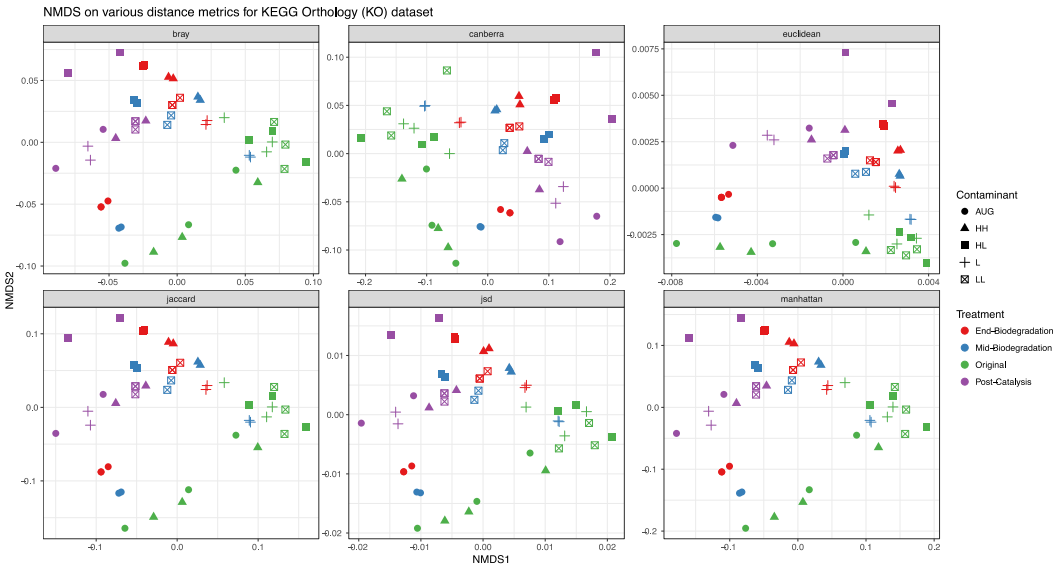

Figure 6.88. Dynamics of functions at each time point under all conditions at the 0.97-OTUs level. NMDS showing various distance methods, and the samples were color-coded by treatments (time) and shape-coded by contaminants (conditions).

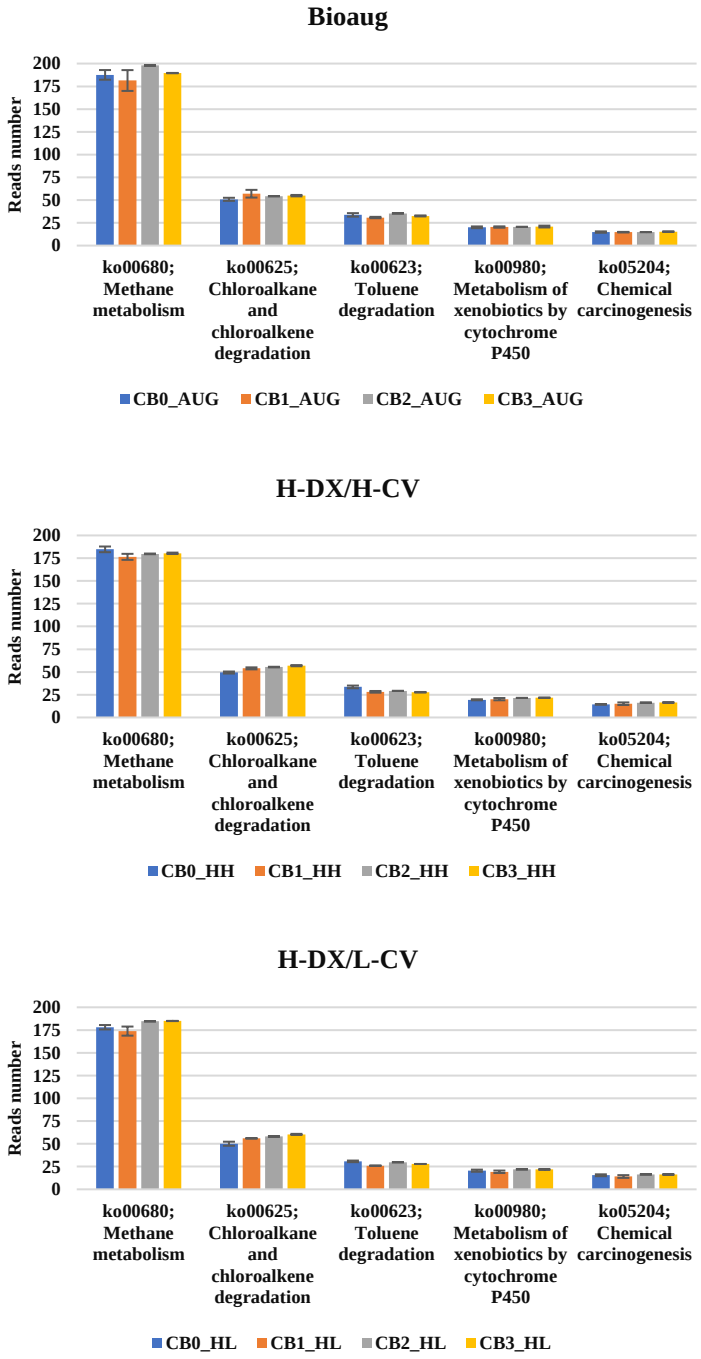

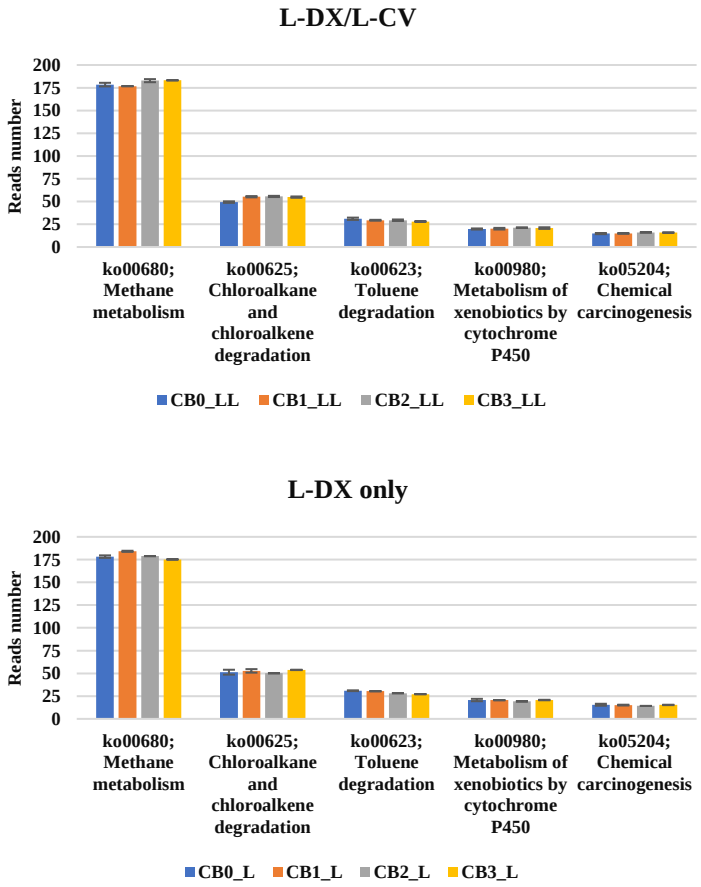

Figure 6.89. Relative abundance of 1,4-dioxane and CVOCs biodegradation related pathways under different conditions during the treatment train. The "Reads number" is the relative abundance multiplying the normalized total reads number of each sample (16000).

The genes encoding enzymes of interest, haloalkane dehalogenase, cytochrome P450 family 125, alkane 1-monooxygenase, haloacetate dehalogenase, and phenol 2-monooxygenase were abundant under the Bioaug condition (Table 6.11). The enzymes under the L-DX only condition showed increased abundance after the catalysis phase (e.g., cytochrome P450 family 125, haloacetate dehalogenase, and haloalkane dehalogenase), indicating elevated biodegradable potentials during the first 2 weeks of biodegradation phase. The decreasing functional features during the remaining biodegradation phase could be explained by the reduction in biodegradable substrates. The relative abundances of methane monooxygenases were stable during the treatment

train, and toluene monooxygenases were dominated by proteins A and E, both of which peaked in the first stage of biodegradation and reduced by the end, and the general monooxygenase [EC:1.14.13.-] abundance was only elevated under the Bioaug condition due to the addition of CB1190 (Table 6.11).

Table 6.21. Relative abundance of 1,4-dioxane and CVOCs biodegradation related genes under different conditions during the treatment train. The "Reads number" is the relative abundance multiplying the normalized total reads number of each sample (16000).

Enzymes	CB0_AUG	CB1_AUG	CB2_AUG	CB3_AUG
alkanal monooxygenase alpha chain [EC:1.14.14.3]	0.00	0.00	0.00	0.00
alkanal monooxygenase beta chain [EC:1.14.14.3]	0.03	0.02	0.02	0.02
alkane 1-monooxygenase [EC:1.14.15.3]	1.90	1.24	2.20	1.72
cytochrome P450 / NADPH-cytochrome P450 reductase [EC:1.14.14.1 1.6.2.4]	0.94	1.05	1.24	1.16
cytochrome P450 monooxygenase	0.05	0.03	0.02	0.02
cytochrome P450, family 142, subfamily A, polypeptide 1	0.92	0.75	1.66	1.16
cytochrome P450, family 51 (sterol 14-demethylase) [EC:1.14.13.70]	0.86	0.72	1.51	1.05
haloacetate dehalogenase [EC:3.8.1.3]	1.72	1.79	2.02	1.91
haloalkane dehalogenase [EC:3.8.1.5]	2.87	3.01	3.94	3.54
2-haloacid dehalogenase [EC:3.8.1.2]	2.53	2.80	2.35	2.54
methane monooxygenase component A alpha chain [EC:1.14.13.25]	0.35	0.42	0.53	0.45
methane monooxygenase component A beta chain [EC:1.14.13.25]	0.22	0.26	0.32	0.28
methane monooxygenase component A gamma chain [EC:1.14.13.25]	0.01	0.01	0.02	0.02
methane monooxygenase component C [EC:1.14.13.25]	0.19	0.14	0.17	0.16
methane monooxygenase subunit A [EC:1.14.13.25]	0.03	0.00	0.02	0.02
methane monooxygenase subunit B [EC:1.14.13.25]	0.10	0.03	0.02	0.03
methane monooxygenase subunit C [EC:1.14.13.25]	0.22	0.07	0.09	0.10
phenol 2-monooxygenase [EC:1.14.13.7]	0.88	1.23	1.31	1.17
phenol hydroxylase P3 protein [EC:1.14.13.-]	0.71	0.50	0.40	0.43
toluene monooxygenase system protein A [EC:1.14.13.-]	0.33	0.28	0.30	0.29
toluene monooxygenase system protein B [EC:1.14.13.-]	0.04	0.03	0.03	0.04
toluene monooxygenase system protein D [EC:1.14.13.-]	0.08	0.07	0.07	0.07
toluene monooxygenase system protein E [EC:1.14.13.-]	0.23	0.19	0.18	0.19
monooxygenase [EC:1.14.13.-]	3.94	3.29	5.73	4.37

Enzymes	CB0_HH	CB1_HH	CB2_HH	CB3_HH
alkanal monooxygenase alpha chain [EC:1.14.14.3]	0.00	0.00	0.00	0.00
alkanal monooxygenase beta chain [EC:1.14.14.3]	0.03	0.02	0.03	0.02
alkane 1-monooxygenase [EC:1.14.15.3]	1.93	0.95	0.81	0.64
cytochrome P450 / NADPH-cytochrome P450 reductase [EC:1.14.14.1 1.6.2.4]	0.87	0.99	0.98	1.11
cytochrome P450 monooxygenase	0.05	0.03	0.04	0.03
cytochrome P450, family 142, subfamily A, polypeptide 1	0.86	0.41	0.11	0.11
cytochrome P450, family 51 (sterol 14-demethylase) [EC:1.14.13.70]	0.83	0.42	0.09	0.09
haloacetate dehalogenase [EC:3.8.1.3]	1.58	1.59	1.83	1.79
haloalkane dehalogenase [EC:3.8.1.5]	2.83	2.76	2.09	2.30
2-haloacid dehalogenase [EC:3.8.1.2]	2.32	2.60	3.37	3.39
methane monooxygenase component A alpha chain [EC:1.14.13.25]	0.32	0.33	0.35	0.37
methane monooxygenase component A beta chain [EC:1.14.13.25]	0.21	0.21	0.23	0.24
methane monooxygenase component A gamma chain [EC:1.14.13.25]	0.01	0.01	0.01	0.02
methane monooxygenase component C [EC:1.14.13.25]	0.19	0.13	0.16	0.13
methane monooxygenase subunit A [EC:1.14.13.25]	0.03	0.01	0.01	0.01
methane monooxygenase subunit B [EC:1.14.13.25]	0.09	0.05	0.13	0.09
methane monooxygenase subunit C [EC:1.14.13.25]	0.23	0.11	0.35	0.23
phenol 2-monooxygenase [EC:1.14.13.7]	0.83	1.08	0.79	0.81
phenol hydroxylase P3 protein [EC:1.14.13.-]	0.78	0.51	0.69	0.49
toluene monooxygenase system protein A [EC:1.14.13.-]	0.34	0.29	0.32	0.26
toluene monooxygenase system protein B [EC:1.14.13.-]	0.04	0.04	0.05	0.04
toluene monooxygenase system protein D [EC:1.14.13.-]	0.09	0.07	0.09	0.07
toluene monooxygenase system protein E [EC:1.14.13.-]	0.24	0.21	0.23	0.18
monooxygenase [EC:1.14.13.-]	3.84	2.28	1.50	1.46

Enzymes	CB0_HL	CB1_HL	CB2_HL	CB3_HL
alkanal monooxygenase alpha chain [EC:1.14.14.3]	0.00	0.00	0.00	0.00
alkanal monooxygenase beta chain [EC:1.14.14.3]	0.04	0.01	0.02	0.02
alkane 1-monooxygenase [EC:1.14.15.3]	1.22	0.68	0.92	0.65
cytochrome P450 / NADPH-cytochrome P450 reductase [EC:1.14.14.1 1.6.2.4]	0.83	0.88	1.19	1.26
cytochrome P450 monooxygenase	0.06	0.02	0.03	0.03
cytochrome P450, family 142, subfamily A, polypeptide 1	0.05	0.25	0.42	0.21
cytochrome P450, family 51 (sterol 14-demethylase) [EC:1.14.13.70]	0.06	0.24	0.37	0.19
haloacetate dehalogenase [EC:3.8.1.3]	1.66	1.37	1.97	1.90
haloalkane dehalogenase [EC:3.8.1.5]	1.85	2.26	2.54	2.73
2-haloacid dehalogenase [EC:3.8.1.2]	2.94	2.80	3.42	3.54
methane monooxygenase component A alpha chain [EC:1.14.13.25]	0.25	0.32	0.42	0.40
methane monooxygenase component A beta chain [EC:1.14.13.25]	0.17	0.20	0.27	0.25
methane monooxygenase component A gamma chain [EC:1.14.13.25]	0.01	0.02	0.02	0.02
methane monooxygenase component C [EC:1.14.13.25]	0.20	0.09	0.14	0.13
methane monooxygenase subunit A [EC:1.14.13.25]	0.04	0.00	0.01	0.01
methane monooxygenase subunit B [EC:1.14.13.25]	0.13	0.03	0.10	0.12
methane monooxygenase subunit C [EC:1.14.13.25]	0.32	0.08	0.27	0.27
phenol 2-monooxygenase [EC:1.14.13.7]	0.73	1.03	0.96	0.83
phenol hydroxylase P3 protein [EC:1.14.13.-]	0.93	0.30	0.48	0.38
toluene monooxygenase system protein A [EC:1.14.13.-]	0.37	0.19	0.27	0.22
toluene monooxygenase system protein B [EC:1.14.13.-]	0.05	0.03	0.03	0.03
toluene monooxygenase system protein D [EC:1.14.13.-]	0.10	0.05	0.07	0.05
toluene monooxygenase system protein E [EC:1.14.13.-]	0.28	0.12	0.18	0.14
monooxygenase [EC:1.14.13.-]	1.62	1.57	1.63	1.89

Enzymes	CB0_L	CB1_L	CB2_L	CB3_L
alkanal monooxygenase alpha chain [EC:1.14.14.3]	0.00	0.00	0.00	0.00
alkanal monooxygenase beta chain [EC:1.14.14.3]	0.04	0.02	0.03	0.03
alkane 1-monooxygenase [EC:1.14.15.3]	1.22	1.24	1.09	0.84
cytochrome P450 / NADPH-cytochrome P450 reductase [EC:1.14.14.1 1.6.2.4]	0.91	1.14	0.82	0.91
cytochrome P450 monooxygenase	0.06	0.03	0.03	0.02
cytochrome P450, family 142, subfamily A, polypeptide 1	0.13	0.80	0.13	0.12
cytochrome P450, family 51 (sterol 14-demethylase) [EC:1.14.13.70]	0.14	0.73	0.14	0.12
haloacetate dehalogenase [EC:3.8.1.3]	1.72	1.80	1.44	1.52
haloalkane dehalogenase [EC:3.8.1.5]	2.03	3.27	2.08	2.21
2-haloacid dehalogenase [EC:3.8.1.2]	3.15	2.60	2.32	2.63
methane monooxygenase component A alpha chain [EC:1.14.13.25]	0.27	0.40	0.23	0.26
methane monooxygenase component A beta chain [EC:1.14.13.25]	0.19	0.25	0.16	0.17
methane monooxygenase component A gamma chain [EC:1.14.13.25]	0.01	0.02	0.02	0.02
methane monooxygenase component C [EC:1.14.13.25]	0.19	0.13	0.15	0.13
methane monooxygenase subunit A [EC:1.14.13.25]	0.03	0.01	0.04	0.03
methane monooxygenase subunit B [EC:1.14.13.25]	0.06	0.05	0.07	0.05
methane monooxygenase subunit C [EC:1.14.13.25]	0.17	0.13	0.18	0.13
phenol 2-monooxygenase [EC:1.14.13.7]	0.69	1.08	0.78	0.81
phenol hydroxylase P3 protein [EC:1.14.13.-]	0.88	0.40	0.62	0.47
toluene monooxygenase system protein A [EC:1.14.13.-]	0.36	0.28	0.31	0.25
toluene monooxygenase system protein B [EC:1.14.13.-]	0.05	0.03	0.05	0.04
toluene monooxygenase system protein D [EC:1.14.13.-]	0.10	0.07	0.08	0.06
toluene monooxygenase system protein E [EC:1.14.13.-]	0.27	0.18	0.22	0.17
monooxygenase [EC:1.14.13.-]	1.75	3.32	1.56	1.61

Enzymes	CB0_LL	CB1_LL	CB2_LL	CB3_LL
alkanal monooxygenase alpha chain [EC:1.14.14.3]	0.00	0.00	0.00	0.00
alkanal monooxygenase beta chain [EC:1.14.14.3]	0.04	0.02	0.02	0.02
alkane 1-monooxygenase [EC:1.14.15.3]	1.26	0.99	1.01	0.86
cytochrome P450 / NADPH-cytochrome P450 reductase [EC:1.14.14.1 1.6.2.4]	0.91	0.95	1.03	1.08
cytochrome P450 monooxygenase	0.07	0.04	0.04	0.04
cytochrome P450, family 142, subfamily A, polypeptide 1	0.07	0.45	0.35	0.22
cytochrome P450, family 51 (sterol 14-demethylase) [EC:1.14.13.70]	0.09	0.40	0.31	0.18
haloacetate dehalogenase [EC:3.8.1.3]	1.70	1.64	1.86	1.76
haloalkane dehalogenase [EC:3.8.1.5]	1.88	2.98	2.34	2.38
2-haloacid dehalogenase [EC:3.8.1.2]	3.06	2.91	3.19	3.06
methane monooxygenase component A alpha chain [EC:1.14.13.25]	0.27	0.28	0.36	0.31
methane monooxygenase component A beta chain [EC:1.14.13.25]	0.19	0.18	0.23	0.20
methane monooxygenase component A gamma chain [EC:1.14.13.25]	0.01	0.01	0.01	0.01
methane monooxygenase component C [EC:1.14.13.25]	0.21	0.13	0.15	0.15
methane monooxygenase subunit A [EC:1.14.13.25]	0.03	0.00	0.01	0.01
methane monooxygenase subunit B [EC:1.14.13.25]	0.06	0.10	0.13	0.17
methane monooxygenase subunit C [EC:1.14.13.25]	0.19	0.20	0.33	0.39
phenol 2-monooxygenase [EC:1.14.13.7]	0.70	0.99	0.86	0.80
phenol hydroxylase P3 protein [EC:1.14.13.-]	0.99	0.53	0.58	0.55
toluene monooxygenase system protein A [EC:1.14.13.-]	0.40	0.30	0.31	0.29
toluene monooxygenase system protein B [EC:1.14.13.-]	0.05	0.04	0.05	0.04
toluene monooxygenase system protein D [EC:1.14.13.-]	0.11	0.08	0.08	0.07
toluene monooxygenase system protein E [EC:1.14.13.-]	0.31	0.21	0.21	0.19
monooxygenase [EC:1.14.13.-]	1.57	2.39	2.25	1.86

6.3.3.5 Species-Species and Genera-Functions Associations

The correlations between predicted functional features and the top 20 abundant genera under four naturally simulated conditions were used to show potential carriers of specific genes (Figure 6.35). The dominant *Pseudomonas* showed significant positive correlation with genes encoding toluene and alkanal monooxygenases alpha and beta chains, while negatively with cytochrome P450 families. However, *Sphingomonas*, *Rhodococcus*, and *Lacibacter* were positively correlated with genes encoding cytochrome P450 families and negatively correlated with toluene and alkanal monooxygenases. For CVOC-related functional enzymes, haloacetate and haloacid dehalogenases were positively correlated with *Ramlibacter*, *Methylobacillus*, *Bradyrhizobium*, and *Acidovorax*, while haloalkane dehalogenase was mainly positively correlated with *Sphingomonas*, *Rhodococcus*, and *Methylobacillus*. Additionally, alkanal monooxygenases correlations were only significantly positive with *Pseudomonas* and *Variovoras*, but tended to be negative with other genera, and the dehalogenases were significantly and widely distributed in various microbes.

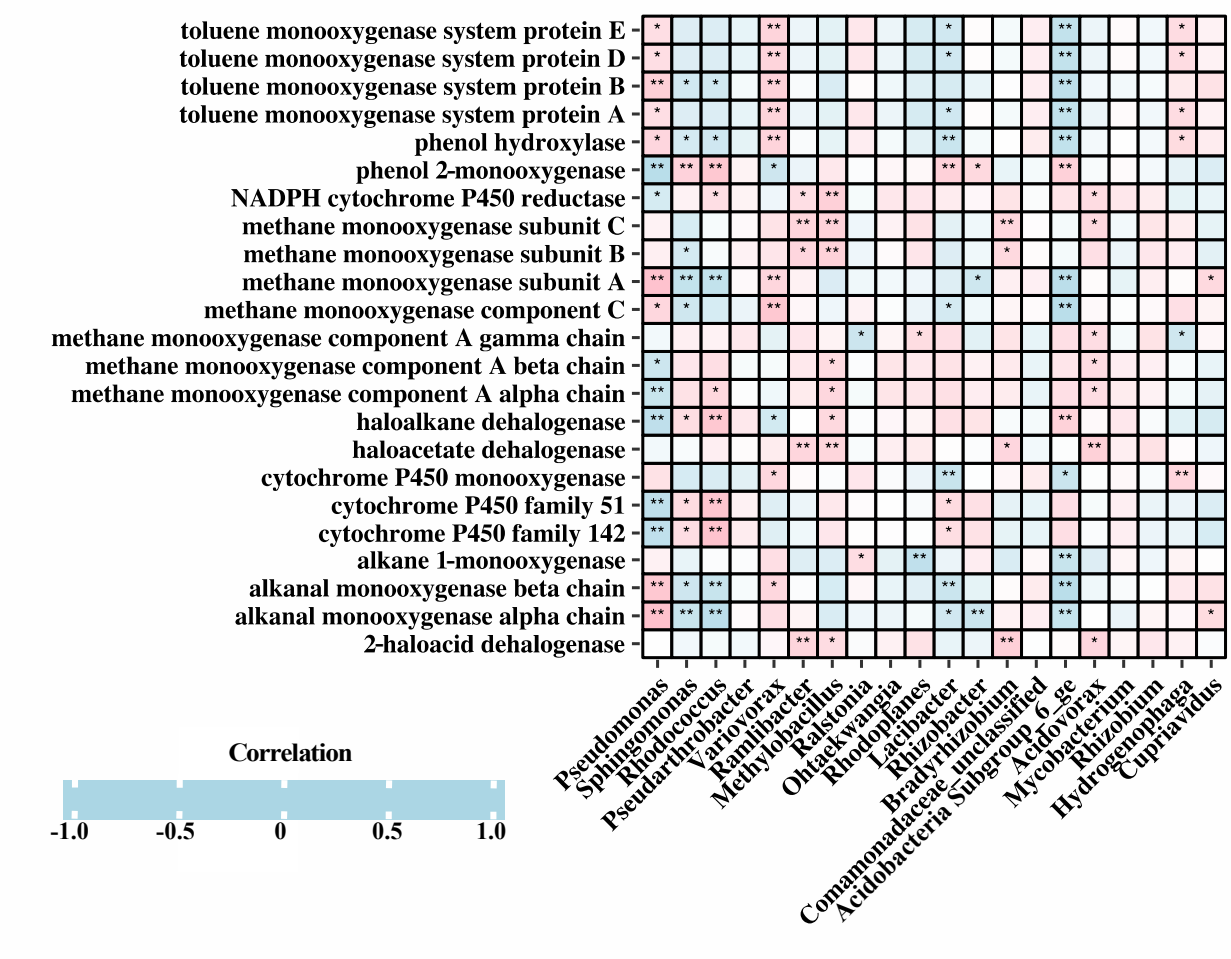

Figure 6.90. Significance of correlation among genera under biostimulated conditions. * indicates $p<0.05$, and ** indicated $p<0.01$. The top 20 abundant genera under biostimulated condition were pooling together and calculated with Spearman's rank correlation coefficient.

Co-occurrence and co-exclusion were represented by positive and negative Spearman's correlations, respectively, and the network among species (OTUs) only incorporated taxa under mimic-natural conditions in the biodegradation phase (CB1-CB3). The strong ($\rho > 0.8$) and significant (P-value < 0.01) positive correlations consisted of 112 nodes and 377 edges, including 9 modules (modularity = 0.583) (Figure 6.36D). Module III, VIII, and IX were isolated without any edges to other modules, but occupied with different phyla (Figure 6.36A). Phylum Proteobacteria mainly occupied module II, IV, V, and IX, and shared modules II, IV, V with

Actinobacteria and module VI with Bacteroidetes. Interestingly, module IV and VI had no direct connections with module II and V; even Proteobacteria spread in these modules. The most abundant genus *Pseudomonas* (OTU1, 2, 3) distributed in three modules (II, V, IX) and mainly connected with *Ramlibacter* (OTU9, 15), *Acidovorax* (OTU8), *Bradyrhizobium* (OTU12), *Variibacter* (OTU45, 92), *Methylobacillus* (OTU10), and *Rhizobium* (OTU31, 56). However, *Sphingomonas* (OTU14, 18, 35, 48, 64, 145), *Rhodococcus* (OTU5), and *Lacibacter* (OTU7) were found co-occurring in module IV and VI. Additionally, *Acidovorax* (OTU8), *Bradyrhizobium* (OTU12), and *Variibacter* (OTU45, 92) were the densely connected nodes within module V, while *Sphingomonas* (OTU35) was the bridge between module IV and VI (Figure 6.36B). Furthermore, the peak abundance of each OTU was used to show the abundance trends among CB1, CB2, and CB3. The OTUs peaking at CB1 mainly distributed in module IV, VI, and VII, while OTUs with peak abundance at CB2 and CB3 were mixed and spread in module II and V, indicating that abundance of species changed less in the second stage of biodegradation (Figure 6.36C). The negative strong ($\rho < -0.8$) and significant (P-value < 0.01) correlations contained 56 nodes and 112 edges, and were separated into 7 modules (modularity = 0.408) (Figure 6.37C). Genera *Pseudomonas* (OTU1) and *Sphingomonas* (OTU18) were in the same module II, and negatively connected, indicating their potential competition, that were also observed between *Pseudomonas* (OTU1) and *Rhizobacter* (OTU13) in module II, *Rhizobium* (OTU31) and *Rhizobacter* (OTU13) in module II, as well as *Sphingomonas* (OTU35) and *Ramlibacter* (OTU9) in module I. Besides, *Sphingomonas* (OTU35) also negatively connected with *Pseudarthrobacter* (OTU6) in different modules (Figure 6.37B).

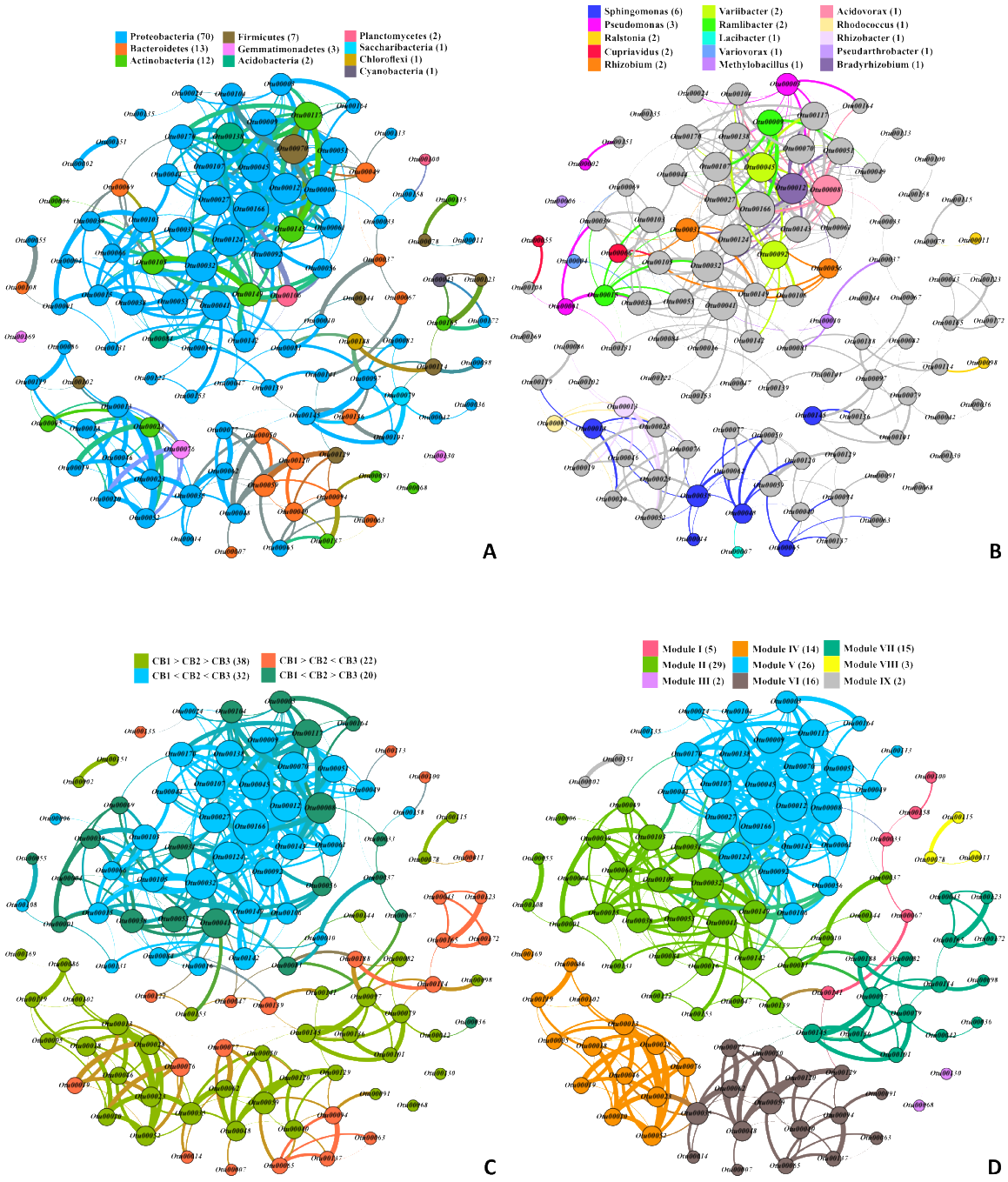

Figure 6.91. Correlation-based network analysis of species co-occurrence patterns in biostimulated samples from CB1 to CB3, with significant (p-value < 0.01) and strong correlations (R > 0.8) between 0.97-OTUs. The size of each node (0.97-OTUs) is proportional to the number of connections, and the thickness of each edge between two nodes is proportional to the strength

of correlation. A: network colored by phylum; B: network colored by genus; C: network colored by rankings of average relative abundance of an OTU at three time points; D: network colored by modules calculated by Gephi modularity toolkit, and nodes within the same module were more densely connected together than to the rest of the network.

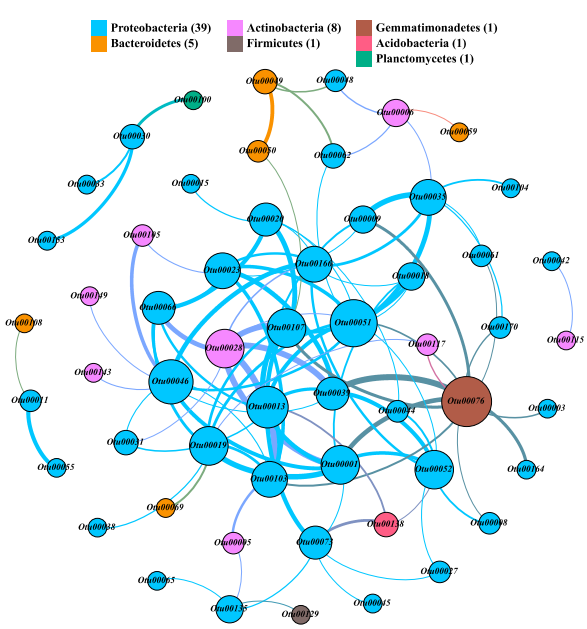

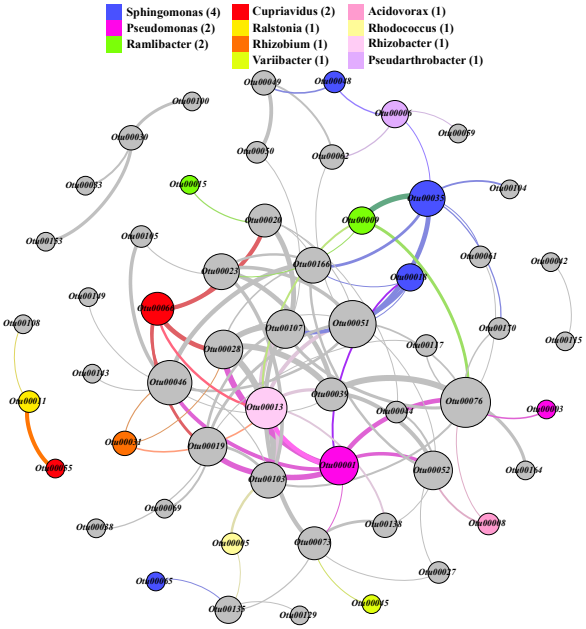

A **B**

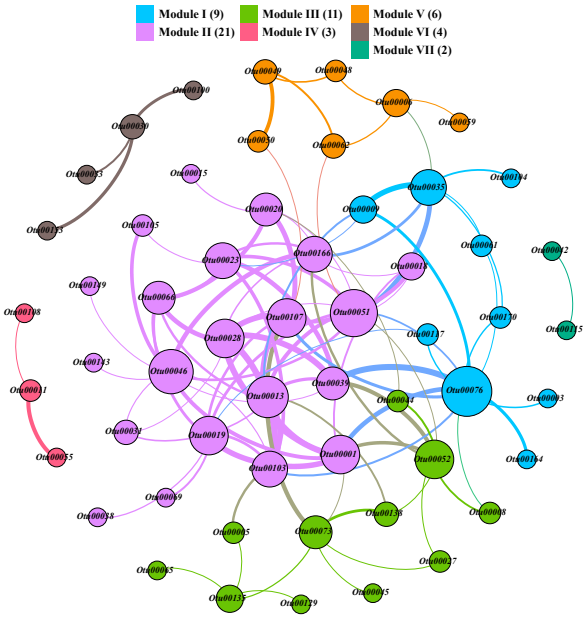

C

Figure 6.92. Correlation-based network analysis of species co-exclusive patterns in biostimulated samples from CB1 to CB3, with significant (p-value < 0.01) and strong correlations (R < -0.8) between 0.97-OTUs. The size of each node (0.97-OTUs) is proportional to the number of connections, and the thickness of each edge between two nodes is proportional to the strength of correlation. A: network colored by phylum; B: network colored by genus; C: network colored by modules calculated by Gephi modularity toolkit, and nodes within the same module were more densely connected together than to the rest of the network.

6.3.3.6 Predictions of Microbial Community Dynamics Using Random Forests

The relative abundance of all OTUs were used to construct RF regression models, that were utilized to predict the distributions of microbes during the treatment process, and the ideal distribution should be on the diagonal where prediction days are equal to actual days. When putting H/H and H/L conditions together as the training dataset and data in L/L and L-DX only conditions using as input (R^2=0.63, MAE = 20.82), the first two time points (day 0 and 1) were beyond the diagonal, and samples at day 63 and 119 were predicted below the diagonal and near to each other (Figure 6.38A), and the similar prediction (R^2=0.67, MAE=19.27) was obtained after switching the training and testing datasets (Figure 6.38B). However, when only inputting Bioaug samples into the naturally simulated model, microbes were predicted to be consistent during the biodegradation phase, showing the potential impacts and dominance of spiked CB1190 in the microbial community (Figure 6.39A). The sooner stabilization of microbial community was also predicted by using model with naturally simulated data (Figure 6.39B).

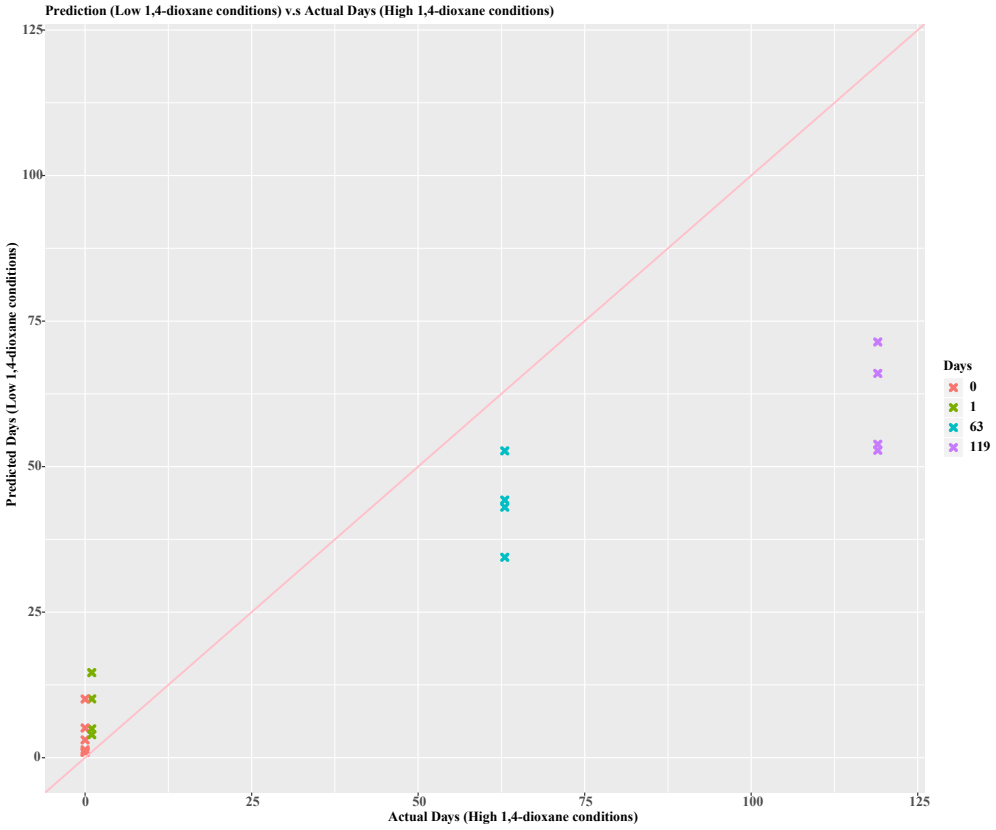
Prediction (Low 1,4-dioxane conditions) v.s Actual Days (High 1,4-dioxane conditions)
Predicted Days (Low 1,4-dioxane conditions)
Actual Days (High 1,4-dioxane conditions)
0
25
50
75
100
125
Days
0
1
63
119

A

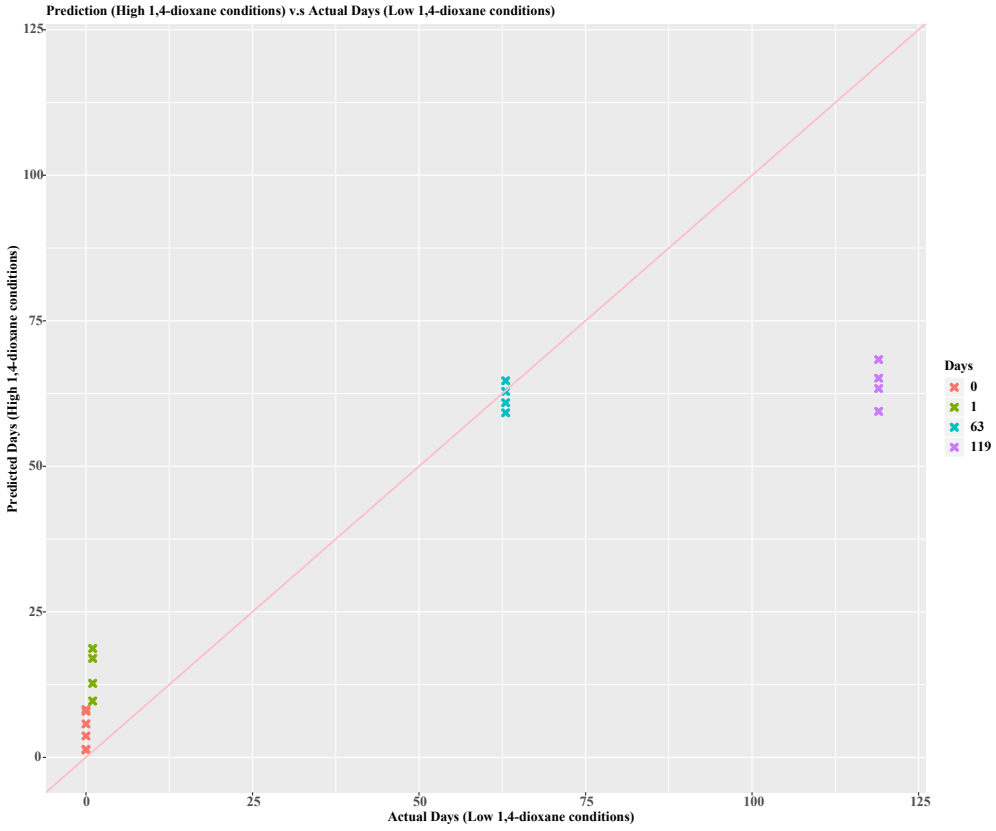
Prediction (High 1,4-dioxane conditions) v.s Actual Days (Low 1,4-dioxane conditions)
Predicted Days (High 1,4-dioxane conditions)
Actual Days (Low 1,4-dioxane conditions)
0
25
50
75
100
125
Days
0
1
63
119

B

Figure 6.93. Random Forest regression models built from relative abundance of all microbes (OTUs) in the entire microbial community under different 1,4-dioxane concentrations. A: Model was trained on samples belonged to high-level 1,4-dioxane conditions and tested on samples belonged to low-level 1,4-dioxane conditions; B: Model was trained on samples belonged to low-level 1,4-dioxane conditions and tested on samples belonged to high-level 1,4-dioxane conditions. CB0=day 0, CB1=day 1, CB2=day 63, and CB3=day 119.

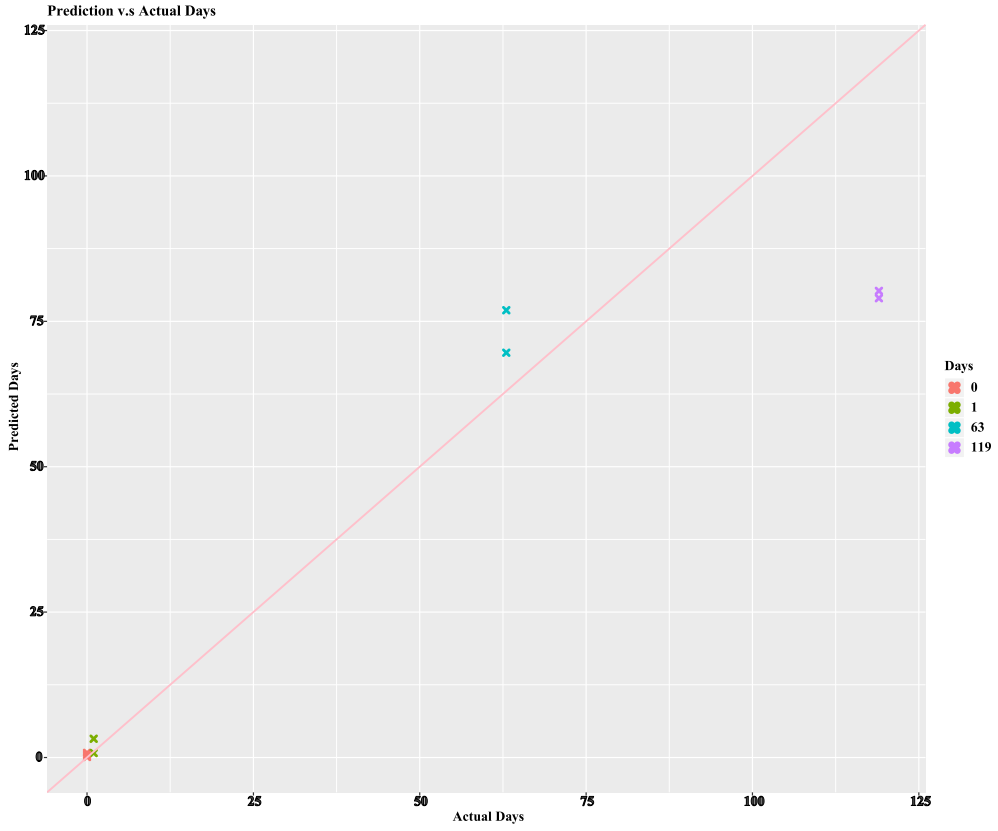

A

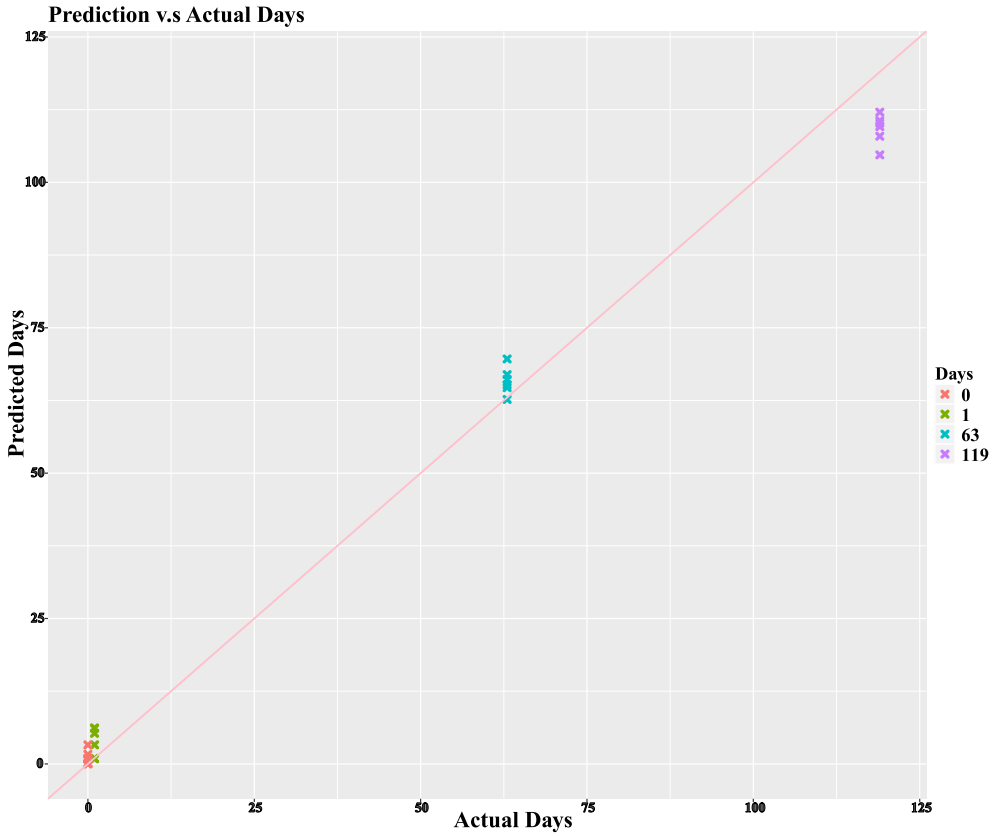

B

Figure 6.94. Random Forest regression models built from relative abundance of all microbes (OTUs) in the entire microbial community under different contaminated conditions. A: Model was trained on biostimulated samples and tested on Bioaug samples. B: Model was trained on biostimulated samples and tested on randomly picked samples. CB0=day 0, CB1=day 1, CB2=day 63, and CB3=day 119.

6.4 Discussion

6.4.1 Oxidation and Catalysis Treatment Train

This study explored the efficiency of a combined oxidation and catalysis treatment train for combined 1,4-dioxane and CVOC contaminations. The oxidation process could rapidly removal 85% of initial 1,4-dioxane regardless of CVOC presence or concentration, even higher than the 50% removal target, validating that hydroxyl radicals decomposed from H_2O_2 could destroy the structure of 1,4-dioxane (Ikehata et al., 2016). The oxidation process was conducted at pH 4.5, which

additionally promoted the activity of WO_x/ZrO_2, and some potential catalyst inhibitors (such as thiols) were mineralized to less deactivating species (Adamson et al., 2017).

Even though the microcosms had similar removal performances after each treatment process, the residual amount of 1,4-dioxane varied under different conditions, because of the different initial concentrations, that would induce shifts in the microbial community. Moreover, Eberle et al. (2016) found that 1,4-dioxane had lower degradation rate than TCE, but higher than 1,1,1-TCA when using peroxone activated persulfate, indicating the potential of residual CVOCs in the microcosms that could be another driver of microbial shifts. The biodiversity directly showed microbial responses to treatment trains, and oxidation-depressing diversity was only found under the H-DX/H-CV condition. This was consistent with a previous study showing that in-situ chemical oxidation (ISCO) could reduce soil diversity (Munakata-Marr et al., 2011, Medina et al., 2018), and peroxide used as a disinfection reagent could reduce diversity in wastewater treatment (Yang et al., 2017). However, the relatively weak impacts of oxidation were found under H-DX/L-CV and L-DX/L-CV conditions, where the biodiversity was as high as the original state, indicating the adverse impact of CVOCs on diversity during oxidation in this study, consistent with a previous study that found lower biodiversity in perchloroethene (PCE) contaminated wells (Munakata-Marr et al., 2011). Furthermore, a lower dose of H_2O_2 applied in microcosms may be insufficient to induce obvious diversity reductions but may be sufficient with 1,4-dioxane and CVOCs to reduce biomass based on 16S rRNA gene copies. Chen et al. (2016) demonstrated that even the addition of 3% peroxide seemed to cause slight reductions in microbial abundance. In addition, biodiversity increased after oxidation under the L-DX condition similar to H_2O_2 treatment of diesel-contaminated soil (Chen et al., 2016), which might increase oxidant-tolerant bacteria by horizontal gene transfer (HGT) (Wilson and Metcalf, 2005). Sutton et al. (2014) also indicated that bacterial diversity could

temporarily increase with the addition of Fenton's reagent. The two-day catalysis process decreased biodiversity under all conditions, indicating that the added catalyst could not only further remove contaminant mixtures, but also simultaneously eliminate fragile microorganisms.

The change of dominant bacteria under different conditions during treatment trains help explain the changes of biodiversity. Genus *Pseudomonas* is generally the dominant bacteria in soil, and it is known to be capable of co-metabolizing cis-DCE and TCE (Li et al., 2015), while some species such as *P. aeruginosa* (Santiago et al., 2016) and *P. plecoglossicida* (Li et al., 2015) have been found to be inhibited by H_2O_2. The oxidation stimulated genus *Massilia* was enriched after the oxidation process based on taxonomic classification and LEfSe, confirming its oxidative tolerance. The further enrichment of *Massilia* under H-DX/H-CV condition also showed potential tolerance to 1,4-dioxane and CVOCs, which was also reported with reductive dehalogenation (Xu et al., 2018). Another oxidative tolerant genus *Rhodococcus* found during this study was previously reported to have oxidative tolerance conferred by the *KatA* catalase gene (Bidaud et al., 2012). Moreover, as a co-metabolizer, *Rhodococcus* could degrade 1,4-dioxane with tetrahydrofuran (THF) as a primary carbon source (Inoue et al., 2016). Thus, *Rhodococcus* had higher abundance under lower CVOCs spiked conditions. Similarly, genus *Rhizobacter* as a plant growth promoter could express ROS-scavenging enzymes (Gururani et al., 2013), but was only enriched under L-DX condition, indicating weak CVOC tolerance. Meanwhile, *Paenibacillus* and *Bacilli*, which can resist peroxide by forming endospore (Dingman, 2011) and secreting bacillithiol (Handtke et al., 2014) respectively, also showed CVOC tolerance, due to their enrichment after oxidation under H-DX/H-CV condition. However, *Williamsia* was capable of oxidative tolerance but less CVOC tolerance in this study under L-DX condition. Genera *Cylindrospermum* and *Novosphingobium* showed catalyst tolerance based on the accumulated abundance after catalysis process, who were also reported to work as biocatalysts

(Hall and Bell, 2015). However, the lower relative abundance of these two genera under L-DX condition suggest their potential CVOC tolerance. Genera *Sphingomonas* and *Devosia* were confirmed catalyst tolerant by both relative abundances and LEfSe, and both have been reported to carry dehydrogenases as biocatalysts (Zheng et al., 2017). Also, these two genera were enriched under L-DX condition after the catalysis process, which is inconsistent with their previous characterizations as chlorinated organic pollutant degraders (San Miguel et al., 2014), and may be caused by the added catalyst and intermediates after oxidation process. Thus, the community during the post-treatment state had a higher potential for CVOC degradation compared with the original microbiome. In addition, studies have shown that the Genera *Cylindrospermum* and *Novosphingobium* demonstrate nitrogen fixing (Padhy et al., 2014) and aromatic hydrocarbons degrading (Fida et al., 2017) characteristics, respectively. Under the H-DX/L-CV and L-DX/L-CV conditions, complex impacts on the microbial community were observed with no clear patterns, possibly due to accumulation of unknown degradation byproducts and intermediates that differed when compared with other conditions. Thus, fewer genera were highlighted by the LEfSe under H-DX/L-CV and L-DX/L-CV conditions.

The cluster analysis and PCoA clearly demonstrated the treatment train and CVOC impacts on the microbial community. Chen et al. (2016) reported that peroxide showed weak adverse effects on native microbes, but when coupled with 1,4-dioxane and CVOCs, as done in this study, peroxide may drive the microbial community shifts. The initially spiked 1,4-dioxane and CVOCs could be transformed into bioavailable products after exposure to peroxide, which could be used by some non-dominant microbes (Chen et al., 2016). Moreover, Eberle et al. (2016) confirmed that the degradation rate followed the sequence TCE > 1,4-dioxane > 1,1,1-TCA, thus L-DX condition without any CVOCs had no CVOCs-degradation products to stimulate microbes, and induced the

isolation of microbiomes under L-DX condition that was observed in the cluster analysis and PCoA. This mechanism could explain community shifts after the catalysis process due to residual 1,4-dioxane and CVOCs, as well as oxidation-produced byproducts, which could be further degraded by microbes. Because the catalysis process was also initialized by H_2O_2, the differences in microbial community changes between treatments might be related to the different peroxide concentrations, which has been reported by Richardson et al. (2011) when using persulfate in phenanthrene contaminated soil. Furthermore, microbiomes under L-DX after catalysis tended to approach the other conditions in cluster analysis, which may be due to catalyst impacts and the lower substrate amounts, and the self-rebound or recovery of the microbial community after oxidation, that have been observed after peroxide (Chen et al., 2016) and Fenton (Laurent et al., 2012) oxidation. This is in line with the PCoA based on unweighted Unifrac, that membership under L-DX condition were controlled more by the catalysis process, and approached the other conditions. While microbial abundances shown on weighted Unifrac PCoA depended more on the amount of substrates, since the L-DX group were still highly separated from other conditions. The multidimensional analysis showed a connection with LEfSe, in that more enriched unique genera were found under the L-DX condition that led to increased community diversity, but higher taxonomic ranks were shared in the rest conditions.

6.4.2 Oxidation and Biodegradation Treatment Train

Bioremediation is generally inhibited by co-contaminate CVOCs; with only a few specific bacterial taxa reported to metabolize or cometabolize 1,4-dioxane being unaffected. In this study, chemical oxidation as a non-selective treatment demonstrated 50-80% 1,4-dioxane removal regardless of the initial CVOCs stress. Post-oxidation bioaugmentation with 1,4-dioxane degrader *Pseudonocardia dioxanivorans* CB1190 (CB1190) removed the remaining 1,4-dioxane. TCE and

DCE were rapidly removed during the 12 hours oxidation phase, while 1,4-dioxane was depleted by 70-80%. This is consistent with oxidation studies that 1,4-dioxane was more difficult to degrade than chlorinated solvents (Eberle et al., 2016), but hydroxyl radicals generated during H_2O_2 decomposition could destroy the structure of 1,4-dioxane (Ikehata et al., 2016). H_2O_2 alone has been reported to be not as effective compared with O_3/H_2O_2 and UV/H_2O_2 technologies (Ikehata et al., 2016, Andaluri and Suri, 2017), but a dose of 0.96 mM successfully achieved the treatment goal for the biodegradation phase that followed oxidation. 1,1,1-TCA was only detected post-oxidation under the H-DX/H-CV condition. This condition also exhibited lower 1,4-dioxane removals, indicating lower susceptibility of TCA to chemical oxidation (Eberle et al., 2016) and its negative impact on 1,4-dioxane degradations. During the following 9-week biodegradation phase, the treatment objective of nearly complete 1,4-dioxane removal was accomplished only under the bioaugmentation condition (Bioaug), while no statistically significant 1,4-dioxane degradation was observed for the remaining non-bioaugmented conditions.

The systems that were bioaugmented with CB1190 degraded 1,4-dioxane completely, which is supported by the detection of dioxane monooxygenase (DXMO) encoding gene *dxmB* and aldehyde dehydrogenase (ALDH) encoding gene *aldH* (Gedalanga et al., 2014). This is consistent with the findings of Kim and Lee (2012) that biodegradation as a second step will achieve higher efficiency due to the addition of microorganisms expressing the appropriate biodegradative enzymes, which is in line with the objective of bioaugmentation. Unfortunately, both *dxmB* and *aldH* were not detected in the native samples during the incubation process, indicating a general lack of 1,4-dioxane degraders in the indigenous microbiomes in site materials. Both biomarker genes were detected in recent work that tracked a CVOC-free 1,4-dioxane plume with reasonable accuracy, and strongly suggested that the presence of these biomarkers was associated with 1,4-dioxane and

that microorganisms containing these biomarkers were degrading 1,4-dioxane (Gedalanga et al., 2016). The incomplete removals under non-bioaugmented conditions can likely be attributed to insufficient time to grow a sufficient population, in part because the initial abundance of metabolizing or co-metabolizing 1,4-dioxane degraders was low. In addition, the oxidation process may have released dissolved organic carbon (DOC) that was preferentially biodegraded by microorganisms over 1,4-dioxane; this process has been reported in oil-contaminated soil (Sutton et al., 2014). Moreover, the oxidation process appears to have inhibited intrinsic microorganisms which potentially biodegrade 1,4-dioxane due to microbial mortality and inactivation in the presence of hydroxyl radicals (Silva-Castro et al., 2013), and has been similarly reported for a diesel-contaminated site (Chen et al., 2016). 1,4-Dioxane oxidation by-products, including formaldehyde and glycolaldehyde, were reported to have geno- and cyto-toxicity (Li et al., 2018) that can also impact native bacteria as well as affect public and ecological health. By reducing the oxidant dose and thus reducing the expense and potential inhibitory effects associated with an oxidation-only treatment approach, the results of this study demonstrated that an oxidation-bioaugmentation strategy is able to completely remove 1,4-dioxane while reducing the economic and environmental concerns.

The biodiversity and richness generally decreased immediately after oxidation under each condition, and this pattern is consistent with previous studies that report dramatic declines in species richness and diversity after AOPs (Silva-Castro et al., 2013, Medina et al., 2018). However, the H-DX/H-CV condition showed no significant change, which could be related to the higher residual levels of 1,4-dioxane and TCA, indicating weaker oxidative effects on the microbial community in the presence of background 1,4-dioxane and TCA. The continuously decreasing biodiversity and richness were detected under H-DX/H-CV, H-DX/L-CV and L-DX/L-CV

conditions, and Medina et al. (2018) also found the similar post-oxidation decreases even for 1 month, while microorganisms under L-DX condition showed rapid recovery from OB2 to OB3. This comparison demonstrated that the initial CVOCs had negative impacts on the recovery of the microbial community even after the oxidation phase, potentially due to the accumulation of epoxide intermediates or byproducts of oxidized CVOCs (Li and Zhu, 2016). Moreover, the spiked CB1190 improved the richness and diversity even under Bioaug condition, showing the potential co-occurrence of species in the microcosms. A notable recovery of richness and diversity under all conditions was observed in the 9-week incubation, and this could be attributed to the adaption of functional microorganisms to the highly bioavailable oxidative products (Silva-Castro et al., 2013), and diverse communities tended to stabilize and contributed to ecosystem functions and service (Bell et al., 2005). This general decreasing-increasing biodiversity trend is consistent with previous studies with different oxidants, such as Fenton (Laurent et al., 2012), permanganate (Luhrs et al., 2006) and persulfate (Richardson et al., 2010), where microbial populations and diversity were reduced after oxidation, but recovered during post-treatment periods. Additionally, the oxidation phase might also induce mutations in microorganisms which could be transferred by horizontal gene transfer (HGT) and increase the community's overall tolerance to chemical oxidation (Wilson and Metcalf, 2005).

For the dynamics of taxonomic classification, taxa responded differently with various initial 1,4-dioxane and CVOCs. Members of Proteobacteria, especially the class Betaproteobacteria, were found to increase only under H-DX/H-CV condition, in line with the resistance to chlorinated compounds (Kao et al., 2016). However, both Beta- and Gamma-proteobacteria fluctuated during the post-AOP process, while only Alphaproteobacteria showed the same increasing trend after oxidation under all conditions, and dominated at OB4, indicating higher competitive capability.

The remaining TCA after oxidation under H-DX/H-CV induced slower recoveries of Firmicutes and Actinobacteria compared with other conditions, and inhibited Bacteroidetes, which thrived at OB4 under other conditions, indicating weak competition and sensitivity to chlorinated compounds (Lin et al., 2016). Furthermore, Cyanobacteria showed general tolerance to oxidative stress with increasing abundance, because they are equipped with glutaredoxin enzymes, ferredoxin enzymes, and fur-like regulators (Cassier-Chauvat and Chauvat, 2015). Interestingly, Firmicutes and Actinobacteria demonstrated oxidative tolerance with backgrounds of high 1,4-dioxane and low CVOCs, respectively. Bioaugmented CB1190 (belonging to Actinobacter) had simplified the composition and driven the change of phyla.

More specific to the genera level, some originally highly abundant genera, including *Pseudomonas, Massilla, Aquabacterium*, and *Variovorax*, were inhibited by the oxidation phase and decreased further in biodegradation phase, indicating that those genera were unable to overcome oxidative stress (Medina et al., 2018). However, the dominant *Pseudomonas* were composed of two main OTUs that showed opposite trends, and *Pseudomonas azotoformans* strain NBRC 12693 thrived after oxidation, which has been reported to have oxidative tolerance, while both *Pseudomonas* strains were inhibited during the biodegradation phase, indicating the co-exclusion with other microorganisms. Many more genera were found to resist oxidation, i.e., *Ralstonia, Gloeobacter*, *Pelomonas*, and *Streptococcus*, etc. Among them, *Ralstonia* was reported as a plant pathogen, and carries oxidative stress response regulator, *OxyR*, which was essential for the hydrogen peroxide stress response (Flores-Cruz and Allen, 2011). In addition, *Ralstonia* was also enriched in the dioxane-degrading consortia (He et al., 2017), which may also have been selected because of the remaining 1,4-dioxane. However, the substance and species information was uncertain in microcosms, and the CVOCs and chemical oxidation process might have impacts

on monooxygenase expression. Thus, the presence of *Ralstonia* does not necessarily indicate removal of 1,4-dioxane in this study. *Gloeobacter* belonging to *Cyanobacteria* was reported to be able to persist in ClO_2 conditions (Walden et al., 2015), and was confirmed to have tolerance to oxidation in this study. Moreover, along with the surge of biodiversity, more genera were classified during the 9-week incubation, represented by *Afipia*, *Pseudolabrys*, *Sphingomonas*, and *Cupriavidus*, etc. He et al. (2017) reported *Afipia* and *Cupriavidus* were enriched together from uncontaminated soil by using 1,4-dioxane, indicating the selection and stimulation of these microorganisms during our study by the remaining 1,4-dioxane in the microcosms, as well as their abilities to outcompete other microbes for resources. Despite *Afipia sp*. D1 demonstrated ability to degrade 1,4-dioxane as the sole carbon and energy source (Sei et al., 2013), the species in *Afipia* information was uncertain and accumulated genus *Afipia* in this study might need an extended incubation period. Besides, *Pseudolabrys*, *Sphingomonas*, and *Cupriavidus* were ubiquitous in hydrocarbon-rich soil, and identified as hydrocarbon degraders (Aislabie et al., 2006, Yang et al., 2014, Medina et al., 2018). These thriving genera imply that the remaining 1,4-dioxane and oxidized DOC provided rich carbon sources for competitive microorganisms. These types of detailed taxonomic information can help further evaluation of remediation work, and serve as a foundation for future ecosystem research.

The whole dynamic change and succession of microbial community during the combined treatment trains under each condition could also be explained by using analogous r/K-strategy (Medina et al., 2018), which described the relatively fast/unstable/competitive (r-Strategist) and slow/stable/equal (K-Strategist) growth conditions of microorganisms (Cycon et al., 2013). In this study, dominant microbes after oxidation at OB2 had higher resistance capability and less competition, identifying the K-Strategists under each condition. Afterward, the community

transferred from K- to r-strategy because of the initial adaption and competition during the early part of the biodegradation process. Samples from OB2 to OB3 were weak (thinner edges) or disordered connected, e.g., OB2_LL connected OB3_HH, OB2_L connected OB3_AUG, and this indicated an unstable or erroneous development of microbial community. More importantly, with the different levels of 1,4-dioxane and CVOCs, their degradation intermediates with various concentrations and compositions would also induce the versatile r-Strategists under different conditions, explaining the uneven distribution of microbial community and rebound of biodiversity at OB3. This was also defined as intermediate disturbance hypothesis (IDH), that intermediate levels of disturbance under different conditions would create patches at different levels of succession, promoting coexistence of microbes and competitors at the specific regime (Roxburgh et al., 2004). At the end of treatment train, more thriving genera/species increased and outcompeted weak ones after 9-weeks, and tended to be equitable with the indicator of higher richness and biodiversity, showing the signs of K-Strategy (Cycon et al., 2013). Moreover, samples within each condition at OB4 had stronger connections that were shown on thinner edges (Figure 4A), and connected with same condition samples at OB3 (e.g., OB3_L and OB4_L), but less connections with other samples, indicating the relatively stable status of microbial community at OB4.

Based on the dynamic successions, PCoA showed that the microbiomes under all conditions followed temporal succession and shared relatively similar developments of compositions and diversities along with operations. The membership of community (unweighted-Unifrac) at different time points grouped separately, and was evident with the biodiversity, indicating the deviation of microbiomes were more dependent on treatment progress. However, when the abundances of the community were taken into account, more overlaps were observed among groups, explicating that the successions were intercepted slightly by the different conditions within

the timelines. Thus, the populations followed the treatment trains changes that were relatively independent of the contaminant concentrations. This chronological change was defined as a deterministic process, and Vanwonterghem et al. (2014) similarly suggested that deterministic processes drove the community assembly with highly synchronized population dynamics in three individual cellulose-degrading bioreactors. Moreover, Ju et al. (2017) also described that the operating time, rather than physicochemical conditions (e.g., VFAs and NH_4-N) and operational parameters (i.e., SRT and OLR) directed the community variations and shifting trends. However, the level of contaminants could also play minor roles in determining and differentiating the detailed microbial progress just within the deterministic process. Interestingly, based on the weighted-Unifrac PCoA, samples at OB4 seemed to group along with the different conditions. Thus, cluster analysis grouping samples based on the relative dissimilarity showed that the microbial community developed in different ways at the end of biodegradation, as compared with other time points. This confirms that the richness and biodiversity thrived and blossomed, and also illustrates the impacts of conditions on the evolution of microbiomes. In addition, community at OB2 and OB3 tended to cluster together, indicating the transferred period of the system, partly in line with the above K-r transition. And the competition during the transition was also reflected in the network, that OTUs belonged to the same taxa were forcedly adaptive to different niches, and the turnover of OTUs among different niches, implicating the competition in guiding the structures (Ju et al., 2017). Moreover, co-exclusion was found even within same phylum, reflecting competition among these microorganisms for limited resources of essential growth factors (Nielsen et al., 2012). The inter-species co-occurrences could be due to the enzymatic associations within distinctive pathway modules, which has been revealed in carbohydrate metabolisms in wastewater treatment plants (Xia et al., 2015). Besides, inter-taxa connections in the same niche

were promoted with co-existences and interactions. Ju and Zhang (2015) suggested that inter-taxa co-occurrences among taxonomically distanced bacteria in activated sludge could be explained as species interactions (i.e., commensalism or mutualism). Phyla Cyanobacteria and Proteobacteria contained genes for sulfur compounds oxidation, that were found to co-occur in oxygenated environments (Wasmund et al., 2017), similar to oxidation condition in this study. Co-occurring multispecies were studied to make efficient use of limited resources through metabolite exchange due to temporal variation in nutritional availability, then provided a survival or thrived environments and enabled coexistence in diverse niches (Zelezniak et al., 2015). Thus, various competitions and metabolically complementary developments of microorganisms emerged during biodegradation phase (Li et al., 2018).

Under the Bioaug condition, the inoculated CB1190 removed 1,4-dioxane efficiently and showed negative correlations with species belonging to *Gloeobacter*, *Ralstonia*, *Mycobacterium*, *Janthinobacterium*, and *Variovorax*, etc., and the network analysis showed that CB1190 only had strongly positive connections with a few co-occurring taxonomically distanced genera (i.e., *Cupriavidus*) at the same modularity, demonstrating the valuable information that CB1190 and its distinct microorganisms were closely bound ecologically (Li et al., 2018). Coupled with the decreasing relative abundance, the survival and growth of CB1190 were compressed by other self-adaptive bacteria, even with additional CB1190 amendments, and this was partially agreeable with the inter-genera competition theory and the highlights of niche differences, which was reported in soil environment (Barberan et al., 2012). More importantly, in this study, the strong inter-order co-occurrence correlations implicated and projected the survival of pure and mixed bacterial cultures applied for bioaugmentation into specific environmental biogeochemical conditions.

6.4.3 Catalysis and Biodegradation Treatment Train

1,4-Dioxane and CVOCs have been widely reported co-contaminants in groundwater plumes across multiple contaminated sites (Adamson et al., 2015), and the inhibitory impact of individual/mixed CVOCs on the biodegradation kinetics of 1,4-dioxane has also been studied (Zhang et al., 2016). Therefore, the concept of the treatment train with combined catalytic oxidation and biological degradation mechanisms was used in this study, in order to reduce 1,4-dioxane and CVOC levels before biodegradation. The WO_x/ZrO_2-H_2O_2 system used 310 µM H_2O_2 to achieve ~20% 1,4-dioxane removals, which is a lower dosage than would be needed for pure H_2O_2 oxidation to achieve equivalent 1,4-dioxane removals (Miao et al., 2018). Andaluri and Suri (2017) also found that the oxidative efficiency of H_2O_2 alone for 1,4-dioxane was lower than that of the O_3/H_2O_2 process. Moreover, 1,4-dioxane decreased continuously even after the quench of the 24-hour catalytic oxidation phase, indicating the potential photoactivity of WO_x/ZrO_2 (Cheng et al., 2016). Similarly, chlorinated compounds were also mainly degraded by hydroxyl radicals, which was observed during electrochemical oxidation (Jasmann et al., 2017). More importantly, chlorinated compounds have been reported to be degraded using SO_4^{2-}/Fe_2O_3 catalysts (Zhang et al., 2018) and persulfate oxidation (Chang et al., 2018), but this study is the first to demonstrate TCE, 1,1-DCE, and cis-1,2-DCE catalysis by WO_x/ZrO_2. The higher removal efficiency of TCE than that of 1,4-dioxane was in line with the findings of Eberle et al. (2016) that TCE had a higher oxidative degradation rate than 1,4-dioxane. However, 1,1-DCE accumulated in the microcosms at higher levels than cis-1,2-DCE, suggesting that some combination of limited 1,1-DCE catalytic degradation occurred and/or 1,1-DCE was produced as a byproduct of TCE degradation. Furthermore, TCE and cis-1,2-DCE were completely degraded during the biodegradation phase under all conditions, indicating that aerobic bacteria removed these CVOCs by utilizing dissolved

oxygen from decomposed H_2O_2 (Li et al., 2015) and potential photoactivity. The increasing gene abundances of *dxmB* and *aldH* in the first four weeks after the CB1190 spike corresponded to the metabolism of 1,4-dioxane, and the higher *aldH* abundance indicated the availability of a diversity of carbon sources (Gedalanga et al., 2014). However, the non-detection of genes *dxmB and aldH* in naturally simulated microcosms indicates a lack of intrinsic 1,4-dioxane metabolizers. Additionally, the potential intrinsic 1,4-dioxane-co-metabolizing bacteria could have been reduced by the catalysis process and inhibited by produced hydroxyl radicals (Silva-Castro et al., 2013). The biodegradation of CVOCs is likely related to the intermediates produced during the catalysis phase, which acted as carbon sources to induce co-metabolism of CVOCs over 1,4-dioxane, that has been observed during the oxidation-bioremediation of a diesel-contaminated soil (Sutton et al., 2014).

The in-depth microbial community analysis explored the behavior of microbial communities under different 1,4-dioxane and CVOCs conditions over time. The original dominant genera, *Pseudomonas* and *Ralstonia*, were described by Sheu et al. (2018) to biodegrade chlorinated compounds in soil. However, both of these were reduced but not completely eliminated by the catalysis phase due to their weak peroxide tolerances or potentially lower oxidative stress regulators. However, the higher recovery of *Pseudomonas* during the biodegradation phase under the L-DX only condition suggests that *Pseudomonas* could consume the catalysis-produced intermediates, due to carrying alkanal monooxygenases alpha and beta chains, but had weak CVOC tolerances in this study. Genus *Sphingomonas* replaced *Pseudomonas* as the dominant genus after the catalysis phase, which was reported to remain active even after 500 mg/L H_2O_2 exposure (Dziga et al., 2018). Genera *Sphingomonas* and *Rhodococcus* were also reported to increase after chloropicrin fumigation in soil remediation, and thus utilized for the biodegradation of

toxic environmental contaminants (Li et al., 2017), that might be as hosts of cytochrome P450 families. However, genera *Rhodococcus* and *Variovorax* were found to be abundant after the first 9-week stage of the biodegradation phase, potentially due to their capabilities for co-metabolizing CVOC (Sercu et al., 2013), and they positively correlated with different enzymes. Moreover, *Ramlibacter* and *Methylobacillus*, both of which belong to Betaproteobacteria with many members that can degrade light hydrocarbons, increased during the biodegradation phase, and were identified in olive mill wastewaters (Kavroulakis and Ntougias, 2011), demonstrating potential consumptions of catalytic transformation products. Overall, besides the previously mentioned bacteria, the microbes that were enriched after 17 weeks of incubation were generally more capable of utilizing catalysis-produced intermediates and 1,4-dioxane/CVOC biodegradation products, e.g., *Ohtaekwangia* in hydrocarbon degradation (Ma et al., 2015), *Acidovorax* in carbon tetrachloride and trichloroethylene degradation (Kwon et al., 2016), and *Bradyrhizobium* in chlorinated compounds remediation (Krzmarzick and Novak, 2014), showing strong potential for long-term natural attenuation after engineered remediation. Even with the increasing absolute degradation gene abundances, the relative abundance of CB1190 decreased during the second stage of biodegradation, attributed to the potentially weak competition capability of CB1190 with other native microbes (Miao et al., 2019).

The stimulated biodiversity after catalytic oxidation was inconsistent with previous work that species richness and diversity dramatically declined after AOPs (Medina et al., 2018), which could be attributed to the lower dosage of H_2O_2 used in this study. On the other hand, WO_x/ZrO_2 and H_2O_2 might selectively impact the microbes that were the most abundant in the original microbial community (*Pseudomonas*), allowing the tolerant species to survive and increase in abundance to the point of detection, resulting in the compensation of microbial diversity (Miao et al., 2018),

identified by more representative microbes after catalysis on LEFSE analysis. The continuously increasing biodiversity in the first stage of biodegradation can be attributed to the generation of catalytic byproducts with enhanced solubility and biodegradability (Zhu et al., 2015) as well as reduced toxicity (Carboneras et al., 2018) that could better support microbial growth. The remaining CVOCs or degradation products under H/H conditions inhibited microbial richness and diversity during the second stage of biodegradation, and Liu et al. (2018) also observed decreasing diversity in vinyl chloride enriched groundwater. Tardy et al. (2014) suggested that biodiversity might increase with available soil resources, and enhanced functional and structural stability, explaining the CVOCs removals under lower H/H, H/L, and L/L-DX conditions. Overall, the biodiversity under each condition was enhanced after the whole treatment train, leading to a more stable microbial ecosystem in the soil for long-term resistance to future contaminant shocks.

The predicted functional features were not separated over the course of time except for the catalysis phase, and this was described as the functional redundancy that increased functional stability (Vanwonterghem et al., 2014), reflected on the stable abundances of pathways. The significant correlations between dehalogenases and multiple genera indicated the presence of widespread CVOC degradation potential, as well as the presence of phylogenetically distinct microbes that were able to fulfill the same functional group with potential functional redundancy (Myers et al., 2018). The high abundance of methane metabolism and methane monooxygenases could be attributed to ubiquitous methane-oxidizing bacteria (e.g., Proteobacteria), and catalytic oxidation improved bioavailability and oxygen content (Chen et al., 2018). Although 1,4-dioxane can be degraded by monooxygenase-containing bacteria (Mahendra et al., 2007), mesophilic methanotrophs, which are also known for cometabolic oxidation of halogenated compounds (Weigold et al., 2016), can rapidly oxidize TCE but not 1,4-dioxane during natural attenuation or

enhanced biodegradation (Hatzinger et al., 2017). The increasing abundance of chloroalkane and chloroalkene degradation in CVOC-containing conditions indicates a potential pathway for CVOC degradation, which has been previously identified as abundant in PCE/TCE-contaminated groundwater (Kao et al., 2016), and chlorinated hydrocarbon-contaminated sites (Kappell et al., 2014). Specifically, high abundances of haloalkane, haloacetate, and 2-haloacid dehalogenases could correspond to the existence of CVOCs (Weigold et al., 2016) and potential oxidative intermediate haloacetic acids from TCE (Chang et al., 2018). Moreover, cytochrome P450 family was found to carry peroxidase (Hrycay and Bandiera, 2012) that made it abundant, except for the H/H condition where CVOCs negatively impacted cytochrome P450. However, the remaining catalysts may also destroy cytochrome P450 (Hrycay and Bandiera, 2012) and contribute to its decreasing trends during the biodegradation phase. The stable abundances of methane and toluene monooxygenases had no improvement on 1,4-dioxane removals, likely due to the impacts of CVOCs on monooxygenase-driven degradation (Zhang et al., 2016) or invalidly expressed monooxygenases to 1,4-dioxane degradation (Mahendra and Alvarez-Cohen, 2006).

Although specific microbes changed among different conditions, a common temporal succession pattern in microbial assembly (including memberships and abundances) was shared across conditions over time, indicating the population dynamics in the complex community were mainly synchronized over time (Vanwonterghem et al., 2014), which is consistent with the findings from Ju et al. (2017) that shifts in the microbial community present an anaerobic biogas digestor were more dependent on operating time rather than physiochemical and operational parameters. This niche-based (e.g., nutrient/substrate availability, environmental selection, biological competition) deterministic temporal succession (Jiao et al., 2017) is supported by the PCoA and NMDS analyses that showed that microbes were temporally clustered. In addition, the LEFSE

analysis could only pick up changes in representative microbes between phases instead of between conditions. The initial catalysis phase removed contaminants to different levels, and microbes were separately clustered (CB0 vs. CB1), depicting the catalysis impact on microbial deterministic succession. Shi et al. (2018) also found the deterministic process in places with distinct environments that contained a few interchangeable bacteria. In the following first stage of the biodegradation phase, microbes were separated because of the access to the remaining oxidative products, while community compositions approached each other in similarity during the second stage, indicating the slow succession that could be attributed to decreasing availability of carbon sources, which has also been observed in microbial communities after heat disturbance (Jurburg et al., 2017). Moreover, the L-DX only condition exhibited the most dissimilar community post-treatment train, indicating that CVOCs can play minor roles in determining and differentiating the individual microbial progress just within the deterministic process. Vanwonterghem et al. (2014) indicated that even if microbial communities had minor differences at the specific time point, the communities as a whole would still follow similar trajectories, and Jiao et al. (2017) also observed similar dynamic patterns of microbial communities induced by individual or mixed contaminants (e.g., phenanthrene, n-octadecane). Furthermore, the microbes from CB1 to CB2 were dominated by r-strategists (fast/unstable/competitive condition) that led to relatively faster succession, because of the shocks caused by the H_2O_2 or the photoactivity of the remaining WO_x/ZrO_2. After this step, the increasing stability indicated by higher biodiversity and slower deviations between microbial communities indicated that the microcosms were occupied by K-strategists (slow/stable/same condition) (Jurburg et al., 2017) from CB2 to CB3. The gradual shift from r- to K-strategists along successional gradients has recently been shown for microbes in mercury- (Tardy et al., 2014) and hydrocarbon-contaminated (Medina et al., 2018) soils. Additionally, the

predictions from RF models also support the deterministic succession that the more similar distributions at day 63 and 119 indicates slower succession compared to the first stage of succession. The predicted microbes under the Bioaug condition were stable from day 63 to 119, showing the potential impacts and dominance of spiked CB1190 in the microbial community, and (Jiao et al., 2017) also reported that temporal microbial turnovers were mainly controlled by abundant bacteria which was mainly driven by deterministic processes.

Combined with taxonomy and functions, the dominant taxa might contribute primary functions in the community, while the rare/minor microbes could act as a source of functional diversity (Jiao et al., 2017). *Pseudomonas*, the dominant genus that rebounded during the biodegradation phase, was observed to co-occur with a diversity of minor community members, which is consistent with flower microbiota where the most prominent microbe co-occur with minor members (Shade et al., 2013). This inter-genera co-occurrence could be attributed to microbial interactions (e.g., commensalism or mutualism) (Ju and Zhang, 2015). Moreover, the minor microbes (e.g., *Bradyrhizobium* and *Variibacter*) also appear to be crucial in the co-occurring network by constructing connections among genotype-specific microbes, a pattern that has also been observed in lettuce root microbiota (Cardinale et al., 2015). Genera *Sphingomonas*, *Rhodococcus*, and *Lacibacter* were phylogenetically distinct and positively correlated in networks and identified catalytic tolerant in relative abundances, as determined by their functional relevance (Cardinale et al., 2015) in microcosms and confirmed by their carrying dehalogenases and cytochrome P450, simultaneously. Thelusmond et al. (2016) also reported that *Sphingomonas* and Rhodobacteraceae were linked to carbamazepine degradation. This phenomenon might result from their sharing the similar niches (e.g., environmental conditions), similar to what has been observed at a uranium contaminated site (Myers et al., 2018). Furthermore, *Pseudomonas* (OTU1) &

Sphingomonas (OTU18) and *Pseudomonas* (OTU1) & *Rhizobacter* (OTU13) were co-exclusive with each other and inter-taxa co-exclusion were prevalent in taxonomically distinct species (Ju and Zhang, 2015). The predicted functional feature showed that *Pseudomonas* (toluene monooxygenase) carried different genes from *Sphingomonas* (cytochrome P450) and *Rhizobacter* (methane monooxygenase), respectively, suggesting that the hosts might not carry toluene and alkanal monooxygenases with cytochrome P450 simultaneously. However, these enzymes were functionally equivariant, and fierce competition would happen among these microbes for limited nutrients, carbon substrates (e.g., 1,4-dioxane, CVOCs, and intermediates in this study), or other factors (Ju and Zhang, 2015). The network analysis also supports the deterministic process observed in this study that ecological niches, bacterial interactions, microbial competitions, and substrate availabilities, etc. could guide the community assembly and dynamics (Vanwonterghem et al., 2014). Additionally, the microbial turnovers (peaked abundances) along with time from Module III, V, VI to Modules I and IV in the co-occurrence networks suggested the gradual microbial shifts during the biodegradation phase, which highlights the role of interspecies competition for resources in intensifying community dynamics. These shifts have also been observed in anaerobic biogas digesters (Ju et al., 2017) and heat disturbed soil (Jurburg et al., 2017). The 1,4-dioxane and the CVOC-mediated deterministic process could also be related to high biodiversity, both of which corresponded to the microbial stability and high CVOCs removals.

6.5 Conclusions

In this study, 1,4-dioxane removal with co-contaminant CVOCs by novel oxidation-catalysis treatment train was achieved, and the effects of those contaminant levels and treatments on microbial community were evaluated. The oxidation process removed 85% of initial 1,4-dioxane under all conditions, and subsequent catalysis step extended the removal to 90%. The overall microbial

community analysis based on multidimensional analyses directly showed that H_2O_2 and WO_x/ZrO_2 caused population shifts away from the original community even with similar high removals. The taxonomic classification combined with LEfSe was used to determine the predominant microbes during the treatment train, and confirmed the potential oxidative tolerant genera, such as *Massilia* and *Rhodococcus*, as well as WO_x/ZrO_2 tolerant genera *Sphingomonas* and *Devosia*. The oxidation-catalysis treatment train shows promising results for future in-situ and *ex situ* field applications. This study is the first to assess microbiome shifts associated with an oxidation-catalysis treatment train for 1,4-dioxane and CVOC removal, and provides valuable guidance for the regulation and optimization of post-treatment bioremediation or microbial community recovery in groundwater and soils contaminated with solvent mixtures.

Chemical oxidation followed by bioaugmentation completely degraded 1,4-dioxane even in the presence of CVOC mixtures, confirming the effectiveness of treatment trains. Shifts in microbial community structures were in the course of treatment process, and influenced by contaminant concentrations at individual time points, and accompanied by r-K strategy transitions. Various microbial groups recovered after exposure to peroxide, a microbicide, and evolved during the biodegradation with deterministic factors, including competition, interaction and niche differentiation. Biodiversity and richness were inhibited right after oxidation process, but increased again during subsequent biodegradation process. It is important to consider the impact of abiotic and biological remediation technologies on the microbial ecology to predict success of short-term active treatment as well as long-term passive attenuation processes.

This study also evaluated the impacts of combined catalysis and biodegradation treatment trains for removing 1,4-dioxane and CVOCs on the microbial community under a selected set of contamination conditions. The data suggests that 1,4-dioxane degradation by CB1190 could be

catalytically enhanced, while CVOCs could be continuously removed during the post-catalysis biodegradation phase by intrinsic microbes regardless of the initial concentrations. This combined technology is an innovative approach to simultaneously degrade refractory pollutants using a combination of bioaugmented and intrinsic microbes that may serve as a promising alternative in-situ remediation strategy for practitioners. Moreover, the microbial community analysis indicated a more stable structure under all conditions after the treatment train with a higher biodiversity of microbes with biodegradation capabilities. The predicted functional features found that reads belonging to monooxygenases remained constant during the biodegradation phase while reads belonging to dehalogenases increased, and this pattern corresponded to increasing CVOC removals. The population dynamics followed deterministic temporal succession even under different contamination conditions, which was supported by the PCoA analysis and random forests models. The network analysis further emphasized deterministic factors, such as ecological niches or microbial competitions, overwhelmed contaminants combinations matrix, dominating and guiding the microbial assembly. The above findings offer novel insights into the ecological mechanisms underlying the effects of 1,4-dioxane and CVOCs on short-term and long-term remediation performance. Combined, the compositions of bacterial communities, as well as the associations among the members of those communities, established in this study could serve as the theoretical foundation for improved treatment applications.

6.6 References

Adamson, D., Newell, C., Mahendra, S., Bryant, D., Wong, M., 2017. In situ treatment and management strategies for 1,4-dioxane-contaminated groundwater. GSI Environmental Inc. Houston United States. SERDP Project ER-2307.

Adamson, D.T., Anderson, R.H., Mahendra, S., Newell, C.J., 2015. Evidence of 1,4-dioxane attenuation at groundwater sites contaminated with chlorinated solvents and 1,4-dioxane. Environmental Science & Technology, 49 (11), 6510-6518.

Aislabie, J., Saul, D.J., Foght, J.M., 2006. Bioremediation of hydrocarbon-contaminated polar soils. Extremophiles, 10 (3), 171-179.

Andaluri, G., Suri, R., 2017. Removal of 1,4-dioxane and volatile organic compounds from groundwater using ozone-based advanced oxidation process. Ozone-Science & Engineering, 39 (6), 423-434.

Anderson, R.H., Anderson, J.K., Bower, P.A., 2012. Co-occurrence of 1,4-dioxane with trichloroethylene in chlorinated solvent groundwater plumes at US Air Force installations: Fact or fiction. Integrated Environmental Assessment and Management, 8 (4), 731-737.

Aßhauer, K.P., Wemheuer, B., Daniel, R., Meinicke, P., 2015. Tax4Fun: Predicting functional profiles from metagenomic 16S rRNA data. Bioinformatics, 31 (17), 2882-2884.

Barberan, A., Bates, S.T., Casamayor, E.O., Fierer, N., 2012. Using network analysis to explore co-occurrence patterns in soil microbial communities. The ISME Journal, 6 (2), 343-351.

Barndok, H., Hermosilla, D., Han, C., Dionysiou, D.D., Negro, C., Blanco, A., 2016. Degradation of 1,4-dioxane from industrial wastewater by solar photocatalysis using immobilized NF-TiO_2 composite with monodisperse TiO_2 nanoparticles. Applied Catalysis B: Environmental, 180, 44-52.

Bastian, M., Heymann, S., Jacomy, M., 2009. Gephi: an open source software for exploring and manipulating networks. Proceedings of the Third International ICWSM Conference.

Belk, A., Xu, Z.Z., Carter, D.O., Lynne, A., Bucheli, S., Knight, R., Metcalf, J.L., 2018. Microbiome data accurately predicts the postmortem interval using random forest regression models. Genes, 9 (2), 104.

Bell, T., Newman, J.A., Silverman, B.W., Turner, S.L., Lilley, A.K., 2005. The contribution of species richness and composition to bacterial services. Nature, 436 (7054), 1157-1160.

Bidaud, P., Hebert, L., Barbey, C., Appourchaux, A.C., Torelli, R., Sanguinetti, M., Laugier, C., Petry, S., 2012. *Rhodococcus equi*'s extreme resistance to hydrogen peroxide is mainly conferred by one of its four catalase genes. Plos One, 7 (8), e42396.

Carboneras, M.B., Cañizares, P., Rodrigo, M.A., Villaseñor, J., Fernandez-Morales, F.J., 2018. Improving biodegradability of soil washing effluents using anodic oxidation. Bioresource Technology, 252, 1-6.

Cardinale, M., Grube, M., Erlacher, A., Quehenberger, J., Berg, G., 2015. Bacterial networks and co- occurrence relationships in the lettuce root microbiota. Environmental Microbiology, 17 (1), 239-252.

Cassier-Chauvat, C., Chauvat, F., 2015. Responses to oxidative and heavy metal stresses in *Cyanobacteria*: Recent advances. International Journal of Molecular Sciences, 16 (1), 871-886.

Chang, Y.-C., Chen, T.-Y., Tsai, Y.-P., Chen, K.-F., 2018. Remediation of trichloroethene (TCE)-contaminated groundwater by persulfate oxidation: a field-scale study. RSC Advances, 8 (5), 2433-2440.

Chao, Y.Q., Liu, W.S., Chen, Y.M., Chen, W.H., Zhao, L.H., Ding, Q.B., Wang, S.Z., Tang, Y.T., Zhang, T., Qiu, R.L., 2016. Structure, variation, and co-occurrence of soil microbial communities in abandoned sites of a rare earth elements mine. Environmental Science & Technology, 50 (21), 11481-11490.

Chen, K.F., Chang, Y.C., Chiou, W.T., 2016. Remediation of diesel-contaminated soil using in situ chemical oxidation (ISCO) and the effects of common oxidants on the indigenous microbial community: A comparison study. Journal of Chemical Technology and Biotechnology, 91 (6), 1877-1888.

Chen, T., Rodrigues, S., Golding, S.D., Rudolph, V., 2018. Improving coal bioavailability for biogenic methane production via hydrogen peroxide oxidation. International Journal of Coal Geology, 195, 402-414.

Cheng, M., Zeng, G.M., Huang, D.L., Lai, C., Xu, P., Zhang, C., Liu, Y., 2016. Hydroxyl radicals based advanced oxidation processes (AOPs) for remediation of soils contaminated with organic compounds: A review. Chemical Engineering Journal, 284, 582-598.

Chitra, S., Paramasivan, K., Cheralathan, M., Sinha, P.K., 2012. Degradation of 1,4-dioxane using advanced oxidation processes. Environmental Science and Pollution Research, 19 (3), 871-878.

Choi, P.G., Nunotani, N., Imanaka, N., 2017. High catalytic efficiency in liquid-phase oxidation of 1,4-dioxane using a Pt/CeO_2-ZrO_2-SnO_2/SBA-16 catalyst. International Journal of Applied Ceramic Technology, 14 (1), 9-15.

Cycon, M., Markowicz, A., Piotrowska-Seget, Z., 2013. Structural and functional diversity of bacterial community in soil treated with the herbicide napropamide estimated by the DGGE, CLPP and r/K-strategy approaches. Applied Soil Ecology, 72, 242-250.

Deng, D., Lin, X., Ou, J., Wang, Z., Li, S., Deng, M., Shu, Y., 2015. Efficient chemical oxidation of high levels of soil-sorbed phenanthrene by ultrasound induced, thermally activated persulfate. Chemical Engineering Journal, 265, 176-183.

Dingman, D.W., 2011. Inactivation of *Paenibacillus larvae* endospores by a hydrogen peroxide/peroxyacetic acid biocide. Journal of Apicultural Research, 50 (2), 173-175.

Dziga, D., Maksylewicz, A., Maroszek, M., Marek, S., 2018. Combined treatment of toxic cyanobacteria *Microcystis aeruginosa* with hydrogen peroxide and microcystin biodegradation agents results in quick toxins elimination. Acta Biochimica Polonica, 65, 133-140.

Eberle, D., Ball, R., Boving, T.B., 2016. Peroxone activated persulfate treatment of 1,4-dioxane in the presence of chlorinated solvent co-contaminants. Chemosphere, 144, 728-735.

Feng, Y., Lee, P.H., Wu, D.L., Shih, K.M., 2017. Surface-bound sulfate radical-dominated degradation of 1,4-dioxane by alumina-supported palladium (Pd/Al_2O_3) catalyzed peroxymonosulfate. Water Research, 120, 12-21.

Fida, T.T., Moreno-Forero, S.K., Breugelmans, P., Heipieper, H.J., Röling, W.F., Springael, D., 2017. Physiological and transcriptome response of the polycyclic aromatic hydrocarbon degrading *Novosphingobium* sp. LH128 after Inoculation in soil. Environmental Science & Technology, 51 (3), 1570-1579.

Flores-Cruz, Z., Allen, C., 2011. Necessity of *oxyR* for the hydrogen peroxide stress response and full virulence in *Ralstonia solanacearum*. Applied and Environmental Microbiology, 77 (18), 6426-6432.

Gedalanga, P., Madison, A., Miao, Y., Richards, T., Hatton, J., DiGuiseppi, W.H., Wilson, J., Mahendra, S., 2016. A multiple lines of evidence framework to evaluate intrinsic biodegradation of 1,4-dioxane. Remediation Journal, 27 (1), 93-114.

Gedalanga, P.B., Pornwongthong, P., Mora, R., Chiang, S.Y.D., Baldwin, B., Ogles, D., Mahendra, S., 2014. Identification of biomarker genes to predict biodegradation of 1,4-dioxane. Applied and Environmental Microbiology, 80 (10), 3209-3218.

Gu, Z.G., Eils, R., Schlesner, M., 2016. Complex heatmaps reveal patterns and correlations in multidimensional genomic data. Bioinformatics, 32 (18), 2847-2849.

Gururani, M.A., Upadhyaya, C.P., Baskar, V., Venkatesh, J., Nookaraju, A., Park, S.W., 2013. Plant growth-promoting *Rhizobacteria* enhance abiotic stress tolerance in solanum tuberosum through inducing changes in the expression of ROS-scavenging enzymes and improved photosynthetic performance. Journal of Plant Growth Regulation, 32 (2), 245-258.

Hall, E.A., Bell, S.G., 2015. The efficient and selective biocatalytic oxidation of norisoprenoid and aromatic substrates by CYP101B1 from *Novosphingobium aromaticivorans* DSM12444. RSC Advances, 5 (8), 5762-5773.

Handtke, S., Schroeter, R., Jurgen, B., Methling, K., Schluter, R., Albrecht, D., van Hijum, S.A.F.T., Bongaerts, J., Maurer, K.H., Lalk, M., Schweder, T., Hecker, M., Voigt, B., 2014. *Bacillus pumilus* reveals a remarkably high resistance to hydrogen peroxide provoked oxidative stress. Plos One, 9 (1), e85625.

Hatzinger, P.B., Banerjee, R., Rezes, R., Streger, S.H., McClay, K., Schaefer, C.E., 2017. Potential for cometabolic biodegradation of 1,4-dioxane in aquifers with methane or ethane as primary substrates. Biodegradation, 28 (5-6), 453-468.

He, Y., Mathieu, J., Silva, M.L., Li, M., Alvarez, P.J., 2017. 1,4- Dioxane- degrading consortia can be enriched from uncontaminated soils: Prevalence of *Mycobacterium* and soluble di-iron monooxygenase genes. Microbial Biotechnology, 11 (1), 189-198.

Heck, K.N., Wang, Y., Wu, G., Wang, F., Tsai, A.-l., Wong, M.S., 2018. Hydrogen peroxide degrades 1,4-dioxane in the presence of metal oxide catalysts. Environmental Science & Technology Letters (Submitted).

Hrycay, E.G., Bandiera, S.M., 2012. The monooxygenase, peroxidase, and peroxygenase properties of cytochrome P450. Archives of Biochemistry and Biophysics, 522 (2), 71-89.

Ikehata, K., Wang-Staley, L., Qu, X.Y., Li, Y., 2016. Treatment of groundwater contaminated with 1,4-dioxane, tetrahydrofuran, and chlorinated volatile organic compounds using advanced oxidation processes. Ozone-Science & Engineering, 38 (6), 413-424.

Inoue, D., Tsunoda, T., Sawada, K., Yamamoto, N., Saito, Y., Sei, K., Ike, M., 2016. 1,4-Dioxane degradation potential of members of the genera *Pseudonocardia* and *Rhodococcus*. Biodegradation, 27 (4-6), 277-286.

Jasmann, J.R., Gedalanga, P.B., Borch, T., Mahendra, S., Blotevogel, J., 2017. Synergistic treatment of mixed 1,4-dioxane and chlorinated solvent contaminations by coupling electrochemical oxidation with aerobic biodegradation. Environmental Science & Technology, 51 (21), 12619-12629.

Jiao, S., Luo, Y., Lu, M., Xiao, X., Lin, Y., Chen, W., Wei, G., 2017. Distinct succession patterns of abundant and rare bacteria in temporal microcosms with pollutants. Environmental Pollution, 225, 497-505.

Jiao, S., Zhang, Z., Yang, F., Lin, Y., Chen, W., Wei, G., 2017. Temporal dynamics of microbial communities in microcosms in response to pollutants. Molecular Ecology, 26 (3), 923-936.

Ju, F., Lau, F., Zhang, T., 2017. Linking microbial community, environmental variables, and methanogenesis in anaerobic biogas digesters of chemically enhanced primary treatment sludge. Environmental Science & Technology, 51 (7), 3982-3992.

Ju, F., Zhang, T., 2015. Bacterial assembly and temporal dynamics in activated sludge of a full-scale municipal wastewater treatment plant. The ISME Journal, 9 (3), 683-695.

Jurburg, S.D., Nunes, I., Stegen, J.C., Le Roux, X., Priemé, A., Sørensen, S.J., Salles, J.F., 2017. Autogenic succession and deterministic recovery following disturbance in soil bacterial communities. Scientific Reports, 7, 45691.

Kao, C.-M., Liao, H.-Y., Chien, C.-C., Tseng, Y.-K., Tang, P., Lin, C.-E., Chen, S.-C., 2016. The change of microbial community from chlorinated solvent-contaminated groundwater after biostimulation using the metagenome analysis. Journal of Hazardous Materials, 302, 144-150.

Kappell, A.D., Wei, Y., Newton, R.J., Van Nostrand, J.D., Zhou, J., McLellan, S.L., Hristova, K.R., 2014. The polycyclic aromatic hydrocarbon degradation potential of Gulf of Mexico native coastal microbial communities after the deepwater horizon oil spill. Frontiers in Microbiology, 5, 205.

Kaufman, L., Rousseeuw, P.J. (2009). Finding groups in data: an introduction to cluster analysis, 344, John Wiley & Sons, New York.

Kavroulakis, N., Ntougias, S., 2011. Bacterial and β-Proteobacterial diversity in *Olea europaea* var. *mastoidis*- and *O. europaea* var. *koroneiki*-generated olive mill wastewaters: influence of cultivation and harvesting practice on bacterial community structure. World Journal of Microbiology and Biotechnology, 27 (1), 57-66.

Kim, I., Lee, M., 2012. Pilot scale feasibility study for in-situ chemical oxidation using H_2O_2 solution conjugated with biodegradation to remediate a diesel contaminated site. Journal of Hazardous Materials, 241, 173-181.

Klindworth, A., Pruesse, E., Schweer, T., Peplies, J., Quast, C., Horn, M., Glöckner, F.O., 2013. Evaluation of general 16S ribosomal RNA gene PCR primers for classical and next-generation sequencing-based diversity studies. Nucleic Acids Research, 41 (1), e1.

Krzmarzick, M.J., Novak, P.J., 2014. Removal of chlorinated organic compounds during wastewater treatment: Achievements and limits. Applied Microbiology and Biotechnology, 98 (14), 6233-6242.

Kwon, K., Shim, H., Bae, W., Oh, J., Bae, J., 2016. Simultaneous biodegradation of carbon tetrachloride and trichloroethylene in a coupled anaerobic/aerobic biobarrier. Journal of Hazardous Materials, 313, 60-67.

Lan, R.S., Smith, C.A., Hyman, M.R., 2013. Oxidation of cyclic ethers by alkane- grown *Mycobacterium vaccae* JOB5. Remediation Journal, 23 (4), 23-42.

Laurent, F., Cebron, A., Schwartz, C., Leyval, C., 2012. Oxidation of a PAH polluted soil using modified Fenton reaction in unsaturated condition affects biological and physico-chemical properties. Chemosphere, 86 (6), 659-664.

Lefevre, E., Bossa, N., Wiesner, M.R., Gunsch, C.K., 2016. A review of the environmental implications of in situ remediation by nanoscale zero valent iron (nZVI): Behavior, transport and impacts on microbial communities. Science of the Total Environment, 565, 889-901.

Li, B., Wu, W.M., Watson, D.B., Cardenas, E., Chao, Y., Phillips, D.H., Mehlhorn, T., Lowe, K., Kelly, S.D., Li, P., Tao, H., Tiedje, J.M., Criddle, C.S., Zhang, T., 2018. Bacterial community shift and coexisting/coexcluding patterns revealed by network analysis in a uranium-contaminated site after bioreduction followed by reoxidation. Applied and Environmental Microbiology, 84 (9), e02885-02817.

Li, B.Z., Zhu, J., 2016. Simultaneous degradation of 1,1,1-trichloroethane and solvent stabilizer 1,4-dioxane by a sono-activated persulfate process. Chemical Engineering Journal, 284, 750-763.

Li, H., Zhang, S.-y., Wang, X.-l., Yang, J., Gu, J.-d., Zhu, R.-l., Wang, P., Lin, K.-f., Liu, Y.-d., 2015. Aerobic biodegradation of trichloroethylene and phenol co-contaminants in groundwater by a bacterial community using hydrogen peroxide as the sole oxygen source. Environmental Technology, 36 (5), 667-674.

Li, J., Huang, B., Wang, Q., Li, Y., Fang, W., Yan, D., Guo, M., Cao, A., 2017. Effect of fumigation with chloropicrin on soil bacterial communities and genes encoding key enzymes involved in nitrogen cycling. Environmental Pollution, 227, 534-542.

Li, J.H., Lu, Q.H., de Toledo, R.A., Lu, Y., Shim, H., 2015. Effect of toluene concentration and hydrogen peroxide on *Pseudomonas plecoglossicida* cometabolizing mixture of cis-DCE and TCE in soil slurry. Environmental Geochemistry and Health, 37 (6), 985-995.

Li, M.Y., Conlon, P., Fiorenza, S., Vitale, R.J., Alvarez, P.J.J., 2011. Rapid analysis of 1,4-dioxane in groundwater by frozen micro-extraction with gas chromatography/mass spectrometry. Ground Water Monitoring and Remediation, 31 (4), 70-76.

Li, M.Y., Fiorenza, S., Chatham, J.R., Mahendra, S., Alvarez, P.J.J., 2010. 1,4-Dioxane biodegradation at low temperatures in Arctic groundwater samples. Water Research, 44 (9), 2894-2900.

Li, M.Y., van Orden, E.T., DeVries, D.J., Xiong, Z., Hinchee, R., Alvarez, P.J., 2015. Bench-scale biodegradation tests to assess natural attenuation potential of 1,4-dioxane at three sites in California. Biodegradation, 26 (1), 39-50.

Li, W., Xu, E., Schlenk, D., Liu, H.Z., 2018. Cyto- and geno- toxicity of 1,4-dioxane and its transformation products during ultraviolet-driven advanced oxidation processes. Environmental Science: Water Research & Technology, 4 (9), 1213-1218.

Lin, Y.W., Li, D., Zeng, S.Y., He, M., 2016. Changes of microbial composition during wastewater reclamation and distribution systems revealed by high-throughput sequencing analyses. Frontiers of Environmental Science & Engineering, 10 (3), 539-547.

Liu, X., Wu, Y., Wilson, F.P., Yu, K., Lintner, C., Cupples, A.M., Mattes, T.E., 2018. Integrated methodological approach reveals microbial diversity and functions in aerobic groundwater microcosms adapted to vinyl chloride. FEMS Microbiology Ecology, 94 (9), fiy124.

Lobo, M.C., Pérez-Sanz, A., Gil-Diaz, M.M., Plaza, A. (2014). Encyclopedia of Applied Electrochemistry. Kreysa, G., Ota, K.-i. and Savinell, R. F. (eds), pp. 1982-1988, Springer New York, New York, NY.

Luhrs, R., Lewis, R., Huling, S., 2006. ISCO's long-term impact on aquifer conditions and microbial activity. Proceedings of the fifth international conference on remediation of chlorinated and recalcitrant compounds. Battelle, Monterey, pp D-48.

Ma, Q., Qu, Y.-Y., Zhang, X.-W., Shen, W.-L., Liu, Z.-Y., Wang, J.-W., Zhang, Z.-J., Zhou, J.-T., 2015. Identification of the microbial community composition and structure of coal-mine wastewater treatment plants. Microbiological Research, 175, 1-5.

Mahendra, S., Alvarez-Cohen, L., 2005. *Pseudonocardia dioxanivorans* sp nov., a novel actinomycete that grows on 1,4-dioxane. International Journal of Systematic and Evolutionary Microbiology, 55, 593-598.

Mahendra, S., Alvarez-Cohen, L., 2006. Kinetics of 1, 4-dioxane biodegradation by monooxygenase-expressing bacteria. Environmental Science & Technology, 40 (17), 5435-5442.

Mahendra, S., Grostern, A., Alvarez-Cohen, L., 2013. The impact of chlorinated solvent co-contaminants on the biodegradation kinetics of 1,4-dioxane. Chemosphere, 91 (1), 88-92.

Mahendra, S., Petzold, C.J., Baidoo, E.E., Keasling, J.D., Alvarez-Cohen, L., 2007. Identification of the intermediates of in vivo oxidation of 1, 4-dioxane by monooxygenase-containing bacteria. Environmental Science & Technology, 41 (21), 7330-7336.

McMurdie, P.J., Holmes, S., 2013. Phyloseq: An R package for reproducible interactive analysis and graphics of microbiome gensus data. Plos One, 8 (4), e61217.

Medina, R., Gara, P.M.D., Fernandez-Gonzalez, A.J., Rosso, J.A., Del Panno, M.T., 2018. Remediation of a soil chronically contaminated with hydrocarbons through persulfate oxidation and bioremediation. Science of the Total Environment, 618, 518-530.

Metcalf, J.L., Xu, Z.Z., Weiss, S., Lax, S., Van Treuren, W., Hyde, E.R., Song, S.J., Amir, A., Larsen, P., Sangwan, N., Haarmann, D., Humphrey, G.C., Ackermann, G., Thompson, L.R., Lauber, C., Bibat, A., Nicholas, C., Gebert, M.J., Petrosino, J.F., Reed, S.C., Gilbert, J.A., Lynne, A.M., Bucheli, S.R., Carter, D.O., Knight, R., 2016. Microbial community assembly and metabolic function during mammalian corpse decomposition. Science, 351 (6269), 158-162.

Miao, Y., Johnson, N.W., Gedalanga, P.B., Adamson, D., Newell, C., Mahendra, S., 2019. Response and recovery of microbial communities subjected to oxidative and biological treatments of 1,4-dioxane and co-contaminants. Water Research, 149, 74-85.

Miao, Y., Johnson, N.W., Heck, K., Guo, S., Powell, C.D., Phan, T., Gedalanga, P.B., Adamson, D.T., Newell, C.J., Wong, M.S., Mahendra, S., 2018. Microbial responses to combined oxidation and catalysis treatment of 1,4-dioxane and co-contaminants in groundwater and soil. Frontiers of Environmental Science & Engineering, 12 (5), 1-13.

Miao, Y., Liao, R.H., Zhang, X.X., Wang, Y., Wang, Z., Shi, P., Liu, B., Li, A.M., 2015. Metagenomic insights into Cr(VI) effect on microbial communities and functional genes of an expanded granular sludge bed reactor treating high-nitrate wastewater. Water Research, 76, 43-52.

Miao, Y., Wang, Z., Liao, R.H., Shi, P., Li, A.M., 2017. Assessment of phenol effect on microbial community structure and function in an anaerobic denitrifying process treating high concentration nitrate wastewater. Chemical Engineering Journal, 330, 757-763.

Miao, Y., Zhang, X.-X., Jia, S., Liao, R., Li, A., 2018. Comprehensive analyses of functional bacteria and genes in a denitrifying EGSB reactor under Cd(II) stress. Applied Microbiology and Biotechnology, 1-10.

Mohr, T.K.G., Stickney, J.A., DiGuiseppi, W.H. (2010). Environmental investigation and remediation: 1,4-Dioxane and other solvent stabilizers, CRC Press, Taylor & Francis Group, Boca Raton, Florida.

Munakata-Marr, J., Sorenson, K.S., Petri, B.G., Cummings, J.B., 2011. Principles of combining ISCO with other in situ remedial approaches. In Situ Chemical Oxidation for Groundwater Remediation, 285-317.

Myers, M., Johnson, N.W., Zerecero-Marin, E., Pornwongthong, P., Liu, Y., Gedalanga, P.B., S., M., 2018. Abiotic and bioaugmented granular activated carbon for the treatment of 1,4-dioxane-contaminated water. Environmental Pollution, 240, 916-924.

Nemecek, J., Pokorny, P., Lhotsky, O., Knytl, V., Najmanova, P., Steinova, J., Cernik, M., Filipova, A., Filip, J., Cajthaml, T., 2016. Combined nano-biotechnology for in-situ remediation of mixed contamination of groundwater by hexavalent chromium and chlorinated solvents. Science of the Total Environment, 563, 822-834.

Nielsen, P.H., Saunders, A.M., Hansen, A.A., Larsen, P., Nielsen, J.L., 2012. Microbial communities involved in enhanced biological phosphorus removal from wastewater - a model system in environmental biotechnology. Current Opinion in Biotechnology, 23 (3), 452-459.

Padhy, R.N., Nayak, N., Rath, S., 2014. Antagonism at combined effects of chemical fertilizers and carbamate insecticides on the rice-field N_2-fixing cyanobacterium *Cylindrospermum* sp. in vitro. Interdisciplinary Toxicology, 7 (1), 5-11.

Pornwongthong, P., Mulchandani, A., Gedalanga, P.B., Mahendra, S., 2014. Transition metals and organic ligands influence biodegradation of 1,4-dioxane. Applied Biochemistry and Biotechnology, 173 (1), 291-306.

Pornwongthong, P., Mulchandani, A., Gedalanga, P.B., Mahendra, S., 2014. Transition metals and organic ligands influence biodegradation of 1,4-dioxane. Applied Biochemistry and Biotechnology, 173 (1), 291-306.

Richardson, S.D., Lebron, B.L., Miller, C.T., Aitken, M.D., 2010. Recovery of phenanthrene-degrading bacteria after simulated *in situ* persulfate oxidation in contaminated soil. Environmental Science & Technology, 45 (2), 719-725.

Roxburgh, S.H., Shea, K., Wilson, J.B., 2004. The intermediate disturbance hypothesis: Patch dynamics and mechanisms of species coexistence. Ecology, 85 (2), 359-371.

San Miguel, A., Roy, J., Gury, J., Monier, A., Coissac, E., Ravanel, P., Geremia, R.A., Raveton, M., 2014. Effects of organochlorines on microbial diversity and community structure in *Phragmites australis* rhizosphere. Applied Microbiology and Biotechnology, 98 (9), 4257-4266.

Santiago, A.J., Ahmed, M.N.A., Wang, S.L., Damera, K., Wang, B.G., Tai, P.C., Gilbert, E.S., Derby, C.D., 2016. Inhibition and dispersal of *Pseudomonas aeruginosa* biofilms by combination treatment with escapin intermediate products and hydrogen peroxide. Antimicrobial Agents and Chemotherapy, 60 (9), 5554-5562.

Schloss, P.D., Westcott, S.L., Ryabin, T., Hall, J.R., Hartmann, M., Hollister, E.B., Lesniewski, R.A., Oakley, B.B., Parks, D.H., Robinson, C.J., Sahl, J.W., Stres, B., Thallinger, G.G., Van Horn, D.J., Weber, C.F., 2009. Introducing mothur: open-source, platform-independent, community-supported software for describing and comparing microbial communities. Applied and Environmental Microbiology, 75 (23), 7537-7541.

Segata, N., Izard, J., Waldron, L., Gevers, D., Miropolsky, L., Garrett, W.S., Huttenhower, C., 2011. Metagenomic biomarker discovery and explanation. Genome Biology, 12 (6).

Sei, K., Kakinoki, T., Inoue, D., Soda, S., Fujita, M., Ike, M., 2010. Evaluation of the biodegradation potential of 1,4-dioxane in river, soil and activated sludge samples. Biodegradation, 21 (4), 585-591.

Sei, K., Miyagaki, K., Kakinoki, T., Fukugasako, K., Inoue, D., Ike, M., 2013. Isolation and characterization of bacterial strains that have high ability to degrade 1,4-dioxane as a sole carbon and energy source. Biodegradation, 24 (5), 665-674.

Sekar, R., Taillefert, M., DiChristinaa, T.J., 2016. Simultaneous transformation of commingled trichloroethylene, tetrachloroethylene, and 1,4-dioxane by a microbially driven fenton reaction in batch liquid cultures. Applied and Environmental Microbiology, 82 (21), 6335-6343.

Sercu, B., Jones, A.D., Wu, C.H., Escobar, M.H., Serlin, C.L., Knapp, T.A., Andersen, G.L., Holden, P.A., 2013. The influence of in situ chemical oxidation on microbial community composition in groundwater contaminated with chlorinated solvents. Microbial Ecology, 65 (1), 39-49.

Shade, A., McManus, P.S., Handelsman, J., 2013. Unexpected diversity during community succession in the apple flower microbiome. MBio, 4 (2), e00602-00612.

Sheu, Y.-T., Tsang, D.C., Dong, C.-D., Chen, C.-W., Luo, S.-G., Kao, C.-M., 2018. Enhanced bioremediation of TCE-contaminated groundwater using gamma poly-glutamic acid as the primary substrate. Journal of Cleaner Production, 178, 108-118.

Shi, Y., Li, Y., Xiang, X., Sun, R., Yang, T., He, D., Zhang, K., Ni, Y., Zhu, Y.-G., Adams, J.M., 2018. Spatial scale affects the relative role of stochasticity versus determinism in soil bacterial communities in wheat fields across the North China Plain. Microbiome, 6: 27, 1-12.

Silva-Castro, G.A., Rodelas, B., Perucha, C., Laguna, J., Gonzalez-Lopez, J., Calvo, C., 2013. Bioremediation of diesel-polluted soil using biostimulation as post-treatment after oxidation with Fenton-like reagents: Assays in a pilot plant. Science of the Total Environment, 445, 347-355.

Simonin, M., Richaume, A., 2015. Impact of engineered nanoparticles on the activity, abundance, and diversity of soil microbial communities: A review. Environmental Science and Pollution Research, 22 (18), 13710-13723.

Soultanidis, N., Zhou, W., Psarras, A.C., Gonzalez, A.J., Iliopoulou, E.F., Kiely, C.J., Wachs, I.E., Wong, M.S., 2010. Relating n-pentane isomerization activity to the tungsten surface density of WO_x/ZrO_2. Journal of the American Chemical Society, 132 (38), 13462-13471.

Suthersan, S., Quinnan, J., Horst, J., Ross, I., Kalve, E., Bell, C., Pancras, T., 2016. Making strides in the management of "Emerging Contaminants". Ground Water Monitoring and Remediation, 36 (1), 15-25.

Sutton, N.B., Grotenhuis, T., Rijnaarts, H.H.M., 2014. Impact of organic carbon and nutrients mobilized during chemical oxidation on subsequent bioremediation of a diesel-contaminated soil. Chemosphere, 97, 64-70.

Sutton, N.B., Langenhoff, A.A., Lasso, D.H., van der Zaan, B., van Gaans, P., Maphosa, F., Smidt, H., Grotenhuis, T., Rijnaarts, H.H., 2014. Recovery of microbial diversity and activity during bioremediation following chemical oxidation of diesel contaminated soils. Applied Microbiology and Biotechnology, 98 (6), 2751-2764.

Tardy, V., Mathieu, O., Lévêque, J., Terrat, S., Chabbi, A., Lemanceau, P., Ranjard, L., Maron, P.A., 2014. Stability of soil microbial structure and activity depends on microbial diversity. Environmental Microbiology Reports, 6 (2), 173-183.

Thelusmond, J.-R., Strathmann, T.J., Cupples, A.M., 2016. The identification of carbamazepine biodegrading phylotypes and phylotypes sensitive to carbamazepine exposure in two soil microbial communities. Science of the Total Environment, 571, 1241-1252.

Vainberg, S., McClay, K., Masuda, H., Root, D., Condee, C., Zylstra, G.J., Steffan, R.J., 2006. Biodegradation of ether pollutants by *Pseudonocardia* sp strain ENV478. Applied and Environmental Microbiology, 72 (8), 5218-5224.

Vanwonterghem, I., Jensen, P.D., Dennis, P.G., Hugenholtz, P., Rabaey, K., Tyson, G.W., 2014. Deterministic processes guide long-term synchronised population dynamics in replicate anaerobic digesters. The ISME Journal, 8 (10), 2015-2028.

Vanwonterghem, I., Jensen, P.D., Dennis, P.G., Hugenholtz, P., Rabaey, K., Tyson, G.W., 2014. Deterministic processes guide long-term synchronised population dynamics in replicate anaerobic digesters. The ISME Journal, 8 (10), 2015.

Walden, C., Carbonero, F., Zhang, W., 2015. Preliminary assessment of bacterial community change impacted by chlorine dioxide in a water treatment plant. Journal of Environmental Engineering, 142 (2), 04015077.

Wang, F.F., van Halem, D., Liu, G., Lekkerkerker-Teunissen, K., van der Hoek, J.P., 2017. Effect of residual H_2O_2 from advanced oxidation processes on subsequent biological water treatment: A laboratory batch study. Chemosphere, 185, 637-646.

Wasmund, K., Mussmann, M., Loy, A., 2017. The life sulfuric: Microbial ecology of sulfur cycling in marine sediments. Environmental Microbiology Reports, 9 (4), 323-344.

Weigold, P., El-Hadidi, M., Ruecker, A., Huson, D.H., Scholten, T., Jochmann, M., Kappler, A., Behrens, S., 2016. A metagenomic-based survey of microbial (de) halogenation potential in a German forest soil. Scientific Reports, 6, 28958.

Wilson, M.M., Metcalf, W.W., 2005. Genetic diversity and horizontal transfer of genes involved in oxidation of reduced phosphorus compounds by *Alcaligenes faecalis* WM2072. Applied and Environmental Microbiology, 71 (1), 290-296.

Xia, Y., Chin, F.Y., Chao, Y., Zhang, T., 2015. Phylogeny-structured carbohydrate metabolism across microbiomes collected from different units in wastewater treatment process. Biotechnology for Biofuels, 8 (1), 172.

Xu, J.L., Deng, X., Cui, Y.W., Kong, F.X., 2016. Impact of chemical oxidation on indigenous bacteria and mobilization of nutrients and subsequent bioremediation of crude oil-contaminated soil. Journal of Hazardous Materials, 320, 160-168.

Xu, X.H., Liu, X.M., Zhang, L., Mu, Y., Zhu, X.Y., Fang, J.Y., Li, S.P., Jiang, J.D., 2018. Bioaugmentation of chlorothalonil-contaminated soil with hydrolytically or reductively dehalogenating strain and its effect on soil microbial community. Journal of Hazardous Materials, 351, 240-249.

Yang, S.Z., Wen, X., Zhao, L., Shi, Y.L., Jin, H.J., 2014. Crude oil treatment leads to shift of bacterial communities in soils from the deep active layer and upper permafrost along the china-russia crude oil pipeline route. Plos One, 9 (5), e96552.

Yang, Y., Cheng, D., Li, Y.N., Yu, L., Gin, K.Y.H., Chen, J.P., Reinhard, M., 2017. Effects of monochloramine and hydrogen peroxide on the bacterial community shifts in biologically treated wastewater. Chemosphere, 189, 399-406.

Zelezniak, A., Andrejev, S., Ponomarova, O., Mende, D.R., Bork, P., Patil, K.R., 2015. Metabolic dependencies drive species co-occurrence in diverse microbial communities. Proceedings of the National Academy of Sciences of the United States of America, 112 (20), 6449-6454.

Zhang, S., Gedalanga, P.B., Mahendra, S., 2016. Biodegradation kinetics of 1,4-dioxane in chlorinated solvent mixtures. Environmental Science & Technology, 50 (17), 9599-9607.

Zhang, S., Gedalanga, P.B., Mahendra, S., 2017. Advances in bioremediation of 1,4-dioxane-contaminated waters. Journal of environmental management, 204, 765-774.

Zhang, Z., Huang, J., Xia, H., Dai, Q., Gu, Y., Lao, Y., Wang, X., 2018. Chlorinated volatile organic compound oxidation over SO_4^{2-}/Fe_2O_3 catalysts. Journal of Catalysis, 360, 277-289.

Zheng, Y.G., Yin, H.H., Yu, D.F., Chen, X., Tang, X.L., Zhang, X.J., Xue, Y.P., Wang, Y.J., Liu, Z.Q., 2017. Recent advances in biotechnological applications of alcohol dehydrogenases. Applied Microbiology and Biotechnology, 101 (3), 987-1001.

Zhu, R., Mao, Y., Jiang, L., Chen, J., 2015. Performance of chlorobenzene removal in a nonthermal plasma catalysis reactor and evaluation of its byproducts. Chemical Engineering Journal, 279, 463-471.

Chapter 7 Conclusions and Future Work

7.1 Summary

This research comprehensively evaluated bioremediation of 1,4-dioxane and co-contaminants impacted groundwater and soil in bench- and pilot-scale studies, and revealed the molecular mechanisms behind the biodegradation processes by using next-generation sequencing technologies.

The multiple lines of evidence (MLOE) framework outlined in this research combined new technologies with traditional data analyses and successfully demonstrated that intrinsic biodegradation of 1,4-dioxane occurred at a landfill site. Molecular biological tools demonstrated that microorganisms capable of metabolizing 1,4-dioxane as well as methanotrophs capable of co-metabolizing 1,4-dioxane were present and abundant at the site. Notably, the detections of dioxane monooxygenase (*dxmB*) and aldehyde dehydrogenase (*aldH*) genes tracked the shrinking 1,4-dioxane plume with reasonable accuracy, strongly suggesting that the presence of 1,4-dioxane stimulated these markers and implying the microorganisms were degrading 1,4-dioxane. The detections of genes coding for soluble methane monooxygenase (sMMO) were widespread and non-specific to 1,4-dioxane, which was expected because co-metabolism is stimulated by the primary substrate (in this case, methane) rather than by the degradation of the co-metabolic substrate. Compound-specific stable isotope analysis (CSIA) implied a weak enrichment of ^{13}C in 1,4-dioxane as it was depleted with distance downgradient and provided additional evidence that a biochemical degradation process was active at this site. Coupled with the historical data that demonstrated that 1,4-dioxane concentrations and plume mass had declined, the results from this case study confirmed that intrinsic biodegradation of 1,4-dioxane was occurring at that site.

This research supported the first attempt of pilot-scale in-situ bioaugmentation to biodegrade 1,4-dioxane with well-characterized 1,4-dioxane-metabolizing bacteria *Pseudonocardia dioxanivorans* CB1190. The feasibility study indicated that injected CB1190 cells (> 10^7 copies/mL) were distributed at least 10 feet away from the injection well and followed preferential pathways, while only low cell densities were detected, supported by biomarker genes abundances and transcripts either in groundwater (< 242 copies/mL), or on Biotrap beads (122-674 copies/beads), or in the soil (141-433 copies/g). The second phase was implemented with higher injection cell density, along with oxygen and diammonium phosphate nutrient sources. However, the abundance and activity of the injected CB1190 steadily decreased in groundwater plume over 8 weeks, resulting in low to no 1,4-dioxane degradation after 6 weeks of the study. Subsequently, in-situ bioreactor (ISBR) contained CB1190-augmented Bio-sep beads were used on site and achieved stable CB1190 abundance and activity over 6 months. During this time, 1,4-dioxane was removed from 2.5 μg/bead to below 0.5 μg/bead, and the 1,4-dioxane in groundwater was degraded to below 30-50 μg/L. Thus, this step wise pilot study validated the feasibility of in-situ bioaugmentation by injecting liquid CB1190 culture as well as placing a bioreactor embedded with CB1190-augmented beads, while the long-term operation may be needed to obtain continuous 1,4-dioxane removal through ISBR.

In another project, effective remediation strategies using bioaugmentation with 1,4-dioxane-metabolizing or co-metabolizing bacteria, as well as oxygen, propane, and nutrient biostimulation were evaluated. Both bioaugmentation cultures degraded approximately 90% 1,4-dioxane in 1.5 days, with 1,4-dioxane falling below detection limits (< 4 μg/L) within 7 days. On day 15, 1,4-dioxane was added again but was undetectable by day 30. However, biostimulation with propane resulted in 1,4-dioxane removal only after sufficient nutrients were added, but oxygen amendments

did not stimulate 1,4-dioxane biodegradation even with added nutrients. Genes related to 1,4-dioxane degradation, *dxmB*, *aldH*, and *prmA*, were all upregulated after nutrient addition. Microbial community analysis showed that augmented genera *Pseudonocardia* and *Rhodococcus* were overwhelmed by other native bacteria over time with *Pseudonocardia* being outcompeted faster than *Rhodococcus*. After nutrient addition, the genera *Mycobacterium* and *Methyloversatilis* accumulated in propane-stimulated microcosms, but microbiomes distributed similarly in microcosms that were stimulated by oxygen and supplemented with nutrients. The predicted functions indicated that the gene allocation for xenobiotics metabolism and lipid metabolism was enhanced when high 1,4-dioxane degradation rates were observed, while the overall profiles of functions under bioaugmentation and biostimulation conditions depicted the similar pathway abundances over time. This indicated the potential functional redundancy and decoupling between metabolic functions and taxonomic community, and explained the community restoration and low 1,4-dioxane removal performances.

Several laboratory-scale treatment trains were tested that applied short-term chemical reactions to 1,4-dioxane and chlorinated solvent contaminated groundwater and soil prior to bioaugmentation processes. The combined chemical treatments were first tested so that the oxidation process removed 85% of initial 1,4-dioxane under all conditions, and subsequent catalysis step extended the removal to 90%. The overall microbial community analysis based on multidimensional analyses directly showed that H_2O_2 and WO_x/ZrO_2 caused population shifts away from the original community even with similar high removals. The biodiversity was changed depending on the contaminant levels after oxidation process, while WO_x/ZrO_2 catalysis reduced biodiversity across all conditions. The taxonomic classification combined with Linear discriminant analysis Effect Size (LEfSe)

confirmed the potential oxidative tolerant genera, such as *Massilia* and *Rhodococcus*, as well as WO_x/ZrO_2 tolerant genera *Sphingomonas* and *Devosia*.

The effectiveness of oxidation-bioaugmentation treatment trains was also revealed by the complete removal of 1,4-dioxane in the presence of chlorinated volatile organic compounds (CVOCs). The shifts in microbial community structures occurred in the course of time. They were influenced by contaminant concentrations only at individual time points and accompanied by r-K strategy transitions. Various microbial groups recovered after exposure to peroxide, a microbicide, and evolved during the biodegradation with deterministic factors, including competition, interaction, and niche differentiation, which were also reflected by increased biodiversity during the post-oxidation biodegradation process.

The catalysis-bioaugmentation treatment train showed the similar efficiency towards 1,4-dioxane and CVOC degradation, indicating that 1,4-dioxane biodegradation by CB1190 could be catalytically enhanced, while CVOCs could be continuously removed during the post-catalysis biodegradation phase by intrinsic microbes regardless of the initial concentrations. Moreover, the microbial community analysis indicated a more stable structure under all conditions after the treatment train with a higher biodiversity of microbes with biodegradation capabilities. The composition of microbiomes tended to be similar regardless of complex contaminants during the post-catalysis biodegradation phase, indicating a r-K scheme transition attributed to the shock experienced during catalysis and the subsequent incubation. The predicted functional features found that reads belonging to monooxygenases remained constant during the biodegradation phase while reads belonging to dehalogenases increased, and this pattern corresponded to increasing CVOC removals. The population dynamics followed deterministic temporal succession even under different contamination conditions, which was supported by the PCoA analysis and random forests models,

that microbial community tended to be similar during the biodegradation process. The network analysis further emphasized deterministic factors, such as ecological niches or microbial competitions, overwhelmed contaminants combinations matrix, dominating and guiding the microbial assembly. The above findings offered novel insights into the ecological mechanisms underlying the effects of 1,4-dioxane and CVOCs on short-term and long-term remediation performance.

Collectively, this research comprehensively evaluated natural and enhanced bioremediation technologies at 1,4-dioxane contaminated sites and validated the 1,4-dioxane degradation by metabolic and co-metabolic bioaugmentation as well as oxygen-, propane-, nutrient-amended biostimulation from both bench- and pilot-scale studies. Additionally, chemical treatment followed by bioaugmentation was developed as an effective synergistic treatment for 1,4-dioxane in the presence of high CVOC concentrations. Besides, applying parallel sequencing technologies revealed the microbial community and function as well as molecular mechanisms, and assessed the microbial ecology along with the ongoing and post-remediation processes. These results will be valuable for predicting treatment synergies that lead to cost savings and improve remedial outcomes in short-term active remediation as well as long-term changes to the environmental microbial communities.

7.2 Significance of the Research

This research systematically explored monitored natural attenuation, bioaugmentation, and biostimulation strategies for 1,4-dioxane treatment, across bench- to pilot-scale studies, coupled with microbial community and function analyses, explicating the following insights.

1. Advanced molecular biological tools, including biomarkers of 1,4-dioxane metabolism, and improved compound-specific stable isotope analysis (CSIA) techniques are critical and accurate in demonstrating intrinsic degradation for 1,4-dioxane.
2. The first pilot-scale *Pseudonocardia dioxanivorans* CB1190 bioaugmentation effort validated the applicability of in-situ metabolic biodegradation of 1,4-dioxane and provided important design and selection considerations for future full-scale demonstration at various contaminated sites.
3. Various investigations of 1,4-dioxane-metabolizing and co-metabolizing bacteria, as well as doses of oxygen, propane, and nutrients in laboratory-scale reactors provided quantitative data for design and decision-making for full-scale ex-situ bioreactors and in-situ bioremediation applications.
4. The treatment trains indicated that oxidation-catalysis, oxidation-bioaugmentation, and catalysis-bioaugmentation could completely remove 1,4-dioxane even in the presence of chlorinated compounds.
5. Analyses of microbial community structure before, during, and after active remediation are valuable for identifying functionally-important bacteria, metabolic pathways, and microbial trajectories and for predicting treatment synergies that lead to cost savings and improved remedial outcomes in short-term active remediation as well as long-term changes to the environmental microbial communities.

7.3 Directions of Future Research

7.3.1 Field-scale Applications and Long-Term Monitoring

The results of our bench-scale microcosms and pilot-scale demonstrations indicated that bioremediation should be considered as an alternative to or in conjunction with other abiotic

remediation strategies. Bioaugmentation with CB1190 or other 1,4-dioxane-metabolizing bacteria can be viable, especially in in-situ or ex-situ bioreactors. The ISBR technology showed promising results in the in-situ pilot test, which could be scaled-up and applied more widely in the remediation of various contaminant mixtures. While metabolic degradation approach has the advantages of supporting the growth of bacteria involved in bioremediation, generation of non-toxic terminal products, and lower requirements of substrate addition, co-metabolism-based processes might be preferred in dilute plumes or when 1,4-dioxane concentrations are very low. Since biostimulation with propane and nutrients was tested successfully in the bench-scale microcosms, propane biosparging should be considered as an option for in-situ 1,4-dioxane treatment in groundwater, even though this approach was not very effective in previous work (Lippincott et al., 2015, Chu et al., 2018). Other liquid or gaseous organic substrates, such as methane, ethane, butanol, or various ethers should be evaluated for inducing 1,4-dioxane co-metabolism in laboratory as well as field settings.

A comprehensive monitoring program is necessary to track not only the contaminant removals, but also changes in bacterial population, activity, and community structure. As long-term monitoring data become available to better support degradation processes using a multiple lines of evidence (MLOE) framework, community analysis can reveal the dominant microbiomes in natural or engineered conditions that impact or are impacted by environmental factors.

7.3.2 Microbial Community and Function Analysis at Post in-situ Treatment Sites

Any in-situ treatment, including biotic and abiotic strategies, will be in contact with the indigenous microbes living in the 1,4-dioxane contaminated soil and groundwater, which are key drivers in various fundamental biogeochemical processes as well as decontaminating processes. However, conventional in-situ remediation process pays more attention to eliminating the

pollutants, which would decide the success of the engineered work. However, the goals of remediation are not only to remove pollutants from soil and groundwater but also to restore the capacity of the soil ecology to function at its potential (Epelde et al., 2009). Thus, post-treatment revisit focusing on microbial diversity, core microbes, and functions in the former remediated areas could re-evaluate the ecological health from the microbial point of view. Moreover, the post-treatment dynamic changes of microbial community will suggest the new isolates or consortia for future bioremediation work targeting the sites with similar characteristics.

7.3.3 Nexus of -Omics Technologies, Microbiology, and Biochemistry

Even as the metagenomics technologies along with bioinformatics tools have been rapidly developed, some limitations might still hamper the normal use of metagenomics. In the current blooming usage of "-omics", microbial community profiled by 16S rRNA sequencing is the quickest and cheapest avenue. However, a complete and "all-in-one" analysis of phylogenetic and functional shifts in polluted ecosystems is needed because datasets only reflect the taxonomic and the functional diversity of microbial communities, while the interactions among community members are usually highly dynamic over time (Prosser, 2015, Bouhajja et al., 2016). However, metagenomics alone will always describe the taxonomic and functional abundances of communities with specific research objectives (Bouhajja et al., 2016). To address this issue, Franzosa et al. (2015) suggested to combine different "-omics" approaches, such as metatranscriptomics to analyze the mRNA of a community by cDNA massive sequencing (Prosser, 2015), metaproteomics to analyze the protein composition (Pan and Banfield, 2014), and using metabolomics to analyze the metabolite in the pathway (Longnecker et al., 2015). The synergistic "-omics" could provide a global overview of the nature, the evolution and the expression of microbial catabolic pathways in polluted environments (Bouhajja et al., 2016).

More generally, the full exploitation of the potentials of meta-omics will also require multiple and creative benchmarking methodologies and reverse engineering of reference soils, among other reductionist and holistic approaches (Nesme et al., 2016). The increasing number of novel putative protein sequencing revealed and annotated in metagenomic reads are emphasized in the diversity and richness of environmental functions, which however lack evidence of their actual function due to the limited number of reference proteins in databases. Therefore, conventional microbiology (isolation and cultivation of pure strains) and biochemistry (characterization of proteins), to validate the actual functions of annotated sequencing in the experiments, are also need to couple with "-omics". Bioremediation-related engineered work can benefit from these rare proteins expressed in species adapted to contaminated environments.

7.4 References

Bouhajja, E., Agathos, S.N., George, I.F., 2016. Metagenomics: Probing pollutant fate in natural and engineered ecosystems. Biotechnology Advances, 34 (8), 1413-1426.

Chu, M.Y.J., Bennett, P.J., Dolan, M.E., Hyman, M.R., Peacock, A.D., Bodour, A., Anderson, R.H., Mackay, D.M., Goltz, M.N., 2018. Concurrent treatment of 1,4-dioxane and chlorinated aliphatics in a groundwater recirculation system via aerobic cometabolism. Ground Water Monitoring and Remediation, 38 (3), 53-64.

Epelde, L., Mijangos, I., Becerril, J.M., Garbisu, C., 2009. Soil microbial community as bioindicator of the recovery of soil functioning derived from metal phytoextraction with sorghum. Soil Biology & Biochemistry, 41 (9), 1788-1794.

Franzosa, E.A., Hsu, T., Sirota-Madi, A., Shafquat, A., Abu-Ali, G., Morgan, X.C., Huttenhower, C., 2015. Sequencing and beyond: integrating molecular 'omics' for microbial community profiling. Nature Reviews Microbiology, 13 (6), 360-372.

Lippincott, D., Streger, S.H., Schaefer, C.E., Hinkle, J., Stormo, J., Steffan, R.J., 2015. Bioaugmentation and propane biosparging for in situ biodegradation of 1,4-dioxane. Ground Water Monitoring and Remediation, 35 (2), 81-92.

Longnecker, K., Futrelle, J., Coburn, E., Soule, M.C.K., Kujawinski, E.B., 2015. Environmental metabolomics: Databases and tools for data analysis. Marine Chemistry, 177, 366-373.

Nesme, J., Achouak, W., Agathos, S.N., Bailey, M., Baldrian, P., Brunel, D., Frostegard, A., Heulin, T., Jansson, J.K., Jurkevitch, E., Kruus, K.L., Kowalchuk, G.A., Lagares, A., Lappin-Scott, H.M., Lemanceau, P., Le Paslier, D., Mandic-Mulec, I., Murrell, J.C., Myrold, D.D., Nalin, R., Nannipieri, P., Neufeld, J.D., O'Gara, F., Parnell, J.J., Puhler, A., Pylro, V., Ramos, J.L., Roesch, L.F.W., Schloter, M., Schleper, C., Sczyrba, A., Sessitsch, A., Sjoling, S., Sorensen, J., Sorensen, S.J., Tebbe, C.C., Topp, E., Tsiamis, G., van Elsas, J.D., van Keulen, G., Widmer, F., Wagner, M., Zhang, T., Zhang, X.J., Zhao, L.P., Zhu, Y.G., Vogel, T.M., Simonet, P., 2016. Back to the future of soil metagenomics. Frontiers in Microbiology, 7.

Pan, C., Banfield, J.F. (2014). Environmental Microbiology, pp. 231-240, Springer.

Prosser, J.I., 2015. Dispersing misconceptions and identifying opportunities for the use of 'omics' in soil microbial ecology. Nature Reviews Microbiology, 13 (7), 439-446.